PPHMF-IV

Proceedings of

Physical Phenomena at High Magnetic Fields - IV

Editors

G. Boebinger

Z. Fisk

L. P. Gor'kov

A. Lacerda

J. R. Schrieffer

World Scientific

This page is intentionally left blank

Proceedings of

Physical Phenomena at High Magnetic Fields - IV

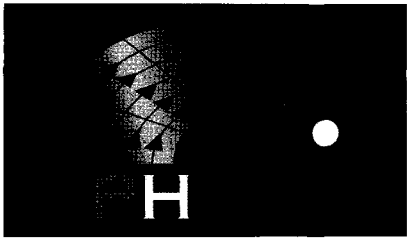

Proceedings of

Physical Phenomena at High Magnetic Fields - IV

Santa Fe, New Mexico, USA 19–25 October 2001

Editors

G. Boebinger
Los Alamos National Laboratory, New Mexico, USA

Z. Fisk
National High Magnetic Field Laboratory, Florida State University, USA

L. P. Gor'kov
National High Magnetic Field Laboratory, Florida State University, USA

A. Lacerda
Los Alamos National Laboratory, New Mexico, USA

J. R. Schrieffer
National High Magnetic Field Laboratory, Florida State University, USA

World Scientific
Singapore • New Jersey • London • Hong Kong

Published by

World Scientific Publishing Co. Pte. Ltd.

P O Box 128, Farrer Road, Singapore 912805

USA office: Suite 1B, 1060 Main Street, River Edge, NJ 07661

UK office: 57 Shelton Street, Covent Garden, London WC2H 9HE

British Library Cataloguing-in-Publication Data
A catalogue record for this book is available from the British Library.

PHYSICAL PHENOMENA AT HIGH MAGNETIC FIELDS–IV

ISBN 981-02-4896-2

Printed in Singapore.

PREFACE

Physical Phenomena at High Magnetic Fields-IV (PPHMF-IV) was the fourth conference sponsored by the National High Magnetic Field Laboratory (NHMFL). The previous conferences were held in May, 1991, 1995, and 1998. These meetings brought together experts in scientific research areas where high magnetic fields could make an important impact.

PPHMF-III devoted substantial time to reviewing the state of many fields in regard to the role of high magnetic fields, such as semiconductors, heavy fermions, superconductivity, and molecular conductors. Since these topics have been thoroughly examined in PPHMF-III, it was felt that the present conference should be devoted to recent developments in these fields.

The conference which took place in October, 2001, at Santa Fe Convention Center in Santa Fe, NM, was organized with invited lectures in the morning and late afternoon and poster sessions in the early afternoon. This schedule permitted extensive discussion with the poster contributors and was judged to be an effective format by the 150 participants in attendance.

As in the past conferences, World Scientific was chosen to be the publisher of the proceedings because of their excellent handling of the prior proceedings.

The editors of these proceedings are pleased to acknowledge their gratitude to the many who worked so hard to bring about this most successful conference. We wish to thank the staff of the NHMFL, especially Wally Thorner of the NHMFL Educational Media Department, LeeRoy Herrera, Marion Hutton, Lou Miller and Alice Hobbs for taking care of the correspondence and travel arrangements. We would also like to warmly thank Julie Gallegos and Mary Layne, for their outstanding help in organizing this conference, and handling the production issues of these proceedings

Finally, our heartfelt thanks to those who put behind them the fears and concerns of the September 11, 2001 events and boarded plans, trains, cars and made the PPHMF-IV conference a tremendous success.

This page is intentionally left blank

CONTENTS

---

* Abstract only

---

* Abstract only

Part II Heavy Fermions

---

* Abstract only

---

* Abstract only

Part III Molecular Conductors

---

* Abstract only

---

* Abstract only

---

* Abstract only

---

* Abstract only

---

* Abstract only

---

* Abstract only

---

* Abstract only

---

* Abstract only

---

* Abstract only

---

* Abstract only

* Abstract only

Part I

Semiconductors/QHE

This page is intentionally left blank

QUANTUM HALL EFFECT IN AlAs 2D ELECTRON SYSTEMS

E. P. DE POORTERE, E. TUTUC, Y. P. SHKOLNIKOV, K. VAKILI and M. SHAYEGAN
Department of Electrical Engineering, Princeton University, Princeton, NJ 08544

E. PALM and T. MURPHY
National High Magnetic Field Laboratory, Tallahassee, FL 32310

We report on fabrication of two-dimensional electrons in AlAs quantum wells with mobilities up to 31 m^2/Vs. Magnetoresistance measurements reveal fractional quantum Hall states at high-order filling factors, and up to $\nu = 11/3$. Shubnikov-de Haas oscillations of high-density samples suggest that electrons occupy two X-point valleys. We also study properties of hysteretic resistance spikes occurring at transitions between quantum Hall ferromagnets in AlAs quantum wells, and show that the spike hysteresis depends sensitively on the number of occupied energy levels involved in the transition.

1 Introduction

Although a great deal of work has been done on two-dimensional electron systems (2DESs) in GaAs quantum wells, little attention has been given to the electronic properties of clean 2DESs confined to AlAs quantum wells. In the vast majority of GaAs/AlAs structures, the electrons are confined in the GaAs while AlAs, or more commonly AlGaAs, is used as the barrier material. The electrons in this case occupy the conduction band minimum at the Γ-point of the Brillouin zone (see Fig.1

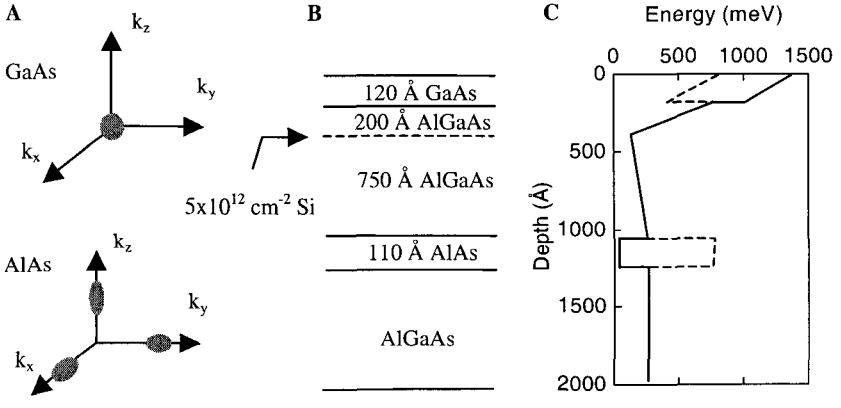

Figure 1: (A) Fermi surfaces of conduction electrons in GaAs and AlAs. (B) Schematic cross-section and (C) conduction band diagram of the AlAs quantum well. In (C), X-point and Γ-point conduction band edges are indicated by solid and dashed lines, respectively.

1). However, in a structure containing a pure AlAs quantum well and selectively-doped AlGaAs barriers with an Al mole fraction greater than about 40%, one can confine electrons to the AlAs layer.[1-5] In this case, the electrons occupy the X-point conduction band valleys and have properties that are quite distinct from GaAs 2DESs.

Bulk AlAs has a six-fold degenerate conduction band minimum at the Brillouin zone X-point, giving rise to ellipsoidal Fermi surfaces for conduction electrons (Fig. 1(A)). The electrons have a large and anisotropic effective mass (m_l = 1.1, m_t = 0.19) in contrast to the much lighter and isotropic mass (m^* = 0.067) of electrons in GaAs (all effective masses are given in units of the free electron mass).[6] The effective Landé g-factor of electrons in AlAs (g^* = 2) is also much larger and of a different sign than in GaAs (g^* = -0.44). Moreover, the electrons occupy multiple conduction band valleys in AlAs. These three main characteristics also differentiate 2D electrons in modulation-doped AlAs quantum wells from those in GaAs quantum wells, and lead to novel phenomena, examples of which are shown in Figs. 2 to 4 and are discussed in the following sections.

The layer structure near the surface of a typical sample is shown in Fig. 1(B). A pure AlAs layer is sandwiched between layers of $Al_{0.40}Ga_{0.60}As$, and is modulation-doped with a Si delta layer placed at a distance of 75 nm away. Figure 1(C) depicts the conduction band edge as a function of distance from the surface. Four AlAs quantum wells are presented here: samples A and B, with an AlAs well width of 150 Å, and samples C and D, 110 Å-wide quantum wells. Sample A was grown on a (411)B GaAs substrate, while samples B-D were grown on (100) GaAs. AuGeNi pads alloyed at 440 °C provided contacts to the 2D electron gas. Samples were also fitted with a back gate and (for all but sample B) with a 300 Å-thin front gate. We performed transport measurements down to T = 30 mK in a dilution refrigerator and in magnetic fields up to 42 T. Using a combination of illumination and front/back gate biasing, we were able to vary carrier density from 1.0 x 10^{11} cm^{-2} to 9.4 x 10^{11} cm^{-2}. The highest mobility reached in these samples is 31 m^2/Vs (see Ref. [7]), a factor of ten higher than in previous samples.[3]

2 Ising Transitions between Integer Quantum Hall States

In a past publication,[8] we have described how near all integer filling factors larger than or equal to 3, transitions between quantum Hall ferromagnets in AlAs give rise to sharp resistance spikes that are hysteretic in magnetic field. Such transitions are observed when samples are submitted to both parallel ($B_{||}$) and perpendicular ($B_{\perp}$) magnetic fields (Fig. 2(C)). As the angle θ between the sample and the magnetic field (B_{tot}) is increased, energy levels cross or come into "coincidence" for several values of the tilt angle, all within easily accessible experimental range. Magnetic transitions, and their corresponding resistance spikes, occur at these level crossings.

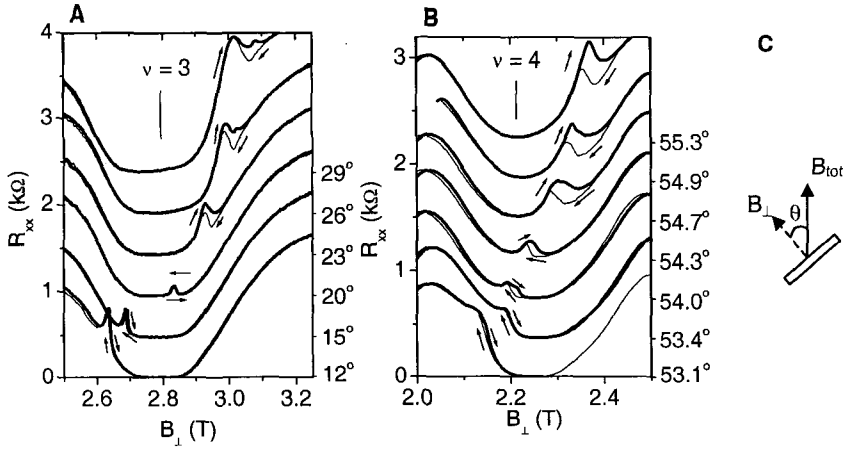

Figure 2: Resistance spikes near integer filling factors in an AlAs 2DES with density $n \cong 2 \times 10^{11}$ cm^{-2} at $T \sim 30$ mK, in tilted magnetic fields (Sample A). Spikes occur at transitions between quantum Hall ferromagnets

The resistance spikes, and their associated hysteresis, are linked to the magnetic domain morphology at the transition, and are thus of prime interest for the study of Ising ferromagnetism.[9-15] We also note that the values of the magnetic field at which resistance spikes occur can be measured with precision, a fact which enables us to derive the change in exchange energy of the electron system as it undergoes the Ising transition.[8] We show here how the hysteresis strength depends on the exact filling factor of the 2DES at the transition.

Coincidences occurring near $\nu = 3$ and $\nu = 4$ are plotted in Fig. 2, which illustrates the sensitivity of the spike position to the tilt angle. Figure 2 also shows the dependence of hysteresis on the exact filling factor at which the transition takes place. We observe that the spikes at $\nu = 3 - \varepsilon$ and at $\nu = 4 - \varepsilon$ are strongly hysteretic, while for $\nu = 3 + \varepsilon$ and $\nu = 4 + \varepsilon$, they are not ($0 < \varepsilon < 1/2$). A possible reason for this variation in hysteresis is that for $\nu < 3$ or $\nu < 4$, the transition involves flipping spins of electrons contained in only one Landau level, while for $\nu > 3$ or $\nu > 4$, one of the two levels involved in the transition is filled while the other is partially occupied. In the latter configuration, electrons in the top two occupied Landau levels flip their spin across the transition, which may imply a different, non-hysteretic, mechanism for the formation of domains. More measurements are needed to fully understand the nature of the transitions, such as temperature and density dependences.

3 Fractional Quantum Hall Effect

Figure 3(A) shows the longitudinal resistivity of sample B at $T \sim 100$ mK. Strong ρ_{xx} minima are observed at fractional fillings $\nu = 2/3$, 3/5, and 2/5 beyond $\nu = 1$, and at $\nu = 4/3$ and 5/3 at higher fillings, while shallower minima are present at $\nu = 3/7$, 4/7 and 4/9. Besides $\nu = 2/3$, none of these FQH states have previously been reported in AlAs. Interestingly, 2D electrons with similar mobilities and densities

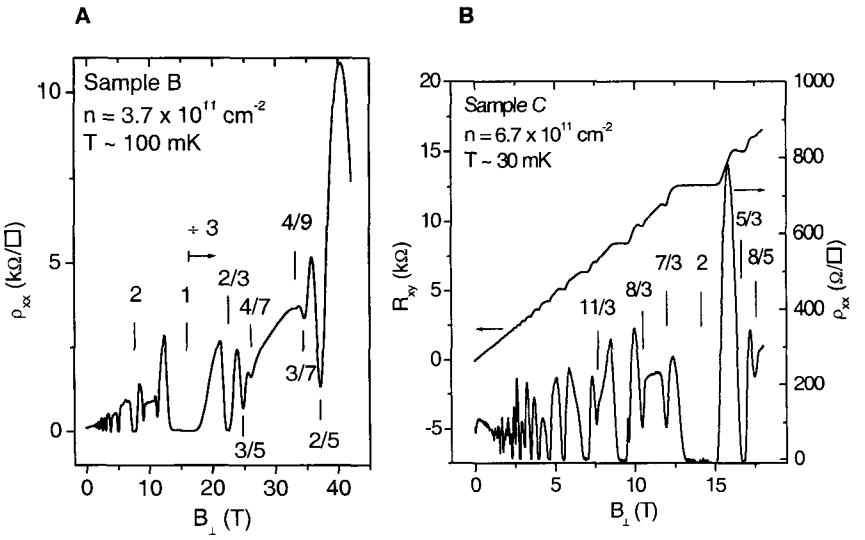

Figure 3: Magnetoresistance of AlAs 2D electrons at $\theta = 0°$: (A) at a density $n = 3.7 \times 10^{11}$ cm^{-2} and $\mu \cong 18$ m^2/Vs, showing developing fractional quantum Hall states up to $\nu = 4/9$; and (B) at $n = 6.7 \times 10^{11}$ cm^{-2} and $\mu \cong 13$ m^2/Vs, exhibiting fractional quantum Hall states at filling factors up to $\nu = 11/3$.

in GaAs show fewer and weaker FQH resistance minima.[16] This is surprising in view of the fact that AlAs 2D electrons, due to their smaller cyclotron energy, are subjected to stronger Landau level mixing, which should weaken the FQH gaps.[17] As noted above, the deeper FQH minima in AlAs might be related to the higher effective mass in this material, which enhances the effect of the Coulomb interaction. We note that similarly, an anomalously large FQH energy gap has been reported in 2D holes in tetracene,[18] which also have a larger m^*. Results in AlAs and tetracene thus both call for a better understanding of the FQH in high-mobility 2D systems with a large effective mass.

Magnetoresistance data from our higher-density sample (C) are plotted in Fig. 3(B). Strong Shubnikov-de Haas oscillations are visible down to $B = 0.5$ T, corresponding to a filling factor greater than 55. Beating is also observed in the magnetoresistance oscillations, indicating that more than one subband is occupied. Because the quantum well has a narrow width of 110 Å, we do not expect a second electric subband to be occupied at the density present in this sample; we suggest instead that electrons in this sample occupy more than one X-valley. Further evidence for multi-valley occupancy is provided in the next section.

Also seen in Fig. 3(B) are FQH states at higher filling factors ($2 < \nu < 4$): these develop at $\nu = 7/3$, 8/3, and 11/3. Moreover, when we tilt the sample in magnetic field at higher carrier densities, we observe small dips in ρ_{xx} at $\nu = 13/3$, 14/3, and 17/3, suggesting the development of a FQH state at these fillings as well. To the best we know, states at such high fillings have not been observed in other materials, including in the highest-quality GaAs 2D electrons.[19] As a tentative explanation for the presence the $\nu = 11/3$ FQH state, e.g., we suggest that at $\nu = 11/3$: (1) two valleys are occupied and (2) electrons are distributed in a 2:(5/3) ratio between the

valleys. In other words, the 11/3 state is composed of a $\nu = 2$ state in one valley and a $\nu = 5/3$ state in the other valley. Verification of this conjecture of course requires further work, but we would like to mention that similar hybrid states have been reported in bilayer systems.[20]

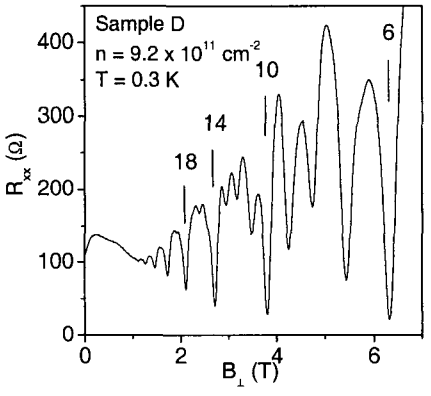

Figure 4: Magnetoresistance of 2D electrons in an AlAs quantum well where two nearly-degenerate X-valleys are occupied. Strong resistance minima are seen at every fourth integer Landau level filling.

4 Multi-Valley Occupancy

In Fig. 4 we plot Shubnikov-de Haas oscillations of 2D electrons in sample D, where the electron density is 9.2 x 10^{11} cm^{-2} and the mobility 19 m^2/Vs. Strongest resistance minima occur at $\nu = 6$, 10, 14, 18, 22, etc., indicating that levels are grouped in near-degenerate quadruplets. Since we do not expect a second electric subband to be occupied at a density of 9.2 x 10^{11} cm^{-2} in this sample, we suggest that electrons occupy more than one X-valley, which together with the spin-splitting of Landau levels, can account for the quadruplet grouping of energy levels. Magnetotransport measurements performed in tilted fields, the results of which will be published elsewhere,[21] also confirm the occupation of a second valley by AlAs 2D electrons. Altogether, these results contrast with former studies of 2D electrons in similar AlAs quantum wells, where electrons were seen to occupy only one of the two X valleys.[22] Van de Stadt *et al.*,[5] have reported double-valley occupancy in a high-density 80 Å-wide AlAs quantum well, though the mobility in these samples was limited to 1.5 m^2/Vs. We also mention that most other Hall bar samples (with front gates) we have measured show double-valley occupancy as well, though the energy splitting between valleys seems to vary greatly from sample to sample. A possible cause for this variation in valley splitting is that the relative positions of the conduction band minima in AlAs are highly sensitive to strain in the quantum well.[4]

In addition, this strain might be anisotropic in the plane of the 2DEG. Further work needs to be done to determine the influence of strain on valley splitting in AlAs 2D electrons.

5 Conclusion

We measured magnetoresistance of high-mobility 2D electrons in AlAs quantum wells with mobilities up to 31 m^2/Vs. Magnetotransport measurements in gated Hall bars, such as in samples C and D, show that at high electron densities, more than one X-valley are occupied by electrons. We also observe, for the first time in this material, fractional quantum Hall states up to the fourth order and at high fillings (e.g. $\nu = 11/3$), the latter likely resulting from double valley occupancy. In addition, we investigated the hysteretic properties of resistance spikes at ferromagnetic transitions in AlAs. We observe that magnetic hysteresis of the spikes is strongest when only one of the crossing levels is occupied.

This work was supported by the NSF.

References

1. T. P. Smith III *et al., Surf. Sci.* **88**, 287 (1987).
2. K. Maezawa *et al., Appl. Phys. Lett.* **62**, 3120 (1993).
3. T. S. Lay *et al., Appl. Phys. Lett.* **62**, 3120 (1993).
4. S. Yamada *et al., Physica B* **201**, 295 (1994).
5. A. F. W. van de Stadt *et al., Surf. Sci.* **361/362**, 521 (1996).
6. S. Adachi, *J. Appl. Phys.* **58**, R1 (1985).
7. E. P. De Poortere *et al., Appl. Phys. Lett.* (in press).
8. E. P. De Poortere *et al., Science* **290**, 1546 (2000).
9. T. Jungwirth *et al., Phys. Rev. B* **63**, 035305 (2001).
10. T. Jungwirth *et al.*, e-Print available at xxx.lanl.gov/abs/cond-mat/0104334.
11. H. Cho *et al., J. Phys. Rev. Lett.* **81**, 2522 (1998).
12. T. Jungwirth *et al., Phys. Rev. Lett.* **81**, 2328 (1998).
13. V. Piazza *et al., Nature* **402**, 638 (1999).
14. J. Eom *et al., Science* **289**, 2320 (2000).
15. J. H. Smet *et al., Phys. Rev. Lett.* **86**, 2412 (2001).
16. See, e.g., E. E. Mendez *et al., Phys. Rev. B* **30**, 7310 (1984).
17. D. Yoshioka, *J. Phys. Soc. Japan* **55**, 885 (1986).
18. H. Schön *et al., J. Phys. Cond. Matt.* **13**, L163 (2001).
19. W. Pan *et al., Phys. Rev. Lett.* **83**, 820 (1999).
20. H. C. Manoharan *et al., Phys. Rev. Lett.* **79**, 2722 (1997).
21. Y. P. Shkolnikov *et al., in preparation.*
22. S. J. Papadakis *et al., Phys. Rev. B* **59**, R12743 (1999).

TUNNELING IN A QUANTUM HALL EXCITONIC CONDENSATE

J. P. EISENSTEIN,[1] I. B. SPIELMAN,[1]
L. N. PFEIFFER[2] and K. W. WEST[2]
[1]*California Institute of Technology, Pasadena, California 91125, USA*
[2]*Bell Laboratories, Lucent Technologies, Murray Hill, New Jersey 07974, USA*

Recent experiments on the tunneling conductance between parallel 2D electron gases at total Landau level filling $\nu_{tot} = 1$ are described. When the two layers are close enough together the ground state of the system may be viewed as a Bose condensate of excitons consisting of electrons in one layer paired with (conduction band) holes in the other. The measured tunneling conductance exhibits a spectacular resonance around zero bias which resembles the dc Josephson effect. This resonance is a signature of long wavelength Goldstone collective modes in the phase coherent ground state. Experiments performed with an added in-plane magnetic field have demonstrated the expected linear dispersion of this mode.

QUANTUM HALL LIQUID CRYSTALS

M. M. FOGLER

Department of Physics, Massachusetts Institute of Technology, 77 Massachusetts Avenue, Cambridge, MA 02139, USA

The stripe phase of a two-dimensional electron system in a weak magnetic field bears a close analogy to liquid crystals. However, reduced dimensionality and unusual dynamics give rise to important differences. At finite temperature they cause divergent fluctuations and nonperturbative renormalization of hydrodynamic parameters. Such effects can be verified in microwave experiments. At low temperatures the physics is dominated by quantum fluctuations. When they are large, the transition to a novel quantum nematic phase may occur, driven by quantum proliferation of dislocations. It will be signaled by an additional low-frequency resonance in the microwave response.

1 Introduction

Historically, most of the research in the area of the quantum Hall effect has been focused on the case of very strong magnetic fields B where all the electrons reside at the lowest Landau level (LL). Recently, it has been discovered that moderate and weak magnetic fields, i.e., high LLs, is also a realm of very interesting physics.[1] A partially filled high LL undergoes a charge-density wave (CDW) transition below a temperature $T_c^{mf} \sim 0.06e^2/\kappa R_c$ where $R_c \propto 1/B$ is the classical cyclotron radius and κ is the bare dielectric constant. Near half-filling, $\nu \sim 2N + \frac{1}{2}$, the resultant CDW is a unidirectional, i.e., the *stripe phase*. At other filling fractions, the CDW has a symmetry of the triangular lattice and is called the *bubble phase*. At low temperatures the system becomes divided into depletion regions where the local filling fraction is equal to $2N$, and stripe- or bubble-shaped domains with the local filling fraction $2N + 1$. The CDW periodicity is set by the wavevector[1] $q_* \approx 2.4/R_c$. In the quasiclassical limit of large LL indices N the CDW is well described by the mean-field theory.[1,2] At moderate N there are sizeable fluctuations around the mean-field solution, which may lead to a new physics described below. At such N the CDW phases compete with Laughlin liquids and other fractional quantum Hall (FQH) states. A combination of analytic and numerical tools[1,3,4,5] suggests that the FQH states lose to the CDW at $N \geq 2$. The existence of the stripe phase as a physical reality was evidenced by a conspicuous magnetoresistance anisotropy observed near half-integral fractions of high LLs.[6,7] This stimulated a considerable amount of theoretical work devoted to the stripes. It led to the understanding that the "stripes" may appear in several distinct

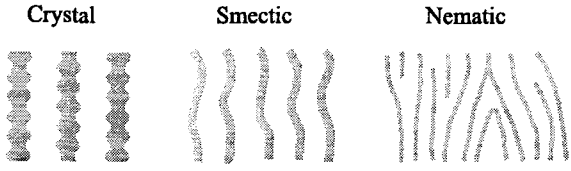

Figure 1. Sketches of possible stripe phases.

forms: an anisotropic crystal, a smectic, and a nematic (Fig. 1). These phases succeed each other in the order listed as the magnitude of either quantum or thermal fluctuations increases. The general structure of a phase diagram that includes these novel phases was discussed in the important paper of Fradkin and Kivelson[8] (for $T = 0$). The most intriguing are the phases which bear the liquid crystal names: the smectic and the nematic.

The smectic is a liquid with the 1D periodicity, i.e., a state where the translational symmetry broken only in one spatial direction.[9] An example of such a state is the original Hartree-Fock stripe solution[1] although a stable quantum Hall smectic must have a certain amount of quantum fluctuations around the mean-field state.[10,11] The necessary condition for the smectic order is the continuity of the stripes. If the stripes are allowed to rupture, the dislocations are created. They destroy the 1D positional order and convert the smectic into a nematic.[12]

By definition, the nematic is an anisotropic liquid.[9] There is no long-range positional order. As for the orientational order, it is long-range at $T = 0$ and quasi-long-range (power-law correlations) at finite T. The nematic is riddled with dynamic dislocations.

It is often the case that the low-frequency long-wavelength physics of the system is governed by an effective theory involving a relatively small number of dynamical variables. In the remaining sections I will discuss such type of theories for the quantum Hall liquid crystals.

2 Smectic state

The collective variables in the smectic are (i) the deviations $u(x, y)$ of the stripes from their equilibrium positions and (ii) long-wavelength density fluctuations n about the average value n_0. The latter fluctuations may originate, e.g., from width fluctuations of the stripes. Let us assume that the stripes are aligned in the $\hat{\mathbf{y}}$-direction, then the symmetry considerations fix the effective

Hamiltonian for u and n to be[9,13]

$$H = \frac{Y}{2}\left[\partial_x u - \frac{1}{2}(\nabla u)^2\right]^2 + \frac{K}{2}(\partial_y^2 u)^2 + \frac{1}{2} n V n, \tag{1}$$

where Y and K are the phenomenological compression and the bending elastic moduli, and $V(r) = e^2/\kappa r$ should be understood as the integral operator. The dynamics of the smectic is dominated by the Lorentz force and is governed by the Largangean[14]

$$\mathcal{L} = p\partial_t u - H, \quad \partial_y p = -m\omega_c(n + n_0 \partial_x u) \tag{2}$$

where m is the electron mass and $\omega_c = eB/mc$ is the cyclotron frequency.

It is natural to start with the harmonic approximation where one replaces the first term in H simply by $(Y/2)(\partial_x u)^2$. Solving the equations of motion for n and u we obtain the dispersion relation for the phonon-like vibrations of the stripes (referred to as *magnetophons* in what follows):[13]

$$\omega(\mathbf{q}) = \frac{\omega_p(q)}{\omega_c}\frac{q_y}{q}\left[\frac{Y q_x^2 + K q_y^4}{m n_0}\right]^{1/2}. \tag{3}$$

Here $\omega_p(q) = [n_0 V(q) q^2/m]^{1/2}$ is the plasma frequency and $\theta = \arctan(q_y/q_x)$ is the angle between the propagation direction and the $\hat{\mathbf{x}}$-axis. For Coulomb interactions $\omega_p(q) \propto \sqrt{q}$. Unless propagate nearly parallel to the stripes, $\omega(\mathbf{q})$ is proportional to $\sin 2\theta\, q^{3/2}$. One immediate consequence of this dispersion is that the largest velocity of propagation for the magnetophonons with a given q is achieved when $\theta = 45°$.

At any finite T, harmonic fluctuations of the stripe positions become larger than the interstripe separation at distances exceeding $\xi_y \sim \sqrt{YK}/k_B T q_*$ and $\xi_x = (Y/K)^{1/2}\xi_y^2$ along the $\hat{\mathbf{y}}$- and $\hat{\mathbf{x}}$-directions, respectively. The stripe positions are also disordered by the dislocations. The dislocations in a 2D smectic have a finite energy $E_D \sim K$. At $k_B T \ll E_D$ the density of thermally excited dislocations is of the order of[12] $\exp(-E_D/k_B T)$ and the average distance between dislocations is $\xi_D \sim q_*^{-1}\exp(2k_B T/E_D)$. At low temperatures $\xi_x, \xi_y \ll \xi_D$; therefore, the following interesting situation emerges (Fig. 2). On the lengthscales smaller than ξ_y (or ξ_x, whichever appropriate) the system behaves like a usual smectic where Eqs. (1–3) apply. On the lengthscales exceeding ξ_D it behaves[a] like a nematic.[12] In between the system is a smectic but with very unusual properties. It is topologically

[a] In a more precise treatment,[15] the lengthscales $\xi_{Dx} \propto \xi_D^{6/5}$ and $\xi_{Dy} \propto \xi_D^{4/5}$ are introduced such that $\xi_{Dx}\xi_{Dy} = \xi_D^2$.

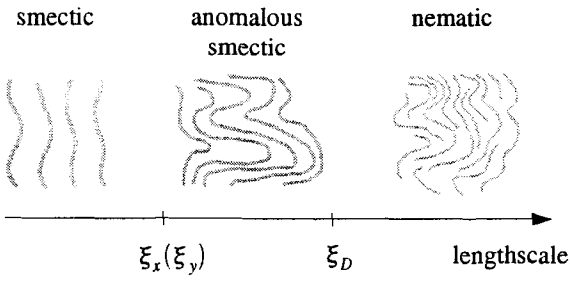

Figure 2. Portraits of the stripe phase on different lengthscales.

ordered (no dislocations) but possesses enormous fluctuations. In these circumstances the harmonic elastic theory becomes inadequate and anharmonic terms must be treated carefully. The calculations[15,13] show that the anharmonisms cause power-law dependence of the parameters of the effective theory on the wavevector $\mathbf{q}$, e.g.,

$$Y \sim Y_0(\xi_x q_x)^{1/3}, \quad K \sim K_0(\xi_x q_x)^{-1/3}, \tag{4}$$

for $q_x \ll \xi_x^{-1}$ and $q_y \ll \xi_y^{-1}(q_x\xi_x)^{2/3}$. The scaling behavior (4) breaks down above the lengthscale ξ_D where the crossover to the thermodynamic limit of the nematic behavior commences.

The scaling shows up not only in the static properties such as Y and K but also in the dynamics. For example, the spectrum of the magnetophonon modes changes to[13]

$$\omega(\mathbf{q}) \sim \sin\theta \cos^{7/6}\theta\,(\xi_x q)^{5/3} \frac{\omega_p(\xi_x^{-1})}{\omega_c \xi_x} \sqrt{\frac{Y_0}{mn_0}}. \tag{5}$$

Compared to the predictions of the harmonic theory, Eq. (3), the $q^{3/2}$-dispersion changes to $q^{5/3}$. Also, the maximum propagation velocity is achieved for the angle $\theta \approx 53°$ instead of $\theta = 45°$. These modifications, which take place at long wavelengths, are mainly due to the renormalization of Y in the static limit and can be obtained by combining Eqs. (3) and (4). Less obvious dynamical effects peculiar to the quantum Hall smectics include a novel dynamical scaling of Y and K as a function of frequency and a specific q-dependence of the magnetophonon damping.[13]

3 Nematic

The collective degree of freedom associated with the nematic ordering is the angle $\phi(\mathbf{r}, t)$ between the local normal to the stripes $\mathbf{N}$ and the $\hat{\mathbf{x}}$-axis orientation. The effective Hamiltonian for $\mathbf{N}$ is dictated by symmetry to be

$$H_N = \frac{K_1}{2}(\nabla \mathbf{N})^2 + \frac{K_3}{2}|\nabla \times \mathbf{N}|^2. \tag{6}$$

The coefficients K_1 and K_3 are termed the splay and the bend Frank constants[9]. Note that in the smectic phase $\phi = -\partial_y u$. This entails the relation $K_3 \simeq K$ between the parameters of the nematic and its parent smectic. On the other hand, the value of K_1 is expected to be determined largely by the properties of the dislocations[12].

Another obvious degree of freedom in the nematic are the density fluctuations $n(\mathbf{r}, t)$. A peculiar fact is that in the static limit n is totally decoupled from $\mathbf{N}$, and so it does not enter Eq. (6). Since the nematic is a rather weak form of ordering, the question about extra low-energy degrees of freedom or additional quasiparticles is nevertheless relevant. I believe that different types of quantum Hall nematics are possible in nature. In the simplest case scenario $\mathbf{N}$ and n are the only low-energy degrees of freedom. This type of state has been studied by Balents[16] and recently by the present author[14]. It was essentially postulated that the effective Largangean takes the form

$$\mathcal{L} = \frac{1}{2}\gamma^{-1}(\partial_t \mathbf{N})^2 - H. \tag{7}$$

(As hinted above, the full expression contains also couplings between $\partial_t \mathbf{N}$ and mass currents but they become vanishingly small in the long-wavelength limit). The collective excitations are charge-neutral fluctuations of the director. They have a linear dispersion,

$$\omega(\mathbf{q}) = q\sqrt{K_1 \gamma \cos^2\theta + K_3 \gamma \sin^2\theta}. \tag{8}$$

One interesting question is the nature of the zero-temperature smectic-nematic transition. It is likely to be dislocation-mediated, which can be studied[14] combining classical[12,17] and quantum[18] theories of topological disordering. One prediction[14] of this scenario is the existence of a second gapped excitation branch in the nematic. This mode is a descendant of the magnetophonon mode of the parent smectic.

Very recently, Radzihovsky and Dorsey[19] formulated a qualitatively different theory of the quantum Hall nematics, whose predictions disagree with our Eqs. (7) and (8). To resolve some of the controversy it is imperative to

bring the discussion from the level of effective theory to the level of quantitative calculations. One promising direction is to investigate some concrete trial wavefunctions of quantum nematics.[20,21] It is worth mentioning that the quantum phase transition(s) from the smectic to an isotropic state may also occur directly, without the intermediate nematic phase.[22]

Acknowledgments.— I would like to thank A. A. Koulakov, B. I. Shklovskii, and V. M. Vinokur for previous collaboration on the topics discussed and the MIT Pappalardo Fellowships Program in Physics for support.

References

1. A. A. Koulakov, M. M. Fogler, and B. I. Shklovskii, Phys. Rev. Lett. **76**, 499 (1996); M. M. Fogler, A. A. Koulakov, and B. I. Shklovskii, Phys. Rev. B **54**, 1853 (1996).
2. R. Moessner and J. T. Chalker, Phys. Rev. B **54**, 5006 (1996).
3. M. M. Fogler and A. A. Koulakov, Phys. Rev. B **55**, 9326 (1997).
4. E. H. Rezayi, F. D. M. Haldane, and K. Yang, Phys. Rev. Lett. **83**, 1219 (1999); Phys. Rev. Lett. **85**, 5396 (2000).
5. N. Shibata and D. Yoshioka, Phys. Rev. Lett. **86**, 5755 (2001).
6. M. P. Lilly, K. B. Cooper, J. P. Eisenstein, L. N. Pfeiffer, and K. W. West, Phys. Rev. Lett. **82**, 394 (1999).
7. R. R. Du, D. C. Tsui, H. L. Störmer, L. N. Pfeiffer, and K. W. West, Solid State Commun. **109**, 389 (1999).
8. E. Fradkin and S. A. Kivelson, Phys. Rev. B **59**, 8065 (1999).
9. P. G. de Gennes and J. Prost, *The Physics of Liquid Crystals* (Oxford University Press, New York, 1995).
10. A. H. MacDonald and M. P. A. Fisher, Phys. Rev. B **61**, 5724 (2000).
11. H. A. Fertig, Phys. Rev. Lett. **82**, 3693 (1999).
12. J. Toner and D. R. Nelson, Phys. Rev. B **23**, 316 (1981).
13. M. M. Fogler and V. M. Vinokur, Phys. Rev. Lett. **84**, 5828 (2000).
14. M. M. Fogler, cond-mat/0107306.
15. L. Golubović and Z.-G. Wang, Phys. Rev. Lett. **69**, 2535 (1992).
16. L. Balents, Europhys. Lett. **33**, 291 (1996).
17. J. Toner, Phys. Rev. B **26**, 462 (1982).
18. M. P. A. Fisher and D. H. Lee, Phys. Rev. B **39**, 2756 (1989).
19. L. Radzihovsky and A. T. Dorsey, cond-mat/0110083.
20. K. Musaelian and R. Joynt, J. Phys. Cond. Mat. **8**, L105 (1996).
21. O. Ciftja and C. Wexler, cond-mat/0108119.
22. E. H. Rezayi and F. D. M. Haldane, Phys. Rev. Lett. **84**, 4685 (2000).

ULTRAFAST MANIPULATION OF ELECTRON SPIN COHERENCE IN QUANTUM WELLS

J. A. GUPTA and D. D. AWSCHALOM*
University of California, Santa Barbara, CA 93106
**E-mail: awsch@physics.ucsb.edu*

R. KNOBEL and N. SAMARTH
The Pennsylvania State University, University Park, PA 16802

A recently developed technique is reviewed with the potential for all-optical coherent control over electron spins in semiconductors. In these experiments, ultrafast laser pulses "tip" electron spins by generating effective magnetic fields via the optical Stark effect. Measurements of Stark shifts have provided estimates of the net tipping angle as a function of tipping pulse energy, intensity, and polarization. Background contributions to the measured tipping angle arise from the undesirable excitation of additional carriers by the tipping pulse.

1 Introduction

Interest in exploiting the spin degree of freedom in semiconductors for both classical and quantum information processing is fueled by the promise of new devices with improved speed and functionality.[1] The ability of spin to exist in superpositions of eigenstates is at the heart of recent proposals for spin-based "quantum bits" comprising quantum dots[2-3] and nuclear spins.[4] Experimental realizations of useful computation based on such units rely on the ability to perform a large number ($>10^4$) of single and multiple quantum bit operations within the limit imposed by the spin coherence time.[5] With an eye toward optimizing spin coherence times, environmental contributions to decoherence can be studied with ultrafast optical techniques on ensembles. Such experiments have identified relevant spin scattering mechanisms in regimes of semiconductor doping where electron spin coherence times can be extended by several orders of magnitude (up to ~100ns) (see Ref. [6]). Related measurements in semiconductor quantum dots revealed nanosecond spin coherence times that persist to room temperature, but are limited by inhomogeneous dephasing due to the ensemble of QDs probed.[7] To reverse dephasing effects and learn more about homogeneous spin coherence times, an extension of spin echo pulse methods to semiconductor quantum structures is desirable.[8] Unfortunately, direct application of conventional pulsed microwave fields is currently impractical for conduction-band electrons due to the short coherence times and small amount of sample present in such quantum structures.

Here we review recent experiments showing that optical methods for producing coherent spin rotations are possible on 100fs time scales.[9] This development may enable one to perform many operations on quantum bits within typical coherence times. The mechanism for this process relies on the generation of an effective magnetic field by a below-bandgap laser pulse through the optical Stark effect.[10-11] When the pulse is circularly polarized, initially degenerate states in the conduction band experience different Stark shifts, resulting in meV-scale spin splittings that correspond to effective field strengths of up to 20T. Any net torque between an existing electron spin population and the effective field then leads to an impulsive "tip" of the electron spin by angles up to ~ $\pi/2$.

2 Experimental results and methods

2.1 *Quantum well samples*

Samples consisted of 10x150 Å wide $Zn_{1-x}Cd_xSe$ (x~0.33) quantum wells grown by molecular beam epitaxy using a digital approach that enables high Cd concentrations (needed to satisfy the laser tuning range) while retaining optical quality.[12] Undoped, modulation-doped, and Mn-doped multiple quantum well samples were studied that demonstrate a range of electronic and magnetic environments in which this technique can be applied.[9] The results presented here were similar for all three samples.

2.2 *The optical Stark effect*

First observed in atoms,[13] the optical Stark effect for excitonic transitions in semiconductors results from virtual excitations induced by intense pulses of sub-resonant photons.[14] The end result is a shift ΔE, of the absorption spectrum toward higher energy that lasts for the duration of the pump-probe correlation time (200-500 fs). The shift is proportional to the photon intensity and inversely proportional to the photon detuning, in our case defined as $\Delta \equiv E_{hh} - E_p$, where E_{hh} and E_p are the hh-exciton and pump energies respectively. The dependence of the Stark shift on the relative polarizations of the pump and probe can be predicted from optical selection rules familiar for ordinary optical transitions.[15]

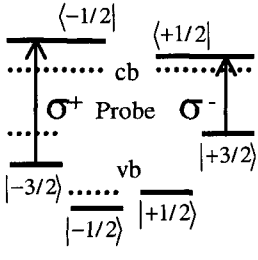

Figure 1: Shifts of conduction and valence band levels in a zinc-blende type semiconductor quantum well produced by a below-bandgap, σ^+-polarized pump pulse. The different shifts measured by co- (σ^+) and counter-polarized (σ^-) probe pulses at E_{hh} are primarily due to optical transition matrix elements.

As a result, a σ^+ polarized sub-resonant pump couples more strongly to σ^+ hh-excitons than to σ^+ lh-excitons (Fig. 1). Measurements of shifts for co- and counter-polarized probe pulses at E_{hh} can be used to calculate the net conduction-band spin splitting, giving an effective magnetic field strength that reaches 20T for non-magnetic samples.[9]

To measure Stark shifts, an optical parametric amplifier produces ~150fs pump pulses tunable across the visible spectrum and probe pulses of a white light continuum. Because the probe pulses are a continuum, direct measurements of Stark shifts > ~1meV can be made by collecting complete absorption spectra with a dual-channel photodiode array detector at each value of pump-probe delay.[16] For better signal-to-noise, differential spectra representing pump-induced changes in the absorption spectrum are recorded at fixed energies using a photomultiplier tube and lock-in amplifiers.[16] Stark shifts in these samples were characterized as functions of pump energy, intensity, and polarization.[9]

Figure 2 shows absorption spectra of the undoped QW sample taken at three time delays between pump and probe pulses. Here a Stark shift of ~3.5 meV can be directly read from the graph by comparing the spectrum at zero time delay with spectra at positive and negative delays. Although the spectrum at positive delay largely matches the spectrum at negative delays (as expected from a process based on virtual excitations), small but significant differences exist[9] that reflect the undesirable excitation of real carriers by the sub-resonant pump photons, discussed below.

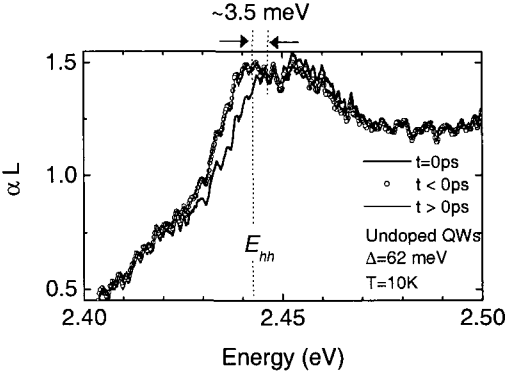

Figure 2: Absorption spectra of the undoped QW sample, directly resolving a Stark shift obtained with co-circularly polarized pump and probe pulses. The corresponding shift for counter-polarized pulses is ~0.7meV (not shown). E_p=2.3787 eV, I_p=0.65 GW/cm^2.

2.3 *Measurements of all-optical spin manipulation*

In these experiments, two synchronized optical parametric amplifiers were used to produce independently tunable pump and "tipping pump" (TP) pulses (Fig. 3). The pump pulse is tuned above the semiconductor bandgap and excites electrons that are spin polarized along the laser direction. The Faraday rotation, θ_F, of a linearly

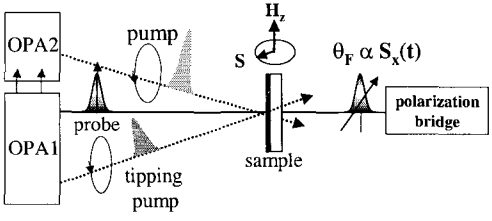

Figure 3: The probe Faraday rotation is detected using a polarization bridge. All beams are modulated with optical choppers and lock-in amplifiers are used to detect pump- and tipping-pump induced changes in the bridge difference signal.

polarized probe pulse is proportional to this component of spin magnetization, S_x. In the presence of a transverse magnetic field H_z, the pump-excited spins precess about the field at a Larmor frequency determined by the electron g-factor. As a result, the Faraday rotation oscillates as a function of the pump-probe time delay, yielding information on the transverse spin relaxation time, T_2^*. It is because T_2^* typically contains contributions from ensemble dephasing[7] and longitudinal spin relaxation, that all-optical spin echo techniques are desirable. Toward this end, below-bandgap tipping pulses are also incident onto the sample that modify the precession dynamics of the pump-excited electron spins through the effective magnetic field associated with the optical Stark effect, $H_{Stark}\hat{x}$.

In order for H_{Stark} to coherently rotate the electron spins as they precess about the static field, there must be a nonzero torque given by $\vec{\tau} \propto \vec{S} \times \vec{H}_{Stark}$. This condition is only met when the TP is incident on the sample at a time delay Δt_{TP} such that $\vec{S}(\Delta t_{TP}) \| \pm\hat{y}$, a situation that occurs at zero crossings in the detected Faraday rotation signal. Figure 4A shows a scan comparing the spin precession taken with and without the TP in the magnetic QW sample.[9] The tipping pulse

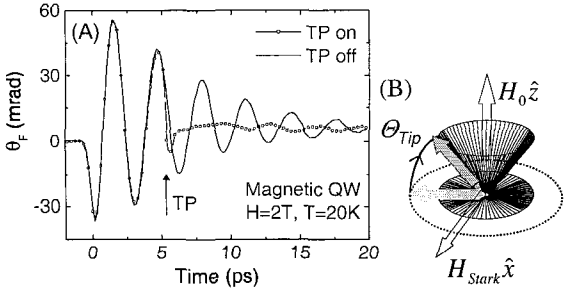

Figure 4: (A) ~ $\pi/2$ spin rotations produced by TP (Δt_{TP} = 5.1ps) when positioned at a zero crossing in θ_F. The pump initiates spin precession at t = 0ps, and the probe time delay is scanned. E_p=2.446eV, I_p=10 MWcm^{-2}, E_{TP}=2.385eV, I_{TP}=0.6 GWcm^{-2}. (B) Schematic showing action of TP with nonzero torque.

rotates the spin magnetization out of the *x-y* plane; precession following the tipping event traces a cone about H_0 (Fig. 4B), thus giving a reduced value of S_x. *A priori*, the angle of rotation can be calculated from the relation: $\Theta_{tip} = ArcCos(A/A_0)$, where A and A_0 are the amplitudes of precession with and without the TP respectively.[9] Such a calculation for the data in Fig. 4 yields a value for Θ_{tip} that exceeds $\pi/2$.

The undesirable excitation of real carriers by the sub-resonant TP complicates this analysis by adding a background contribution to A that must be subtracted.[9] Figure 5 compares the amplitude of spin precession *initiated* by the TP (taken in reference to the TP modulation frequency) with and without a preceding pump pulse for the undoped QW sample. The sharp spike in the data reflects the Stark shift (detected through Faraday rotation), and marks the arrival of the TP. Here Δt_{TP} = 908ps, well beyond T_2^* (~100ps), but within the carrier recombination time (~1ns), so that spin-relaxed carriers excited by the pump still fill states in the conduction

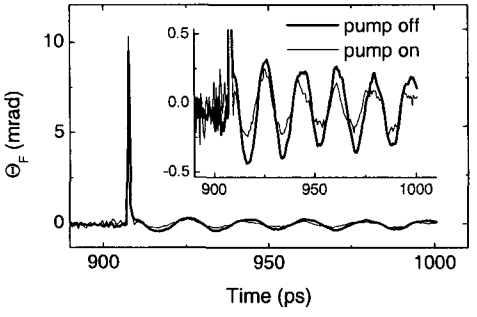

Figure 5: Faraday rotation data showing spin precession initiated by the TP. Data are taken in the undoped QW sample at H=4T, T=100K. E_p= 2.4314eV, E_{TP}= 2.3755eV, I_{TP}= 0.5 GWcm^{-2}. The change in amp-litude caused by the preceding pump pulse results in a background contribution to the net tipping angle. The data for t >908ps have been averaged for clarity.

and valence bands that would otherwise be available to carriers excited by the TP. As a result, the TP excites fewer carriers (lower precession amplitude) when preceded by the pump than if the pump were absent, a difference that necessarily appears in data concurrently taken in reference to the pump modulation frequency. This background contribution to A represents a ~10% effect that can in principle be subtracted,[9] problems arise at high TP intensities when the real-carrier excitation density becomes comparable to that of the pump itself. Although energetically unfavorable, absorption of sub-resonant photons may involve two-photon processes, low-energy states, or phonon-assistance.[9] The preservation of spin coherence (evidenced by the oscillations in Fig. 5) may preclude two-photon processes, but the exact origin of this signal remains an open question.[9]

3 Conclusions and Outlook

The optical Stark effect could provide a way to perform spin-coherent operations on femtosecond time scales. Although not discussed here, measurements using two tipping pumps have verified the coherent nature of the rotation.[9] The net rotation angle has also been characterized as a function of tipping pump intensity and detuning, with dependencies qualitatively (but not quantitatively) consistent with expectations from measurements of optical Stark shifts. Future experiments will seek to overcome limitations on TP intensity and detuning imposed by the semiconductor absorption linewidth. Extension to measurements on single spins using optical techniques with high spatial resolution (e.g. near field microscopy) is feasible, although experimentally difficult. Stark shifts have been observed in bulk materials, quantum dots, and quantum wells, providing ample opportunity for the development of structures with tailored optical properties.

This work was supported by DARPA/ONR N00014-99-1-1096, DARPA MDA972-01-1-0027, ONR N00014-99-0077, and NSF DMR-0071888.

References

1. G. A. Prinz, *Physics Today* **48**, 58 (1995).
2. D. Loss and D. P. DiVincenzo, *Phys.* Rev. A **57**, 120 (1998).
3. A. Imamoglu *et al., Phys. Rev. Lett.* **83**, 4204 (1999).
4. B. E. Kane, *Nature* **393**, 133 (1998).
5. J. Preskill, http://xxx.lanl.gov/abs/quant-ph/9712048 (1997).
6. J. M. Kikkawa and D. D. Awschalom, *Phys. Rev. Lett.* **80**, 4313 (1998).
7. J. A. Gupta *et al., Phys. Rev. B* **59**, 10421 (1999).
8. E. L. Hahn, *Phys. Rev.* **80**, 580 (1950).
9. J. A. Gupta *et al., Science* **292**, 2458 (2001).
10. C. Cohen-Tannoudji and J. Dupont-Roc, *Phys. Rev. A* **5**, 968 (1972).
11. M. Rosatzin, D. Suter and J. Mlynek, *Phys. Rev. A* **42** 1839 (1990).
12. O. Ray *et al., Appl. Phys. Lett.* **76**, 1167 (2000).
13. C. Cohen-Tannoudji and S. Reynaud, *J. Phys. B* **10**, 345 (1977).
14. A. Mysyrowicz *et al., Phys. Rev. Lett.* **56**, 2748 (1986).
15. M. Joffre *et al., Phys. Rev. Lett.* **62**, 74 (1989).
16. J. A. Gupta and D. D. Awschalom, *Phys Rev. B.* **63**, article # 085303 (2001).

ZERO-BIAS CONDUCTANCE ANOMALY IN BILAYER QUANTUM HALL SYSTEMS

Y. N. JOGLEKAR and A. H. MACDONALD
Department of Physics, Indiana University, Bloomington, Indiana 47405, and University of Texas at Austin, Austin, Texas 78705
Email: yojoglek@physics.utexas.edu

Bilayer quantum Hall system at total filling factor $\nu=1$ shows a rich variety of broken symmetry ground states because of the competition between the interlayer and intralayer Coulomb interactions. When the layers are sufficiently close, a bilayer system develops spontaneous interlayer phase-coherence that manifests itself through a spectacular enhancement of the zero-bias interlayer tunneling conductance. We present a theory of this tunneling conductance anomaly, and show that the zero-bias conductance is proportional to the square of the *quasiparticle* tunneling amplitude.

1 Introduction

Bilayer systems consist of two 2D electron gases separated by a distance d comparable to the typical distance between electrons within one layer, and have been intensely investigated over the past decade.[1] Weakly disordered bilayer quantum Hall systems at *total* filling factor $\nu=1$ undergo a quantum phase transition from a compressible state to a $\nu=1$ quantum Hall state with spontaneous interlayer phase-coherence when the layers are sufficiently close.[1] It is conventional to use a pseudospin to represent the layer index, where pseudospin "up" denotes a state in the top layer, and pseudospin "down" denotes a state in the bottom layer. In the pseudospin language, the phase-coherent state can be viewed as an easy-plane ferromagnet with its pseudospin polarization $\boldsymbol{M}$ along the x-axis, $M_x=1$. In analogy with ferromagnets, the low-lying excitations of a phase-coherent bilayer system are long-wavelength fluctuations of the ordered moment, *i.e.* pseudospin waves. These collective modes transfer charge from one layer to the other, and have a linear dispersion at long wavelengths when the interlayer tunneling amplitude Δ_t is zero.[1] The close similarity between phenomenological effective theory of a phase-coherent bilayer system and that of a Josephson junction has led to suggestions that the phase-coherent bilayers should exhibit a D. C. Josephson effect in interlayer tunneling measurements.[2,3]

The first *direct* experimental signature of the phase-coherent state and the linearly dispersing collective mode was observed by Spielman *et al.*, who discovered a dramatic enhancement of the zero-bias tunneling conductance G_T as the layer separation d (measured in units of magnetic length) was reduced.[4,5] Although this dramatic enhancement is reminiscent of the tunneling characteristics of a

Josephson junction, it is not yet clear whether the finite width and height of the peak is intrinsic, or is governed by the temperature and experimental limitations.

Here we present a theory of the zero-bias conductance G_T that is non-perturbative in the tunneling amplitude Δ_t. We find that the tunnel conductance G_T is given by Fermi's Golden rule for the *quasiparticles* in the phase-coherent state, and that the breakdown of Fermi's Golden rule for the *bare* electrons is therefore expected. In the following sections we first discuss the physical picture that underlies our theory, and then present the results of an approximate but fully microscopic calculation. The details of this calculation are available elsewhere.[6]

2 Physical Picture

Let us consider a bilayer quantum Hall system at total filling factor $\nu=1$ with tunneling amplitude Δ_t. In the pseudospin picture, the tunneling amplitude acts as a field along the x-axis in the pseudospin-space, whereas a bias-voltage or a random disorder potential acts as a field along the z-axis. In the mean-field approximation, the interlayer exchange Coulomb interaction enhances the splitting between symmetric and antisymmetric single-particle energies, $\Delta_{qp} = \Delta_t + M_0 \Delta_{sb}$, where M_0 is the dimensionless order-parameter for the phase-coherent state. This exchange-enhancement $M_0\Delta_{sb}$ survives in the limit $\Delta_t \to 0$ and gives rise to spontaneous interlayer phase-coherence.[1] We will call the exchange-enhanced splitting Δ_{qp} as the *quasiparticle* tunneling amplitude.

The tunneling amplitude Δ_t is the only term in the microscopic Hamiltonian that does not conserve the charge in each layer separately. Recent theoretical work[3,7-9] has shown that $\lim_{\Delta t \to 0} G_T/\Delta_t^2$ diverges in the phase-coherent state. Evaluation of G_T therefore requires a non-perturbative theory like the one we present here. Our finding, that G_T is finite once the presence of low-energy quasiparticle excitations at finite temperature and with disorder even at zero temperature is acknowledged, is at odds with the prediction that this system should show a dc Josephson effect. In usual dc Josephson effect systems, the persistent currents are maintained by a current-direction order-parameter phase-slip barrier that has no analog in bilayer quantum Hall systems.

Now let us examine the possibility of persistent currents in a bilayer system when we treat the interlayer tunneling non-perturbatively. First we recall that the interlayer current operator is given by $I = eNM_0\Delta_t M_y$, where N is the total number of electrons. Thus, a current-carrying initial state corresponds to the pseudospin lying in the x-y plane with a nonzero y-component and a concurrent field Δ_t along the x-axis. Since the bilayer system has an easy-plane anisotropy, it is clear that in steady state the pseudospin must relax and point along the x-axis or, equivalently, that the initial-state current must decay. In other words, in the absence of bias-voltage, a state with nonzero interlayer current cannot be a steady state. *This physical picture*

underlies our theory, and provides a transparent way to see why persistent currents are impossible in the presence of a finite interlayer tunneling.

In a steady state the rate of change of interlayer current is zero. This constraint allows us to express the zero-bias tunnel conductance G_T in terms of a phenomenological lifetime τ for the interlayer current,

$$G_T = e^2 N M_0 \Delta_t \tau. \quad (1)$$

At a microscopic level, there are several possible channels for the decay of the current; disorder broadening of the quasiparticle bands, local density fluctuations leading to puddles of compressible regions, etc. In the present calculation, we assume that the broadening of the mean-field quasiparticle bands because of disorder leads to a finite density of states at the Fermi energy and provides a channel for the current to decay into particle-hole pairs. It is then possible to extract the relaxation time τ for the interlayer current from the dynamical response function χ_{yz},

$$\tau = M_0 \Re [\chi_{yz}]^{-1} (\omega \to 0) \quad (2)$$

and obtain the dependence of the zero-bias conductance G_T on interlayer tunneling amplitude Δ_t by using Eq.(1).

3 Results and Discussion

We evaluate the response function χ_{yz} using disorder vertex corrections and the generalized random phase approximation, which capture the physics of collective excitations in the presence of a random disorder potential. A straightforward calculation[9] shows that the zero-bias tunnel conductance is given by the Fermi's Golden rule for the *mean-field quasiparticles*

$$G_T \propto \Delta^2_{qp} = (\Delta_t + M_0 \Delta_{sb})^2 . \quad (3)$$

Figure 1 shows the results for the zero-bias conductance as a function of interlayer tunneling amplitude Δ_t for various disorder strengths. We characterize the strength of disorder by the suppression of the mean-field order parameter M_0 from its clean limit value, $M_0 = 1$. When the system is barely phase-coherent ($M_0 << 1$) we find that $G_T \propto \Delta^2_t$; however, as the interlayer phase-coherence develops, the conductance G_T remains finite as $\Delta_t \to 0$. This result is clearly non-perturbative in the tunneling amplitude Δ_t, and consistent with the breakdown of Fermi's Golden rule for the bare electrons. The inset in Fig. 1 shows the dependence of the zero-tunneling-amplitude conductance G_T ($\Delta_t = 0$) on the order-parameter M_0. We see that the quadratic dependence is consistent with the general result, Eq.(3).

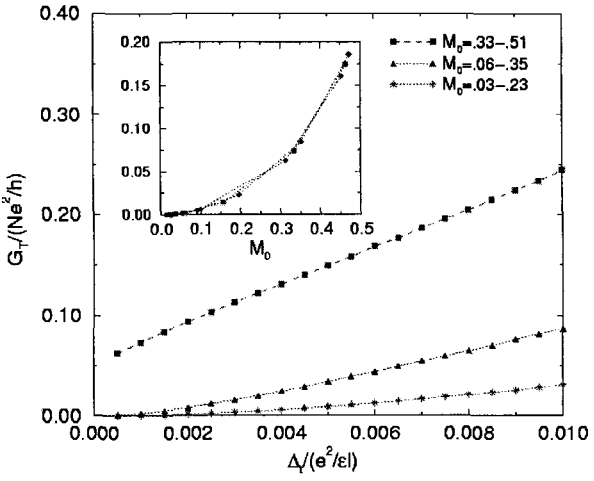

Figure 1: Zero-bias conductance G_T as a function of interlayer tunneling amplitude Δ_t for various disorder strengths. The strength of disorder is characterized by the suppression of the order parameter M_0 from its clean limit value M_0 =1. The inset shows the $\Delta_t \to 0$ limit of G_T as a function of the order parameter M_0.

Thus, we find that the zero-bias conductance of a bilayer system is proportional to the square of the *quasiparticle* tunneling amplitude. This result provides further support for the idea that a weak-coupling (Hartree-Fock) description of the phase-coherent state is indeed reliable.

This work was supported by the Welch Foundation, the Indiana 21st Century Fund, and the NSF grant no. DMR 0115947.

References

1. See, for example, S, Das Sarma and E. Demler, *Solid State Comm.* **117**, 141-147 (2001) and references therein.
2. X. –G. Wen A. and Zee, *Phys. Rev. Lett.* **69**, 1811-1815 (1992).
3. M. M. Fogler and F. Wilczek, *Phys. Rev. Lett.* **86**, 1833-1837 (2001).
4. Spielman *et al.*, *Phys. Rev. Lett.* **84**, 5808-5812 (2000).
5. Spielman *et al.*, *Phys. Rev. Lett.* **87**, 036803 (2001).
6. Y. N. Joglekar A. H. and MacDonald, *Phys. Rev. Lett.* **87**, 196802 (2001)
7. L. Balents, L. and Radzihovsky, *Phys. Rev. Lett.* **86**, 1825-1829 (2001).
8. A. Stern *et al.*, *Phys. Rev. Lett.* **86**, 1829-1833 (2001).
9. Y. N. Joglekar and A. H. MacDonald, *cond-mat*/0107016.

SOME FRACTIONS ARE MORE SPECIAL THAN OTHERS: NEWS FROM THE FRACTIONAL QUANTUM HALL ZONE

W. PAN,[1,2] H. L. STORMER,[3,4] D. C. TSUI,[1] L. N. PFEIFFER,[4] K. W. BALDWIN,[4] and K. W. WEST[4]

[1]*Department of Electrical Engineering, Princeton University, Princeton, NJ 08544*
[2]*National High Magnetic Field Laboratory, Tallahassee, FL 32310*
[3]*Department of Physics and Department of Applied Physics, Columbia University, New York, NY 10027*
[4]*Bell Labs, Lucent Technologies, Murray Hill, NJ 07974*

We report observation of new fractions: 4/11, 5/13, and 6/17 between ν=2/5 and ν=1/3, 4/13 and 5/17 between ν=1/3 and ν=2/7, and 4/19 between ν=2/9 and ν=1/5. The ν=4/11 state was studied in detail. The tilting magnetic field data show that its ground state is spin-polarized.

1 Introduction

Over the last twenty years, many fractional quantum Hall effect (FQHE) states have been observed in the first and second Landau levels.[1-3] For example, in the first Landau level, FQHE sequences of $\nu=p/(2p\pm1)$ and $\nu=p(4p\pm1)$ form around ν=1/2 and ν=1/4, and of $\nu=2-p/(2p\pm1)$ and $\nu=1-p/(4p\pm1)$ around ν=3/2 and ν=3/4, respectively. In a recent experiment, preliminary results also showed the possible FQHE sequences of $p/(6p\pm1)$ around ν=1/6 (see Ref. [4]). In the second Landau level, the peculiar FQHE states at ν=5/2 and ν=7/2 are so far the only even-denominator FQHE states.[5-7] Also between the ν=2 and ν=3, the well-developed 2+p/3 (p=1,2) FQHE states are confirmed,[6] and the developing FQHE states at ν=2+p/5 (p=1,4) were observed.[4,7] Around ν=7/2, Eisenstein *et al.*,[7] reported the formation of ν=3+p/5 (p=1,4) FQHE states, however very surprisingly, no 3+p/3 (p=1,2) FQHE states are found.

While the search for new FQHE state continues, the question as to the end of the FQHE sequence has consistently been raised. Numerous experiments and theories have showed that the FQHE states should eventually give way to the Winger crystal state at $\nu\leq$1/7 (see Refs. [8,9]). More over, no FQHE states have been found in the third and higher Landau levels. There, the two-dimensional electron system (2DES) forms stripe or bubble states.[10-14]

In the past several years, there has been a big improvement in the GaAs/AlGaAs sample quality. This provides us a timely opportunity to search for new fractions. In this paper, we present our recent observations of new fractional states at ν=4/11, 5/13, 6/17 between ν=2/5 and ν=1/3, as well as the ν=4/13 and 5/17 states between

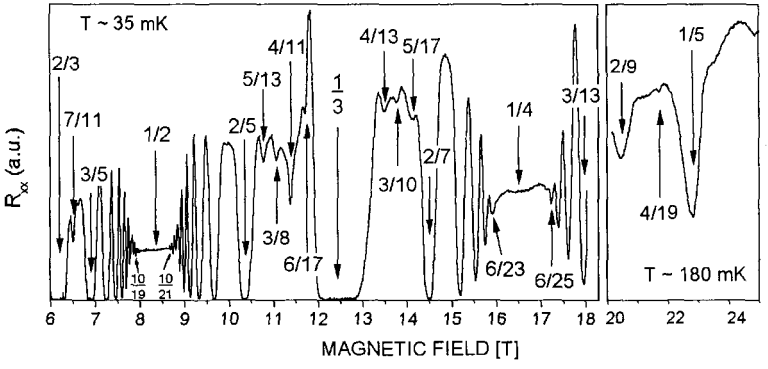

Figure 1: R_{xx} in the regime of 2/3>ν>3/13 and in the regime of 2/9>ν>1/5. Two traces were taken at different magnet run.

ν=1/3 and ν=2/7. We have also observed a weak R_{xx} minimum at ν=4/19 between ν=2/9 and ν=1/5. The observation of these new fractions may provide initial glimpses of a yet richer spectrum of FQHE states to come.

2 Experimental results

The experiments were carried out in an exceptionally high quality GaAs/AlGaAs quantum well sample of density $n \sim 1 \times 10^{11}$ cm^{-2}. Figure 1 shows two experimental traces of R_{xx} in the regime of 2/3> ν u>3/13, taken at T ~ 35 mK, and in the regime of 2/9> ν >1/5, taken at T ~ 180 mK. The exceptionally high sample quality is manifested by the appearance of the high order FQHE states at ν=10/19 and 10/21 around ν=1/2, and ν=6/23 and ν=6/25 around ν=1/4. More remarkably, the weak structure, previously observed between ν=1/3 and 2/5 (see Ref. [15]), is resolved into clear and strong R_{xx} minima at ν=5/13, 3/8, 4/11, and 6/17. R_{xx} minima are also observed at fractions ν=4/13, 3/10, and 5/17 between =1/3 and 2/7, and even at ν=4/19 between ν=2/9 and 1/5.

Of these new fractions, the ν=4/11 state is particularly interesting. Within the framework of the composite fermion (CF) model,[3,16,17] Halperin, Lee, and Read[17] showed that CFs form at ν=3/8 and have fractional charges. The ν=4/11 state is the ν*=1 integer QHE state (where ν* is the effective Landau level filling factor of the CFs at ν=3/8), and its ground state is spin-polarized. However, Wojs and Quinn[18] showed in their few-particle calculation that the spin-polarized state at ν=4/11 is not stable. Later Park and Jain[19] proposed that the ν=4/11 state can be viewed as a mixed state of the CFs with two flux-quanta and the CFs with four flux-quanta. Its ground state is probably partially spin-polarized or a spin-singlet. In the following, we present detail experimental results on this state.

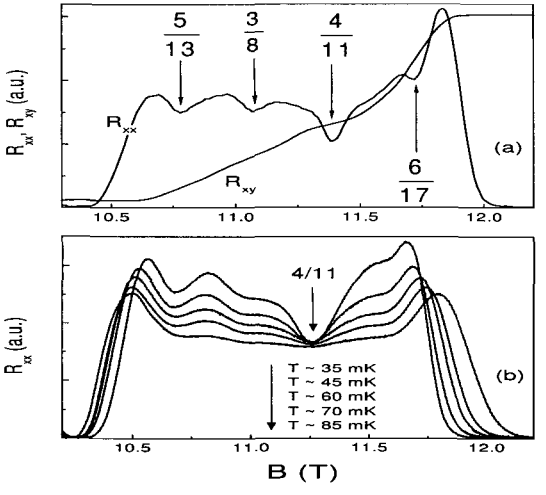

Figure 2: (a): R_{xx} and R_{xy} around ν=4/11. (b) Temperature dependence around ν=4/11.

Figure 2(a) shows the R_{xx} and R_{xy} around ν=4/11. The dashed line is the Hall trace. A clear slope change is apparent in R_{xy} at ν=4/11, although the quantization value remains ill defined as in the early stages of many developing fractions. The strong R_{xx} minima at ν=4/11 and the accompanying developing Hall plateau point to the formation of FQHE states at this fraction.

Figure 2(b) is the T-dependent data for the ν=4/11 state. Five temperature traces are shown. Unlike the well-developed FQHE states, R_{xx} at exactly ν=4/11 barely changes with temperature. On the other hand, the strength of the whole

ν=4/11 feature decreases markedly with increasing temperature. This T-dependent behavior is reminiscent of the initial T-dependence of many FQHE states. A characteristic energy of approximately 30-50mK is obtained .[20] We believe that the true activation energy gap of the ν=4/11 state is roughly in a similar range.

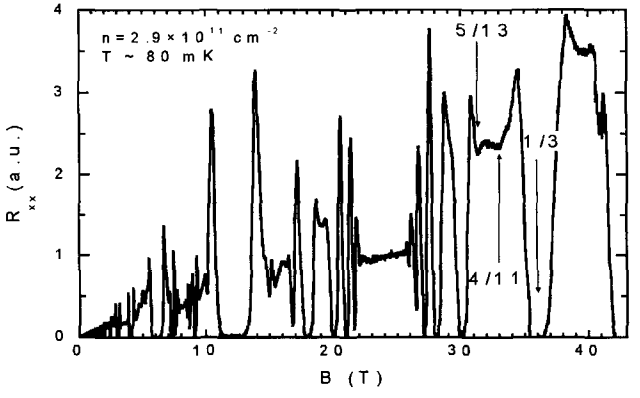

Figure 3: R_{xx} of a higher density sample, taken at T ~ 80 mK in a hybrid magnet.

At B~11T the Zeeman energy of electrons in GaAs is ~3K. It is vastly larger than the characteristic energies (mK). Already at this point it appears highly unlikely that ν=4/11 is spin unpolarized. To further strengthen this assertion we tilted the sample, *in situ*, in a magnetic field. For tilts up to θ=42.2° the magneto-resistance R_{xx} show practically no variation in the strength nor does the shape of the ν=4/11 state vary noticeably .[20] From this result we infer that no spin transition occurs as a result of such tilts and hence that the ν=4/11 state is always spin polarized. The assertion is further strengthened by the observation of the ν=4/11 state at a magnetic field as high as 33T, shown in Fig. 3, taken in the Hybrid magnet at the National High Magnetic Field Laboratory. Such a high magnetic field should create a polarized spin state.

Between $\nu=2/3$ and 3/5, a strong minimum appears at $\nu=7/11$ and an additional feature around $\nu=5/8$ are observed, in Fig. 1. Indications of a $\nu=7/11$ state had been seen earlier.[21]

3 Discussions

The newly found fractions do not belong to any principle FQHE sequences around $\nu=1/2$ or $\nu=1/4$. Their existence provides initial glimpses of a yet richer spectrum of FQHE states to come. One intuitive way to understand these new fractions is to interpret them as the FQHE states of CFs. In this sense, they are the FQHE states in the first Landau level of CFs. In analogy to the normal 2D electron system, one may ask whether the FQHE states of CFs exist in the second or higher Landau levels of CFs. To answer this question, higher quality samples are essential and more experiments are necessary

4 Conclusions

In an exceptional sample, we observed new fractions of 4/11, 5/13, and 6/17 between $\nu=2/5$ and $\nu=1/3$, and 4/13, 5/17 between $\nu=1/3$ and $\nu=2/7$. In a separate experiment, 4/19 between $\nu=2/9$ and 1/5 was also observed. The temperature dependent and tilted magnetic field studies of the $\nu=4/11$ state show that its ground state is spin-polarized.

We would like to thank the E. Palm, T. Murphy, and S. Hannahs for experimental help. We are grateful to J. K. Jain, K. Park, and J. Moore for useful discussions. A portion of this work was performed at the National High Magnetic Field Laboratory, which is supported by NSF Cooperative Agreement No. DMR-9527035 and by the State of Florida. D.C.T. and W.P. are supported by the AFOSR, the DOE, and the NSF.

References

1. H. L. Stormer *et al., Rev. Mod. Phys.* **71**, S298 (1999).
2. *The Quantum Hall Effect*, R. E. Prange and S. M. Girvin (Eds.), Springer, New York (1990).
3. *Perspectives in Quantum Hall Effect*, S. Das Sarma and A. Pinczuk (Eds.), Wiley, New York (1996).
4. W. Pan *et al.*, unpublished.
5. R. L. Willett *et al., Phys. Rev. Lett.* **59**, 1779 (1987).
6. W. Pan *et al., Phys. Rev. Lett.* **83**, 3530 (1999).
7. J.P. Eisenstein *et al.*, cond-mat/0110477.

8. M. Shayegan, in Reference [3].
9. H. A. Fertig, in Reference [3].
10. M. P. Lilly *et al., Phys. Rev. Lett.* **82**, 394 (1999).
11. R. R. Du *et al., Solid State Commun.***109**, 389 (1999).
12. W. Pan *et al.,* Phys. Rev. Lett. **83**, 820 (1999).
13. M. P. Lilly *et al., Phys. Rev. Lett.* **83**, 824 (1999).
14. K. B. Cooper *et al., Phys. Rev. B* **60**, 11285 (1999).
15. H. L. Stormer *et al., Physica E* **3**, 38 (1998).
16. J. K. Jain *et al., Phys. Rev. Lett.* **63**, 199 (1989); *Phys. Rev. B* **41**, 7653 (1990); *Phys. Today* **53** (4), 39 (2000).
17. B. I. Halperin, P. A. Lee, and N. Read, *Phys. Rev. B* **47**, 7312 (1993).
18. A. Wojs and J. J. Quinn, *Phys. Rev. B* **61**, 2846 (2000).
19. K. Park and J. K. Jain, *Phys. Rev. B* **62**, 13274 (2000).
20. W. Pan *et al.,* submitted for publication.
21. V. J. Goldman and M. Shayegan, *Surface Science* **229**, 10 (1990).

POSSIBLE NEW PHASES OF COMPOSITE FERMIONS

V. W. SCAROLA, S. Y. LEE and J. K. JAIN

Department of Physics, 104 Davey Laboratory, The Pennsylvania State University, University Park, Pennsylvania 16802

When the effective filling factor of composite fermions is an integer, the residual interaction between them can often be neglected because the ground state of the non-interacting model is unique and incompressible. However, at non-integer composite fermion (CF) filling factors the ground state of composite fermions is enormously degenerate if the interaction between them is neglected, and consideration of the inter composite fermion interaction is necessary for determining the true ground state. In this article, we summarize certain results regarding what new states the inter composite fermion interaction can possibly produce. More details can be found in Refs. [11] and [12].

1 Introduction

A hypothetical system of *non-interacting* electrons in two dimensions, exposed to a high magnetic field, would only show the integral quantum Hall effect, because gaps appear only at integral filling factors, due to Landau level quantization of the kinetic energy. At non-integral filling factors, the ground state of non-interacting electrons is extremely highly degenerate, and interactions play a crucial role in lifting the degeneracy and determining the true ground state.

The essential consequence of the interaction is to produce composite fermions, electrons bound to and even number of quantum vortices of the many body wave function.[1,2] The simplest approximation, in which the composite fermions are assumed to be non-interacting, has been quite successful in explaining the phenomenology. The integral quantum Hall effect of composite fermions carrying $2p$ vortices (called ^{2p}CFs) at effective filling $\nu^*=n$ corresponds to the fractional quantum Hall effect (FQHE) (see Ref. [3]) of electrons at $\nu = n/(2pn\pm1)$, which are the most prominently observed fractions. At $\nu=1/2p$, the $n\rightarrow\infty$ limit of the above sequences, a Fermi Sea of composite fermions is obtained,[4] which, in the absence of CF-CF interactions, has no gap. This explains the lack of FQHE at the simplest even denominator fractions; the existence of the CF Fermi sea has been confirmed in several experiments.[5]

However, at $\nu^*\neq n$, the ground state for the model system of non-interacting composite fermions is highly degenerate, and it is crucial to take account of the CF-CF interaction to determine the nature of the true ground state. Would the composite fermions capture more vortices to become higher order composite fermions to show more FQHE, or would they form some new state?

2 Variational States

We have explored this question in the context of filling factors $\nu=(2n+1)/[4(n+1)]$, which correspond to $\nu^*=n+1/2$ of composite fermions. The n filled Landau levels of composite fermions are treated as inert, and the problem is mapped into fermions at half filling.

We proceed in a variational approach, considering the following plausible states:

(i) ^{4}CF Fermi sea: The ^{2}CFs capture two additional vortices to convert into ^{4}CFs, which experience no magnetic field and form a Fermi sea. This state is well described by the wave function

$$\Psi_{FS}=P_{LLL}\Phi_1^2\Phi_\infty \tag{1}$$

where Φ_∞ is the Fermi sea wave function at zero magnetic field, Φ_1 is the wave function of the lowest filled Landau level, and P_{LLL} is the lowest Landau level projection operator. The base particles in Φ_∞ are ^{2}CFs, so Ψ_{FS} is a Fermi sea of ^{4}CFs.

(ii) ^{4}CF paired state: The ^{2}CFs capture two additional vortices to convert into ^{4}CFs, which pair up. A gap opens up due to pairing, which results in a FQHE. This mechanism appears to be relevant for the FQHE at $\nu=5/2$.(see Ref.[6]) A satisfactory approximation for this state is the Pfaffian wave function[7]

$$\Psi_{PS}=\Phi_1^2 Pf[M] \tag{2}$$

where $Pf[M]$ is the Pfaffian of the NxN antisymmetric matrix M with components $M_{jk}=(z_j-z_k)^{-1}$, and $z=x-iy$ denotes the position of a particle in the plane. $Pf[M]$ is a real space BCS wave function, so Ψ_{PS} describes a paired state of composite fermions.

(iii) ^{2}CF unidirectional charge density wave: The ^{2}CFs phase separate into stripes of alternating FQHE states. A Hartree-Fock wave function for this state can be written and its energy evaluated.[8]

(iv) ^{2}CF two-dimensional charge density wave: The ^{2}CFs form what is called a bubble crystal.[8] Again, the energy of this state can be estimated in the Hartree-Fock approximation.

The last two states are not unique, in the sense that the period of the stripe or the crystal (which depends on the number of particles in each bubble) is variable, and the lowest energy must be determined in each case variationally. The methods for obtaining the energies of the paired and Fermi sea states as well as the charge density wave states have been described in detail in the literature.[8-10]

It ought to be noted that the above states are fantastically complicated, correlated states when viewed in terms of electrons. For example, in (ii): first all electrons at $\nu=(2n+1)/4(n+1)$ capture vortices to become ^{2}CFs at $\nu^*=n+1/2$; those

in the topmost half filled ^{2}CF Landau level capture two additional vortices to transform into ^{4}CFs that see no magnetic field; these would normally form a ^{4}CF Fermi sea, which is here unstable to pairing due to a weak residual interaction between the ^{4}CFs; a gap opens up due to pairing and the FQHE is produced.

3 CF-CF Interaction

In order to determine the lowest energy state, we need a model for the effective interaction between the composite fermions in the topmost half filled CF Landau level. Given the strongly correlated nature of the problem, the interaction is complicated and is expected to contain two, three, and higher body terms. In order to make progress, we will neglect all but the two-body term, which we will determine by placing only two CFs in the nth CF Landau level, while filling the lower CF Landau levels completely. The validity of this approximation is discussed in Refs.[11,12] The wave function for this state is uniquely given by the composite fermion theory as a function of the relative angular momentum, from which one can work backward to obtain a real space interaction. The detailed method has been explained in the literature.[10,11,13]

4 Results

We consider two situations. First, we assume that the external magnetic field is sufficiently high that the system is fully spin polarized. Fig. 1 shows the energies of the paired CF state as well as the CF Fermi sea as a function of $1/N$, where N is the number of composite fermions in the topmost CF Landau level. The thermodynamic limit is obtained by linear extrapolation. The energies of the stripe and bubble phases are found in the Hartree-Fock approximation, which directly gives the thermodynamic limit.

A comparison of the energies shows that stripes have the lowest energy at total fillings 3/8, 5/12, and 7/16, which lie between 1/3 and 2/5, 2/5 and 3/7, and 3/7 and 4/9, respectively. The anisotropic transport observed in higher electronic Landau levels has been interpreted in terms of the formation of stripes.[14] A similar anisotropy between fractions will indicate the formation of stripes alternating between n and $n+1$ filled Landau levels of composite fermions.

The conditions for the observation of CF stripes in the FQHE regime are obviously more stringent than those for the observation of electron stripes in higher Landau levels, just as the conditions for the observation of the fractional quantum Hall effect are than the integral quantum Hall effect. The effective interaction between the composite fermions is approximately an order of magnitude smaller than that between electrons in higher Landau levels, indicating that the temperatures at which the CF stripes become observable might also be reduced similarly. The

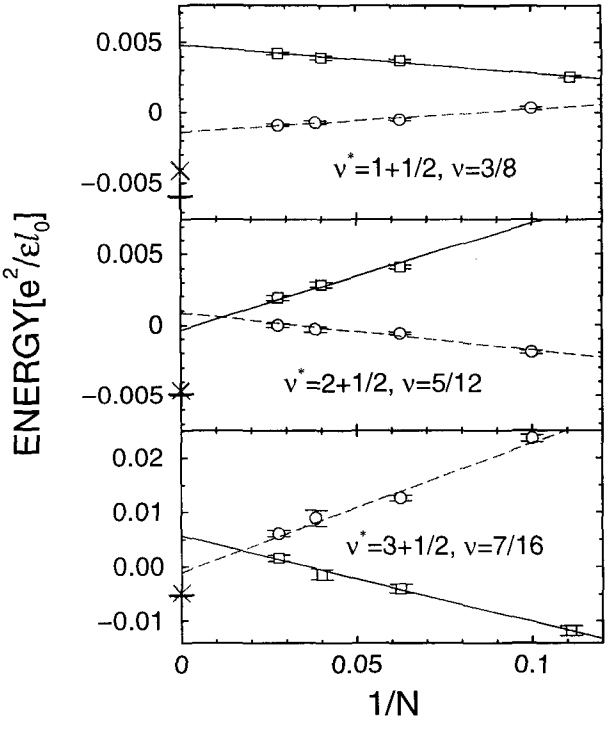

Figure 1: The energy per particle for the CF Fermi sea (squares) and the CF paired state (circles) as a function of N, the number of composite fermions in the $(n+1)$st spin up CF Landau level. The thermodynamic energies are also indicated for the CF stripe and bubble phases by dashes and crosses on the y-axis. All energies are measured relative to the uncorrelated uniform density state.

period of the CF stripes is also much larger: 10, 28, and 34 in units of the magnetic length for ν=3/8, 5/12, and 7/16, respectively. The reason is that the CF stripes involve density oscillations of much smaller amplitude than the electron stripes in the integral quantum Hall regime, as the neighboring FQHE states have very similar densities.

Next we consider the situation when the composite fermions in the topmost CF Landau level have spin opposite to composite fermions in the fully occupied CF Landau level. This state would be irrelevant in the $B\rightarrow\infty$ limit, but could occur for typical or small magnetic fields. The calculation proceeds as before, but with a different effective interaction, appropriate for spin reversed composite fermions.

Figure 2 shows how the thermodynamic energies of the Fermi sea, paired state, and the stripe state vary at ν=3/8 as the first pseudopotential[15] of the effective interaction, V^{eff}, is changed. V^{eff} is the effective interaction obtained from the microscopic method described above. It is seen that when the short range part is enhanced the Fermi sea wins; when it is significantly reduced the stripe phase has the lowest energy; but there is a range of parameters where the paired state is the relevant state. Further calculations[12] have confirmed this result for the above model, but show that the paired state is rather delicate, with an extremely small excitation gap.

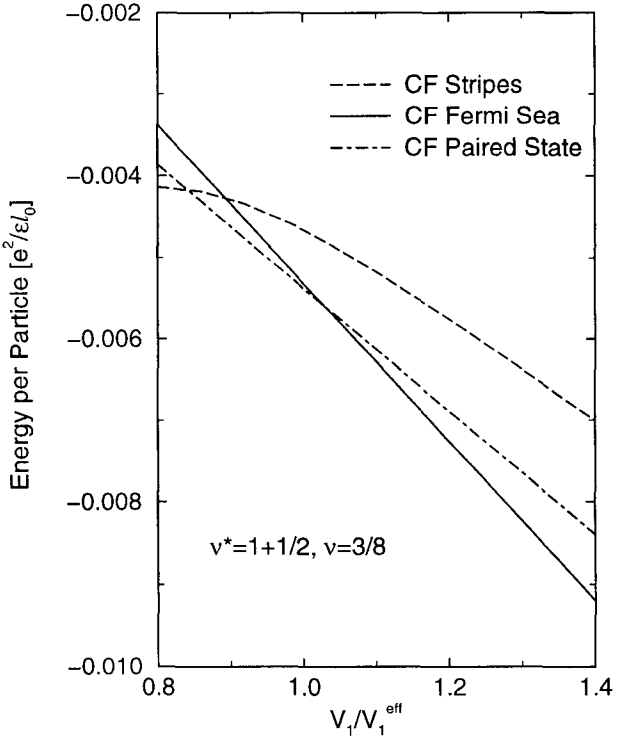

Figure 2: The thermodynamic energies of the CF stripe (dashed line), CF Fermi sea (solid line), and CF paired (dot-dashed line) states as a function of the first pseudopotential for the interaction modeling one full spin up CF Landau level and a half filled spin down CF Landau level (ν*=1+1/2; ν=3/8). The energies are measured relative to the uncorrelated uniform density state.

In summary, out studies suggest the possibility of new structure *between* the principal FQHE sequences, due to either stripe formation or pairing of composite fermions. The energy scale associated with these phases is estimated to be rather low, approximately an order of magnitude below the analogous states in higher Landau levels. This work was supported in part by the National Science Foundation under grants DMR-9986806 and DGE-9987589.

References

1. *Composite Fermions*, ed. by O. Heinonen (World Scientific, New York, 1998); *Perspectives in Quantum Hall Effects*, ed. by D. Das Sarma and A. Pinczuk (Wiley, New York, 1997).
2. J. K. Jain, Phys. Rev. Lett. **63**, 199 (1989); Phys. Rev. B **41**, 7653 (1990).
3. D. C. Tsui, H. L. Stormer and A. C. Gossard, Phys. Rev. Lett. **48**, 1559 (1982).
4. B. I. Halperin, P. A. Lee and N. Read, Phys. Rev. B **47**, 7312 (1993); V. Kalmeyer and S. C. Zhang, Phys. Rev. B **46**, 9889 (1992).
5. R. L. Willet *et al.*, Phys. Rev. Lett. **71**, 3846 (1993); W. Kang *et al.*, Phys. Rev. Lett. **71**, 3850 (1993); V. J. Goldman *et al.*, Phys. Rev. Lett. **72**, 2065 (1994).
6. R. L. Willet *et al.*, Phys. Rev. Lett. **59**, 1779 (1987).
7. G. Moore and N. Read, Nucl. Phys. B **360**, 362 (1991).
8. A. A. Koulakov, M. M. Fogler, and B. I. Shlovskii, Phys. Rev. Lett. **76**, 499 (1996); M. M. Fogler and A. A. Koukalov, Phys. Rev. B. **55**, 9326 (1997).
9. J. K. Jain and R. K. Kamilla, Int. J. Mod. Phys. B **11**, 2621 (1997); Phys. Rev. B **55**, R4895 (1997).
10. K. Park *et al.*, Phys. Rev. B **58**, R10167 (1998).
11. S. Y. Lee, V. W. Scarola and J. K. Jain, Phys. Rev. Lett., in press.
12. V. W. Scarola, E. H. Rezayi, and J. K. Jain, unpublished.
13. J. J. Quinn and A. Wojs, J. Phys. Cond. Mat. **12**, R265 (2000); I. Szlufarska, A. Wojs and J. J. Quinn, cond-mat/0105294 (2001).
14. M. P. Lilly *et al.*, Phys. Rev. Lett. **82**, 394 (1999); R. R. Du *et al.*, Solid State Commun. **169**, 389 (1999).
15. F. D. M. Haldane, Phys. Rev. Lett. **51**, 605 (1983).

INTERSUBBAND MAGNETOPHONON RESONANCES IN QUANTUM CASCADE STRUCTURES

D. SMIRNOV, O. DRACHENKO, J. LEOTIN

Laboratoire National de Champs Magnétiques Pulsés et Laboratoire de Physique de la Matière Condensée, 143 Avenue de Rangueil, 31432 Toulouse, France

H. PAGE, C. BECKER, C. SIRTORI

Laboratoire Central de Recherches Thalès, 91404 Orsay, France

V. APALKOV, T. CHAKRABORTY

Max-Plank-Institut fur Physik komplexer Systeme, 01187 Dresden, Germany

We report on magnetotransport measurements of GaAs/GaAlAs quantum cascade structures in magnetic fields up to 62 T parallel to the current. We observe novel quantum oscillations series in tunneling current that are periodic in reciprocal magnetic field and have field positions *independent* of the applied bias. These oscillations are explained as intersubband magnetophonon resonance due to electron relaxation by emission of optical or acoustic phonons.

The magnetophonon effect is a powerful tool to investigate electron-phonon interaction in semiconductor systems, particularly in confined structures.[1] For the in-plane transport in a two dimensional (2D) electron gas of a quantum well (QW), quantization of the carrier motion into discrete Landau levels (LLs) gives rise to quantum oscillations at elevated temperatures due to resonant absorption of LO phonon.[2] The resonance field positions are at $B_N=\frac{1}{N}\frac{m^*}{e}\omega_{LO}$. In the case of perpendicular transport, magnetotunneling measurements in 2D double barrier (DB) quantum well structures have evidenced optical-phonon-assisted tunneling from 2D LLs emitter states into LLs of the DB central well.[3] However, these measurements did not show any evidence of intersubband resonant relaxation via optical phonon inside the central QW of the DB. This relaxation scheme occurs when electrons injected in the Landau ground state of a j-th subband $E_{j,0}$ relax by resonant emission of a LO phonon into a Landau state of an i-th subband $E_{i,N}=E_i+N\hbar\omega_C$. This magnetophonon resonance process is characterized by the equation $\hbar\omega_{LO}=E_j-(E_i+N\hbar\omega_C)$, which defines field positions at $B_N=\frac{1}{N}\frac{m^*}{e}\left(\frac{E_j-E_i}{\hbar}-\omega_{LO}\right)$. In this case, the intersubband distance in the central well must exceed the optical phonon energy $\hbar\omega_{LO}$. We report in this paper the intersubband magnetophonon effect in vertical transport measurements of DB structures based on GaAs/GaAlAs.

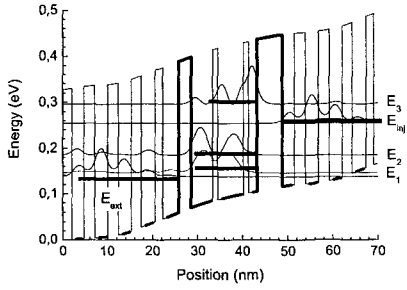

Figure 1: Electronic structure of a GaAs/GaAlAs QCL sequence biased at 117 mV per period. Ground state subband energy levels and wave functions of the DB system are displayed.[6]

For this purpose, we used a specific DB structure, which is implemented in quantum cascade lasers (QCLs) (see Ref. [4]).

The QCLs consist of sequences of DB-like structures, each consisting of a central QW structure between a 2D emitter and collector. When a suitable high bias voltage is applied to the QCL, the upper subband in the central QWs becomes populated by tunneling injection while the ground state is quickly emptied by tunneling collection. In this voltage bias range, the current becomes dependent on electron recombination rates inside the central QWs. This opens up the possibility to detect intersubband magnetophonon resonance as current oscillations under constant voltage bias or conversely voltage oscillations at constant current. Considering the constant current situation, we have a fixed electron supply rate into the central well which is equal to the recombination rate into the QWs ground state: n/τ , n being the upper subband electron population and τ its lifetime. As a result, if the relaxation rate $1/\tau$ increases, the electron population in the QW decreases. This builds up a positive charge in the well which in turn decreases the bias across the emitter barrier and consequently across the entire QCL sample.

Magneto-tunneling measurements were performed in magnetic fields up to 62T generated by a pulsed magnet with total pulse duration of 100ms (see Ref. [5]). GaAs/GaAlAs QCL samples including forty periods[6] were measured at 4.2K with constant DC current applied parallel to the magnetic field. Figure 1 depicts the electronic structure along a sequence Emitter-QWs-Collector of the QCL structure under applied bias. In this system, the central QWs include three coupled wells developing three subbands E_1, E_2 and E_3. Emitters and the collectors are identical multi-quantum-wells structures which are degenerately n-doped in their central portion at the concentration of $6 \cdot 10^{11}$ cm^{-3}. The electronic structure was obtained by a self-consistent calculation including electron charge transfer across the DB sequence. The calculated intersubband separations agree well with our optical measurements data: $E_3 - E_2 = 108.7$ meV, and $E_3 - E_1 = 147$ meV.

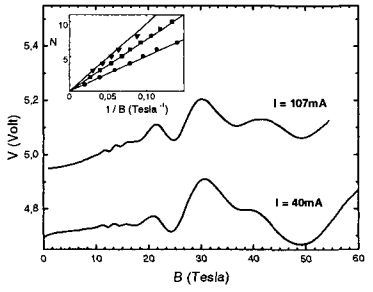

Figure 2: (a) Voltage across the QCL biased at 40 mA and 107 mA. The inset shows three series given by resonance numbers versus the inverse magnetic field curve.

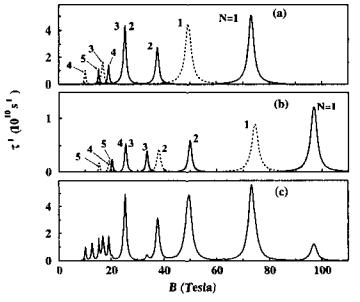

Figure 3: LO phonon (a) and acoustic-phonon (b) emission rate as a function of the applied magnetic field. Transitions into E_1 and E_2 subbands are shown by solid and dotted lines, respectively. The total electron relaxation rate is shown in (c).

In the following, we focus on the magneto-tunneling study in the range of current where the electrons are injected into the E_3 subband. Figure 2 shows two recordings of the voltage across the structure measured at 40mA and 107mA. Resonances are labeled as voltage minima, which means relaxation rate maxima. One series of oscillations dominates with a fundamental field near 50 T. Two other series become clearly visible on the second derivative curve. We observed that magnetic field resonance positions are independent of bias in this current range.

The three series are identified in the inset, which plots integer N versus reciprocal magnetic fields. The fundamental fields are obtained from the slopes at the values $B_1^{(1)}$ =50T, $B_1^{(2)}$ =75.5T, and $B_1^{(3)}$ =95T. From these fields, we derive cyclotron energies $\varepsilon^{(i)}=\hbar eB_1^{(i)}/m^*$ by using effective mass values measured in 2D GaAs electron gas in the same magnetic field range, in order to account for non parabolicity.[7] We obtain (within 3% experimental accuracy): $\varepsilon^{(1)}$=72meV, $\varepsilon^{(2)}$=109meV, and $\varepsilon^{(3)}$=149meV. These energy values must be only related to the central QWs electronic structure since they are insensitive to the Emitter-Collector bias. Remarkably, $\varepsilon^{(1)}+\hbar\omega_{LO}=E_3-E_2$ and $\varepsilon^{(2)}+\hbar\omega_{LO}=E_3-E_1$ which is a clear signature of intersubband magnetophonon resonance while $\varepsilon^{(3)}=E_3-E_1$ is supporting the idea of an elastic scattering process from E_3 into E_1 subbands.

Theoretical results presented below account for all observed series, assuming the two inelastic series are caused by the LO phonon emission, and the elastic one by acoustic phonon emission. Figure 3 displays electron scattering rates from $E_{3,0}$

into $E_{i,N}$ LLs subbands by the emission of LO or acoustic phonons as calculated in Ref. [8]. The LO phonon emission rate plotted in Figure 3(a) as a function of the magnetic field for N=1–5 shows sharp resonances when $E_3-E_2-\hbar\omega_{LO}$ or $E_3-E_1-\hbar\omega_{LO}$ equal $N\hbar\omega_C$. Similarly, Figure 3(b) gives the total rate of acoustic phonon emission. Finally, in Fig. 3(c) shows the total electron relaxation rate due to emission of acoustic and optical phonons. The model explains the observed resonance field positions fairly well. For example, the optical phonon emission series agree within ~1% with the data for the B_N^1 series (relaxation into E_2 subband), and within ~3% with the data for the B_N^2 series (relaxation into E_1 subband). Notice that, this later inelastic series into the E_1 subband coincide with the elastic series into E_2 subband because $E_2-E_1\approx\hbar\omega_{LO}$. This explains why only three and not four series are viewed in our QCL structure.

In summary, intersubband magnetophonon oscillation series were identified in the tunneling current across a GaAs/GaAlAs DB structure based on a QCL.

References

1. A. Yu *et al., Landau Level Spectroscopy*, eds: G. Landwehr, E. I. Rashba (Elsevier, Amsterdam, 1192 (1991)); R. J. Nicholas, *ibid.*, 779.
2. D. C. Tsui *et al.,* Phys. Rev. Lett. **44**,341 (1980).
3. M. L. Leadbeater *et al., Phys. Rev. B,* **39**, 3438 (1989), G. S. Boebinger *et al., Phys.Rev.Lett*, **65**, 235 (1990).
4. J. Faist *et al., Science* **264**, 553 (1994) J. Faist *et al., Phys. Rev. Lett.* **76**, 411 (1996).
5. O. Portugal *et al.,* Physica B **294-295**, 579 (2001).
6. P. Kruck *et al., Appl. Phys. Lett.* **76**, 3340 (2000).
7. S. P. Najda *et al.,* Phys. Rev. **40**, 6189 (1989).
8. D. Smirnov *et al., cond-mat/0109109* (2001).

INTERFERENCE AND DECOHERENCE OF COMPOSITE FERMIONS IN THE QUANTUM HALL EFFECT

A. STERN
Weizmann Institute of Science, Dept of Condensed Matter Physics, Rehovot, 76100, Israel

In this talk I will discuss quantum interference phenomena of composite fermions in quantum Hall systems. In particular, I will focus on huge mesoscopic fluctuations of non-linear response and of Coulomb drag in single and bi-layer systems. Finally, I will give a simple physical picture of dephasing (de-coherence) of composite fermions, with simple expressions for their coherence length.

Most of the talk will be based on work done in collaboration with I. Aleiner and B. Narozhny (Stony Brook).

(Note: if time permits I will also comment on Coulomb drag in strongly coupled bi-layers at $\nu=1$, following experiments carried out by Eisenstein's group.)

CURRENT-DRIVEN MAGNONS IN MAGNETIC MULTILAYERS

M. TSOI
Department of Physics and Astronomy, Michigan State University, East Lansing, MI
and
Grenoble High Magnetic Field Laboratory, MPI-FKF, CNRS, Grenoble, France

Spin waves, or magnons, are intrinsic excitations in magnetic materials and have attracted considerable attention since introduced by Bloch in 1930.[1] Recently ideas of spintronics have impacted this field dramatically. Berger[2] and Sloczewski[3] introduced completely new aspects of the physics of metallic ferromagnets in the presence of an electric current of high density. Excitation of magnons by an electric current has been predicted and seen in magnetic multilayers,[4-6] where the driving force for the excitations is the spin-momentum transfer associated with an electric current flow. We have developed a microcontact technique (magnetic microcontact spectroscopy) to investigate the current-driven magnon generation.[4,5] In our experiments we inject current densities as high as 10^9 A/cm^2 into a Co/Cu multi-layer through a point contact made using a sharpened Ag wire carefully brought into contact with a multi-layer film. We observe current-driven magnons in multi-layers with both ferromagnetic[4,5] and antiferromagnetic[7] configuration of the adjacent layer magnetizations.

Some further interesting applications of the technique, particularly, for studying fluctuation phenomena, resonant magnon generation, acoustic wave generation, etc., will be presented.

*Indispensable contributions of A. G. M. Jansen, J. Bass, V. Tsoi, and P. Wyder to this work are gratefully acknowledged.

1. F. Bloch, *Z. Phs.* **61**, 206 (1930).
2. L. Berger, *Phys. Rev. B* **54**, 9353 (1996).
3. J. C. Slonczewski, *J. Magn. Magn. Matt.* **159**, L1 (1996).
4. M. Tsoi, *et al., Phys. Rev. Lett.* **80**, 4281 (1998).
5. M. Tsoi, *et al., Nature* **406**, 46 (2000).
6. J. A. Katine, *et al., Phys. Rev. Lett.* **84**, 3149 (2000).
7. M. Tsoi, *et al.,* to be published.

This page is intentionally left blank

Contributed Papers

This page is intentionally left blank

THEORY OF SURFACE-ACOUSTIC-WAVE PROPAGATION IN THE $\nu = 5/2$ FRACTIONAL QUANTUM HALL STATE

K. C. FOSTER,[1] N. E. BONESTEEL,[1] and S. H. SIMON[2]
[1]*Department of Physics and NHMFL, Florida State University, Tallahassee, Florida 32310, USA*
[2]*Lucent Technologies, Bell Labs, Murray Hill, New Jersey 07974, USA*

There is compelling theoretical evidence[1] that the $\nu = 5/2$ fractional quantum Hall state is a Moore-Read state[2] - a state which can be viewed as a spin-polarized p-wave superconductor of composite fermions. The question remains, how can one test this hypothesis experimentally? To address this we have developed a semi-phenomenological description of this state in which the Halperin-Lee-Read[3] theory of the half-filled Landau level is modified by adding a p-wave pairing interaction between composite fermions by hand. The electromagnetic response functions for the resulting mean-field p-wave superconducting state are then calculated and used in an RPA calculation of the physical electronic response. In particular, we predict the wave-vector and frequency dependence of the longitudinal conductivity $\sigma_{xx}(\mathbf{q},\omega)$ which can be measured in surface-acoustic-wave propagation experiments.[4]

Work is supported in part by US DOE Grant No. DE-FG02-97ER45639.

1. R. Morf, *Phys. Rev. Lett.* **80**, 1505-1508 (1998).
2. G. Moore and N. Read, *Nucl. Phys.* B **360**, 362 (1991).
3. B. I. Halperin, P. A. Lee and N. Read, *Phys. Rev. B* **47**, 7312 (1993).
4. R. L. Willett, *Adv. in Phys.* **46**, 447 (1997).

HIGH MAGNETIC FIELD DEPENDENT DIAMAGNETIC SHIFTS IN $Al_xGa_{1-x}As$ SEMICONDUCTOR ALLOYS

E. D. JONES and J. L. RENO

Sandia National Laboratories, Albuquerque, NM, USA
E-mail: edjones@sandia.gov

S. CROOKER

NHMFL, Los Alamos National Laboratory, Los Alamos, NM, USA
E-mail: crookers@lanl.gov

K. K. BAJAJ and G. COLI

Physics Department, Emory University, Atlanta, GA, USA
Email: phskkb@physics.emory.edu

Low temperature diamagnetic shifts and FWHM linewidths of excitonic transitions in $Al_xGa_{1-x}As$ alloys are reported as a function of magnetic field (50T maximum) at 4K using photoluminescence spectroscopy. Two samples with aluminum compositions of 5 and 20%, are discussed. The slope of the diamagnetic shift at high fields allows a direct measure of the excitonic reduced mass μ

1 Introduction

Because of their importance in applications for electronic and optoelectronic devices, ternary semiconductor alloys such as $Al_xGa_{1-x}As$ have been thoroughly studied.[1-3] Because of the close lattice matching between GaAs and AlAs, the $Al_xGa_{1-x}As$ system can be grown over the whole range of alloy compositions with excellent physical properties using a variety of epitaxial growth techniques, such as molecular beam epitaxy (MBE), metal organic chemical vapor deposition, and liquid phase epitaxy.

One of the most commonly used optical characterization techniques to assess the quality of a semiconductor alloy is low temperature photoluminescence (PL) spectroscopy. At liquid helium temperatures, the PL linewidth of an excitonic transition defined as the full-width-at-half-maximum (FWHM) in semiconductor alloys is considerably larger than those observed in their binary components. This broadening has been attributed to the compositional disorder[4] which is inevitably present in these systems. In addition, the FWHM linewidth can be broadened by the application of an external magnetic field.[4] This is due to the fact that the application of a magnetic field shrinks the excitonic wave function and thus enhances the value of the FWHM linewidth. However, studies of the change of the exciton emission energy by applying a magnetic field (diamagnetic shift) has not been extensively reported.

In this paper we present an observation of the variations of the 4K diamagnetic shift of the excitonic transition energy and FWHM linewidth as a function of magnetic field in AlGaAs using PL spectroscopy and a 50T pulsed magnet. Because of the large magnetic field, the observed high-field diamagnetic shifts are greater than the exciton binding energies (~1-3 meV), the slope of the high-field diamagnetic shift can yield information about the exciton reduced mass μ.

2 Experimental

Two $Al_xGa_{1-x}As$ samples reported here were grown on (001) oriented undoped GaAs substrates by MBE at 590°C. The structure consisted of a 300-nm-thick epilayer of GaAs grown on top of the GaAs substrate followed by a double heterostructure of undoped $Al_{x+0.1}Ga_{1-x-0.1}As/Al_xGa_{1-x}As$ with 50-nm-thick barriers and a 50-nm-thick $Al_xGa_{1-x}As$ alloy. In this manner, the $Al_{x+0.1}Ga_{1-x-0.1}As$ barriers, whose composition was always 10% greater than that of the $Al_xGa_{1-x}As$ alloy under study, provided carrier confinement and therefore prevented carriers and/or excitons from diffusing to GaAs. A 10-nm-thick undoped cap-layer of GaAs was grown on top of the AlGaAs double heterostructure to prevent oxidation. The compositions were verified by comparing the sample's lattice constants of the samples obtained from double x-ray scattering, with the well known composition dependence of the band gap energy for these alloys.[1-4]

Figure 1 shows the low-temperature zero-field PL spectra for the 5% (EA0571) and the 20% (EA0517) AlGaAs samples. The FWHM linewidths are respectively 0.95 meV and 3.1 meV both of which are in agreement with linewidth calculations based on the alloy fluctuation model.[4]

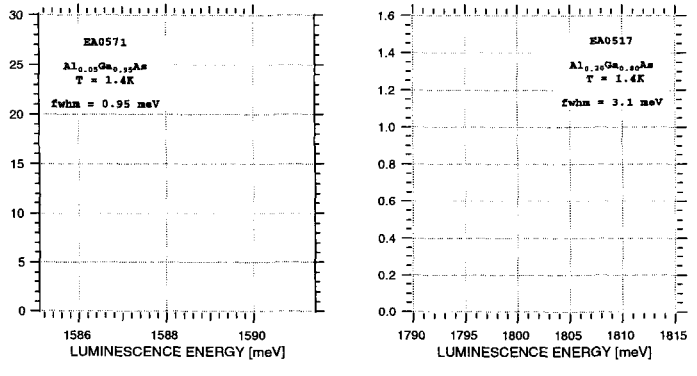

Figure 1: Zero-field PL spectra at 1.4K for the 5% and 20% AlGaAs samples. The FWHM linewidths are indicated in the figure.

3 Discussion

The pulsed-magnetic field dependent PL energies and FWHM linewidths are shown in Fig. 2. For all magnetic fields, the line shapes were nearly gaussian. The FWHM leveling off at high magnetic fields for these samples has also been observed for PL data taken in DC magnetic fields in the same range.[5]

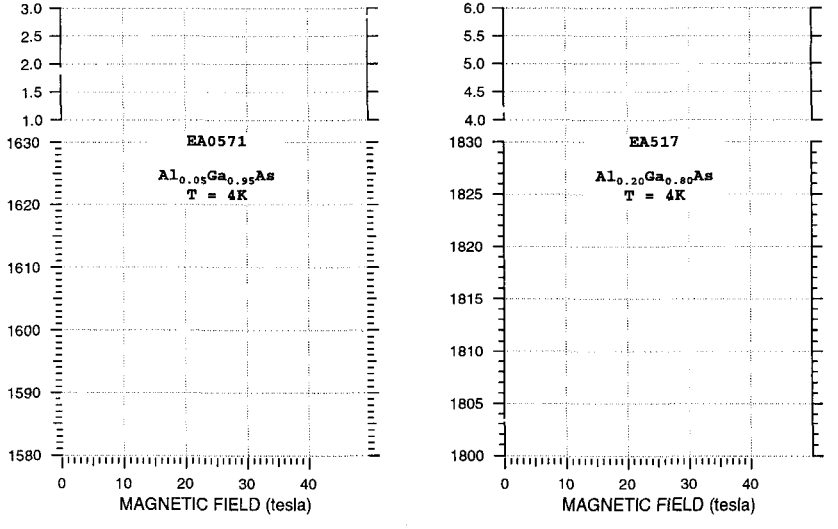

Figure 2: Pulsed-magnetic field dependent PL energy and FWHM at 4K for the 5% (EA0571) and the 20% (EA0517) AlGaAs samples. The respective high field slopes for the 5% and 20% diamagnetic shifts are 0.723 meV/T and 0.527 meV/T respectively.

From an analysis of the high field data, the slope $\alpha = \partial E/\partial H$ for the diamagnetic shifts are respectively 0.723 meV/T and 0.527 meV/T for the 5% and 20% samples. The reduced exciton mass μ can be calculated from the high-field slope α, i.e., $\mu = (\mu_\beta/\alpha)$ where μ_β is the Bohr the magneton with the result that for the 5% sample, the $\mu = 0.080$ and for the 20% samples, $\mu = 0.11$. These values for the exciton reduced mass are consistent with the expectation that μ should increase as the Al concentration X is increased. Further measurements with differing alloy compositions are required before a determination of the experimental dependence of the reduced mass as a function of X can be made. An estimate for the valence-band mass m_v could be made if the conduction-band mass m_c values were known. The concentration dependence for the conduction-band mass $m_c(x)$ is given by[1]

$$m_c(x) = 0.0657 + 0.0174x + 0.145x^2. \quad (1)$$

For the 5% sample, $m_c = 0.067$ and for the 20% sample, $m_c = 0.075$ both values are less than their associated reduced exciton masses μ and therefore, estimates for the valence-band masses cannot be made. At the present time, these difficulties are not understood unless the excitons are localized. Currently, similar measurements on other $Al_xGa_{1-x}As$ samples are being performed at high magnetic fields and these results will be reported at a later date.

The "*leveling-off*" of the FWHM at high magnetic fields may be an indication that the exciton ground state radius is smaller than the alloy fluctuation coherence length. If we use the FWHM data shown in Fig. 2, the magnetic length,

$$\ell = \sqrt{\frac{\hbar c}{eH}}, \tag{2}$$

at the field at which the FWHM "*leveling-off*" occurs perhaps can be used as a measure of when the exciton radius is smaller than the alloy fluctuation coherence length. With these speculations and assumptions in mind, we find values for this length scale of 66Å (~15T) for the 5% sample and 51Å (~25T) for the 20% sample. In order to corroborate these observations (and speculations), temperature dependent and magnetic field dependent studies for the FWHM a series of $Al_xGa_{1-x}As$ samples are currently underway and the results will be reported at a later date.

The authors wish to thank Dr. Yong Zhang for valuable comments. Sandia is a multiprogram laboratory operated by Sandia Corporation, a Lockheed Martin Company, for the United States Department of Energy under contract DE-AC04-94AL85000.

References

1. S. Adachi, Properties of Aluminum Gallium Arsenide, EMIS Datareviews Series **7** (INSPEC, UK, 1993)
2. L. Pavesi and M. Guzzi, *J. Appl. Phys.* **75**, 4779-4842 (1994).
3. I. Vurgaftman,J. R. Meyer and L. R. Ram-Mohan, *J. Appl. Phys.* **89**, 5815-5875 (2001).
4. K. K. Bajaj, *Mat. Sci. Engineering* B **79**, 203-243 (2001).
5. E. D. Jones, Unpublished.

EFFECT OF STRONG TERAHERTZ RADIATION ON MAGNETOCONDUCTIVITY IN TWO DIMENSIONS

R. A. LEWIS and W. XU
Institute for Superconducting and Electronic Materials, University of Wollongong, NSW 2522, Australia
E-mail: roger_lewis@uow.edu.au

P. M. KOENRAAD
COBRA Inter-University Research Institute, Eindhoven University of Technology, P.O. Box 513 5600 MB Eindhoven, The Netherlands

I. V. BRADLEY
FOM Institute Rijnhuizen, NL-3430 BE Nieuwegein, The Netherlands

The interaction between strong THz radiation from a free electron laser and an electron sheet in a high-mobility, low-density, GaAs/AlGaAs structure has been investigated in magnetotransport experiments over a wide range of wavelengths, intensities, magnetic fields, and temperatures. Photovoltage and photocurrent effects are evident in both longitudinal and transverse potential differences. Broad cyclotron resonance is observed to high temperature and connected with a decrease in electron density. The change in electron temperature under THz radiation is estimated from changes in the magnitude of the magnetoresistivity oscillations at low lattice temperature. The effect of the magnetic field is to suppress the rise in electron temperature relative to the zero field case.

1 Introduction

The longitudinal and transverse electrical conductivities of a high-mobility, (μ = 1 x 10^6 cm^2/V-s), low-density (n = 5 x 10^{11} cm^{-2}) GaAs/AlGaAs-based two-dimensional electron gas (2DEG) have been investigated over magnetic field range 0 – 14 T and temperature range 4.2 – 75 K under THz radiation of wavelengths 50 – 110 μm from a linearly polarized, pulsed (10 ps width, 25 MHz or 1 GHz repetition) free electron laser of peak intensity >10 MW/cm^2. The laser is described in detail elsewhere.[1] We distinguish the electron temperature T_e of the 2DEG from the lattice temperature T_L. Where not specified, temperature refers to lattice temperature. The 2DEG and the phonons interact by phonon emission and absorption and by phonon-induced changes to the electron mobility. The direct effect of the THz radiation is to heat the electron gas, but the interaction between electrons and phonons is significant.

2 Experiment

We measure magnetoconductivity in a conventional Hall bar and determine the carrier number density. This allows us to tell to what extent the observed laser-induced changes in conductivity are due to changes in carrier concentration and to what extent they are due to changes in mobility. We use the Shubnikov-de Haas (SdH) oscillations in magnetoresistivity to determine the 2DEG electron temperature. We observe cyclotron resonance (CR) at the cyclotron field and from the CR width the cyclotron scattering time and the cyclotron mobility are deduced. Magnetophonon resonances (MPR) or its variants are not observed here as the temperatures (<75 K) are too low for a sufficient phonon population to exist.

3 Results and Discussion

The effect of THz illumination on the magnetotransport is illustrated in Fig. 1. This data was taken at 75 K. Such an "intermediate" temperature is too high for SdH oscillations to appear and too low for the MPR oscillations to appear; magnetotransport in the dark is largely featureless. Under THz illumination, an increase in resistivity is observed when the cyclotron condition is fulfilled: for λ = 94 μm, at B = 8.6 T. CR is observed at this rather high temperature; normally the condition $\omega\tau > 1$ requires low temperatures. CR is observed in both magnetoresistance R_{xx} and Hall resistance R_{xy}. The CR field allows the

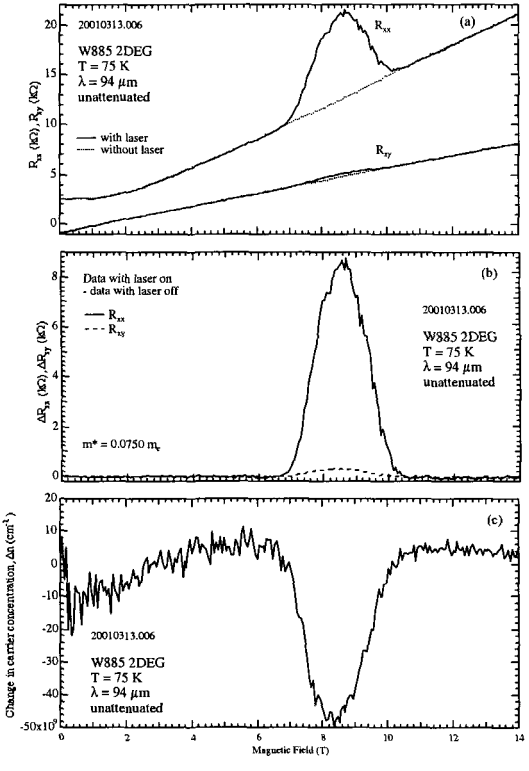

Figure 1

cyclotron mass to be determined to be $m_{CR} = 0.0750m_e$. This value is conspicuously greater than that measured in a similar sample under low-intensity conditions in a conventional spectrometer[2] of $m_{CR} = 0.0693m_e$, due to band non-parabolicity. The shape of the resistance peak is Gaussian rather than Lorentzian, indicating a range of contributions. By fitting the magnetoresistance peak (light - dark), Fig. 1(b), the resonance width is determined. It is found to be (1.05±0.01) T. This corresponds to a scattering time of (4.09±0.04) x 10^{-13} s, corresponding to optical mobility μ_{CR} = (0.95±0.01) x 10^4 cm^2/V-s. This is considerably less than the electrical mobility. The increase in resistance under illumination corresponds to a removal of electrons from the 2DEG. As shown in Fig. 1 (c), it is calculated that $n = 0.5 \times 10^{11}$ cm^{-2} electrons are removed. This amounts to about one-tenth of the 2DEG electron population.

The effect of intense THz illumination on the magnetoconductivity of the 2DEG at lower temperatures is illustrated in Fig. 2 for T = 4.2 K and for T = 18 K.

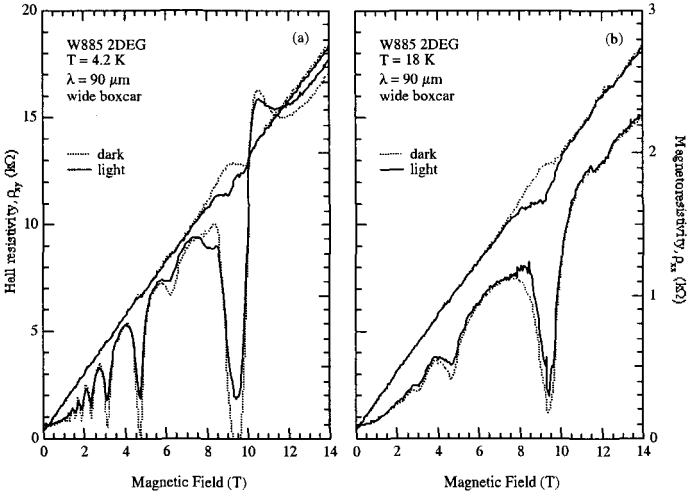

Figure 2

As at T = 75 K (Fig. 1), CR is observed at B = 8.6 T. This is now clearer in R_{xy} than R_{xx}. In both R_{xy} and R_{xx}, but more markedly in the latter, changes occurs on illumination that we attribute to laser heating. The changes are most prominent at the magnetic fields corresponding to integral N; that is, at the SdH oscillations. Similar changes in resistivity observed in another 2DEG sample under somewhat different conditions (T = 5 K, I = 5 μA, λ = 27.4 μm) have been reported earlier.[3] A comparison of the SdH oscillations at 4.2, 9, 20, and 50 K with the present data allows an estimation to be made of the electron gas heating as a result of the laser illumination. We deduce that the effect of the laser on the 2DEG at 4.2 K is to raise

the electron temperature to >9 K but to <18K and estimate T_e = 15±5 K. Likewise, the effect at 18 K is to raise T_e to 25±5 K. We thus have directly determined from magnetotransport data the electron temperature increase upon THz irradiation.

We compare the change in electron temperature T_e with the results of previous experimental and theoretical work. Asmar *et al.*[4] report electron temperatures deduced from photoluminescence (PL) measurements for 0.68 THz = 440 μm radiation of field strength E = 1 - 12 kV/cm for a sample at T_L = 10 K. They deduce $T_{e,PL}$ is 28 - 239 K over this range. The radiation field strengths do not reach ours of 74 kV/cm, but at the largest strength reported, namely 12 kV/cm, they obtain $T_{e,PL}$ = 239 K. This is much larger than our data of $T_{e,SdH}$ = 15 K for T_L = 4.2 K and $T_{e,SdH}$ = 25 K for T_L = 18 K. Our data are in rather better agreement with the results of Lei[5] calculated using an energy-balance approach. Lei presents data in the range 1 - 9 THz, embracing our results which fall in the range 3 - 6 THz. Lei gives T_e as a function of E for various values of lattice temperature and radiation frequency. The data sets closest to ours are for 3 THz ~ 100 μm and for T_L = 10 K and 77 K. For T_L = 10 K, Lei shows T_e rises steeply from 10 K at E = 0 to 35 K at E ~ 2 kV/cm then remains rather constant to E ~ 9 kV/cm, after which it rises steeply. For T_L = 77 K, T_e hardly changes up to E ~ 10 kV/cm. While the change in T_e at T_L = 4.2 K we observe is slightly smaller than that predicted by Lei at T_L = 10 K and the change in T_e at T_L = 18 K somewhat larger than that predicted by Lei at T_L = 77 K, the overall behavior agrees well. The electron temperature rise we observe here in strong magnetic field is much less than that observed and calculated in the absence of magnetic field. Clearly the magnetic field greatly suppresses T_e.

This work was supported in part by the Australian Research Council and the University of Wollongong. We gratefully acknowledge the support of the *Stichting voor Fundamenteel Onderzoek der Materie* (FOM) in providing the required beam time on FELIX and highly appreciate the skilful assistance by the FELIX staff, in particular Dr A. F. G. van der Meer. This work was supported in part by the Australian Research Council, the University of Wollongong, and the EPSRC (UK).

References

1. D. Oepts *et al.*, *Infrared Phys. Technol.* **36**, 297 (1995).
2. P. M. Koenraad *et al.*, *Physica B* **256-258**, 268 (1998).
3. R. A. Lewis *et al.*, *Physical Phenomena at High Magnetic Fields – III* (Eds. Z. Fisk, L. Gor'kov, R. Schrieffer), World Scientific, 642 (1999).
4. N. G. Asmar *et al.*, *Appl. Phys. Lett.* **68**, 829 (1996).
5. X. L. Lei, *J. Phys.: Condens. Matter* **10**, 3201 (1998).

TUNNELING ZERO-BIAS ANOMALY IN THE ULTRA-QUANTUM LIMIT

D. L. MASLOV and S.-W. TSAI
Institute for Fundamental Theory and Department of Physics, University of Florida, Gainesville, FL, USA
E-mail: tsai@phys.ufl.edu, maslov@phys.ufl.edu

L. I. GLAZMAN
Theoretical Physics Institute, University of Minnesota, Minneapolis, MN, USA
E-mail: glazman@physics.umn.edu

Effects of the electron-electron interaction on tunneling into a metal in a very strong magnetic field (ultra-quantum limit) are considered. It is shown that for short-range repulsive interactions, tunneling is dominated by the renormalization of the coupling constant leading eventually to the CDW instability. Near the gap, the conductance g_T assumes a universal form. For the long-range interaction, there exists an intermediate energy E_{PL} such that for $\Delta << E \leq E_{PL}$ the conductance obeys a power-law scaling form, similar to that of a 1D Luttinger liquid. For smaller energies, scaling breaks down and g_T is again dominated by the CDW-instability. It is also shown that the energy dependence of g_T may be *non-monotonic*: whereas g_T is always suppressed by the interaction at lower energies, at higher energies it may also be *enhanced* above its non-interacting value. Such an unusual behavior gets a natural explanation in terms of multiple scattering from the Friedel oscillation near the surface.

Low-dimensional systems exhibit "zero-bias anomalies" in tunneling (non-linearities of the current-voltage characteristics at small biases), which reflect the renormalization of the density of states by the electron-electron interaction. Tunneling into a one-dimensional (1D) metal is characterized by a power-law suppression of the tunneling conductance, g_T, characteristic for a Luttinger Liquid (LL). A three-dimensional metal placed in a strong magnetic field that depopulates all but one Landau level (ultra-quantum limit UQL) provides an example of a very interesting quasi-1D system. In particular, it is known that repulsive interactions result in opening of the charge-density wave (CDW) gap,[1] whose magnitude depends strongly on the magnetic field. On the other hand, it has recently been shown that in the case of long-range (Coulomb) interaction g_T exhibits a power-law (LL-like) behavior at sufficiently high energies with the field-dependent exponent.[2] In this paper, we combine the approaches of Refs. [1] and [2] to study the behavior of g_T in the whole energy interval from the Fermi energy down to the CDW gap (Δ).

First we review the procedure of finding the effect of the electron-electron interactions on the tunneling conductance of a metal in the UQL (see Ref. [2]). The contact plane (z=0) separates two metallic sides and the field is perpendicular to this plane. We consider both the symmetric (when both sides are in the UQL) and asymmetric (when one of the sides is made of a high-carrier concentration and/or dirty metal so that the magnetic field does not affect that side) configurations. The

transmission and reflection amplitudes for non-interacting electrons, t_0 and r_0, are assumed to be known. Backscattering of magnetically quantized electrons at the barrier gives rise to a Friedel oscillation whose amplitude decays away from the barrier as z^{-1}. Correspondingly, the exchange, $V_{ex}(\vec{r},\vec{r}')$, and Hartree, $V_H(\vec{r})$, potentials, calculated using exact (in the presence of the barrier) but otherwise free wavefunctions, also exhibit rapid $2k_F$-oscillations and decay as z^{-1} away from the barrier. The first-order correction to the wavefunction due to interaction is given by $\delta\Psi(\vec{r}) = \int d\vec{r}'d\vec{r}''G(\vec{r},\vec{r}';E)[V_{ex}(\vec{r}',\vec{r}'') + \delta(\vec{r}'-\vec{r}'')V_H(\vec{r}'')]\Psi^{(0)}(\vec{r}'')$, where $G(\vec{r},\vec{r}';E)$ is Green's function in the presence of the magnetic field. Evaluation of the integral leads to a logarithmic singularity ($\propto \ln E$) in $\delta\Psi(\vec{r})$, and thus in δt. At the next order, one re-calculates V_{ex} and V_H using the corrected wavefunctions, etc. Summation of the most divergent corrections to t in all orders of the perturbation theory is achieved via the renormalization group (RG) Eq. (3)

$$\frac{dt}{d\xi} = -c\Gamma(\xi)t(1-|t|^2), \xi \equiv \ln W/E, t(0) = t_0, \qquad (1)$$

where $c = 1(1/2)$ for a symmetric (asymmetric) configuration and $\Gamma(\xi)$ is related to the interaction vertex $\Gamma(\vec{q}_\perp,\xi)$ as $\Gamma(\xi) = \Gamma(0,\xi)$. Renormalization of $\Gamma(\vec{q}_\perp,\xi)$ is described by another RG Eq. (1)b:

$$\frac{d\Gamma(\vec{q}_\perp,\xi)}{d\xi} = \Gamma^2(\vec{q}_\perp,\xi) - \int d\vec{k}_\perp d\vec{k}_\perp' \Gamma(\vec{k}_\perp,\xi)\Gamma(\vec{k}_\perp',\xi)e^{i[\vec{q}_\perp\wedge(\vec{k}_\perp-\vec{k}_\perp')+\vec{k}_\perp\wedge\vec{k}_\perp']} \qquad (2)$$

where the first and second term correspond to the Peierls and Cooper channels of interaction, respectively. (Here and in what follows we set $\hbar$ and the magnetic length equal to one.) The initial condition for Eq. (2) $\Gamma(\vec{q}_\perp,0) = \Gamma(\vec{q}_\perp)$ is expressed via the Fourier transform of the interaction potential $U_0(q_Z,\vec{q}_\perp)$:

$$\Gamma_0(\vec{q}_\perp) = \frac{1}{(2\pi)^2\nu_F}\left[\int\frac{d\vec{k}_\perp}{2\pi}e^{i\vec{q}_\perp\cdot\vec{k}_\perp - k_\perp^2/2}U_0(0,\vec{k}_\perp) - U_0(2k_F,\vec{q}_\perp)e^{-q_\perp^2/2}\right]. \qquad (3)$$

The first and second terms in Eq. (3) are the exchange and Hartree contributions, respectively. Eqs.(1, 2 and 3) give a full description of tunneling in the UQL.

Equation (2) was analyzed in Ref. [1] for the case of a short-range interaction, when the $\vec{q}_\perp$ -dependence of U_0 can be neglected: $U_0(0,\vec{q}_\perp) \to u_0$, $U_0(2k_F,\vec{q}_\perp) \to u_{2k_F}$, and $\Gamma_0(\vec{q}_\perp) = \gamma_0 e^{-q_\perp^2/2}$, where $\gamma_0 \equiv (u_0 - u_{2k_F})/(2\pi)^2 v_F$. For repulsive interactions, the solution of Eq. (2) with the Peierls term alone is $\Gamma(\vec{q}_\perp,\xi) = (\Gamma_0^{-1}(\vec{q}_\perp) - \xi)^{-1}$ and the CDW gap is determined from the position of the pole at $\vec{q}_\perp = 0$: $\Delta = W\exp(-1/\gamma_0)$ (see Ref. [1]). Inclusion of the Cooper term merely changes the magnitude of the gap (see Ref. [1]b). Substituting $\Gamma(\vec{q}_\perp,\xi)$ into (1), we obtain for t:

$$t = \frac{t_0 f(E)}{\sqrt{|r_0|^2 + |t_0|^2 f^2(E)}}, \tag{4}$$

where $f(E) \equiv (\gamma_0\theta(E-\Delta)\ln E/\Delta)^c$. Near the gap ($E \approx \Delta$), the tunneling conductance $g_T \propto |t|^2$ assumes a *universal* form $g_T \propto (E-\Delta)^{2C}\theta(E-\Delta)$.

For the case of a long-range Coulomb potential $U_0(q_z,\vec{q}_\perp) = 4\pi e^2/(q_z^2 + q_\perp^2 + \kappa^2)$ with $\kappa \ll 1$, the gap is of order $\Delta = W\exp(-av_F/e^2)$ with $a \sim 1$. (For a single-band metal in the UQL, $\kappa^2 \sim e^2/v_F$, so there is only one small parameter controlling the validity of our weak-coupling approach: $e^2/v_F \ll 1$). In this case there exists a characteristic energy E_{PL} such that $\Delta \ll E_{PL} \sim W(\Delta/W)^{|\ln\kappa|^{-1}} \ll W$. For $E \gg \Delta$, the renormalization of the interaction vertex is not yet important and Eq. (1) can be solved with $\Gamma(\xi)$ replaced by its initial value Eq. (3). This results in t given by Eq. (4) with $f(E) = (E/W)^\alpha$, $\alpha = (ce^2/\pi v_F)[|\ln\kappa| - (4k_F^2 + \kappa^2)^{-1}]$. This high-energy regime corresponds to the Luttinger-liquid behavior (power-law scaling of the conductance) discussed in Ref. [2]. Note that exponent α is *not* necessarily positive: if k_F is sufficiently small (the lowest Landau level is strongly depleted), the second term in α, resulting from the Hartree (backscattering) channel, dominates and $\alpha < 0$. This means *enhancement* of g_T above its non-interacting value. The Hartree channel dominates because, being just an interaction of an electron with a z-dependent charge modulation near the surface, it does not involve the momentum transfer parallel to the surface ($q_\perp = 0$), whereas the exchange channel, being a non-

local interaction, involves transfers $q_\perp \sim \kappa$ which makes the effective interaction weaker.

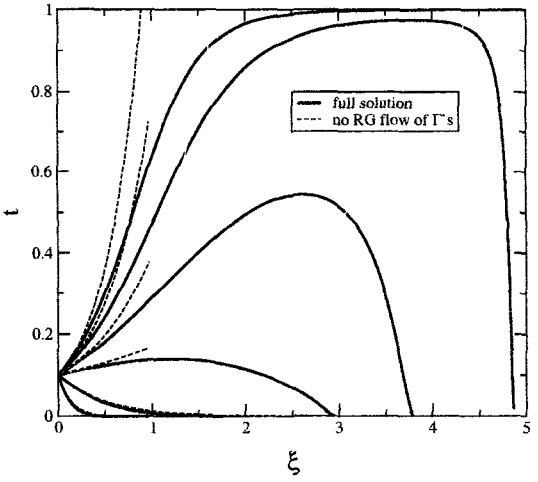

Figure 1: – Solid lines correspond to numerical solution of the full RG equations for the case of screened Coulomb potential Eqs. (1, 2 and 3). Different curves correspond to different values of κ (from the top curve to the bottom one κ =0.8, 0.7, 0.6, 0.5, 0.3, 0.1). Dashed lines are solutions of Eq. (1) without including RG flow of the coupling $\Gamma(\xi)$. Here ξ is in units of $2\pi^2 v_F/e^2$ and k_F =0.5.

The power-law scaling is cut off at energies $E \sim \Delta$, when the renormalization of the vortex becomes important. At smaller energies, the energy dependence of the conductance is determined by the proximity of the CDW instability. Full solution of Eqs. (1, 2 and 3) illustrating various regimes of the $t(E)$-dependence for a screened Coulomb potential is presented in Fig. 1.

We are grateful to V. M. Yakovenko for very useful discussions. D. L. M. acknowledges support from the NHMFL In-House Research Program, NSF DMR-9703388 and Research Corporation (RI0082). L. I. G. acknowledges support from NSF DMR-9731756.

1. ReferencesS. A. Brazovskii, *Zh. Eksp. Teor. Fiz.* **61**, 2401 (1971) [*Sov. Phys. JETP* **34**, 1286 (1972)], V. M. Yakovenko, *Phys. Rev. B* **47**, 8851 (1993).
2. C. Biagini et *al., Europhys. Lett.* **55**, 383 (2001).
3. D. Yue, L. I. Glazman and K. A. Matveev, *Phys. Rev. B* **49**, 1966 (1994).

HIGH MAGNETIC FIELD OPTICAL STUDIES OF CHARGED EXCITON IN CdTe 2D ELECTRON GASES

N. NEGRE,[1] S. A. CROOKER,[1] A. WOJS,[2] and G. KARCZEWSKI[3]
[1]*NHMFL/LANL, Los Alamos, NM 87545*
[2]*Institute of Physics, Wroclaw University of Technology, Wroclaw, Poland*
[3]*Institute of Physics, Polish Academy of Science, Warsaw, Poland*

Photoluminescence (PL) and reflectivity spectroscopy in magnetic fields up to 60 Tesla are used to investigate the excitonic optical transitions within CdTe/(Cd,Mg)Te 2D electron gases. The samples are 100 A and 200 A wide quantum well (QW) wherein the electron density is varied smoothly from $1x10^{11}$ to $4.5x10^{11}$ cm^{-3} across the wafer. This allows us to follow the energy diagram of the neutral exciton (X_0) and the charged exciton singlet and triplet spin states (X^-_s, X^-_t) versus magnetic field and the electron density. We observe a weak PL peak above 12 T (15 T) for the 200 A QW (100 A) at the low energy side of the spectra in addition to the X^-_0 and X^-_S PL. This peak could be the signature of a fundamental dark triplet state recently predicted (*Phys. Rev. B* **62**, 4630). Moreover, for high density samples a balance of PL intensity between the X^-_S and an other X^-_t occurs in the 25T-30T range. These results are interpreted on the basis of the calculations by Wojs *et al.* (*Phys. Rev. B* **62**, 4630) taking account the Zeeman energy of the charged exciton.

INCREASE OF QUANTUM HALL PLATEAU WIDTHS DUE TO ELECTRON-PHONON INTERACTION

J. RIESS, T. DUGUET and P. MAGYAR

Centre de Recherches sur les Très Basses Températures, CNRS, BP 166, 38042 Grenoble Cedex 9, France
E-mail: riess@labs.polycnrs-gre.fr

D. BICOUT

Lab of Chemical Physics, NIDDK, NIH, Bethesda, MD 20892

We calculate the conductivities for a model system of the integer quantum Hall effect including electron-phonon interactions, with a substrate potential chosen such that microscopic processes can be understood in detail. We find that in general the macroscopic Hall current is not only composed of velocities arising from the Schrödinger time evolution but also of velocities generated by electron-phonon interactions and that the latter can contribute to the formation of the quantized Hall plateaus. We show that for typical quantum Hall systems the phonon induced contributions lead to Hall plateaus which are somewhat larger than the plateaus of the dissipative conductivity. Experimentally this difference has been known for a long time, but it seemed unexplained so far. In the case where the substrate potential has no spatial fluctuations in the direction of the macroscopic electric field, all states are conducting and the dissipative conductivity vanishes only near integer filling factors. Nevertheless, the calculated Hall conductivity shows broad quantized plateaus, which here are entirely generated by velocities arising from phonon induced relaxation processes. These results show that absence of dissipation is not indispensable for the existence of quantized Hall plateaus.

We investigate the nature of the processes which generate the conductivity curves of the integer quantum Hall effect. We study electrons in a relatively simple substrate potential V(x,y) which is chosen such that the time dependent Schrödinger equation can be solved in very good approximation. In addition, the electrons are coupled to a heat bath of acoustic phonons. The Hamiltonian can be expressed as

$$H = [1/(2m)]\{(\hbar/i)\nabla - (e/c)[\boldsymbol{A}(\boldsymbol{r},t) - c\boldsymbol{E}t]\}^2 + V(\boldsymbol{r}), \qquad (1)$$

where curl $\boldsymbol{A}(\boldsymbol{r}) = \boldsymbol{B} = (0,0,B)$ and $\boldsymbol{E}$ is the macroscopic electric field (taken to be $(0,E_y,0)$). As in Ref. [1], our substrate potential $V(x,y)$ consists of a term $V(x)$ describing a sequence of hills and valleys, varying slowly over a magnetic length, and of a term $V'(x,y)$ representing more rapid spatial fluctuations. The solutions of the time-dependent Schrödinger equation are expressed as time-dependent linear combinations of solutions in the absence of V', which to a good approximation are Landau functions $\psi_p(x,y,t)$, which are plane waves in y direction and Gaussians in x direction (centered at $x_p(t) = chp/(eBL_y) + cE_yt/B$ + const., where L_y is the length of

the system (subdomain) in y direction and p is an integer). The corresponding energies are $E_p(t) \approx \hbar\omega_C(n + 1/2) + V[x_p(t)]$ + const.

For the macroscopic current it is sufficient to express the total time evolution in terms of transition rates between the fixed basis functions $\psi_p = \psi_p(x,y,t=0)$. When $V^I(x,y)$ is chosen sufficiently small (weak disorder approximation)[1] the transition rates $W^{Sch}_{p,p'}$ due to the Schrödinger time evolution can be expressed explicitly.[2] The presence of $V^I(x,y)$ leads to insulating states in the tails of the broadened Landau band (characterized by $W^{Sch}_{p,p'} = 0$ for $p \neq p'$). In the center of the band the electrons have velocities composed of a classical part and in general also of a nonclassical part due to elastic scattering in the potential V(x,y). Inelastic scattering with the phonons causes additional transition rates $W^{e-p}_{p,p'} = A(|p-p'|, B, c_L, \ldots)(n_{\boldsymbol{q}} + 1/2 \pm 1/2)$. Here the + (-) sign holds for emission (absorption) of a phonon with energy $\hbar\omega_{\boldsymbol{q}} = \hbar c_L|\boldsymbol{q}|$, and $n_{\boldsymbol{q}} = 1/[\exp(\hbar\omega_{\boldsymbol{q}})/k_B T - 1]$ is the Bose-Einstein distribution of the phonons at temperature T. $A(\ldots)$ is given explicitly in Ref. [2].

By means of these transition rates the total time evolution is described by a master equation for the occupation numbers $f_p(t)$ of the states ψ_p. The steady state solution f_p is obtained numerically. The *dissipative current density* has the form

$$j_y = \sum_{\substack{p \\ p'}} f_p W^{Sch}_{p,p'} (E_{p'} - E_p)/(2LL_y E_y), \tag{2}$$

where $2L$ is the length in x-direction of the unit cell of the substrate potential $V(x,y)$. The *Hall current density* j_x can be expressed as

$$j_x = [e/(L_y)] \Bigg\{ - \sum_{\substack{p \\ p' \\ x_{p'} - x_p > L}} f_p [W^{Sch}_{p,p'} + W^{e-p}_{p,p'} (1 - f_{p'})]$$

$$+ \sum_{\substack{p \\ p' \\ x_p - x_{p'} > L}} f_p [W^{Sch}_{p,p'} + W^{e-p}_{p,p'} (1 - f_{p'})] \Bigg\}. \tag{3}$$

Here the sum runs over $x_p\ x_{p'} \in [0,\ 2L]$. The Hall current density j_x contains a contribution which is generated by electron-phonon interaction.

The resulting conductivities σ_{xy} and σ_{yy} have been calculated numerically for all filling factors and as a function of temperature.[2] A remarkable result is that the plateaus of σ_{xy} became sensibly larger than those of σ_{yy}. This is illustrated in Fig. 1(a) for T = 1 K. Experimentally, such a phenomenon has been known for a long time, but it seemed unexplained so far. Our analysis shows that this effect has the following origin: Due to the electric field E_y the electrons in the conducting states get a Hall velocity component in positive x direction. Hence their energy increases for states localized on a positive slope of V(x) and decreases for states on a negative slope. If the Fermi level ε_F is in a range of conducting states, this creates an out of equilibrium situation, which is reduced by inelastic scattering (with phonon emission) from the momentarily energetically highest occupied states (on positive slopes) to the lowest unoccupied states (on negative slopes). It follows finally that for $\nu >$ half integer, the relaxation corresponds to hopping in the direction of the classical Hall velocity (cE_y/B, 0) and for $\nu <$ half integer it represents hopping in the opposite direction.

In general, $\sigma_{xy}(\nu)$ is the sum of three contributions : a Schrödinger contribution from the unperturbed, classical part of the Hall velocities (denoted σ_{xy}^{Sch1} in Fig. 1(a) and σ_{xy}^{Sch} in Fig. 1(b)); a Schrödinger contribution from the non-classical part of the Hall velocities (σ_{xy}^{Sch2}); the phonon induced contribution discussed above, denoted $\sigma_{xy}^{(e-p)}$, which is $\sigma_{xy}(\nu)$ restricted to the terms in Eq. (3) containing $W_{p,p'}^{e-p}$. In the region of a quantized Hall plateau, the current corresponding to the last two contributions is called "*compensating current*".

Fig. 1(a) shows the case, where conducting *and* insulating states are present (as in typical QH systems). Here the *compensating current* is to a great extent composed of nonclassical Schrödinger velocities and only to a small amount of phonon induced hopping (near the edges of the Hall plateau). Fig. 1(b) shows the special situation where the part V^I of the substrate potential $V(x,y)$ is zero. Here all states are conducting, with Schrödinger velocities describing only *classical* motion, which themselves lead to the straight line $\sigma_{xy}^{Sch} = (e^2/h)\nu$. But the total σ_{xy} (where $\sigma_{xy}^{(e-p)}$ is included) shows very large quantized plateaus similar to Fig. 1(a). This means that in Fig. 1(b) the phonon induced contribution generates the *totality* of the compensating current. Indeed, σ_{xy}^{Sch} is here exactly annihilated by $\sigma_{xy}^{(e-p)}$ when $\nu < 1/2$ and exactly completed to e^2/h when $\nu > 1/2$.

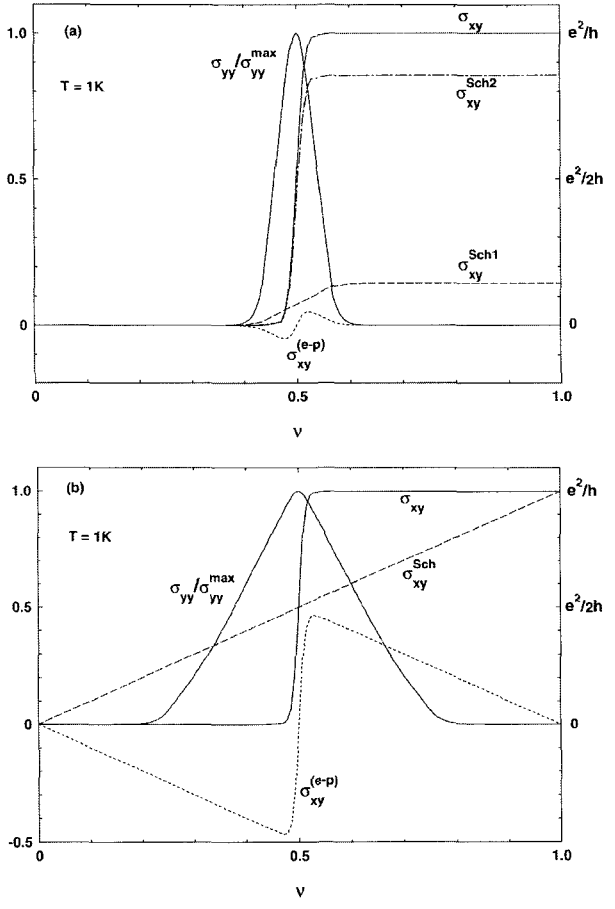

Figure 1: The full lines are numerical results of $\sigma_{yy}(\nu)/\sigma_{yy}^{max}$(units given on the left hand side) and of $\sigma_{xy}(\nu)$ (units given on the right hand side) for the following cases : a) $V^I(x,y) \neq 0$, b) $V^I(x,y) = 0$. The significance of σ_{xy}^{Sch}, σ_{xy}^{Sch1}, σ_{xy}^{Sch2}, $\sigma_{xy}^{(e-p)}$, is explained in the text. ν denotes the filling factor of the highest occupied Landau band. In Figs. 1(a) and (b), the values σ_{yy}^{max} are 16s, 64s, respectively, where s is a constant defined in Ref. [2].

References

1. J. Riess, Z. *Phys. B* **77**, 69 (1989); *J. Phys. France* **51**, 815 (1990).
2. D. Bicout, P. Magyar and J. Riess, *Phys. Rev. B* **57**, 7228 (1998).
3. J. Riess, D. Bicout and T. Duguet, *Physics Lett. A* **252**, 205 (1999).

SEARCH FOR SUPERLUMINAL PROPAGATION IN HIGH MAGNETIC FIELDS

J. RIESS

Centre de Recherches sur les Très Basses Températures, CNRS, BP 166, 38042 Grenoble Cedex 9, France
E-mail: riess@labs.polycnrs-gre.fr

We investigate the possibility of superluminal propagation of massive particles in high magnetic fields. Formal arguments suggest that this could occur in the quantum Hall regime near zero temperature, since here a few conducting states in the center of a broadened Landau band carry a macroscopic Hall current. We investigate the microscopic processes which lead to the high velocities of conducting states in the quantum Hall effect and ask what are the highest possible velocities which can be generated in that way. Our analysis shows that in typical quantum Hall systems at the most a tiny fraction of a carrier wave function can describe superluminal behaviour but that the center of mass velocity is far below the velocity of light. On the other hand, on pure theoretical grounds we can construct special systems (with « exotic » parameters) where the Schrödinger equation does admit solutions with superluminal center of mass velocities. The described propagation has no analogy in classical physics. Einstein's causality is not violated. The time evolution of the corresponding wave function is similar to that of a recently observed superluminal light pulse.[1] We discuss analogies and differences between the two phenomena.

In the past decade superluminal propagation has been observed in transmitted evanescent electromagnetic waves. Here the major part of a wave packet is reflected and the average, i. e., the « center of mass » velocity of the total wave packet is not superluminal. But recently superluminal « center of mass » propagation has been observed for light.[1] In this paper we will investigate whether such an effect is also possible for *massive* particles, at least in theory (see also Ref. [2]).

In particular, we will investigate quantum Hall and related systems. High particle velocities can occur in the quantum Hall regime where a few conducting states in the center of a broadened Landau band carry a macroscopic current. We consider non-interacting electrons (charge e) on a strip in x-direction (of width L_y) in the presence of a strong magnetic field $\boldsymbol{B} = (0,0,B)$, a macroscopic electric field $\boldsymbol{E} = (0,E_y,0)$ and a substrate potential $V(x,y)$. The Hamiltonian can be written as

$$H = (1/2\mathrm{m})\left\{ [(\hbar/i)(\partial/\partial x)]^2 + [(\hbar/i)(\partial/\partial y) - (e/c)\,[Bx + \phi(t)/L_y]]^2 \right\} + V(x,y), \qquad (1)$$

where $\phi(t) = -cE_yL_yt$. We chose periodic boundary conditions in y-direction. In typical quantum Hall systems $V(x,y)$ is composed of a smooth part $V^s(x,y)$, which is composed of hills and valleys which vary slowly over the magnetic length $\lambda_B = |\hbar c/eB|^{1/2}$, and of a more rapidly varying part $V^r(x,y)$. In the absence of V^r the wave functions can be approximately described semi-classically by Landau type wave functions with localization centers on equipotential lines of $V^s(x,y)$. Due to the

presence of $\boldsymbol{E} = (0,E_y,0)$ their guiding centers move with a velocity component $v_d = (cE_y/B,0,0)$ (in addition to the local Hall velocity arising from the local electric field $-(1/e)\mathrm{grad}V^s(x,y)$). Now one has to distinguish between *two different basic situations*:[3] Either the orbitals are on a tangential surface of $V^s(x,y)$ which is perpendicular to $\boldsymbol{E} = (0,E_y,0)$ or on a tangential surface parallel to $\boldsymbol{E}$. The second case is crucial for the following. To study this case, let us for a moment consider a simplified smooth potential $V(x)$ depending only on x. The wave functions are then in good approximation Landau functions

$$\psi_p(x,y,t) = (L_y)^{-1/2}\exp(-i2\pi py/L_y)u_p(x,t), \quad p \text{ integer.} \tag{2}$$

For the moment we omit the Landau index n. The functions $u_p(x,t)$ are proportional to Gaussians with localization centers

$$x_p(t) = chp/(eBL_y) - \phi(t)/(BL_y) - mc^2V'(x_p)/(e^2B^2), \tag{3}$$

which move in x direction with the classical Hall velocity cE_y/B (we restrict ourselves to the non-relativistic case where $E_y/B << 1$). V' denotes $dV(x)/dx$ and m is the effective mass. The corresponding energies

$$E_p(t) = \hbar\omega_c(n + 1/2) + V[x_p(t)] + (m/2)[cV'(x_p)/(eB)]^2. \tag{4}$$

increase or decrease as a function of t, depending on the sign of $V'[x_p(t)]$, leading to intersecting levels $E_p(t)$, $E_{p'}(t)$ when x_p, $x_{p'}$ are on *opposite* slopes of $V(x)$ (Fig. 1).

The true substrate potential varies also in y direction. This represents a deviation $V^l(x,y)$ from the potential $V(x)$ and leads in general to *anticrossing* of the adiabatic energies (see Fig. 1). The time evolution can then become entirely non-classical. Within the « anticrossing » time $\tau/2 = |h/2eE_yL_y|$ an adiabatic state transforms from ψ_p localized at x_p to $\psi_{p'}$ localized at $x_{p'}$ on the opposite slope of $V(x)$. This transformation is most complete if $V^l(x,y)$ is sufficiently small such that

$$|V^l_{pp'}| = f|E_p(t) - E_p(t + \tau)| \quad (= fV'|x_{p+1} - x_p|) \quad \text{with } f << 1, \tag{5}$$

(for simplicity we choose $V(x)$ symmetric with respect to the top of a hill or the bottom of a valley). In this *weak disorder case* the energy gap Δ between adjacent adiabatic levels is $\Delta = \Delta_{pp'} = 2|V^l_{pp'}|$. The corresponding *adiabatic* time evolution from x_p to $x_{p'}$ leads to the *non-classical velocity*

$$v_{nc} = |x_{p'} - x_p|/(\tau/2) = |(x_{p'} - x_p)2eE_yL_y|/h, \tag{6}$$

Equation (6) can be much larger than cE_y/B. It determines an *upper limit* for the

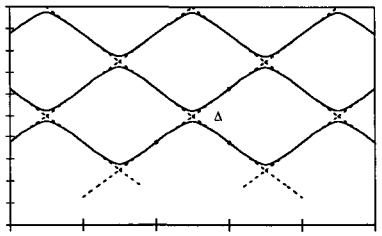

Figure 1: The full lines show the adiabatic energies as a function of time t (t in units of τ.) After the time interval $\tau/2$ an initial state A develops into a linear combinaion of B and C (if Δ is small, see text).

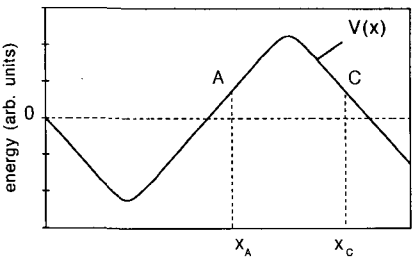

Figure 2: Schematic illustration of the type of smooth potential $V(x)$ used in the explicit calculations and of the potential energies and spatial positions of the states A and C.

Hall velocities in a quantum Hall system.[2] It is valid for the *adiabatic* evolution in the weak disorder case. The time evolution is *adiabatic* if the probability $P_{pp'}$ for the non-adiabatic transition from A to B in Fig. 1 is close to zero. $P_{pp'}$ can be calculated by the Zener formula[4] which takes here the form

$$P_{pp'} = \exp\{-|4\pi^2|V^I_{pp'}|^2 B/[V'(x_p)chE_y]|\}. \tag{7}$$

In order to have an *average* particle velocity greater than c during the time interval $\tau/2$, the physical parameters must be such that $v_{nc} > c$, and further that $1 - P_{pp'} \approx 1$, i. e., $|V^I_{pp'}|$ has to be sufficiently big such that $P_{pp'} << 1$ and sufficiently small such that the weak disorder condition Eq. (5) is fulfilled (see above).

Let us now estimate the *upper limit* of the Hall velocity *in typical quantum Hall samples*. Here the highest slopes of the potential $V^s(x,y)$ are about 10^3 Vcm^{-1}. The average distance between potential hills (wells) is roughly 1500 - 2000 Å since the magnitude of $|V^s(x,y)|$ is bounded by $\hbar\omega_c$. The greatest possible distance between two points x_p and $x_{p'}$ of equal energy, situated on nearest opposite slopes, is near the bottom of a hill (or the rim of a well). This distance is thus about 800 Å. Further we take an electric field E_y = 10 Vcm^{-1}, which is relatively close to the value where the IQHE breaks down (50 - 100 Vcm^{-1}), and L_y = 1cm. With these parameter values one obtains $v_{nc} = 1.3c$, which does exceed c. However, within a wave function, v_{nc} occurs only with the probability $1 - P_{pp'}$. which turns out to be extremey small since in the weak disorder condition (5) the highest possible value of f is about 0.2 leading to $|V^I_{pp'}| = 1.4\text{x}10^{-9}$ eV. With a typical value B = 6 T we obtain then $P_{pp'} = 0.9999999989$. The average Hall velocity in the time interval $\tau/2$ becomes then $P_{pp'}cE_y/B + (1 - P_{pp'})v_{nc} = 5.5\text{x}10^{-7}c$, which is far below c.

It is, however, possible to achieve superluminal center of mass propagation from the described mechanism with physical parameters chosen independently of

their realizability in a laboratory. For example let us ask that $P_{pp'} = 0.1$ and $v_{nc} = 2c$. The corresponding system of Eqs. (5) (with $f = 0.2$), (6) and (7) can then be satisfied, for instance with the following set of parameters : B = 6T, E_y = $3{,}24 \times 10^6 \mathrm{Vcm}^{-1}$, L_y = 0.0210μm, e = 4.8×10^{-10} esu (the charge of the electron), $|V| = 3 \times 10^6$ eVcm^{-1}. The length $|x_{p'} - x_p|$ becomes 1833 Å and the magnetic length 105 Å . This would give a *center of mass velocity* $P_{pp'}cE_y/B + (1 - P_{pp'})v_{nc} = 1.82c$.

Due to the high value of $|V|$ the broadened Landau bands now overlap if m is the effective mass of typical quantum Hall systems. This may lead to additional energy anticrossings *during the transition interval of length* $\tau/2$. In order to avoid this and to ensure that only the two considered functions $\psi_{0p}(t)$ and $\psi_{0p'}(t)$ mix in the previously described time-dependent way, we take for $V(x)$ a potential well centered at $x = 0$ and $V^1(x,y)$ in the special form

$$V^1(x,y) = d\delta(x - 0)\cos(2\pi 2py/L_y), \tag{8}$$

and we chose the origin of t such that for $t = 0$ we have $E_{0p} = E_{0-p}$, i. e., we have now $p' = -p$. The constant d is determined from the weak disorder condition Eq. (5) with $f = 0.2$. The form Eq. (8) effectivly restricts then the mixing to levels ψ_{nq} and $\psi_{n'q'}$ with $|q - q'| = 2p$. In particular, there remains a possible undesired mixing of $\psi_{0p}(t)$ with $\psi_{n-p}(t)$ $(n > 0)$ and of $\psi_{0-p}(t)$ with $\psi_{np}(t)$ $(n > 0)$, which can be avoided if the energy difference $\hbar\omega_c = \hbar eB/(mc)$ between adjacent Landau levels is larger than the maximum possible energy difference of the $n = 0$ levels $E_{0p}(t)$, $E_{0-p}(t)$ in the considered « quasi-degeneracy » interval $\{E_{0p}(-\pi/4), E_{0p}(\pi/4\}$. With the parameter values obtained above from Eqs. (5), (6) and (7), this can be achieved with a mass m which is not larger than 1.4×10^{-4} times the electron mass.

The time evolution leading to the non-classical velocity v_{nc} is similar to that of the superluminal light pulse observed in Ref. [1]. In both cases a moving Gaussian wave packet is shifted forward in time. However, in Ref. [1] this effect results from *classical interference* between the different frequency components in a region of anomalous dispersion, whereas in our case it originates from a *quantum mechanical* mechanism which has no classical analogy. In both cases the superluminal propagation does not violate Einstein causality since already the initial Gaussian wave packet has a tail which extends to « infinity », hence no wave front travels faster than c.

References

1. L. J. Wang, A. Kuzmich and A. Dogariu, *Nature* **406**, 277 (2000).
2. J. Riess, *Phys. Lett. A* **282**, 53 (2001).
3. D. Bicout, P. Magyar and J. Riess, *Phys. Rev. B* **57**, 7228 (1998).
4. C. Zener, *Proc. R. Soc. London Ser. A* **137**, 696 (1932).

IMPURITIES IN A MAGNETIC-FIELD-INDUCED LUTTINGER LIQUID

S.-W. TSAI and D. L. MASLOV

Institute for Fundamental Theory and Department of Physics, University of Florida, Gainesville, FL, USA

E-mail: tsai@phys.ufl.edu, maslov@phys.ufl.edu

L. I. GLAZMAN

Theoretical Physics Institute, University of Minnesota, Minneapolis, MN, USA

E-mail: glazman@physics.umn.edu

We study the effect of dilute impurities on a system of interacting electrons subject to a quantizing magnetic field. For the case of point impurities, the calculation of the scattering cross section can be mapped onto a 1D problem of tunneling conductance through a barrier for interacting electrons. We find that the electron-electron interaction produces temperature-dependent corrections to the cross-section, and thus to the tensor of conductivities. Upon summation of the most diverging corrections in all orders of perturbation theory, a scaling behavior of the conductivities emerges. This behavior is similar to that of 1D Luttinger liquid. The scaling exponents depend on the magnetic field and are calculated explicitly in the weak-coupling limit. The limitations on the scaling behavior due to the formation of a charge-density wave are also discussed.

The effective dimensionality of charge carriers in a bulk metal may be reduced from 3D to 1D by applying a strong magnetic field. Such a reduction leads to formation of a strongly correlated state.[1] If the interaction among electrons is long-range, certain characteristics of this state, e. g., tunneling density of states, exhibit a high-energy behavior similar to that of a 1D Luttinger liquid.[2] Here we investigate the effect of dilute impurities on such a "magnetic-field-induced Luttinger liquid". We first find the conductivities for free electrons in the ultra-quantum limit (UQL), when only the lowest Landau level is occupied, and then calculate the renormalization corrections due to the electron-electron interaction. The second part is done by an exact mapping onto a pure 1D (no magnetic field) problem of tunneling for interacting electrons, solved by Yue, Glazman and Matveev.[3] We find that in a certain temperature range the dissipative conductivities scale as power-laws of the temperature: $\sigma \propto T^{2\alpha\varepsilon}$, where $\varepsilon = 1$ (-1) is for the electric current parallel (perpendicular) to $\vec{B}$. The exponent α is determined by the effective strength of the electron-electron interactions. Our analysis is valid for temperatures $T >> 1/\tau$, where τ is the mean free time for scattering off impurities. In this regime, a typical electron-electron interaction time is shorter than τ, and the effect of interaction on the impurity scattering may be considered for a single impurity at a time.

First, we discuss scattering of free electrons from a single, axially-symmetric impurity. As the angular momentum $\vec{L}$ is conserved in the scattering process, the scattering cross-section Σ is completely determined by a set of backscattering amplitudes, $\{ r_m \}$, for each component m of $\vec{L}$ (see Ref. [4]):

$$\Sigma = 2\pi\ell_B^2 \sum_{m=0}^{\infty} | r_m |^2 \qquad (1)$$

where ℓ_B is the magnetic length. Amplitudes r_m are simply reflections coefficients obtained from the solution of a set of 1D Schrodinger equations. There is one such an equation for each value of m and the corresponding 1D potential is $V_m(z) = \langle m | V(\vec{r}) | m \rangle$. A short-range impurity potential ($a << \ell_B$, where a is the range of the potential) can be modeled by an effective delta-function potential. This is an especially simple case as all but the $m = 0$ component vanish.

Now we turn to the calculation of the interaction correction to Σ. The free-electron scattering state Ψ_0 for a point impurity is specified by the reflection and transmission amplitudes r_0 and t_0 for a 1D delta-function potential. The first-order correction to Ψ_0 due to exchange and Hartree potentials is given by:

$$\delta\Psi(\vec{r}) = \iint d\vec{r}'\, d\vec{r}''\, G(\vec{r},\vec{r}';E)[V_{ex}(\vec{r}',\vec{r}'') + V_H(\vec{r}'')\delta(\vec{r}'-\vec{r}'')]\Psi_0(\vec{r}''). \qquad (2)$$

The scattering problem is now formally equivalent to the tunneling problem in the UQL [2]. The latter, on its own turn, can be reduced to a pure 1D case, with no **B** field, solved by Yue, Glazman and Matveev.[3] Correction (2) leads to a logarithmically divergent correction to the transmission amplitude

$$\delta t = \alpha t_0 | r_0 |^2 \ln(| E | / W)$$

where (here and in what follows $\ell_B = 1$):

$$\alpha = \frac{e^2}{\pi v_F}[F(\kappa) - F(\sqrt{\kappa^2 + 4k_F^2})] \geq 0,$$

E is the energy reckoned from the Fermi energy E_F, v_F (k_F) is the Fermi velocity (momentum), $W \sim E_F$ is the effective bandwidth, κ is the screening wavevector,

and $F(x) = e^{x^2/2} E_1(x^2/2)$ with $E_1(z) = \int_z^\infty dy e^{-y}/y$. The physical reason for a singularity at $E = 0$ is a nearly 1D form of the Friedel oscillation around an impurity in the strong magnetic field. Consequently, both the exchange and the Hartree potentials decay as $1/z$ along the field, hence the log-singularity.

The higher order corrections to the transmission amplitude can be summed up via the renormalization group procedure, derived in Ref. [3]. The flow of t is described by the equation

$$dt/d\zeta = -\alpha t(1-|t|^2) \tag{3}$$

where the "RG time" $\xi \equiv \ln(W/E)$. Assuming that α itself does not flow, this equation results in a power-law scaling of t with E. The renormalized cross-section is now written in terms of the renormalized reflection amplitudes.

For the current parallel to $\vec{B}$, the conductivity is given by $\sigma_\parallel = ne^2\tau/m \propto 1/\Sigma(|E| = T)$, so that

$$\sigma_\parallel = \sigma_{\parallel U}^0 + (\sigma_\parallel^0 - \sigma_{\parallel U}^0)[T/W]^{2\alpha(B)}, \tag{4}$$

where $\sigma_\parallel^0$ is the conductivity for free electrons and $\sigma_{\parallel U}^0$ is the conductivity for free electrons in the unitary limit, *i.e.*, for an infinitely strong impurity. As $T \to 0$, the conductivity approaches the unitary limit but our calculation is expected to be valid only for $T >> 1/\tau$. For the current perpendicular to $\vec{B}$, the conductivity is $\sigma_\perp = e^2 \upsilon_F D_\perp \propto \Sigma \propto \sigma_\parallel^{-1}$.

When deriving Eq. (4), we assumed that the coupling constant is not renormalized. This assumption breaks down at low energies, as the ground state of (repulsively) interacting electrons in the UQL is unstable with respect to the formation of a charge-density wave (CDW) (see Ref. [1]). For Eq. (4) to have a region of validity, there should exist an interval of intermediate energies, in which the renormalization of α due to CDW fluctuations is not yet important but the power-law renormalization of the transmission amplitude t is already significant. Such an interval exists for a long-range Coulomb interaction ($|\kappa| << 1/\ell_B = 1$). The RG equation for the flow of the coupling constant was derived in Ref. [1]. It follows from this equation that the renormalization of the coupling constant becomes significant at energies of order of the CDW gap Δ. If the lowest Landau level is not depleted too strongly, *i.e.*, $k_F \leq 1$, one can show that $\xi_{CDW} \equiv \ln(W/\Delta) \sim \nu_F/e^2$. On

the other hand, the power-law for t forms at such energy E_{PL} that $\xi_{PL} \equiv \ln(W / E_{PL}) \sim \alpha^{-1} \sim v_F / e^2 \,|\ln\kappa|$. We see that in terms of the "RG time" the power-law renormalization of t occurs *earlier* than the renormalization of the coupling constant: $\xi_{CDW} / \xi_{PL} \sim |\ln\kappa| \geq 1$. Thus there exists an energy interval ($\Delta << E << W$) in which the conductivity has a scaling form given by Eq. (4). This conclusion is supported by a numerical solution of the RG equation for the coupling constant[1] for the case of a long-range Coulomb interaction.[5] This solution demonstrates that the ratio ξ_{CDW} / ξ_{PL} can be as large as 7 if κ is sufficiently small (~0.1) and k_F is close to 1. As the lowest Landau level is depleted further (k_F decreases), the ratio ξ_{CDW} / ξ_{PL} decreases. However, the decrease is rather slow: *e.g.*, for $\kappa = 0.1$, ξ_{CDW} / ξ_{PL} becomes equal to one only at $k_F = 0.05$. A detailed study of the crossover region between the power-law scaling and the CDW behavior is currently in progress.[5]

Experiments on heavily doped semiconductors (InSb and InAs) in the UQL (see Ref. [6]) do show rather strong T-dependences of $\sigma_{\parallel,\perp}$. The signs of observed $d\sigma_{\parallel,\perp} / dT$ agree with Eq. (4). A more detailed analysis is required, however, to connect the theory presented here to these experimental results because the concentration of charged impurities is very high. In these cases localization has been argued to play an important role.[6] Low carrier density semi-metals such as bismuth or graphite would be better candidates for observing the effect studied here.

We are grateful to V. M. Yakovenko for very useful discussions. D. L. M. acknowledges support from the NHMFL In-House Research Program, NSF DMR-9703388 and Research Corporation (RI0082). L. I. G. acknowledges support from NSF DMR-9731756.

References

1. S. A. Brazovskii, *Zh. Eksp. Teor. Fiz.* **61**, 2401 (1971) [*Sov. Phys. JETP* **34**, 1286 (1972)], V. M. Yakovenko, *Phys. Rev. B* **47**, 8851 (1993).
2. C. Biagini, D. L. Maslov, M. Yu. Reizer and L. I. Glazman, *Europhys. Lett.* **55**, 383 (2001).
3. D. Yue, L. I. Glazman and K. A. Matveev, *Phys. Rev. B* **49**, 1966 (1994).
4. D. G. Polyakov, *Zh. Eksp. Teor. Fiz.* **83**, 61 (1982) [*Sov. Phys. JETP* **56**, 33 (1982)].
5. S.-W. Tsai, D. L. Maslov and L. I. Glazman, unpublished.
6. see, *e.g.,* S. S. Murzin, *Usp. Fiz. Nauk.* **170**, 387 (2000) [*Sov. Phys. Usp.* **43**, 349 (2000)] and references therein.

RECONSTRUCTION OF FRACTIONAL QUANTUM HALL EDGES

X. WAN,[1] K. YANG[1] and E. H. REZAYI[2]

[1]*NHMFL and Department of Physics, Florida State University, Tallahassee, Florida 32306, USA*

[2]*Department of Physics, California State University, Los Angeles, California 90032, USA*

Edge reconstruction has been a well-known effect for integer quantum Hall liquids in the presence of both electron interactions and a confining potential generated by charged background. At more generic fractional fillings, we point out that confined two-dimensional interacting electrons can exhibit the similar reconstruction effect. Our exact diagonalization results show that, in a fractional quantum Hall system with a sharp cleaved edge potential, the electron density oscillation near the edge increases with the distance between the electron gas and the background charge layer. As a result, the outermost hump can detach from the bulk beyond certain point. We suggest that the edge reconstruction effect is relevant to the recent edge tunneling experiments,[1] as well as the microwave absorption experiment on two-dimensional electrons in an antidot array.[2] Calculating the finite-temperature density profiles, we estimate the temperature above which the edge reconstruction disappears to further discuss the relevance to the microwave absorption experiment.

1. Grayson *et al., Phys. Rev. Lett.* **80**, 1062 (1998); A.M. Chang *et al., Phys. Rev. Lett.* **86**, 143 (2001); M. Hilke *et al., cond-mat*/0104533.
2. D. Ye *et al., cond-mat*/0103127.

SAMPLE COOLING AND ROTATION AT ULTRA-LOW TEMPERATURES AND HIGH MAGNETIC FIELDS

J. S. XIA,[1,2] E. D. ADAMS,[1,2] N. S. SULLIVAN,[1,2] W. PAN,[2,3]
H. L. STORMER,[4] and D. C. TSUI[3]

[1] *Microkelvin Laboratory, Department of Physics, University of Florida, Gainesville, FL 32611-8440, USA*

[2] *National High Magnetic Field Laboratory, Tallahassee, FL 32310, USA*

[3] *Princeton University, Department of Electrical Engineering, Princeton, NJ 08544, USA*

[4] *Columbia University, Department of Physics and Department of Applied Physics, New York, NY 10027, USA and Bell Labs, Lucent Technologies, Murray, NJ 07974, USA*

A rotator, made from polycarbonate and operated hydraulically using liquid helium, has been developed at the High B/T Facility of the National High Magnetic Field Laboratory (NHMFL) in Gainesville, It can be tilted more than 90 degrees by applying a pressure of several bars. The frictional heating was found to be negligible down to 8.0 mK. The sintered silver powder heat exchangers, specially designed for the cooling of the two-dimensional electron gas (2DEG) system in the fractional quantum Hall effect (FQHE) experiment,[1,2] are also attached to the rotator. We have conducted an angular-dependent study of the even-denominator FQHE state at $\nu = 5/2$. Our preliminary data showed that the rotator performed well at ultra-low temperatures and high magnetic fields. This technique should be applicable for other transport measurements at such extreme experimental conditions.

1 Introduction

It is of great interest to study the spin polarization of the even-denominator fractional quantum Hall effect state at $\nu = 5/2$, by measuring the angular dependence of its energy gap. Since the energy gap at $\nu = 5/2$ is rather small, this kind of experiment is technically extraordinarily challenging, duo to the requirement of the *in situ* rotation of the sample at ultra-low temperatures ($T<10$ mK). Several *in situ* rotating devices have been reported,[3-6] but none of them is suitable for ultra-low temperatures and achieved by a nuclear demagnetization refrigerator. We have developed a miniature sample rotator, which to our knowledge is the first device that operates below 10 mK. It rotates the sample about one axis more than 90 degrees with an accuracy of 0.2 degrees. The details of the construction and performance are described in this article.

In this unique device, the main objective is concentrated on the minimization of the thermal dissipation generated by frictional motion. Most of the parts are made of plastic, polycarbonate, to reduce eddy current heating in magnetic fields. Commercially available ruby, sapphire vee jewels, and nivapoint pivots[7] are used as frictional bearings in all moving joints. Hydraulic pressure is chosen as the driving force to avoid a heat load from high temperatures. Indeed, with these advantages the

rotator performed well without significant heating down to our dilution refrigerator base temperature of 8.0 mK.

2 Construction

The rotator is attached at the bottom of the experimental cell, which is thermally connected to the nuclear refrigerant stage, as shown in the lower part of Fig. 1. The rotation mechanism is driven by compressed liquid helium three (^{3}He) through a capillary from a heat exchanger--- thermally anchored onto the top of the nuclear stage --- with a small capacitive strain gauge contained in as an indicator of the liquid pressure. The ^{3}He is condensed through a capillary at 1 K pot, cooled in the heat exchanger and compressed into the rotator. The liquid pressure is controlled by hand through a needle valve from room temperature.

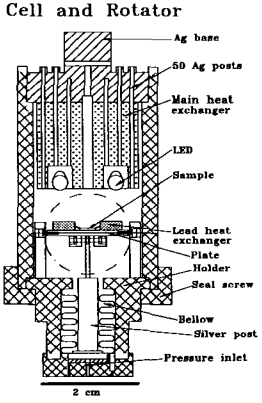

Figure 1: Experimental cell and rotator

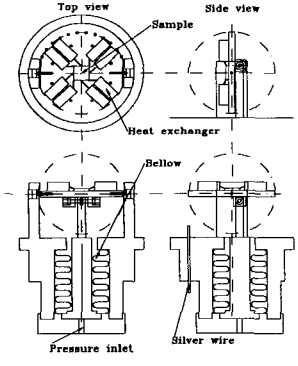

Figure 2: Construction details of the rotator

The mechanical details of rotator are shown schematically in Fig. 2 with views from different angles. It consists of a BeCu bellow,[8] two pure silver posts (one large and one small in diameter), a sample plate and a holder both made of polycarbonate. One end of the bellow is glued to the holder with Stycast 2850 and other end is soft soldered to the large silver post. The small silver post, with sapphire ring jewel in one end, and a sapphire rod together form a "T" shaped joint connected to the sample plate. The initial position of the sample plate can be adjusted by the screw joint between the two silver posts.

The 4.0 mm x 4.0 mm x 0.5 mm GaAs/$Al_xGa_{1-x}As$ sample is mounted in the center of the plate. Eight sintered silver powder heat exchangers are used to cool the

two-dimensional electron gas (2DEG) with the same construction as Re. (see Ref. [2]), but are shorter to fit the plate and are tied down on the plate with cotton threads. Each electrical contact of the sample is directly soldered to the center silver wire of the heat exchanger with indium. To make the electrical connection from the leads coming from outside of the cell, 14 silver wires, with diameter in 0.25 mm, are fed through the holder. Fine copper wires with proper length then make the connections between the heat exchangers and the silver wires.

3 Performance

The rotator was first tested and calibrated at the liquid nitrogen temperature by directly measuring the change of angle of the sample plate with a capacitive pressure sensor and the driving pressure. An Andeen-Hagerling 2500 A capacitance bridge and a Parocientific Digiqurtz pressure gauge were used to read the capacitance and the applied pressure, respectively. The initial angle of sample plate was positioned at negative 10 degrees with the pressure of zero bar, and it turned to vertical at 5.240 bar. Hysteresis was found to be rather small and negligible during pressure increasing and decreasing.

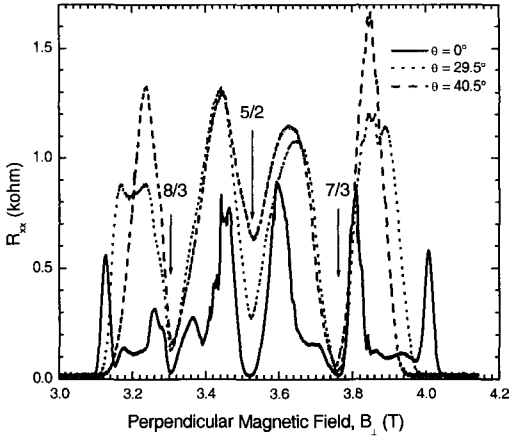

Figure 3: R_{xx} versus perpendicular magnetic field at different angles. Sample is a GaAs/AlGaAs quantum well.

At 8.0 mK, the rotator was operated up to full pressure and down to zero several times. It showed excellent reproducibility and precision of the pressure and capacitance. Approximately one hour is required to turn the sample to 90° from 0°.

The turning speed is limited by the slow condensing of ^{3}He gas. During this time the change of the temperature was found to be less than 50 μK as indicated by a calibrated ^{3}He melting pressure thermometer (MPT).

In this particular experiment, the tilt angle of the sample was monitored by the magnetic field position of resistance minimum at $\nu = 5/2$. It depends only on the perpendicular magnetic field, $B_{perp} = B_{total} \times \cos(\theta)$, where B_{total} is the total field and θ is the tilt angle. The angular dependence of R_{xx} around $\nu = 5/2$ at 8.0 mK is shown in Fig. 3. It clearly demonstrated the possibility of performing angular-dependent measurements at such extreme conditions. The calculated θ and the angle converted from the pressure agreed to within 0.2 degrees.

Reference

1. W. Pan *et al., Phys. Rev. Lett.* **80**, 3530-3533 (1999).
2. J. S. Xia *et al., Physica B* **280**, 491-492 (2000).
3. E. C. Palm *et al., Rev. Sci. Instrum.* **70**, 237-239 (1999).
4. G. R. Ashton *et al., Rev. Sci. Instrum.* **48**, 1402-1404 (1977).
5. B. G. Pazol *et al., Rev. Sci. Instrum.* **59**, 776-777 (1988).
6. E. Haas *et al., Rev. Sci. Instrum.* **67**, 1930-1932 (1996).
7. Swiss Jewel Company, Lafayette Building, Philadephia, PA 19106.
8. Mini-Flex Corporation, 2472 Eastman Avenue, Unit 29, Ventura, CA 93003.

This page is intentionally left blank

Part II

Heavy Fermions

This page is intentionally left blank

DOES THE HEAVY ELECTRON MAINTAIN ITS INTEGRITY AT QUANTUM CRITICAL POINT?

P. COLEMAN
Center for Materials Theory, Rutgers University, University Heights, Newark, New Jersey 07102, USA

This talk will discuss non-Fermi liquid and quantum critical behavior in heavy fermion materials, focussing on the mechanism by which the electron mass appears to diverge at the quantum critical point. Is the quantum critical point merely a case of electron diffraction off a quantum critical spin density wave, or does it involve a fundamental break-down in the composite nature of the heavy electron place at the quantum critical point? We discuss the nature of the critical langrangian and show that the Hall constant changes continuously in the first scenario, but may "jump" discontinuously at a quantum critical point where the composite character of the electron quasiparticles changes.

1. P. Coleman *et al., J. of Phys.: Cond. Matt.* **13**, 723, (2001).
2. A. Schroeder *et al., Nature*, **407**, 351-355 (2000).
3. A. Schroder *et al., Phys. Rev. Lett.*, **80**, 5623 (1998).

OBSERVATION OF A SECOND ENERGY SCALE IN $YbAl_3$ ABOVE 40 T

A. L. CORNELIUS

University of Nevada, Las Vegas, Department of Physics, Las Vegas, Nevada, 89154-4002, E-mail: cornel@physics.unlv.edu

T. EBIHARA

Shizuoka University, Department of Physics, Faculty of Science, 836 Ohya, Shizuoka 422-8529, Japan
E-mail: sptebih@ipc.shizuoka.ac.jp

J. M. LAWRENCE

University of California, Irvine, Department of Physics, Irvine, CA 92697, USA
E-mail: jmlawren@uci.edu

P. S. RISEBOROUGH

Temple University, Department of Physics, Philadelphia, PA 19122, USA
E-mail: prisebor@astro.temple.edu

J. D. THOMPSON

Materials Science and Technology Division, Los Alamos National Laboratory, Los Alamos, NM 87545, USA
E-mail: jdt@lanl.gov

$YbAl_3$ is an intermediate valent compound with a Kondo temperature T_K in excess of 500 K and a rather low conduction electron density of ~0.5/atom. Recent measurements are suggestive of a second energy scale T_{coh} of order 50 K that dominates the low temperature ($T << T_{coh}$) thermodynamic properties. Previous de Haas-van Alphen (dHvA) measurements on $YbAl_3$ in magnetic fields to 17 T reveal a fairly simple Fermi surface with 6 branches having effective masses m* ranging from 8 to 24 m_0 (see Refs. [2-3]). We report magnetization and dHvA results on $YbAl_3$ in pulsed magnetic fields up to 60 T. For $T << T_{coh}$ we indeed find that the magnetization "crosses" over from the zero field energy scale (T_{coh}) to the high temperature energy scale T_K at a magnetic field $B^* \approx 40$ T ($\approx k_B T_{coh}/\mu_B$). For $B > B^*$, we find dHvA oscillations when magnetic field is applied along the <100>, <110> and <111> directions. For magnetic field applied along <111>, the Fermi surface changes very little for $B > B^*$, and the effective masses are all reduced by a factor of 2-3 relative to their low field values. This is due to the large change in the characteristic temperature, which goes from T_{coh} below B^* to T_K above B^*. We believe this is the first work to directly observe the two energy scales and to observe the crossover in the dominant energy scale as a function of magnetic field.

1 Introduction

The f-electrons in Ce and Yb compounds are known to interact very strongly with the conduction electrons. The number of f-electrons per atom n_f in Ce compounds varies between 0 and 1. In a similar manner, the number of f-holes per atom n_f in Yb compounds varies from 0 to 1. A great deal of experimental and theoretical

work has been performed both in the Kondo limit (n_f=1) and the intermediate valent (IV) limit (n_f<1) as a function of the number of conduction electrons per atom n_c to gain a better understanding of these complicated systems. A standard starting point for these materials is the Anderson Impurity Model (AIM). In the AIM the f-electrons are considered to interact only with the conduction electrons and not each other. This assumption of non-interacting f-electrons is clearly not valid as Yb and Ce compounds have a regular lattice of impurities that gives rise to the name Anderson lattice model (ALM).

The temperature dependence of thermodynamic properties (magnetic susceptibility and heat capacity) and n_f along with the energy dependence of the dynamic susceptibility in both the AIM and ALM are qualitatively similar.[1-2] The low temperature transport properties are quite different in the two models as the AIM predicts an increase in the scattering at low temperatures while the ALM has a vanishing resistance due to the formation of a coherent Fermi liquid state. Typically the magnetic f-electrons are believed to behave as localized electrons above T_K and form the coherent state below T_K.

Recently, theoretical studies have shown that the AIM and ALM give different results as the conduction electron density n_c decreases. Firstly, the crossover from the high temperature local moment to the Fermi liquid state is slower in the ALM than the AIM with the disparity being larger for smaller values of n_c (see Refs. [2-4]). Also, as n_c decreases theory predicts that a new low temperature scale T_{coh}<<T_K arises for the onset of Fermi liquid coherence[5] with $T_{coh}/T_K = n_f/(2J+1)$, where J is the total spin, being independent of n_c (see Ref. [6]). Due to the formation of a second energy scale, it is expected that measurements will show evidence of two energy scales. For example, two peaks in the magnetic susceptibility; one corresponding to T_K at high temperatures and the other T_{coh} at low temperatures to would be expected. Indeed, preliminary results on $YbAl_3$ seem to be suggestive of two energy scales and a slow crossover.[6]

By extending the range of applied magnetic fields to 60 T, magnetization and de Haas-van Alphen (dHvA) results on $YbAl_3$ are found to be consistent with the existence of two energy scales. In particular, at low temperatures, the application of a magnetic field of 40 T, which is of the order $k_B T_{coh}/\mu_B$ is sufficient to cause the system to go from the T_{coh} energy scale to the T_K energy scale without a significant change in Fermi surface geometry.

2 Methods

The samples used in the current study were single crystals of $YbAl_3$. The single crystals were grown by a "self-flux" technique that uses excess Al as the flux. The samples were found to be of high quality as determined by the ratio of the resistance at room temperature to that at 2 K being in excess of 60 and the existence of well-defined dHvA oscillations.[7-8]

The magnetization and dHvA effect were measured using counter wound highly compensated pickup coils in the 60 T short pulse magnet at the National High Magnetic Field Laboratory, Los Alamos. Throughout the dHvA experiments, the sample was immersed in a ^{3}He environment in which the temperature could be varied between 0.49 K and 2.1 K. The magnetization measurements were performed both in a commercial SQUID magnetometer using a 1 kOe applied field and in a ^{3}He gas environment to 60 T both for sample in and sample out to determine the magnetization of the sample only. In pulsed field measurements, the raw inductive signal S is proportional to dM/dB so the magnetization is found by integrating S as a function of B. Small oriented single crystals were used for the dHvA measurements while a fine powder consisting of ground single crystals was used in the magnetization measurement to minimize heating effects.

3 Experimental Results

3.1 Magnetization Measurements

Figure 1 shows the magnetization as a function of applied magnetic field at temperatures above and below T_{coh} (~40 K). The solid lines are linear fits to the data

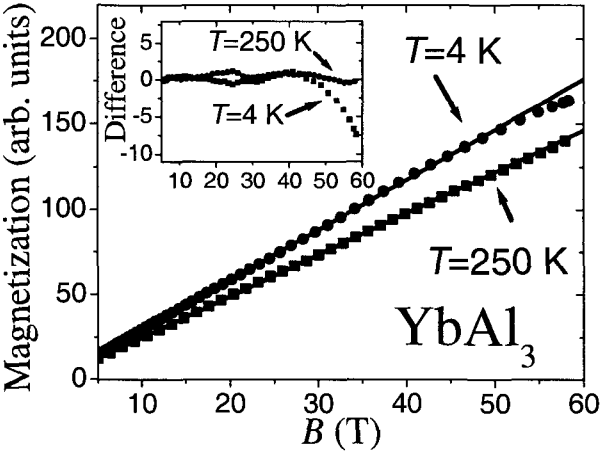

Figure 1: Magnetization as a function of applied magnetic field B for $YbAl_3$. The solid lines are linear fits to the data in the range 10 T<B<35 T, and the inset shows the difference between the fits and the raw data.

in the magnetic field range 10 T<B<35 T. The difference between the linear fits and the raw data is shown in the inset. At both temperatures, the data display linear

behavior for B<40 T. Above 40 T, there is a clear change in slope for the 4 K data while the 250 K data retains its linearity. As the slope is simply the magnetic susceptibility χ, there is clearly a reduction in χ above 40 T at 4 K. The data is found to be linear in the field range 47 T<B<57 T.

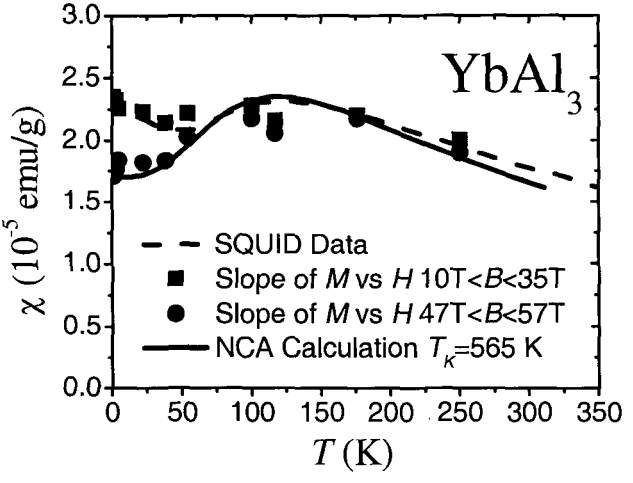

Figure 2: Magnetic susceptibility χ as a function of temperature T for $YbAl_3$. The dashed line is the SQUID magnetometer while the solid line is a fit to the data above 50 K as described in the text. The symbols represent the slope of the M versus B curves in two different field ranges.

Figure 2 shows a summary of the magnetization results. The dashed line is the SQUID magnetometer data that is taken in a 1 kOe magnetic field. A close examination of the SQUID data reveals two maxima at 110 K and 15 K. As one expects a peak in χ to be directly related to the germane energy scale, it would appear that there are two energy scales in $YbAl_3$. The solid line is a fit to the high temperature SQUID data above ~50 K using the non-crossing approximation (NCA) in the ALM (for details see Ref. 6 and the references therein) with a characteristic temperature T_K=565 K. The NCA calculation data has been normalized to agree with the peak in the SQUID data, and one can see good agreement with experiment above 75 K. Below 50 K, the SQUID data no longer agrees with the NCA calculation as the second energy scale T_{coh} becomes dominant. The solid symbols represent the slopes of the M versus B curves shown in Figure 1 and are normalized to give the best agreement to the SQUID data. For the low field data (10 T<B<35 T) there is good agreement to the SQUID data. For the high field data (47 T<B<57 T) the data can be fit very well by the NCA calculation. In other words, it appears that

applying a magnetic field $B^* \approx 40$ T ($\approx k_B T_{coh}/\mu_B$) which is of order the coherence energy scale drives the system into behaving according to a single energy scale T_K.

3.2 *Fermi Surface (de Haas-van Alphen) Measurements*

To clarify the nature of the crossover in energy scales at low temperature, we decided to see if the Fermi surface was affected above 40 T. Indeed, one explanation for the observance of two energy scales would be a drastic change in the Fermi surface. The entire Fermi surface of $YbAl_3$ was determined for fields below 16 T by Ebihara *et al.*[7] The main result of that work was the finding of a nearly spherical orbit, labeled β and numerous multiply connected orbits all having relatively enhanced effective masses ($m^*>10\ m_0$ where m_0 is the mass of an electron). A summary of the previous results is given in Table 1 for the magnetic field applied along the <111> direction. We extended the range of the dHvA studies up to 60 T using the pulsed magnetic facilities at NHMFL-LA. Above 40 T, we clearly saw dHvA oscillations when the magnetic field was applied along the <100>, <110> and <111> directions. The results for the <111> direction are included in Table 1. The β, η and α orbits were observed while we were not able to detect the ε orbit

Table 1: Effective masses and frequencies for the de Haas-van Alphen orbits observed in $YbAl_3$ for magnetic fields applied along the <111> direction both below 20 T and above 40 T (the values for the higher fields are in parentheses).

Orbit Label (from Ref. 7)	Frequency (kT) B<20 T (B>40 T)	Effective Mass (m_0) B<20 T (B>40 T)
β	4.1 (4.7)	23.9 (7.7)
η	14.7 (13.5)	14.2 (7.8)
α	15.8 (14.2)	13.5 (6.4)
ε	18.6 (---)	17.4 (---)

The effective masses should scale as the electronic specific heat component γ that in turn can be related to the Kondo temperature T_K by $\gamma \propto m^* \propto 1/T_K$. As we go from low fields (<20 T) to high fields (>40 T) the effective masses are reduced by a factor of 2-3. This implies that γ would decrease and the characteristic temperature would increase at high fields. This latter point was clearly seen the previously mentioned magnetization results which show the characteristic temperature going from ~40 K at low fields to ~565 K at high fields.

4 Conclusion

We have performed magnetization and de Haas-van Alphen measurements on the intermediate valent compound $YbAl_3$. In addition to the slow crossover observed previously [6] we have clearly observed two energy scales T_{coh} and T_K. The dominant energy scale depends on both the temperature and the applied magnetic field. For $T>T_{coh}$ and $B>k_BT_{coh}/\mu_B$, the dominant energy is the Kondo scale T_K, otherwise T_{coh} dictates the thermodynamic energy scale. We believe this is the first work to directly observe the two energy scales and to observe the crossover in the dominant energy scale as a function of magnetic field. Further work in the field range from 20 T<B<40 T is necessary to clarify the nature of the crossover. This work should include both Fermi surface studies and heat capacity measurements.

Acknowledgments

Work at UNLV supported by a DOE EPSCoR-State/National Laboratory Partnership Award (DE-FG02-00ER45835). Work at UC Irvine was supported by UCDRD funds provided by the University of California for the conduct of discretionary research by the Los Alamos National Laboratory and by the UC/LANL Personnel Assignment Program. Work at Los Alamos was performed under the auspices of the DOE.

References

1. N. E. Bickers, D. L. Cox and J. W. Wilkins, *Phys. Rev. B* **36,** 2036 (1987).
2. J. M. Lawrence *et al., Phys. Rev. B* **63**, 054427 (2001).
3. A. N. Tahvildar-Zadeh *et al., Phys. Rev. B* **55**, R3332 (1997).
4. A. N. Tahvildar-Zadeh *et al., Phys. Rev. Lett.* **80**, 516 (1998).
5. S. Burdin, A. Georges and D. R. Grempel, *Phys. Rev. Lett.* **85**, 1048 (2000).
6. J. M. Lawrence *et al.*, cond-mat/0107638.
7. T. Ebihara *et al., J. Phys. Soc. Jpn.* **69**, 895 (2000).
8. T. Ebihara *et al., Physica B* **281&282**, 754 (2000).

HIGH PRESSURE TRANSPORT STUDY OF NON-FERMI LIQUID BEHAVIOUR IN U_2Pt_2In AND $U_3Ni_3Sn_4$

A. DE VISSER and P. ESTRELA

Van der Waals-Zeeman Institute, University of Amsterdam, Valckenierstraat 65, 1018 XE Amsterdam, The Netherlands
E-mail: devisser@science.uva.nl

T. NAKA

National Research Institute for Metals, 1-2-1 Sengen, Ibaraki 305-0047, Japan
E-mail: naka@nrim.go.jp

The strongly correlated metals U_2Pt_2In and $U_3Ni_3Sn_4$ show pronounced non-Fermi liquid (NFL) phenomena at ambient pressure. Here we review single-crystal electrical resistivity measurements under pressure ($p \leq 1.8$ GPa) conducted to investigate the stability of the NFL phase. For tetragonal U_2Pt_2In ($I \parallel a$) we observe a rapid recovery of the Fermi-liquid T^2-term with pressure. The Fermi-liquid temperature varies as $T_{FL} \sim p\text{-}p_c$, where $p_c = 0$ is a critical pressure. The analysis within the magnetotransport theory of Rosch provides evidence for the location of U_2Pt_2In at a $p = 0$ antiferromagnetic quantum critical point (QCP). In the case of cubic $U_3Ni_3Sn_4$ we find $T_{FL} \sim (p\text{-}p_c)^{1/2}$. The analysis provides evidence for an antiferromagnetic QCP in $U_3Ni_3Sn_4$ at a negative pressure $p_c = -0.04 \pm 0.04$ GPa.

1 Introduction

Materials with low-temperature properties that show strong departures from the standard Fermi-liquid behaviour nowadays attract considerable attention. Exemplary compounds to study this so-termed *non-Fermi liquid* (NFL) behaviour are found amongst dense Kondo *f*-electron systems. A mechanism of much general interest that may lead to NFL behavior is the proximity to a magnetic quantum critical point (QCP) (see Ref. [1]). Here a $T = 0$ K electronic instability leads to a phase transition between a strongly renormalized Fermi liquid and a magnetically ordered phase. The *quantum phase transition* can occur spontaneously or may be induced by tuning the magnetic ordering temperature to 0 K by an external parameter, such as hydrostatic or chemical pressure. Magnetic quantum phase transitions in correlated metals are often discussed in terms of the "weak-coupling" Hertz-Millis model, in which the QCP is treated as a magnetic instability of the Fermi surface.[1] The Kondo-screened heavy quasiparticles undergo an antiferromagnetic (AF) spin-density wave transition. NFL behaviour is due to Bragg diffraction of the electrons off a critical spin-density wave. Recently, Coleman and coworkers[2] proposed an alternative "strong-coupling" local-moment model, which starts from the magnetic side and treats the metal as a local-moment

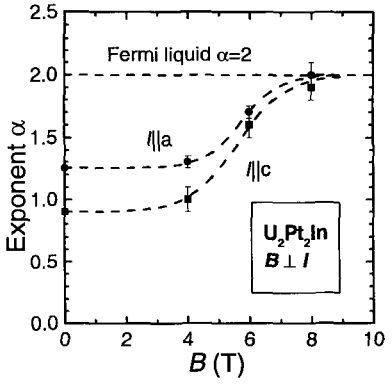

Figure 1: Field dependence of the resistivity exponent α of U_2Pt_2In. Dashed lines are to guide the eye.

antiferromagnet, that becomes disordered when the effective Kondo temperature, T_K^*, is large enough to form the dense Kondo state. At the QCP the Kondo-bound states decompose and T_K^* vanishes.

Magnetotransport under pressure is an excellent experimental tool to explore the NFL phase. By comparing the experimental data to the predictions of a new magnetotransport theory by Rosch[3] for metals close to an AF QCP, a stringent test of the Hertz-Millis scenario can be made. One of the major assets of the Rosch theory is that it takes into account the effect of disorder. Considering that spin fluctuations are destroyed at the temperature scale Γ, where Γ is typically of the order of T_K or the coherence temperature T_{coh}, the following scaling form of the resistivity is derived:[3] $\rho = \rho_0 + \Delta\rho = \rho_0 + T^{3/2} f(T/\rho_0, (\delta-\delta_c)/\rho_0, B/\rho_0^{3/2})$. Here ρ_0 is the residual resistivity, B the magnetic field and δ-δ_c the distance to the QCP in the non-ordered (paramagnetic) side of the phase diagram, with δ_c the critical control parameter. The scaling form of the resistivity allows one to delineate the NFL ($\Delta\rho \sim T$ and $\Delta\rho \sim T^{3/2}$) and Fermi-liquid ($\Delta\rho \sim T^2$) regimes as a function of the distance to the QCP (here measured by the pressure p) and the amount of disorder in the material, $x \sim \rho_0/\rho_{RT}$. For instance, T_{FL}, i.e. the temperature below which $\Delta\rho \sim T^2$, varies initially as $T_{FL} = a_1 (p\text{-}p_c)$, with a cross-over to $T_{FL} = a_2 (p\text{-}p_c)^{1/2}$ at higher distances, where p_c is the pressure at the QCP. Predictions for the NFL resistivity exponents in the local-moment model[2] are not available yet. However, the model predicts a discontinuity in the Hall constant at the QCP when the heavy-fermions decompose.

In this paper we review electrical resistivity measurements under pressure ($p \leq 1.8$ GPa), conducted to investigate the stability of the NFL phase in the heavy-electron compounds U_2Pt_2In and $U_3Ni_3Sn_4$. U_2Pt_2In belongs to the group of U_2T_2X compounds, where T is a transition metal and X is In or Sn (see Ref. [4]). It does

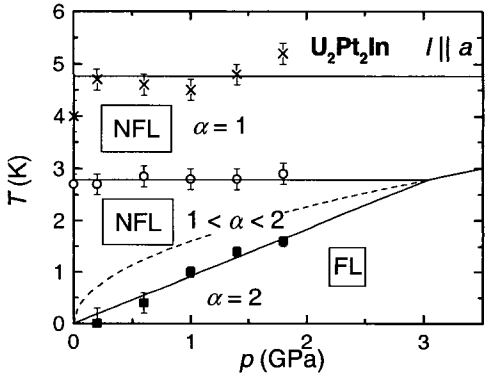

Figure 2: Pressure dependence of T_{FL} (closed squares) and of the temperature range in which $\rho \sim T$ (between (o) and (x)) for U_2Pt_2In ($I \parallel a$). The solid lines delineate NFL and FL regimes with exponents α. The dashed line shows the $T_{FL} = a_2 (p-p_c)^{1/2}$ dependence.[8]

not show magnetic order and is the heaviest compound in this series ($c/T = 0.41$ J/(mol-U)K^2 at $T = 1$ K). $U_3Ni_3Sn_4$ belongs to the family of isostructural cubic stannides $U_3T_3Sn_4$, where T = Ni, Cu, Pt or Au. It is a moderate heavy-electron compound ($c/T = 0.09$ J/(mol-U)K^2) (see Ref. [5]).

2 Resistivity of U_2Pt_2In under pressure

U_2Pt_2In shows robust NFL behaviour.[6-7] The NFL properties are summarized by: (i) the specific heat varies as $c(T) \sim -T\ln(T/T_0)$ over almost two decades of temperature ($T = 0.1$-6 K), (ii) the magnetic susceptibility shows a weak maximum at $T_m = 8$ K for $B \parallel c$ (tetragonal structure), while it increases as $T^{0.7}$ when $T \to 0$ for $B \parallel a$, and (iii) the electrical resistivity obeys a power law T^{α} with $\alpha = 1.25 \pm 0.05$ ($T < 1$ K) and 0.9 ± 0.1 ($T \to 0$), for the current along the a and c axis, respectively. Moderate magnetic fields strongly influence the NFL state. The Fermi-liquid value $\alpha = 2$ is recovered in an applied magnetic field of ~ 8 T as shown in Fig. 1 (see Ref. [7]). Muon spin relaxation experiments exclude the absence of (weak) static magnetic order down to 0.05 K (see Ref. [7]). We have carried out high-pressure transport measurements on single-crystalline U_2Pt_2In (see Ref. [8]). For $I \parallel c$ $\rho(T)$ increases with pressure and develops a relative minimum at low temperatures ($T_{min} \sim 4.8$ K at 1.8 GPa). In the following, we concentrate on the low-temperature data for $I \parallel a$.

A detailed analysis has been presented in Ref. 8. In Fig. 2 we show how the results compare to the transport theory of Rosch[3] for materials with considerable disorder (for our U_2Pt_2In crystal $x \sim 0.6$). The different NFL and FL regimes are

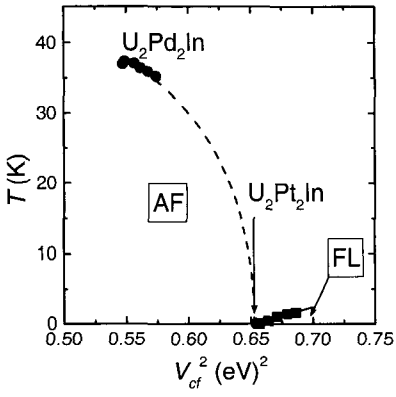

Figure 3: Tentative Doniach-type diagram for U_2Pt_2In (squares: $T_{FL}(p)$) and U_2Pd_2In (circles: $T_N(p)$. AF= antiferromagnetic order, FL = Fermi-liquid regime. The lines serve to guide the eye.

deduced by fitting the resistivity under pressure to a T^2 term at the lowest temperatures and a term linear in T at higher temperatures. Figure 2 shows that the data are consistent with T_{FL} being a linear function of pressure with $p_c = 0$. The cross-over to a $T_{FL} = a_2 (p-p_c)^{1/2}$ dependence is expected near 3.0 GPa. The $\Delta\rho \sim T$ region is predicted to occur in the reduced temperature range $x < T/\Gamma < x^{1/2}$ ($x < 1$). From Fig. 2 we extract that the $\Delta\rho \sim T$ region is found in the temperature range 2.8-4.7 K, from which it follows $x = 0.34$ and $\Gamma = 8.1$ K. The agreement between the calculated value $x = 0.34$ and the experimental value $x \sim 0.6$ is, given the rather simple data treatment, satisfactory. The temperature-pressure diagram presented in Fig. 2 is consistent with the scaling diagram for the resistivity presented by Rosch. Hence, we conclude that the compound U_2Pt_2In has an AF QCP at a critical pressure $p_c = 0$.

It is of interest to compare the pressure effects on U_2Pt_2In and the isoelectronic compound U_2Pd_2In. U_2Pd_2In is an antiferromagnet with $T_N = 37.5 \pm 0.5$ K, which decreases under pressure to $T_N = 35.2 \pm 0.5$ K at $p = 1.8$ Gpa (see Ref. [7]). In Fig. 3 we show a tentative Doniach-like diagram for the compounds U_2Pt_2In and U_2Pd_2In under pressure. Here the relative increase of V_{cf}, i.e. the hybridization matrix element for the total conduction electron hybridization at the f atom, was calculated using a simple model.[7] With a compressibility value $\kappa = 6.82 \times 10^{-3}$ GPa^{-1}, we calculate for U_2Pt_2In that V_{cf} increases by 2.3% in the pressure range 0-1.8 GPa. Thus by applying a moderate pressure of 1.8 GPa, U_2Pt_2In is shifted considerably into the non-magnetic region of the Doniach-like diagram. A similar calculation for U_2Pd_2In results in an increase of V_{cf} of 2.4% at 1.8 GPa. According to Fig. 3, a very rough estimate of the pressure needed to tune U_2Pd_2In to a QCP is ~ 7 GPa.

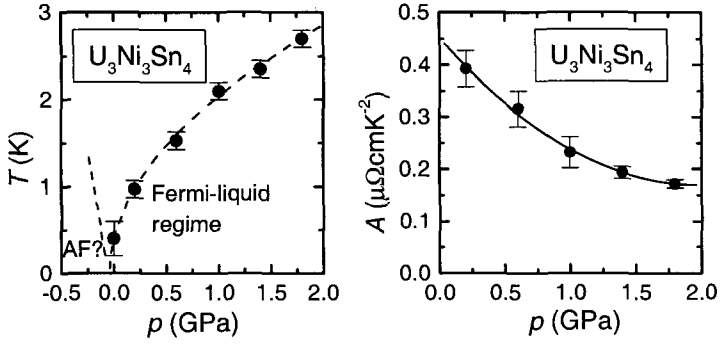

Figure 4: T_{FL} and the coefficient A as function of pressure for $U_3Ni_3Sn_4$ (see Ref. [10]).

3 Resistivity of $U_3Ni_3Sn_4$ under pressure

For $U_3Ni_3Sn_4$, evidence for the proximity to an AF instability is predominantly provided by specific-heat experiments.[9] Data taken on a single-crystalline sample in the temperature range $T = 0.3$-5 K, revealed the presence of a NFL electronic term of the form $c_{el}/T \sim \gamma_0 - \alpha T^{1/2}$. Such a $\alpha T^{1/2}$ correction to the standard Fermi-liquid coefficient has been predicted for a 3D AF QCP by Millis. Subsequent measurements, showed that the electronic specific heat below $T = 0.4$ K is best described by the modified Fermi-liquid expression $c_{el}/T \sim \gamma_0 + \delta T^3 \ln(T/T^*)$, with $\gamma_0 = 0.130$ J/(mol-U)K^2. This led to the conclusion that $U_3Ni_3Sn_4$ has a FL ground state, with a crossover to NFL behaviour near $T \sim 0.5$ K. NFL-like temperature dependencies have also been observed in the magnetic and transport properties.

The electrical resistivity of single-crystalline $U_3Ni_3Sn_4$ under pressure ($p \leq 1.8$ GPa) was measured in the temperature range 0.3-300 K (see Ref. [10]). The residual resistivity, ρ_0, at ambient pressure equals ~7 μΩcm and $\rho_{RT}/\rho_0 = 55$, which shows that $U_3Ni_3Sn_4$ is a relatively clean material. The observed temperature variation of the resistivity at ambient pressure is typical for dense Kondo systems. The coherence temperature, T_{coh}, estimated by the temperature of the maximum in $d\rho/dT$, amounts to 20 K. The qualitative behavior of $\rho(T)$ does not change in the range of pressures applied. In the following we focus on the low-temperature behaviour. Under pressure the FL temperature interval increases. In Fig.4, we show T_{FL} extracted by fitting the resistivity data to the expression $\rho = \rho_0 + AT^2$. T_{FL} shows a strong variation with pressure. Within the theory of Rosch the linear dependence $T_{FL} \sim (p - p_c)$ is restricted to the immediate vicinity of the QCP, while at further distances to the QCP T_{FL} shows a cross-over to $T_{FL} = a\,(p-p_c)^{1/2}$. The data obtained for our relatively clean sample of $U_3Ni_3Sn_4$ are consistent with the latter

dependence. The solid line in Fig.4 represents the function $T_{FL} = a\,(p-p_c)^{\nu}$, with fit parameters p_c = -0.04±0.04 GPa, ν = 0.50±0.07 and a = 2.0±0.1 KGPa$^{-\nu}$. Thus the analysis of the pressure variation of T_{FL} within the magnetotransport theory of Rosch is consistent with $U_3Ni_3Sn_4$ being located close to an antiferromagnetic QCP, with the QCP located at a *negative* critical pressure of ~ -0.04 GPa. Figure 4 also shows that the coefficient A of the T^2 term increases strongly upon approaching the QCP.

4 Conclusions

Resistivity measurements under pressure of the NFL correlated metals U_2Pt_2In and $U_3Ni_3Sn_4$ show that Fermi liquid properties are rapidly recovered. A comparison of the data with the magnetotransport theory of Rosch provides evidence for an AF QCP at ambient pressure in U_2Pt_2In, and at a negative pressure of –0.04±0.04 GPa in $U_3Ni_3Sn_4$. Additional high-pressure experiments on samples with different amounts of disorder would be extremely useful to further investigate the scenario of a Hertz-Millis AF QCP as origin of the NFL properties in these materials.

Acknowledgments

The authors acknowledge support within the EC-TMR and ESF-FERLIN programs.

References

1. J. A. Hertz, Phys. Rev. B **14**, 1165 (1976); A. J. Millis, *Phys. Rev. B* **48**, 7183 (1993).
2. P. Coleman, *Physica B* **259-261**, 353 (1999); P. Coleman *et al.*, *J. Phys.: Con. Mat.* **13**, R723 (2001).
3. A. Rosch, *Phys. Rev. B* **62**, 4945 (2000).
4. L. Havela *et al.*, *J. Appl. Phys.* **76**, 6214 (1994).
5. T. Takabatake *et al.*, *J. Phys. Soc. Jpn.* **59**, 4412 (1993).
6. P. Estrela *et al.*, *J. Phys. Cond. Mat.* **10**, 9465 (1998).
7. P. Estrela, Ph.D. *Thesis*, University of Amsterdam, 2000.
8. P. Estrela *et al.*, *Physica B* **281-282**, 381 (2000); P. Estrela *et al.*, *Physica B*, in print (e-print LANL *cond-mat*/0106292); P. Estrela *et al.*, *Euro Phys. J. B*, in print (e-print LANL *cond-mat*/0009324).
9. L. Shlyk *et al.*, *J. Phys. Cond. Mat.* **11**, 3525 (1999); L. Shlyk *et al.*, *Physica B* **292**, 89 (2000).
10. P. Estrela *et al.*, *Phys. Rev. B* **63**, 212409 (2001).

THE DE HAAS-VAN ALPHEN EFFECT IN $CeMIn_5$ (WHERE M = Rh AND Co)

D. HALL, T. P. MURPHY, E. C. PALM, S. W. TOZER,
Z. FISK, and N. HARRISON
National High Magnetic Field Laboratory, 1800 E. Paul Dirac Dr., Tallahassee, FL 32310
E-mail: hall@magnet.fsu.edu

R. G. GOODRICH and U. ALVER
Department of Physics and Astronomy, Louisiana State University, Baton Rouge, LA 70803
E-mail: goodrich@rouge.phys.lsu.edu

J. L. SARRAO
Los Alamos National Laboratory, Los Alamos, NM 87545

To understand the electronic structure of the heavy fermion superconductors $CeMIn_5$, we have performed a comprehensive magnetic study of these materials.[1-4] Our quantum oscillation studies reveal that the Fermi surface becomes systematically more 2-d (and displays heavier effective masses) as one progresses from M=Rh to M=Ir to M=Co, consistent with the observed increase in superconducting T_c. Furthermore, dilution studies show that the *f*-electrons in $CeRhIn_5$ are substantially localized whereas in $CeIrIn_5$ and $CeCoIn_5$ a more itinerant character is observed.

Superconductivity and Magnetism

The $CeMIn_5$s are heavy fermion (HF) anti-ferromagnets (AFs) and superconductors (SCs) where 4*f* electrons play a significant role in determining the thermodynamic properties. In cases where superconductivity and magnetism coexist,[5] the 4*f* electrons are localized and do not interact strongly with the conduction electrons.[6] However, our work on $Ce_xLa_{1-x}RhIn_5$ paints another picture:[3] when the 4*f* electrons are localized, anti-ferromagnetism occurs. Alternately, when the 4*f* wave functions mix with conduction band electrons, superconductivity occurs.[7] The most interesting alloy in this family is $CeRh_{1-x}Ir_xIn_5$ where superconductivity and magnetism coexist for a concentration range of 0.25 to 0.60 (see Ref. [8]).

The particular attraction of these materials is that they appear to be quasi-2D variants of $CeIn_3$, an ambient pressure antiferromagnet in which superconductivity can be induced at 25 kbar and 200 mK (see Ref. [9]) and have properties of unconventional superconductivity. Movshovich *et al.*,[10] have shown a power law temperature dependence in the specific heat and thermal conductivity suggesting strongly that the superconductivity in $CeCoIn_5$ is unconventional. If one can demonstrate that the reduced dimensionality is responsible for the factor of 10 increase in superconducting T_c (as compared to the ambient pressure T_c of $CeIrIn_5$), the impact of these compounds on the physics of superconductivity will far exceed that of just another family of heavy fermion superconductors.

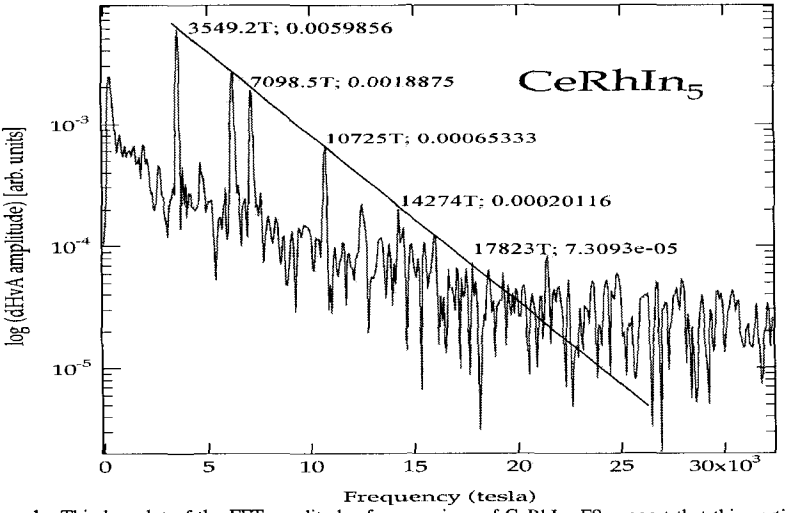

Figure 1: This log plot of the FFT amplitudes for one piece of $CeRhIn_5$ FS suggest that this particular sheet arises from a single spin direction.

$CeRhIn_5$

$CeRhIn_5$ orders anti-ferromagnetically at 3.8 K at ambient pressure. Superconductivity can be induced under the application of pressure. Pressures of about 16 kbar will produce a first-order phase transition from the magnetically ordered state into the superconducting state at 2.1 K.

The motivation for de Haas-van Alphen (dHvA) studies of this material is to investigate the dimensionality of the Fermi surface (FS) in order to determine its effect on the fluctuation spectra. We have found that these materials exhibit large directional anisotropies in the effective mass of the charge carriers.[1] Additionally, based on a harmonic analysis of the Fourier amplitudes of the dHvA effect, the oscillatory magnetization of at least one FS sheet in $CeRhIn_5$ is observed to be spin polarized, a shown in Fig. 1.

Direct evidence of a spin polarized FS comes from a measurement of the Fourier amplitudes of the harmonics.[13] When only one spin sheet is present, each successive Fourier harmonic is reduced by some exponential factor related to the harmonic index. This follows from the fact that the harmonic index enters into the thermal and Dingle reduction factors, both of which are approximately exponential in form.[14,15] When two spins are present on the FS sheet, an extra reduction factor due to electron spin must be factored in. This spin reduction term oscillates as a function of harmonic index, thus avoiding the exponential decay of the harmonic amplitudes. The log plot shown in Fig. 1 demonstrates this exponential reduction as a function of increasing harmonic number.

$CeCoIn_5$

$CeCoIn_5$ has a very high transition temperature compared to most heavy fermion superconductors at 2.3 K. Like $CeIrIn_5$, it has a superconducting ground state at ambient pressure. Below 1.4 K the transition from the normal state to the superconducting state as a function of magnetic field in $CeCoIn_5$ has been found to be first order at ambient pressure.[4]

dHvA measurements on $CeRhIn_5$ (see Ref. [1]) and $CeIrIn_5$ (see Ref. [11]) show multiple branches for rotations in the [001] -[100] and [001] - [110] planes of the tetragonal structure. Most of these branches are associated with large quasi-2D undulating cylinders that show the expected $1/\cos(\theta)$ dependence with θ being the angle at which the field is applied away from the [001] axis. Band structure calculations, both in Ref. [1] and in Ref. [11] show, in addition, that several small pieces of FS should exist in both $CeRhIn_5$ and $CeIrIn_5$.

We find a similar situation in $CeCoIn_5$ in that the there are three sheets closely spaced in frequency near 6 kT, corresponding to extremal areas on an open 2 D undulating cylinder extending along the [001] direction,[2] see Fig. 2. However, fewer frequencies are observed for $CeCoIn_5$ than is the case for $CeRhIn_5$ or $CeIrIn_5$. Based on comparisons of these closely spaced frequencies, the magnitude of this undulation in $CeCoIn_5$ is approximately 50% less than that observed in the other materials.

Some of the frequencies observed in these two cases are attributed to holes in the cylinders and the band structure calculations bear out this assignment. Because the mass enhancements expected in all of these materials is comparable, based on heat capacity data,[12] the reduced number of observed frequencies seen here cannot be attributed to particularly heavy carriers in $CeCoIn_5$. The cylindrical surface in $CeCoIn_5$ appears to be closed with no holes, and much more 2 D like than in either of the other two cases. In addition, the number of low frequencies in $CeCoIn_5$ is much smaller than in either the Rh or Ir analogs so there are a smaller number of electrons exhibiting 3 D behavior.

These results indicate that many of the transport properties and cooperative phenomena that are seen in $CeCoIn_5$ should be much more 2 D in character than those found in either $CeRhIn_5$ or $CeIrIn_5$. The fact that the T_c in $CeCoIn_5$ is 5 times higher than that observed in $CeIrIn_5$ would suggest that the increasingly two-dimensional electronic structure has a direct correlation with enhanced T_c.

Studies of the Fermi surface of $CeRhIn_5$ at pressures adequate to produce superconductivity would be valuable in confirming this supposition because the T_c of $CeRhIn_5$ under pressure is comparable to that of $CeCoIn_5$. Already, we have measured the evolution of the FS of $CeRhIn_5$ up to 13 kbar. Preliminary analysis indicates very small changes in the cross-section of the undulating cylinders; however, this study is not yet complete and will be the subject of a forthcoming article.

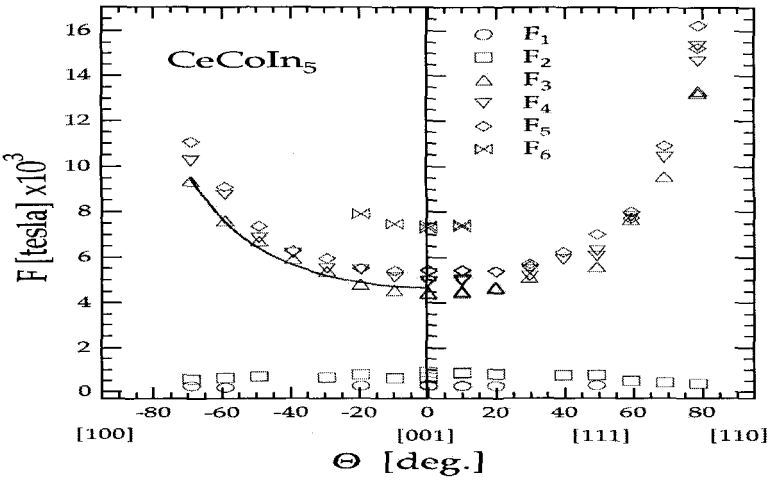

Figure 2: The frequency of the dHvA oscillations plotted as a function of angle show a mostly 2 D FS with only a few small 3 D pockets.

This work was supported in part by the National Science Foundation under Grant No. DMR-9971348 (Z. F.). A portion of this work was performed at the National High Magnetic Field Laboratory, which is supported by NSF Cooperative Agreement No. DMR-9527035 and by the State of Florida. Work at Los Alamos was performed under the auspices of the U. S. Dept. of Energy.

References

1. D. Hall *et al., Phys. Rev. B.* **64**, 064506 (2001).
2. D. Hall *et al., Phys. Rev. B.* **64**, 212508 (2001).
3. U. Alver *et al., Phys. Rev. B.* **64**, 180402 (2001),. *cond-mat/*0106522.
4. T. P. Murphy *et al.*, submitted to *Phys. Rev. B.*, cond-mat/0104179.
5. J. E. Crow, R. P. Guertin and R. D. Parks, *Physical Review Letters* **19**, 77 (1967) and references therein.
6. R. H. Heffner, *Comm. Condens. Matt. Phys.* **17**, 361, (1996).
7. R. G. Goodrich and N. Harrison, private communication
8. P. Pagliuso *et al., Phys. Rev. B.* **64**, 100503 (2001).
9. N. D. Mathur *et al., Nature* **394**, 39 (1998).
10. R. Movshovich *et al.,. preprint, condmat/*001135, 2001.
11. Y. Haga *et al.*, preprint (2000).
12. C. Petrovic *et al.*,. preprint (2001) cond-mat/0012261.
13. N. Harrison *et al., Phys. Rev. Lett.* **81**, 870 (1998).
14. I. M. Lifshitz and A. M. Kosevich, *Sov. Phys. JETP* **2**, 636 (1956).
15. D. Shoenberg, *Magnetic Oscillations in Metals*, (Cambridge University Press, Cambridge, England, 1984).

SUPERCONDUCTING AND NORMAL STATE PROPERTIES OF THE HEAVY FERMION COMPOUND $PrOs_4Sb_{12}$

P.-C. HO, V. S. ZAPF, E. D. BAUER, N. A. FREDERICK, and M. B. MAPLE

Department of Physics and Institute for Pure and Applied Physical Sciences, University of California, San Diego, La Jolla, CA 92093, USA

G. GIESTER and P. ROGL

Institut für Physikalische Chemie und Institut für Kristallographie und Mineralogie der Universitaet, Wien, Austria

S. T. BERGER, C. H. PAUL and E. BAUER

Institut für Experimentalphysik, Technische Universität Wien, 1040 Wien, Austria

The filled skutterudite compound $PrOs_4Sb_{12}$ displays superconductivity with a critical temperature $T_c \approx 1.85$K which appears to involve heavy fermion quasiparticles with an effective mass $m^* \sim 50 - 100\ m_e$, as inferred from the slope of the upper critical field curve near T_c and the specific heat. New measurements of electrical resistivity $\rho(T)$ in applied magnetic fields, thermoelectric power, and X–ray diffraction are presented. A peak appears in the $d\rho/dT$ data for magnetic fields above 4 T that suggests the occurrence of a phase transition in the normal state of $PrOs_4Sb_{12}$ below ~ 1K.

1 Introduction

The filled skutterudite compound $PrOs_4Sb_{12}$, which crystallizes in the cubic $LaFe_4P_{12}$ structure, was recently found to be a heavy fermion superconductor with an effective mass $m^* \sim 50 - 100\ m_e$ and a superconducting transition temperature $T_c \approx 1.85$ K (see Refs. [1-3]). As the first example of a Pr-based heavy fermion superconductor, $PrOs_4Sb_{12}$ joins the ranks of other filled skutterudite compounds that have sparked interest in scientists and engineers alike due to the wide variety of strongly correlated electron phenomena they exhibit[4,5] and their potentially useful thermoelectric properties.[6]

Superconductivity in $PrOs_4Sb_{12}$ was previously observed by means of measurements of electrical resistivity $\rho(T)$, magnetic susceptibility $\chi(T)$, and specific heat C(T), all of which displayed features at ~ 1.85K associated with the onset of superconductivity.[1-3] The coefficient of the electronic contribution to the specific heat γ was estimated to be between ~ 350 and ~ 750mJ/mol-K^2. These values are consistent with the formation of a heavy fermion state in this compound. The $\chi(T)$ and C(T) data also displayed pronounced peaks at ~ 3K, indicating that the 9-fold degeneracy of the J = 4 Hund's rule multiplet of Pr^{3+} is lifted by the cubic

crystalline electric field (CEF) (see Ref. [7]). An analysis of the $\chi(T)$ and C(T) data within the framework of the cubic CEF model of Lea, Leask and Wolf (LLW) (see Ref. [7]) yielded a Pr^{3+} energy level scheme consisting of a nonmagnetic Γ_3 doublet ground state (0 K), a Γ_5 triplet first excited state (11 K), and higher energy Γ_4 triplet (139 K) and Γ_1 singlet (313 K) excited states. Inelastic neutron scattering experiments[3] revealed peaks in the excitation spectra at 0.71meV (8.2 K) and 11.5 meV (133.5 K) that are consistent with the Pr^{3+} energy level scheme Γ_3 (0 K), Γ_5 (8.2 K), Γ_4 (133.5 K) and Γ_1 (320 K), in excellent overall agreement with the energy level scheme inferred from $\chi(T)$ and C(T). It is conceivable that the heavy fermion state originates from the interaction between the Pr^{3+} electric quadrupole moments associated with the Γ_3 nonmagnetic doublet ground state and the charges of the conduction electrons, as has been suggested for the heavy fermion compound $PrInAg_2$ (see Ref. [8]). A possible mechanism for the heavy fermion state is the quadrupolar Kondo model.[9,10]

In this paper, we report further results of our investigation of the physical properties of $PrOs_4Sb_{12}$ in the normal and superconducting states. We present new $\rho(H,T)$ measurements at temperatures down to ~ 0.1K and in magnetic fields H up to 10T. Analysis of these data yields a more complete upper critical field H_{c2} vs T phase diagram, as well as intriguing features in the normal state above 4T that suggest the occurrence of some type of phase transition below ~ 1K. We also present measurements of the thermoelectric power S(T) and of the lattice structural parameters determined from single crystal X-ray diffraction.

2 Experimental Details

The $PrOs_4Sb_{12}$ single crystals were prepared in an antimony flux as described in Ref [11]. X-ray diffraction measurements confirmed that the $PrOs_4Sb_{12}$ samples have the $LaFe_4P_{12}$-type BCC structure with a lattice parameter a = 9.3068 Å. Single crystral X-ray intensity data were collected on a four circle Nonius Kappa diffractometer equipped with a CCD area detector employing graphite monochromated Mo K_α radiation (0.71073 Å). Orientation matrix and unit cell parameters were derived from the first ten frames using the program DENZO (see Ref. [12]) and absorption corrections were taken from the SORTAV (see Ref. [12]) program. The structure was refined with the aid of the SHELXS-97 program.[13]

Measurements of $\rho(H,T)$ were performed at various values of H (0T – 10T) using a standard 4 - wire technique in a transverse geometry in a ^3He - ^4He dilution refrigerator at temperatures between ~ 0.1 K and 2.5 K. Resistance measurements were made with a Linear Research LR 700 4 - wire ac bridge operating at 16Hz with a constant current of 100 μA.

Temperature dependent measurements of S(T) were performed using the differential method where Pb serves to determine the absolute S(T) values.

3 Results and Discussion

Displayed in Fig.1 are $\rho(H,T)$ data for $PrOs_4Sb_{12}$. Shown in Fig.1(a) are ρ vs T data between ~ 0.1 K and 2.5 K in various fixed magnetic fields H between 0 T and 10 T. The electric resistivity $\rho(T)$ in the normal state is nearly linear for $H \leq 0.5$ T, and develops positive curvature as H is increased. For $H \geq 2.3$ T, the superconductivity is completely suppressed by the magnetic field. For H ~ 4T, a shoulder begins to develop in $\rho(T)$ in the neighborhood of 0.75K. At magnetic fields high enough to suppress superconductivity ($2.3\ T \leq H \leq 10$ T), the $\rho(T)$ measurements below 1 K reveal a power law dependence $\rho(T) = \rho_0 + BT^n$ with an exponent n that decreases slightly with magnetic field from n ~ 3 at 2.5 T to n ~ 2.6 at 10 T (Fig.1(b)). Shown in Fig.1(c) are the $d\rho(T)/dT$ data. A peak appears in $d\rho/dT$ at ~ 0.75 K and attains a maximum value at H ~ 8 T. The feature in $\rho(T)$ and $d\rho(T)/dT$ at ~ 0.75 K suggests the occurrence of a phase transition, presumably involving ordering of either Pr^{3+} magnetic dipole or electric quadrupolar moments.

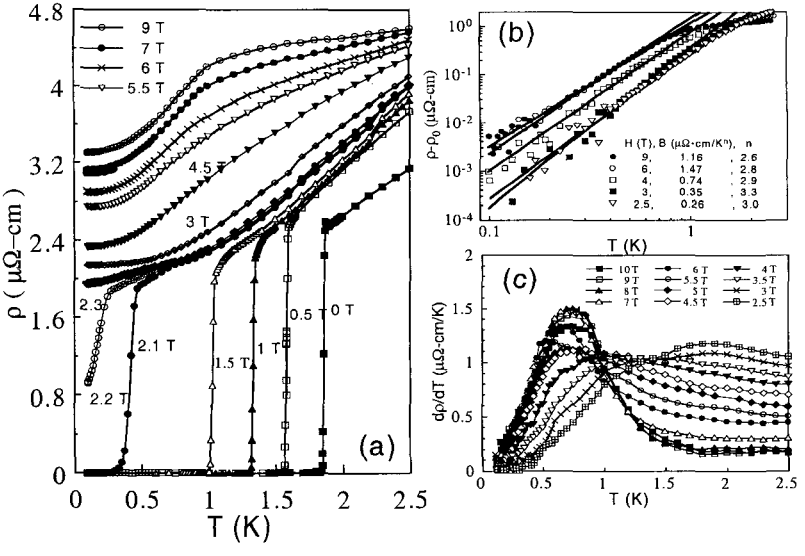

Figure 1: A selection of the electrical resistivity $\rho(H,T)$ data for $PrOs_4Sb_{12}$. Panel (a): ρ vs T at constant fields H from 0T to 9T. Panel (b): ρ-ρ_0 vs T on a log-log scale. The solid lines are fits of a power law ρ-$\rho_0 = BT^n$ to the data. Panel (c): $d\rho/dT$ vs T in the normal state of $PrOs_4Sb_{12}$ at constant fields from 2.5T to 10T. A peak begins to develop at ~ 0.74 K for fields H > 4.5T.

The $H_{c2}(T)$ curve for $PrOs_4Sb_{12}$, derived from $\rho(T)$ measurements in various magnetic fields, is shown in Fig. 2. The $H_{c2}(T)$ curve is consistent with the previously reported $H_{c2}(T)$ curve,[2,3] but contains more data, especially near T_c. Disregarding the slight positive curvature in H_{c2} near T_c, a linear fit to the data yields the initial slope $(dH_{c2}/dT)_{Tc} \sim -2.03$ T/K. The zero temperature value of the orbital critical field can be determined from the relation $H_{c2}^*(0) = 0.693 (-dH_{c2}/dT)_{Tc}T_c$ (see Ref. [14]), yielding $H_{c2}^*(0) \sim 2.57$ T. From the equation $H_{c2}^*(0) = \Phi_0/(2\pi\xi_0^2)$, the zero-temperature superconducting coherence length ξ_0 is estimated to be ~ 113Å. If each Pr atom contributes 3 valence electrons to the conduction band, the Fermi wavevector can be derived using a spherical Fermi surface approximation $k_F = (3\pi^2Z/v)^{1/3} \sim 6.04\times10^7$ cm^{-1}, where v is the unit cell volume (~ 8.1×10^{-22}cm^3) and Z is the number of electrons per unit cell (= 6). Using the results from the BCS theory, $\xi_0 = \hbar v_F/[\pi\Delta(0)]$ and $\Delta(0) = 1.764k_BT_c$, the Fermi velocity v_F is estimated to be ~ 1.5×10^6 cm/s. From the relation $m^* = \hbar k_F/v_F$, we obtain an effective mass $m^* \sim 47m_e$. This value of m^* is consistent with the values $m^* \sim 46m_e$ - $98m_e$ inferred from the values of γ (~ 350 – 750 mJ/mol-K^2) estimated from specific heat measurements[2,3] according to the relation $\gamma = m^*k_B^2k_F/(3\hbar^2)$ based on the free electron model.

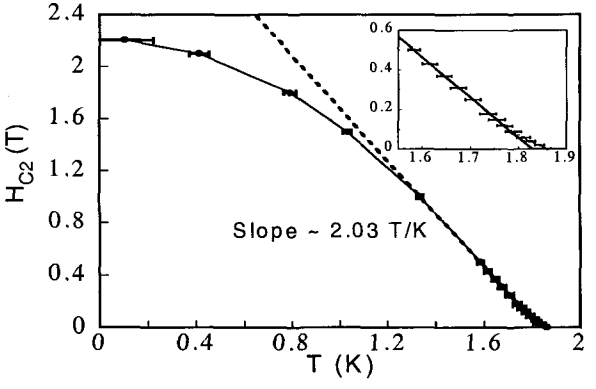

Figure 2: Upper critical field H_{c2} vs T of $PrOs_4Sb_{12}$. The horizontal bars indicate the 10% and 90% values of the superconducting transition. Inset: H_{c2} between H = 0 T and 0.6 T.

Selected values of the single crystal X-ray diffraction data are tabulated in Table 1. A simple single ion CEF analysis of $\chi(T)$ data for $PrOs_4Sb_{12}$ (see Ref. [2]) yielded a reduced value of the Landé g-factor $g_J \approx 0.58$, corresponding a reduced effective magnetic moment $\mu_{eff} \equiv g_J\sqrt{J(J+1)}\,\mu_B$, where J = 4, of ~ $2.6\mu_B$ per Pr^{3+} ion, smaller than the free ion value of $3.58\mu_B$. Since the X-ray diffraction results show that lanthanide sites are fully occupied by Pr ions, this eliminates the possibility that the reduced value of μ_{eff} is due to Pr vacancies. As expected for a

typical skutterudite compound, the Pr ion "rattles" with quite a large amplitude about its lattice site (thermal displacement factor U_{ij} ~ 0.036 Å^2). The filled skutterudites have attracted much attention recently as potential candidates for thermoelectric applications as a result of their thermoelectric properties and the reduction of the lattice contribution to the thermal conductivity by the "rattling" of the lanthanide ions.[6]

The S(T) data are shown in Fig. 3. S(T) is nearly linear for T < 50 K and T > 170K and displays a plateau at ~ 65 K. Below ~ 40 K, S(T) is negative. The overall shape of S(T) does not resemble a typical heavy fermion system,[15] but appears to be similar to a number of lanthanide-antimony based skutterudites like $PrFe_4Sb_{12}$, $NdFe_4Sb_{12}$ or $EuFe_4Sb_{12}$ which are also characterized by a crossover from positive to negative values of the Seebeck coefficient. The positive values of S(T) at elevated temperatures indicates that holes are the dominant charge carriers. This picture is corroborated by a simple carrier count, where the holes created by Os are just partially compensated by the electropositive Pr^{3+} ion. According to Mahan, Sales and Sharp,[6] for a correlated metal to be a viable thermoelectric material, S must be greater than 156 μV/K. Thus, the thermoelectric power of $PrOs_4Sb_{12}$ is too small for application purposes below 300 K.

Table 1: Details of the single X-ray data collections and structure refinements for $PrOs_4Sb_{12}$.

a = 9.3068(1) Å	ρ_x = 9.743 g cm^{-3}
Space group: $Im\bar{3}$	Formula units/cell : 2
Pr in 2a (0,0,0); occ. : 0.99(1)	U_{11}=U_{22}=U_{33} : 0.0363(9)Å^2
Os in 8c; occ. : 1.00(1)	U_{11}=U_{22}=U_{33} : 0.0008(1) Å^2
Sb in 24g (0,y,z) y = 0.15603(4), z = 0.34035(4)	U_{11} (Å^2); U_{22} (Å^2); U_{33} (Å^2) 0.0009(2); 0.0027(2); 0.0046(2)

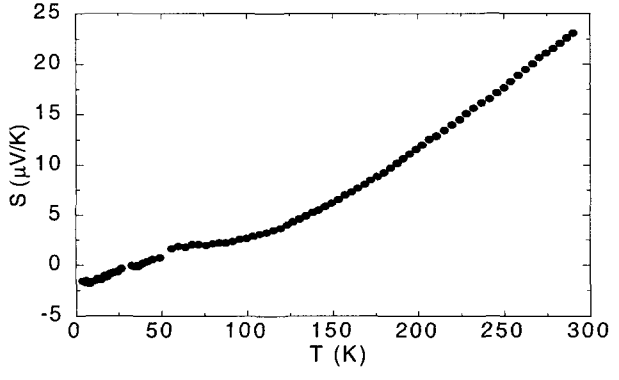

Figure 3: Thermoelectric power S vs T of $PrOs_4Sb_{12}$.

Acknowledgments

This research was supported by the U. S. Department of Energy under Grant No. DE FG03-86ER-45230, the U. S. National Science Foundation under Grant No. DMR 00-72125, and the NEDO international Joint Research Program.

References

1. M. B. Maple *et al., Acta Physica Polonica B* **32**, 3291-3301 (2001).
2. E. D. Bauer *et al., Phys. Rev. B: Rapid Comm.* (2001) to be published.
3. M. B. Maple *et al., J. Phys. Soc. Japan* (2002) to be published.
4. M. B. Maple *et al., Physica B* **259-61**, 8-9 (1999).
5. E. D. Bauer *et al., J. Phys. Cond. Matt.* **13**, 5183-5193 (2001) and references therein.
6. G. Mahan *Physics Today* **50**, 42-47 (1997).
7. K. R. Lea *et al., J. Phys. Chem. Solids* **23**, 1381-1405 (1962).
8. A. Yatskar *et al., Phys. Rev. B* **61**, 1831-1835 (2000).
9. P. D. Sacramento *et al., Phys. Lett.* A **142**, 245-250 (1989) .
10. D. L.Cox D. L., *Phys. Rev. Lett.* **59**, 1240-1243 (1987).
11. E. D. Bauer *et al., J. Phys. Cond. Matt.* **13**, 4495-4503 (2001).
12. NONIUS KAPPA CCD package COLLECT, DENZO, SCALEPACK, SORTAV, Nonius Delft, The Netherlands (1998).
13. G. M. Sheldrick, SHELXS-97, Program for Crystal Structure Refinement, University of Göttingen, Germany (1998); Windows version by McArdle, Natl. Univ. Galway, Irland.
14. R. R. Hake, *Appl. Phys. Lett.* **10**, 189-192 (1967).
15. A. C. Hewson A. C., *The Kondo problem to heavy fermions*, (Cambridge, New York, 1993) ch. 9, 281-283.

SPECIFIC HEAT ANOMALY FOR H ≥ 28.5 T IN $CeIrIn_5$

J. S. KIM, J. ALWOOD, P. KUMAR and G. R. STEWART

Department of Physics, University of Florida, Gainesville, FL 32611-8440

Recently Takeuchi reported a weak, 'metamagnetic-like' increase in the magnetization around 42 T in single crystals of $CeIrIn_5$ for field in the c-direction. We report specific heat measurements on single crystal $CeIrIn_5$, H parallel c-axis, measured in the dc hybrid magnet at NHMFL in Tallahassee between 1.4 and 10 K. A clear anomaly in C/T in 35 T is observed to peak at 1.8 K, with an entropy of 6% of Rln2. This anomaly grows in size *and* shifts upwards in temperature (both monotonically) with increasing H until at 45 T T_{peak}=4.1 K, with the entropy associated with the transition equal to 14 % of Rln2. C/T data at 32 T show[3] only the high temperature side of the peak occurring above 1.4 K, while C/T data at 28.5 T show no anomaly down to 1.4 K. This is consistent with our T_{peak} vs H data, which imply $T_{peak} \rightarrow 0$ at 26 T.

1 Introduction

Recently, a new group of heavy-fermion compounds has been discovered that form in a layered, tetragonal structure[1] with chemical composition $CeMIn_5$, where M= Ir, Co, and Rh. Characteristic of heavy-fermion systems, each member exhibits a large Sommerfeld coefficient γ ($\equiv C/T$ as $T \rightarrow 0$) in the specific heat C. $CeIrIn_5$ (see Ref. [2]) and $CeCoIn_5$ (see Ref. [3]) are bulk superconductors with transition temperatures at T_c = 0.4 K and 2.3 K and normal-state values of $\gamma \approx 750$ mJ/molK^2 and $\approx$ 1200 mJ/molK^2, respectively. $CeRhIn_5$ displays heavy-fermion antiferromagnetism with[4] T_N = 3.8 K. Recently, we reported[5] non-Fermi liquid behavior in both $CeIrIn_5$ and $CeCoIn_5$, implying the presence of strong, long range in space and time electron-electron correlations presumably magnetic in nature. Coupled with the heavy fermion superconductivity present in these two compounds, such strong correlations would be consistent with the superconductivity being of the non-conventional variety, as had already been proposed.[2-3,6]

One possible source for strong magnetic correlations in a system is its being 'nearly', in a phase diagram sense, magnetic. Takeuchi *et al.*,[7] reported a small, ~0.05 μ_B, and rather broad jump in the magnetization centered at about 42 T for field along the c-axis direction and labelled it metamagnetic-like, (see Fig. 1). The term "metamagnetic transition" is used to describe a variety of field induced transitions, with a much broader range of behavior than envisioned by Wohlfarth and Rhodes, the originators of the phrase. "Metamagnetism" has been used to describe systems where a staggered magnetization vanishes in a phase transition at $H_{metamag}$, spin-flop antiferromagnets, as well as various highly correlated electron systems; all of these examples have the common feature of a jump (either sharp or

broad) in the magnetization at a particular applied field, see Fig. 1 for an comparison of three well known examples with the data for $CeIrIn_5$.

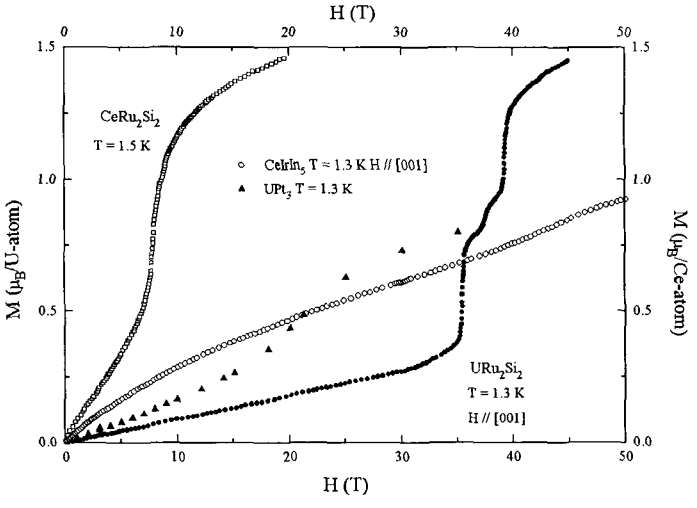

Figure 1: Magnetization vs applied field data for $CeRu_2Si_2$[8], UPt_3[9], URu_2Si_2[10], and $CeIrIn_5$[7] show a wide variety of behavior for the size and breadth of the increase at $H_{metamag}$.

Some metamagnetic systems show more localized electron behavior above $H_{metamag}$. For example, de Haas van Alphen measurements on $CeRu_2Si_2$ have been described[11] as consistent with localized f-electron behavior above $H_{metamag}$ with a definite decrease in the measured effective masses. A somewhat more recent work[12] describes the nature of the $H>H_{metamag}$ state in $CeRu_2Si_2$ as unresolved. In UPt_3, Shubnikov de Haas measurements[13] indicate that the large, zero field effective mass ('heavy Fermion') state persists above $H_{metamag}$. All of these systems show evidence of strong magnetic fluctuations in their zero field state.

In order to help clarify the magnetic properties of $CeIrIn_5$, we present here the specific heat of single crystal $CeIrIn_5$ with field in the c-axis direction up to 45 T.

2 Results and Discussion

Specific heat data in applied field up to 45 T for field parallel to the c-axis of single crystal $CeIrIn_5$ (see Ref. [5] for preparation) are shown in Fig. 2.

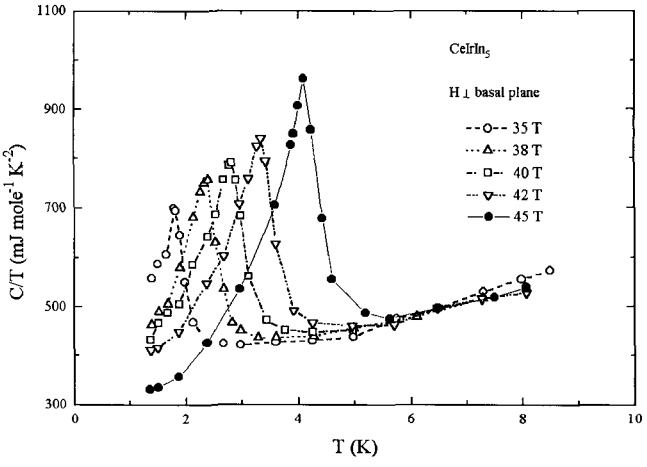

Figure 2: Specific heat divided by temperature vs temperature for field parallel to the c-axis for $CeIrIn_5$. Note the essentially linear with field increase of T_{max} of the anomaly, as well as the monotonic increase of $\Delta C/T_{max}$ with increasing field.

As may be seen from Fig. 2, field induces an anomaly in $CeIrIn_5$ already at 35 T. If we extrapolate T_{max} vs H, $T_{max} \rightarrow 0$ at approximately 26 T. A field of ~ 32 T would cause the anomaly in C/T to occur at 1.3 K – thus, we would expect to see some feature in the magnetization data of Takeuchi *et al.*, which were taken at 1.3 K, at around 32 T. Even when the data shown in Fig. 1 for $CeIrIn_5$ are expanded, the most that can be identified around this field in the magnetization data is the possibility of an inflection point in the M vs H graph. The actual faster-than-linear increase in the magnetization first occurs at approximately 40 T.

The specific heat data in Fig. 2 allow the entropy as a function of temperature to be calculated and plotted. When this is done, the entropy shows a broad, faster than linear in T increase as a function of temperature over the temperature range where the anomaly occurs, followed by a linear increase of the entropy with temperature above the anomaly. The breadth of the increase in entropy aside, these entropy data give a ΔS that, coupled with the magnetization jump ΔM and the slope of T_{max} with field derived from Fig. 2, agrees with the Ehrenfest relation for a first order phase transition.

The magnitude of ΔS for H=45 T is approximately 14% of Rln2. Thus, only a fraction of the f-electron/Ce-atom is participating in the field induced transition.

How this transition develops at higher field, keeping in mind that the magnetization data of Takeuchi *et al.* show a finish to the transition at ~ 50 T, must await further investigation. At this point, the size of ΔS, but not the breadth of the specific heat anomaly, is reminiscent of the specific heat results[14] below the third metamagnetic transition at 39.6 T in URu_2Si_2.

In conclusion, while we have confirmed the existence of a metamagnetic-like transition in $CeIrIn_5$ in fields between 32 and 45 T and at temperatures around 4 K, the specific details of the nature of the transition remain to be understood.

Acknowledgments

Work at the University of Florida supported by the United State Department of Energy, contract # DE-FG05-86ER45268. We thank J. Thompson and J. Sarrao for suggesting this work. The National High Magnetic Field Laboratory is supported by the National Science Foundation, cooperative Agreement #DMR-0084173, and by the State of Florida.

References

1. E. G. Moshopoulou *et al., Solid State Chem.* **158**, 55 (2001).
2. C. Petrovic *et al., Europhys. Lett.* **53**, 354 (2001).
3. C. Petrovic *et al., J. Condens. Mat. Phys.* **13**, L337 (2001).
4. N. J. Curro *et al., Phys. Rev. B* **62**, 6100 (2000); W. Bao *et al., Phys. Rev. B* **62**, 14621(2000); W. Bao *et al., Phys. Rev. B* **63**, 219901(E) (2001).
5. J. S. Kim *et al., Phys. Rev. B* **64**, 134524 (2001).
6. R. Movshovich *et al., Phys. Rev. Lett.* **86** 5152 (2001).
7. T. Takeuchi *et al., J. Phys. Soc. Japan* **70** 877 (2001).
8. P. Haen *et al., J. Magn. Magn. Matt.* **63 & 64** 202 (1987).
10. K. Sugiyama *et al., J. Phys. Soc. Japan* **59** 3331 (1990).
11. H. Aoki *et al., Phys. Rev. Lett.* **71** 2110 (1993).
12. F. S. Tautz *et al., Physica B* **206 & 207**, 29 (1995).
13. S. R. Julian *et al., Phys. Rev. B* **46**, 9821(1992).
14. J. S. Kim and G. R. Stewart, unpublished.

THERMODYNAMIC STUDIES OF THE FIELD-INDUCED GAP IN THE QUASI-ONE-DIMENSIONAL S = ½ ANTIFERROMAGNET Yb_4As_3

M. LANG, S. ZHERLITSYN and B. WOLF

Physikalisches Institut, J. W. Goethe-Universität, Frankfurt/Main, Germany
E-mail: Michael.Lang@Physik.uni-frankfurt.de

H. AOKI, T. CICHOREK, P. GEGENWART, B. SCHMIDT and F. STEGLICH

Max-Planck-Institut für Chemische Physik fester Stoffe, Dresden, Germany

A. OCHIAI

Center for Low Temperature Science, Tohoku University, Japan

The quasi-onedimensional S = ½ antiferromagnet Yb_4As_3 is studied by using low-temperature measurements of the specific heat C(T,B), thermal expansion α(T,B) and longitudinal elastic mode c_{11}(T,B). As has been previously shown [M. Köppen *et al.*, Phys. Rev. Lett. **82**, 4548 (1999)], finite magnetic fields perpendicular to the spin chains induce a gap in the spin-excitation spectrum (reminiscent of massive, soliton-like excitations) which manifests itself in distinct anomalies in the specific heat and thermal expansion. In this paper, we present an extension of the above work placing special emphasis on the lattice response and the evolution of the gap at higher fields. The main observations are: (i) the field-induced gap causes a minimum in the c_{11} elastic constant both as a function of temperature and field. Applying a simple two-level model allows for a determination of the gap value $\Delta(B)$ as well as the constant $G(B) = \partial\Delta/\partial\varepsilon$ introduced to account for the spin-lattice coupling. (ii) At $B \leq 9$ T, the $\Delta(B)$ values derived from the various quantities are consistent with $\Delta(B) \propto B^{2/3}$ as predicted by the quantum sine-Gordon model. (iii) Measurements of C(T,B = const) in dc-fields up to 18 T and of c_{11}(T = const, B) in pulsed fields up to 50 T, however, reveal deviations from this behavior at higher fields. (iv) Isothermal measurements of $c_{11}(B)$ show a sharp increase above 35 T which is almost T-independent for $T \leq 10$ K and whose origin is unknown.

1 Introduction

Quasi-one-dimensional (1D) quantum magnets continue to be fascinating objects for both theorists and experimentalists owing to their richness of interesting many-body phenomena. Well-known examples are the appearance of an excitation gap in antiferromagnetic (afm) chains with integer spins[1] and the gapless two-spinon excitations for the uniform 1D S = ½ Heisenberg antiferromagnet.[2] Recent interest has been focusing on S = ½ chains where unexpected behavior occurs in finite magnetic fields: in the 3d-ions-containing organic complexes Cu-benzoate[3] and Cu-pyrimidine[4] as well as the rare-earth-pnictide compound Yb_4As_3 (see Ref. [5]), fields perpendicular to the chains were found to induce a gap in the magnetic excitation spectrum. The observed field dependences of the gap (in not too high

magnetic fields) are consistent with $\Delta(B) \propto B^{2/3}$ as predicted by a quantum sine-Gordon (SG) model.[6] Here we present results of our thermodynamic studies on the field-induced gap in Yb_4As_3 with particular attention paid to the elastic response and the evolution of the gap at high fields. While the specific heat[7] and thermal expansion[5] data have been published already, the results on the elastic constants are new.

2 Charge-Ordering Transition

While in the above-mentioned insulating Cu-complexes the magnetic chains are dictated by the crystal structure, in Yb_4As_3 it is a charge-ordering (CO) transition near room temperature which leads to 1D magnetism.[8] At high T, Yb_4As_3, crystallizing in the cubic anti-Th_3P_4 structure, is a homogeneous intermediate-valent metal where charge balance requires a valence ratio of $Yb^{2+}/Yb^{3+} = 3:1$. The Yb ions are residing statistically on four families of chains along the cubic space diagonals. At $T_{co} \approx 295$ K, a first-order phase transition into a trigonal state takes place where the Yb^{3+} ($4f^{13}$) and Yb^{2+} ($4f^{14}$) ions spatially order. Coulomb repulsion between the $4f^{13}$ holes along with a strong deformation-potential coupling cause the Yb^{3+} ions to order along one of the four cubic space diagonals[9] which results in a slight shrinkage of this axis. Unless uniaxial pressure of the order of 100 bar[8] is applied to one of the <111> axes prior to cooling through T_{co}, the crystals adopt a multidomain low-T structure. At sufficiently low T (< 20 K), where almost all of the Yb^{3+} ions are in their J = 7/2 crystal-field ground-state doublet,[10] the system can be considered to consist of weakly coupled afm S = ½ chains. According to inelastic neutron scattering (INS) (see Ref. [11]), the low-energy excitations at B = 0 agree well with the des Cloizeaux-Pearson spectrum of an afm S = ½ Heisenberg chain with nearest-neighbour coupling J = -2.2meV (= $-k_B \cdot 25.5$ K) (see Ref. [10]).

3 Field-induced spin gap

In Fig. 1 we show low-T specific heat (a) and thermal expansion (b) data of polydomain Yb_4As_3 crystals in varying fields. The large, in-T linear specific heat at zero field, γT with $\gamma \approx 200$ $mJK^{-2}mol^{-1}$, is consistent with the low-energy spin excitations of the Yb^{3+} chains.[9] In a finite field, however, C/T becomes progressively reduced at low T and a maximum develops at slightly higher temperatures indicating the opening of a spin gap.[5] The gap values derived from these measurements[7] as well as from INS (see Ref. [11]) are plotted in the inset. Corresponding anomalies were found also in the coefficient of thermal expansion $\alpha(T,B)$, although there the B-induced maximum is much more strongly pronounced compared to that in C(T,B) and grows almost linearly with the field. A detailed analysis of the $\alpha(T,B)$ data on various multi-domain crystals with different domain

configurations revealed that a finite-field component perpendicular to the S = ½ chains is required to induce this anomaly.[5] Consequently, the B-induced features in $\alpha_{\perp<111>}$ (B ∥ <111>) on a multi-domain crystal, cf. Fig. 1(b), are due to those domains which enclose a finite angle (≈ 70°) with respect to the measuring direction, cf. (SEE Ref. [5]).

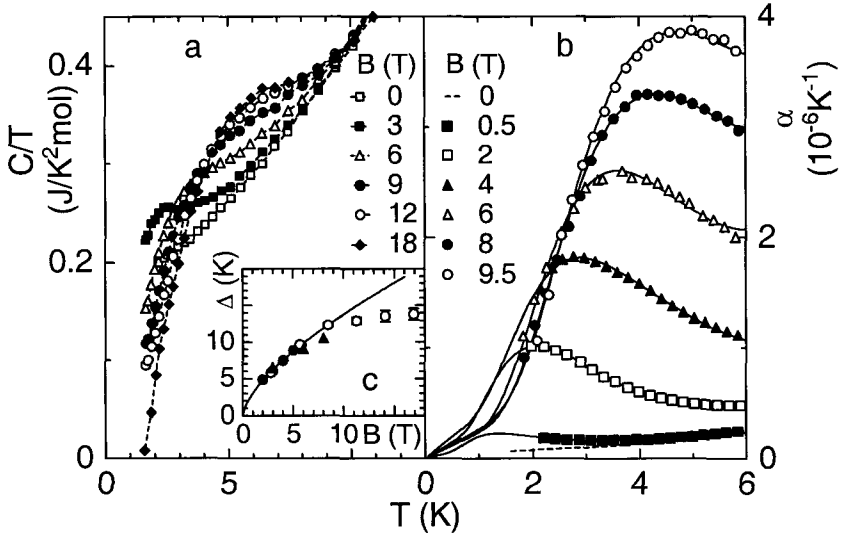

Figure 1: Specific heat as C(T,B)/T vs T (a) and thermal expansion as α(T,B) vs T (b) of multi-domain Yb_4As_3 crystals at varying magnetic fields applied parallel to one of the four cubic space diagonals. Inset: B-dependence of the spin-excitation gap as derived from INS (•) (see Ref. [11]), C(T,B=const) (○) (see Ref. [7]) and c_{11}(T,B=const) measurements (▲), see text. Solid line represents $\Delta(B) \propto B^{2/3}$.

Figure 2 displays relative changes of the c_{11} elastic constant as a function of temperature at varying fields. In these experiments, magnetic fields were aligned parallel to the acoustic wave vector **k** (being ∥ to the polarization **u**) which was normal to the S = ½ chains (i.e. parallel to [100] in the low-T trigonal structure). A mono-domain configuration was achieved by applying uniaxial pressure of about 150 bar along one of the cubic <111> directions while cooling the crystal down to low temperatures. Similar to C(T,B) and α(T,B) we find clear B-induced anomalies in c_{11}(T,B= const): a pronounced minimum that grows in size and shifts to higher temperatures with increasing B. To follow the evolution of this feature to higher fields, isothermal measurements have been conducted in both slowly varying fields for B ≤ 6T and pulsed fields for B ≤ 50 T using our pulse-field facility,[12] cf. Fig. 3: upon increasing the field a minimum develops in Δc_{11} which grows in size and shifts

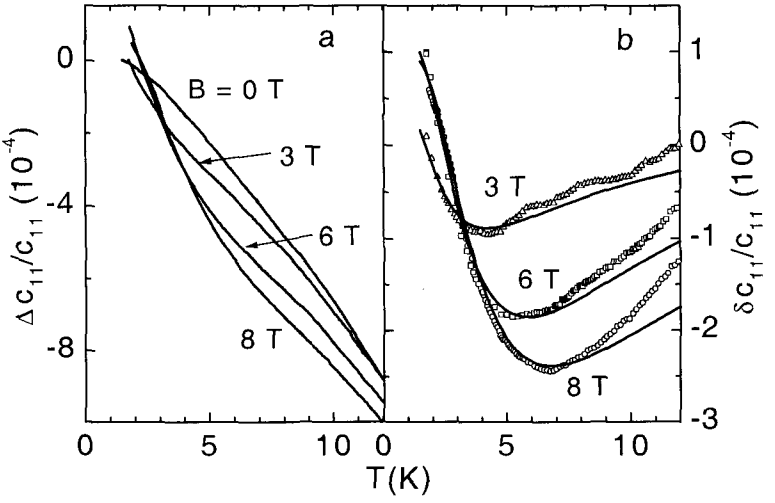

Figure 2: T-dependence of the c_{11} elastic mode as $\Delta c_{11}/c_{11} = (c_{11}(T,B) - c_{11}(T_{min},0))/c_{11}(T_{min},0)$ (a) and $\delta c_{11}/c_{11} = (c_{11}(T,B) - c_{11}(T,0))/c_{11}(T_{min},0)$ (b) at varying fields applied perpendicular to the spin chains of mono-domain Yb_4As_3; T_{min} being the lowest temperature of the measurement. Solid lines in (b) represent fits according to eq. (1), see text.

to higher field values with increasing T. At T = 1.35 K (not shown), a positive contribution (maximum) is superimposed at low fields which - though substantially reduced - is still present in the data at 2 K. Its origin is still unclear but might be related to weak inter-chain-interaction effects which become relevant at low T (see Ref. [7]). Another, more strongly pronounced positive contribution shows up at very high fields, cf. Fig 3(b), which may have its correspondence in a hump observed in the magnetoresistivity at about the same field.[7] Our preliminary pulse-field measurements indicate that the rapid increase above 35 T is almost T-independent for $T \leq 10$ K.

4 Discussion

Lacking a microscopic model that specifies the spin-lattice coupling in the present compound, it is useful to parameterize the B-induced anomalies in the elastic properties by considering a simple two-level model: an excited state is separated from the ground state by a field- and strain- dependent energy gap $\Delta(B,\varepsilon)$. This results in a partition function $Z = 1 + \exp(-\Delta(B,\varepsilon)/k_BT)$ and an elastic constant

$$c(T,B) = c_0 - G^2 \frac{N}{k_B T V}\left(\frac{Z-1}{Z^2}\right), \qquad (1)$$

where c_0 is the background elastic constant, V the volume and N the number of particles. The constant $G = \partial\Delta/\partial\varepsilon$ measuring the strain (ε) dependence of the energy gap Δ accounts for the spin-lattice coupling. As can be seen in Fig. 2(b), Eq. (1) - with G(B) and Δ(B) as adjustable parameters - provides a reasonable description of

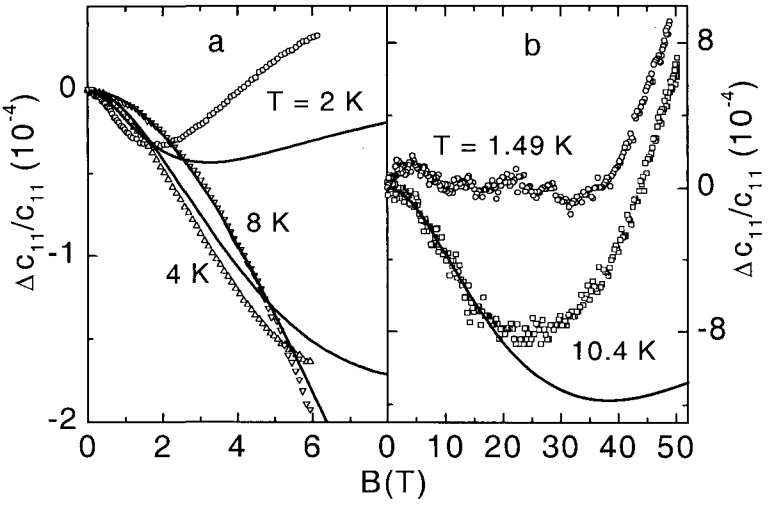

Figure 3: Relative change of the c_{11} elastic constant vs B in slowly varying fields (a) and in pulsed fields (b). Solid lines represent fits according to eq. (1), see below.

the data at constant B. The growth of the c_{11} anomaly with field is reflected in a coupling constant $|G(B)|$ which rises from 71 to 124 and 141 K on going from 3 to 6 and 8 T. The Δ(B) values obtained agree satisfactorily with those found in our specific heat measurements, cf. inset Fig. 1 and are consistent with $\Delta(B) \propto B^{2/3}$. Using the same field dependence and $|G(B)| \propto B$ as suggested from the low-field data, Eq. (1) also allows for a description of the isothermal measurements at T = 4 and 8 K for $B \leq 6$ T, cf. Fig. 3(a), but fails to describe the position and high-B side of the minimum, cf. solid line in Fig. 3(b). These deviations might indicate a gap that becomes reduced (or even closes) at higher fields. Such a field dependence of Δ would also be consistent with the tendency seen in Δ(B) extracted from our high-field C(T,B) measurements. Alternatively, the poor quality of the fit might come from a B dependence of the coupling constant G which is different from $|G(B)| \propto B$ at high fields. The anomalous steep increase in c_{11} above 35 T, the origin of which is still unclear, makes a definite statement on this point rather difficult.

In Ref. [5] it was shown that the B-induced maxima in C(T,B) and α(T,B) in Yb_4As_3 are well described by soliton-like (i.e. massive) excitations of an afm

Heisenberg chain with (weak) easy-plane anisotropy. While the classical SG model used there predicts a field dependence of the soliton rest energy or - equivalently - the gap $\Delta \propto B^{\nu}$ with $\nu = 1$, $\nu = 2/3$ - as obtained by the quantum version of the SG model - was found to be much better for describing the experimental results. The quantum SG model has been applied to Yb_4As_3 by Oshikawa *et al.*[6] where the spin gap was related to the presence of a B-induced staggered field due to (i) an alternating g-tensor and (ii) the Dzaloshinskii-Moriya (DM) interaction. By considering an effective Hamiltonian that describes the low-energy physics of the Yb^{3+} chains in this compound, Shiba *et al.*,[13] uncovered a hidden symmetry so that (i) and (ii) are not independent from each other. As a result of the staggered DM term, finite transverse fields induce a staggered field which thus may account for the field-induced gap in Yb_4As_3. The limitations of the quantum SG model as an effective low-energy model valid only at $k_BT \ll J$ have been overcome recently by a finite-T density-matrix renormalization-group treatment of the problem.[14] According to their calculations, the $\Delta(B) \propto B^{2/3}$ result of the quantum SG model should be valid up to 24 T, the highest field considered in their study. This is, however, in contrast to our C(T,B) results where above 9 T $\Delta(B)$ starts to level off. Deviations from the $\Delta(B) \propto B^{2/3}$ dependence at elevated fields might also be indicated by our preliminary pulse-field experiments. A further open problem related to $\Delta(B)$ is the origin of the response in the elastic properties that grows with B. In our simple model this is accounted for by the coupling constant $G(B) = \partial\Delta/\partial\varepsilon$ that increases almost linearly with the field at least at low fields. We stress that the application of this model to the coefficient of thermal expansion ($\alpha \propto G \cdot \Delta \cdot T^{-2} \cdot (Z-1) \cdot Z^{-2}$) using the same G(B) parameters provides a reasonable quantitative description of the $\alpha(T,B)$ data as well.

References

1. F.D.M. Haldane, Phys. Rev. Lett. **50**, 1153 (1983).
2. J. Des Cloizeaux and J. J. Pearson, Phys. Rev. **128**, 2131 (1962).
3. D. C. Dender *et al.*, Phys. Rev. Lett. **79**, 1750 (1997).
4. R. Feyerherm *et al.*, J. Phys.: Condens. Matter **12**, 8495 (2000).
5. M. Köppen *et al.*, Phys. Rev. Lett. **82**, 4548 (1999).
6. M. Oshikawa *et al.*, J. Phys. Soc. Jpn. **68**, 3181 (1999).
7. P. Gegenwart *et al.*, Physica B (in press).
8. A. Ochiai, T. Suzuki and T. Kasuya, J. Phys. Soc. Jpn. **59**, 4129 (1990).
9. P. Fulde *et al.*, Europhys. Lett., **31**, 323 (1995).
10. M. Kohgi *et al.*, Phys. Rev. B **56**, R11388 (1997).
11. M. Kohgi *et al.*, Phys. Rev. Lett. **86**, 2439 (2001).
12. B. Wolf *et al.*, Physica B **294-295**, 612 (2001).
13. H. Shiba *et al.*, J. Phys. Soc. Jpn. **69**, 1493 (2000).
14. N. Shibata and K. Ueda, J. Phys. Soc. Jpn. (submitted).

TWO-COMPONENT SUPERCONDUCTIVITY OF HEAVY FERMIONIC MATERIAL UPt_3

V. P. MINEEV and T. CHAMPEL
Commissariat a l'Energie Atomique, DRFMC/SPSMS,
17 rue des Martyrs, 38054, Grenoble, France

The theory of the Abrikosov lattice structures in the unconventional superconductor UPt_3 under magnetic field parallel to the hexagonal crystal axis is presented. Only the two-component E_2 superconducting state among the other states of different symmetry is proved to be compatible with the recent observations[1] of the flux lattice in the A phase misaligned with crystallographic directions. Unlike to the one-dimensional superconductivity where anisotropic interactions caused by non-local electrodynamic corrections are essential for the vortex ordering the formation of slightly distorted triangular flux lattice in UPt_3 due to the two-dimensional nature of its superconducting state can be described already in local electrodynamics.[2]

1. A. Huxley *et al., Nature* (London) **406**, 160 (2000).
2. T. Champel, V. P. Mineev, *Phys. Rev. Lett.* **86**, 4903 (2001)

$CeMIn_5$ (M=Co, Ir, Rh) HEAVY FERMION SUPERCONDUCTORS AND THE UTILITY OF HIGH MAGNETIC FIELDS

J.L. SARRAO

Los Alamos National Laboratory, Los Alamos, NM 87545, USA

E-mail: sarrao@lanl.gov

We review the properties of the recently discovered $CeMIn_5$ (M=Co, Ir, Rh) heavy fermion superconductors and discuss the present state of our understanding of these materials. A particular focus is the role that magnetic fields have played in elucidating the properties of these materials. Specifically, we discuss quantum oscillation measurements on $CeMIn_5$, the influence of applied field on the linear coefficient of specific heat, γ, and the nature of the H-T phase diagrams in both the normal and superconducting states of these materials.

1 Introduction

The response of heavy fermions to applied magnetic fields has significantly contributed to our understanding of these materials.[1] The recent availability of magnetic fields on the order of 100 Tesla, which corresponds to Zeeman energies on the order of 100 K, a scale which often exceeds those characteristic of heavy fermion ground states and a growing suite of available measurement techniques only serves to increase this impact.[2] In particular, the dependence of the conduction electron effective mass, most simply probed by measurements of the linear-in-T coefficient of the low-temperature heat capacity, on applied field allows one to separate mass enhancements due to spin fluctuation behavior from 'real' heavy fermion character.[3] Furthermore, the appearance, or not, of field-induced metamagnetic transitions in heavy fermion compounds allows insights to be gained into the degree of f-electron localization or itineracy, an open and material-specific issue in heavy fermions.[4] Finally, at least in some circumstances, the availability of high magnetic fields facilitates quantum oscillation studies of the fermi surfaces of these materials.[5] In what follows, we review the recent discovery of the $CeMIn_5$ family of heavy fermion compounds and discuss the ways in which field-dependent measurements have contributed to our understanding of these materials.

2 Basic properties of $CeMIn_5$

The $CeMIn_5$ (M=Co, Ir, Rh) family of compounds are the first heavy fermion materials in which structural layering can be demonstrated to play an important role. Each of these materials is a tetragonal derivative of $CeIn_3$, and their ground state properties depend on both the effective hydrostatic and uniaxial pressure created by

the tetragonal stacking of $CeIn_3$ and MIn_2 layers. Co, Ir, and Rh are isovalent so, although these materials bear remarkable similarities to the cuprates, carrier-density tuning does not play an explicit role in determining their ground state properties.

At ambient pressure, $CeRhIn_5$ orders antiferromagnetically at 3.8 K. T_N increases weakly with applied pressure, an unconventional dependence, until it vanishes abruptly near 16 kbar, at which point superconductivity, with a T_c of 2.1 K, is observed.[6] The superconductivity is bulk as evidenced by heat capacity[7] and nuclear magnetic resonance,[8,9] and the observed temperature dependencies are consistent with unconventional, d-wave pairing. The value of C/T just above T_N and T_c is ~ 400 mJ/molK^2 in both cases, confirming that $CeRhIn_5$ is a heavy fermion.

$CeIrIn_5$ displays bulk superconductivity at 0.4 K that develops out of a state with γ ~ 700 mJ/molK^2 (see Ref. [10]). Again, heat capacity, thermal transport, and nuclear magnetic resonance measurements provide strong evidence for line nodes in the superconducting gap.[11-13] An interesting wrinkle regarding $CeIrIn_5$ is that its resistivity vanishes near 1 K, well above the bulk T_c. The detailed origin of this filamentary state remains unclear,[14] but it is robust as a function of applied magnetic field and displays the same crystallographic anisotropy as the bulk transition. Furthermore, the zero-resistance transition in $CeIrIn_5$ "reveals" the value of bulk T_c that can be approached with either pressure[15] or chemical doping.[16]

With an ambient-pressure T_c of 2.3 K, $CeCoIn_5$ displays the highest transition temperature of any heavy Fermion superconductor.[17] Again, the implication is d-wave superconductivity.[11,13,18] Applied pressure can further increase T_c to 2.6 K (at a pressure of 15 kbar).[19] The observed C/T of 300 mJ/molK^2 at T_c is rather modest, but the application of a magnetic field greater than Hc_2 reveals that γ is not fully developed at $T_c(H=0)$, and, in fact, the field-induced normal state γ ~ 1000 mJ/molK^2 is quite large.

An additional surprising feature of $CeMIn_5$ is the robustness of intermediate alloys, e.g., $CeM_{1-x}M'_xIn_5$ (M or M' = Co, Ir, Rh) (see Ref. [20]). Single crystals can be grown for the full range of x for all M and M' without apparent degradation of sample quality; neither clustering nor gross phase segregation has been observed. Thus, one is presented with the opportunity of exploring the competition and interaction of diverse ground states, e.g., magnetism and superconductivity.[16,20,21] The range of x for which superconductivity can be observed is remarkable, ~ 0.7 for Rh-Ir alloys, and is rivaled only by the cuprates in terms of the flexibility of chemical tuning.

3 Trends in electronic anisotropy deduced from dHvA measurements

3.1 Fermi surface evolution with M

Because of the high quality of single crystals that result from flux growth-based crystal growth, substantial progress has been made in quantum oscillation studies of

$CeMIn_5$ (see Refs. [22-26]). From a broad perspective, reasonable agreement is found between LDA band structure calculations and de Haas-van Alphen oscillation measurements. Three pieces of fermi surface (FS) are calculated and observed, a relatively small quasi-spherical sheet, a quasi-cylindrical sheet, and a third more complex, larger-volume sheet. More important are the trends that emerge on evolution from $CeRhIn_5$ to $CeIrIn_5$ to $CeCoIn_5$. As the ambient pressure ground state evolves from antiferromagnet to low-T superconductor to higher-T superconductor, the degree of quasi-2d character - thought to play an important role in the enhanced T_c of these materials relative to $CeIn_3$ – increases substantially, as judged by the decreased variation in extremal areas measured on the quasi-cylindrical FS sheet. Furthermore, increased effective masses, consistent with the known increases in C/T, are observed. However, the heaviest orbits and M-dependent mass enhancement are not observed on the quasi-cylindrical FS, but rather on the larger piece of FS, complicating the interpretation that high-T_c heavy fermion superconductivity derives from the quasi-2d character of these materials.

3.2 Degree of f-electron localization

It has also proved possible to observe quantum oscillations in a wide range of alloys, in particular $Ce_{1-x}La_xMIn_5$ (see Refs. [27,28]). Such measurements provide a model-free measure of the degree of f-electron localization in heavy fermion materials. Because Ce possesses one f-electron whereas La has none, replacing Ce with La should result in a change in FS volume if the f-electron is itinerant and contributes to the FS. On the other hand, if the f-electron is highly localized, no such change in FS volume is expected. Similar La-dilution studies have been performed in a wide range of heavy fermion materials, and a general trend in which heavy fermion antiferromagnets possess localized f-electrons and heavy fermion superconductors possess itinerant f-electrons seems to emerge. Our measurements of $Ce_{1-x}La_xRhIn_5$ may confirm this trend.[27] Both the observed dHvA frequencies, which measure the FS area, and the measured effective masses depend only weakly on La concentration, suggesting highly localized f-electrons. However, although the data are not as complete, $CeIrIn_5$ and $CeCoIn_5$ appear to display a similar degree of localization.[28] This strong degree of f-electron localization is also revealed by the bulk magnetic properties of $CeMIn_5$, which appear to be dominated by crystal-electric-field effects.[29,30] Interestingly, preliminary dHvA measurements as a function of pressure in $CeRhIn_5$, in which the observed effective masses and, perhaps, the extremal areas are seen to vary near the antiferromagnetic-superconducting transition, reveal a greater degree of variation in f-electron localization.[31] Unfortunately, although data exist,[32] insufficient progress has been made in $CeM_{1-x}M'_xIn_5$ dHvA studies to determine whether similar changes are observed as a function of doping.

4 H-T phase diagram in $CeCoIn_5$

Partially in the process of performing dHvA measurements in $CeCoIn_5$, a remarkable H-T phase diagram has emerged.[33] $CeCoIn_5$ possesses upper critical fields that are very large and anisotropic. For a T_c of 2.3 K, simple estimates predict a critical field of ~ 4.6T (see Ref. [34]). $CeCoIn_5$, however, displays $Hc_2[001]$ ~ 5T and $Hc_2[100]$ ~ 12T. Furthermore, the angular and temperature evolution of these critical fields is anomalous.[33,35] When field is applied along the c-axis, first-order transitions are observed in temperature and field sweeps for $4.6\ T < H < Hc_2$ in thermal expansion and specific heat data, suggesting Pauli limiting.[36]

The in-plane behavior of Hc_2 in $CeCoIn_5$ is even more anomalous.[33] Rotating the applied field from [001] into the plane at lowest temperatures reveals different behaviors for rotation into [100] and [110], respectively. The angular variation of Hc_2 from [001] to [100] is that expected from the anisotropic effective masses deduced from quantum oscillation measurements. [001]-[110] rotations, on the other hand, follow a form expected for thin films rather than 3-d superconductors and suggest 2-d character. The temperature evolution of Hc_2 for field applied along [110] is even more anomalous. For $T < 0.6T_c$, a step-like transition in magnetization is observed at Hc_2 (determined resistively) that, for decreasing field sweeps, remains step-like but occurs at fields lower than Hc_2. For $T>0.6T_c$, the conventional behavior is recovered, the magnetization vanishes smoothly at Hc_2 independent of field-sweep direction. These observations provide strong evidence for the realization of an inhomogeneous Fulde-Ferrell-Larkin-Ovchinikov (FFLO) state in $CeCoIn_5$.

A metamagnetic transition is also observed in the normal state of $CeCoIn_5$. For temperatures at least as high as 25 K, and extending down to $0.6T_c$ in the field induced normal state, a step-like transition is observed in magnetization for fields near 9 T. The positive step in magnetization suggests the possibility of field-induced ferromagnetism. Although the detailed nature of this transition remains unclear, a (partial) spin polarization of the FS is a possibility. This metamagnetic transition also might be related to similar phenomena observed in $CeIrIn_5$, albeit at higher fields, by Stewart *et al.*[37] Finally, it is worth noting that the FFLO behavior observed in the superconducting state emerges from the field-induced ferromagnetic state and may, in fact, be stabilized by it.

5 General trends in applied fields

Finally, we discuss the field-dependent evolution of the heavy fermion state itself in $CeMIn_5$. Measurements of heat capacity in fields as high as 28.5 T reveal that γ is suppressed by 33% and 50% in $CeIrIn_5$ and $CeCoIn_5$, respectively.[38] Although the suppression of γ is significant, substantial mass enhancement does persist to high

fields, consistent with observations from dHvA measurements, confirming that the enhanced heat capacity is attributable to heavy fermion behavior rather than magnetic correlations resulting from proximity to a phase transition. Because T_N depends only weakly on field in $CeRhIn_5$, similar estimates of $\gamma(H)$ are difficult, but it is clear that heavy-fermion mass enhancement comparable to that of $CeIrIn_5$ and $CeCoIn_5$ are present in $CeRhIn_5$. Another normal-state feature of $CeMIn_5$ revealed by high-field measurements is the ubiquitous presence of metamagnetic transitions. $CeRhIn_5$ (see Refs. [22,39]), $CeIrIn_5$ (see Ref. [37]) and $CeCoIn_5$ (see Ref. [33]) all display field-induced transitions in heat capacity or magnetization.

6 Conclusions

In summary, high magnetic field measurements have played an important role in our present understanding of the $CeMIn_5$ family of heavy fermion superconductors. Heat capacity measurements as a function of field reveal that the low-T mass enhancement is due to heavy fermion behavior. Quantum oscillation measurements confirm this point and further reveal trends as a function of M that suggest that a quasi two-dimensional electronic structure exists and may play a role in determining T_c in these materials. Finally, applied fields provide another thermodynamic axis along which ground-state properties can be mapped. Not only are metamagnetic transitions observed in the paramagnetic states of $CeIrIn_5$ and $CeCoIn_5$ but also anomalous evolution of the Neel state in $CeRhIn_5$ as well as candidate FFLO behavior in the superconducting state of $CeCoIn_5$ is revealed.

Acknowledgments

I thank R. G. Goodrich, D. Hall, N. Harrison, T. P. Murphy, E. C. Palm, G. R. Stewart, J. D. Thompson, and S. W. Tozer for important contributions to this effort. Work at Los Alamos was performed under the auspices of the U.S. Department of Energy. Work at the NHMFL, where many of the high-field measurements discussed above were performed, is supported by the N.S.F. and the State of Florida.

References

1. B. Andraka *et al., Phys. Rev. B* **39**, 6420 (1989).
2. M. Jaime *et al, Nature* **405**, 160 (2000).
3. G. R. Stewart *et al., Phys. Rev. B* **37**, 3344 (1988).
4. A. Schroder *et al., Nature* **413**, 297 (2000).
5. R. G. Goodrich *et al., Phys. Rev. Lett.* **82**, 3669 (1999).
6. H. Hegger *et al., Phys. Rev. Lett.* 4986 (2000).

7. R. A. Fisher *et al.*, submitted to Phys. Rev. Lett. (2001); cond-mat/0109221.
8. T. Mito *et al.*, Phys. Rev. B **63**, 220507 (2001).
9. Y. Kohori *et al.*, Eur. Phys. J. B **18**, 601 (2000).
10. C. Petrovic *et al.*, Europhys. Lett. **53**, 354 (2001).
11. R. Movshovich *et al.*, Phys. Rev. Lett. **86**, 5152 (2001).
12. G. Q. Zheng *et al.*, Phys. Rev. Lett. **86,** 4664 (2001).
13. Y. Kohori *et al.*, Phys. Rev. B **64,** 134526 (2001).
14. A. Bianchi *et al.*, to appear in Phys. Rev. B (2001); cond-mat/0108081.
15. G. Sparn *et al.*, to appear in Physica B (2001).
16. P. G. Pagliuso *et al.*, Phys. Rev. B **64**, 100503 (2001).
17. C. Petrovic *et al.*, J. Phys. Cond. Matt. **13**, L337 (2001).
18. K. Izawa *et al.*, Phys. Rev. Lett. **87**, 057002 (2001).
19. M. Nicklas *et al.*, J. Phys. Cond. Matt. **13**, L905 (2001).
20. P. G. Pagliuso *et al.*, to appear in Physica B (2001); cond-mat/0107266.
21. V. S. Zapf *et al.*, to appear in Phys. Rev. B (2001).
22. A. L. Cornelius *et al.*, Phys. Rev. B **62**, 14181 (2001).
23. D. Hall *et al.*, Phys. Rev. B **64**, 064506 (2001).
24. Y. Haga *et al.*, Phys. Rev. B **63**, 060503 (2001).
25. D. Hall *et al.*, to appear in Phys. Rev. B (2001); cond-mat/0102533.
26. R. Settai *et al.*, J. Phys. Cond. Matt. **13**, L627 (2001).
27. U. Alver *et al.*, Phys. Rev. B **64**, 180402 (2001).
28. R. G. Goodrich *et al.*, unpublished (2001).
29. N. J. Curro *et al.*, Phys. Rev. B **64**, 180514 (2001).
30. P. G. Pagliuso *et al.*, to appear in Physica B (2001).
31. Y. Onuki private communication (2001).
32. R. G. Goodrich *et al.*, unpublished (2001).
33. T. P. Murphy *et al.*, submitted to Phys. Rev. Lett. (2001); cond-mat/0104179.
34. A. M. Clogston Phys. Rev. Lett. **9**, 266 (1962).
35. N. Oeschler *et al.*, unpublished (2001).
36. A. Bianche *et al.*, unpublished (2001).
37. G. R. Stewart *et al.*, these proceedings.
38. J. S. Kim *et al.*, Phys. Rev. B **64**, 134524 (2001).
39. T. Takeuchi *et al.*, J. Phys. Soc. Jpn. **70**, 877 (2001).

QUANTUM CRITICAL FLUCTUATIONS IN HEAVY FERMION COMPOUNDS

A. SCHROEDER,[1,2] G. AEPPLI,[3] P. COLEMAN,[4]
R. RAMAZASHVILI,[5] R. COLDEA,[6,7] M. ADAMS,[7]
E. BUCHER,[8] D. F. MCMORROW,[9] H. V. LÖHNEYSEN,[2,10]
and O. STOCKERT,[2,11]

[1]*Physics Department, Kent State University, Kent, OH 44242, U.S.A.*
[2]*Physikalisches Institut, Universität Karlsruhe, D-76128 Karlsruhe, Germany*
[3]*NEC Research, 4 Independence Way, Princeton, NJ 08540, U.S.A.*
[4]*Serin Laboratory, Rutgers University, Piscataway, NJ 08855-0849, U.S.A.*
[5]*Department of Physics, University of Illinois, Urbana, IL,U.S.A.*
[6]*Clarendon Laboratory, University of Oxford, Oxford, UK*
[7]*ISIS Facility, CCLRC, Rutherford-Appleton Laboratory, Didcot, UK.*
[8]*Bell Laboratories, Lucent Technologies, Murray Hill, NJ 079 74, U.S.A.*
[9]*Risø National Laboratory, DK-4000 Roskilde, Denmark*
[10]*Institut für Festkörperforschung, Forschungszentrum Karlsruhe, D-76021 Karlsruhe, Germany*
[11]*Max-Planck-Institute for Chemical Physics of Solids, D-01187 Dresden, Germany*

The electronic properties of heavy fermion alloys are dominated by spin fluctuations which are expected to become critical when tuned by pressure to a quantum critical point (QCP), entering a magnetic ordered state. Apart from the onset of exotic superconductivity, unexpected "normal conducting" behavior is found close to the QCP, which does not seem only to escape the conventional view of metals (Fermi liquids) but also the "conventional view" of an antiferromagnetic quantum phase transition in these f-metals. So far only few compounds have been investigated by neutron scattering to directly reveal the critical fluctuations spectrum. In $CeCu_{5.9}Au_{0.1}$ the fluctuations develop an unusual energy dependence, characterized by an exponent $\alpha = 0.75$, which persist over the entire Brillouin zone, provoking an unexpected local non Fermi liquid behavior. The same unusual exponent derived from *E/T* scaling determines the *H/T* scaling of the uniform magnetization. Recent neutron scattering data in magnetic fields further confirm this picture of nearly free local magnetic moments (modified by α) emerging at the antiferromagnetic QCP in this strongly correlated electron system.

While some time ago heavy fermion compounds (HFC) attracted attention as an extreme example of a highly correlated electron system to behave essentially like a non interacting electron system following the Fermi liquid (FL) concept - although the highly renormalized mass may exceed the free electron mass by three orders of magnitude - in recent years their potential in studying systematic deviation from the Fermi liquid is being exploited. The origin of so called non-Fermi liquid (NFL) behavior, manifesting in "unusual" low energy excitations, remains diverse and is approached by trying to separate the effects of purely local, distributional and correlated nature. The most "pure" correlated effect is expected close to a magnetic instability. Many HFC can be tuned by real or chemical pressure (through chemical

substitution) from a paramagnetic to a magnetic ordered phase (mostly an antiferromagnet (AF)). The onset of long-range correlations is believed to set in at a quantum critical point (QCP), that the approach to understand the "unusual" low energy (NFL) excitations lays in the characterization of the quantum critical magnetic fluctuation spectrum.[1] There are only few examples studied in detail. Several pure pressure-driven Ce-compounds (like $CePd_2Si_2$, $CeIn_3$) develop a low temperature superconducting phase[2] close to the expected QCP somehow avoiding the QCP. But also here, the "normal conducting" phase shows an anomalous power in the T-dependence of $\rho(T)$ (see Ref. [2]), clearly different from FL behavior, but also different from the expected power close to an AF QCP in three dimension (3d) (see Ref. [3]). The most systematic study has been performed at the HFC $CeCu_{6-x}Au_x$ focussing on the direct observation of spin fluctuations by neutron scattering,[5,6,7,12] which is presented below. $CeCu_6$ remains paramagnetic and shows a huge specific heat coefficient described by one renormalized energy scale of $T_K = 5$ K. Tuned by chemical substitution $CeCu_{6-x}Au_x$ (see Ref. [4]) evolves long range AF order for $x_c > 0.1$ (without any spin glass phase) (see Fig. 1(d)). At $x_c = 0.1$ typical NFL excitation are observed like $C/T \sim \log(T_0/T)$ or $\Delta\rho \sim T$ (see Ref. [4]), but not the one expected for a 3d AF QCP (see Ref. [3]), which would essentially lead to a recovery of FL behavior of the majority of the Fermi surface except some "hot lines" connected by the finite wave vector, where critical AF fluctuations evolve forming a spin density wave. Is the assumption of critical 3d AF correlations not appropriate, and/or are distributional effects (like different local environments) or local effects (no conventional Kondo effect) important? The neutron scattering data of $CeCu_{5.9}Au_{0.1}$ indeed do not confirm ideal 3d AF correlations and neither ideal local excitations, but they can be described in a very simple picture (enforced through diverse scaling analysis)[5,7] suggesting a new kind of AF QCP occurring in this HFC(see Ref. [8]).

The main neutron scattering and magnetization study presented here was performed at $CeCu_{5.9}Au_{0.1}$ single crystals at TAS7 in Risø and IRIS in ISIS, and Karlsruhe (as described in Refs. [5,7]) yielding the magnetic susceptibility $\chi(Q,E,T,H)$ at a wide range of wave vectors Q, energy transfers E (down to 0.02 meV), temperatures T (down to 0.05 K) and magnetic fields H. Correlated magnetic fluctuations below and magnetic order above x_c occur essentially in the neighborhood of the zone boundary at Q = (100). But in effect the most intense scattering at x_c is found in an extended Q-region containing the incommensurate wave vector Q = B, where long range order sets in for $x \geq 0.15$ (see Ref. [10]), but also part of the a*-axis giving rise to this "butterfly" shape (sketched in Fig. 1(c)). χ'' at a very low E (see Figs. 1(a) and 1(b)) shows still the smooth Q-dependence along the "wings" and the pronounced Q-dependence across the wings. Such weak correlation in one direction and strong correlations in the other two dimensions may be regarded as AF correlation with a apparent reduced dimensionality ($d < 3$). This might already question the realization of an ideal 3d AF QCP in this otherwise 3d material regarding the electronic properties.[6]

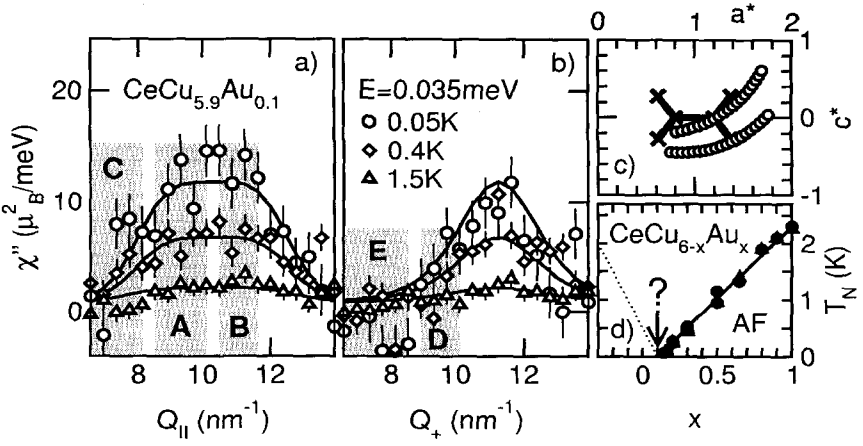

Figure 1: a) b) Wave vector dependence of magnetic fluctuations along the trajectories indicated in c) for a small energy transfer of E = 0.035 meV at different temperatures. Lines correspond to Eq.(3) with a T-independent f(q) expanded in even powers of Q. The letters A-D label specific Q-regions referred to in this paper. c) shows the "butterfly" shaped critical Q-region observed for x = 0.1 including the wave vector of 3d AF order for x > 0.1 (Q=B marked by crosses). D) Néel temperature T_N (see Ref.[4]) of $CeCu_{6-x}Au_x$ vs concentration x vanishing at x_c=0.1.

But what is even more unexpected is the dynamic evolving towards the QCP. Within this extended critical Q_c-region, the same energy dependence of the magnetic scattering is observed. The high energy tail of the dynamic response is expressed by a modified power different from 1 like $\chi''(E > k_BT) \sim E^{\alpha}$ with $\alpha = 0.75$ inconsistent with a single Lorentxain lineshape. The width of this distribution narrows down following the absolute k_BT-scale. More precisely, all data at Q_c collapse on one scaling plot (see Fig. 2a)

$$\chi'' \sim T^{-\alpha} g''(E/T), \qquad (1)$$

exhibiting simple E/T-scaling, when α is chosen to be 0.75. The solid line represents the scaling function g derived from a modified Curie law

$$g \sim (1 - iE/aT)^{-\alpha}, \qquad (2)$$

(with $a = 0.8\ k_B$) where α is consistently $\alpha = 0.75$. This simple scaling is expected close to a QCP, but only if the effective dimension D (including the time scale) of the system does not exceed its upper critical dimension d_{uc}. But the consistent scenario derived for a 3dAF (see Ref. [3]), holds for d above d_{uc} (where $D = 3+2 > d_{uc} = 4$), that corrections to the Gaussian fluctuations lead to a different

scaling power E ~ $T^{3/2}$ (see Ref. [3]), which cannot be confirmed by these $CeCu_{5.9}Au_{0.1}$- data.

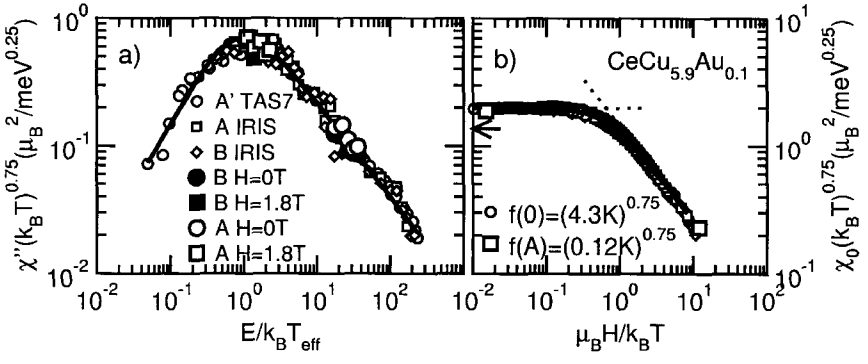

Figure 2: E/T_{eff} scaling plot of χ'' and H/T scaling plot of χ_0. Lines are fits described in the text.

Turning to the dynamic outside Q_c, surprisingly the same unusual exponent $\alpha = 0.75$ remains. The most convincing evidence comes from precise χ_{bulk}-data with Q = 0 far away from Q_c. χ_{bulk} can be expressed by a modified Curie Weiss law of the form, $1/\chi \sim f(0) + T^{\alpha}$, where the same unusual exponent $\alpha = 0.75$ determines the T-dependence down to 0.1K for H < 0.1 T (which also holds for the harder axes like H || a and H || b). The general form

$$1/\chi \sim f(Q) + (T - iE/a)^{\alpha} \qquad (3)$$

still fits the available neutron data in a large range of Q, as shown in Fig. 3(a) for E = 0, where χ' vs T^{α} results in parallel straight lines shifted by f(Q). This simple form demonstrates that the unconventional dynamic is not restricted to certain hot spots but rather extended over the whole Brillouin zone originating from unusual local dynamic evolving at this QCP. This contradicts the conventional view,[3] that the local excitations remain unaffected at the QCP and rather suggest, that the screening of the magnetic moments brakes down.[8]

The character of nearly free local moments, just modified by α, can be further manifested by the H-dependence. The fact that real free local moments exhibit a Curie Weiss law and also H/T-scaling with a scaling power of 1, immediately suggest to probe H/T-scaling here. Fig. 3b shows $1/\chi_{bulk}$ vs T^{α} in small fields ($\mu H^{\alpha} < f(0)$) leading to a gradual saturation for $k_BT < \mu_BH$, different than the Q- or x-dependence,[7] where $1/\chi$ is just shifted. Decoupling the correlations by subtracting f(0) from $1/\chi$ allows to check for the singular part χ_0 from the χ_{bulk} data. Indeed χ_0 exhibits H/T scaling (see Fig. 2b) if $\alpha = 0.75$. For $\mu_BH > k_BT$ the H-dependence of χ_0 is the same as the T - or E-dependence namely just a simple power law $\chi_0 \sim H^{-\alpha}$

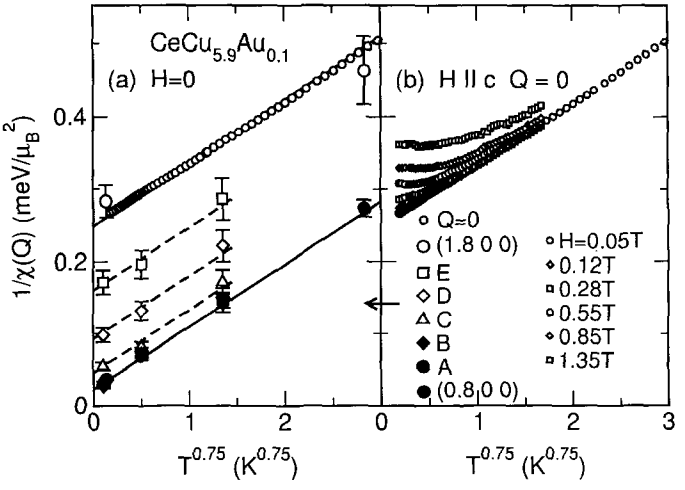

Figure 3: Inverse susceptibility $\chi(E=0,Q,T)^{-1}$ vs T^{α} with $\alpha = 0.75$ for diverse wave vectors Q at $H \approx 0$ (a) and in different magnetic fields $H \parallel c$ at $Q = 0$ (b).

χ_0 is the same as the T- or E-dependence namely just a simple power law $\chi_0 \sim H^{-\alpha}$ reproducing again the same power α. The best scaling function is achieved by replacing T by T_{eff} with

$$T_{eff} = (T^2 + (\mu H/k_B)^2)^{1/2}. \quad (4)$$

The only new parameter, the effective moment μ, is in the order of $1\mu_B$ consistent with an atomic moment. The assumption that f(Q) is now also H-independent (for $\mu H < f(0)^{1/\alpha}$), was addressed in a further neutron scattering study[12] to probe the critical fluctuation directly in a magnetic field. The present data confirm, that the H-dependence at Q = A and Q = B are indistinguishable and that the same description can be applied to describe the data by just replacing T by $\mu H/k_B$ in the limit $\mu H > k_B T$. Also μ is consistent with the χ_{bulk} measurements. These neutron data fit perfectly in the E/T and H/T-scaling plots (replacing E/T by E/T_{eff}, see Fig. 2(b)).

$CeCu_{5.9}Au_{0.1}$ allows the observation of critical correlated AF fluctuations at x_c revealed by neutron scattering. But the quantum critical fluctuations are less correlated in space and more correlated in time then ideally assumed for a 3d AF QCP. Instead of finding a clear separation between the hot spots and an unaffected Fermi surface containing the screened f-electrons, we see an extended Q-range (butterfly), where χ tends to diverges, and more severely the whole Fermi surface evolving a modified dynamic. The clear experimental evidence of E/T and H/T scaling supports the picture of nearly free local moments, which are becoming unscreened at the QCP, where the complex interactions seem to be contained in the simple parameter, the exponent α. In this compound an "ideal" 3d AF QCP is

avoided. The picture of the purely correlated mechanism has to incorporate now the local degree of freedom.[8,9] Do we have to deal here with a local and correlated instability simultaneously?[9] Might this in fact be typical for these f-metals or is the nature of these QCP delicately depending on structural properties and its deviations (introduced by e.g. impurities)? Such unusual space and/or time correlations could account for unusual exponents in ρ observed close to a QCP in the "pure" pressure driven Ce-compounds. The simple H/T scaling including an exponent $\alpha = 0.7$ is already observed for a "cleaner" compound $YbRh_2Si_2$ (see Ref. [11]). But how general this kind of QCP might occur and how general this scaling exponent α is, cannot be decided until the AF fluctuations have been directly observed and characterized in different compounds.

References

1. S. Sachdev, *Quantum phase transitions*, Cambridge University Press (1999).
2. S. Julian, J. *Magn. Magn. Mater.* **177-181**, 265 (1998) and N. D. Mathur *et al.*, Nature **394**, 39 (1998).
3. J. Hertz, *Phys. Rev. B* **14**, 1165(1976) and A. Millis, *Phys. Rev. B* **48**,7183 (1993).
4. H. V. Löhneysen, *J. Phys. Condens. Matter* **8**, 9689 (1996) and refs therein.
5. A. Schröder *et al.*, *Phys.Rev.Lett.* **80**, 5623 (1998).
6. O. Stockert *et al.*, *Phys.Rev.Lett.* **80**, 5627 (1998) p. 5627.
7. A. Schröder *et al.*, *Nature* **407**, 351 (2000).
8. P. Coleman, C. Pepin, Q. Si, R. Ramazashvili, *J. Phys. Condens. Matter* **13**, R723(2001).
9. Q. Si, S. Rabello, K. Ingersent, J. L. Smith, *Nature* **413**, 804 (2001).
10. H. V. Löhneysen, C. Pfleiderer, A. Schröder, O. Stockert, *Acta Physica Polonica B* 3313 (2001).
11. O. Trovarelli *et al*, *Phys. Rev. Lett.* **85**, 626 (2000) and O. Trovarelli, to be published.
12. A. Schroeder, G. Aeppli, D. F. McMorrow, E. Bucher, *Physica B*, in press.

ULTRASONIC MEASUREMENTS AT THE METAMAGNETIC TRANSITION IN URu_2Si_2

A. SUSLOV,* D. DASGUPTA, J. R. FELLER, B. K. SARMA

Department of Physics, University of Wisconsin-Milwaukee, P.O. Box 413 Milwaukee, WI 53201, U.S.A.
E-mail: alexei@uwm.edu

J. B. KETTERSON

Department of Physics and Astronomy, Northwestern University, Evanston, IL 60208, U.S.A.

D. G. HINKS

Materials Science and Technology, Argonne National Laboratory, Argonne, IL 60439, USA

M. JAIME, F. BALAKIREV, A. MIGLIORI, A. LACERDA

NHMFL, Los Alamos National Laboratory, Los Alamos, NM 87545, U.S.A.

Ultrasonic velocity measurements were performed on a single crystal of URu_2Si_2 at various temperatures in the 20 ms 50T pulsed magnets at the NHMFL, Los Alamos, NM. At 4 K a three-fold splitting of the metamagnetic transition is seen; corresponding features were observed earlier in magnetization studies. As the temperature is raised, the three-fold splitting evolves first into two features, then into a single broad dip, after which it disappears entirely.

1 Introduction

URu_2Si_2 is compound showing most the interesting low temperature properties that are characteristics of heavy fermion systems: superconductivity (1.2-1.4K), antiferromagnetism (17.5K), and metamagnetism (35-40). The metamagnetism is evidenced by an increase in magnetization: in this case there is a three-step structure in the field range 35-40 T (see Refs. [1,2]). Experiments above 33 T must usually be performed on fast pulsed magnets, thus limiting the number of techniques that can be used. Ultrasound is a powerful tool for studying phase transitions in superconductors and magnetic systems. Recently we have assembled various ultrasonic spectrometers designed for fast data acquisition in pulsed fields[3] which were used here to study metamagnetism in URu_2Si_2.

2 Experiment

The ultrasonic measurements were performed at NHMFL, Los Alamos, on the 20ms 50T magnets. Longitudinal sound was propagated both along the c-axis and in the basal plane of a URu_2Si_2 single crystal (2.8mm x 3.7mm x 1.7mm). The c-axis measurements were somewhat difficult to do because of the short length of the crystal in this direction. The sample was bathed in helium and measurements performed in the frequency range 15-200MHz and at temperature from 4-45K. A small pick up coil of 5 turns close to the sample was used to measure the flux during the magnet pulse, from which the magnetic field was determined. At temperatures 4K and above, there was no apparent heating during the magnet pulse.

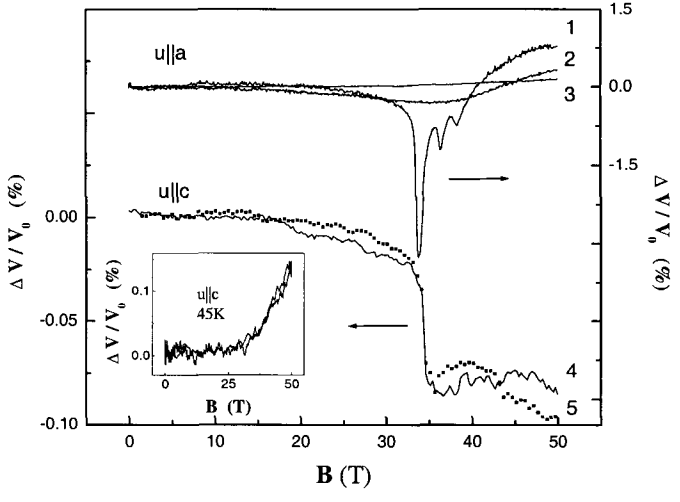

Figure 1: Relative velocity change in the vicinity of the metamagnetic transition in URu_2Si_2 for different temperatures, frequencies and directions of sound propagation: 1 - 4K, 27MHz, 2 – 20K, 27MHz, 3 – 45K, 27MHz, 4 – 4K, 50MHz, 5 – 4K, 115MHz. Insert: Measurements at 45K (curve 3) at expanded scale (×40); the field was swept both up and down.

3 Results and discussion

Metamagnetic behavior is seen when magnetic field is applied along the c-axis. No such behavior is seen with field in the basal plane. This agrees well with the earlier magnetic susceptibility measurements[1] and recent ultrasonic measurements.[4] As in

the case with UPt_3, a softening of the lattice is seen at the metamagnetic transition (Fig. 1). However the easy axis in URu_2Si_2 is the c-axis, whereas in UPt_3 the easy axis is in the basal plane. There is a softening of the lattice (a dip in the velocity) at the metamagnetic transition. At 4K there is a 3 percent change in the velocity of longitudinal sound propagating along the a-axis, accompanied by a three fold splitting (which has also been seen in magnetic susceptibility measurements).[1] As the temperature is raised, the magnitude of the dips decreases, the three dips merge into two (at about 14 K), then one, and finally disappear (see the inset on Fig. 1).

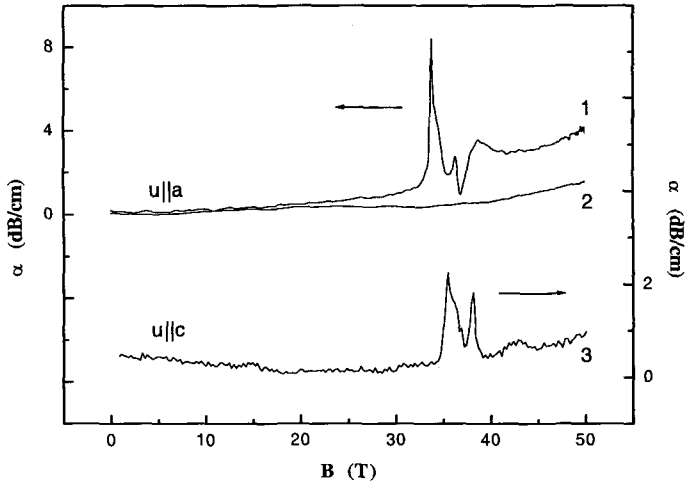

Figure 2: Magnetic field dependence of the ultrasound attenuation in URu_2Si_2 at different temperatures, frequencies and sound propagation directions: 1–4K, 27MHz, 2–20K, 27 MHz, 3–50MHz.

For sound along the c-axis, the change in velocity is much smaller. There seems to be a step decrease at 35 T (50 times smaller than the dip for sound along the a-axis), which, after background subtraction, may be interpreted as a dip. The corresponding attenuation is shown in Fig. 2. For sound along the a-axis there is a corresponding attenuation peak associated with the velocity dips. For sound along the c-axis there is a two-peak behavior in the attenuation.

Acknowledgments

This work is supported by the National Science Foundation under grant numbers DMR-9971123 and DMR-9704020. The NHMFL is supported by the NSF, the State of Florida and the U. S. Department of Energy.

* Permanent address: A. F. Ioffe Physical-Technical Institute, Russian Academy of Sciences, St.Petersburg, Russia.

References

1. K. Sugiyama *et al., J. Phys. Soc. Jpn.* **68**, 3394 (1999).
2. A. de Visser *et al., Solid State Comm.* **64**, 527 (1987).
3. A. Suslov *et al., Ultrasonic spectrometers for condenced matter studies at very high magnetic fields*, these proceedings.
4. B. Wolf *et al., J. of Mag. Mag. Mat.* **226-230**, 107-109 (2001).

Contributed Papers

This page is intentionally left blank

HIGH-FIELD MAGNETIZATION, LONGITUDINAL AND TRANSVERSE MAGNETORESISTANCE OF UIrGe

S. CHANG[†]

MST-10, Los Alamos National Laboratory, MS K764, Los Alamos, NM 87545, USA

H. NAKOTTE and A. M. ALSMADI

Physics Department, New Mexico State University, MSC-3D, Las Cruces, NM 88003,USA

A. H. LACERDA and M. H. JUNG[†]

National High Magnetic Field Laboratory, Pulsed Field Facility, Los Alamos National Laboratory, Los Alamos, NM 87545, USA

M. MIHALIK

Institute of Experimental Physics, Slovak Academy of Sciences, 04354 Košice, and Slovak Republic

K. PROKEŠ[‡]

Hahn-Meitner-Institute, SF-2, Glienickerstrasse 100, D-141 09 Berlin, Germany

J. C. P. KLAASSE, E. BRÜCK, F. R. DE BOER

Van der Waals-Zeeman Instituut, Universiteit van Amsterdam, Valckenierstraat 65, 1018 XE, Amsterdam, The Netherlands

UIrGe crystallizes in the orthorhombic TiNiSi structure and undergoes an antiferromagnetic transition around 14.1 K. The low-temperature longitudinal magnetoresistance (I // B) exhibits a pronounced field-induced step at about 13 T (14 T) and a much weaker step at about 17 T (out of field range) for B // *b* axis (*c* axis). No transition was seen for B // a. Here, we report on the magnetization results in fields up to 38 T applied along the principle directions. In addition, we present new magnetoresistance results taken in the transverse (I ⊥ B) configuration in fields up to 18 T applied along the *c* axis. The data show intriguing differences in comparison to those taken in the longitudinal configuration. The results are discussed in terms of field-induced magnetic transitions and/or Fermi-surface changes.

Isostructural UTX (T = transition metal, X= p-electron element) compounds that crystallize in the orthorhombic TiNiSi structure display a rich variety of moment configurations, unlike those with the hexagonal ZrNiAl structure, which exhibit strong uniaxial *c*-axis magnetism.[1-4] Despite intensive studies of both of these isostructural groups, the detailed mechanisms that determine the moment configuration and magnetic anisotropy in UTX compounds remain unclear. Of the UTX compounds with the TiNiSi structure, UIrGe is one of the most puzzling examples. Bulk studies on polycrystalline UIrGe showed metallic transport behavior

but is inconsistent with single-crystal studies in which the resistivity increased sharply below 14 K, indicating the formation of an antiferromagnetic gap in the Fermi surface.[5] Recent pressure experiments suggest internal pressure as an explanation of the apparent contradictions between the behavior of poly- and single-crystalline UIrGe but the idea remains speculative.[6] Further, bulk single-crystal studies that indicated an antiferromagnetic ground state were supported by muon spin resonance experiments, while all neutron diffraction experiments, to date, have failed to verify long-range magnetic order.[7-9]

Here, we present magnetization measurements in magnetic fields applied along the principal axes. Further, we compare new magnetoresistance results for B // c axis, taken in the transverse (I $\perp$ B) configuration, with previous data that were measured in the longitudinal (I // B) configuration. It is worth noting that the measurements were performed on the same set of single crystals used for our previous magnetoresistance studies.[10]

We measured the high-field magnetization of UIrGe in fields up to 38 T applied along the principle axes at the High Field Facility, Van der Waals-Zeeman Institute, University of Amsterdam. The magnetic response of an 11 mg sample of UIrGe was measured using an experimental set-up with a sensitivity of about 3×10^{-6} A m^2. Figure 1(a) shows the high-field magnetization with fields applied along the principle axes at 4.2 K. For B // *a* axis, we observed a linear magnetization with a value of about 0.2 Bohr-magneton at 38 T, which is about 5 and 3 times smaller than the *b*- or *c*-axis response, respectively. For B // *b* axis, a single sharp metamagnetic transition with a step size of approximately 0.2 μ_B appears at about 12.3 T. No additional step-like transition is seen but there is some indication of a change in the slope of the magnetization curve at about 18 T. In the case of B // *c* axis, the slope of the magnetization curve clearly increases around 13 T and the step-like transition, again with a step size of about 0.2 μ_B follows at about 20 T. The transition fields are consistent with phase boundaries derived from magnetoresistance and specific heat measurements.[10]

The magnetoresistance of UIrGe was measured in fields up to 18 T applied along the *c* axis, using the 20 T superconducting magnet at the Pulsed Field Facility, National High Magnetic Field Laboratory, Los Alamos National Laboratory. A standard four-point technique was employed in the transverse configuration. We measured the temperature dependence of the resistivity at various fixed fields and the field dependence at various fixed temperatures. The overall results were similar to previous data taken in the longitudinal configuration but with some striking differences. At 2.1 K, a field induced transition around 14 T results in a drop in the magnetoresistance to about 85% of the zero field value. The transition field corresponds well with the longitudinal data, but the magnitude of the drop is only a third of what was seen in the longitudinal data. The second metamagnetic transition was out of the available field range but is clearly visible at slightly higher

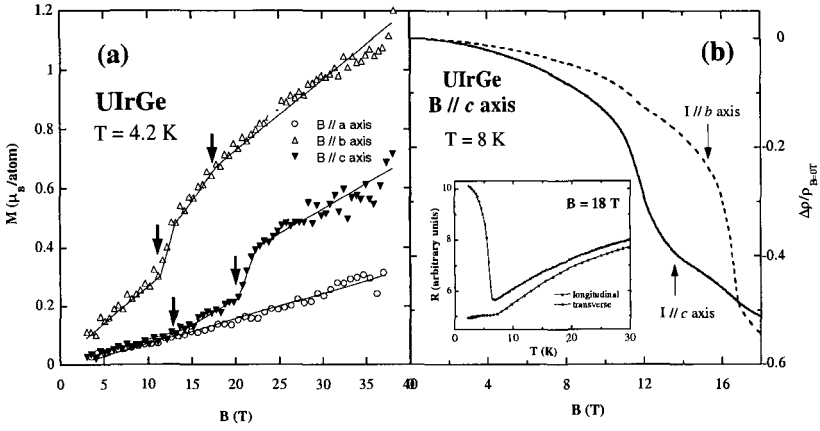

Figure 1: (a) High field magnetization of UIrGe at 4.2 K. The *a*-axis magnetization is linear while for B // *b* and *c* axis, a step-like metamagnetic transition appears at about 12.3 T and 20 T, respectively. A slight change in slope may be discerned at about 18 T for B // b axis and about 13 T for B // c axis. (b) A comparison of longitudinal and transverse magnetoresistance of UIrGe at 8 K. Both curves exhibit two metamagnetic transitions but the relative magnitudes of the responses are inverted in going from the longitudinal to the transverse configurations. The inset of (b) shows the temperature dependence of the resistivity of UIrGe at 18 T. The sharp upturn in the low-temperature resistivity, indicative of an antiferromagnetic super-zone gap, is suppressed in the longitudinal configuration.

temperatures. Figure 1(b) shows the magnetoresistance at 8 K. Here, a small step in the magnetoresistance around 12 T is followed by a drastic fall around 16.5 T to less than 50% of the zero field value. This is, in some sense, inverse of the longitudinal configuration case, in which a pronounced drop in the magnetoresistance was followed by a much weaker transition at higher fields. In temperature scans at fixed fields, the resistivity increases below $T_N \approx 14.4$ K and the transition moves to lower temperatures with increasing applied fields, in good agreement with measurements taken in the longitudinal configuration. The inset of Figure 1(b) shows the temperature dependence of the resistivity in a field of 18 T applied along the *c* axis. Unlike the data taken in the longitudinal configuration, the upturn in low temperature resistivity, which is believed to be connected to an opening of an antiferromagnetic gap in the Fermi surface, is not suppressed by application of a field up to 18 T. Furthermore, we observed only one clear anomaly in the temperature scans, whereas data taken in the longitudinal configuration showed two transitions in the fixed field range of 11 – 13 T (see Ref. [10]).

To summarize, we have measured the high-field magnetization of UIrGe in fields up to 38 T applied along the principle axes and extended our previous magnetoresistance studies to measurements in the transverse configuration for fields applied along the *c* axis. We observed substantial differences between the two sets of magnetoresistance data (transverse and longitudinal configurations), which

suggests a highly anisotropic Fermi surface in UIrGe. In addition, given that only one metamagnetic transition appears clearly in the magnetization curves, one may speculate that only one of the metamagnetic transitions involves a change in the magnetic structure. However, an unambiguous description of even the zero-field structure has still not been established. Clearly, a microscopic determination of the magnetic structures is necessary to clarify the nature of the transitions in UIrGe.

Acknowledgments

This work was supported by a grant from NSF (grant number: DMR-0094241). Work at the National High Magnetic Field Laboratory in Los Alamos was performed under the auspices of the NSF (INT-9722777), the US Department of Energy and the State of Florida.

References

[†]Also at the Physics Department, New Mexico State University
[‡]On Leave from the Department of Electronic Structures, Charles University, 12116 Prague 2, the Czech Republic

1. K. H. J. Buschow *et al., J. Appl. Phys.* **67**, 5212 (1990).
2. V. Sechovsky *et al., Physica B* **136**, 103 (1990).
3. L. Havela *et al.,Physica B* **177**, 159 (1992).
4. V. Sechovsky *et al.,Physica B*, **177**, 164 (1992).
5. K. Prokeš *et al.,Phys Rev* B, **60**, 9532 (1999).
6. A. M. Alsmadi *et al.*, submitted to *J. Appl. Phys.*
7. K. Prokeš *et al.*, (unpublished)
8. V. H. Tran *et al., Solid State Commun,* **98**, 111 (1996).
9. R. A. Robinson *et al., MLNSC-LANSCE Progress Report*, (1993).
10. S. Chang *et al., J. Appl.Phys.*, **89**, 7186 (2001).

High Field Magnetotransport in $CeRh_{1-x}Ir_xIn_5$ Heavy Electron Alloys

A. D. CHRISTIANSON* and A. H. LACERDA
National High Magnetic Field Laboratory, MS E536, Los Alamos National Laboratory, Los Alamos, NM 87545, USA

P. G. PAGLIUSO, N. O. MORENO, M. F. HUNDLEY, and J. L. SARRAO
Condensed Matter and Thermal Physics Group, MS K764, Los Alamos National Laboratory, Los Alamos, NM 87545, USA

**Also of the Manuel Lujan Jr. Neutron Scattering Center, Los Alamos National Laboratory, Los Alamos, NM 87545 and the Physics Department, Colorado State University, Fort Collins, CO 80523*

The interplay of magnetism and superconductivity has been a recurring theme in heavy fermion compounds. Recently, alloys of $CeRhIn_5$ (antiferromagnet at 3.8 K) and $CeIrIn_5$ (superconductor at 0.4 K) have been grown, i.e. $CeRh_{1-x}Ir_xIn_5$. For x = 0.5, specific heat and magnetic susceptibility measurements indicate at ~3.6 K an antiferromagnetic transition occurs. Decreasing temperature still further, a superconducting transition is observed at 0.8 K. Thus this alloy series offers the possibility of exploring the coexistence of superconductivity and magnetism in a Ce-based heavy fermion system. We have initiated a magnetotransport study from 1.4 to 300 K with applied fields to 18 T, to probe the behavior of these systems at temperatures above the possible coexistence region. In this paper we will focus on comparing the high field magnetotransport properties of $CeRh_{0.9}Ir_{0.1}In_5$ to the end compounds $CeRhIn_5$ and $CeIrIn_5$.

1 Introduction

Recently a new family of tetragonal (space group P4/mmm) Ce-based heavy fermions was discovered.[1] This family has a generalized chemical formula, $CeMIn_5$, where M is Rh, Ir, or Co. Interesting properties in this series of compounds include magnetic ordering and pressure induced superconductivity in $CeRhIn_5$ (see Ref. [1]), ambient pressure superconductivity at 0.4 K in $CeIrIn_5$ (see Ref. [2]), and the highest ambient pressure T_c of 2.3 K for a heavy fermion superconductor in $CeCoIn_5$ (see Ref. [3]). This new family of compounds offers the opportunity to explore new examples of Ce-based heavy fermion superconductors and the role played by high magnetic fields on the ground state properties.

$CeRhIn_5$ first attracted attention due to its unusual pressure induced superconductivity.[1] In contrast to $CeIn_3$ (see Ref. [4]), the antiferromagnetic transition temperature (3.8 K at ambient pressure) remains essentially pressure independent until disappearing and giving way to a superconducting state at 2.1 K and 16 kbars.[1] At ambient pressure the magnetic structure is an incommensurate spiral along the c-axis with the moments ($0.37\mu_B$) lying completely in the basal plane of the tetragonal structure.[5] Upon alloying with $CeIrIn_5$, the antiferromagnetic transition temperature remains roughly constant until about x = 0.45, after which T_N

drops sharply.[6] At x = 0.3 a superconducting state begins to emerge at low temperature until at x = 0.5 the superconducting transition temperature has risen close to 1 K (see Ref. [6]). In the possible region of coexistence of superconductivity and magnetism, a separate anomaly in the specific heat is observed at the magnetic and superconducting transition temperatures.[6] This indicates at least two possibilities: one is that the magnetism gives way to a superconducting ground state and another that superconductivity and magnetism coexist. Preliminary neutron diffraction studies of $CeRh_{1-x}Ir_xIn_5$ for $0 < x < 0.5$ suggest that the magnetic wave vector, q_M = (1/2, 1/2 ,0.29), remains nearly the same as $CeRhIn_5$ at ambient pressure.[7] In order to better understand the possible region of coexistence, we have initiated a magnetotransport study of the normal state in these materials. Previous magnetotransport studies have revealed several interesting properties of the heavy fermion ground state in $CeRhIn_5$ (see Ref. [8]) and $CeIrIn_5$ (see Ref. [9]). In this paper we will focus on comparing the high field magnetotransport properties of $CeRh_{0.9}Ir_{0.1}In_5$ to the end compounds $CeRhIn_5$ and $CeIrIn_5$.

2 Results and Discussion

Sample preparation and experimental details have been reported previously in Ref [8]. An overview of the magnetotransport is displayed in Fig. 1: (a) displays the resistivity at 0 and 18 T for $CeRhIn_5$. A rapid decrease in the resistivity is observed at ~ 40 K which is due to the combined effects of the onset of coherence and crystal fields.[5] The resistivity at 18 T crosses the zero field data at ~20 K. The inset displays the low temperature behavior in which the resistive signature of the antiferromagnetic transition may be observed as slight downturn in the resistivity (the arrows indicate the inflection point in the resistivity). (b) displays the resistivity at 0 and 18 T for $CeIrIn_5$. A broad maximum occurs at 50 K after which the resistivity drops rapidly down to the lowest temperature measured for both 0 and 18 T. The inset displays the low temperature behavior. The low temperature data (2 - 10 K) may be fit with a power law obtaining exponents of 0.91 for 0 and 1.5 for 18 T. This may be an indication that the effect of higher applied magnetic fields is to cause the recovery of T^2 behavior in the resistivity at low temperatures. (c) displays the resistivity at zero and 18 T for $CeRh_{0.9}Ir_{0.1}In_5$. The downturn in the resistivity due to the combination of the onset of coherence and crystal fields has almost become a maximum similar to $CeIrIn_5$. The magnetoresistance centered around 20 K is the largest of the three compounds in this paper. The signature of the antiferromagnetic transition remains even at 18 T.

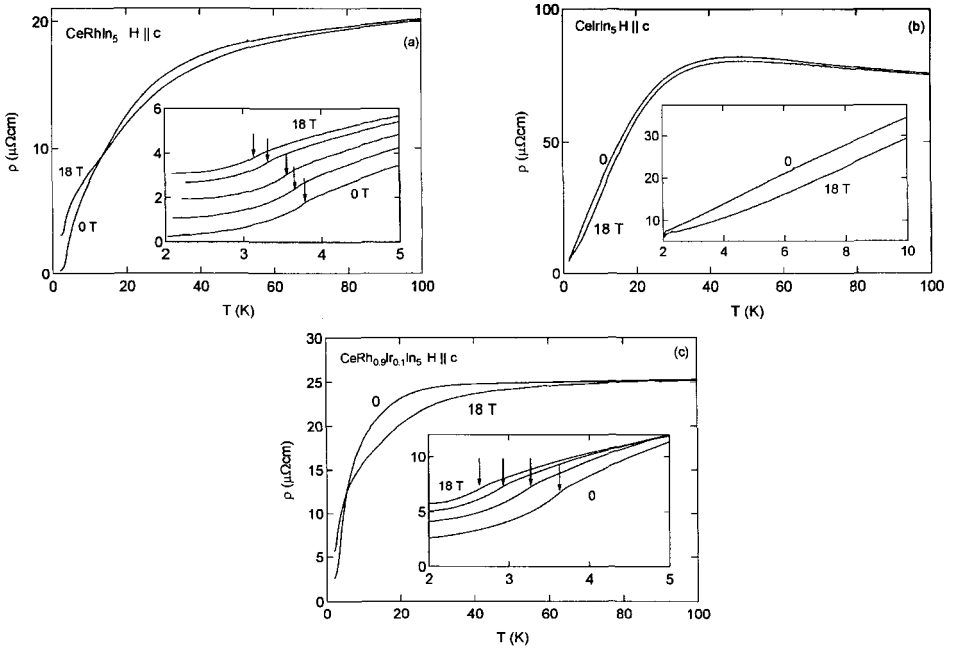

Figure 1: Temperature dependence of the resistivity of CeRhIn5 (a), CeIrIn5 (b), CeRh0.9Ir0.1In5 (c). In the inset in (a) and (c) the arrows indicate the inflection point in the resistivity signifying the antiferromagnetic transition. The curves in the inset correspond to 0, 5, 10, 15, 18 T (a) and 0, 10, 15, 18 T (c). The inset in (b) displays the low temperature resistivity of CeIrIn5.

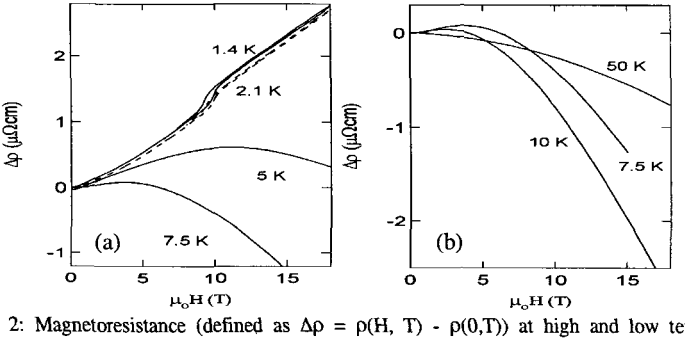

Figure 2: Magnetoresistance (defined as $\Delta\rho = \rho(H, T) - \rho(0,T)$) at high and low temperature for $CeRh_{0.9}Ir_{0.1}In_5$.

Figure 2 displays the low (a) and high (b) temperature magnetoresistance of $CeRh_{0.9}Ir_{0.1}In_5$. At low temperature the magnetoresistance is similar in magnitude and shape as $CeRhIn_5$ (see Ref. [5]). A small feature, which exhibits hysteresis appears at ~9.5 T in the 1.4 and 2.1 K data. At 5 K the magnetoresistance exhibits a broad maximum. At higher temperatures the negative term in the magnetoresistance becomes increasingly more important until at high temperatures only a negative magnetoresistance is observed. The negative magnetoresistance which is observed at high temperatures likely corresponds to a single impurity-like regime developing above about 10 K, in contrast to the single impurity regime which develops at somewhat higher temperatures in $CeRhIn_5$ (see Ref. [5]).

In conclusion we have presented magnetotransport data for $CeRhIn_5$, $CeIrIn_5$, and $CeRh_{0.9}Ir_{0.1}In_5$. By replacing only 10% of Rh with Ir, the sharp downturn in the resistivity of $CeRhIn_5$ due to the combined effects of the onset of coherence and crystal fields has already become qualitatively similar to that of $CeIrIn_5$. The behavior of the magnetoresistance of CeRhIn5 and $CeRh_{0.9}Ir_{0.1}In_5$ is similar at low temperature. The magnetoresistance in the high temperature single impurity-like regime in $CeRhIn_5$ is comparable to the magnetoresistance above 10 K in $CeRh_{0.9}Ir_{0.1}In_5$. Future studies will focus on extending the magnetotransport measurements across the alloy series as well as investigating the behavior down to lower temperatures.

Acknowledgments

We gladly acknowledge useful discussions with S. Kern (Colorado State University). The work at the National High Magnetic Field Laboratory, Los Alamos Facility, was performed under the auspices of the National Science Foundation, State of Florida, and the U.S. Department of Energy.

References

1. N. D. Mathur *et al.*, *Nature* **394**, 39 (1998).
2. H. Hegger *et al.*, *Phys. Rev. Lett.* **84**, 4986 (2000).
3. C. Petrovic *et al.*, *Europhys. Lett.* **53**, 354 (2001).
4. C. Petrovic *et al.*, *J. Phys.: Condens. Matter* **13**, L337–L342 (2001).
5. W. Bao *et al.*, *Phys. Rev. B* **62**, 14621 (2000); **63**, 219901(E) (2001).
6. P. G. Pagliuso *et al.*, *Phys. Rev. B* **64**, 100503(R) (2001).
7. A. D. Christianson *et al.*, *unpublished.*
8. A. D. Christianson, *et al.*, submitted to *Phys. Rev. B*, cond-mat/0109062.
9. A. D. Christianson, *et al.*, *in preparation.*

dHvA MEASUREMENTS ON $La_{1-x}Ce_xMIn_5$ WHERE M=Rh, Ir AND Co

R. G. GOODRICH,[1] U. ALVER,[1] N. HARRISON,[2] J. L. SARRAO,[3] D. HALL,[4] and Z. FISK[4]

[1]*Louisiana State University, Department of Physics, 202 Nicholson Hall, Baton Rouge, LA 70803*

[2]*Los Alamos National Laboratory, NHMFL, MS E536, Los Alamos, New Mexico 87545, USA*

[3]*Los Alamos National Laboratory, Condensed Matter and Thermal Physics, MS K764, Los Alamos, New Mexico 87545, USA*

[4]*NHMFL-Tallahassee, Florida State University, 1800 E. Paul Dirac Dr., Tallahassee, Florida, 32310USA*

Measurements of the de Haas-van Alphen effect in $Ce_xLa_{1-x}MIn_5$ show that x dependence for the three different values of M behaves quite differently. The Ce $4f$ electrons remain localized and have little interaction for all x in the Rh alloys, but strongly interact with the conduction electrons in both the Ir and Co alloys. Both the dependence on x of the observed frequencies and the effective masses are presented. Preliminary measurements on $CeRh_{1-x}Ir_xIn_5$ will also be given.

ANISOTROPIC PROPERTIES OF SINGLE-CRYSTALLINE $CeNiGe_2$

M. H. JUNG,* N. HARRISON and A. H. LACERDA
National High Magnetic Field Laboratory – Pulse Facility, Los Alamos National Laboratory, MS E536 Los Alamos, NM 87545, USA
E-mail: mhjung@lanl.gov

P. G. PAGLIUSO, J. L. SARRAO and J. D. THOMPSON
Condensed Matter and Thermal Physics, Los Alamos National Laboratory, MS K764 Los Alamos, NM 87545, USA

The anisotropic properties of $CeNiGe_2$ with a layered crystal structure have been studied by measurements of electrical resistivity, magnetic susceptibility and magnetization. It is confirmed that $CeNiGe_2$ undergoes two-step antiferromagnetic transition at T_N^{I} = 4 K and T_N^{II} = 3 K as reported earlier on polycrystalline samples. $CeNiGe_2$ is found to exhibit highly anisotropic properties with an easy magnetization axis along the longest crystallographic *b* direction. The magnetization ratio $M(H//b)/M(H\perp b)$ is estimated to be about 15 at 5 T. The in-plane resistivity $\rho_{\perp b}(T)$ shows double maxima typical of that expected when an interplay of crystal-field and Kondo effects plays a role. The low-*T* maximum at 4 K in $\rho_{\perp b}(T)$ is strongly suppressed with increasing magnetic field. This negative magnetoresistance is a result of the strong reduction of magnetic scattering by the ferromagnetic alignment of Ce magnetic moments.

Ce-based intermetallics are of fundamental importance for the understanding of their various ground states. The type of magnetic ground state in heavy-fermion compounds is controlled by the competition between the indirect RKKY exchange (T_{RKKY}) and on-site Kondo (T_K) interactions. For the strong-hybridization limit ($T_K > T_{RKKY}$), the ground state is nonmagnetic as found in $CeCu_6$ (see Ref. [7]). In the limit of medium to week hybridization ($T_K \approx T_{RKKY}$), different ground states can be found. CePdSn is a typical Kondo antiferromagnet with T_N = 7 K (see Ref. [9]), while $Ce_2Ni_3Ge_5$ exhibits two magnetic phase transitions at T_{N1} = 5.1 K and T_{N2} = 4.5 K (see Ref. [5]). For the weak-hybridization limit ($T_K < T_{RKKY}$), the system orders magnetically.

In the present paper, we report magnetization, magnetic susceptibility and electrical resistivity measurements on a single crystal of $CeNiGe_2$ grown by Sn-flux method. This material crystallizes in the orthorhombic $CeNiSi_2$-type layered structure with the lattice parameters of a = 4.25(3) Å, b = 16.78(9) Å, and c = 4.21(0) Å, close to those reported previously.[6] It has been reported that for polycrystalline samples of $CeNiGe_2$, a large Sommerfeld coefficient of γ = 220 mJ/K^2mol is obtained.[3] The magnetic susceptibility and specific heat measurements indicated two antiferromagnetic phase transitions at T_N^{I} = 4 K and T_N^{II} = 3 K (see Ref. [8]). However, the nature of two-step antiferromagnetic ordering below 4 K has not yet been elucidated. Furthermore, one can expect anisotropic properties in response to the direction of magnetic field along and perpendicular to the plane.

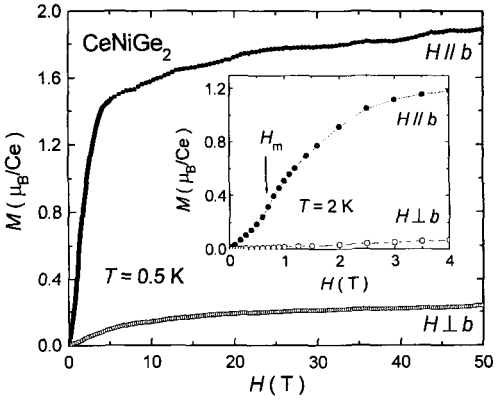

Figure 1: Isothermal magnetization $M(H)$ to 50 T of $CeNiGe_2$ single crystal measured at 0.5 K ($H//b$ and $H\perp b$). The inset shows the low-field data at 2 K.

Figure 1 displays the anisotropic behavior of the magnetization $M(H)$ of $CeNiGe_2$, which was measured at 0.5 K in magnetic fields to 50 T applied along the b axis ($H//b$) and in the plane ($H\perp b$). A clear anisotropy with an easy magnetization direction along the b axis is observed. In the inset of Fig. 1, $M(H//b)$ at 2 K shows a metamagnetic-like behavior around H_m = 0.7 T and then saturates rapidly to a value of 1.2 μ_B/Ce at 3 T. The high-field measurement indicated that $M(H//b)$ at 0.5 K reaches 2 μ_B/Ce at 50 T. On the other hand, $M(H\perp b)$ increases linearly with increasing magnetic field. At 5 T, the magnetization ratio of $M(H//b)/M(H\perp b)$ is estimated to be about 15.

The inverse of magnetic susceptibility $\chi^{-1}(T)$ in a field of 0.1 T for $H//b$ and $H\perp b$ as a function of temperature from 2 to 350 K is shown in Fig. 2. As expected from the $M(H)$ observations, the b-axis magnetic susceptibility $\chi_{//b}$ is much larger than the in-plane magnetic susceptibility $\chi_{\perp b}$ over all temperature range. Above 100 K, the data obey the Curie-Weiss law, $\chi = C / (T - \theta_P)$ with the paramagnetic Curie temperatures of $\theta_{//b}$ = 31.9 K and $\theta_{\perp b}$ = −168.2 K. This might indicate a development of ferromagnetic and antiferromagnetic exchange interactions for $H//b$ and $H\perp b$, respectively. From the value of $\theta_P = (\theta_{//b} + 2\theta_{\perp b}) / 3$, we can estimate the Kondo temperature $T_K \sim |\theta_P / 2|$ (see Ref. [1]), obtaining T_K = 51 K. The high-temperature slopes of χ^{-1} yield the effective magnetic moments of $\mu_{//b}$ = 2.11 μ_B and $\mu_{\perp b}$ = 2.22 μ_B, which is slightly smaller than the theoretical value (2.54 μ_B) expected for the free Ce^{3+} ion. This implies that the magnetic moments of Ce ions are well localized

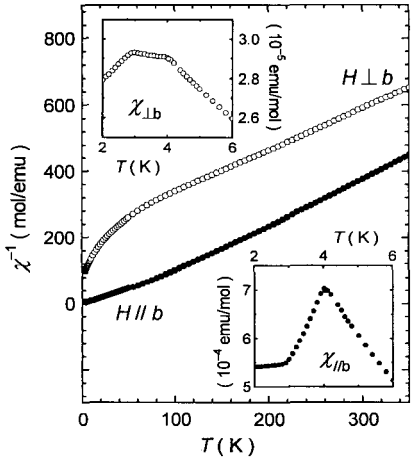

Figure 2: Inverse magnetic susceptibility $\chi^{-1}(T)$ of $CeNiGe_2$ in an applied magnetic field of 0.1 T ($H//b$ and $H \perp b$). The inset shows the low-temperature data.

in this material. However, it is important to notice that the deviation from the Curie-Weiss behavior below 100 K could be attributed to the crystal field effect. In the insets of Fig. 2, the low-temperature data of $\chi_{//b}$ and $\chi_{\perp b}$ exhibit two anomalies at 4 and 3 K indicating antiferromagnetic orderings.

In Fig. 3, we have plotted the in-plane resistivity $\rho_{\perp b}(T)$ as a function of temperature. A broad peak around 100 K, followed by a minimum at ~ 20 K, and a steep decrease below 4 K are observed. The resistivity features are typical under the influence of crystal field effect on the Kondo effect.[2] The steep decrease below 4 K could be attributed to the combined effect of the reduction of spin-disorder scattering and the development of coherence, as found in other Kondo antiferromagnetic compounds.[4,5,9] In the inset of Fig. 3, the maximum structure at 4 K is suppressed with increasing magnetic field. This negative magnetoresistance could be associated with the arrangement of magnetic spins, since the change of magnetoresistance coincides with the slope change of $M(H)$. However, the magnetic scattering in a ferromagnetic state is much weaker than that in an antiferromagnetic state, and thus the negative magnetoresistance could be a result of the strong reduction of scattering by the ferromagnetic alignment of Ce magnetic moments.

In summary, we have measured the magnetization, magnetic susceptibility and electrical resistivity on a single crystal of $CeNiGe_2$. This material can be classified

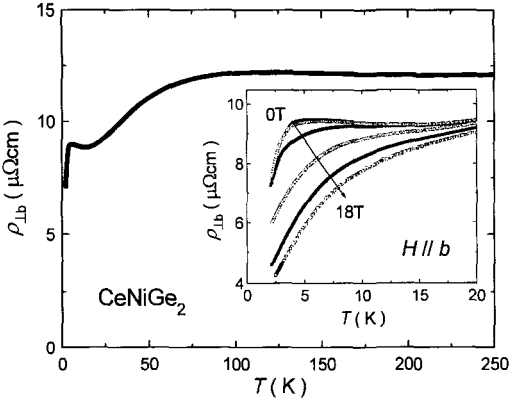

Figure 3: In-plane resistivity $\rho_{\perp b}(T)$ for $CeNiGe_2$. The inset shows $\rho_{\perp b}(T)$ at static fields of zero, 2, 5, 10, 15 and 18 T for *H//b*.

as a Kondo antiferromagnet (T_N^I = 4 K and T_N^{II} = 3 K) with a strong anisotropy arising from the quasi-2D crystal structure. It is found that the easy magnetization axis is parallel to the longest crystallographic *b* direction. The double maximum structure of the in-plane resistivity $\rho_{\perp b}(T)$ hints that the interplay of crystal-field and Kondo effects plays a role. The low-T maximum at 4 K in $\rho_{\perp b}(T)$ is suppressed with increasing magnetic field. This negative magnetoresistance is a result of the strong reduction of scattering by the ferromagnetic alignment of Ce magnetic moments.

We thank Prof. H. Nakotte for his helpful discussion. One of us (MHJ) acknowledges partial support from LANSCE - LANL.

References

* *Department of Physics, New Mexico State University, Las Cruces, NM 88003*

1. N. B. Brandt and V. V. Moshchalkov, *Adv. Phys.* **33**, 273 (1984).
2. B. Cornut and B. Coqblin, *Phys. Rev. B* **5**, 4541 (1972).
3. C. Geibel *et al.*, *J. Magn. Magn. Mater.* **108**, 207 (1992).
4. Z. Hossain *et al.*, *Phys. Rev. B* **60**, 10383 (1999).
5. Z. Hossain *et al.*, *Phys. Rev. B* **62**, 8950 (2000).
6. A. V. Morozkin *et al.*, *J. Alloys Com.* **264**, 190 (1998).
7. Y. Onuki *et al.*, *J. Phys. Soc. Jpn.* **53**, 1210 (1984).
8. V. K. Pecharsky *et al.*, *Phys. Rev. B* **43**, 10906 (1991).
9. J. Sakurai *et al.*, *J. Magn. Magn. Mater.* **84**, 157 (1990).

"HIGH-TEMPERATURE" OSCILLATIONS OF BISMUTH CONDUCTIVITY IN THE ULTRA-QUANTUM LIMIT

V. B. KRASOVITSKY
Institute for Low Temperature Physics and Engineering,
47 Lenin Ave. 61103 Kharkov, Ukraine
krasovitsky@ilt.kharkov.ua

The special quantum oscillations of the kinetic coefficients in magnetic field ("high-temperature" oscillations – HTO) discovered by the author in 1974 have been considered. The oscillations are periodic in the reciprocal magnetic field and are characterized by a frequency higher then that of Shubnikov–de Haas (SdH) oscillations. The results of joint studies of SdH oscillations and HTO of the magnetoresistance for pure Bi and alloy BiSb in magnetic field up to 33 T are presented. The oscillations are measured for different magnetic field directions at temperature 4 – 30 K. It was found that SdH holes oscillations and holes HTO reached its quantum limit at the same value of magnetic field. The analysis of the experimental data verified one of two alternative models of HTO.

1 Introduction

A new type of quantum oscillations of static conductivity of bismuth in a magnetic field was discovered by the author in 1974 (see Ref. [1]). The new oscillations are periodic in reciprocal magnetic field and are characterized by a frequency higher than that of Shubnikov-de Haas (SdH) oscillations. In contrast to SdH oscillations observed at $T \leq 4$ K, the new oscillations were registered in temperature range 6–65 K and were referred to as "high-temperature" oscillations (HTO) (see Ref. [2]). At high temperatures, HTO are observed for $T > \hbar \Omega_c$ (Ω_c is the characteristic cyclotron frequency), when SdH oscillations are exponentially small. HTO are investigated on bismuth samples of various quality, in compensated alloys $Bi_{1-X}Sb_X$ and in not compensated alloys $Bi_{1-X}(Te, Sn)_X$. The thermo-emf HTO in a magnetic field has also been studied.

The correlation between the HTO frequency F and the concentration n of charge carriers ($F \sim n^{2/3}$) was established in experiments carry out with bismuth and compensated bismuth semimetallic bismuth-based alloys.[3] In the more general case of semimetallic alloys of bismuth with different numbers of electrons and holes, it was found that $F \propto \varepsilon^e_F + \varepsilon^h_F = \varepsilon_p$ (see Ref. [4]) (ε^e_F and ε^h_F are the Fermi energy of electrons and holes and ε_p is of the energy bands overlapping region). Thus, the characteristic feature of HTO distinguishing them from other quantum oscillations in a magnetic field is the independence of the HTO frequency of the Fermi energy.

HTO differ basically from SdH oscillations in peculiar temperature dependence: the HTO amplitude rapidly attains its peak value at $T \approx 10$ K and then decreases slowly upon heating.[4] It was found[5] that the existence of a peak on the HTO amplitude ρ (T) dependence is determined by the relation $(\tau_{ep}^m)^{-1} >> (\tau_i^m)^{-1}$,

where $(\tau_{ep}^{m})^{-1} \sim \exp(-\vartheta_m/T)$ is the frequency of the intergroup electron-hole transitions associated with inelastic scattering by acoustic phonons, and $(\tau_i^{m})^{-1}$ is the frequency associated with quasielastic scattering at the impurities ($\vartheta_m = \hbar S q_m / k_B$, q_m being the phonon wave vector corresponding to the separation between the characteristic points on the electron and hole branches of the spectrum).

The oscillations period for quasi-elastic scattering in the simplest case of quadratic dispersion law for charge carriers is given by $\Delta B^{-1} = e \hbar / m^{*}_{e,h} c \varepsilon_p$. For inelastic scattering of electrons by acoustic phonons the following expressions were received (see Ref. [5]): $\Delta B^{-1} = e \hbar / m^{*}_{e,h} c (\varepsilon_p \pm k_B \vartheta_m)$.

Recently two alternative models tried to explain qualitatively of the HTO nature.

According to[6] the HTO emerge due to the electron-hole transitions near the boundaries of the energy bands in the L and T points of the Brillouin zone. Every time the Landau subband extremum for the hole band of the spectrum appears near the bottom of the conduction band, the collision frequency suffers a discontinuity because the density of electron states below the bottom of the conduction band is equal to zero. This is also true for transitions between the Landau levels of the electron branch of the spectrum and the top of the valence band (point T). Authors[6] suppose that in the temperature region $T << \varepsilon_F / k_B$ the number of unoccupied states below the Fermi level ε_F (and the number of occupied states above ε_F) is not exponentially small but one is determined by the broadening of the energy levels due to relaxation processes (both elastic and inelastic).

In paper[9] an alternative model[6] for explanation of the HTO nature was offered. According to[9] oscillations of conductivity are a result of electron–hole transitions close to a Fermi level. The necessary condition for HTO appearance in model[9] is that the effective electron and hole masses must be commensurable ($k m_e^* \approx k' m_h^*$ with integers k and k'). In this case the appropriate extrema of electron and hole Landau subbands have a simultaneous tangent in the vicinity of the Fermi level.

For final confirmation conclusions concerning the HTO physical nature it is necessary to carry out a set of joint measurements of Shubnikov-de Haas hole frequency oscillations and hole ``high-temperature`` oscillations in a monocrystals bismuth and alloy BiSb in strong magnetic fields (up to 30-40 T). Shubnikov-de Haas hole oscillations reached its quantum limit when magnetic fields is so high. Under these conditions according to the holes HTO behavior it will be possible to obtain the appropriate conclusions on their nature.

2 Experiment and evaluation of results

The measurements of SdH oscillations and HTO were made in stationary magnetic fields up to 33T on pure bismuth and alloy $Bi_{1-X}Sb_X$ (x =2.6 at. %) samples under the conditions when $I \,||\, X \,||\, C_2$, $B \perp C_2$ ($C_3 \,||\, Z$, C_2 and $C_1 \,||\, Y$ – trigonal, binary and bisector crystallographic axes, respectively and I is the current). Since the HTO

amplitude does not normally exceed 0,1–1 % of the monotonic magnetoresistance component, we used in our measurements the following peculiar property of the nondiagonal component ρ_{yx} of the magnetoresistance tensor:[7] the monotonic component of the even part ρ_{yx} vanishes in view of symmetry for exact orientation B $||C_3$, while the oscillating component remains unchanged. For this reason, SdH oscillations and HTO were measured in the angular interval ±10° relative to direction B $||C_3$. In the temperatures 4–15K SdH oscillations prevail in the dependencies $\rho_{yx}(H)$, while HTO dominate above ~15K.

The results for SdH oscillations (4.3 K) and HTO (15 K) are presented in Fig.1.

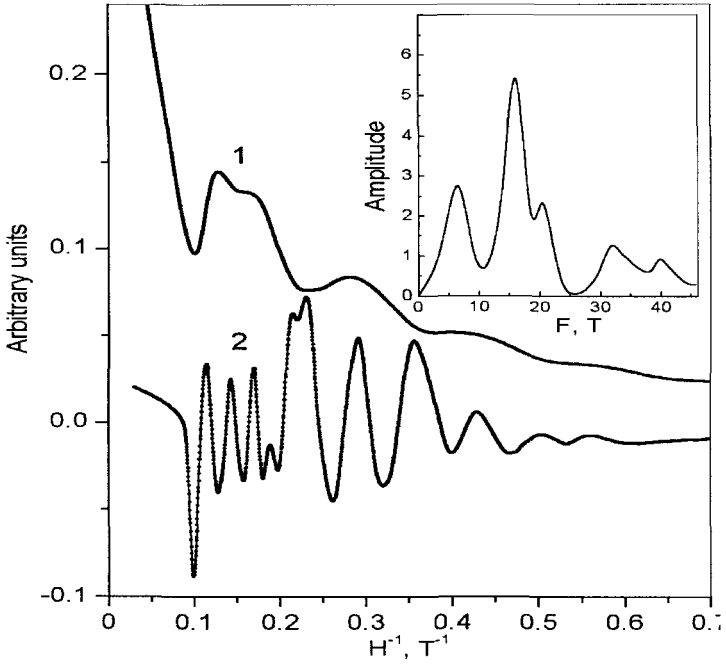

Figure 1: Dependence of ρ_{yx} at 4.3 K(curve 1) and ρ''_{yx} at 15 K (curve 2) on the reciprocal magnetic field, B $||C_3$.

The SdH oscillations' ρ_{yx} period of bismuth as a function of the inverse magnetic field is $\Delta(1/B) = 0.155\ T^{-1}$.This value corresponds to the area of the extremal section of the hole Fermi surface.[8] The last minimum at ~10 T corresponds to the crossing of the Fermi surface of the level (1, +) (a ratio between the Zeeman energy to the cyclotron energy close to 2).

"High-temperature" oscillations can be detected reliably on the second derivative ρ_{yx}'' obtained as a result of computer processing of the corresponding curve $\rho_{yx}(B)$. The dependence $\rho_{yx}''(B^{-1})$ is shown in Fig.1 (curve 2). Fourier

analysis of oscillations on curve 2 indicates the presence of periods of SdH for holes $P_h = 0.155\ T^{-1}$ ($F_h = 6.45$ T) as well as HTO periods $P_1^{HTO} = 0.062\ T^{-1}$ ($F_1^{HTO} = 16$ T) and $P_2^{HTO} = 0.051\ T^{-1}$ ($F_2^{HTO} = 19.8$ T) attributed to holes (see the frequency spectrum in the inset to Fig.1). As is usually the case with bismuth, HTO are observed as a superposition of two frequencies differing by a factor 1.22. The frequency of oscillations also displays second harmonics of fundamental frequencies $2\ F_1^{HTO} = 32$ T and $2\ F_2^{HTO} = 39.6$ T.

As is seen from Fig.1 the quantum limit for SdH oscillations and the last minimum HTO will be realized by the same value of the magnetic field $B^{-1} \approx 0.1\ T^{-1}$. Given measurements of SdH oscillations and HTO in the sample $Bi_{1-X}Sb_X$ (x =2.6 at. %) allow drawing such a conclusion. At the same time, the model proposed in[6] predicts for this case observable HTO until the condition $0.5\ \hbar\ \Omega_c > \varepsilon_p$ is fulfilled. Thus, the results obtained in the present work allow showing preference for HTO model similar to.[7]

These researches were carrying out in collaboration with National High Magnetic Field Laboratory in framework of the NIS/NHMFL Program.

References

1. Yu. A. Bogod, Vit. B. Krasovitsky and V. G. Gerasimechko, *Sov. Phys. JETP* **39**, 667+672 (1974).
2. Yu. A. Bogod, Vit. B. Krasovitsky and S. A. Mironov, *Sov. Phys. JETP* **51**, 554-560 (1980).
3. Yu. A. Bogod, Vit. B. Krasovitsky and E. T. Lemesevskaya, *Sov. J. Low Temp. Phys.* **9**, 431-438 (1983).
4. Yu. A. Bogod, Vit. B. Krasovitsky and E. T. Lemesevskaya,. *Sov. J. Low Temp. Phys.* **12**, 345-348 (1986).
5. Yu. A. Bogod and Bit. B. Krasovitsky, *Sov. J. Low Temp. Phys.* **16**, 527-530 (1990).
6. Yu. A. Bogod, L. Yu. Gorelik and A. A. Slutskin, *Sov. J. Low Temp. Phys.* **13**, 353-356 (1987).
7. V. M. Polianovskii, *Ukr. Fiz. Zh.* **33** 1575-1580 (1988); **34**, 459-462 (1989).
8. Yu. A. Bogod and Vit. B. Krasovitsky., *Phys. Status Solidi* B **65** 847 (1974).
9. R. D. Brown, *Phys. Rev.* B **2**, 928-937 (1970).

HIGH-FIELD MAGNETIZATION IN THE MOTT-HUBBARD SYSTEM $(Y,Ca)VO_3$

H. NAKOTTE and A. M. ALSMADI
Physics Department, New Mexico State University
Las Cruces, NM 88003
E-mail: hnakotte@nmsu.edu

H. KAWANAKA
AIST, Tsukuba, Ibaraki 305, Japan

K. KINDO and K. GOTO
Kyokugen Osaka University, Toyonaka Osaka, 560-8531, Japan

We measured the magnetization of $Y_{1-x}Ca_xVO_3$ compounds with 0 Ω x Ω 0.6 in pulsed magnetic fields up to 56 T. YVO_3 exhibits a slightly S-shaped magnetization curve with an inflection point at B_c = 42 T. The critical field B_c was found to decrease with increasing calcium content, and no sign of an S-shape is seen for the compound with x = 0.6, which is at the boundary of the metal-to-insulator transition. Our data provide further evidence that the metal-to-insulator transition in this system coincides with the transition from a paramagnetic to a magnetic ground state.

1 Introduction

Strong on-site Coulomb repulsion between *3d* electrons can cause an integer-filled ($3d^N$) system to be insulating. This leads to a possible formation of a Mott inuslator, where the charge gap is determined by the Hubbard splitting (U) of the *d* band.[1] YVO_3 is such a Mott insulator and it exhibits two magnetic transitions at about 120 and 85 K (see Ref. [2]). The interactions in the phase AF1 (85 K < T < 120 K) are predominantly antiferromagnetic, while an additional small but significant ferromagnetic component was established for the low-temperature magnetic phase AF2 (T < 85 K). The Mott-Hubbard compound $CaVO_3$, on the other hand, is non-magnetic and it exhibits metallic conductivity at low temperatures.[3] Substitution of calcium onto the yttrium sites in YVO_3 causes an insulator-to-metal transition at about 60% of calcium content.[4]

2 Sample Preparation and Characterization

We prepared 11 different $Y_{1-x}Ca_xVO_3$ compounds with increasing Ca content with a step size of x = 0.1. All samples were prepared by mixing stoichiometric amounts of high-purity starting material of Y_2O_3, V_2O_3, CaO and VO. After subsequent annealing under Ar and H atmosphere at 1000-1300°C, the polycrystals were grown using the floating-zone method. The quality and homogeneity of the samples was checked by X-ray diffraction, and the oxygen content was determined by thermal-gravity analysis. In all cases, we found single-phase samples with the desired oxygen content close to 3 (within 2%).

Next, we measured the magnetic susceptibility and electrical resistivity of all $Y_{1-x}Ca_xVO_3$ samples. Two magnetic transitions were found in YVO_3 and $Y_{0.9}Ca_{0.1}VO_3$, while only one magnetic transition could be identified for compounds with 0.2 Ω x Ω 0.6. No magnetic ordering was detected for compounds with x > 0.6. The transport measurements revealed high room-temperature resistivity values and insulating behaviour for x Ω 0.6, while samples with higher Ca content show a more metallic behaviour. The results are summarised in Fig. 1.

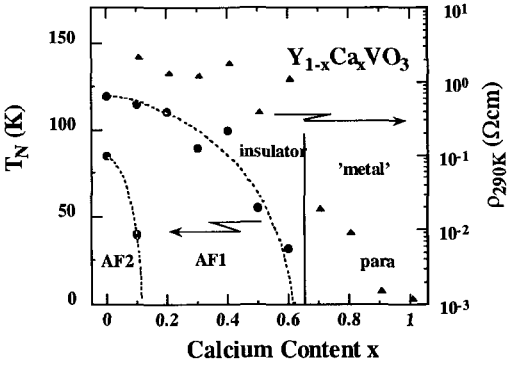

Figure 1: Concentration dependence of the ordering temperatures (circles, left axis) and room-temperature resistivity values (triangles, right axis) of $Y_{1-x}Ca_xVO_3$ compounds. Note, that a metal-to-insulator transition occurs around x = 0.65, which is close to a paramagnetic-to-(antiferro)magnetic transition. Lines are guides to the eye.

3 High-Field Magnetization: Procedure and Results

The magnetically-ordered $Y_{1-x}Ca_xVO_3$ compounds with 0 Ω x Ω 0.6 were ground to fine powders, which could be considered to consist of single-crystalline particles.

The magnetization experiments were performed at 4.2 K on powders with particles free to be rotated by the applied field using a pulsed magnet at the High-Field Facility in Osaka, Japan. Data were collected on field-oriented powders during the field-down sweep. This way, the magnetic response is believed to represent the easy-axis response of the material.

Figure 2(a) shows the change in the magnetic response of YVO_3 and $Y_{0.9}Ca_{0.1}VO_3$. Compared to YVO3, $Y_{0.9}Ca_{0.1}VO_3$ exhibits a substantially large high-field susceptibility. Since only the change in magnetization is recorded, these experiments do not provide any measure of a possible spontaneous moment that is present in the AF2 phase, which is believed to be the ground state of these two compounds. Both compounds exhibit slightly S-shaped magnetization curves with inflection points B_c that we determined from the maxima in the derivative dM/dH (see inset of Fig. 2(a)). In Fig. 2(b), the magnetic response of the other $Y_{1-x}Ca_xVO_3$ is shown. For these compounds (with an AF1 ground state), the overall magnetization decreases with increasing Ca content. Similarly to the former two compounds, we find an S-shaped magnetization curve for all samples except for $Y_{0.4}Ca_{0.6}VO_3$. For the other compounds, the inflection points B_c are found decrease approximately linear with increasing Ca content (see Fig. 3), and an extrapolation indicates that $B_c \cong 0$ T for $Y_{0.4}Ca_{0.6}VO_3$.

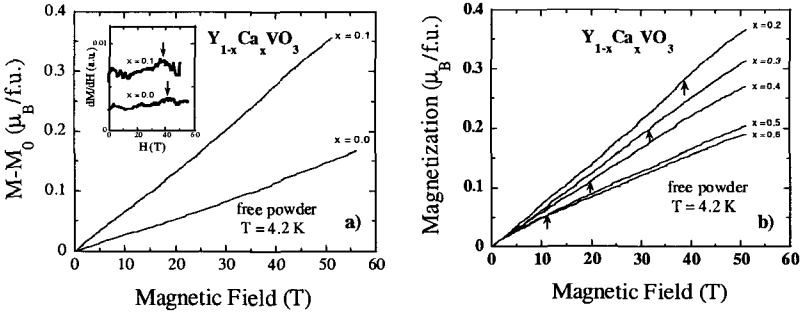

Figure 2: Magnetic response of $Y_{1-x}Ca_xVO_3$ compounds at 4.2 K with Ca concentration x of a.) 0.0 and 0.1 and b.) 0.2, 0.3, 0.4, 0.5 and 0.6. In the inset, the derivative of the magnetization as a function of applied field is shown for the first two compounds. The arrows indicate the positions of the critical fields B_c.

4 Conclusion

We measured the magnetic response of magnetically-ordered $Y_{1-x}Ca_xVO_3$ compounds in magnetic fields up to 56 T. S-shaped magnetization curves provide evidence of a critical field B_c, at which antiferromagnetic interactions start to break up. However, these compounds show no (or little) tendency toward saturation even

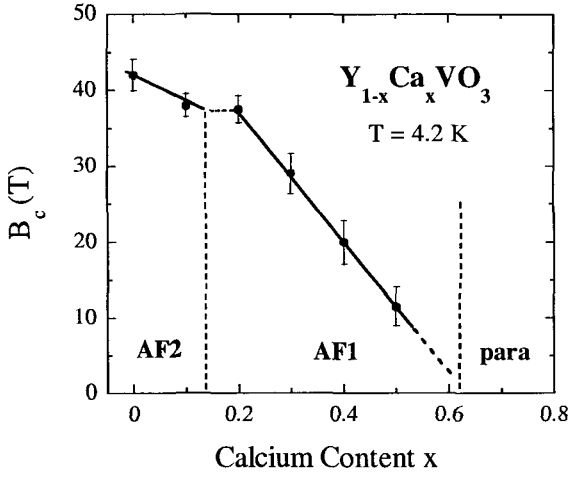

Figure 3: Concentration dependence of the critical field B_c in magnetically-ordered $Y_{1-x}Ca_xVO_3$ compounds.

at the highest field applied. Increasing the Ca content decreases the critical field B_c, and no S-shape is found for $Y_{0.4}Ca_{0.6}VO_3$ which is at the boundary of the insulator-to-metal transition. Thus, we may argue that strong antiferromagnetic interactions are responsible for the insulator-to-metal transition in the $Y_{1-x}Ca_xVO_3$ system.

This work was supported by a grant from NSF (grant number: DMR-0094241). HN would also like to acknowledge some support from the Science and Technology Agency (STA), Japan.

References

1. T. Arima, Y. Tokura and J.B. Torrance, *Phys. Rev. B* **48**, 17006-17009 (1993).
2. H. Nakotte, L. Laughlin, H. Kawanaka, D. N. Argryriou, R. I. Sheldon and Y. Nishihara, *J. Appl. Phys.* **85**, 4850-4852 (1999).
3. I. H. Inoue, I. Hase, Y. Aiura, A. Fujimori, Y. Haruyama, T. Maruyama and Y. Nishihara, *Phys. Rev. Lett.* **74**, 2539-2542 (1995).
4. M. Kasuya, Y. Tokura, T. Arima and S. Uchida, *Phys. Rev. B* **47**, 6197-6203 (1993).

INELASTIC NEUTRON SCATTERING FROM ANISOTROPIC SUPERCONDUCTORS

P. S. RISEBOROUGH

Dept. of Physics, Temple University, 1900 North 13th Street, Philadelphia PA 19122, E-mail: prisebor@astro.temple.edu

The magnetic fluctuation spectra are calculated for various phases of anisotropic superconductors. Both singlet and triplet superconducting phases can support anti-ferromagnetic fluctuations For small values of the Coulomb repulsion, the spectra show power law frequency dependencies due to the nodes in the superconducting order parameter. For larger strengths of the Coulomb interaction, low energy critically damped collective excitations develop from the quasi-particle density of states in the gap. The q and ω dependence of the spectra can be used to deduce the character of the superconducting order parameter.

1 Introduction

Most heavy fermion superconductors[13-15] exhibit strong magnetic correlations, ranging from anti-ferromagnetic fluctuations in UBe_{13}, to both paramagnetic and anti-paramagnetic fluctuations in UPt_3 (see Refs. [1,3]). In addition these materials exhibit multiple superconducting phases,[4,16] and show non-exponential temperature dependencies signifying the presence of a finite density of states within the superconducting "gap". The presence of nodes in the superconducting parameter should result in a region of power law temperature dependencies of the specific heat, spin susceptibility, N.M.R. relaxation rate and thermal conductivity.[5,7,8,9,17] However, the effects of non-magnetic impurities in anisotropic superconductors are pair breaking and produce a finite density of states at the Fermi-energy which obscures the power law dependencies in T expected for a pure system.[6,12] Pair breaking may be responsible for the small sample dependent linear T term found in the specific heat of many heavy fermion superconductors. As the change in the low energy density of states caused by elastic impurity scattering posses complications for the interpretation of thermodynamic and transport measurements, it is proposed that inelastic neutron scattering may be a more efficient probe of the symmetry of the superconducting order parameter since this directly measures the density of excitations. In particular, the reduction of the low energy superconducting quasi-particle density of states may result in the low energy neutron spectrum showing a narrow resonance with an anisotropic q dependence. The energy dependence of the quasi-particle density of states is manifested in the line shape of the resonance. In the next section, the calculation of the inelastic neutron scattering spectrum for an anisotropic superconductor is briefly outlined, and the effects of the critical scattering are ascertained and discussed.

2 The Model and Calculation

The heavy superconducting quasi-particles are modeled by a single band tight binding Hubbard model, with nearest neighbor hopping matrix elements t_i, and a residual on-site interaction U. The lattice sites have tetragonal symmetry. The superconducting pairing interaction was treated in the mean field approximation. Cases of singlet or triplet superconducting order parameters are considered. The dynamic susceptibility tensor was evaluated in the Random Phase Approximation. We shall examine the magnetic fluctuations where the occupation of the band was chosen to be half filled. It is expected that in this case, the anti-ferromagnetic nature of the correlations will be maximized due to the perfect nesting condition being satisfied in the normal state. The inelastic cross-section for triplet unitary phases of $\Gamma^-_1(A_{1u})$, $\Gamma^-_2(A_{2u})$ and $\Gamma^-_5(E_u)$ symmetry were calculated. In Fig.1 the spectra are shown at $Q = \pi$ (1,1,1) which corresponds to anti-ferromagnetic correlations. The scattering is large at this q value. The scattering shows a low energy damped collective excitation that softens and grows in intensity as U is increased. A small intensity second peak is observed slightly above the maximum gap. The ω^2 dependence of the leading edge of the peak is a consequence of the point nodes in the superconducting order parameter. The correlation length is large and anisotropic.

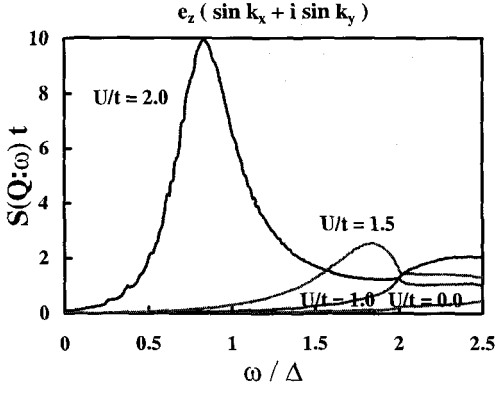

Figure 1: The inelastic scattering spectra from the triplet ABM-like state at momentum transfer (π,π,π), for various values of U/t.

The corresponding resonance peak for the polar-like state of $\Gamma^-_1(A_{1u})$, which has line nodes in the superconducting order parameter, is shown in Fig. 2. It is seen that the spectrum for the polar-like state experiences comparable enhancements to the ABM-like state, for similar values of U/t, but varies linearly with ω at low frequencies. The spectra exhibit a second small intensity peak just above the

maximum superconducting gap 2 Δ, which is more pronounced for large values of U/t. The large U/t spectrum show similarities to those observed in inelastic neutron scattering experiments on UPd_2Al_3 (see Refs. [2,11]).

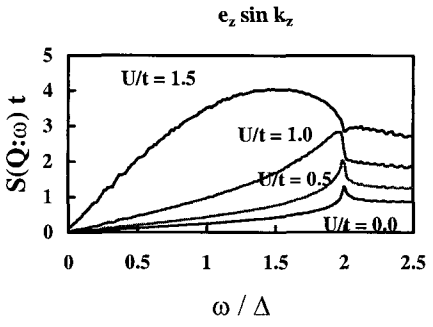

Figure 2: The inelastic scattering spectra from the triplet polar-like state at momentum transfer (π,π,π), for various values of U/t.

The singlet states investigated were chosen as the non-degenerate $\Gamma^+_3(B_{1g})$ and $\Gamma^+_4(B_{2g})$ states. In these cases, the low energy magnetic peak is confined to the corners of the Brillouin zone. The vanishing at the zone center is a consequence of ferromagnetic correlations being suppressed by spin singlet superconductivity. The spectra at momentum transfer Q are linear in ω, at low ω, which is caused by the presence of line nodes of the gap. Furthermore, in contrast to the polar phase, the spectra show no discernable structure or second peak.

3 Conclusions

The calculations show that triplet unitary superconducting phases are compatible with strong anti-ferromagnetic correlations and ferromagnetic correlations, which show up as critically damped spin wave modes for energies below the superconducting gap. For non-s wave singlet phases, a similar magnetic correlation appears, but only at the corners of the Brillouin zone corresponding to anti-ferromagnetic fluctuations. These peaks develop from the broad q independent quasi-elastic peaks found in the normal state, and are caused by the reduction in the low energy quasi-particle density of states in the superconductor, below the "gap". The intensity of magnetic scattering at the nuclear Bragg peaks, can serve to distinguish singlet from triplet superconductivity, while the ω dependence of the leading edge of the resonance peak can be correlated with the presence of point or line nodes in the superconducting order parameter.

References

1. G. Aeppli, E. Bucher and G. Shirane, *Phys. Rev. B*, **32**, 7579 (1985).
2. N. R. Bernhoeft *et al.*, *Physica B* **259-261**, 614 (1999).
3. N. R. Bernhoeft and G. G. Lonzarich, *J. Phys. CM* **7**, 7325 (1995).
4. R. A. Fisher *et al., Phys. Rev. Letts.* **62**, 1411 (1989).
5. J. J. M. Franse *et al., Phys. B* **59**, 15 (1985).
6. L. P. Gor'kov and P. A. Kalugin, *J.E.T.P. Lett.* **41**, 253 (1985).
7. D. Jaccard *et al., J. Phys. (Paris)* **46**, L 811 (1985).
8. Y. Kohori *et al.,J. Phys. Soc. Jpn.* **56**, 2263 (1987).
9. D. E. MacLaughlin *et al., Phys. Rev. Letts.* **53**, 1833 (1984).
10. N. Metoki *et al., J. Phys. Soc. Jpn.* **66**, 2560 (1997).
11. N. K. Sato *et al., Nature* **410**, 340 (2001).
12. S. Schmitt-Rink *et al.,Phys. Rev. Letts.* **57**, 2575 (1986).
13. G. R. Stewart *et al.,Phys. Rev. Letts.* **52**, 679 (1984).
14. F. Steglich *et al., Phys. Rev. Letts.* **43**, 1982 (1979).
15. H. R. Ott *et al., Phys. Rev. Letts.* **50**, 1595 (1983).
16. H. R. Ott *et al., Phys. Rev. B* **31**, 1651 (1985).
17. H. R. Ott *et al., Phys. Rev. Letts.* **52**, 1915 (1984).

ULTRASONIC AND MAGNETIZATION STUDIES AT THE METAMAGNETIC TRANSITION IN UPt_3

A. SUSLOV,* D. DASGUPTA, J. R. FELLER and B. K. SARMA

Department of Physics, University of Wisconsin-Milwaukee, P.O. Box 413 Milwaukee, WI 53201, U.S.A.
E-mail: alexei@uwm.edu

J. B. KETTERSON

Department of Physics and Astronomy, Northwestern University, Evanston, IL 60208, U.S.A.

D. G. HINKS

Materials Science and Technology, Argonne National Laboratory, Argonne, IL 60439, U.S.A.

The velocity and attenuation of longitudinal ultrasound were measured on two single crystals of UPt_3 in magnetic fields up to 33 T and temperatures down to 40 mK. For fields applied in the basal plane, a strong dip in the velocity is seen at a field of 20 T in both samples and is accompanied by a simultaneous increase in the dc magnetization. At lower temperatures the dip gets more pronounced and sharper. At a temperature around 0.6 K the velocity dip develops a second feature at a slightly higher field of ~21.6 T.

1 Introduction

Some of the Cerium and Uranium based heavy fermion compounds show a multitude of interesting low temperature properties like superconductivity, antiferromagnetism, metamagnetism, etc. Ultrasonic velocity has proved to be a useful technique to study these phenomena.

2 Experiment

We have developed ultrasonic spectrometers[1] specifically for measurements in high magnetic fields. Using this instrumentation, measurements have been made on two single crystals of UPt_3. The measurements on one of these samples was reported previously[2] (henceforth referred to as sample A). Here we report simultaneous ultrasonic and (VSM) magnetization measurements on a second single crystal (sample B, acquired earlier). We believe sample A to be of a higher quality as evidenced from the superconducting T_c measurements. In addition we performed magnetization measurements on a third sample (sample C), which was obtained

from the same single crystal rod as sample A and shaped in the form of a sphere. The studies were carried out in DC magnetic fields up to 33 T and temperatures down to 40 mK at the Tallahassee site of the National High Magnetic Filed Laboratory (NHMFL). Velocity measurements were also carried out on the 20ms 50 T pulsed magnet at Los Alamos, with the intent of testing a new ultrasonic spectrometer designed for fast data acquisition in the pulsed magnetic fields.[1]

3 Results and discussion

The relative velocity change was measured as a function of magnetic field at various temperatures on samples A and B at temperatures down to 40 mK and fields up to 33 T. Sound waves were propagated in the basal plane and parallel to the applied magnetic field. Figure 1 shows the data on sample A. Strong metamagnetic behavior (MMT), characterized by a large and sharp dip in the sound velocity (and a peak in the attenuation) is seen at 20 T. As the temperature is

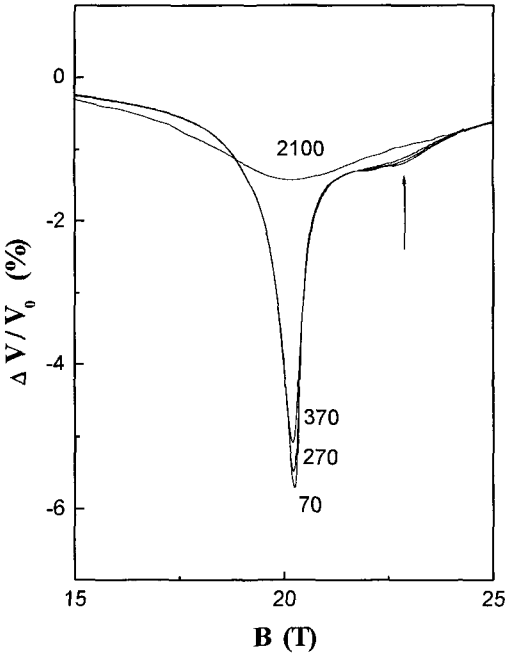

Figure 1: Relative velocity change in UPt_3 in vicinity of metamagnetic transition in the sample B at different temperatures indicated (in mK) near each curve. The arrow shows position of the second dip.

lowered to 0.6 K, a new feature (a second dip) shows up at a slightly higher field of 21.6 T, which becomes more pronounced as the temperature is further lowered. This is associated with an increase in the attenuation. We believe this is the first observation of this feature using any technique. Measurements on the second sample B, also show qualitatively the same features; however the second dip at higher fields is less prominent. We believe the second dip to be an intrinsic property of UPt_3. It is interesting to note that velocity measurements at the metamagnetic transition in the heavy fermion compound URu_2Si_2 show a softening in the velocity in the field range 35 T – 40 T (see Ref. [3]). At low temperatures three dips in the velocity are seen which however merge to two and then one as the temperature is raised. This splitting of the velocity dip agrees well with the observed steps in the magnetization measurements. These observations imply that magnetization measurements in UPt_3 at very low temperatures would prove equally interesting.

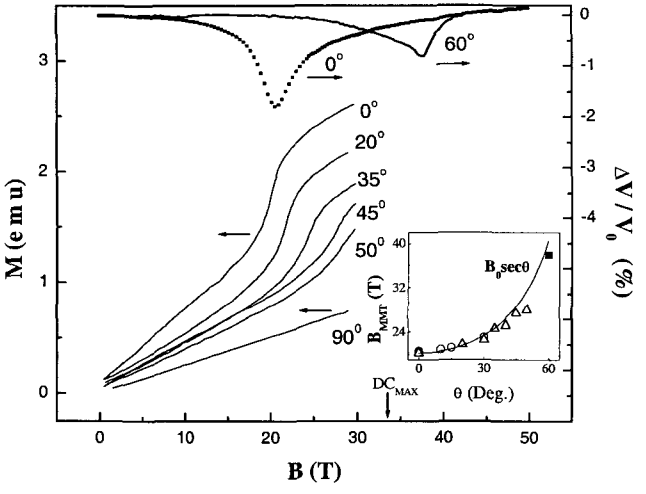

Figure 2: Anisotropy of magnetization and ultrasonic velocity measurements in UPt_3. Inset: angular dependence of the metamagnetic transition field extracted from these data.

Magnetization measurements were done on two of the UPt_3 samples (B and C) with a vibrating sample magnetometer in fields up to 30 T, and using a pumped helium-4 refrigerator.[4] A step increase in the dc magnetization is seen at the metamagnetic transition, the steps becoming sharper at lower temperatures (Fig. 2). The measurements were done for various orientations of the magnetic field with respect to the basal plane of the crystal (the angle θ is measured from the basal plane). The inset shows the anisotropy of B_{MMT} with respect to this angle for measurements on both samples (open circles for the spherical sample C, and open

triangles for sample B). The velocity measurements (upper curve) on sample B in the 50 T short pulse magnet are also shown for the 0^0 and 60^0 orientations. The solid curve is a fit to the form $B_{MMT} = B_0(\cos\Theta)^{-1}$, which would be the expected field of the MMT if the component of the applied field in the basal plane must be B_0, as was assumed in.[5] The 60^0 data shows the strength of the velocity measurement technique in a pulsed field. Magnetization measurements would be very difficult, because of the large dB/dt (rate of change of flux) through the pick-up coils.

Acknowledgments

This work is supported by the National Science Foundation under grants DMR-9971123 and DMR-9704020. The NHMFL is supported by the NSF, the State of Florida and the US Department of Energy.

*) Permanent address: A. F. Ioffe Physical-Technical Institute, Russian Academy of Sciences, St.-Petersburg, Russia.

References

1. A. Suslov *et al., these proceedings.*
2. J. R. Feller *et al., Phys. Rev. B* **62**, 11538-11544 (2000).
3. A. Suslov *et al.,* A., *these proceedings.*
4. A. Suslov *et al., J. Low Temp. Physics* **121**, 221-226 (2000).
5. A. de Visser *et al., Physica B* **147**, 81-160 (1987).

This page is intentionally left blank

Part III

Molecular Conductors

This page is intentionally left blank

MAGNETIC-FIELD-INDUCED SUPERCONDUCTIVITY IN LAYERED ORGANIC MOLECULAR CRYSTALS WITH LOCALIZED MAGNETIC MOMENTS

O. CEPAS, R. H. MCKENZIE, J. MERINO
Department of Physics, University of Queensland, Brisbane, 4072, Australia

The synthetic organic compound $\lambda(BETS)_2FeCl_4$ undergoes successive transitions from an antiferromagnetic insulator to a metal and then to a superconductor as a magnetic field is increased. We use a Hubbard-Kondo model to clarify the role of the Fe^{3+} magnetic ions in these phase transitions. In the high-field regime, the magnetic field acting on the electron spins is compensated by the exchange field H_e due to the magnetic ions. This suggests that the field-induced superconducting state is the same as the zero-field superconducting state which occurs under pressure or when the Fe^{3+} ions are replaced by non-magnetic Ga^{3+} ions. We show how H_c can be extracted from the observed splitting of the Shybnikov-de Haas frequencies. Furthermore, we use this method of extracting H_e to predict the field range for field-induced superconductivity in other materials. We also show that at high fields the spin fluctuations of the localized spins are not important.

This work was supported by the Australian Research Council.

PERSISTENT CURRENTS AT FIELDS ABOVE 23T

N. HARRISON

NHMFL, Los Alamos National Laboratory, MS-E536,

Los Alamos, New Mexico 87545, USA

E-mail: nharrison@lanl.gov

Experimental studies made on organic conducting salts of the composition α-(BEDT-TTF)$_2M$Hg(SCN)$_4$ (where M = K, Tl and Rb) indicate that they exhibit persistent currents at magnetic fields exceeding 23T. The presence of currents cannot be explained by the quantum Hall effect, while superconductivity seems unlikely. All indications point towards a new type of dissipationless current flow involving relative gradients in the pinning of a CDW and quantized orbital magnetism.

In high purity two-dimensional itinerant electron systems, Landau quantization often leads to an orbital magnetization that dominates all other contributions at high magnetic fields.[1] This is certainly established to be true in the majority of molecular conducting systems,[2] where the present experimental techniques do not lend themselves favourably to the detection of spin paramagnetic effects. Thus, if magnetic hysteresis is observed at high magnetic fields, one can assume with confidence that it is the orbital magnetism that is hysteretic; whether it corresponds to (1) first order phase transitions across which the orbital magnetism changes or (2) persistent currents.

Molecular conductors of the form α-(BEDT-TTF)$_2M$Hg(SCN)$_4$ (where M = K, Tl or Rb) have become known to be plagued by hysteresis effects at high magnetic fields.[3] Most notable, is an abrupt change in the pattern of Landau quantization at and around fields of 23T (for M = K), thought to be of the type (1) above. A change in shape and size of the de Haas-van Alphen (dHvA) oscillations[4] results from a change in the electronic structure caused by a transition between commensurate and incommensurate charge-density wave (CDW) phases.[5,6] Although this transition is driven primarily by changes in the spin paramagnetism of the groundstates,[7,8] it is the ancillary change in orbital magnetism that is detected experimentally.[3,4]

Another form of hysteresis comes into prominence at fields exceeding 23T (for M = K), manifesting itself as a vertical offset in the dHvA oscillations between rising and falling fields.[3] This can be shown to be of type (2), above, by monitoring the behaviour of the irreversible magnetization as the magnetic field is cycled.[3,9,10] Figure 1(A) depicts a model hysteresis loop for a cylindrical sample of radius r within which currents flow at a critical current density j_c (see Ref. [11]). On the rising magnetic field (point 1) the irreversible magnetization is saturated at a negative value $M_{sat} = -j_c r/3$. On reversing the direction in which the applied magnetic field $\mu_0 H$ is swept (point 2), the irreversible magnetization changes according to the susceptibility $\chi' = -\eta$. As the magnetic field changes further, the

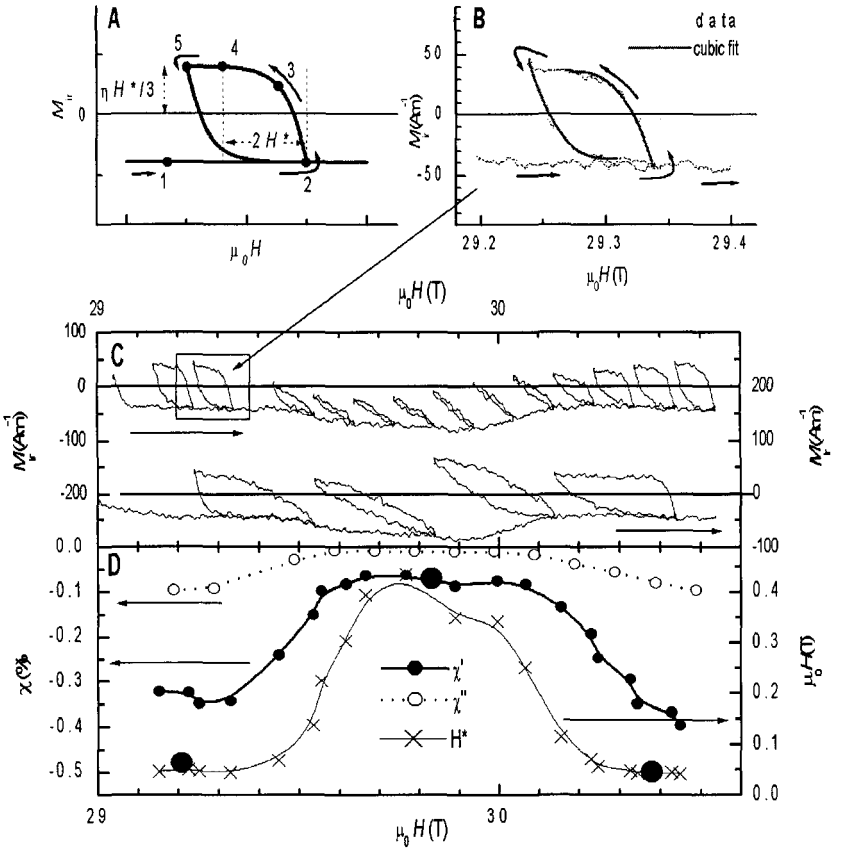

Figure 1: The irreversible magnetic properties of α-(BEDT-TTF)$_2$KHg(SCN)$_4$. (A) Model irreversible magnetization M_{ir} due to currents, as observed in type II superconductors. The dependence of M_{ir} on the magnetic sweep history as explained in the text. (B) An example of M_{ir} measured in α-(BEDT-TTF)$_2$KHg(SCN)$_4$ at 85 mK using magnetic torque with the angle between the applied magnetic field and the normal to the conducting planes being 18°. (C) A series of loops measured over an extended range of field. (D) χ' χ'' and H^* extracted from M_{ir} in (C). Enlarged symbols correspond to the model calculations.

polarity of the currents becomes reversed within the sample, penetrating inwards in the form of a concentric flux-reversal front. The inductive response of the sample collapses quadratically, leading to a cubic lineshape in the irreversible magnetization

(point 3). Finally the magnetization saturates again at $M_{sat} = + j_c r/3$ (point 4), having taken an interval in field equivalent to twice the coercion field $H^* = \eta M_{sat}$ to fully reverse all currents. Figure 1(B) shows actual data taken from magnetic torque measurements made on a sample of α-(BEDT-TTF)$_2$KHg(SCN)$_4$ (see Ref. [10]). The cubic formula derived by Bean for type II superconductors fits the change in the irreversible magnetization in the flux reversal regime perfectly well,[11] implying that the inductive response of the sample collapses quadratically as in the simple model in Fig. 1(A).

The primary implication of the fits in Fig. 1(B) is that the sample sustains a uniform gradient in the orbital magnetization $\nabla \times \mathbf{M}_{orb}$, with its orientation depending on the magnetic field history. By Maxwell's equations, this gradient is irreducibly equivalent to a current density $\mathbf{j}$ that attains a critical value $\mathbf{j}_c$. The origin of the current is subject to debate. Two kinds of effect, namely the quantum Hall effect[12] and superconductivity,[13] are commonly known to give rise to persistent or long-lived currents in metals with magnetic fields present. Both appear to be unlikely for the following reasons:

Quantum Hall effect:[12] Long-lived currents, here, occur orthogonal to a Hall electric field that is sustained owing to the absence of quasiparticle scattering effects orthogonal to the current. The failure of transport experiments to detect a persistent Hall electric field in static magnetic fields weighs heavily against the quantum Hall effect as a likely mechanism. Furthermore, the absence of quasiparticle scattering processes orthogonal to the current is normally achieved when the chemical potential μ is situated in a Landau gap. This cannot be the case at all filling factors at all magnetic fields: note that in Fig. 1(C), hysteresis loops are observed in α–(BEDT-TTF)$_2$KHg(SCN)$_4$ at all filling factors and at all fields above 23T. It should also be noted that currents are carried by surface states in the quantum Hall effect: they are not expected to permeate the bulk as the experiments in Fig. 1(B) indicate.

Superconductivity:[13] Persistent currents, here, are sustained in equilibrium when the vortex density gradient is held in place by vortex-impurity interactions. The magnetic behaviour in Fig. 1(B) and transport behaviour in Ref. [14] are both consistent with an inhomogeneous superconducting phase. The primary argument against such an explanation is that superconductivity tends to be destroyed by a magnetic field. Superconductivity is induced by a magnetic field only in rare instances where an internal antiferromagnetic exchange field is compensated by the applied field.[15] Evidence for significant internal magnetic fields have not been reported in any of the α–(BEDT-TTF)$_2M$Hg(SCN)$_4$ salts.[16,17] The electron g-factors are also too high to enable more exotic forms of field-induced superconductivity.[18]

Should neither of the above conventional mechanisms satisfactorily explain the experimental data in Fig. 1, more exotic explanations must be considered, even if these explicitly involve the CDW groundstate. A mechanism involving the spontaneous sliding of CDWs (a variant of Fröhlich superconductivity) has been

considered.[14] The extreme anisotropy of such a phase could account for the survival of the persistent currents to very high magnetic fields (at least approaching 100T). It, nevertheless, requires the existence of unprecedented quantum depinning effects.

Manifestly similar effects to Fröhlich superconductivity can result even if the CDW is pinned. A model has recently been proposed that can explain why certain aspects of the behaviour of α–(BEDT-TTF)$_2$*M*Hg(SCN)$_4$ salts exhibit parallels with both the quantum Hall effect and type II superconductivity.[19] Orbital magnetism resulting from Landau quantization is an essential component of this model. Organic conducting salts of the form α–(BEDT-TTF)$_2$*M*Hg(SCN)$_4$ are subject to Landau quantization owing to the existence of a quasi-two-dimensional section of Fermi surface in addition to the quasi-one-dimensional sheets that become nested.[20] As a consequence of the strong variations in the density of states with field accompanying Landau quantization, carriers flow back and forth between the sections of Fermi surface as the magnetic field is swept.[21] The optimum nesting vector **Q** on the quasi-one-dimensional section of Fermi surface therefore undergoes oscillations in response to oscillations in the number of carriers between the quasi-one-dimensional sheets, causing the CDW to become periodically stretched and compressed like a concertina. Magnetic hysteresis results when this process is impeded by the pinning of the CDW to impurities.[19]

The hysteresis, here, is parameterized by a differential chemical potential $2\Delta\mu$ between the two Fermi surface sheets: a change in the chemical potential $-\Delta\mu$ of the quasi-two-dimensional Fermi surface pocket is compensated by an equal and opposite change $\Delta\mu$ in that of the quasi-one-dimensional Fermi surface sheets.[19] Rather than being uniform, however, the differential chemical potential exists in the form of a gradient, $2\nabla(\Delta\mu)$. If this were not the case, the hysteresis would be accompanied by a surface current that would exceed the critical current density. This is related to the characteristic CDW sliding threshold electric field by means of the formula $\mathbf{j}_c = (\mathbf{E}_t \times \mathbf{nz})/\rho_{xy}$ (see Ref. [19]). Such behaviour results from the fact that the chemical potential gradients on the two sections of Fermi surface exist in equilibrium and oppose each other, while the gradient that exists on the quasi-one dimensional Fermi surface sheets is electrostatically limited such that $\nabla(\Delta\mu) < e\mathbf{E}_t$. The relation between $\mathbf{j}_c$ and $\mathbf{E}_t$, described above, is similar to the relation between **j** and **E** in the quantum Hall effect,[12] except that, here, there exists *zero* net electric field across the sample. A consequence of this behaviour is that the current becomes uniformly distributed within the interior of the sample upon saturation of the magnetization. The manner in the sample responds to changes in magnetic field is therefore similar to that of a type II superconductor, giving rise to hysteresis loops consistent with the Bean model, like those in Fig. 1(B).[11]

Figure 1(C) shows a series of hysteresis loop measurements made on a sample of α–(BEDT-TTF)$_2$KHg(SCN)$_4$ (see Ref. [10]). Several quantities can be extracted from these data: the irreversible susceptibility χ', the losses incurred by the

hysteresis χ", the coercion field H^* and the irreversible saturation magnetization M_{sat}. The quantities χ', χ" and H^*, thus extracted, are shown in Fig. 1(D). χ' and H^* are especially sensitive to the Landau level filling factor F/B, but can be accounted for by the model described in Ref. [19]. On reversing the direction of sweep of the magnetic field, CDW pinning initially prevents the CDW from sliding, except in the regions closest to the sample surface. The temporal dHvA susceptibility of the quasi-two dimensional Fermi surface becomes characteristic of a system in which there are no quasi-one dimensional Fermi surface states.[21] It is because the pinning disrupts the process be which quasiparticles flow back and forth between the two Fermi surface sheets that the susceptibility becomes hysteretic.[19] This effect can be modeled and estimates of χ' made from such a model (calculated in Ref. [19]) at integral and half-integral filling factors are indicated by oversized filled circular symbols in Fig. 1(D). The agreement between experiment and theory can be seen to be rather good.

The experimental results displayed in Figure, therefore, amount to compelling evidence for persistent currents occurring orthogonal to the charge polarization field of a CDW. The mechanism that gives rise to these currents appears to be unprecedented and quite unlike that giving rise to superconductivity or the quantum Hall effect.

This work is supported by the National Science Foundation, Florida State University and the U.S. Department of Energy.

References

1. D. Shoenberg, *Magnetic Oscillations in Metals* (Cambridge University Press, Cambridge, 1984).
2. J. Wosnitza, *Fermi Surfaces of Low-Dimensional Organic Metals and Superconductors of Springer Tracts in Modern Physics* (Springer-Verlag, Berlin, 1996).
3. See N. Harrison *et al., Phys. Rev. B* **62**, 14212-14223 (2000) and references therein.
4. N. Harrison *et al., Phys. Rev. B* **63**, 195102 (2001).
5. P. Christ *et al., Pis'ma Zh. Éksp. Teor. Fiz.* **71**, 437 (2000) [*JETP Lett.* **71**, 303 (2000)].
6. J. S. Qualls *et al., Phys. Rev. B* **62** 10008 (2000).
7. R. H. McKenzie, *cond-mat*/9706235 (unpublished).
8. N. Harrison, *Phys. Rev. Lett.* **83**, 1395-1398 (1999).
9. N. Harrison *et al., Phys. Rev. Lett.* **86**, 1586-1589 (2001).
10. A. Ardavan *et al.*, (to be published).
11. C. P. Bean, *Rev. Mod. Phys.* **36**, 31 (1964).

12. Chakraborty *The Quantum Hall Effects: Integral and Fractional*, Second Edition (Springer-Verlag, 1995).
13. M. Tinkham, *Introduction to Superconductivity*, Second Edition (McGraw-Hill, 1996).
14. N. Harrison *et al., J. Phys.: Condens. Mat.* **13**, L389 (2001).
15. S. Uji, *Nature* **410**, 908 (2001).
16. F. L. Prat *et al., Phys. Rev. Lett.* **74**, 3892 (1995).
17. K. Miyagawa, A. Kawamoto and K. Kanoda, *Phys. Rev. B* **56**, R8487 (1997).
18. Z. Tesanovic, M. Rasolt and X. Lei, *Phys. Rev. B* **43**, 288 (1991).
19. N. Harrison, *cond-mat/*0110278 (unpublished).
20. N. Harrison *et al., J. Phys. Condens.: Mat.* **11**, 7227 (1999).
21. N. Harrison *et al., Phys. Rev. B* **54**, 9977 (1996).

HIGH-MAGNETIC-FIELD TESTS FOR REDUCED DIMENSIONALITY IN ORGANIC SUPERCONDUCTORS: JUST HOW VALID ARE THE MOTT-IOFFE-REGEL AND ANDERSON CRITERIA?

J. SINGLETON,[1,2,*] P. A. GODDARD,[2] A. ARDAVAN,[2] N. HARRISON,[1]
S. J. BLUNDELL,[2] J. A. SCHLUETER [3] and A. M. KINI,[3]

[1]*National High Magnetic Field Laboratory, LANL, MS-E536, Los Alamos, New Mexico 87545, USA*
[2]*The Clarendon Laboratory, Parks Road, Oxford OX1 3PU, United Kingdom*
[3]*Materials Science Division, Argonne National Laboratory, Argonne, Illinois 60439, USA*
j.singleton1@physics.ox.ac.uk

The interlayer transfer integrals of various organic superconductors have been deduced using high-magnetic-field techniques. The measurements demonstrate the inappropriateness of criteria used to denote incoherent interlayer transport.

1 Introduction

Most of the correlated-electron systems which excite current interest have very anisotropic electronic bandstructure. Examples include the "high-T_c" cuprates,[1,2] layered ruthenates,[3] and crystalline organic metals.[2-4] Such systems may be described by a tight-binding Hamiltonian in which the ratio of the interlayer transfer integral $t_\perp$ to the average intralayer transfer integral $t_\parallel$ is << 1) (see Refs. [2, 4, 5]).

Values of $t_\perp$ in such systems are often compared with a one-dimensional form of the Mott-Ioffe-Regel criterion;[6]

$$h/2\pi\tau > t_\perp \tag{1}$$

where τ^{-1} is the quasiparticle scattering rate.[1,2,5] The inequality is often found to apply, suggesting that the quasiparticles scatter more frequently than they tunnel between layers. Similarly, under standard laboratory temperatures T, the inequality

$$k_B T > t_\perp \tag{2}$$

often holds, hinting that thermal smearing will wipe out details of the interlayer periodicity (Anderson'scriterion).[7] The question has thus arisen as to whether the interlayer charge transfer is coherent or incoherent in these materials, i.e. whether or not the Fermi surface extends in the interlayer direction.[2,4,5] Incoherent interlayer transport is used as a justification for proposed non-Fermi-liquid behaviour (see Refs. [2, 7]). Moreover, models for unconventional superconductivity in κ-phase BEDT-TTF salts invoke the nesting properties of the Fermi surface;[8-10] [the degree

of nesting might depend on whether the Fermi surface is a 2D or 3D entity (see Ref. [4], Section 3.5).

It is, therefore, of considerable interest to derive a test for coherent interlayer transport. However, many apparently solid experimental tests for coherence in organic superconductors have been deemed to be inconclusive,[5] e.g. semiclassical models can reproduce angle-dependent magnetoresistance oscillation (AMRO) (see Ref. [12]) and Fermi-surface-traversal resonance (FTR) data[11] equally well when the interlayer transport is coherent or "weakly coherent".[5] We describe below a reliable experimental test which shows that the criteria given in Eqs. 1 and 2 are a very poor guide to interlayer incoherence. We also compare data for four organic conductors.

2 Experiment and Discussion

A simple tight-binding expression is often used to simulate the interlayer (z-direction) dispersion in Q2D organic conductors;[4]

$$E(k_z) = -2t_\perp \cos(k_z a). \tag{3}$$

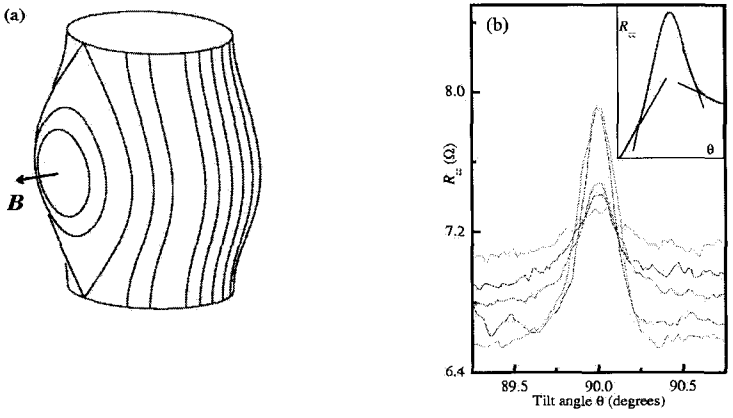

Figure 1: (a) Illustration of the effect of introducing interlayer dispersion on a Q2D Fermi-surface section; the cross-section of the Fermi surface varies in the interlayer (k_z) direction. The lines on the sides of the Fermi surface illustrate some of the quasiparticle orbits caused by an in-plane field. (b) Interlayer resistance R_{zz} (proportional to ρ_{zz}) of a κ-(BEDT-TTF)2Cu(NCS)$_2$ sample as a function of magnetic-field orientation (θ=90° corresponds to magnetic field exactly in-plane). Data for temperatures T = 0.48 K, 1.4 K, 3.0 K, 4.4 K and 5.1 K are shown. The background magnetoresistance increases with increasing T, whereas the peak at θ=90° becomes smaller. The inset shows the intersections of the linear extrapolations used to determine the peak width (after Ref. [15]).

In an applied magnetic field, the quasiparticles undergo orbits defined by the Lorentz force $(h/2\pi)(d\mathbf{k}/dt) = -e\mathbf{v} \times \mathbf{B}$, where $\mathbf{v}$ is given by $(h/2\pi)\mathbf{v} = \nabla_k E(\mathbf{k})$; here $E(\mathbf{k})$ is the quasiparticle energy.[4,12] This results in orbits on the Fermi surface, in a plane perpendicular to $\mathbf{B}$ (see Ref. [12]). Thus, if the Fermi surface is extended in the z direction, a magnetic field applied exactly in the intralayer (xy) plane can cause a variety of orbits on the sides of the Fermi surface, as shown schematically in Fig.1(a). It has been proposed that the closed orbits about the belly of the Fermi surface[13] or the "self-crossing orbits" found under the same conditions[14] are very effective in averaging the interlayer component of the velocity. Therefore, the presence of such orbits will lead to an increase in the resistivity component ρ_{zz} (see Refs. [13, 14]). On tilting $\mathbf{B}$ away from the intralayer direction, the closed and "self-crossing" orbits cease to be possible when $\mathbf{B}$ has turned through an angle Δ, where

$$\Delta(\text{in radians}) \approx v_\perp / v_\parallel. \qquad (4)$$

Here $v_\perp$ is the maximum of the interlayer component of the quasiparticle velocity, and $v_\parallel$ is the intralayer component of the quasiparticle velocity in the plane of rotation of $\mathbf{B}$. Therefore, on tilting $\mathbf{B}$ around the in-plane orientation, one expects to see a peak in ρ_{zz}, of angular width 2Δ, if (and only if Ref. [5]) the Fermi surface is extended in the z direction. As $v_\perp \propto 2t_\perp$ (see Eq. 3), the angular width of the peak is pleasingly proportional to $t_\perp$. By using Eq. 4 and measured details of the intralayer Fermi-surface topology (which give $v_\parallel$), it is therefore possible to use Δ to deduce $t_\perp$ (see Refs. [15, 16, 17]).

Figure 1(b) shows typical data for κ-(BEDT-TTF)$_2$Cu(NCS)$_2$. The observation of a peak in ρ_{zz} close to θ=90° demonstrates that the interlayer transport is coherent. The intralayer Fermi-surface parameters of κ-(BEDT-TTF)$_2$Cu(NCS)$_2$ are well known,[14,15] allowing the interlayer transfer integral to be estimated to be $t_\perp \approx 0.04$ meV (see Ref. [15]) (c.f. intralayer transfer integrals ~150 meV (see Ref. [15])). Already it is plain that the criterion given in Eq. 2 is not a good guide to interlayer incoherence. At the maximum temperature of 5 **K**, $k_B T \approx 10\, t_\perp$, and yet the peak in ρ_{zz} shown in Fig. 1(b) unambiguously demonstrates a 3D Fermi-surface topology.

It is next instructive to compare $t_\perp$ with τ^{-1}. The sample used in Fig. 1 has been studied using Shubnikov-de Haas (SdH) oscillations at $|\mathbf{B}| \leq 15$ T (see Ref. [15]). At such fields, the oscillatory magnetoresistance is much less than the nonoscillatory component, and magnetic breakdown is a minor consideration.[4] Hence, the 2D form of the Lifshitz-Kosevich formula may be used to extract τ (see Ref. [4]), giving $\tau \approx 3$ ps (see Ref. [15]). Another estimate can be derived from studies[11] of the FTR due to quasiparticles crossing the Q1D FS sheets, which use samples from the same batch. In the data of,[11] the FTR appears at $B \approx 10$ T, with a full-width at half-maximum of $\Delta B \approx 7$ T. If we assume that $\omega\tau \sim B/\Delta B$ (see Ref. [15]), where $\omega = 2\pi \times 70 \times 10^9$ rad s^{-1} (see Ref. [11]), we obtain $\tau \sim 3$ ps, close to the SdH values. Thus, $1/\tau \approx 0.24$ meV, $\sim 6\, t_\perp$. In such circumstances, Eq. 1 leads one to

expect incoherent interlayer transport, and yet the peak in ρ_{zz} unambiguously demonstrates the opposite.[19]

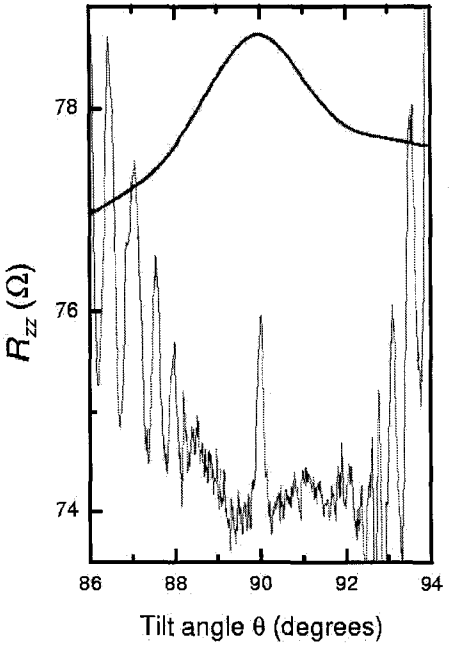

Figure 2: Peaks in the interplane resistance R_{zz} (proportional to ρ_{zz}) close to $\theta = 90°$ in λ- $(BETS)_2GaCl_4$ (thick line; $T = 1.4$ **K**, $B = 30$ **T** [16]) and κ-$(BEDT\text{-}TTF)_2Cu(NCS)_2$ (fine line; $T = 520$ m**K**, $B = 42$ **T** (see Ref. [15]). In the case of κ-$(BEDT\text{-}TTF)_2Cu(NCS)_2$ the rapid oscillations at the edges of the figure are angle-dependent magnetoresistance oscillations (AMROs).

Figure 2 compares the peaks observed in intralayer magnetic fields in λ-$(BETS)_2GaCl_4$ (see Ref. [16]) and κ-$(BEDT\text{-}TTF)_2Cu(NCS)_2$ (see Ref. [15]). Such a comparison is interesting because the two superconductors possess similar intralayer Fermi-surface topologies, and almost identical quasiparticle effective masses.[16] Note how the peak at 90° is much wider in λ-$(BETS)_2GaCl_4$ than in κ-$(BEDT\text{-}TTF)_2Cu(NCS)_2$; given the similarity of their intralayer Fermi-surface properties, this immediately suggests a larger $t_\perp$ in λ-$(BETS)_2GaCl_4$, and indeed, simulations of the data give $t_\perp \approx 0.21$ meV (see Ref. [16]). The greater "three

dimensionality" of the bandstructure of λ-$(BETS)_2GaCl_4$ compared to κ-(BEDT-TTF)$_2$Cu(NCS)$_2$ is manifested in their superconducting behaviour (e.g. c.f. Figs.(9) and (10) of Ref. [16]). Whereas λ-$(BETS)_2GaCl_4$ exhibits 2D-3D dimensional crossover in its H_{c2} (T) behaviour, $H_{c2}(T)$ in κ-(BEDT-TTF)$_2$Cu(NCS)$_2$ is entirely characteristic of a Q2D superconductor.

By contrast, we have been unsuccessful in observing peaks in the resistivity of β"-(BEDT-TTF)$_2SF_5CH_2CF_2SO_3$ and α-(BEDT-TTF)$_2$KHg(SCN)$_4$ in intralayer magnetic fields, even at temperatures as low as 470~mK and in magnetic fields of up to 33T (see Ref. [17]).

This observation might suggest that these BEDT-TTF salts have considerably smaller values of $t_\perp$ than those mentioned above; certainly, the behaviour of the low-temperature resistivity of β"-(BEDT-TTF)$_2SF_5CH_2CF_2SO_3$ is very similar to that of weakly-coupled semiconductor quantum wells[18] Alternatively, as both salts show evidence for density-wave (DW) groundstates at low temperatures,[4,18] some aspect of the DW formation might suppress the mechanism for the resistivity peak described above.

The work is supported by the Department of Energy, the National Science Foundation (NSF) and the State of Florida (USA), and by EPSRC (UK). Work at Argonne National Laboratory is supported by US-DOE under contract W-31-109-ENG-38.

References

1. L. B. Ioffe and A. J. Millis, *Science* **285**, 1241 (2000).
2. D. G. Clarke and S. P. Strong, *Adv. Phys.* **46**, 545 (1997).
3. C. Bergemann *et al.*, *Phys. Rev. Lett.* **84**, 2662 (2000).
4. J. Singleton, *Rep. Prog. Phys.* **63**, 1111 (2000).
5. R. H. McKenzie and P. Moses, *Phys. Rev. Lett.***81**, 4492 (1998*); Phys. Rev. B* **60**, 11241 (1999).
6. N. F. Mott and E. H. Davies *Electronic properties of non-crystalline materials* (Taylor and Francis, London, 1975); A. F. Ioffe and A. R. Regel, *Prog. Semicond.*, **4**, 237 (1960).
7. See e.g. *The theory of superconductivity in the high T_c cuprates*, P. W. Anderson (Princeton University Press, 50 (1997)).
8. K. Kuroki and H. Aoki, *Phys. Rev. B* **60**, 3060 (1999).
9. J. Schmalian, *Phys. Rev. Lett.* **81**, 4232 (1998).
10. S. Louati *et al Phys. Rev. B* **62**, (2000).
11. J. M. Schrama *et al.*, J. *Phys. Condens.* **13** 2235 (2001).
12. M. S. Nam *et al.*, *J. Phys: Cond.. Matt.* **13**, 2271 (2001).
13. T. Osada *et al.*, *Phys. Rev. Lett.* **77**, 5261 (1996); N. Hanasaki *et al.*, *Phys. Rev. B* **57**, 1336 (1998); *ibid.* **60**, 11210 (1999)
14. V. G. Peschansky and M. V. Kartsovnik, *Phys. Rev. B* **60**, 11207 (1999); I. J. Lee and M. J. Naughton, *Phys. Rev. B* **57**, 7423 (1998).

15. John Singleton *et al.*, *preprint cond-mat* 0104570; P. Goddard *et al.*, this conference.
16. C. Mielke *et al.*, *J. Phys. Cond. Matt.* **13**, 8325 (2001).
17. J. Symington *et al.*, to be published.
18. M-S. Nam *et al.*, *Phys. Rev. Lett.* **87**, 117001 (2001).
19. An interesting possibility is that the broadening of the Shubnikov-de Haas and de Haas-van Alphen oscillations is mainly due to local variations in the potential experienced by the quasiparticles, and not conventional scattering; hence the true scattering rate is much smaller. This is discussed in J. Singleton *et al.*, *J. Phys. Cond. Matt.*, in press, which also shows that such considerations can account for the broadness of the superconducting transition.

MAGNETIC PHASE DIAGRAM IN FIELD INDUCED SUPERCONDUCTORS λ-$(BETS)_2Fe_xGa_{1-x}Cl_4$

S. UJI, C. TERAKURA, T. TERASHIMA, T. YAKABE, Y. IMANAKA and Y. TERAI

National Institute for Materials Science, Tsukuba, Ibaraki 305-0003, JAPAN
E-mail: UJI.Shinyac@nims.go.jp

S. YASUZUKA

National Institute for Materials Science Hokkaido University, and National Institute for Materials Science, JAPAN

M. TOKUMOTO

National Institute of Advanced Industrial Science and Technology, JAPAN

A. KOBAYASHI

Graduate School of Science, The University of Tokyo, JAPAN

F. SAKAI

Institute for Solid State Physics, The University of Tokyo, JAPAN

H. TANAKA and H. KOBAYASHI

Institute for Molecular Science, JAPAN

L. BALICAS and J. S. BROOKS

National High Magnetic Field Laboratory, Florida State University, USA

Electronic states have been investigated under high magnetic fields for quasi-two-dimensional organic conductors λ-$(BETS)_2Fe_xGa_{1-x}Cl_4$ (x=1.0, 0.47, 0.45, 0). Under magnetic field parallel to the c-axis, various electronic states appear, depending on x, field, and temperature. The global phase diagram for this alloy is presented and the evidence of the strong internal field due to the Fe moments is shown.

1 Introduction

Recently, magnetic field induced superconductivity was discovered for a magnetic organic conductor λ-$(BETS)_2FeCl_4$, where BETS is bis (ethylenedithio) tetraselenafulvalene.[1] At zero magnetic field, λ-$(BETS)_2FeCl_4$ shows the metal-insulator (M-I) transition around 8 K, which is associated with the antiferromagnetic order of the Fe spins (S=5/2) (see Refs. [2-5]). The insulating (I) phase for λ-$(BETS)_2FeCl_4$ is destabilized by the magnetic field above ~10 T, where paramagnetic state of the Fe moments is induced by the field. When the magnetic field is applied exactly parallel to the conduction plane, superconductivity (S) is

induced above 17 T below 1 K and then metallic (M) state is recovered above 42 T (see Ref. [6]). This field induced superconductivity is destroyed when the magnetic field component perpendicular to the conduction layers exceed ~3 T. In contrast, the isostructural non-magnetic salt λ-$(BETS)_2GaCl_4$ remains metallic and shows a superconducting transition at ~6 K (see Refs. [2,7,8]).

For the alloy system λ-$(BETS)_2Fe_xGa_{1-x}Cl_4$, the M-I transition is suppressed as the concentration of the magnetic Fe ion x decreases, and then the ground state becomes superconducting for $x<0.35$ (see Ref. [7]). A striking feature is that the metal-superconductor-insulator transition takes place for $0.35<x<0.5$. The variety of the magnetic phases apparently originates from the interaction between the Fe magnetic moments and the electrons on the BETS molecules. In order to investigate the field induced superconductivity, we have performed the resistance measurements for λ-$(BETS)_2Fe_xGa_{1-x}Cl_4$ and determined the global phase diagram.

2 Experiment

The single crystals are needle-like, elongating along the c axis. The Fe and Ga concentrations of the crystals of λ-$(BETS)_2Fe_xGa_{1-x}Cl_4$ were determined by electron probe microanalysis. The error is less than 10 %. The resistance was measured by a conventional four-probe ac technique with electric current along the b*-axis, which is perpendicular to the ac-plane. The experiments were made with 20 T superconducting and 30 T resistive magnets at NIMS, or 33 T resistive and 43 T hybrid magnets at NHMFL.

3 Results

Semi-log plots of the resistance curves for λ-$(BETS)_2Fe_xGa_{1-x}Cl_4$ ($x=0.47$) for B//c (B in the conduction layers) Å is shown in Fig. 1. At 0.6 K, as field increases, the resistance suddenly decreases by more than eight orders of magnitude around 5 T and then reaches zero within experimental error. As the field further increases, the resistance comes back to a metallic state value, ~1 Ω. The resistive transition curves show hysteresis around 5 T but not at the high field S-M transitions. At 0.6 K, the resistance shows a small bump at 6 T in the down sweep. This anomaly may suggest that the M phase intervenes between the I and S phases. In the superconducting transitions, kink behavior is seen, indicated by arrows. The behavior may be a vortex lattice melting transition as observed in high Tc superconducting cupurates : once the flux lattice is formed completely, the resistance sharply drops down to zero. At higher temperatures, the transition becomes broad, which is probably due to the enhance of the thermally activated flux motion. We have performed the resistance measurements for some alloys, and

obtained the global phase diagram for B//c as shown in Fig. 2.

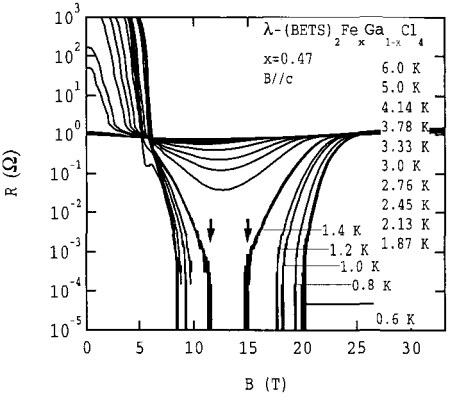

Figure 1: Semi-log plots of the resistance curves for λ-$(BETS)_2Fe_xGa_{1-x}Cl_4$ (x=0.47). The arrows indicate the kinks in the resistive transitions.

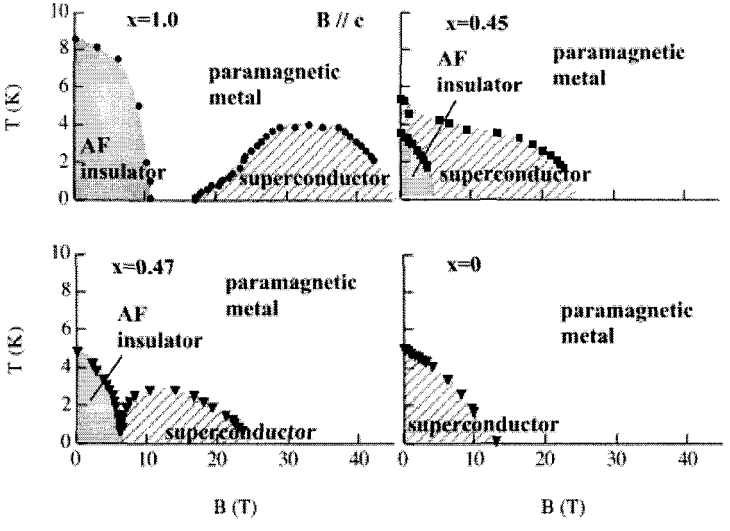

Figure 2: Global phase diagrams of λ-$(BETS)_2Fe_xGa_{1-x}Cl_4$ for B//c.

We define the midpoint of the resistive transition and the onset of the sharp increase in the resistance curve as the transition fields to the S and I phases,

respectively. For x=1, the I and S phase are well separated. As x decreases the field region of the S phase shifts to a lower field. For x=0.47, both the I and S phases are touching each other below 1 K. For x=0.45, the phase diagram seems very anomalous. The I phase is completely surrounded by the S phase. The S phase appears in a very wide temperature and field region, and survives up to 25 T at least, which is comparable to that for x=0.47. For x=0, the S phase is observed below 13 T, which is consistent with the reported one.[8]

4 Discussion

The field induced superconductivity has been discussed in terms of Jaccarino-Peter compensation mechanism.[6-9] In the M phase of λ-$(BETS)_2Fe_xGa_{1-x}Cl_4$, the localized Fe moments are paramagnetic. If the exchange interaction J between the Fe moments and the conduction electrons on the BETS molecules is negative, the external magnetic field can be compensated with the internal magnetic field B_J created by the Fe moments. The evidence of such strong internal field is obtained in the Shubnikov de Haas (SdH) experiments,[10] which was first pointed out by Cepas et al.[11] When the internal field B_J due to the exchange interaction is present, the spin splitting factor S in Lifshitz-Kosevich formula is modified.[12] When there exists only one cylindrical Fermi surface, the resultant oscillatory term is given by

$$R_{osc} \propto A_1 \cos\left[2\pi\left(\frac{F}{B}-\frac{1}{2}\right)+\pi S\right]+A_2\cos\left[2\pi\left(\frac{F}{B}-\frac{1}{2}\right)-\pi S\right], \quad (1)$$

$$S=\frac{1}{2}g\frac{m_{eff}}{m_0}\left(1-\frac{B_J}{B}\right), \quad (2)$$

where F is the SdH frequency corresponding to the cylindrical Fermi surface, m_{eff} is the effective mass, and g is the g-factor. The prefactors A include the temperature and Dingle reduction factors. Because of B_J/B in Eq. (2), we obtain two different SdH frequencies, F-$2B_J$ and F+$2B_J$, using m_{eff}/m_o=4 (see Ref. [10]), and g=2.

In Fig 3(a), the oscillatory parts of the resistance (SdH oscillations) are shown for two different salts, x=0 and 1.0 when the field is applied perpendicular to the conduction plane (B//b*). The spectra calculated by maximum entropy method (MEM) are shown in Fig. 3(b). For x=1.0, two frequencies are evident although a single frequency for x=0. The frequency 660T for x=0 corresponds to the area of 15% in the first Brillouin zone. This value is consistent with the results of the band calculations.[3-5] The difference of the two frequencies for x=1.0 is 128 T, which gives B_J =32 T. The phase diagram for x=1.0 has the maximum transition temperature at 32 T, and seems almost symmetric around 32 T, suggesting B_J =32 T. Therefore, we can conclude that Jaccarino-Peter effect is the main mechanism of the field induced superconductivity. However, we have still some important problems

to be solved; the mechanism of the Cooper pairs (electron-phonon interaction, magnetic fluctuation, or anything else?), the symmetry of the energy gap (s-wave, p-wave, or d-wave?), and so on. Further studies are now in progress.

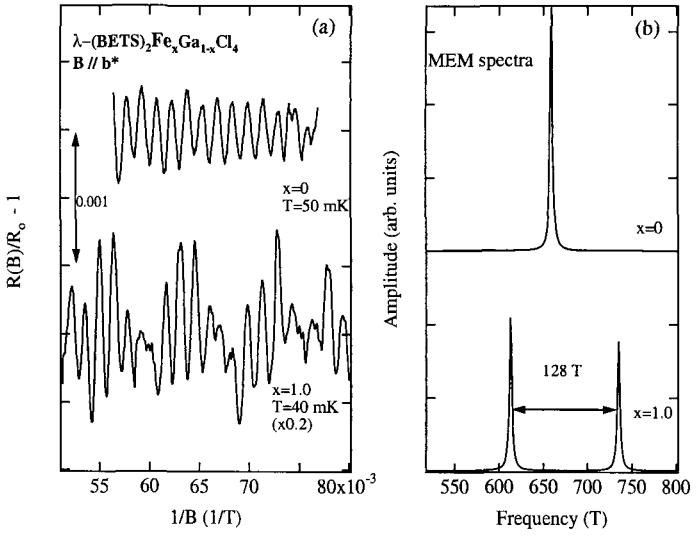

Figure 3: (a) Oscillatory part of the resistance (SdH oscillation. (b) MEM spectra of the SdH oscillations.

References

1. S. Uji *et al., Nature*, **410**, 908-910 (2001).
2. A. Kobayashi *et al., Chem. Lett.* 2179-2182 (1993).
3. H. Kobayashi *et al., J. Am. Chem. Soc.* **118**, 368-377 (1996).
4. M. Tokumoto *et al., Synth. Met.* **86**, 2161-2162 (1997).
5. L. Brossard *et al., Eur. Phys. J. B*, **1**, 439-452 (1998).
6. L. Balicas *et al., Phys. Rev. Lett.* **87**, 067002-1-4 (2001).
7. A. Sato *et al.*, Chem. Lett., 673-674 (1998) .
8. A. Tanatar *et al., J. Supercond*, **12**, 511-514 (1999).
9. V. Jaccarino and M.Peter, *Phys. Rev. Lett.* **9**, 290-292 (1962).
10. S. Uji *et al., Phys. Rev. B*, **64**, 024531-1-5 (2001).
11. O. Cepas and R. H. Mckenzie, J. Merino, preprint.
12. D. Shoenberg, *Magnetic Oscillations in Metals* (Cambridge University Press, 1984)

THE QUANTUM HALL EFFECT IN QUASI-ONE-DIMENSIONAL ORGANIC CONDUCTORS

V. M. YAKOVENKO
Department of Physics, University of Maryland, College Park, Maryland 20742-4111

Theoretical overview of the quantum Hall effect in quasi-one-dimensional (Q1D) organic conductors $(TMTSF)_2X$ will be presented.[1] The emphasis will be on the recent developments, such as the temperature evolution of the Hall effect[2,3] and the chiral edge states.[4] Time permitting, a theory of the nonchiral electron edge states in a Q1D triplet superconductor[5] and the holon edge states in the charge-gap regime[6] will be presented too.

1. V. M. Yakovenko and H.-S. Goan, *J. Phys. I* (France) **6**, 1917 (1996).
2. V. M. Yakovenko, H-S. Goan, J. Eom, and W. Kang, *J. Phys. IV* (France) **9**, Pr10-195 (1999).
3. T. Vuletic *et al.*, *Eur. Phys. J. B* **21**, 53 (2001).
4. K. Sengupta, H.-J. Kwon, and V. M. Yakovenko, *Phys. Rev. Lett.* **86**, 1094 (2001).
5. K. Sengupta *et al.*, *Phys. Rev. B* **63**, 144531 (2001).
6. A. V. Lopatin and V. M. Yakovenko, *cond-mat*/0106516.

NMR STUDY OF THE ANTIFERROMAGNETIC TO SUPERCONDUCTOR PHASE TRANSITION IN $(TMTSF)_2PF_6$

W. YU and S. E. BROWN

Department of Physics and Astronomy UCLA, Los Angeles, CA 90095, E-mail: brown@physics.ucla.edu

F. ZAMBORSZKY

MST Division, Los Alamos National Laboratory, Los Alamos, NM 87545

I. J. LEE and P. M. CHAIKIN

Department of Physics, Princeton University, Princeton, NJ 08544

The pressure-tuned quantum phase transition from spin-density wave (SDW) to Fermi Liquid (FL) ground states is studied in $(TMTSF)_2PF_6$ by NMR relaxation and spectroscopy. As for recent transport measurements, we find evidence in the distribution of local hyperfine fields for phase segregation, from which we conclude the transition between normal and SDW phases is discontinuous. A tricritical point (TCP) is identified. A crossover to FL behavior identified by spin-lattice relaxation measurements intersects the normal to SDW phase boundary very close to the TCP.

1 Introduction

Correlated electron systems are often characterized by their tunability by a single parameter, for example by adjusting the doping level or by the application of pressure. In many cases, the tuning gives access to a magnetic phase that is competing with a Fermi Liquid, or even superconductivity. In principle, the nature of the transition between magnetic and superconducting phases depends on the broken symmetries involved, which follow from the properties of the system under consideration. Opportunities to study this type of transition arise in various families of correlated materials. A particularly familiar example is $(TMTSF)_2PF_6$, well-known as the first organic conductor that was also superconducting.[1] In this system, an ambient-pressure spin-density wave (SDW) phase is easily suppressed by a modest applied pressure, and superconductivity appears at temperatures below about 1K at the boundary of the magnetic phase.

Assuming that the transition from the normal phase to the SDW phase is continuous, we expect that the phase diagram that includes superconducting and antiferromagnetic phases will feature a quantum critical point (QCP), a bicritical point (BCP), or a tetracritical point. The possibility for phase coexistence and a tetracritical point has been ruled out theoretically.[2,3] Experimental support for that

point of view came from the observation of reentrant superconductivity,[4] which was offered as evidence for a line of first order transitions terminated by a BCP. However, the results of a recent transport study were appeared to contradict the accepted scenario.[5] Instead, it was proposed that the normal/SDW phase line should not be considered as a line of continuous transitions. At pressures sufficiently close to the critical pressure P_c for suppressing the SDW, it was inferred that phase segregation occurs. The two phases are the normal, metallic phase and the fully-gapped SDW. At lower temperatures, superconductivity occurs in the volume fraction that was metallic. The phase segregation indicates that there is a line of first-order phase transitions separating the normal and SDW phases. Segregation disappears at lower pressures, suggesting that the line of first order transitions terminates at a tricritical point (TCP). Below we describe solid state NMR experiments, primarily ^{1}H NMR spectroscopy and ^{77}Se T_1^{-1} measurements, which demonstrate the microscopic phase segregation, and which seem to link a crossover to Fermi Liquid (FL) behavior to the TCP.

2 Experimental results and discussion

Single crystals of $(TMTSF)_2PF_6$ used in these experiments were prepared by the standard electrolysis method at UCLA, and the NMR measurements were performed at 10.5MHz, corresponding to (B_0=0.25T for ^{1}H nuclei and B_0=1.32T for ^{77}Se). In all cases, the magnetic field was applied along the crystallographic **b′** direction, with an uncertainty of ±0.5deg.

Two sets of NMR measurements gave the appropriate description of the low-temperature phases: AF-ordered or Fermi Liquid. Loosely speaking, the signature for the former is an inhomogeneous line broadening, which results from the development of static magnetism. Both ^{1}H spectroscopy and ^{77}Se T_1^{-1} were used for that purpose. For $P<P_c$, the SDW transition is identified by a sharp increase in T_1^{-1} attributable to slowing down of thermal magnetic fluctuations. A Korringa-like spin-lattice relaxation rate (*i.e.*, proportional to the temperature) serves as the FL identifier on the high-pressure side of P_c. The onset of superconductivity was identified by observing changes in the reflected power of the NMR tank circuit, and the superconducting transition temperature of Pb, placed within a second coil in the pressure cell, determined the pressure. Construction of the phase diagram in Fig. 1 follows.

The phase diagram includes a crossover line $T_{FL}(P)$ on the high-pressure, metallic, side of P_c that is described elsewhere in more detail[6]. Summarizing those results, T_{FL} is defined by fitting to

$$\frac{1}{T_1} = A\frac{1}{1+\frac{T_{FL}}{T}}, \qquad (1)$$

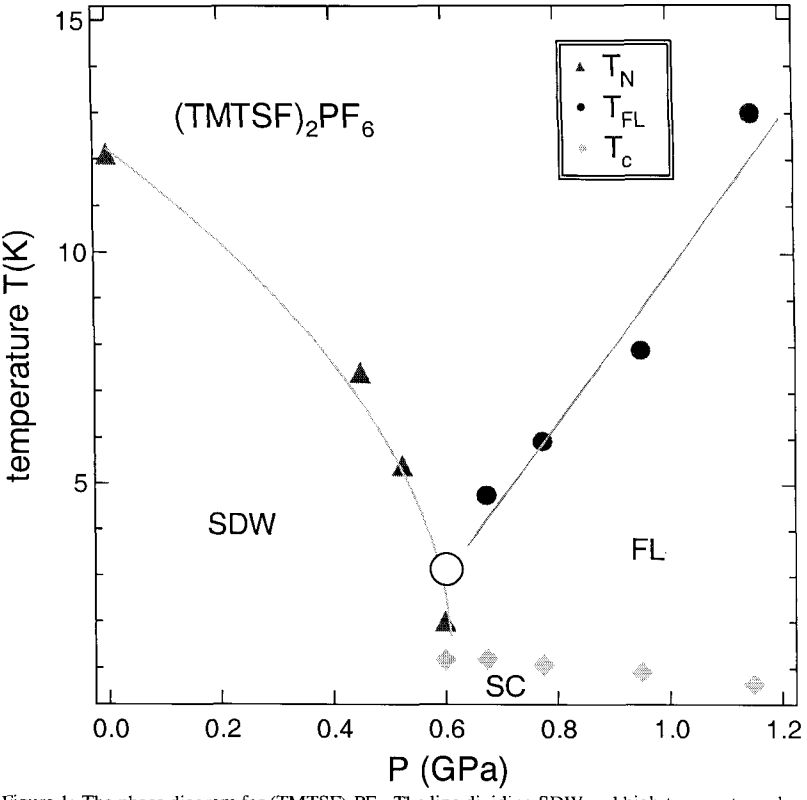

Figure 1: The phase diagram for $(TMTSF)_2PF_6$. The line dividing SDW and high-temperature phases is a line of continuous transitions. The circle is the proposed tricritical point at T*, beyond which the second-order line becomes first order. The line dividing the FL and high-temperature phases is a crossover.

where A is found to be a pressure-independent constant. As indicated by Eq. (1), the ^{77}Se T_1^{-1} is only weakly dependent on temperature for $T>T_{FL}$ as it would be for low-dimensional, quantum critical, spin fluctuations.[7,8] At lower temperatures, $^{77}T_1^{-1} \propto T$. The intersection of the crossover line T_{FL} and the SDW transition temperature T_{SDW} at a temperature T* is just less than T=3K. On the other hand, we expect T*=0K if the QCP exists, so it remains to identify the reason for avoiding it. A possible starting point is provided by a recent discussion of the quantum phase transition associated with $2k_F$ instabilities,[9] where it was suggested that large fluctuations in such systems will induce a first-order transition between ordered and normal phases.

(The idea of a fluctuation-induced first-order phase transition was originally presented in the context of isotropic instabilities).[10] Independently, an explanation for the heterogeneous mixing that depends strictly on band parameters, which change as a result of coupling to the lattice, was proposed to explain the transport results.[5]

Whatever the mechanism, the distribution of local fields obtained from ^{1}H NMR spectroscopy verifies the phase segregation. The top frame of Fig. 2 shows the change in the spectrum on lowering the temperature from T=5K to 1.5K for a pressure within the phase-segregated region. The change from high- to low-temperature is the development of wings, or a broad part of the spectrum, which is indicative of the *nonuniform* onset of static magnetic moments. In the bottom frame of Fig. 2 are plotted two pieces of information obtained from the temperature dependence of the absorption in the broad part. On the left vertical axis is the full extent of the wings, determined by the maximal range of the local hyperfine field distribution (and therefore is proportional to the range of local electronic moments). On the right-hand axis is the relative weight of the absorption in the broad part, giving a measure of the volume-fraction seeing static magnetism. To within experimental uncertainty, the moment increases discontinuously at T_{SDW} and the volume-fraction increases linearly in T_{SDW}-T. Both results are expected for a phase segregation scenario in the appropriate experimental situation. For example, a clean, stoichiometric system under controlled volume conditions is susceptible to phase segregation, and the situation is different under controlled pressure conditions. In our case, the pressure medium is solidified at a much higher temperature so there is no reason *a priori* to insist on idealized controlled pressure conditions.

Finally, we comment on the possibility that the existence of a nonzero pressure gradient within the cell is sufficient to explain the results above. In the simplest case, a gradient will lead to well-separated volume fractions for the two phases, for example at opposite ends of the sample. And while we have observed similar behavior in a number of samples of different shapes, there is at least one counterargument to this scenario. The important experimental fact is that there is a substantial increase of the upper critical field H_{c2}, for fields H||c, of the superconducting phase when the pressure is very close to P_c[11]. Where H_{c2} becomes large, the temperature dependence develops an unusual upward curvature. These observations were accounted for in a model[11] that depends on the formation of micro-domains of SDW and superconducting phases. The size of the superconducting domains would have to be on a length scale of the order of the coherence length, or less, to prevent vortex penetration into the superconducting fraction, which leads to screening currents and pairbreaking if the field is high enough. It indicates that phase segregation into domains much smaller than the sample size is very likely to occur under some circumstances.

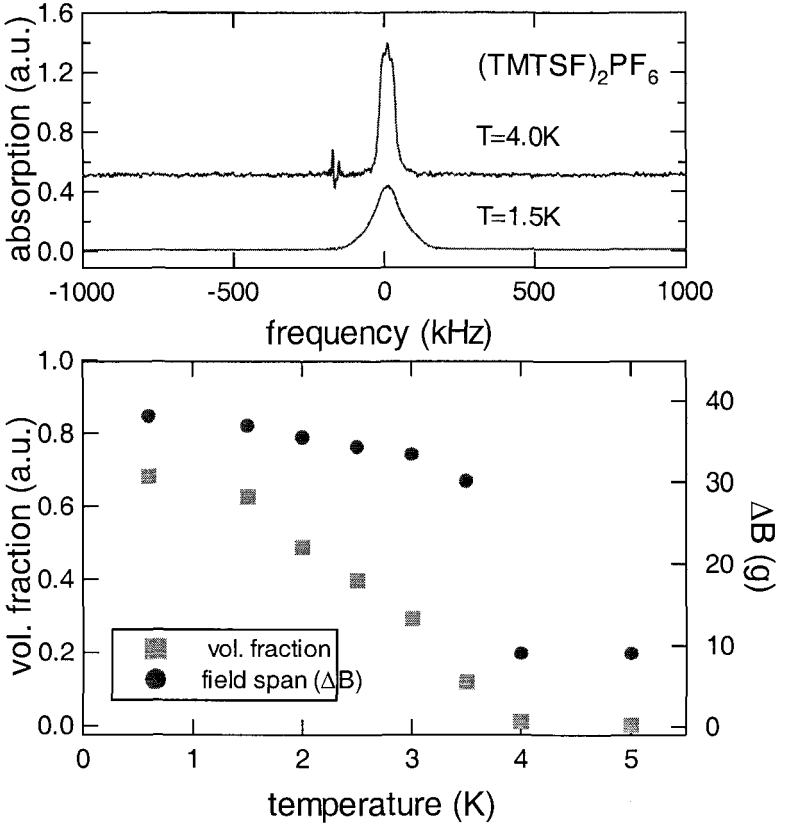

Figure 2: (a) The proton NMR spectrum for a pressure less than the critical pressure Pc $\approx$ 0.6 GPa at T=5K and 1.5K. The spectra have been normalized by correcting for temperature effects. (b) Maximum magnitude of the observed local field variation developing in the fraction with SDW order (right vertical axis), and *unnormalized* volume fraction developing the static magnetism (left vertical axis).

3 Conclusions

The observation of phase segregation supports a scenario for the magnetic/non-magnetic phase transition as first-order as T$\rightarrow$0, and a tricritical point at T* $\approx$3K. The observations appear consistent with the proposal that the SDW/normal metal transition becomes first order as T$\rightarrow$0. The intersection of the quantum-critical$\rightarrow$FL crossover temperature T_{FL} with the tricritical point at T* is a natural expectation, yet overall the pressure-dependence of $^{77}T_1^{-1}$ is consistent with the predictions of Ref.

[8] for tuning close to an AF QCP. The effect of disorder should not be ignored. Suppose we consider a simple weak-coupling picture for density wave formation. Applied pressure simply weakens the nesting condition, thereby reducing T_{SDW} and with it the gap parameter Δ_{SDW}. However, a relatively sharp SDW transition occurs only in the clean limit, $\xi << \ell$. And when $T_{SDW} \rightarrow 0$, the condition is more difficult to satisfy. Experiments in intentionally disordered materials will clarify the impact of disorder on the appearance of the phase diagram, and in particular the extent of the measured quantum-critical behavior.

Acknowledgments

We thank Steve Kivelson and Sudip Chakravarty for several discussions. This work was supported in part by the National Science Foundation and the In-house Research Program of the National High Magnetic Field Laboratory.

References

1. D. Jérome, A. Mazaud, M. Ribault and K. Bechgaard, *J. Phys. Lett.* **41**, L95, (1980).
2. K.Yamaji, *J. Phys. Soc. Japan* **52**, 1361 (1983).
3. Y. Hasegawa and H. Fukuyama, *J. Phys. Soc. Japan* **55**, 3978 (1986).
4. L. J. Azevedo, J. E. Schirber, J. M. Williams, M. A. Bono and D. R. Stephens, *Phys. Rev. B* **30**, 1570 (1984).
5. T.Vuletic, P. Auban-Senzier, C. Pasquier, S. Tomic, D. Jerome, M. Heritier and K. Bechgaard, *Eur. Phys. J. B* **21**, 53 (2001).
6. W. Yu, F. Zamborszky, B. Alavi, C. A. Merlic, A. Baur, D. J. Tantillo and S. E. Brown (*to be published*).
7. C. Bourbonnais, *J. Phys. I.* **3**, 143 (1993).
8. T. Moriya and K. Ueda, *J. Phys. Soc. Japan* **63**, 1871 (1994).
9. B.L. Altshuler, L.B. Ioffe and A.J. Millis, *Phys. Rev. B* **52**, 5563 (1995).
10. S. A. Brazovskii, *JETP* **68**, 175 (1975).
11. I.J. Lee, M.J. Naughton and P.M. Chaikin (submitted to *Phys. Rev. Lett.*).

This page is intentionally left blank

Contributed Papers

This page is intentionally left blank

THE EFFECTS OF PRESSURE AND MAGNETIC FIELD ON THE CONDUCTIVITY OF $FeCl_4$ DOPED POLYACETYLENE: THE INFLUENCE OF SCATTERING BY LOW-ENERGY EXCITATIONS

A. N. ALESHIN, T. J. KIM, D.-S. SUH and Y. W. PARK

School of Physics and Condensed Matter Research Institute, Seoul National University, Seoul 151-747, Korea
E-mail: aleshin@phya.snu.ac.kr

H. KANG and W. KANG

Department of Physics, Ewha Womans University, Seoul 120-750, Korea
E-mail: wkang@mm.ewha.ac.kr

The effects of hydrostatic pressure and magnetic field on the conductivity of oriented polyacetylene films doped with $FeCl_4$- up to metallic state have been studied at T = 0.35-300 K. It was found that application of pressure up to 10 kBar increases the conductivity at 300 K by a factor of 1.3 and suppresses the resistivity minimum in $\rho(T)$ at 270 - 280 K. At $T < 2$ K the temperature dependence of resistivity $\rho(T) \sim \ln T$ (at ambient pressure and at 10 kBar) which remains unaltered by a magnetic field up to 14 Tesla. Transverse magnetoresistance (MR) was found to be negative, linear and temperature independent at $T < 2$ K (at ambient and high pressure). We attribute the observed $\rho(T)$ and MR behavior to weak localization accompanied by effect of electron dephasing time saturation due to scattering by two-level systems of a special type. More strong behavior of $\rho(T)$ and MR at $T > 2$ K related to further suppression of weak localization due to scattering by low-energy excitations of a "glassy" type.

1 Introduction

The effects of hydrostatic pressure and magnetic field on the charge transport of heavily iodine and potassium doped polyacetylene (PA) have been studied intensively.[1,2] Most results have been treated in the framework of well-known interaction-localization or heterogeneous models. However some disagreements of experimental data obtained for heavily doped polymers with both of these models at $T < 1$ K allow to propose the influence of strong inelastic scattering by low-energy excitations (related to an initial chemical structure of conducting polymers) on the low-temperature conductivity.[3] Low temperature transport mechanism of $FeCl_4^-$ doped PA remains the subject of great interest because of its pronounced metallic behavior[4,5] and possible contribution from scattering by low-energy excitations.

In this paper we present and analyze the effects of pressure (up to 14 kBar) and magnetic field (up to 14 T) to the charge carrier transport of oriented heavily doped with $FeCl_4^-$ PA films in the temperature region 0.35 - 300 K.

2 Samples and Methods

The Naarmann type high-density PA films were synthesized by the modified Shirakawa method.[6] The samples were oriented by stretching with l/l_0~3-4. The $FeCl_4^-$ doping was done from solution up to saturation level (~ 7-8 wt %). The dc conductivity was measured in the temperature range 0.35 - 300 K with the standard four-probe method. High-pressure (up to 14 kBar) transport studies were carried out in a self-clamped beryllium-copper pressure cell using a sample holder with platinum contact wires. Manganin wire was placed inside the cell to determine the pressure during experiment. The hydrostatic pressure-transmitting medium was Fluorinert^{TM}. After pressuring the cell was clamped at 300 K and then cooled down to 350 mK in a ^{3}He cryostat system. Magnetic field up to 14 T was applied perpendicular to the sample surface and current direction.

3 Results

Figure 1 presents the typical pressure dependence of the normalized conductivity $\sigma(P)/\sigma$(ambient pressure) of $FeCl_4^-$ doped PA. As can be seen from Fig. 1, the conductivity at 300 K increases from 9100 S/cm up to 11720 S/cm (by a factor of 1.3) with pressure increase up to 10 kBar, while at higher pressure the conductivity decreases. The typical temperature dependencies of the normalized resistivity

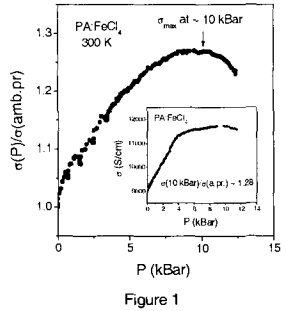

Figure 1

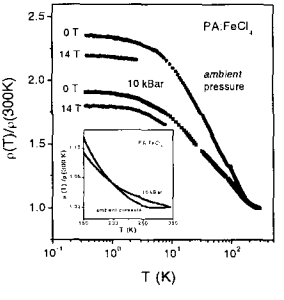

Figure 2

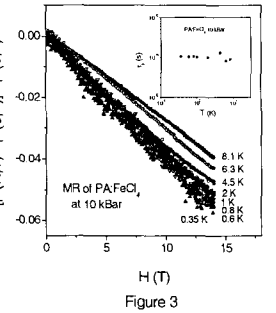

Figure 3

Figure 1, 2 and 3: Pressure dependence of the normalized conductivity (Fig. 1); temperature dependence of the normalized resistivity (Fig. 2), and transverse magnetoresistance of $FeCl_4^-$ doped PA.

$\rho(T)/\rho(300\ K)$ of $FeCl_4$ doped PA at ambient pressure and at 10 kBar are shown in Fig. 2. It is evident from Fig. 2 that application of pressure 10 kBar decreases the resistivity ratio $\rho_r = \rho(0.37\ K)/\rho(300\ K)$ from 2.4 down to 1.9. The resistivity minimum - a characteristic feature of heavily doped PA - was observed at $T^* \sim 280$ K at ambient pressure only. Application of pressure suppresses the

resistivity minimum. $FeCl_4^-$ doped PA samples demonstrate $\rho(T)/\rho(300\ K) \sim \ln T$ at $T < 2$ K, at ambient pressure and at 10 kBar, which is almost unaltered by a magnetic field. As can be seen from Fig. 2, a magnetic field (14 T) decreases the ρ_r at ambient pressure and at 10 kBar. The starting temperature T_0 of the $\rho(T)/\rho(300\ K) \sim \ln T$ dependence shifts by a magnetic field up to higher temperatures. Fig. 3 shows that at 10 kBar the MR of $FeCl_4^-$ doped PA is negative, linear and almost temperature independent at $T < 2$ K.

4 Discussion

We attribute the initial increase of $\sigma(P)/\sigma(\text{ambient pressure})$ in $FeCl_4^-$ doped PA to an enhancement of interchain interactions while the following decrease reflects the creation of structural defects. The suppression of the resistivity minimum at $T^* \sim 280$ K by pressure can be related to a pressure-dependent spatial imhomogeneity. The $\rho(T)/\rho(300\ K) \sim \ln T$ dependence at $T \leq 2$ K and negative MR at $T = 0.35 - 8.1$ K are similar to those observed in 2D systems.[7] However, our PA films are 3D because their thickness is far an excess of the diffusion length L_φ. Negative MR indicates that the transport dominates by weak localization (WL) with weak spin-orbit coupling. Hence the phase coherence time τ_φ can be estimated from the WL theory by fitting magnetoconductivity (MC): $\Delta\sigma(H) = \sigma(H) - \sigma(0) \sim H^2$ near zero magnetic field.[7] For 3D systems (at $\tau_\varphi << \tau_{SO}$):

$$\Delta\sigma(H) = \sigma(H) - \sigma(0) = (e^2/96\pi^2\hbar)(4DeH\tau_\varphi/\hbar c)^{3/2}(eH/\hbar c)^{1/2}$$

Were D is the diffusion coefficient estimated from the Einstein relation $\sigma = e^2N(E_F)D$ where $N(E_F)$ is a density of states at the Fermi level. For our samples with $\sigma \sim 10^4$ S/cm the electron concentration $n \sim 10^{22}$ cm^{-3}, thus one obtains $D \sim 4$ cm^2/s. The $\tau_\varphi(T)$ plot calculated for $FeCl_4^-$ doped PA at 10 kBar was found to be saturated (inset to Fig.3). This saturation behavior of $\tau_\varphi(T)$ at $T < 2$ K is similar to that found recently in variously doped PA at ambient pressure[8] as well as in some crystalline semiconductors.[9] We suggest that saturation of dephasing observed in $FeCl_4^-$ doped PA at high hydrostatic pressure originating from a presence of two-level systems (TLS) (see Ref. [10]) of a special type.[8] Such TLS originating from initially symmetric defect configurations, where the symmetry is partially lifted by the disorder. The model implies that the phase variation between different acts of inelastic scattering by TLS is small and the dephasing at low temperatures is due to phase diffusion involving many acts of electron-TLS scattering.[8] At temperatures $T > 2$ K the further stronger $\rho(T)/\rho(300\ K)$ behavior associated with another dephasing mechanisms originating from scattering by the TLS of a "glassy" type related to the amorphous properties of the polymer, i.e. to a presence of soft

interatomic potentials.[10] Pressure decreases the number of the density of states of soft localized modes with their conversion into TLS. This phenomenon may affect the inelastic scattering of electrons by TLS at low temperatures in PA, leading to higher metallic conductivity of PA fibril-like structure under high hydrostatic pressure.

Acknowledgments

We thank V. I. Kozub for discussions. Partial support for A.N.A. is from the BK-21 Program of Ministry of Education (MOE), Korea.

References

1. N. Basescu *et al., Nature* **327**, 403-405 (1987).
2. M. R. Anderson *et al., Phys. Rev. B* **47**, 9238-9242 (1993).
3. V. I. Kozub *et al., Phys. Rev. B* **59**, 11322-11327 (1999).
4. T. Masui *et al., Phys. Rev. B* **58**, 4352-4361 (1998).
5. E. S. Choi *et al., Synth. Met.* **100**, 3-12 (1999).
6. K. Akagi *et al., Synth.Met.* **27-29**, D1-D10 (1989).
7. B. L. Altshuler *et al., Sov. Phys.- JETP* **54**, 411-419 (1981).
8. A. N. Aleshin *et al., Phys. Rev. B* **64** (2001) in press.
9. P. Mohanty *et al., Phys. Rev. Lett.* **78**, 3366-3369 (1997).
10. Yu. Galperin *et al., Adv. Phys.* **38** 669-737 (1989).

HIGH FIELD PHASE DIAGRAM OF THE FIELD-INDUCED SUPERCONDUCTING STATE OF λ-(BETS)$_2$FeCl$_4$

L. BALICAS, J. S. BROOKS, and K. STORR
National High Magnetic Field Laboratory, Florida State University, Tallahassee-FL 32306
E-mail: balicas@magnet.fsu.edu

S. UJI
National Research Institute for Metals, Tsukuba, Ibaraki 305-0003, Japan
E-mail: UJI.Shinya@nims.go.jp

M. TOKUMOTO
Nanotechnology Research Institute, National Institute of Advanced Industrial Science and Technology (AIST), Tsukuba, Ibaraki 305-8568, Japan
E-mail: madoka.tokumoto@aist.go.jp

H. TANAKA and H. KOBAYASHI
Institute for Molecular Science, Okazaki, Aichi 444-8585, Japan
E-mail: hayao@ims.ac.jp

A. KOBAYASHI
Research Centre for Spectrochemistry, Graduate School of Science, The University of Tokyo, Bunkyo-ku, Tokyo 113-0033, Japan

V. BARZYKIN and L. P. GOR'KOV
National High Magnetic Field Laboratory, Florida State University, Tallahassee-FL 32306, USA
E-mail: gorkov@magnet.fsu.edu

We investigate by electrical transport the field-induced superconducting state (FISC) in the organic conductor λ-(BETS)$_2$FeCl$_4$. Below 4 K, antiferromagnetic-insulator, metallic, and eventually superconducting (FISC) ground states are observed with increasing in-plane magnetic field. The FISC state survives between 18 and 41 T, and can be interpreted in terms of the Jaccarino-Peter effect, where the external magnetic field *compensates* the exchange field of aligned Fe^{3+} ions. We further argue that the Fe^{3+} moments are essential to stabilize the resulting singlet, two-dimensional superconducting state. Here we provide experimental evidence indicating that this state, as well as the insulating antiferromagnetic ground state, is extremely sensitive to hydrostatic pressure.

1 Introduction

Superconductivity is usually destroyed by induced diamagnetic currents and by the so-called Clogston-Chandrasekhar paramagnetic limit[1,2] in the presence of strong magnetic fields. Nevertheless, and despite these well known physical limitations, S. Uji *et al.*,[3] have recently reported the observation of a magnetic-field induced

superconducting phase (FISC) in the quasi-two-dimensional organic conductor λ-$(BETS)_2FeCl_4$ for fields exceeding 18 tesla, applied parallel to the conducting layers. This is particularly remarkable since this compound, at zero field, is an antiferromagnetic insulator (AI) below $T_p \cong 8.5$ K (see Ref. [4]). The AI state is suppressed by the application of magnetic fields above 10 tesla at low temperatures.[5]

The present work was motivated by the apparent increase in the critical temperature of the FISC above 18 T with increasing magnetic field.[3] To clarify the nature of the FISC, we have studied the λ-$(BETS)_2FeCl_4$ compound at low temperatures in steady, tilted magnetic fields up to 45 tesla under ambient pressure and a very small amount of hydrostatic

2 Experimental Results

Single crystals of λ-$(BETS)_2FeCl_4$ were obtained by electro-crystallization. Annealed (low strain) gold wires (ϕ = 12.5 μm) were attached with graphite paint in a four-terminal arrangement along the c-axis. An ac current (10 to 100 μA) was used, and the voltage was measured by a conventional lock-in amplifier technique. Samples were mounted in a rotating sample holder in a ^{3}He refrigerator. The measurements were carried out in the Hybrid magnet at the DC Field Facility of the National High Magnetic Field Laboratory. Figure 1 shows Resistance as a function of field for several temperatures and two values of pressure: 1 bar and ε kbar. While Fig. 2 shows the resultant phase diagram.

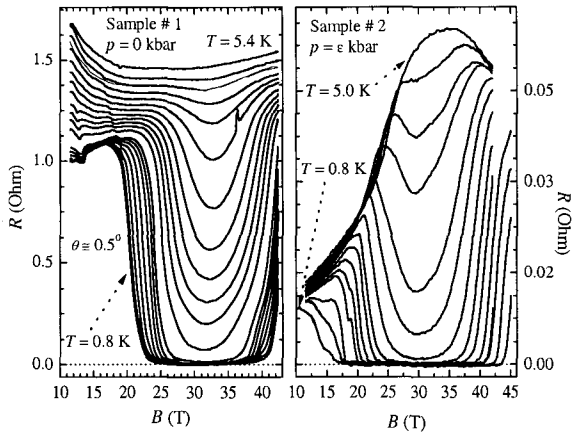

Figure 1: (a) Resistance R as a function of magnetic field B, applied along the in-plane c-axis (± 0.3 degrees) of a λ-$(BETS)_2FeCl_4$ single crystal (sample #1), at ambient pressure and for temperature intervals of approximately 0.25 K, between 5.4 and 0.8 K. The superconducting state develops progressively with decreasing temperature, but is suppressed for fields sufficiently away from (above or below) 33 tesla. (We note that since the Hybrid magnet is composed of a superconducting outsert coil in combination with a Bitter type resistive insert coil, the field generated by the outsert is kept constant at approximately 11.5 tesla, while the field of the insert coil was ramped between 0 and and 31.5 tesla). The FISC transition has a maximum transition temperature $T_c \approx 4.2$ K near 33 tesla. (b) As in (a) R as a function of B, applied along the in-plane c-axis for sample #2. In the present case, the sample is immersed in a fluid medium that induces a very small amount of hydrostatic pressure $p = \varepsilon$ kbar (>> 1 bar) upon cooling. The effect of p is, on one hand, to considerably decrease the resistivity of this compound and, on the other, to widen the range in magnetic fields at which the FISC state is observable.

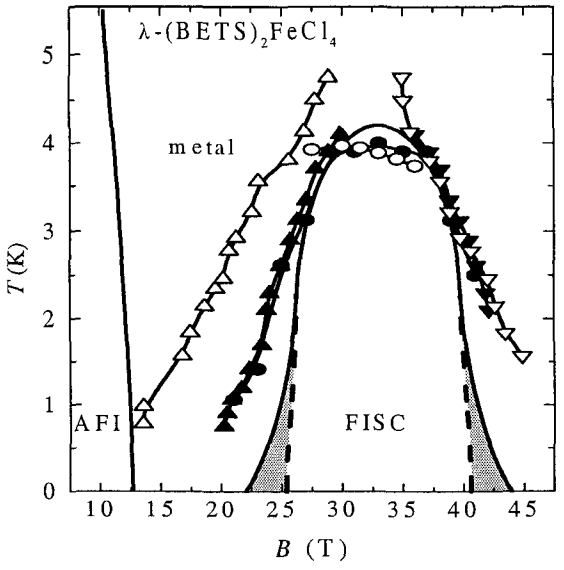

Figure 2: Temperature-magnetic field phase diagram showing the AI, metallic, and FISC states for a λ-$(BETS)_2FeCl_4$ single crystal vs in-plane magnetic field at ambient pressure (solid lines and symbols) . Solid triangles indicate the middle point of the resistive transition as a function of B (from Fig. 1(a)), while solid circles indicate the middle point of the resistive transition as a function of T. Similarly, opened triangles and opened circles describe the T - B diagram of the FISC state under *a very small amount of* hydrostatic pressure (the AFI is displaced to fields $B < 8$ T). The solid line is a theoretical fit[7] to a second order phase transition towards the FISC phase while the dashed line indicates a first order transition from the inhomogeneous so-called LOFF state (after Larkin, Ovchinnikov, Ferrell and Fulde)[7] (shaded area) into the bulk superconducting state.

3 Discussion

The $S = 5/2$ Fe^{3+} magnetic moments, oriented by magnetic field, exert the exchange field $J\langle S\rangle$ on the spins s of the conduction electrons via the exchange interaction, $J\,\mathbf{s} \bullet \mathbf{S}$. Thus, the effective field $H_{\rm eff}$ acting on the electron spin is:

$$I(B) = \mu_B H_{\rm eff} = \mu_B B + J\langle S\rangle \qquad (1)$$

The Jaccarino-Peter effect is the compensation in Eq. (1) of the magnetic field, B, by the exchange field, $J\langle S\rangle$, at $J < 0$, so that the effective field, $H_{\rm eff}$, may become below the Clogston limit[1,2] at higher B.

4 Conclusions

We conclude by noting that λ-$(BETS)_2FeCl_4$ (along with the non-magnetic analog λ-$(BETS)_2GaCl_4$) has provided a rich new area for the study of low dimensional superconductivity and magnetism, where the two mechanisms compete on a very low energy scale. In this paper we have provided a simple theoretical picture that describes the broader features of the newly discovered high field induced superconducting state. We argue that magnetic ions are actually essential to suppress the coupling between planes in the presence of in-plane magnetic fields.
We have also provided evidence clearly indicating that, small values of hydrostatic pressure, have a significant effect on the phase diagram of the high field FISC state. Under pressure the transition towards the FISC phase occurs at significantly lower magnetic fields. While the upper critical field and the transition temperature towards this state, does not seem to be significantly affected by the application of pressure. Pressure seems to be an effective way of changing the value of the exchange interaction between itinerant and localized spins.

Acknowledgments

We would like to thank the Hybrid Magnet Group at the NHMFL for their invaluable assistance during these measurements. One of us (JSB) acknowledges support from NSF-DMR-99-71474 for this work.

References

1. A. M. Clogston, *Phys. Rev. Lett.* **9**, 266 (1962).
2. B. S. Chandrasekhar, *Appl. Phys. Lett.* **1**, 7 (1962).
3. S. Uji, *et al.*, *Nature* **410**, 908 (2001).
4. A. Kobayashi, *et al.*, *Chem. Lett.***12**, 2179 (1993).
5. L. Brossard *et al., Eur. Phys. J. B* **1**, 439 (1998).
6. V. Jaccarino and M. Peter, *Phys. Rev. Lett.* **9**, 290 (1962).
7. L. Balicas, *et al.*, *Phys. Rev. Lett.* **87** (6), 067002 (2001).
8. L. P. Gor'kov and A. I. Rusinov, *Sov. Phys. JETP* **19**, 922 (1964).
9. V. Barzykin and L. P. Gor'kov, *Phys. Rev. Lett.* **84**, 2207 (2000).
10. L. Balents and C. M. Varma, *Phys. Rev. Lett.* **84**, 1264 (2000).
11. A. I. Larkin and Yu. N. Ovchinnikov, *Sov. Phys. JETP* **20**, 762 (1962); P. Fulde and R. A. Ferrell, *Phys. Rev.* **135A**, 550 (1964).
12. L. N. Bulaevskii, *Sov. Phys. JETP* **38**, 634 (1974).

MAGNETIC FIELD-INDUCED DENSITY WAVE TRANSITION IN A τ-PHASE ORGANIC CONDUCTOR

D. GRAF, L. BALICAS and J. S. BROOKS
National High Magnetic Field Laboratory, Tallahassee, FL 32310, USA

C. MIELKE
National High Magnetic Field Laboratory, Pulsed Field Facility, Los Alamos, NM 87545, USA

G. C. PAPAVASSILIOU
Theoretical and Physical Chemistry Institute, National Hellenic Research Foundation, Athens, Greece 116/35

Pulsed magnetic fields to 53 tesla reveal a new high field phase transition in τ-[P-(S,S)-DMEDT-TTF]$_2$($AuBr_2$)($AuBr_2$)$_y$ (where y~.75). This transition appears as an abrupt increase in the magnetoresistance at a threshold field (B_{Th}~44 tesla for T=0.55 K). B_{Th} shifts toward higher magnetic fields with increasing temperature, and there is evidence of higher field sub-phases. Measurements of Shubnikov de Haas oscillations below 33 tesla have provided compelling evidence as to the two-dimensional (2D), metallic nature of this compound. In the following report we discuss this new unexpected state, reminiscent of the field-induced spin density wave (FISDW) behavior in the quasi one-dimensional (Q1D) Bechgaard salts.

1 Introduction

The Tau-phase class of organic conductors go through a metal-insulator transition below T~50 K (see Ref. [1]). Quantum oscillations provide evidence of this low temperature metallic state.[2] A square-like network of cations (in the ab-plane) forms the unique crystal structure (as shown in Fig. 1) of these compounds, with anions appearing at both in-plane and inter-plane sites. The long unit cell is constructed by a four layer repeat pattern with highly anisotropic conductivity. The low temperature Fermi surface (FS) of this material remains uncertain since band structure calculations[3] predict a closed star-shaped FS (Fig. 2), but SdH oscillations show a more complex FS with several closed orbits. This experiment was done to investigate the magnetoresistance of the Tau sample in very high fields, up to 52 tesla. We were surprised to see a new phase transition above 44 tesla, which is quite similar to the field-induced density wave (FIDW) phase transitions seen in the Bechgaard salts. We report on the possibility of an underlying Q1D nature of the FS for the Tau-phase materials.

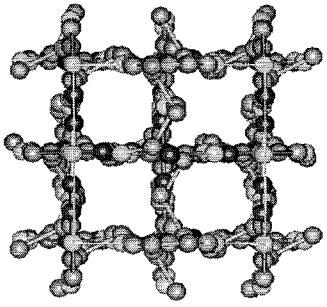

Figure 1: Intersecting molecular planes of the Tau-phase molecular structure in the ab-plane.

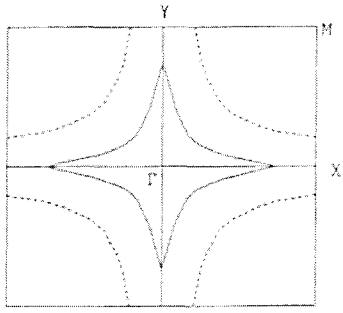

Figure 2: Star-shaped FS determined by band structure calculations. Dotted line indicates y=1. (see Ref. [3]).

2 Experimental Results

The sample was synthesized using electrochemical methods (the same sample used in Ref. [2]). Four terminal DC measurements were made on the τ-[P-(S,S)-DMEDT-TTF]$_2$($AuBr_2$)($AuBr_2$)$_y$ sample using 12 μm gold wire attached with silver paint. Current along the c-axis was set at 300 μA to provide an adequate signal-to-noise ratio. Pulsed magnetic fields, produced at the pulsed magnet facility at LANL, were applied parallel to this axis. A ^{3}He refrigeration system was used to achieve low temperatures.

The sample displays negative magnetoresistance at low fields (Fig. 3), consistent with previous measurements.[2] In our pulsed field results we observe a sharp increase in magnetoresistance above 40 tesla. As the magnetic field increases beyond this point, the resistance reaches a peak and then decreases to its initial value. We define the changes in resistance as the threshold field (B_{Th}), divot (B_D), and the peak (B_P) (shown in Fig. 4). The lowest temperature measurement, taken at T=0.55 K, clearly shows these features. The positively sloped side of the peak has a slight divot, which suggests sub-phases when $B > B_{Th}$. Higher temperature pulses show B_{Th} shift toward higher fields and the peak broaden (ie. B_{Th} ~47 T for T=13.0 K). Though some resistance measurements had random oscillations, no systematic SdH oscillations were observed. This is not completely unexpected due to the noisy nature of pulsed field measurements.

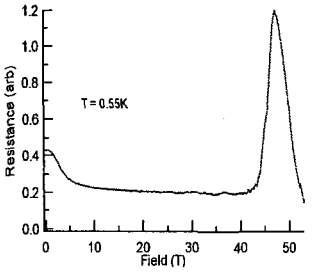

Figure 3: Magnetoresistance measurement of the Tau-phase sample at T=0.55 K.

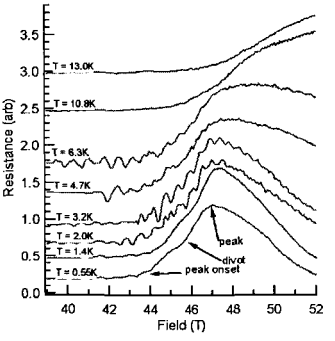

Figure 4: Magnetoresistance measurements to 52 T at temperatures (curves are offset for clarity).

A proposed phase diagram for a FIDW, derived from the features in figure 4, is shown in figure 5. A clear tendency towards higher fields with increasing temperature is seen for all three features

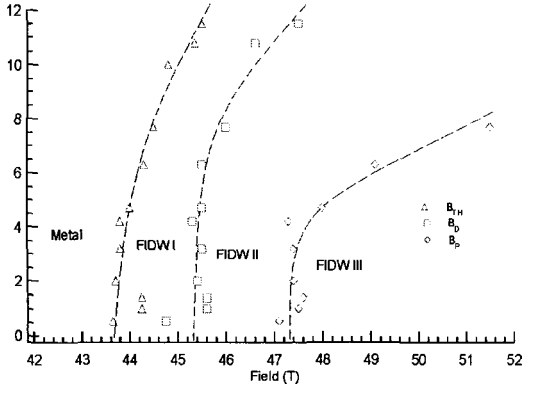

Figure 5: Phase diagram for τ-[P-(S,S)-DMEDT-TTF]$_2$(AuBr$_2$)(AuBr$_2$)$_y$.

3 Discussion

The FIDW transition at high fields introduces a new Q1D phase that is unexpected in this Tau-phase organic conductor since previous studies have clearly shown 2D properties, in the form of SdH oscillations. The resulting phase diagram of this experiment is surprisingly similar to that of (TMTSF)$_2$X (where X=ClO_4, PF_6),

which also suppress a metallic state through FISDW transitions. In the Tau-phase material, the sample resistance decreases after B_P, which is at odds with the behavior of the Bechgaard salts where the resistance continues to increase after the transition. Pressure data would be useful to continue this comparative study with the Bechgaard salts since B_{Th} is suppressed to higher fields.[4]

Measurements of temperature dependence at even higher fields would answer the question of re-entrant behavior from FIDW back to a conducting phase.[5] Further tight-binding calculations need to be completed for low temperatures to determine if they are in better agreement with experiment results.

An important question is the origin of the Q1D behavior in the 2D case of the Tau-phase conductor. Following Whangbo, this shift in dimensionality may be due to a "hidden" Q1D nature in the FS.[6] Using this concept, the sides of a star or diamond-shaped FS could be viewed as Fermi sheets which nest in the presence of high magnetic fields. A clearer view of the FS topology of this compound is necessary before this theory can be applied.

Acknowledgments

We would like to acknowledge the LANL Pulsed Magnetic Field Facility for their expertise and technical support as well as the National Science Foundation (NSF-DMR-99-71474) for their financial sponsorship.

References

1. G. C. Papavassiliou *et al.*, *Synth. Met.* **86**, 2043 (1997).
2. K. Storr *et al.*, *Phys. Rev. B* **64**, 045107 (2001).
3. A. Terzis *et al.*, *Synth. Met.* **42**, 1715 (1991).
4. W. Kang *et al.*, *Phys. Rev. Let.* **70**, 3091 (1993).
5. M. Naughton *et al.*, *Phys. Rev. Let.* **61**, 621 (1988).
6. M. H. Whangbo *et al.*, *Science* **252**, 96 (1991).

ELECTRON MAGNETIC RESONANCE FERMI SURFACE IMAGING: APPLICATIONS TO ORGANIC CONDUCTORS AND Sr_2RuO_4

S. HILL and A. KOVALEV

Department of Physics, University of Florida, Gainesville, FL 32611
E-mail: hill@phys.ufl.edu

M. M. MOLA and C. PALASSIS

Department of Physics, Montana State University, Bozeman, MT 59717

Z. Q. MAO and Y. MAENO

Department of Physics, University of Kyoto, Kyoto 606-8502, Japan, and CREST-JST, Kawaguchi, Saitama 332-0012, Japan

J. S. QUALLS

Department of Physics, Wake Forest University, Winston-Salem, NC 27109

We report detailed angle dependent studies of the metallic state microwave (40 to 200 GHz) magneto-conductivity of single crystal samples of the α-$(BEDT\text{-}TTF)_2KHg(SCN)_4$ organic charge density wave conductor, and the perovskite superconductor Sr_2RuO_4. We observe series' of resonant absorptions which we attribute to periodic orbit resonances - a phenomenon closely related to cyclotron resonance. By performing measurements on several samples, and in different electromagnetic field configurations, we are able to couple to different orbital modes (+ harmonics), which derive from deformations (warpings) of the quasi-one and quasi-two-dimensional Fermi surfaces of these compounds. These studies provide vital information concerning interlayer dispersion which, in turn, affects the Fermi surface nesting characteristics which are believed to play a crucial role in the low temperature physics of these exotic materials.

1 Introduction

A detailed knowledge of the Fermi surface (FS) topologies of low-dimensional conductors is an essential starting point for understanding the mechanisms that drive the various electronic instabilities which result in, *e.g.* the magnetism or superconductivity in these systems. For example, recent theoretical studies have shown that the symmetry of the superconducting state in quasi-2D (Q2D) and quasi-1D (Q1D) systems is extremely sensitive to the nesting characteristics of the FS (see Refs. [1,2]). Although there exists an extensive array of experimental techniques for probing FS topology, few possess the necessary resolution to profile the small (often $< 1\%$) deformations (warpings) that arise due to weak dispersion along the low conductivity axis (axes) of Q2D (Q1D) systems.

We have recently developed new methods for determining the FS topologies of quasi-low-dimensional systems using a millimeter-wave spectroscopic technique.[3] A novel type of cyclotron resonance (CR) is predicted to occur, which is fundamentally different from the conventional CR observed in normal metals. This technique, which was first considered by Osada *et al.*,[4] essentially corresponds to high frequency ($\omega \sim \omega_c$) Angle-dependent Magneto-resistance Oscillations (AMRO). The periodic *k*-space motion (over the FS) induced by the application of a magnetic field, translates into periodic modulations of the real space quasiparticle velocities as they traverse either Q1D or Q2D warped FSs in a plane perpendicular to the applied field; in particular, the velocity components along the low-conductivity directions undergo dramatic oscillations. GHz measurements then couple resonantly to these real space oscillations, resulting in so-called Periodic Orbit Resonances (POR). Just as in the DC case, different angle dependences are predicted for the Q1D and Q2D cases. However, additional harmonic AMRO/POR series are expected, corresponding to the higher harmonic content of the FS warping.[4,5] Thus, GHz AMRO offer an novel means for extracting minute, albeit essential, details of the FS topologies of low-dimensional conductors.

2 Experimental

Single crystals of α-(BEDT-TTF)$_2$KHg(SCN)$_4$ and the perovskite Sr_2RuO_4, with dimensions ranging from 2×1×0.05 to 0.5×0.5×0.05 mm^3, have been used in these investigations. Both materials possess layered structures, and exhibit Q2D conducting behavior. However, as we will show, the POR observed in Sr_2RuO_4 reflect its Q2D FS while, in the organic compound, a Q1D POR behavior is seen.

Measurements were performed using a cavity perturbation technique covering the frequency range from 18 to 200 GHz; for experimental details see Ref. [6]. A single sample was placed within a cylindrical resonator such that a combination of in-plane and interlayer currents were excited; a detailed discussion of the electrodynamics is published elsewhere.[7] Interlayer currents penetrate deep (100 μm – 1 mm) into the sample due to the low conductivity in this direction. Dissipation then depends on the ratio of the intelayer and in-plane conductivities, as well as the relative dimensions of the sample. For this experimental geometry, we have shown unambiguously that this dissipation is dominated by the interlayer conductivity for the highly anisotropic organic conductors,[7] whereas the measured dissipation is equally sensitive to the in-plane (conventional CR) and interlayer (POR) conductivities for the slightly less anisotropic Sr_2RuO_4 system.[8]

A combination of the resistive magnets at the National High Magnetic Field Laboratory (up to 33 T) and a superconducting split-pair (7 T) were used in these investigations. The magnetic field was either swept at constant orientation with respect to the sample, or the orientation of a fixed magnetic field is swept relative to the cavity containing the sample.

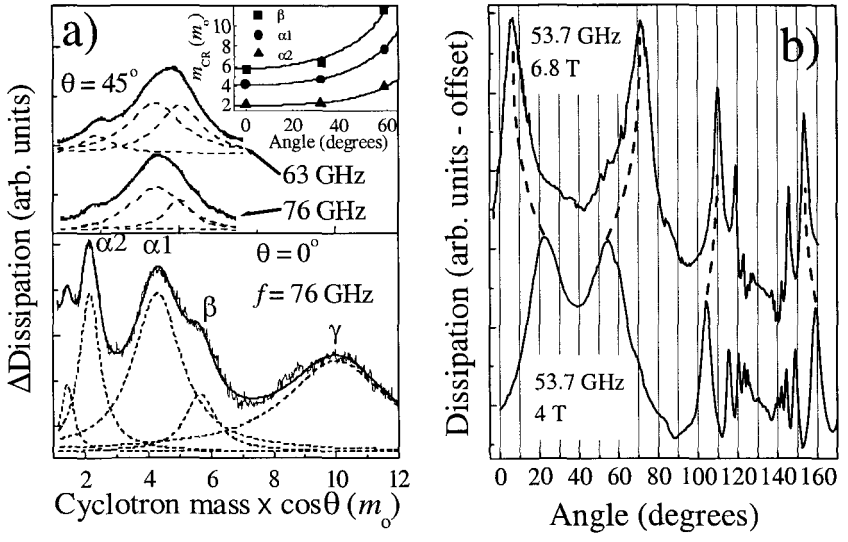

Figure 1(a): Scaled angle dependent dissipation (+ fits) measured in Sr_2RuO_4 (T = 2 K), showing several POR branches, plus harmonics. b) Angle dependent oscillations in the magneto-conductivity, at T = 2 K, of α-(BEDT-TTF)$_2$KHg(SCN)$_4$; note the field dependence of the dissipation (∝ conductivity) maxima.

3 Results and discussion

Figure 1(a) shows angle dependent POR for Sr_2RuO_4. Several branches (+ harmonics) are observed, corresponding to the three well known FSs (α, β, and γ), with effective masses of $m_\alpha = 4.3\ m_o$, $m_\beta = 5.76\ m_o$, and $m_\gamma = 9.73\ m_o$. A detailed account of the analysis of this data may be found in Ref. [8], including a determination of the symmetry of the FS warping. The important point to note is the fact that the measured effective masses scale as 1/cosθ, where θ is the angle between the applied field and the normal to the conducting layers. This confirms the Q2D nature of the FSs of Sr_2RuO_4, and settles a recent controversy regarding the origin of the resonances observed in the mm-wave magneto-conductivity of this compound.[8,9]

Figure 1(b) shows the first measurements (a preliminary study) of dissipation versus angle for α-(BEDT-TTF)$_2$KHg(SCN)$_4$. The sharp peaks correspond to conductivity resonances, or PORs. The data show symmetry about ≈40° and ≈130°, corresponding approximately to the field applied perpendicular and parallel to the highly conducting layers. The first thing to note is the amazing similarity between this data, and published DC AMRO data.[10] However, most importantly, we observe a systematic shift in the positions (angles) of the conductivity resonances for the two

magnetic field strengths. In the DC case, the AMRO conductivity peaks are observed at field independent angles. The reason for the shifts in our data is due to the fact that there exist two similar time scales in the problem, both of which exceed the scattering time – namely the FS traversal period, which depends on the field strength, and the microwave oscillation period. It has been predicted that the AMRO minima (conductivity maxima) depend on the ratio of f/B, where f is the measurement frequency and B the applied field strength.[4,5] For the DC case, this ratio is always zero, and the angles at which AMRO minima are observed do not depend on the field strength.

Another point to note is the strong dependence of the POR frequency on angle in the vicinity of 40° (field ⊥ layers); a 70% increase in the magnetic field (∝ POR frequency) causes the conductivity peaks to move from only about 18° to 33° either side of 40° (see dashed lines). For the 2D case, the POR frequency should scale as 1/cosθ, where θ is measured relative to 40° in our set up, *i.e.* for the 2D case, the observed shift in the peaks would be brought about by only a 13% increase in the field strength. In fact, although preliminary, our measurements are characteristic of Q1D POR, in agreement with AMRO measurements.[10] These are the first measurements of their kind, and a work very much in progress. Future measurements of this kind hold the promise to accurately image minute details of the FSs of a wide range of low-dimensional conductors.

Acknowledgments

This work was supported by the National Science Foundation (DMR 0196461). Stephen Hill is a Cottrell Scholar of the Research Corporation.

References

1. T. Kuwabara and M. Ogata, *Phys. Rev. Lett.* **85**, 4586 (2000).
2. T. Takimoto, *Phys. Rev. B* **62**, R14641 (2000).
3. S. Hill, *Phys. Rev. B* **55**, 4931 (1997).
4. T. Osada, S. Kagoshima and N. Miura, *Phys. Rev. B* **46**, 1812 (1992).
5. S. Blundell, A. Ardavan and J. Singleton, *Phys. Rev. B* **55**, 6129 (1997).
6. M. Mola, S. Hill, P. Goy and M. Gross, *Rev. Sci. Inst.* **71**, 186 (2000).
7. S. Hill, *Phys. Rev. B* **62**, 8699 (2000).
8. S. Hill *et al., Phys. Rev. Lett.* **84**, 3374 (2000); C. Palassis *et al., Physica C* **364-365**, 386 (2001).
9. E. Rzepniewski, A. Ardavanand J. S. Singleton, *Physica B* **294-295**, 379 (2001).
10. S. J. Blundell and J. S. Singleton,. J. S., *Phys. Rev. B* **53**, 5609 (1996).

HIGH FIELD MAGNETOCONDUCTIVITY OF IODINE DOPED HELICAL POLYACETYLENE

D. -S. SUH, T. J. KIM and A. N. ALESHIN

School of Physics and CMRI, Seoul National University, Seoul 151-747, Korea
E-mail: dssuh@phya.snu.ac.kr

Y. W. PARK

School of Physics and CMRI, Seoul National University, Seoul 151-747, Korea and NHMFL, Tallahassee, FL 32310
E-mail: ywpark@phya.snu.ac.kr

G. PIAO, K. AKAGI and H. SHIRAKAWA

Institute of Materials Science and Center for Tsukuba Advanced Research Alliance, University of Tsukuba, Tsukuba, Ibaraki 305-8573, Japan
E-mail:akagi@ims.tsukuba.ac.jp

J. S. QUALLS, S. Y. HAN and J. S. BROOKS

Physics Department and NHMFL, Florida State University, Tallahassee, FL 8544, USA
E-mail: brooks@magnet.fsu.edu

The effect of interfibrillar interaction on the charge transport of doped polyacetylene is investigated by studying the high field magnetoconductivity of iodine doped helical polyacetylene. The zero-field resistivity ratio, $\rho_r = \rho(1.2\ K)/\rho(300\ K)$, is comparable to that of stretch-oriented high-density polyacetylene, which indicates the partial alignment of chains inside a polymer fiber. At low magnetic fields, the small negative component of magnetoconductivity was observed and its magnitude increases as the ρ_r value increases. In the high field region, the magnetoconductivity is positive and it clearly shows the linear dependence on the magnetic field up to H=30 T. The linear field dependence of magnetoconductivity is different from what is expected in the three-dimensional weak localization picture. For the same ρ_r value samples, the magnitude of negative magnetoconductivity of S-polyacetylene is much bigger than that of R-polyacetylene, which could be attributed to the difference in the degree of helicity determining the strength of interfibrillar interaction.

1 Introduction

Magnetotransport of doped polyacetylene has been studied since the first discovery of conducting polymers in order to understand the basic electrical conduction mechanism. In this work we investigated the interfibrillar transport properties of polyacetylene system with special type of films which have the twisted structure of polymer fibers. Helical polyacetylene was synthesized using chiral nematic liquid crystal as a solvent of Ziegler Natta catalyst.[1] There are two types of helical films, R-type and S-type, with opposite helicity to each other. The helical polyacetylene

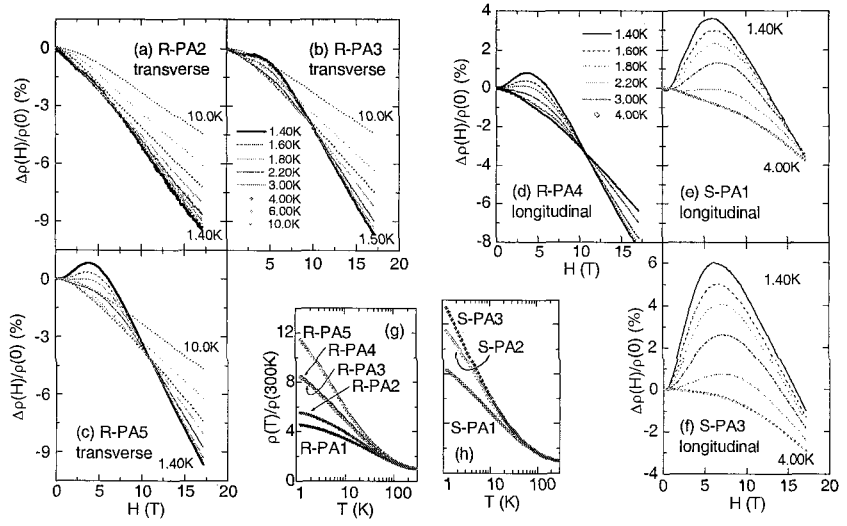

Figure 1: Magnetoresistance and temperature dependence of resistivity of the R-type and the S-type helical polyacetylene films heavily doped with iodine.

has two special features distinguishable from the traditional high-density film. One is that the size of single fiber is approximately 100 nm diameter which is much larger than that of the traditional one. The other is that fibers are twisted to form the ropes.

2 Experimental Results

Magnetoresistance data of several R-type and S-type helical polyacetylene films are plotted in Fig. 1. Highly conducting R-polyacetylene(PA) shows negative magnetoresistance in the overall magnetic field region, which is closely related to the weak localization as in the case of high-density film. As the ρ_r value increases in Fig. 1(g), this negative magnetoresistance in the low field region systematically changes to be positive. See Figs. 1(a), (b) and (c). In the high field region, however, the temperature and the field dependence of magnetoresistance are more or less the same for all R-type samples. In the case of S-PA, the magnetoresistance begins to increase at low fields forming a positive broad peak around H=5-7 T, and it decreases in the high field region. When we compare the data in Fig. 1(e) with Fig. 1(f), the larger ρ_r value gives the larger positive magnetoresistance. From Figs. 1(d) and (e), it is possible to examine the effect of the different morphology between two helical polyacetylene films with approximately the same ρ_r values. The positive

component of S-PA at low fields is much bigger than that of R-PA be attributed to the structural distinction between the R- and the S-PA films. From the circular dichroism spectra,[1] it was clearly shown that not only the direction of helicity is different but also the degree of helicity of S-PA is less than that of R-PA, *i.e.*, the tightness of twisted structure of fibers in S-PA is weaker. Consequently, the interfibrillar coupling strength becomes smaller in S-polyacetylene. It leads to the higher potential barrier for the charge carriers to be delocalized with the applied magnetic field resulting in the bigger positive magnetoresistance in S-polyacetylene than in R-polyacetylene. .

3 Discussion

The low temperature magnetoconductivity of high-density polyacetylene has been discussed in terms of the weak localization in three-dimensional system, where the competition between the localization (giving the positive contribution) and the

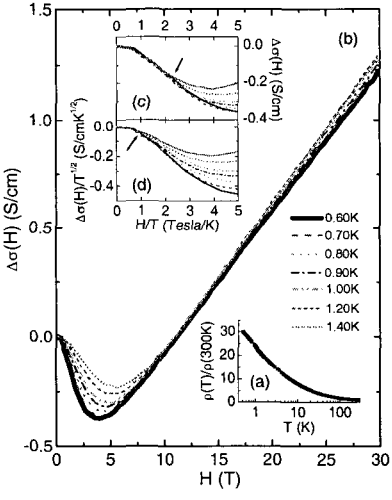

Figure 2: High field magnetoconductivity of iodine doped R-type helical polyacetylene up to H=30 T.

electron-electron interaction effect (resulting in the negative contribution) determines its field dependence.[3] It predicts the $H^{1/2}$ dependence of the positive magnetoconductivity in the high field region. However, in our data given in Fig. 2 up to H=30 T, the linear dependence of magnetoconductivity in the high field region is observed. And it is almost insensitive to the temperature below T=1.40 K. Therefore the three-dimensional localization-interaction picture is not sufficient to describe the obtained results in the region of high magnetic field. And for the low

field data, if the negative magnetoconductivity originates from the electron-electron interaction in isotropic three-dimensional disordered metallic system, the data of the inset (d) in Fig. 2 (showing $\Delta\sigma(H)/T^{1/2}$ vs H/T plot) follow one single curve up to the higher H/T value than the data in the inset (d) as pointed by the arrow in the figure. In the inset (d), all the data start to deviate from each other at H/T~1. However, in the inset (c) in Fig. 2 given in the scheme of $\Delta\sigma(T,H)$ vs H/T, they follow the same line up to H/T~2.4. This implies that the H/T is the single parameter determining $\Delta\sigma(T,H)$ in the low H/T region.

Acknowledgments

This work was supported by KISTEP under the contract No. 98-I-01-04-026, Ministry of Science and Technology, Korea. A portion of this work was performed at NHMFL, Tallahassee, which is supported by NSF Cooperative Agreement No. DMR-95-27035 and by the State of Florida.

References

1. K. Akagi *et al., Science* **282**, 1683-1686 (1998).
2. D. –S. Suh *et al., J. Chem. Phys.* **114**, 7222-7227 (2001).
3. P. A. Lee and T. V. Ramakrishnan, *Rev. Mod. Phys.* **57**, 287-337 (1985).

Part IV

Quantum Solids and Liquids

This page is intentionally left blank

VISCOSITY OF HIGHLY POLARIZED VERY DILUTE ^{3}He -^{4}He MIXTURES

H. AKIMOTO,[A,B] J. S. XIA,[A] E. D. ADAMS,[A] D. CANDELA,[B]
W. J. MULLIN,[B] and N. S. SULLIVAN,[A]

[A]*Microkelvin Laboratory, NHMFL and Physics Department*
University of Florida, Gainesville, FL 32611 USA

[B]*Hasbrouck Laboratory, Department of Physics,*
University of Massachusetts, Amherst, MA 01003 USA

We present vibrating - wire viscosity measurements on a very dilute ^{3}He-^{4}He mixture (x_3 = 150 ppm) in fields up to 14.8 T and temperatures down to 3 mK. The ^{3}He spin polarization is greater than 99% for the highest field and lowest temperature used. In these conditions, the *s*-wave scattering rate decreases due to a lack of quasiparticles with the minority spin state. This enhances all transport coefficients including the viscosity. At the lowest temperature, the hydrodynamic damping of the viscometer in a 14.8 T field was more than 10 times larger than in low fields. This indicates a many-fold increase in the mixture viscosity due to spin polarization.

1 Introduction

At very low temperatures, the properties of dilute ^{3}He -^{4}He mixtures are determined by the ^{3}He quasiparticles since thermal excitation of the ^{4}He is negligible. The ^{3}He quasiparticle system behaves as a weakly interacting Fermi gas.[1] The transport properties are determined by ^{3}He - ^{3}He interactions. The interaction between ^{3}He quasiparticles is short range and is dominated by *s*-wave scattering at sufficiently low temperatures and concentrations. Even though the *s*-wave scattering length is not polarization dependent, polarization decreases the scattering rate due to Fermi statistics.[2] Only anti-parallel pairs of spins can scatter in s-wave orbital states, and the fraction of anti-parallel pairs decreases with increasing spin polarization. Consequently the mean free path becomes longer and the viscosity and thermal conductivity get larger as polarization is increased. In a fully polarized system, *p*-wave scattering would dominate.[2]

Figure 1 shows the polarization calculated for non-interacting Fermions of effective mass $2.255m_3$ for concentrations and magnetic fields used in two previous experiments[3,4] as well as the present one. The dots show the lowest temperature for each experiment. Previously, the polarization-induced viscosity increase had been observed for systems with modest spin polarization, of order one but not close to one. A 50% increase in viscosity in an 8 T field was observed using second sound,[5] and later by using a vibrating wire viscometer.[3] Recently the Nottingham group measured a four-fold increase of viscosity due to 77% polarization in an 11.5 T field.[3] To reach the nearly fully polarized regime (1- P) << 1, we have used both lower ^{3}He concentration and higher magnetic field than in these earlier experiments.

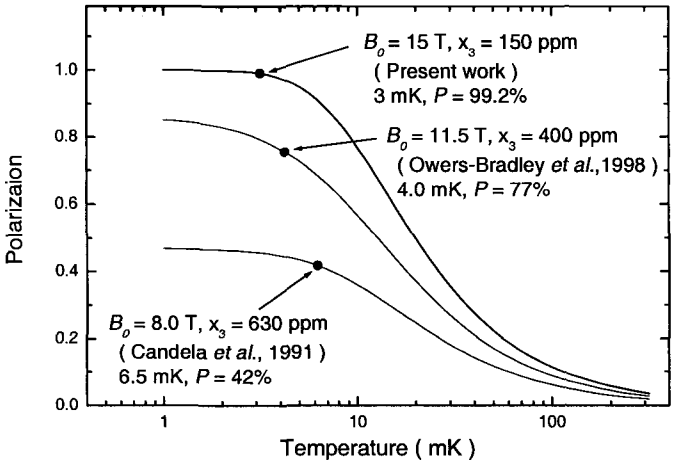

Figure 1: Temperature dependence of the spin polarization of ^{3}He-^{4}He mixtures for concentration (x_3) and field values (B_0) used in three reported experiments.

At low temperatures and concentrations the ^{3}He mean free path increases, presenting a problem for vibrating-wire viscometry. When the mean free path is an appreciable fraction of the wire diameter, the mechanical dissipation deviates from the hydrodynamic prediction. A slip correction[6] can deal with modest mean free path effects, but the slip theory breaks down when the mean free path becomes comparable to or greater than the wire diameter. In this ballistic regime, the wire damping is independent of quasiparticle scattering and no longer reflects the hydrodynamic viscosity. Previous experiments[3,4] used fine viscometer wires (diameter 10-100 μm) to achieve sufficient sensitivity for the viscosity of very dilute ^{3}He-^{4}He mixtures. Consequently significant slip corrections were required. To enable viscosity measurements with the much longer mean free paths occurring in the present experiment, we constructed a novel two-part vibrating-wire viscometer as described below.

In this report we describe our measurement system and preliminary results for viscometer measurements on a very dilute ^{3}He-^{4}He mixture (x_3 = 150 ppm) at very high spin polarization (>99 %). Our viscometer retains sensitivity down to the lowest temperature reached (3 mK), and exhibits hydrodynamic losses over ten times greater at high field than for a non-polarized system.

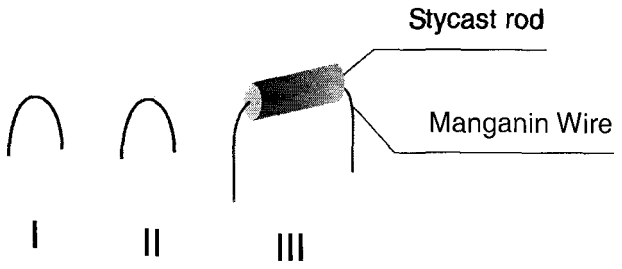

Figure 2: Sketch of the three vibrating-wire viscometers. Viscometers I and II are conventional, while viscometer III incorporates an enlarged section to reduce slip effects.

2 Apparatus

As shown in Figure 1, the present experiments required an extremely high field/temperature ratio B_0/T. To achieve this we used a cryostat combining a powerful nuclear demagnetization stage and a 15 T sample magnet. The nuclear stage contains 92 mol of copper (effectively 46 mol in 8 T) along with 5 mol of $PrNi_5$. The high field experimental base plate is cooled through a high-conductivity silver thermal link. The sample cell is fastened to this plate by titanium screws and has a 40 m^2 sintered heat exchanger. The temperature was monitored by a melting pressure thermometer installed in the low magnetic field region. This was supplemented by a Kapton capacitance thermometer inside the sample cell at high field. Details of the refrigeration and thermometry will appear elsewhere.[7]

Three vibrating-wire viscometers were installed inside the sample cell (Figure 2). Two of the viscometers are conventional semicircular loops of manganin wire (diameters 28 μm and 40 μm). The third viscometer consists of an epoxy rod (Stycast 1266, 0.82 mm dia. by 4 mm long) glued to the central portion of a 40 μm-dia. manganin wire. For this viscometer the exposed manganin "legs" provide a weak restoring force (as required for the low viscosity values measured here), while the epoxy rod is sufficiently large to interact hydrodynamically with the long mean free path quasiparticle gas. Table 1 gives the dimensions and some measured properties of the three viscometers.

3 Results

First we show the resonance line widths of the three viscometers measured in a mixture with x_3 = 150 ppm at 14.8 T (Figure 3). The line width due to the loss of the vibrating wire was subtracted. At temperatures higher than 10 mK, the three viscometers show nearly the same temperature dependence. This includes a shallow

Table 1: Dimensions, resonance frequency f_0, and quality factor Q for the three vibrating wire viscometers in vacuum at $T = 10$ mK, $B_0 = 14.8$ T.

Viscometer	I	II	III
Wire diameter (μm)	28	40	40
Rod diameter (μm)	-	-	820
Distance between legs (mm)	5	5	6
f_0 (Hz)	3245	3438	96.2
Q	7980	7270	22000

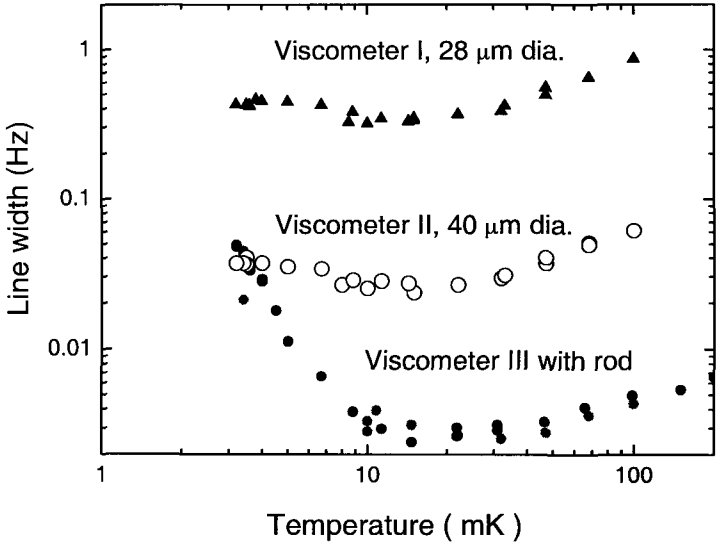

Figure 3: Measured line widths for the three viscometers in a mixture with x_3=150 ppm at field B_0= 14.8 T. The line widths for the two conventional viscometers saturate below 10 mK, while the line width of the third viscometer increases down to the lowest temperature measured.

minimum at about 20 mK. Below 10 mK the line widths of the two conventional viscometers have very little temperature dependence. At these temperatures the mean free path exceeds the diameters of the wires according to our calculation. Conversely, the line width of the third viscometer (with epoxy rod) shows marked temperature dependence to the lowest temperature measured.

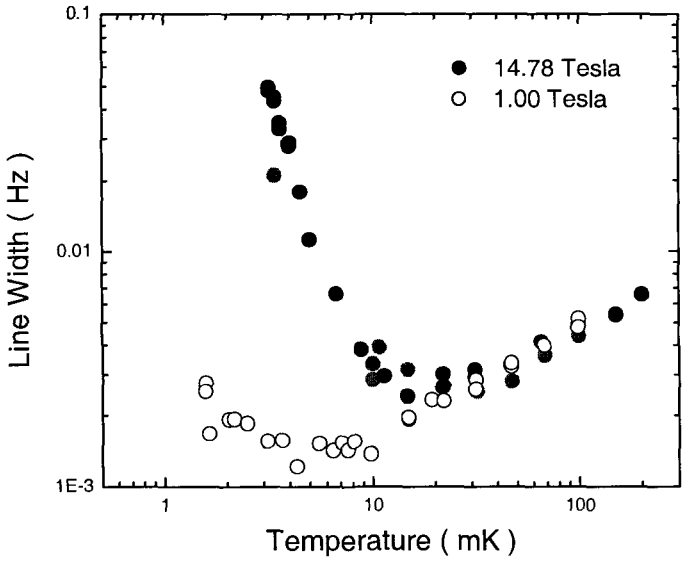

Figure 4: Line width measured for viscometer III in a x_3=150 ppm mixture at two different magnetic fields.

Figure 4 shows the line width for viscometer III in the x_3 = 150 ppm mixture at two fields, 1.0 and 14.8 T. At higher temperature the line width is proportional to $T^{1/2}$, which agrees with the expected temperatur dependence for the viscosity of a dilute gas. The B_0 = 1.0 T line width has a shallow minimum at about 6 mK, corresponding to the expected viscosity minimum in the vicinity of the Fermi temperature of non-polarized system. Our base temperature is not sufficiently low to see the T^{-1} behavior expected at temperatures far below the Fermi temperature. At B_0=14.8 T a large increase of the line width is clearly seen at the lowest temperatures (Figure 4). At the lowest temperature reached at high field, 3 mK, the line width is more than ten times larger than at low field.

The large field-induced increase we observe in the line width of viscometer III suggests that the viscosity of the liquid has increased by a factor about one hundred due to the very large spin polarization. Final reduction of our data to field-dependent viscosity values will require a consideration of the hydrodynamics for our novel viscometer design. The preliminary data shown here demonstrate that it is possible to measure the viscosity of ^{3}He-^{4}He mixtures in these combined

conditions of very low ^{3}He concentration, very low temperature, and very high magnetic field.

This work was supported by the science research program of the National High Magnetic Field Laboratory funded by the NSF-DMR-9016241 and the State of Florida.

References

1. G. Baym and C. Pethick in *The Physics of Liquid and Solid Helium,* ed. by K. H. Bennemann and J. B. Ketterson (Wiley, New York, 1978), Part II.
2. E. P. Bashkin and A. E. Meyerovich, *Adv. Phys.* **30**, 1 (1981).
3. D. Candela, L.-J. Wei, D. R. McAllaster, and W. J. Mullin Phys. Rev. Lett. **67**, 330 (1991) and D. Candela, D. R. McAllaster, L.-J. Wei, and N. Kalechofsky, *J. Low Temp. Phys.* **89**, 307 (1992).
4. J. R. Owers-Bradley, R. M. Bowley, J. H. Naish, P. J. Richardson, A. P. J. Voncken and R. K. Konig, *J. Low Temp. Phys.* **110**, 321 (1998)
5. J. R. Owers-Bradley, P. C. Main, R. J. Church, T. M. Hampton, G. McHale and R. M. Bowley *Phys. Rev. Lett.* **61**, 1619 (1988).
6. H. Smith, in *Progress in Low Temperature Physics Vol. 11,* ed. by W. P. Halperin and L. P. Pitaevskii (Elsevier, Amsterdam, 1991).
7. H. Akimoto *et al., to be published* in J. Low Temp. Phys.
8. A. M. Guenault, T. R. Nichols and G. R. Pickett, *J. Low Temp. Phys.* **81**, 179 (1990).

Contributed Papers

This page is intentionally left blank

INVESTIGATION OF MULTIPLE-SPIN EXCHANGE IN 2D FILMS OF ^{3}He: NMR STUDIES

C. PARKS and N. S. SULLIVAN

Department of Physics, University of Florida, Gainesville, Fl 32611, USA
E-mail: sullivan@phys.ufl.edu

P. STACHOWIAK

Institute for Low Temperature and Structure Research, Wroclaw, Poland
E-mail: p_stach@int.pan.wroc.pl

Results of NMR studies of the nuclear spin-spin relaxation times at low temperatures are reported for commensurate monolayers of ^{3}He physisorbed on hexagonal boron nitride. Temperature independent relaxation rates are observed for $0.11<T<0.56$ K, and are interpreted in terms of the quantum exchange motions of the ^{3}He atoms. The relaxation times and the inferred effective exchange rates were observed to change significantly on replacing the ^{3}He atoms with relatively immobile Ne atoms. This result is understood in terms of a large 3-spin exchange in addition to 2-spin exchange.

1 Introduction

Solid ^{3}He films formed by physisorbtion of atoms on suitable substrates such as exfoliated graphite or hexagonal boron nitride represent one of the most ideal two-dimensional quantum systems. The weak localization of the atoms due to quantum mechanical zero-point motions leads to significant overlap of the atomic wave functions and a resulting high probability of atom-atom exchange. The most remarkable property of the solid heliums, two-dimensional (2D) and three-dimensional (3D), is that exchange is not limited to 2-spin exchange, but 3-spin, 4-spin and higher order cyclical exchanges also occur.

The effective multi-spin exchange (MSE) Hamiltonian is given by

$$H = -\hbar \sum_n (-)^n J_n P_n \qquad (1)$$

J_n and P_n are, respectively, the exchange frequency and permutation operator for cyclic permutations of n atoms. The nuclear magnetism at very low temperatures is dominated by the MSE. At the lowest densities in bulk solid ^{3}He the tendency for the nuclear spin ordering is antiferromagnetic. As the density is increased the system becomes increasingly ferromagnmetic. This is attributed to the rapid change of the relative values of the antiferromagnetic 2-spin exchange compared to the ferromagnetic 3-spin exchange. In 2D films this dependence on local density is even more pronounced[1] and depends on the particular geometry of the center of mass

lattice structure, *i.e.* whether commensurate $\sqrt{3}$ X $\sqrt{3}$ or higher order (10 X 10 or 7 X 7) at higher surface densities. In 2D films, the lowest coverages tend to be ferromagnetic because of the suppression of 2-spin exchange by the corrugation of the absorption potential, then becoming more anti-ferromagnetic on approaching perfect $\sqrt{3}$ X $\sqrt{3}$ coverage, and ferromagnetic on completing the full monolayer coverage.

The MSE model has been successful in describing the observed temperature dependence of the nuclear spin susceptibility, X_N, and the heat capacity, C_N

$$X_N = C/((T-\Theta) \text{ and } C_N = \tfrac{9}{4}(J_{eff}^C/k_BT)^2 \text{ with } \Theta = 3J_{eff}^N \text{ where}$$

$$J_{eff}^N = -(J_2 - 2J_3 + 3J_4 - 5J_5 + \tfrac{5}{8}J_6 + ...) \text{ and}$$

$$J_{eff}^C = J_2 - 2J_3 + \tfrac{5}{2}J_4 - \tfrac{7}{2}J_5 + ...$$

The effective exchange frequencies can also be probed using NMR techniques. NMR is sensitive to the motion of atoms through modulation of the nuclear dipole-dipole interactions which can be written as

$$H_{DD} = D\sum_{kl}\sum_n Y_{2n}(\Theta_{kl},\Phi_{kl})I_{2n}(kl) \tag{2}$$

The Y_{2n} are the spherical harmonics and (Θ_{kl},Φ_{kl}) are the polar angles defining the orientation of the interatomic vector $\vec{r}_{kl}$. The I_{2n} are the irreducible tensorial operators in spin space that transform equivalently to the Y_{2n}, *e.g.* $I_{20}(kl)=(3I_{kz}I_{lz}-I_k\cdot I_l)/\sqrt{6}$.

The spectral densities $G_n(n\omega)$ (Fourier transforms at the nuclear Larmor frequency ω of the autocorrelation functions $<Y^{2n}_{kl}(0)Y^{2n}_{kl}(t)>$ determine the nuclear spin relaxation rates. The relaxation rate (T_2^{-1}) of the transverse magnetization is particularly useful to study.

$$\frac{1}{T_2} = \tfrac{3}{2}G_0(0) + \tfrac{5}{2}G_1(\omega) + G_2(2\omega) \tag{3}$$

At high magnetic fields; $G_0(0) >> G_1(\omega) > G_2(2\omega)$, and T_2 is very simple to analyze.

$\frac{1}{T_2} = \frac{3}{2}G_0(0) = \frac{3}{2}M_2/J_{eff}^{NMR}$ with $J_{eff}^{NMR} = \sqrt{2M_4/\pi M_2}$ where M_2 and M_4 are the second and fourth moments of the NMR line shape. From direct calculations for the triangular lattice, we find

$$J_{eff}^{NMR} = 1.4\left|(J_2 - 2xJ_3 + \tfrac{3}{4}x^2J_4 + ...)\right| \tag{4}$$

where x is the probability that a given site is occupied by a ^{3}He atom in the event of site substitution by an immobile atom (*e.g.* Ne).

2 Experimental Results

Powdered hexagonal boron nitride was used for the high field experiments because the high conductivity and high diamagnetism of graphite interferes with the RF penetration and can seriously distort NMR line shapes at high fields. After careful cleaning, controlled amounts of 99.95% pure ^{3}He were admitted to the sample cell. The boron nitride surface was characterized using adsorption isotherms of HD and para-H_2. (see Ref. [2])

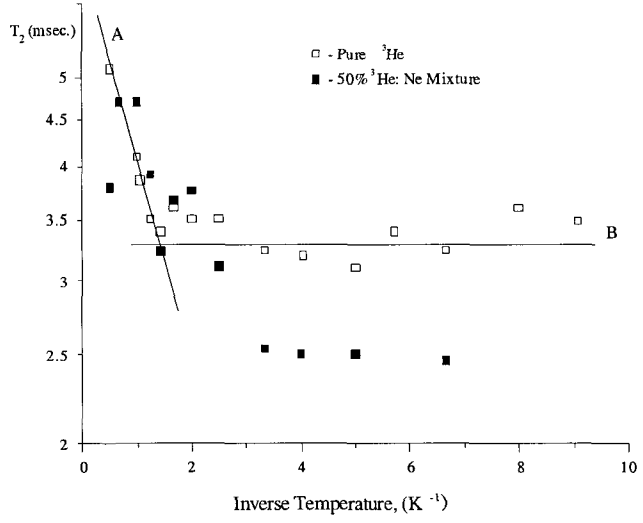

Figure 1: Temperature dependence of nuclear spin-spin relaxation times for commensurate layers of pure ^{3}He and a 50% ^{3}He:Ne mixture on hexagonal boron nitride.

The NMR relaxation rates were measured using standard pulse techniques. The first measurements were carried out at fixed temperature for a range of coverages. A sharp dip in the relaxation time was observed at the completion of a monolayer coverage. This results from the higher rigidity of the perfect lattice with respect to atomic motions compared to that in the presence of excess, or missing, atoms.[3] This sharp and reliable characterization of the commensurate coverage for the boron nitride surface was carried out for both pure ^{3}He and 50% ^{3}He:Ne. The minimum shifted slightly with Ne substitution and was broadened as expected. It is clear that the adsorbed Ne did not form islands.

The observed relaxation times are shown in Fig. 1. At high temperatures an exponential temperature dependence is observed (solid line A in Fig. 1). This dependence is due to the thermal activation of vacancies. The experimental results allow the determination of both the vacancy formation energy and the vacancy-atom

tunneling (or exchange) frequency. The temperature independent region (B of Fig. 1) is attributed to the quantum mechanical exchange motions. Using the expressions given above for J_{eff}^{NMR}, we find for pure ^{3}He, $J_{eff}^{NMR} = |J_3 - 2J_2| = 3.9.10^5$ rad/s., and for the 50% mixture, $J_{eff}^{NMR''} = |2J_2 - 0.5J_3| = 1.3.\ 10^5$ rad/s. where we have neglected J_4, J_5 etc. From these results we deduce $J_2 = 3.25.10^5$ rad/s., and $J_3 = 10.4.10^5$ rad/s.

3 Conclusions

The strong reduction of the nuclear spin-spin relaxation time on diluting the ^{3}He monolayers shows clearly that the overall motional narrowing of the line shapes due to quantum motions is appreciably reduced. For classical rigid lattice systems the dilution would lead to the opposite effect. The results can only be understood if there are strong competing multi-particle exchange rates with 2-spin and 3-spin exchange rates of comparable magnitude.

Acknowledgments

This work was supported by the NSF under grant no. 9623536.

References

1. M. Roger, C. M. Bauerle, Yu M. Bunkov, A. S. Chen and H. Godfrin, *Phys. Rev. Lett.* **80**, 308-315 (1998).
2. M. D. Evans, N. Patel and N. S. Sullivan, *J. Low Temp. Phys.* **89**, 653-672 (1992).
3. C. Parks, P. Stachowiak and N. S. Sullivan, *J. Low Temp. Phys.* **121**, 489-493 (2000).

ORDER/DISORDER TRANSITIONS OF ORTHO-PARA HYDROGEN MONOLAYERS AT LOW TEMPERATURES

N. S. SULLIVAN

Department of Physics, University of Florida, Gainesville, FL 32611-8440, USA
E-mail: sullivan@phys.ufl.edu

K. KIM

Department of Physics, University of South Alabama, Mobile, AL 36688, USA
E-mail: kkim@jaguar1.usouthakl.edu

V. B. KOKSHENEV

Department of Physics, Universidade Federale de Minas Gerais, MG, Brazil, 30123-970 E-mail: valery@fisica.ufmg.br

Experimental studies of the low temperature behavior of mono-layers of ortho-H_2 - para-H_2 mixtures using low temperature NMR techniques reveal an unusual phase diagram. An extension of the mean field approach is proposed to explain the qualitative features of the observed phase diagram. The competition between the highly frustrated short-range quadrupolar fields and the local crystal fields plays a key role in determining the nature of the ordered structures.

1 Introduction

The orientational ordering of the simplest diatomic molecules (H_2, N_2) in reduced dimensions provides valuable insights into the interplay of geometry and disorder in highly frustrated systems. The molecular centers of mass form well-defined lattice structures, typically triangular close-packed for graphite or boron nitride substrates, but the molecular orientations are determined by weak anisotropic intermolecular forces, principally electrostatic quadrupole-quadrupole (EQQ) interactions. The symmetry properties of these interactions are incompatible with the lattice symmetry, leading to very high frustration for the orientational ordering. Molecular field calculations of Harris and Berlinsky[1] for pure ortho-H_2 predict periodically ordered herring bone (HB) or pinwheel (PW) structures at low temperatures, depending on the sign of the interactions with the substrate. The PW structures have been verified by NMR experiments for high ortho-H_2 concentrations.[2,3] The periodic ordering is, however, fragile with respect to site disorder, and for ortho-H_2 fractions $c<0.69$, only local glass-like ordering is observed.

For concentrations below the critical concentration, $c_p=0.69$, that corresponds to the site-percolation threshold, unusual behaviors are observed for the local order

parameters deduced from NMR studies.[2] For ortho fractions, 0.48<c<0.68, where glass states are observed at low temperatures (T<0.58 K), the high temperature values of the order parameters vary from small and positive to zero at temperatures 0.8<T<1.5, and then become small and negative on further cooling or additional site disorder. The purpose of this report is to examine extensions of the mean field treatment[1] that include fluctuations in the local fields due to the random nature of the site disorder, with a view to explaining this unusual cross-over of the order parameters.

2 Theoretical Considerations

The local ordering is defined by three local axes, L_{Zi} =(x_i, y_i, z_i), and two intrinsic local order parameters for each site i, the alignment $\sigma_i \equiv <\hat{\sigma}_i> = <1-\frac{3}{2}\hat{J}_z^2>$ and the eccentricity, $\eta_i = <\hat{J}_x^2 - \hat{J}_y^2>$. Self-consistent solutions for the temperature dependence of the order parameters are deduced from the mean-field (MF) Hamiltonian

$$H = \sum_i \varepsilon_i \hat{\sigma}_i c_i - \sum_i h_i \hat{\sigma}_i c_i \qquad (1)$$

where $\varepsilon_i = \sum_j J_{ij}\hat{\sigma}_j$ is the molecular field. $J_{ij} = -\frac{3}{2}\Gamma_0 P_{20}(L_{Zi})P_{20}(L_{Zj})$, $P_{20}(L_{Zi})$ is the Legendre polynomial defined by the molecular orientations L_{Zi}. h_i is the static local field due principally to the substrate interactions, and c_i is the occupation number for site *i*. In lowest order approximation, assuming $\eta_i = 0$ at each site, $\varepsilon_0 = -9\Gamma_0\sigma_0$ and $h_0 = \frac{2}{3}V_0$ where Γ_0 is the strength of the EQQ interaction and V_0 is the local substrate interaction or crystal field).[1] The temperature dependence of the alignments obtained from Eq.(1) is given by

$$\frac{1-\sigma_i}{1+2\sigma_i} = \exp[-\frac{3}{2T}(\varepsilon_i + h_i)] \qquad (2)$$

The solution to Eq.(2) proposed in Ref. (1) for $\varepsilon_i = \varepsilon_0$; $h_i = h_0$ does not describe the behavior at the critical concentration nor the high temperature cross-over phenomenon. For a better approximation one needs to consider the fluctuations in the local fields.[4] Using a Gaussian approximation, we find for the order parameter σ_A in the high-temperature para-orientational (PRA) state

$$\frac{1-\sigma_A}{1+2\sigma_A} = \exp[-\frac{3}{2T}(\varepsilon_{1A} + \delta\varepsilon_{1a} + h_a) + \frac{9}{8}(\frac{\varepsilon_{2a}}{T})^2] \,. \qquad (3)$$

$\varepsilon_{1A} = -\frac{3}{2}\gamma_{1A}\Gamma_0 nc^{5/2}\sigma_A$, $\gamma_{mA} = < P_{20}^m(L_{Zi})P_{20}^m(P_{Zj}) >_c$ where <...>$_c$ refers to a configurational average, n is the coordination number, and $\delta\varepsilon_{1A} = \gamma_{2A}^2 nc\sigma_A(1-\sigma_A^2)/T$, $\varepsilon_{2A}^2 = \frac{3}{8}\gamma_{2A}^2\Gamma_0^4 c(1-c)(1-\sigma_A^2)/T^2$. Eq. (3) leads to solutions $0 \le \sigma_A \le 1$ at low temperatures with $\gamma_{1A} = -1/3$ and $\gamma_{2A} = 1$. This result is expected to be valid while quadrupolar field effects dominate the crystal fields. A different situation occurs at low values of c where the fluctuations become important. This is designated as the PRB phase. In this state, ε_{1B} is neglected, and the variance $< h_i^2 >_B = \frac{8}{9}V_0 T_x$ becomes significant.

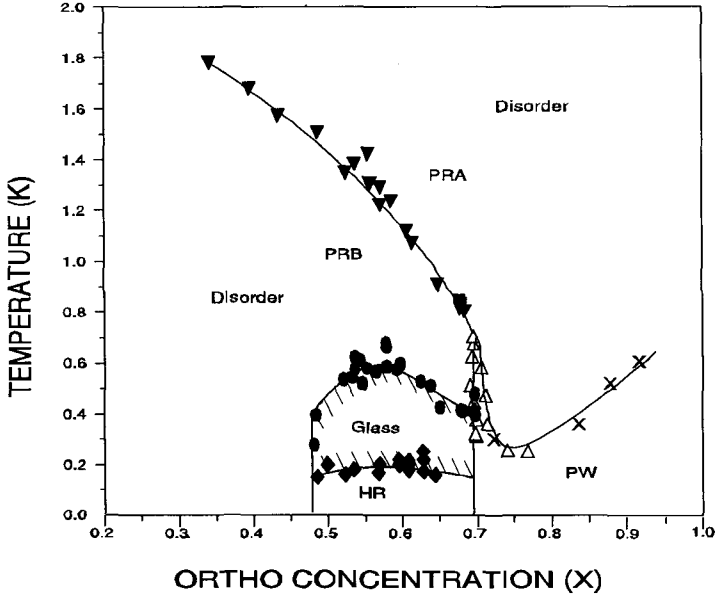

Figure 1: Phase diagram for a commensurate monolayer of H_2 on boron nitride. PW, pinwheel ordering; PRA and PRB two regions of the para-orientational state separated by a crossover at T_x (dashed line); HR, hindered rotor.

The PRB state is therefore determined by the solutions of

$$\frac{1-\sigma_B}{1+2\sigma_B} = \exp[-\frac{3}{2T}(h_B) + \frac{9}{8}(\frac{\varepsilon_{2B}^2 + \Delta h_B^2}{T^2})] \quad (4)$$

At low temperatures the solutions are given by $-\frac{1}{2} \leq \sigma_B \leq 0$, with $\gamma_{1B} = 0$ and $\gamma_{2B} = 1$, which is consistent with experiment. Although there is no fundamental symmetry difference between the PRA and PRB states, this crossover in behavior is seen clearly in experiments through the vanishing of the small doublet in the NMR spectrum at the crossover temperature $T_x(c)$ (dotted line in Fig.1).

There is an anomalous upturn of the phase boundary between the PW phase and the PRA state. This upturn occurs near the critical concentration, c_p, below which periodic order is not realized. This region corresponds to concentration values for which the competing effects of the quadrupolar and crystal field effects are most pronounced. Generally, the mean field equations[1] support the stability of the PW phase in the presence of negative local fields and this narrow region of stability is believe to result in the anomalous upturn.

3 Conclusions

The simplified Hamiltonian for a frustrated triangular array of linear quantum quadrupoles with site disorder has been proposed to determine the onset of local ordering in the paraorientational state and to show how this local order changes with increasing disorder. The local orientational ordering is characterized in terms of a reduced set of local order parameters (Θ_i, σ_i) where Θ_i, defines the polar angle for the orientation of the molecular axis at site i with respect to the substrate, and σ_i is the local alignment with respect to that axis. At high temperatures, the PRA state is characterized by Θ_i=0 with $\sigma_A > 0$. On increasing the disorder the fluctuations in the local field become dominant and we find $\Theta_i = \pi/2$ (principally) with $\sigma_B < 0$. This is the PRB region. The PRA-PRB crossover temperature $T_x(c)$ predicted for this change in behavior is also in qualitative agreement with experiment.

The authors acknowledge support from the NSF under grant no. 9812657 (NSS).

References

1. A. B. Harris A. J. and Berlinsky, *Can. J. Phys.* **57**, 1852-1863 (1979).
2. K. Kim and N. S. Sullivan, *J. Low Temp. Phys.* **114**, 173-189 (1999).
3. P. R. Kubik, W. N. Hardy and H. Glatti, *Can. J. Phys.* **63**, 605-621 (1985).
4. V. B. Kokshenev, *Phys. Rev.* B **53**, 2191-2199 (1996).

Part V

Superconductivity

This page is intentionally left blank

MAGNETOTRANSPORT IN CUPRATES AND RELATED COMPOUNDS IN HIGH MAGNETIC FIELDS:EVIDENCE FOR PREFORMED BIPOLARONS

A. S. ALEXANDROV
Department of Physics, Loughborough University

By extending the BCS theory to the strong-coupling regime with small bipolarons we explain the common origin of the anomalous upper critical field in high-Tc cuprates, in some organic superconductors, spin ladders and cubic oxides. The bipolaron theory accounts well for the normal state c-axis negative magnetoresistance in high magnetic fileds,[1] normal state diamagnetism,[2] c-axis tunneling and Andreev reflection,[3] angle-resolved photoemission,[4] normal gaps and stripes[5] observed in cuprates.

1. V. N. Zavaritsky, M. Springford and A. S. Alexandrov, *EuroPhys. Lett.* **51**, 334 (2000).
2. C. J. Dent, A. S. Alexandrov and V. V. Kabanov, *Physica C* **341**, 153 (2000).
3. A. S. Alexandrov and A. F. Andreev, *EuroPhys. Lett.* **54**, 373 (2001).
4. A. S. Alexandrov and C. J. Dent, *Phys. Rev. B* **60** 15414 (1999).
5. A. S. Alexandrov, Int. *J Mod. Phys. B* **14**, 3298 (2000).

SPINLESS IMPURITIES IN CUPRATES:LOCAL MAGNETISM AND KONDO EFFECT IN THE NORMAL AND SUPERCONDUCTING STATES

H. ALLOUL,[1] J. BOBROFF,[1] P. MENDELS[1] and F. RULLIER-ALBENQUE,[2]
[1]*Physique des Solides, UMR 8502 CNRS,*
Universite Paris-Sud 91405, Orsay (France)
[2]*SPEC/CEA, Orme des Merisiers, 91191 Gif s/ Yvette (France)*

Spinless point defects in the CuO_2 planes of the cuprates have been shown for long to induce a magnetic response on the neighboring copper sites which behaves as a nearly free local moment in the under-doped case.[1,2] In the case of Li^+ substitution on the Cu site, accurate ^7Li NMR shift data allow to evidence that the local moment susceptibility displays a $(T+T_K)^{-1}$ dependence, with a Kondo like temperature T_K which increases abruptly near optimal doping.[3] While a Curie paramagnetic response can be understood on general theoretical grounds in the case of undoped quantum spin systems, the Kondo screening of the moment might directly reflect the influence of charge carriers. This Kondo like behavior is also corroborated by measurements of the fluctuation time of the local moment deduced from ^7Li NMR spin lattice relaxation time.[4] The local moment is found to survive in the superconducting state although a marked reduction of the screening is observed when $T_K > T_c$ (see Ref. [5]), as might be expected from theoretical considerations.

Correlatively it will be shown that the scattering of charge carriers by spinless defects can be studied accurately in single crystals in which such defects are created by electron irradiation. The low T upturns of the resistivity can be associated with a Kondo-like T dependence of the scattering in the under-doped case. In the over-doped case, T_K being very high, the scattering becomes T-independent and 2D weak localization effects dominate.[6]

1. H. Alloul *et al., Phys. Rev. Lett.* **67**, 3140 (1991).
2. A. V. Mahajan *et al., Phys. Rev.* Lett. **72**, 3100 (1994), also *EJPB* 13, 457 (2000).
3. J. Bobroff *et al., Phys. Rev. Lett.* **83**, 4381 (1999).
4. A. MacFarlane *et al., Phys. Rev. Lett.* **85**, 1108 (2000).
5. J. Bobroff *et al., Phys. Rev. Lett.* **86**, 4116 (2001).
6. F. Rullier-Albenque *et al., cond-mat*/0102294, to be published in *Phys. Rev. Lett.*

MAGNETIC FIELD AND IMPURITY EFFECTS IN PSEUDOGAP STATE OF CUPRATES

A. V. BALATSKY
Los Alamos National Laboratory, Los Alamos, NM 87545, USA

Both impurities and magnetic field can be used as a tool to investigate the properties of superconducting state of cuprates. Recent STM tunneling experiments on impurity states in superconducting state provide a new set of results that can be compared with the expectations for d-wave pairing in cuprates. We will argue that impurities and magnetic field could be used to test the nature of the *pseudogap state* (PG).

i) We will present the extension of the theory of impurity on the pseudogap regime. The impurity such as Zn or Ni, will generate resonance state in PG state on very general grounds. Single vs double impurity peak will appear depending on the superconducting vs non-superconducting origin of the PG.

ii) For the particular proposal of the *d- density wave* PG (DDW) we found that out of plane magnetic field will induce complex, proportional to the field, id_{xy}-wave density wave component. Physical properties of this, previously not considered, state will be discussed.

THE FASCINATING NEW PHYSICS OF SOME OLD BCS SUPERCONDUCTORS

V. BARZYKIN

National High Magnetic Field Laboratory, Florida State University, 1800 E. Paul Dirac Dr., Tallahassee, Florida 32310
E-mail: barzykin@magnet.fsu.edu

We consider the pairing state due to the usual Bardeen-Cooper-Schrieffer mechanism in substances where the Fermi surface forms pockets around several points of high symmetry. The symmetry imposed on the multiple pocket positions can give rise to a multidimensional nontrivial superconducting order parameter. A complicated mechanism is not required for unusual superconductivity to exist, just the usual phonon attraction and Coulomb repulsion. Time reversal symmetry is broken, so the superconducting state also has orbital magnetism. In some sense, these superconductors are similar to superfluid ^{3}He, which is known to have an 18-dimensional order parameter and a complicated phase diagram. We suggest several candidate substances where ordering of this kind may appear and discuss how these phases may be identified. Superconductivity in these new materials is expected to be much less sensitive to impurities than in other non s-wave superconductors.[1]

The Bardeen-Cooper-Schrieffer (BCS) theory works very well for conventional superconductors. The BCS theory assumes that the weak attraction between electrons due to electron-phonon interaction is stronger than the Coulomb repulsion, which leads to the Cooper instability of the normal state and the superconducting condensate of electron pairs at low temperatures. The order parameter, the wave function of the condensate, is an s-wave. In terms of the group theory this just means that it is invariant with respect to the transformations of the crystal point group, G, and the time reversal operation, R. The quasiparticle spectrum in the superconducting state has a gap, which has been observed in different experiments. While most superconductors are described by the BCS theory, in several materials, such as ^{3}He, UBe_{13}, UPt_3, the high-T_c cuprates, and Sr_2RuO_4, the pairing state potentially breaks the $G \otimes R$ symmetry of the normal state (see Refs. [2-3] for a review). A well known example is the A-phase of ^{3}He (see Ref. [4]) which is not invariant with respect to rotations or time reversal operation (the B phase of ^{3}He is both rotationally and time reversal invariant). Such unconventional superconductors usually have a gapless excitation spectrum and arise when the interaction itself depends upon the superconducting ground state. For example, in ^{3}He the BCS ground state is the B phase and the spin fluctuation feedback effect is required to stabilize the A phase.[5]

We show below that exotic superconductivity does not require unusual feedback mechanism, and thus could be a lot more common. The multidimensional pairing state can appear within the BCS approach as a result of non-trivial topology of the Fermi surface. The new superconducting state breaks the time-reversal

symmetry, *i.e.*, is magnetic. The effects that we consider are possible in metals with several pockets that are centered at or around some symmetry points of the Brillouin Zone (BZ), although we believe this approach can be formulated for other FS topologies as well. A BCS approximation generalized to the multi-band case will be used. The new point here is that since the form of the interaction parameters describing the two electron scattering on and between different pockets on the Fermi surface (FS) is fixed by symmetry, the resulting superconducting state does not have to be *s*-wave. The non-trivial superconductor of this kind is a spin singlet, but it has a finite orbital moment. This moment is screened by the Meissner effect. One nevertheless expects to have internal domain structure due to the degeneracy of the ground state and the competition between magnetism and superconductivity.

This FS structure is not unusual. Indeed, most real FS in metals are quite complicated and may have topological effects on the BCS order parameter. Below we consider one simplest example in detail: three FS pockets centered about the X-points of a simple cubic lattice. This situation is applicable to LaB_6 (a $T_c \sim 0.1$ K superconductor,[6] (see Fig. 1) and $CeRu_2$ ($T_c \sim 6$ K) (see Ref. [7]). We also briefly discuss the results for $CeCo_2$, a $T_c \sim 1.6$ K (see Refs. [8,9]) superconductor.

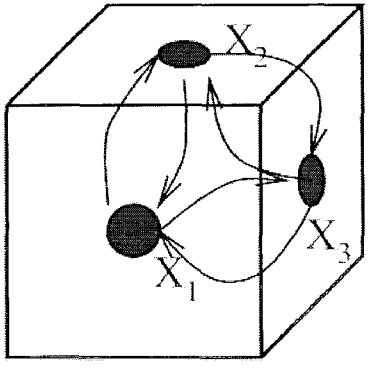

Figure 1: Schematic 3-pocket Fermi surface structure for $Ca_xLa_{1-x}B_6$. The arrows show interactions between Cooper pairs on different pockets which lead to unconventional superconductivity.

We use the generalized Ginsburg-Landau (GL) functional to identify possible nontrivial superconducting phases. The Hamiltonian for several separate pieces of the FS can be written in the following form:

$$H = \Sigma_{\mathbf{p}}\Sigma_{\alpha\sigma}\, \varepsilon(\mathbf{p})\, a^{+}_{\alpha\sigma}(\mathbf{p})\, a_{\alpha\sigma}(\mathbf{p})$$

$$+ (1/2)\ \Sigma_{\mathbf{k'},\mathbf{k},\mathbf{q}}\Sigma_{\alpha\beta\sigma\sigma'}\, \lambda_{\alpha\beta}(\mathbf{q})\, a^{+}_{\alpha\sigma}(\mathbf{k}+\mathbf{q})\, a^{+}_{\beta\sigma'}(\mathbf{k'}-\mathbf{q})\, a_{\alpha\sigma'}(\mathbf{k'})\, a_{\beta\sigma}(\mathbf{k}), \qquad (1)$$

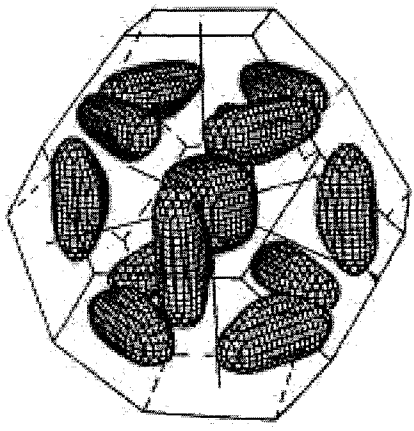

Figure 2: Some FS sheets of $CeCo_2$ (see Ref. [9]).

where σ and σ' are spin indices, $\lambda_{\alpha\beta}(\mathbf{q})$ includes the interaction for scattering two electrons from the pocket α into pocket β which is due to both Coulomb and electron-phonon terms. Introducing the anomalous Green's function $F_{\alpha}(x\text{-}x')$ for each FS sheet α, the corresponding Gor'kov equations can be used to obtain the following solution at finite temperatures for the case of singlet pairing:

$$F_{\alpha}(\omega_n, \mathbf{p}) = \Delta_{\alpha}^{*}(\mathbf{p})\ /\ (\omega_n^2 + \xi^2 + |\Delta_{\alpha}(\mathbf{p})|^2), \qquad (2)$$

where

$$\Delta^{*}_{\alpha}(\mathbf{p}) = -(T/(2\pi)^3)\Sigma_{\beta}\Sigma_{n}\int d\mathbf{k}\ \lambda_{\beta\alpha}(\mathbf{p}-\mathbf{k})\, F_{\beta}(\omega_n, \mathbf{k}). \qquad (3)$$

Expanding Eqs.(2) and (3) in $|\Delta_{\alpha}|$ up to the third order, we obtain the GL equations for the vector order parameter $\Delta_{\alpha}(\mathbf{p})$. For simplicity we assume that each $\Delta_{\alpha}(\mathbf{p})$ is constant along the corresponding FS, and to fourth order in Δ_{α} we can write the GL functional:

$$F_s - F_n = -\Delta^*_\alpha [(\lambda^{-1})_{\alpha\beta} - \delta_{\alpha\beta}(mp_0/2\pi^2)ln(2\gamma\omega_D/\pi T)]\Delta_\beta + 7\zeta(3)(mp_0/32\pi^4T^2)\Sigma_\beta|\Delta_\beta|^4, \quad (4)$$

where $(\lambda^{-1})_{\alpha\beta}$ is the matrix inverse to the interaction $\lambda_{\alpha\beta}$, ω_D is the cutoff (Debye) frequency.

Let us now analyze the simplest example for multiple FS sheets, three X points in a cubic lattice.

The interaction matrix $\lambda_{\alpha\beta}$ for three X points takes the following general form:

$$\lambda_{\alpha\beta} = \lambda\delta_{\alpha\beta} + \mu(1-\delta_{\alpha\beta}). \quad (5)$$

Here λ is the interaction on the same pocket, μ couples any two different pockets. The linearized gap equation, Eqs.(2) and (3) to determines T_c. The three Δ_α transform among each other at cubic symmetry transformations forming a 3D reducible representation of the cubic group O_h, which *is split* into a *1D* A_{1g} and a *2D* E_g irreducible representation. These two representations correspond to different order parameters with two critical temperatures:

$$T_{c,E} = 2(\gamma\omega_D/\pi)\exp(2\pi^2/mp_0(\lambda-\mu)) \quad (2D) \quad (6)$$

$$T_{c,A} = 2(\gamma\omega_D/\pi)\exp(2\pi^2/mp_0(\lambda+2\mu)) \quad (1D) \quad (7)$$

(the terms in the exponents must be negative for the Cooper effect to take place). The basis wave functions for the 2D representation can be chosen as

$$\eta_1 = (\Delta_1+\varepsilon\Delta_2+\varepsilon^2\Delta_3)/\sqrt{3}\ ;\ \eta_2 = (\Delta_1+\varepsilon^2\Delta_2+\varepsilon\Delta_3)/\sqrt{3}. \quad (8)$$

where $\varepsilon = \exp(2\pi i/3)$. If $\lambda-\mu < 0$ and $\mu > 0$, superconductivity belongs to the nontrivial 2D E_g representation, *i.e.*, if the interaction between Cooper pairs on two different FS pockets is dominated by Coulomb repulsion (see Fig. 1). Expanding Eq. (4) to the fourth order, we easily determine the phase of the order parameter: $\eta_2 = 0$ in Eq. (8). Since the wave function η_1 is complex, the time reversal symmetry is broken. The symmetry class (the symmetry of the pair wave function, (see Refs.[2-3]) for definitions) for this phase is $O(D_2)$.

Analysis for $CeCo_2$ is very similar, albeit a little more sophisticated due to the presence of twelve different pockets (see Fig. 2). Since the pockets are not located on the BZ boundary, the resulting multiplicity of the superconducting order parameter is half that. We find that the six-dimensional reducible representation for the multi-component parameter splits into A_{1g} (identical, 1D), E_g (2D), and F_{2g} (3D). For the 2D case the superconducting class is again $O(D_2)$, which allows antiferromagnetic orbital ordering, while in the 3D case the symmetry of the order parameter is $D_3(E)$, which allows ferromagnetic orbital ordering.

The properties of the nontrivial phase are known. Time-reversal symmetry is broken and allows for antiferromagnetic domains and for fractional vortices on domain walls to appear. The existence of domains follows directly from the degeneracy of the order parameter. Thus, inhomogeneous orbital magnetism coexists with superconductivity in these materials. There are magnetic domains and superconducting currents along the domain walls, but magnetism inside the domain is negligible due to the Meissner effect. In principle, point nodes should appear where the FS intersects the cube diagonals. This would lead to the *electronic* contribution in the T^3 behavior for the heat capacity at low temperatures. In our case, however, there is no FS along the diagonals of the cube and the low temperature thermodynamic properties will be determined by the gap of the same magnitude for all three FS sheets. In the presence of another FS, for example, at the Γ-point, the nontrivial order $O(D_2)$ will be induced on it. In such case the point nodes will exist and power laws in thermodynamic properties due to nontrivial superconductivity should be seen experimentally. The anisotropy of the upper critical field (H_{c2}) near T_c for this class also requires that (at least) two vortex lattice phases (with a second order transition between them) exists when the magnetic field is applied along the *(1,1,0)* and equivalent directions.

In some sense, the resulting superconducting states are similar to the BCS s-wave: they have gaps of equal magnitude on each of the FS sheets. Thus, in such a case a Hebel-Slichter peak in $1/T_1$ measurements may be present. The non-trivial representations were stable when the pair interaction between the different sheets was repulsive (independent of the intra-sheet interaction). These exotic phases are considerably less sensitive to impurities, since the Anderson theorem applies, provided that one neglects small inter-pocket scattering terms. Inclusion of these terms leads to standard suppression of T_c (see Ref. [1]).

In summary, we have shown that exotic superconductivity can appear simply as a result of the competition of the phonon and Coulomb interactions if the FS consists of several pockets located at some symmetry points. The time-reversal symmetry is broken for the nontrivial order, meaning that the superconducting transition should be accompanied by orbital magnetic order. The simplest methods to identify these order parameters are, apart from the phase-sensitive measurements, the power law dependence of the heat capacity (due to nodes), measurements of the upper critical field anisotropy $H_{c2}(\theta)$ at T_c, or the observation of transitions between different vortex lattice phases. Note that if the FS pockets are fully isolated then the nodes are absent since the order parameter is then constant on each FS pocket and changes phase as one moves from one pocket to another. Nodes could appear, however, if there are "necks" connecting different sheets or if superconductivity is induced on a FS centered, for example, around the Γ-point. The magnetic order can be observed in μSR measurements or magnetization measurements in small enough samples (where the dimensions are on the order of the penetration depth). These FS sheets are not always centered on the BZ boundary, as, for example, in $CeCo_2$ (see Refs. [8-9]).

This work has been performed in collaboration with D. F. Agterberg and L. P.Gor'kov.[1] We would like to thank Z. Fisk, D. Khokhlov and J. R. Schrieffer for useful discussions and comments. This work was supported by the National High Magnetic Field Laboratory through NSF cooperative agreement No. DMR-9527035 and the State of Florida.

References

1. In collaboration with D. F. Agterberg and L. P. Gor'kov; D. F. Agterberg, V. Barzykin, L. P. Gor'kov, *Phys. Rev. B* **60**, 14868 (1999); *Europhys. Lett.* **48**, 449 (1999).
2. L. P. Gor'kov, *Sov. Sci. Rev., Sect. A* **9**, 1 (1987).
3. M. Sirgist and K. Ueda, *Rev. Mod. Phys.* **63**, 239 (1991).
4. D. D. Osheroff, R. C. Richardson and D. M. Lee, *Phys. Rev. Lett.* **28**, 885 (1972).
5. P. W. Anderson and W. F. Brinkmann, *Phys. Rev. Lett.* **30**, 1108 (1973).
6. A. J. Arko *et al., Int. J. Quantum Chem.* **S9**, 569 (1975).
7. M. Hedo *et al., J. Phys. Soc. Jpn.* **64**, 4535 (1995).
8. H. Sugawara *et al., J. Phys. Soc. Jpn.* **64**, 3639 (1995).
9. H. Sugawara *et al., J. Phys. Soc. Jpn.* **65**, 1744 (1996).

ORBITAL MAGNETISM IN THE CUPRATES

SUDIP CHAKRAVARTY, HAE-YOUNG KEE and CHETAN NAYAK
Department of Physics, University of California Los Angeles, Los Angeles CA 90095, USA
E-mail: sudip@physics.ucla.edu

The pseudogap phase of the cuprate superconductors is argued to be characterized by a hidden broken symmetry of d-wave character in the particle-hole channel that leads to staggered orbital magnetism. This proposal has many striking phenomenological consequences, but the most direct signature of this order should be visible in the neutron scattering experiments. The theoretical underpinning of these experiments is discussed.

1 Introduction

It has been proposed that the pseudogap state is a phase with a broken symmetry and an order parameter,[1,2] not a state with a merely fluctuating order.[3] The distinction between the two is enormous. The order parameter, which is due to a particle-hole condensate with internal "angular momentum" 2, will be termed the d-density wave (DDW). We have predicted that the present day neutron scattering experiments have enough resolution to provide a direct evidence of this order. And, indeed, there are some preliminary neutron scattering measurements in the bilayer $YBa_2Cu_3O_{6.6}$ that appear to have observed the theoretically predicted order parameter.[4,5] There are other experiments on $YBa_2Cu_3O_{6.5}$, which observe a magnetic signal,[6] but appear to be from remnant spins left over from the undoped antiferromagnet. While the experimental situation must be resolved, we shall focus merely on the theoretical predictions because a precise analysis is necessary to make sure that what is being observed is not an artifact. The fundamental signature of this order parameter is an elastic Bragg peak centered at two-dimensional wave vector $\mathbf{Q} = (\pi/a, \pi/a)$, where a is the lattice spacing of the CuO-lattice. Since the magnitude of the staggered orbital fields is of order 10 G, the experiments are difficult.

The neutron scattering from DDW was addressed previously,[7] but the polarized neutron scattering and the important question about the current form factors were not. The current form factors play an important role in polarized neutron measurements, without them one may be led to physically incorrect results. Moreover, the crucial connection to the pseudogap phase was not made, nor was it made clear that such a phase truly survived beyond the

large-N mean field theory due to presumed gauge fluctuations. There is also a proposal[8] of a circulating current phase, which does not break translational symmetry. The similarity with the DDW state is merely superficial. At the very least, the signature, on robust symmetry grounds, is a neutron signal at $Q = 0$ which is fundamentally different. We will have nothing to say about this proposal, as it is not germane to the present set of experiments.

2 Order parameter

The singlet DDW is defined by the order parameter $\Phi_{\mathbf{Q}}$ in terms of a particle-hole condensate[9]

$$\langle c^{\sigma\dagger}(\mathbf{k}+\mathbf{Q},t)c_\rho(\mathbf{k},t)\rangle = i\frac{\Phi_{\mathbf{Q}}}{2}\left(\cos k_x a - \cos k_y a\right)\delta^\sigma_\rho, \tag{1}$$

where σ, ρ are spin indices. The order parameter breaks time reversal, parity, translation by a lattice spacing, and the rotation by $\pi/2$, although the product of any two of these is preserved. Interestingly, DDW does not modulate charge at all, but it modulates currents. The reason it is still called a density wave is because it is a particle-hole condensate, and d-wave refers to the internal form factor of the particle and the hole, which is $(\cos k_x a - \cos k_y a)$. We expect that the magnetic field generated by the circulating currents should be proportional to the pseudogap.[2] A simple estimate results in a tiny field of order 10 G due to currents circulating in a CuO plaquette as shown below:

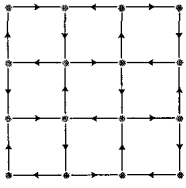

Figure 1. Circulating current pattern in the model where the current is carried by δ-function wires.

Although this simple model captures the correct symmetry, it is crucially deficient in predicting the correct neutron scattering intensities, as we shall see. It is *a priori* clear that the flow of currents cannot be along infinitesimally thin wires, but it must spread out, both because of finite sized atomic orbitals and because of electron-electron interactions. One can model the more realistic current distribution[5] by the form factors $\alpha(\mathbf{q})$ and $\beta(\mathbf{q})$ in the Fourier

transform of the current distribution $\langle \mathbf{j}(\mathbf{q}) \rangle$without destroying the symmetry of the order parameter ($\mathbf{q} \cdot \langle \mathbf{j}(\mathbf{q}) \rangle = 0$), where

$$\langle \mathbf{j}(\mathbf{q}) \rangle \propto \Phi_{\mathbf{Q}} \sum_{\mathbf{G}_\parallel} \delta_{\mathbf{q}_\parallel, \mathbf{G}_\parallel} \; f(\mathbf{q}) \times \left[\left(\alpha(\mathbf{q}) \frac{\hat{\mathbf{x}}}{q_x} - \beta(\mathbf{q}) \frac{\hat{\mathbf{y}}}{q_y} \right) - (\alpha(\mathbf{q}) - \beta(\mathbf{q})) \frac{\hat{\mathbf{z}}}{q_z} \right]. \tag{2}$$

Here, $\mathbf{q}_\parallel = (q_x, q_y)$, $f(\mathbf{q}) = \sin(\frac{q_z d}{2})$, d is the separation between the two CuO-planes within a bilayer complex, and $\mathbf{G}$ is a reciprocal lattice vector. The simplest choice is to take $\alpha(\mathbf{q})$ and $\beta(\mathbf{q})$ to be dependent on q_z only, such that $\alpha(q_z) - \beta(q_z) \sim q_z^2$, as $q_z \to 0$. The choice of this current density was discussed in Ref. 5.

3 Experimental detection of DDW

The DDW is usually hard to detect because

$$\sum_{\mathbf{k}} \langle c^{\sigma\dagger}(\mathbf{k} + \mathbf{Q}) c_\rho(\mathbf{k}) \rangle \propto \sum_{\mathbf{k}} (\cos k_x a - \cos k_y a) = 0 \tag{3}$$

There is no net modulation of charge and spin that could be measured. Contrast this with a d-wave superconductors (DSC) for which a similar momentum sum of the particle-particle condensate also vanishes. Nonetheless, because of broken gauge symmetry, Meissner effect follows, irrespective of the pairing channel. This is not possible for a DDW because the broken symmetry is in the Ising universality class, and experiments seeking to uncover such order must (a) be sensitive to spatial variation of kinetic energy or currents, (b) measure higher order correlations of the charge or spin density as in 2-magnon Raman scattering, nuclear quadrupole resonance, etc.[9] One nice feature of DDW is that a thermodynamic transition is possible in two dimensions due to the Ising nature of the order parameter.

Impurities will mix d-wave order with the s-wave order proportional to the concentration of impurities. This may be an indirect way to reveal the hidden broken symmetry, because the corresponding s-wave order is none other than the conventional charge density wave (CDW). Another possibility is spin-orbit coupling, which will mix spin density wave (SDW) with DDW. In mean field theory,[10] there is some evidence that DDW may incommensurate for higher doping. If this is the case, the charge order must inevitably be mixed in, an idea that can be experimentally probed by scanning tunneling measurements inside the vortex core of the mixed DDW and DSC phase. The detailed nature

of the charge order appear to be highly nonuniversal, and certainly cannot be used as a diagnostic tool for theories of pseudogap.

4 Neutron scattering

4.1 Unpolarized neutron scattering

For unpolarized neutron scattering, the differential scattering cross sections for Bragg scattering from an ordered array of orbital currents is given by[5]

$$\left(\frac{d\sigma}{d\Omega}\right) \propto \frac{|\langle \mathbf{j}(\mathbf{q})\rangle|^2}{q^2}, \tag{4}$$

where $\mathbf{q}$ now is the momentum transfer. We certainly do not know the form factors $\alpha(\mathbf{q})$ and $\beta(\mathbf{q})$ beyond their limiting forms, but a reasonable guess can be made to see the robust features of the intensity modulation as a function of the momentum transfer. For this purpose, we have chosen $\alpha(\mathbf{q}) = f(q)e^{-(\frac{q_z}{q_0})^2}$, and $\beta(\mathbf{q}) = f(q)e^{-(\frac{q_z}{q_1})^2}$. So, the intensity is parametrized by a orthorhombicity parameter $\lambda(\mathbf{q}) = e^{-[(\frac{q_z}{q_0})^2-(\frac{q_z}{q_1})^2]}$ and $\beta(\mathbf{q})$. Note that all other factors, such as the magnitude of the order parameter, drop out if we normalize with respect to a reference Bragg reflection intensity. We then replace $\beta(\mathbf{q})$ by the well known Cu form factor,[11] which is likely to be an upper bound because the orbital currents are more spread out in real space than atomic orbitals. We choose $q_0 = 2\pi/d$ and $q_1 = 0.275q_0$. We shall see that the unpolarized intensity is not sensitive to the choice of the λ-parameter.

There is no question that the unpolarized neutron scattering intensities are dramatically different for orbital currents in comparison to spins lying in the a-b plane as shown in Fig. 2. The scattering from spins pointing along the c-direction can be easily calculated and is similar to the scattering from orbital currents. These two cases can be distinguished by going to higher order Bragg reflections such (H, H, L), for $H > 1/2$, for example $(3/2, 3/2, L)$. The results for orbital currents fall off very rapidly in contrast to spins pointing in the c-direction.

4.2 Polarized neutron scattering

The Bragg scattering intensity for polarized neutrons from orbital currents is given by

$$\left(\frac{d\sigma}{d\Omega}\right)_{i\to f} \propto \frac{1}{q^4}\,|\langle f|\vec{\mu}|i\rangle \cdot \mathbf{q} \times \langle \mathbf{j}(\mathbf{q})\rangle\,|^2, \tag{5}$$

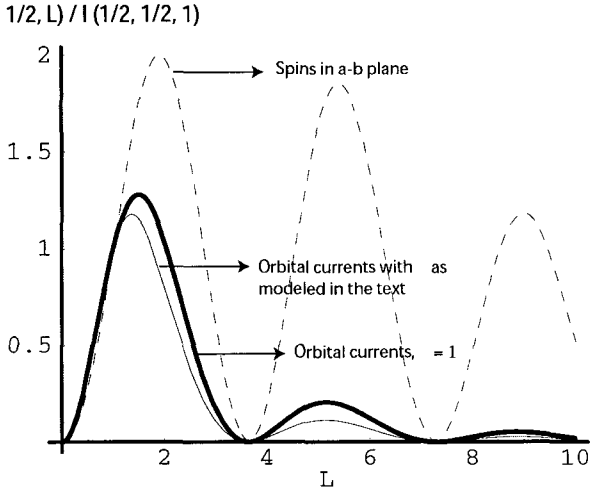

Figure 2. Normalized intensity, I, of Bragg reflections as a function of the perpendicular momentum transfer, q_z. The shorthand notation is $I(H,K,L) \equiv I(2\pi H/a, 2\pi K/a, 2\pi L/c)$. The intensity from spins lying in the a-b plane is obtained from the form factor given in Ref. 11.

where $\vec{\mu}$ is the neutron spin, and $|i\rangle$ and $|f\rangle$ are the initial and the final states of the neutron. It is easy to see that if the scattering vector is parallel to the direction of polarization, the entire scattering is spin flip. This is useful to identify magnetic scattering from non-magnetic scattering and the intensity ratios should follow the same pattern as that of the unpolarized case. When the scattering vector $\mathbf{q}$ is perpendicular to the polarization, there can be both spin-flip and non-spin-flip scattering. This geometry contains additional information, which is the ratio of the spin-flip to non-spin-flip scattering. A common experimental set up is to polarize neutron along along the $[1,\bar{1},0]$ direction as shown in Fig. 3, so that the new x-axis is along $[1,1,0]$, and the new y-axis is along $[0,0,1]$.

Then a simple calculation shows that the ratio of the non-spin-flip to spin-flip scattering intensity, NSF/SF, for Bragg reflection (H,H,L) is

$$\frac{NSF}{SF} = 2\left(\frac{\lambda(L)-1}{\lambda(L)+1}\right)^2 \left(\frac{Hc}{La}\right)^2 \left[1+\frac{1}{2}\left(\frac{La}{Hc}\right)^2\right], \tag{6}$$

which vanishes identically if there is no orthorhombicity, that is, $\lambda(L) = 1$.

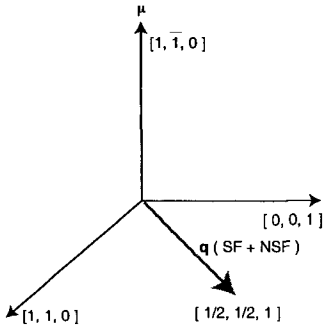

Figure 3. The vertical field geometry.

This is a nontrivial result for orbital current theory.

For the choice of the parameters described earlier, corresponding to $\lambda(L = 1) \approx 0.4$, this ratio for the reflection $(1/2, 1/2, 1)$ turns out to be ≈ 1. Thus, while modeling of the orthorhombicity of the current distribution had very little effect on the unpolarized intensity, its effect on the polarized scattering is striking, turning the ratio (NSF/SF) to order 1 as compared to 0.

5 Concluding remarks

Other possible evidence against spin order is the existence of a spin gap due to the Ising universality class of the DDW order, and the small moment of order $2 \times 10^{-2} \mu_B$ corresponding to the field due to circulating currents. We made an educated guess for the microscopic nature of the current distribution. Clearly, we need a better understanding of it, although the ratio of the intensities as a function of the momentum transfer for unpolarized scattering is very insensitive to the modeling of the current distribution. Thus, we believe that our results are quite robust.

Acknowledgments

We thank H. Mook and P. Dai for many discussions. This work was supported by a grant from the National Science Foundation.

References

1. S. Chakravarty and H. Y. Kee, Phys. Rev. B **61**, 14821 (2000).
2. S. Chakravarty, R. B. Laughlin, D. K. Morr, and C. Nayak, Phys. Rev. B **64**, 094503 (2001).
3. D. A. Ivanov, P. A. Lee, and X. -G. Wen, Phys. Rev. Lett. **80**, 3843 (1998).
4. H. A. Mook, P. Dai, and F. Dogan, Phys. Rev. B **64**, 012502 (2001); H. A. Mook *et al.*, in preparation.
5. S. Chakravarty, H. -Y. Kee, and C. Nayak, Int. J. Mod. Phys. **15**, 2901 (2001).
6. Y. Sidis *et al.*, Phys. Rev. Lett. **86**, 4100 (2001).
7. T. C. Hsu, J. B. Marston, and I. Affleck, Phys. Rev. B **43**, 2866 (1991).
8. C. M. Varma, Phys. Rev. Lett. **83**, 3538 (1999).
9. C. Nayak, Phys. Rev. B **62**, 4880 (2000).
10. E. Cappelluti and R. Zeyher, Phys. Rev. B **59**, 6475 (1999).
11. S. Shamoto *et al.*, Phys. Rev. B **48**, 13817 (1993).

MAGNETISM AND SUPERCONDUCTIVITY IN $YBa_2Cu_3O_{6+x}$ SUPERCONDUCTORS

P. DAI,[1,2] H. A. MOOK,[2] S. M. HAYDEN,[3] A. HIESS,[4]
S.-H. LEE,[5] and F. DOGAN[6]

[1] *Department of Physics and Astronomy, University of Tennessee, Knoxville, TN 37966*
[2] *Solid State Division, Oak Ridge National Laboratory, Oak Ridge, TN 37831-6393*
[3] *H. H. Wills Physics Laboratory, University of Bristol, Bristol BS8 1TL, UK*
[4] *Institut Laue-Langevin, BP 156, 38042 Grenoble, France.*
[5] *NIST Center for Neutron Research, National Institute of Standards and Technology, Gaithersberg, Maryland 20899*
[6] *Department of Materials Science and Engineering, University of Washington, Seattle, WA 98195*

Perhaps the most puzzling attribute of the high-temperature cuprate superconductors is that for underdoped materials the energy gap normally associated with superconductivity is observed well above the superconducting transition temperature T_c. Neutron scattering measurements of $YBa_2Cu_3O_{6.6}$ have identified small moments that increase in strength as the temperature is reduced below the pseudogap temperature T^*. Polarized beam neutron scattering measurements demonstrate that the signal is magnetic in origin. Furthermore, the pattern of neutron intensities found in the experiment is unusual as it is not readily understandable in terms of conventional spin magnetism. Although we have considered the origin of the moment in terms of the orbital bond currents, new experimental data suggest that only part of the signal is consistent with this interpretation. We present detail analysis of polarized neutron data and systematic studies of oxygen chain ordering. Finally, we discuss our most recent results on spin-glass phase of Ca-doped $YBa_2Cu_3O_6$.

FAR-INFRARED HALL EFFECT IN NORMAL STATE OF YBCO

M. GRAYSON,[1*] L. RIGAL,[1] D. C. SCHMADEL,[2] H. D. DREW[2] and P.-J. KUNG,[3]
[1]*Department of Physics, University of Maryland, College Park, Maryland 20742, USA*
[2]*Center for Superconducting Research, University of Maryland, College Park, Maryland 20742, USA*
[3]*Advanced Fuel Research, Inc., East Hartford, Connecticut, USA*

Cuprate superconductors in the normal state exhibit the "anomalous Hall effect",[1] *ie.*, the longitudinal components of the current scattters linearly with T whereas the Hall angle obeys a T^2 scattering, where T is temperature. To help resolve this anomaly, we have developed a technique to measure the Hall angle at far-infrared frequencies. Measuring the magnetotransmission spectrum of polarized light through thin film of YBCO, we are able to independently measure both the real and imaginary parts of the complex Hall response. With a spectral range from dc to 250 cm^{-1}, a lineshape analysis of the Hall response reveals that the Hall angle spectrum has a non-Lorentzian form thereby ruling out Drude-like transport models of the Hall effect. Instead it shows a dominant Loretnzian-squared response, implying a square-scattering behavior with a scattering rate that is linear in T and which *quantitatively fits the linear scattering rate of the longitudinal current.* The experimental results strongly constrain the number of theories that can accurately describe transport in normal state cuprates.

1 .T. R. Chien, D. A. Brawner, Z. Z. Wang and N. P. Ong, *PRB* **43**, 6242 (1991).

*This work was supported in part by NSF.

PSEUDOGAP STATE OF HIGH T_C CUPRATES: A PREDOMINANT ROLE OF SPIN DEGREES OF FREEDOM

L. KRUSIN-ELBAUM and T. SHIBAUCHI[*#]

IBM T.J. Watson Research Center, Yorktown Heights, New York 10598, E-mail: krusin@us.ibm.com

M. P. MALEY

[*]*Superconductivity Technology Center, Los Alamos National Laboratory, Los Alamos, New Mexico 87545, USA*

M. LI and P. H. KES

Kamerlingh Onnes Laboratory, Leiden University, 2300 RA Leiden, The Netherlands

We map the field-temperature (H-T) diagram of the pseudogap state in $Bi_2Sr_2CaCu_2O_{8+y}$ crystals in a wide range of hole doping. By probing the quasiparticle density-of-states with the c-axis interlayer resistivity measurements in fields up to 60 T we make a systematic evaluation of the pseudogap closing field H_{pg} that restores the superconductor to its ungapped state. In contrast to the characteristic fields of the superconducting state, $H_{pg}(T)$ at low temperatures is temperature independent and scales with the pseudogap temperature T^* by a simple Zeeman energy scale, indicating a predominant role of spins over the orbital effects in the formation of the pseudogap.

1 Introduction

The unusual electronic correlations in the normal state of high-T_c superconductors express themselves well above T_c as the anomalous depletion of the quasiparticle density of states (DOS) near the putative Fermi energy.[1] The origin of this normal state partial gap, or pseudogap, is still elusive and understanding the pseudogap phenomenon and establishing whether it is related to, competes with, or is a precursor of the Cooper-pair formation responsible for the superconducting state is the key problem in high-T_c. Since magnetic field strongly couples to the orbital motion of Cooper pairs, a comparison between responses of the pseudogap and the superconducting gap to high magnetic fields over a wide range of carrier doping is an important step toward clarifying this puzzle. Most of spectroscopic techniques probing the pseudogap require dc magnetic fields and thus are restricted to the dc field range where the pseudogap response is weak.[2] Here, we use the c-axis *tunneling* resistivity measurements in the highest field range available in a pulsed mode, to directly access the low-energy DOS. We demonstrate that in the overdoped (OD) regime, close to T^* a 60 T field closes the pseudogap, and that a field that restores DOS to its fully ungapped state shows

strikingly different temperature dependence from the characteristic fields of the superconducting state. The pseudogap closing field and the pseudogap temperature T^* evaluated independently are found to relate through a simple Zeeman energy scaling.

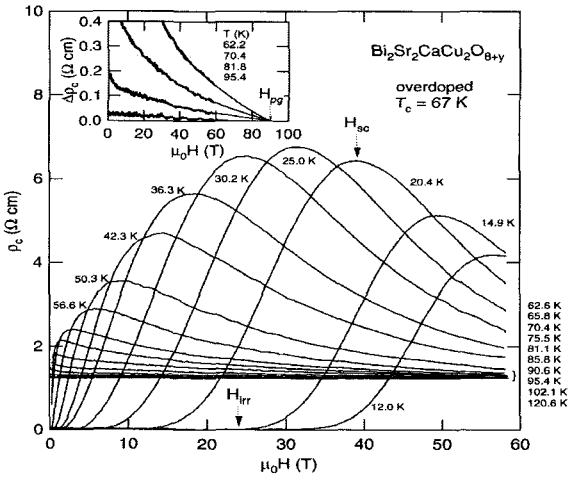

Figure 1: c-axis resistivity ρ_c (labeled by temperatures) *vs* magnetic field $H \parallel c$ in an overdoped BSCCO crystal. In the superconducting state, $\rho_c(H)$ becomes finite above the irreversibility field H_{irr} and exhibits a peak at H_{sc}. The negative MR persists up to T^* (see Fig. 2). Inset: Excess resistivity due to the pseudogap $\Delta\rho_c$ is fitted to a power-law field dependence $[\Delta\rho_c(H) - \Delta\rho_c(0)] \propto H^{\alpha}$. The pseudogap is closed at a field H_{pg} when $\Delta\rho$ is zero. The evaluation of H_{pg} is robust against the specific functional form of the fit.

One of the striking consequences of the pseudogap is the temperature dependence of (anisotropic) normal state resistivity. The in-plane resistivity is linear in temperature in the optimally doped materials but deviates from this behavior in the underdoped regime near the opening of the pseudogap.[1] However, the out-of-plane resistivity, at least in $Bi_2Sr_2CaCu_2O_{8+y}$ (BSCCO), turns from metallic to semiconducting-like at T^* above onset of the T-linear in-plane transport.[3] Recent tunneling spectroscopy data [4] indicate that the "pseudogap temperature" -- identified as the temperature at which the conductance dI/dV develops a dip at zero-bias -- coincides with T^* from the c-axis transport. Furthermore, Watanabe *et al.*,[3] find a close correspondence between pseudogap phase boundaries obtained from the c-axis resistivity ρ_c and from the static susceptibility measurements in overdoped BSCCO. And since ρ_c directly measures Cooper pair or quasiparticle tunneling in both normal and superconducting states, providing *bulk* information about the low-energy quasiparticle DOS, it should be particularly sensitive to the onset of the pseudogap formation, since the DOS depletion is largest at the Fermi energy.

2 Experimental

In this study we used BSCCO crystals grown by the floating-zone method with hole concentration p in the overdoped regime ($0.20 \leq p \leq 0.22$) controlled by the long time anneals in up to 100 atm of O_2 (see Ref. [3]) at 300-400°C. ρ_c was measured in fields $\| c$ up to ~ 32 T in a dc mode at the National High Magnetic Field Laboratory (NHMFL) in Tallahassee, FL, and up to ~ 60 T in a quasi-static mode LP system at NHMFL in Los Alamos, NM. The LP technique with a ~ 2100 ms pulse duration avoided eddy current sample heating $\propto (dB/dt)^2$, as witnessed by the non-hysteretic magnetoresistance at different up- and down-ramp rates and by the consistency with the dc results.

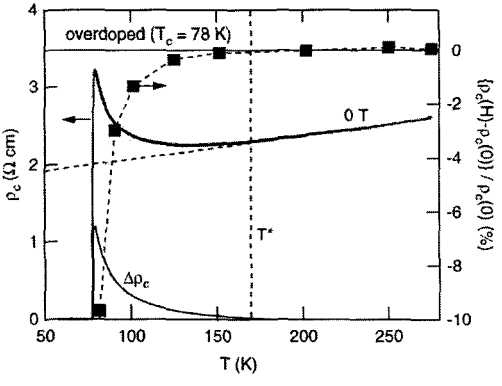

Figure 2: Temperature dependence of ρ_c and the magnetoresistance MR = $[\rho_c(H) - \rho_c(0)]/\rho_c(0)$ at 31.2 T in an overdoped BSCCO. Subtraction of a linear term gives the excess resistivity $\Delta\rho_c$..

3 Results and Discussion

The field dependence of ρ_c for an overdoped BSCCO crystal (p = 0.22) with T_c = 67 K is shown at fixed temperatures in Fig. 1. In the superconducting state, ρ_c becomes finite above the irreversibility field H_{irr}, and exhibits a peak at a characteristic field H_{sc}. We have demonstrated[5] that this peak arises from a competition between two parallel tunneling conduction channels comprising the total interlayer conductivity: of Cooper pairs (Josephson tunneling at low fields) and quasiparticles (mainly at high fields). At H_{sc}, the quasiparticle and the Josephson tunneling currents are comparable. Above the peak, the magnetoresistance (MR) is negative and continues to be negative above T_c. The negative MR eventually vanishes at the temperature at which the zero-field $\rho_c(T)$ also develops a characteristic upward deviation from the metallic dependence, as

illustrated in Fig. 2. This temperature is identified as the pseudogap temperature T^* (see Figs. [3,4]). Thus, negative MR is a result of the field suppression of the pseudogap.

In the crystal of Fig. 1, a magnetic field of ~ 60 T downshifts the semiconducting upturn in $\rho_c(H)$ and the associated T^* by about 20 K (See Fig. [6]). To track the pseudogap closing field at lower temperatures and higher fields, we determine the excess resistivity $\Delta\rho_c$ due to the pseudogap. $\Delta\rho_c$ is obtained by subtracting the T-linear metallic contribution, found by Krasnov *et al.*,[2] to persist down to very low temperatures. A fit to the power-law field dependence[5] of $\Delta\rho_c(H)$ at different T (inset in Fig. 1) allows us to evaluate the pseudogap closing field $H_{pg}(T)$ at which $\Delta\rho_c$ vanishes, even beyond 60 T.

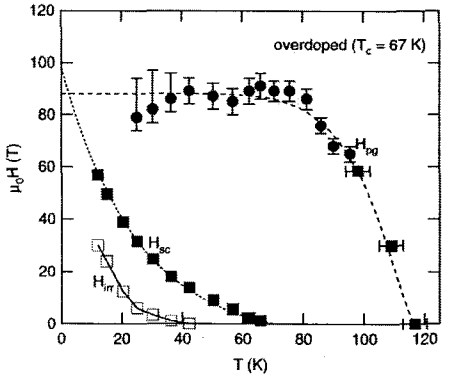

Figure 3: H-T diagram showing the pseudogap closing field $H_{pg}(T)$, the peak field $H_{sc}(T)$, and the irreversibility field $H_{irr}(T)$ in the overdoped BSCCO. Up to 60 T, $H_{pg}(T)$ is directly determined from the down-shifting upturn of $\rho_c(T)$. At lower temperatures, $H_{pg}(T)$ is obtained by extrapolating $\Delta\rho_c(H)$ to zero.

The H-T diagram of the pseudogap in the OD crystal is shown in Fig. 3. At low temperatures H_{pg} is essentially flat, capped at ~ 90 T -- a behavior very different from a strong temperature dependence of the peak $H_{sc}(T)$ and the irreversibility $H_{irr}(T)$ fields in the superconducting state. Note that even in such OD crystal (p ~ 0.22) the pseudogap state dominates the H-T diagram. This is consistent with recent intrinsic tunneling data showing a well-defined pseudogap with energy higher than the superconducting gap for OD BSCCO with $p > 0.20$ [7], but at odds with the conclusions of the specific heat analysis[8] that the pseudogap extinguishes at a `quantum critical point' $p \approx 0.19$.

The doping dependence of the pseudogap closing field $H_{pg}(p)$ and T^* are shown in Fig. 4. H_{pg} and T^* obtained independently in the same crystals in the OD regime, scale through a basic Zeeman energy relation $g\mu_B H_{pg} \approx k_B T^*$ with $g = 2.0$. This implies that magnetic field couples to the pseudogap by the Zeeman energy of the spin degrees of freedom. Consistently, our preliminary experiments also show a very weak field

anisotropy (between the $H \parallel c$ and $H \perp c$ configurations) of H_{pg}. It all indicates a predominant role of spins over the orbital effects in the formation of the pseudogap.

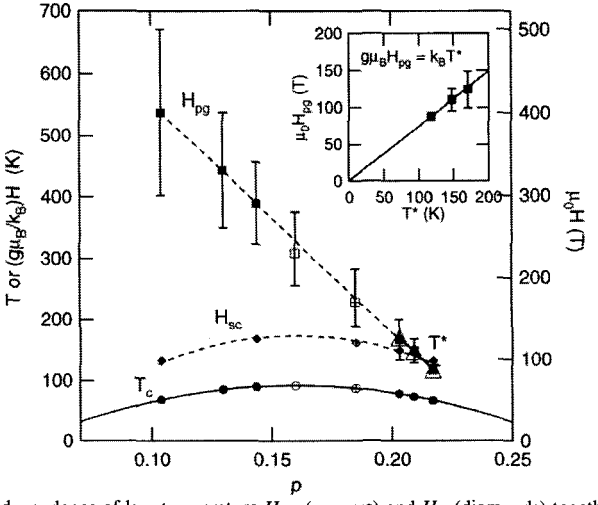

Figure 4: Doping dependence of low-temperature H_{pg} (squares) and H_{sc} (diamonds) together with T^* (open triangles) and T_c (circles). The hole concentration p was obtained from the empirical formula in Ref. [8]. Open and crossed symbols for H_{pg} , H_{sc} , and T_c are from our analysis of $\rho_c(H,T)$ (for details see Ref. [6]). Inset shows H_{pg} as a function of T^* in overdoped BSCCO. Note that the peak field $H_{sc}(p)$ in the low-T limit has a very different doping dependence than $H_{pg}(p)$. At H_{sc} there is still a nonzero Josephson current - a measure of the coherence of the superconducting state. This naturally accounts for the fact that $H_{pg}(p)$ shows a parabolic dependence similar to $T_c(p)$, where the superconducting coherence is established at zero field.

4 Conclusions

Our finding that Zeeman splitting closes the pseudogap implies that the triplet spin excitation at high fields overcomes the singlet pair correlations responsible for the gap in the spin spectrum, and that the orbital contribution is very small. There have been recent reports[9] of vortex-like excitations or superconducting fluctuations well above T_c but still considerably below T^* as defined here. This may imply two different energy scales (gaps), such as appear, for example, in a recent calculation based on strong coupling superconductivity.[10] However, our observation of higher-energy spin gap is most naturally understood[6] within models based on a doped Mott insulator.[11,12]

This work was supported in part by NSF through NHMFL by the Contract No. AL99424-A009, and performed at NHMFL, which is supported by the NSF Cooperative Agreement No. DMR-9527035.

#Present address: Department of Electronic Science and Engineering, Kyoto University, Kyoto 606-8501, Japan.

References

1. T. Timusk and B. Statt, *Rep. Prog. Phys.* **62**, 61-122 (1999).
2. V. M. Krasnov *et al.*, *Phys. Rev. Lett.* **86**, 2657-2660 (2001) and references therein.
3. T. Watanabe, T. Fujii and A. Matsuda, *Phys. Rev. Lett.* **84**, 5848-2116 (2000).
4. M. Suzuki, T. Watanabe and A. Matsuda, *Phys. Rev. Lett.* **82**, 5361-5364 (1999).
5. N. Morozov *et al.*, *Phys. Rev. Lett.* **84**, 1784-1787 (2000).
6. T. Shibauchi *et al.*, *Phys. Rev. Lett.* **86** 5763-5766 (2000).
7. M. Suzuki and T. Watanabe, *Phys. Rev. Lett.* **85**, 4787-4790 (2000).
8. J. L. Tallon and J. W. Loram, *Physica* C **349**, 53-68 (2001).
9. Z. A. Xu, *et al.*, *Nature* **406**, 486-488 (2000).
10. Y. Yanase and K. Yamada, *J. Phys. Soc. Jpn.* **68**, 2999-3015 (1999).
11. V. J. Emery *et al.*, *Phys. Rev.* B **56**, 6120-6147 (1997).
12. P. W. Anderson, cond-mat/0108522 (2001).

VORTEX MAGNETISM IN THE HIGH-TEMPERATURES SUPERCONDUCTOR $LA_{2-X}SR_XCUO_4$

B. LAKE,[1] T. E. MASON,[1] G. AEPPLI,[2] K. LEFMANN,[3] N. B. CHRISTAINSON,[3]
D. F. MCMORROW,[3] K. N. CLAUSEN,[3] H. M. RONNOW,[4] P. VORDERWISCH,[5]
P. SMEIBIDL,[5] N. MAGNKORNTONG,[6] N. E. HUSSEY,[6] T. SASAGAWA,[6]
M. NOHARA,[6] H. TAKAGI,[6] and A. SCHRODER,[7]

[1]*Oak Ridge National Laboratory, Oak Ridge, Tennessee, USA*
[2]*N.E.C. Research Center, Princeton, New Jersey, USA*
[3]*Riso National Laboratory, Roskilde, Denmark*
[4]*CEA-Grenoble, and Inst. Laue-Langevin, Grenoble, Cedex 9, France*
[5]*BENSC, Hahn-Meitner Institute, Berlin, Germany*
[6]*University of Tokyo, Tokyo, Japan*
[7]*University of Karlsruhe, Karlsruhe, Germany*

There is strong evidence that magnetic interactions play a crucial role in the mechanism driving high-temperature superconductivity in cuprate superconductors. To investigate this further we have done a series of neutron scattering measurements on $La_{2-x}Sr_xCuO_4$ (LSCO) in an applied magnetic field. Below T_c the field penetrates the superconductor via an array of normal state metallic inclusions or vortices. Phase coherent superconductivity characterized by zero resistance sets in at the lower field-dependent irreversibility temperature (T_{irr}). We have measured optimally doped LSCO (x=0.16, T_c=38.5 K) and underdoped LSCO (x=0.10, T_c = 29 K); both have an enhanced antiferromagnetic response in a field. Measurements of the optimally doped system at H=7.5 T show that sub-gap spin fluctuations first disappear with the loss of finite resistivity at T_{irr}, but then reappear at a lower temperature with increased lifetime and correlation length compared to the normal state. In the underdoped system elastic antiferromagnetism develops below T_c in zero field, and is significantly enhanced by application of a magnetic field. Phase coherent superconductivity is then established within the antiferromagnetic phase at T_{irr}; thus, the situation in underdoped LSCO is the reverse of that for the optimally doped LSCO where the zero-resistance state develops first before the onset of antiferromagnetism.

MAGNETIC FIELD TUNING OF CHARGE AND SPIN ORDER IN THE CUPRATE SUPERCONDUCTORS

A. POLKOVNIKOV,[1] S. SACHDEV,[1]
M. VOJTA,[2] E. DEMLER[3]

[1]*Department of Physics, Yale University, P.O. Box 208120, New Haven CT 06520-8120, USA*

[2]*Theoretische Physik III, Elektronische Korrelationen und Magnetismus, Universität Augsburg, 86135 Augsburg, Germany*

[3]*Department of Physics, Harvard University, Cambridge MA 02138, USA*

Recent neutron scattering, nuclear magnetic resonance, and scanning tunneling microscopy experiments have yielded valuable new information on the interplay between charge and spin density wave order and superconductivity in the cuprate superconductors, by using a perpendicular magnetic field to tune the ground state properties. We compare the results of these experiments with the predictions of a theory which assumed that the ordinary superconductor was proximate to a quantum transition to a superconductor with co-existing spin/charge density wave order.

1 Introduction

An innovative series of recent experiments[1-4] have shed new light on the nature of strong correlations in the cuprate superconductors. These experiments all use a magnetic field, applied perpendicular to the CuO_2 layers, to tune the low temperature properties of the superconducting state. The results support the idea that ground state correlations in the doped Mott insulator can be described using a framework of competing order parameters.[5-8] In our view, they (especially Ref. [4]) also offer compelling evidence that the orders competing with the superconductivity are spin and charge density waves, and suggest that one or both are present in the insulating state at very high fields.[9]

In the underdoped regime, experimental evidence for spin and charge density ordering, coexisting with superconductivity, has accumulated over the last decade.[5,10-13] With increasing doping, some experimental results in Refs. 13 and 14 can also be explained by proximity to a quantum critical point at which the spin/charge order disappears. At optimal doping, it is widely accepted that the important qualitative characteristics of the ground state are identical to those of a *d*-wave superconductor described in the standard BCS-BdG theory; nevertheless even at such dopings an attractive description of the collective spin and charge excitations is provided by a theory of the vicinity of the spin/charge ordering critical point at lower doping.[15] Such a framework was used recently in Refs 16 and 17 to address the influence of the applied magnetic field, and a number of its specific predictions appear to have been confirmed in subsequent measurements.[2-4] Here we will briefly review aspects of this theory and discuss extensions needed to develop a complete

theory of the remarkable recent scanning tunneling microscopy (STM) measurements of Hoffman *et al.*[4]

2 Order parameters and quantum field theory

We consider a zero temperature transition between a *d*-wave superconductor (SC) and a superconductor with co-existing spin/charge order (SC+SDW/CDW). The density wave order parameters for the transition are defined by the following representations of spin ($S_\alpha(\boldsymbol{r},\tau)$, $\alpha=x,y,z$) and charge density modulation ($\delta\rho(\boldsymbol{r},\tau)$) at imaginary time τ and on the sites, $\boldsymbol{r}$, of a square lattice of unit lattice spacing:

$$S_\alpha(\boldsymbol{r},\tau) = \mathrm{Re}\left(\Phi_\alpha(\boldsymbol{r},\tau)e^{i\boldsymbol{K}_s\cdot\boldsymbol{r}}\right) \quad ; \quad \delta\rho(\boldsymbol{r},\tau) = \mathrm{Re}\left(\phi(\boldsymbol{r},\tau)e^{i\boldsymbol{K}_c\cdot\boldsymbol{r}}\right) \tag{1}$$

where $\boldsymbol{K}_s$ and $\boldsymbol{K}_c$ are the respective ordering wavevectors. A phase with SDW order has $\langle\Phi_\alpha\rangle \neq 0$ and a broken spin rotation symmetry; it is important to note that we use the term 'CDW order' (with $\langle\phi\rangle \neq 0$) in its most general sense: all local observables which are invariant under spin-rotation and time-reversal symmetries (like the on-site energy, or the bond kinetic and exchange energies, or the bond charge density) acquire a spontaneous modulation at wavevector $\boldsymbol{K}_c$ and it is possible that the modulation in the total site charge density itself is quite small. Excluding the case of two sublattice orderings (with wavevectors (π,π), $(\pi,0)$, $(0,\pi)$), the order parameters Φ_α, ϕ are *complex fields*, with their phases representing a sliding degree of freedom of the density wave. This sliding degree of freedom is also present when the ordering is commensurate, but the phases then prefer to take a discrete set of values. We will focus here on the case $\boldsymbol{K}_s=(3\pi/4,\pi)$, $\boldsymbol{K}_c=(\pi/2,0)$ which is experimentally relevant above a doping of about 1/8 (a theoretical rationale for the selection of this value of $\boldsymbol{K}_c$ was provided in Ref. [18]); the generalization to other commensurate and incommensurate wavevectors is immediate. The theory also includes order parameters associated with density waves in the orthogonal direction ($\boldsymbol{K}_{s1}=(\pi,3\pi/4)$, $\boldsymbol{K}_{c1}=(0,\pi/2)$) but we will not write down these terms explicitly in the interest of brevity---this has been done in Ref. 17. A variety of SDW and CDW phases (with background SC order) are possible in models described by the fields Φ_α and ϕ, and some of these have been described in Ref. 19. Here we will focus on the simplest possibility of a transition from SC to SC+SDW driven by the condensation of Φ_α (results are similar in other cases); as discussed in Ref. 19 the condensation of Φ_α also leads to concomitant CDW order with $\boldsymbol{K}_c=2\boldsymbol{K}_s$ (modulo a reciprocal lattice vector), and near the transition we can pin the charge order field to the spin order field by

$$\phi(\boldsymbol{r},\tau) \propto \Phi_\alpha^2(\boldsymbol{r},\tau)\,, \tag{2}$$

where a summation over the repeated index α is implied here and henceforth.

The effective action for Φ_α describing the quantum transition from SC to SC+SDW is:

$$S_\Phi = \int d^2 r d\tau \Big[\left|\partial_\tau \Phi_\alpha\right|^2 + c_x^2 \left|\partial_x \Phi_\alpha\right|^2 + c_y^2 \left|\partial_y \Phi_\alpha\right|^2 + s\left|\Phi_\alpha\right|^2 + \frac{u_1}{2}\left(\left|\Phi_\alpha\right|^2\right)^2 + \frac{u_2}{2}\left|\Phi_\alpha^2\right|^2 + \lambda\left(\left(\Phi_\alpha^2\right)^4 + \text{c.c.}\right)\Big], \tag{3}$$

(see Refs. [6, 7, 15-19]) where $c_{x,y}$ are velocities, and s is a coupling which tunes the system across the SC to SC+SDW transition. We have neglected couplings to the fermionic nodal quasiparticles as we assume they have been suppressed by constraints from momentum conservation.[16,17] The non-linearity u_2 selects between spiral and collinear spin orderings,[19,17] and we assume $u_2<0$, for which case collinear ordering with $\varepsilon_{\alpha\beta\gamma}\left\langle\Phi_\beta\right\rangle\left\langle\Phi_\gamma^*\right\rangle = 0$ is selected, as is the case experimentally. The λ term is special to the value $\boldsymbol{K}_s=(\pi/4,0)$ and prefers that the phase of Φ_α take a set of discrete values: it is permitted for this value of $\boldsymbol{K}_s$ because translations by integer lattice spacings correspond to the transformation (see Eq. (1))

$$\Phi_\alpha \rightarrow \Phi_\alpha e^{in\pi/4}\ ,\ n \text{ integer}, \tag{4}$$

under which all the terms in S_Φ are invariant; the sign of λ chooses between bond and site centered density waves.[17]

The SC phase with no SDW order is realized for s larger than some critical value s_c. An important property of this phase is that the Φ_α quanta constitute a stable excitonic excitation with a *6-fold* degeneracy. At the Gaussian level this is evident from the fact that the quadratic terms in Eq. (3) have a global O(6) symmetry. However, the terms proportional to u_2 and λ are only invariant under O(3) spin rotation symmetry and the discrete symmetry in Eq. (4), but a perturbative computation to all orders easily shows that this symmetry is sufficient to preserve the 6-fold degeneracy. The usual degeneracy of a spin S=1 triplet has been doubled by the additional discrete sliding degree of freedom of the SDW.

Now let us consider the influence of an applied magnetic field, H, on the SC phase. An important early contribution was made by Arovas *et al.*,[20] who focused on cores of the vortices in the SC order introduced by H and argued that, because of a microscopic repulsion between the SC and Neel orders, locally the SC order would "rotate" into an insulating Neel (SDW) phase. The cores have since been examined in a number of experiments[21,22,3] and no clear sign of such behavior emerged: instead, the sub-gap conductance is enhanced in the cores, additional core states appear, and there may be a subdominant pairing amplitude (*e.g.* $d_{x^2-y^2}+id_{xy}$) (see Ref. [23]. The nuclear magnetic resonance (NMR) experiments observed enhanced antiferromagnetic *fluctuations* located *outside* the vortex core, as was originally predicted in Ref. [16] (see below); the formalism of[20] allows static antiferromagnetic

order on scales larger than the core size, and this along with the extension to dynamic antiferromagnetism was discussed recently in.[24]

Two of us and Y. Zhang[16] examined the consequences of the microscopic repulsion between SC and SDW orders, but near a bulk transition between the SC and SC+SDW phases. We argued that effects driven by the strongly relevant $u_{1,2}$ interactions in Eq. (3) implied that the predominant enhancement of the SDW fluctuations in the SC phase, and the consequent lowering of the exciton energy, occurred primarily in the superconducting region outside the vortex cores, driven by the superflow induced by H. (Loosely speaking, this can be understood as follows: as we approach the onset of SDW order by decreasing s, Φ_α initially attempts to condense in the cores of the vortices. However, the quartic self interactions $u_{1,2}$ are most effective in this strongly localized region, and this drives up the effective Hartree potential felt by Φ_α in the core. So Φ_α can only condense in an extended state which is primarily sensitive to the large spatial region outside the core over which the superflow is present. Alternatively stated, the energy of any Φ_α states which may be localized in the core *always* remains at non-zero energies of order of the exchange interaction (and so are probably strongly overdamped), and Bose condensation of Φ_α can only occur in extended states outside the core whose energy can indeed approach zero.)[25] These predictions appear to have been confirmed in subsequent experiments: the NMR experiments of Ref. [3] were noted above, and the recent STM measurements of Ref. [4] observe CDW modulations (which are related to the SDW by Eq. (2)) at distances almost an order of magnitude beyond the point where the superconducting coherence peaks are fully recovered outside the vortex core. The work of Ref. [16] also made predictions on the field-dependence of the elastic Bragg peaks associated in the SC+SDW phase: these are in good accord with subsequent neutron scattering measurements.[2]

We briefly mention the field theory origin of the results of Ref. [16]. As we are focusing on long length scales outside the small vortex cores, a continuum description is possible. For the collective spin/charge excitations we use S_Φ in Eq.(3); for simplicity, we do not include a Zeeman coupling to H in S_Φ because it only modifies physical properties at order H^2 (because, loosely speaking, the average field on the spins in the oscillating SDW vanishes). The infinite diamagnetic susceptibility of the SC order makes its response to H much stronger, and we describe this, and the coupling to Φ_α, by the action S_Φ+S_Ψ (this cannot be applied within the core where the SC wavefunction is perturbed in different ways, as noted above), where

$$S_\Psi = \int d^2\boldsymbol{r}d\tau \left[\left|(\nabla - iA)\Psi\right|^2 - \left|\Psi\right|^2 + \frac{\left|\Psi\right|^4}{2} + \kappa\left|\Psi\right|^2\left|\Phi_\alpha\right|^2 \right], \tag{5}$$

$\Psi(\boldsymbol{r})$ is the superconducting order parameter which is dependent on $\boldsymbol{r}$ but independent of τ, we have chosen various scales to make many couplings in Eq. (5)

unity,[16] A is the vector potential of the applied field, and $\kappa > 0$ is the repulsive coupling between the two orders. The action $S_\Phi + S_\Psi$ provides a theory of the SC to SC+SDW transition, including the ingredients for the repulsive interactions between the excitons and for the lowering of the exciton energy by the superflow.

In the context of the application to the recent STM measurements,[4] a significant property of $S_\Phi + S_\Psi$ is that as long we are in the SC phase (which is evidently the case in Ref. [4]), not only do we have no static SDW order with $\langle \Phi_\alpha \rangle = 0$, but we also have $\langle \phi \rangle = \langle \Phi_\alpha^2 \rangle = 0$, and so there is no local static CDW order even in an external field, even though the energy of thespin/charge exciton has been considerably lowered. This is simply a consequence of the fact that all the terms in Eqs. (3) and (5) are invariant under the sliding symmetryin Eq. (4), and so the phase of the exciton has not been pinned. However, the presence of the vortices clearly breaks the translational symmetry on the lattice scale, and so the continuum theory should be supplemented by additional terms which implement this effect and pin the exciton; a little thought using (1) shows that the simplest such term is

$$S_{\text{lat}} = -\zeta \int d\tau \sum_r |\Psi(r)|^2 \Phi_\alpha^2(r,\tau) e^{i2K_c \cdot r} + \text{c.c.} \tag{6}$$

where ζ is a new coupling constant. Because of the rapidly oscillating $e^{iK_c \cdot r}$ term, Eq.(6) will vanish in any region of space where $\Psi(r)$ is slowly varying. So the pinning of the exciton by Eq. (6) happens mainly in the vortex core (the diameter of the core is of the order of a couple lattice spacings), while the energy of the exciton is lowered by κ term in Eq. (5) by the superflow outside the vortex core. On long scales outside the vortex core it should be acceptable to replace Eq.(6) by

$$S_{\text{lat},1} = -\zeta_1 \int d\tau \Phi_\alpha^2(r=0,\tau) e^{i\delta} + \text{c.c.} \tag{7}$$

for a vortex at $r = 0$, where the phase δ is determined by the microstructure of the vortex on the lattice scale. The term in Eq. (7) breaks the symmetry in Eq. (4), and so it is now possible to have static CDW order in the SC phase in an applied magnetic field. We still have $\langle \Phi_\alpha \rangle = 0$, but Eq.(7) does locally lift the 6-fold degeneracy of the gapped exciton to 3+3. We can compute the static CDW order in the spirit of the calculation of Ref. [16], and in the Gaussian approximation to $S_\Phi + S_\Psi + S_{\text{lat},1}$, and to first order in ζ_1 we find

$$\langle \Phi_\alpha^2(r,\tau) \rangle = \left(\frac{3}{8\pi^{3/2} s_1^{1/4} c^{5/2}} \right) \zeta_1 e^{-i\delta} \frac{e^{-2r_1\sqrt{s_1}/c}}{r_1^{3/2}} \tag{8}$$

where s_1 is the exciton "mass" s renormalized downwards by the superflow via the κ term in Eq. (5) (as in Ref.[16]), $c = \left(c_x c_y\right)^{1/2}$ and $r_1 = c\left[\left(x/c_x\right)^2 + \left(y/c_y\right)^2 \right]^{1/2}$; this implies a static CDW by (1) and (2). The length scale, $\xi_c = c/\left(2\sqrt{s_1}\right)$, over which

this CDW order appears has been significantly increased by the superflow around the vortex core *and* the exciton interactions $u_{1,2}$, while the order has been pinned by the vortex core via Eq. (7). In the absence of the pinning in Eq. (7) we would have $\langle \delta\rho(\boldsymbol{r},\tau)\rangle = 0$ in this SC phase.

3 Quasiparticle density of states

We now discuss the application of the above theoretical framework to the STM measurements in BSCCO of Hoffman *et al.*[4] As we indicated earlier, they report observations of a modulation of period 4 in the local density of states (LDOS) in a small energy window around ±7 meV in the superconducting region (with fully formed coherence peaks) outside the vortex core. Such a modulation can arise by scattering of the quasiparticles off either the SDW or the CDW correlations. The SDW order is dynamic and one of its effects will be an enhancement of the quasiparticle LDOS at energies large enough to allow the quasiparticles to decay by emission of a finite energy spin exciton. It remains to be seen whether the spin excitation spectrum of BSCCO in a magnetic field, as observed in neutron scattering experiments, has spectral weight at low enough energies for this effect to be important. We also note that the modulation in the LDOS will only arise as a consequence of the 3+3 splitting of the spin exciton by the potential in Eqs (6) or (7). Here we only present our results for the simpler case of modulation induced directly by the CDW order; this order is made static by the pinning induced by the vortex cores (as in Eq. (8)), and can serve as an elastic scattering potential for the quasiparticles. The effect of an isolated elastic scattering potential in a *d*-wave superconductor has been well studied,[26] and for large scattering a virtual bound state is formed at low energies; the effect of Eq. (8) can loosely be interpreted as a periodic version of this, with the weaker potential only leading to a periodic 'hump' or 'shoulder' in the quasiparticle LDOS.

This proposal immediately raises a puzzle which we have not fully resolved. In general, symmetry arguments indicate that the presence of the static CDW order in Eq. (8) implies that the quasiparticle LDOS should display a period 4 modulation at *all* energies, and not just on the sub-gap feature at ±7 meV. A possible resolution of this puzzle is provided by an appeal to the effects of disorder: the signal-to-noise for any periodic modulation is largest at sub-gap energies, and that is where the CDW modulation is visible. At higher energies, random fluctuations in the background LDOS of the *d*-wave superconductor, and especially in the energy at which the coherence peaks are present, can mask the presence of a periodic modulation. A further consequence of our proposal is that the CDW order should be visible near any strong short distance imperfection which can provide a pinning potential as in Eq. (7), and not just near vortex cores.

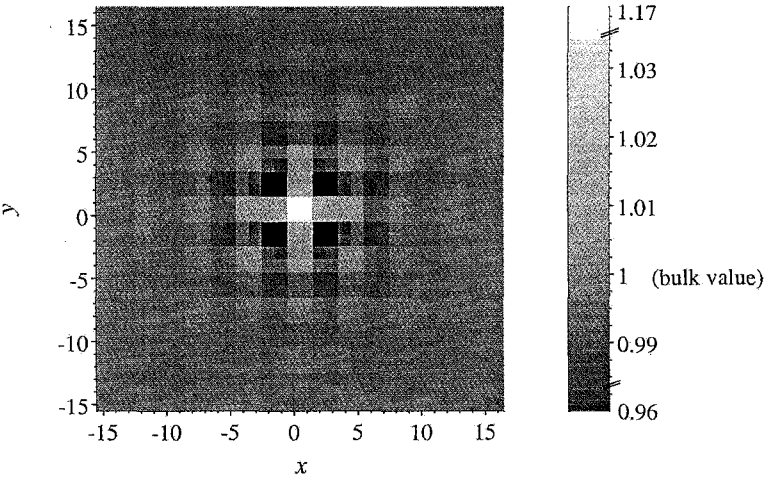

Figure 1: Grayscale plot of the CDW-induced quasiparticle LDOS, integrated over an energy interval $\Delta_0/10 \ldots \Delta_0/3$, where Δ_0 is the size of the bulk d-wave gap. The CDW modulation is plaquette-centered at (0.5,0.5), with wavevectors $\boldsymbol{K}_c=(\pi/2,0)$ and $\boldsymbol{K}_{c1}=(0,\pi/2)$, decay length $\xi_c=6$, and a strength $v_1 = t/5$. For computational reasons we have used a large pairing potential, $V=2t$, but we do not expect qualitative changes for smaller V. A similar modulation is observed at the corresponding energy interval at negative energies.

As promised above, we conclude with a simple calculation of the effect of Eq. (8) on the LDOS. We diagonalized a d-wave BCS Hamiltonian on a square lattice,

$$H = \sum_{ij}\left(-t_{ij}c^{\dagger}_{i\sigma}c_{j\sigma} + \Delta_{ij}c^{\dagger}_{i\sigma}c^{\dagger}_{j,-\sigma} + h.c.\right) + \sum_{i}\left[v(\boldsymbol{r}_i) - \mu\right]c^{\dagger}_{i\sigma}c_{i\sigma}, \qquad (9)$$

where t_{ij} includes nearest-neighbor (t) and next-neighbor (t') hopping, μ is the chemical potential, the pairing amplitude Δ_{ij} is self-consistently determined from $\Delta_{ij} = V_{ij}\left\langle c_{i\sigma}c_{j,-\sigma}\right\rangle$ and V_{ij} is the nearest-neighbor pairing potential. The CDW modulation in Eqs (1), (2), and (8) was implemented via $v(\boldsymbol{r}) = v_1\left\{\cos\left[\boldsymbol{K}_c\cdot(\boldsymbol{r}-\boldsymbol{r}_0)\right] + \cos\left[\boldsymbol{K}_{c1}\cdot(\boldsymbol{r}-\boldsymbol{r}_0)\right]\right\}e^{-|\boldsymbol{r}-\boldsymbol{r}_0|/\xi_c}\left(|\boldsymbol{r}-\boldsymbol{r}_0|^2+1\right)^{-3/4}$. In this initial calculation we did not include the usual modulation of the Δ_{ij} induced directly by the presence of the vortex: we expect this to be important only in the core of the vortex, whose physics we are not attempting to model here, and where the present BCS model is probably inadequate anyway. Figure 1 shows a numerical result for the LDOS, integrated over an interval of sub-gap energies, obtained for a periodic 32×32 system with 20% (bulk) hole doping. The charge-density modulation caused by $v(\boldsymbol{r})$ clearly leads to a period-4 modulation of the sub-gap LDOS.

We are especially grateful to Seamus Davis for communicating the results of Ref. [4] prior to publication, and for useful discussions. We thank Shoucheng Zhang

for valuable comments on the manuscript, and Steve Girvin for helpful discussions. This research was supported by US NSF Grant DMR 0098226 and by the DFG (SFB 484).

References

1. B. Lake *et al., Science* **291,** 1759 (2001).
2. B. Khaykovich *et al.,* submitted to *Nature.*
3. V. F. Mitrovic *et al., Nature* **413**, 501 (2001).
4. J. E. Hoffman *et al.,* submitted to *Science.*
5. J. Zaanen, Physica C **317**, 217 (1999) and references therein; V. J. Emery *et al., Proc. Natl. Acad. Sci. USA* **96**, 8814 (1999) and references therein.
6. S. Sachdev and J. Ye, *Phys. Rev. Lett.* **69**, 2411 (1992); A. V. Chubukov, S. Sachdev and J. Ye, *Phys. Rev. B* **49**, 11919 (1994).
7. S.-C. Zhang, *Science* **275**, 1089 (1997).
8. S. Sachdev, *Science,* **288**, 475 (2000) and references therein.
9. G. S. Boebinger *et al., Phys. Rev. Lett.* **77**, 5417 (1996).
10. C. Panagopoulos *et al., cond-mat*/0007158; C. Panagopoulos *et al., preprint.*
11. Y. S. Lee *et al., Phys. Rev. B* **60**, 3643 (1999).
12. J. E. Sonier *et al., cond-mat*/0108479.
13. P.M. Singer, A.W. Hunt, and T. Imai, *cond-mat*/0108291.
14. G. Aeppli *et al., Science* **278**, 1432 (1998).
15. S. Sachdev, C. Buragohain, and M. Vojta, *Science*, **286**, 2479 (1999); M.Vojta, C. Buragohain, and S. Sachdev, *Phys. Rev. B* **61**, 15152 (2000).
16. E. Demler, S. Sachdev, and Y. Zhang, *Phys. Rev. Lett.* **87**, 067202 (2001).
17. S. Sachdev, *cond-mat*/0108238.
18. M. Vojta and S. Sachdev, *Phys. Rev. Lett.* **83**, 3916 (1999); M. Vojta, Y. Zhang, and S. Sachdev, *Phys. Rev. B* **62**, 6721 (2000).
19. O. Zachar, S. A. Kivelson, and V. J. Emery, *Phys. Rev. B* **57**, 1422 (1998).
20. D. P. Arovas *et al., Phys. Rev. Lett.* **79**, 2871 (1997).
21. Ch. Renner *et al., Phys. Rev. Lett.* **80**, 3606 (1998).
22. S. H. Pan *et al., Phys. Rev. Lett.* **85**, 1536 (2000).
23. M. Franz and Z. Tesanovic, *Phys. Rev. Lett.* **80**, 4763 (1998).
24. J.-P. Hu and S.-C. Zhang, *cond-mat*/0108273.
25. This perspective differs from that of Ref. [24], whose formulation did not account for the strong effects of the quartic exciton self-interactions $u_{1,2}$.
26. A. V. Balatsky *et al., Phys. Rev. B* **51**, 15547 (1995).

ANOMALOUS BEHAVIOR OF SPIN FLUCTUATIONS IN POLYCRYSTALLINE $NdBa_2Cu_3O_7$

A. P. REYES,[1] M. ABDELRAZEK,[1] P. L. KUHNS,[1]
W. G. MOULTON,[1] W. P. HALPERIN[2] and K. KISHIO[3]

[1]*National High Magnetic Field Laboratory, Tallahassee, Florida, USA*
[2]*Northwestern University, Evanston, Illinois, USA*
[3]*Tokyo University, Tokyo, Japan*

Nuclear spin-lattice relaxation rate $1/T_1$ at the planar O(2,3) and bridging O(4) oxygen sites in $NdBa_2Cu_3O_7$ have been measured as a function of temperature in fields up to 42T. Data is characterized by extremely fast relaxation due to Nd. A well-defined peak is observed, indicative of spin freezing, occurring well below T_c and higher than T_N, and whose physical origin is unknown. Extracted T_1 data for Cu(2) shows enhanced Cu-Cu correlations in the superconducting state, suggesting a short-ranged order at lower temperatures.

1 Introduction

One of the most important questions in the study of cuprate superconductors is the nature of the interplay between, and coexistence of, the antiferromagnetic (AF) spin fluctuations and superconductivity. Strong magnetic correlations on the Cu-O planes suggest that the superconducting pairing mechanism is magnetic in nature. In YBCO system, highly magnetic rare-earths doped in place of yttrium has little or no effect on superconductivity while the rare-earths themselves order antiferromagnetically. The fact that these local moments, in spite of their close proximity to the Cu-O planes, fail to break Cooper pairs suggests that they are magnetically isolated from the Fermi liquid by virtue of the small density of states. The bonding energy of the *Zhang-Rice singlet*, a one-component hybridized Cu3*d*–O2*p* state describing the cuprates, is on the order of 1eV, while the exchange energy between the 4*f* moments, J_{4f}, is ~ 10meV (see Ref. [1]). This large difference in energy scales implies that the condensate is very robust against spin-flip scattering from the local moments of the rare-earths.

However, the superconductivity is reduced in the Pr-doped YBCO system, perhaps because of 1) the enhanced *4f–CuO*$_2$ hybridization causing pair-breaking or 2) depletion of the mobile hole-carriers by Pr^{4+} ions. X-ray measurements later revealed that Pr atoms substitute into the Ba site due to atomic size matching. Dow *et al.*, has then argued that the loss of superconductivity is due to the presence of Pr^{3+} ions in close proximity to Cu–O chains which causes magnetic scattering of carriers *residing on the chains.*[2] Although the discovery of superconducting $PrBa_2Cu_3O_7$ supports this idea,[3,4] it has remained largely controversial. Microscopic information on the dynamics of the sample regions influenced by the local moments

is therefore needed in order to resolve this important issue. However, synthesis of superconducting PrBCO has been extremely difficult.[4] NdBCO provides an excellent alternative since it normally superconducts but T_c can also be decreased by allowing Nd to substitute for Ba (see Ref. [5]). The Nd atoms order at $T_N = 0.5$K in this compound.

2 Experimental Techniques

Polycrystalline samples of NdBCO were annealed in flowing ^{17}O and then aligned in 8T magnetic field. The sample has a narrow transition, $T_c \sim 92$K. Field-swept NMR spectra were obtained by spin-echo pulse technique while the relaxation data were obtained from the quadrupolar satellites, as labeled in Fig. 1. Data at 23T has been taken in the high-homogeneity 10ppm Bitter magnet and at 37T and 42T, using the Hybrid magnet at NHMFL.

3 Results and Discussion

3.1 Oxygen spectra

A typical ^{17}O NMR spectrum is shown in Fig. 1 for $H_0 \| c$. The lines have almost identical positions as in YBCO except that the quadrupolar satellites of the O(2) and O(3) lines in NdBCO completely overlap, indicating nearly identical local environments of the two sites along the planar direction.[6] The NdBCO spectrum is invariably broader than YBCO even at high temperatures. Although vortex freezing significantly broadens the spectrum below T_c, the second O(2,3) ⟨5/2–3/2⟩ transitions and the first O(4) ⟨3/2–1/2⟩ transitions remain clearly resolved.

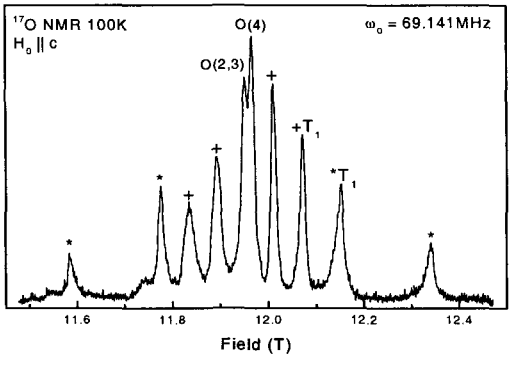

Figure 1: ^{17}O NMR spectrum at 100K; (+) and (*) are O(2,3) and O(4) satellites, respectively.

3.2 ^{17}O *spin-lattice relaxation*

Figure 2 shows the spin-lattice relaxation rate $1/T_1$ as a function of temperature and field for the O(2,3) sites. A peak in the relaxation rate, well below T_c, is also observed in O(4) (not shown). This peak progressively shifts to higher temperature as the field increases, concomitant with a decrease in its magnitude. The O(2,3) relaxation is about an order of magnitude *faster* than those of O(4). In striking contrast to YBCO (see Ref. [7]), neither Korringa or pseudo-gap behavior is observed and the rates are typically two orders of magnitude faster for both sites. These facts indicate that Nd moment fluctuations dominate the oxygen relaxation.

The peak in $1/T_1$ can be understood in terms of critical slowing down of local moment fluctuations. For $T >> T_N$, the relaxation has a Lorentzian form

$$1/T_1 \propto \gamma_n^2 H_o^2 [\tau_c / (1 + \omega_L^2 \tau_c^2)] \quad (1)$$

where γ_n is the nuclear gyromagnetic ratio and ω_L is the Larmor frequency. The system is assumed to have a single correlation time, τ_c which has an activated behavior. A peak in $1/T_1$ occurs when the correlation time becomes longer and becomes comparable to the nuclear precession period, $\omega_L \tau_c \approx 1$. At higher fields, the fluctuations are suppressed owing to magnetic saturation and the peak shifts to higher temperatures. This phenomena is clearly observed in the data, at least qualitatively, up to 42T. However, this presents a physical dilemma since it implies that the Nd atoms are magnetically frozen, which is not observed in any bulk measurements. No sign of any AF order has been seen down to 0.5K.

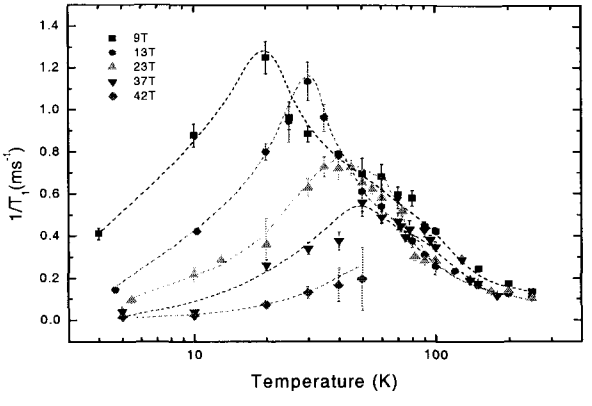

Figure 2: $1/T_1$ versus temperature and field for O(2,3) sites. Dotted lines are guides to the eye.

3.3 ^{63}Cu Relaxation

Copper NMR in NdBCO was inobservable due to short spin dephasing time, but Cu NQR was observed below 50K. The ^{63}Cu(2) $1/T_1$ as a function of temperature is shown in Fig. 3. There is a broad peak around 25K, similar to that seen in ^{17}O $1/T_1$ data at low fields (see Fig. 2).

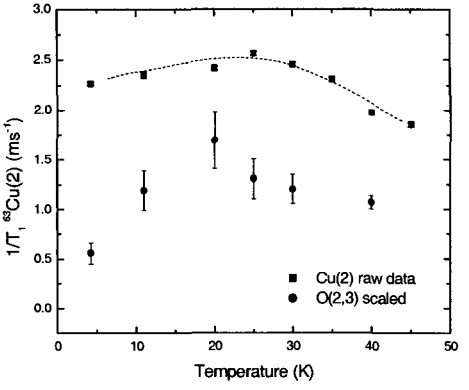

Figure 3: Spin-lattice relaxation rate as a function of temperature for ^{63}Cu(2) (squares). The circles are the calculated Cu(2) relaxation due to Nd, $^{63}1/T_{1d}$ extracted using the O(2,3) data (*see text*).

From these data, we wish to extract the Cu relaxation that is solely due to Nd fluctuations. Assuming a dipolar mechanism, the relaxation rate contribution to α^{th} atom (Cu or O) by the local moments is given by

$$^{\alpha}1/T_{1d} = (2/3)(\sqrt{2}\pi\ ^{\alpha}\gamma_n^2\,\gamma_e^2 / \omega_{ex})\ S(S+1)\ \Sigma_i\ (1/^{\alpha}r_i)^6 \qquad (2)$$

where ω_{ex} is the exchange frequency of the 4*f* moments containing the temperature dependence and $^{\alpha}r_i$ is the distance from the *i*th local moment. The sum is over the nearest-neighbor Nd atoms. If we assume that the oxygen relaxation from copper fluctuations is negligible compared to that from Nd, the Cu relaxation from Nd can be obtained by scaling the oxygen data:

$$^{63}1/T_{1d} = \frac{(^{63}\gamma)^2\,\Sigma_i\,(1/^{63}r_i)^6}{(^{17}\gamma)^2\,\Sigma_i\,(1/^{17}r_i)^6}\ ^{17}1/T_{1d} \qquad (2)$$

This equation automatically takes care of the intrinsic temperature dependence common to both sites. The calculated results scaled to O(2,3) are plotted in Fig. 3 together with the raw data. The intrinsic Cu relaxation, *i.e.* due to Cu AF fluctuations, is the difference $^{63}R = {}^{63}1/T_{1raw} - {}^{63}1/T_{1d}$, as shown in Fig. 4, where the

Cu(2) data in YBCO is also plotted for comparison. Although the NdBCO data is slightly enhanced, both sets of data are in the same order of magnitude, indicating that the character of the Cu AF fluctuations is the same for both materials at this temperature range. However, the NdBCO data shows an upturn below 20 K and continues to increase as the temperature is lowered, suggesting a critical slowing down or perhaps an approach to ordering. One might expect that a Suhl-Nakamura type of interaction among Cu spins will enhance Cu-Cu correlations in the presence of the large Nd moment. This kind of scenario is manifested strongly in PrBCO, where Cu(2) exhibits a very high ordering temperature, T_N(Cu(2)) = 280 K.[10] This data means that strong in-plane magnetic correlations persist deep into the superconducting state.

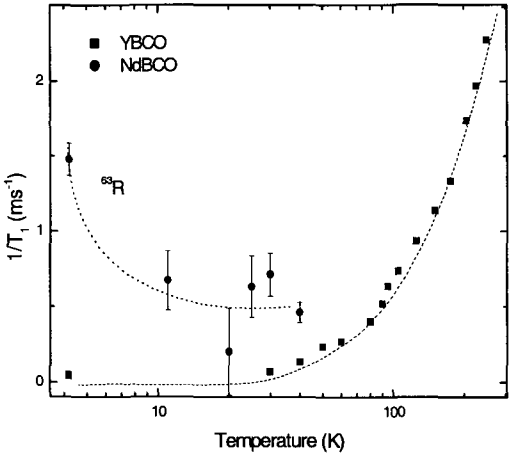

Figure 4: Intrinsic Cu relaxation ^{63}R. The YBCO data is from Ref. 9. Dotted lines are guides to the eye.

4 Conclusions

The results demonstrate a very strong influence of the local moments on the Cu and O relaxation. This important behavior puts into question how is superconductivity unaffected inspite of the very strong local magnetism. The magnetic correlations in the parent compound of REBCO is thought to be reduced by hole-doping. That these correlations survive the superconducting state in the case of NdBCO is clearly evidenced by the Cu T_1 data. On the other hand, it is important to note that the presence of the unquenched AF correlations on the Cu(2) sites is not inconsistent with the idea of *chain-superconductivity.*[2] More data on the chain sites is necessary to clarify this issue.

The exact physical nature of the ^{17}O relaxation remains unclear. A spin-glass-freezing is not expected to lead to antiferromagnetic order[11] at lower temperatures. In fact, any magnetic ordering would drastically shift the resonance lines, which is not observed. Vortex relaxation is far too slow to contribute to this effect. Observation of spin freezing in the striped phase of the $(La_{1-x},Sr/M_x)_2CuO_4$ system is commonly associated with a cluster spin-glass formation and is accompanied by the disappearance of Cu NQR signal.[12] Our observation of Cu NQR discounts the possibility of having a striped phase although the contributions from spin-stripe fluctuations may be expected to be the same order of magnitude and comparable to that of Nd. Since spin or charge stripes have not been observed directly in the (Y/RE)BCO system, a new or exotic relaxation mechanism, probably of stripe-like nature, may have to be invoked. Further analysis of the data is being performed. Future studies involving controlled Nd dopants should help in understanding this interesting behavior.

References

1. F. C. Zhang and T.M. Rice, *Phys. Rev.* B **37**, 3759 (1988).
2. H. A. Blackstead and J. D. Dow, *Phys. Rev.* B **51**, 11830 (1995).
3. H. A. Blackstead, J. D. Dow, D. B. Chrisey, J. S. Horwitz, M. A. Black and P. J. McGinn, A. E. Klunzinger and D. B. Pulling, *Phys. Rev.* B **54**, 6122 (1996).
4. Z. Zou, J. Ye, K. Oka, Y. Nishihara, *Phys. Rev. Lett.* **80**, (1998) 1074.
5. M. J. Kramer, K. W. Dennis, D. Falzgraf, R. W. McCallum, S.K. Malik and W. B. Melon, *Phys. Rev.* B **56**, 5512 (1997).
6. M. Takigawa, P. C. Hammel, R. H. Heffner, Z. Fisk, K. C. Ott and J. D. Thompson, *Phys. Rev. Lett.* **63**, 1867 (1989).
7. P. C. Hammel, M. Takigawa, R. H. Heffner, Z. Fisk and K. C. Ott, *Phys. Rev. Lett.* **63**, 1993 (1989).
8. *see for example*, P. C. Hammel, M. Takigawa, R.H. Heffner and Z. Fisk, *Phys. Rev.* B **38**, 2832(1988).
9. W. W. Warren, Jr., R. E. Walstedt, G. F. Brennert, G. P. Espinosa and J. P. Remeika, *Phys. Rev. Lett.* **50**, 1861 (1987).
10. A. P. Reyes, D. E. MacLaughlin, M. Takigawa, R. H. Heffner, J. D. Thompson, J. E. Crow, A. Kebede, T. Mihalisin and J. Schwegler, *Phys Rev.* B **42**, 2688 (1990).
11. Z. Fisk and D. Pines, *private communications*.
12. M.–H. Julien, A, Campana, A. Rigamonti, P. Carretta, F. Borsa, P. Kuhns, A. P. Reyes, W. G. Moulton, M. Horvatic, C. Berther, A, Vietkin and A. Revcolevschi, *Phys. Rev.* B **63**, 144508 (2001).

This page is intentionally left blank

Contributed Papers

This page is intentionally left blank

LOW-TEMPERATURE NORMAL-STATE HALL EFFECT IN HIGH-T_C $Bi_2Sr_{2-x}La_xCuO_{6+\delta}$ REVEALED BY 60 T MAGNETIC FIELDS

F. F. BALAKIREV, J. B. BETTS and G. S. BOEBINGER

NHMFL, Los Alamos National Laboratory, Los Alamos, NM 87545, USA

S. ONO

Central Research Institute of Electric Power Industry, Tokyo 201-8511, Japan

Y. ANDO and T. MURAYAMA

Central Research Institute of Electric Power Industry, Tokyo 201-8511, Japan, and Dept. of Physics, Science University of Tokyo, Tokyo 162-8601, Japan

We report low-temperature Hall coefficient in the normal state of the high-T_c superconductor $Bi_2Sr_{2-x}La_xCuO_{6+\delta}$. The Hall coefficient was measured down to 0.5 K by suppressing superconductivity with a 60 T pulsed magnetic field. The carrier concentration was varied from overdoped to underdoped regimes by partially substituting Sr with La in a set of five samples. The observed saturation of the Hall coefficient at low temperatures suggests the ability to extract the carrier concentration of each sample. The most underdoped sample exhibits a diverging Hall coefficient at low temperatures, consistent with a depletion of carriers in the insulating ground state. The Hall number exhibits a sharp peak providing additional support for the existence of a phase boundary at the optimal doping.

High-T_c superconductors exhibit a number of anomalous normal state transport properties that does not follow conversional Fermi liquid behavior. One of the most peculiar anomalies observed in High-T_c cuprates is strong temperature dependence of Hall coefficient (R_H), which is far from being understood.[1-3] The study of transport phenomena is further obscured by the onset of superconductivity at low temperatures. Here we report the low temperature properties of Hall coefficient in $Bi_2Sr_{2-x}La_xCuO_{6+\delta}$ (BSLCO) high temperature superconductor. The Hall coefficient was measured down to 0.5 K by suppressing superconductivity with a 60 T pulsed magnetic field.

The properties of BSLCO samples makes it an ideal compound for a comprehensive magnetotransport study of normal state of high-T_c superconductors at low temperatures and high magnetic fields. High quality BSLCO single crystals can be produced within a wide range of carrier concentration by partially substituting Sr with La. The optimal doping, corresponding to highest superconducting transition temperature (T_c), is achieved at La concentration x=0.4. Recently the existence of metal to insulator crossover has been demonstrated in the underdoped regime in BSLCO at low temperatures.[3] Moreover, the insulating behavior exhibits anomalous logarithmic divergence of resistivity with temperature, which was previously observed in $La_{2-x}Sr_xCuO_4$ (see Ref. [4]). Both overdoped (x<0.4) and underdoped (x>0.4) samples have been investigated in present study.

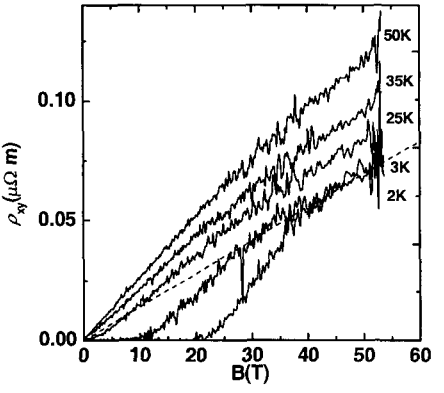

Figure 1: Magnetic field dependence of Hall resistivity in $Bi_2Sr_{2.49}La_{0.51}CuO_{6+\delta}$ sample (T_c=26 K) at temperatures above and below T_c. The dashed line is a best linear fit, $\rho_{xy}(H)= R_H H$, for a high field regime for T=2 K trace.

Single crystal samples of BSLCO were prepared using a floating-zone technique. Resistivity and Hall coefficient were measured in standard 6-probe geometry in a total of 5 samples with nominal La concentrations x=0.23, 0.49, 0.51, 0.73, and 0.84. The measurements where carried out using synchronous digital lockin technique developed at NHMFL. The transport data were obtained during the sweep of magnetic field for two opposite directions of the field for each temperature.

Figure 1 shows a typical field dependence of the Hall resistivity in a BSLCO sample (x=0.51, T_c=26 K). Hall resistivity observes conventional linear in field dependence at temperatures above T_c. At temperatures below T_c the Hall signal is zero at low magnetic field due to superconductivity. As increasing magnetic field suppresses superconductivity, the Hall signal rapidly increases. At magnetic field high enough as to completely suppress superconductivity, conventional linear in field behavior for Hall resistivity is recovered. Thus low temperature Hall coefficient can be determined by a linear fit to Hall resistivity dependence in high field regime, $\rho_{xy}(H)= R_H H$ (dashed line on Fig. 1).

Temperature dependencies oh R_H for 5 BSLCO samples with different levels of La doping are plotted on Fig. 2. The R_H values below T_c where determined from the slope of the $\rho_{xy}(H)$ in a high field regime as outlined above. The fact that there's no noticeable change in $R_H(T)$ dependence between temperature ranges above and below T_c suggests that superconductivity is completely suppressed by high magnetic field and that R_H values plotted on Fig. 2 correspond to the normal state of BSLCO.

We found that at the low temperature limit Hall coefficient becomes independent of temperature in samples with La concentration x=0.49, 0.51, and 0.73. The possible explanation for temperature-independent Hall coefficient could

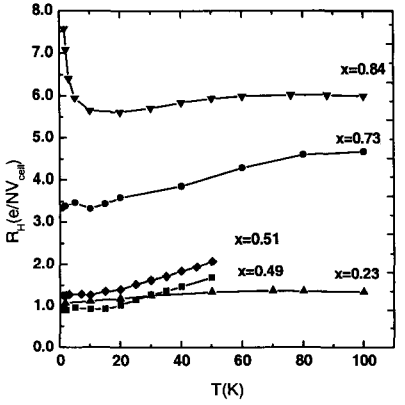

Figure 2: Temperature dependence of R_H in $Bi_2Sr_{2x}La_xCuO_{6+\delta}$ samples with different levels of La doping x. The Hall coefficient is normalized per unit cell.

be that the inelastic scattering channel, which is responsible for the anomalous Hall effect and resistivity at higher temperatures, "freeze out" at low temperatures while only the conventional temperature-independent elastic scattering mechanism remains. The Hall coefficient in the most underdoped sample with x=0.84 rapidly increases as temperature decreases below 10 K perhaps due to the depletion of carriers as metal to insulator transition occurs in this sample at low temperature. The $R_H(T)$ in the underdoped sample (x=0.23) does not saturate down to lowest experimental temperature, but continues to decrease, although the change is small. Similar continuous decrease oh the Hall coefficient as temperature decreases has been reported for overdoped single layer Tl-2201 sample.[5] This data suggest that transport mechanism in underdoped regime could be different from the transport mechanism in the overdoped regime.

Temperature-independent Hall effect can possibly be due to the recovery of the Fermi liquid behavior in the low temperature limit. In a single band Fermi liquid model the Hall number, $n_H = 1/R_H$, reflects the actual number of charge carriers. To check the validity of this interpretation the variation of the low temperature n_H with doping is shown on Fig. 3. The Hall number obtained for near optimally doped samples corresponds to approximately one hole per Cu atom. These values are close to what have been determined in Angular Resolved Photoemission Spectroscopy (ARPES) studies in similar high-T_c compounds.[6] The ARPES reports large Fermi surface, which is supported by the large Hall number in the low temperature ground state reported here.

In the assumption that low temperature Hall number corresponds to the actual number of charge carriers in BSLCO the evolution of the Fermi surface with doping can be traced. The Hall coefficient in the most underdoped sample(x= 0.84)diverges

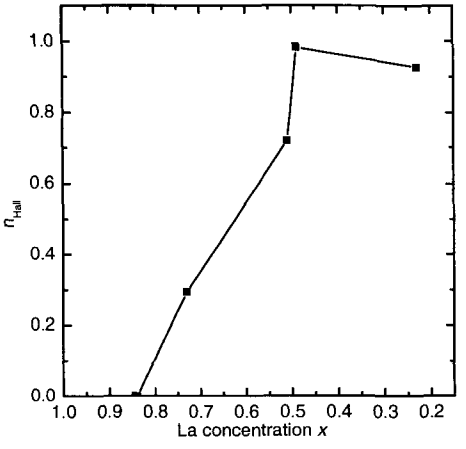

Figure 3: Hall number variation with doping in $Bi_2Sr_{2-x}La_xCuO_{6+\delta}$ at low temperatures. The bottom axes shows the actual La doping level x.

in the T -> 0 limit which suggesting fully gaped ground state at this doping level. The increase in hole doping leads to a formation of a small Fermi surface in a x=0.73 sample corresponding to about 0.3 carriers per Cu atom. The size of the Fermi surface grows rapidly from underdoped to optimally doped regime. The low temperature Hall number value peaks at optimal doping. In the overdoped sample n_H decreases compared to near-optimally doped sample. The sharp peak in n_H dependence near optimal doping provide additional support for the existence of a phase boundary perhaps due to a quantum critical point at the optimal doping.

References

1. T. R. Chien, Z. Z. Wang and N. P. Ong, *Phys. Rev. Lett.* **67**, 2088-2091(1991).
2. Y. Kubo and T. Manako, *Physica C* **197**, 378-384 (1992).
3. S. Ono *et al., Phys. Rev. Lett.* **85**, 638-641(2000).Y. Ando *et al.,*, Y., *Phys. Rev. Lett.* **75**, 4662-4665 (1995).
5. A. P. Mackenzie *et al., Phys. Rev. B* **53**, 5848-5855 (1996).
6. R. Liu *et al., Phys. Rev. B* **45**, 5614-5621 (1992).

TUNNELING SPECTROSCOPY OF THE ELECTRON-DOPED CUPRATE SUPERCONDUCTOR $Pr_{2-x}Ce_xCuO_4$

A. BISWAS, P. FOURNIER, V. N. SMOLYANINOVA, H. BALCI,
J. S. HIGGINS, A. R. C. BUDHANI and R. L. GREENE
Center for Superconductivity Research, Department of Physics, University of Maryland, College Park, Maryland 20742, USA

The properties of electron(n)-doped cuprate superconductors show significant deviations from those of their hold(p)-doped counterparts. Experiments prior to 2000 suggested an s-wave pairing symmetry as opposed to a d-wave pairing symmetry in hole-doped cuprates. Recent experiments have suggested that n-doped cuprates have a d-wave pairing symmetry. However, tunneling spectroscopy of these materials have not revealed a zero bias conductance peak (ZBCP), which is a classic signature of d-wave symmetry. We present the first tunneling spectroscopy data on n-doped $Pr_{2-x}Ce_xCuO_4$ (PCCO) using point contact junctions which show a systematic evolution of the ZBCP. This method of junction fabrication is important as it allows the barrier strength between the normal and the superconducting electrodes to be varied. We show that this is essential to observing the ZBCP. The n-doped cuprates have a low T_c (~25 K) and H_{c2} (~10 T). The low H_{c2} enables us to obtain the normal state in PCCO at low temperatures. We have used this to probe the density of states in the normal state of PCCO. We observe an anomalous gap even in the normal state.[1] This normal state gap (NSG) becomes smaller on the over-doped side. We discuss the behavior of this NSG in the context of the pseudogap which has been observed in hole-doped cuprates.

1. A. Biswas, P. Fournier, V. N. Smolyaninova, R. C. Budhani, J. S. Higgins, and R. L. Greene, *cond-mat*/0103634 (to appear in *Phys. Rev. B*).

*This work was supported by NSF DMR 97-32736.

MAGNETIC FIELD EFFECTS ON T_C AND THE PSEUDOGAP ONSET TEMPERATURE IN CUPRATE SUPERCONDUCTORS

QIJIN CHEN

National High Magnetic Field Laboratory, 1800 East Paul Dirac Drive, Tallahassee, Florida 32310

YING-JER KAO, ANDREW P. IYENGAR and K. LEVIN

James Franck Institute, University of Chicago, Chicago, Illinois 60637

We study the sensitivity of T_c and the pseudogap onset temperature, T^*, to low fields, H, for cuprate superconductors, using a BCS-based approach extended to arbitrary coupling. We find that T^* and T_c, which are of the same superconducting origin, have very different H dependences. The small coherence length makes T^* rather insensitive to the field. However, the presence of the pseudogap at T_c makes T_c more sensitive to H. Our results for the coherence length ξ fit well with existing experiments. We predict that very near the insulator ξ will rapidly increase.

The pseudogap phenomena have been a great challenge to condensed matter physicists since last century. Yet there has been no consensus on the origin of the pseudogap and its relation to the superconducting order parameter. Theories about the pseudogap physics fall into two categories: (1) precursor versus (2) non-precursor superconductivity. For the former, pseudogap forms as a consequence of precursor superconducting pairing, and therefore, shares the same origin as the order parameter. In contrast, for the latter category, pseudogap has a different origin, e.g., a hidden DDW (d-density wave) order.[1]

On the other hand, experiment has revealed different behaviors of T_c and the pseudogap onset temperature T^* in magnetic fields.[2] However, there is still no proper theoretical explanation. This difference has been used as evidence against precursor superconductivity scenarios. Here we show that it can be well explained within the present precursor superconductivity theory.[3,4,5]

Our calculation is based on an extension of BCS theory which incorporates incoherent pair excitations. These pair excitations become increasingly important at large coupling g, and lead to a pseudogap in the single-particle excitation spectrum, as seen in the cuprates. As the temperature increases from $T = 0$, these pairs can survive a higher temperature ($> T_c$) than the condensate, until they are completely destroyed by the thermal effect at T^*. In agreement with experiment, we find that T^* and T_c have very different field (H) dependences. The small coherence length (ξ) makes T^* rather insensitive to the field. However, the presence of the pseudogap at T_c (at optimal and

under- doping) makes T_c relatively more sensitive to H. Our results for the coherence length ξ fit well with existing experiments. Furthermore, we predict that very near the insulator ξ will rapidly increase.

We first consider the zero magnetic field case. We include, in addition to time-reversal state pairing, finite center-of-mass momentum pair excitations in the problem and then treat the interrelated single- and two-particle propagators self-consistently. We truncate the infinite series of equation of motion at the three-particle level, and then factorize the three-particle Green's function G_3 into single-particle (G) and two-particle (G_2) Green's functions.[6]

Here we consider an electron system near half filling on a quasi-two dimensional (2D) square lattice, with tight-binding dispersion $\epsilon_{\mathbf{k}}$. The electrons interact via a separable potential $V_{\mathbf{k},\mathbf{k}'} = g\varphi_{\mathbf{k}}\varphi_{\mathbf{k}'}$, where $\varphi_{\mathbf{k}} = \cos k_x - \cos k_y$ (for d-wave). We use a T-matrix approximation for the self-energy, and have

$$\Sigma(K) = G_0^{-1}(K) - G^{-1}(K) = \sum_Q t(Q)\, G_0(Q-K)\, \varphi^2_{\mathbf{k}-\mathbf{q}/2}\,, \qquad (1)$$

$$t(Q) = -\frac{|\Delta_{sc}|^2}{T}\delta(Q)\theta(T_c - T) + \frac{g}{1+g\chi(Q)}\,, \qquad (2)$$

where Δ_{sc} is the order parameter, and $\chi(Q) = \sum_K G(K)G_0(Q-K)\,\varphi^2_{\mathbf{k}-\mathbf{q}/2}$. For small $Q \neq 0$, $t(Q)$ can be written in a standard propagator form. The pseudogap is given by $\Delta^2_{pg} \equiv -\sum_Q t(Q)$, the total gap[4] by $\Delta = \sqrt{\Delta^2_{sc} + \Delta^2_{pg}}$, and the quasiparticle dispersion by $E_{\mathbf{k}} = \sqrt{\epsilon^2_{\mathbf{k}} + \Delta^2\varphi^2_{\mathbf{k}}}$.

T_c is determined by the superconducting instability condition $1+g\chi(0) = 0$, in conjunction with the number constraint $n = 2\sum_K G(K)$. We obtain a set of three equations.[4] Taking into account that the cuprates is close to the Mott insulator and thus in-plane hopping $t_{\|}(x) = t_0(1-n) = t_0 x$, where x is the doping concentration, we solve for T_c, Δ, chemical potential μ, and Δ_{pg}. The results for T_c, $\Delta_{pg}(T_c)$, and $\Delta(T=0)$ as a function of x are summarized in Fig. 1(a). Our predictions fit experiment well with $-g/4t_0 = 0.045$ and $t_0 \approx 0.6$ eV. For more details, see Refs. 3–5.

In a finite field, the Ginzburg-Landau free energy functional near T_c can be expanded to quadratic order in the order parameter Δ_{sc}:

$$F \sim \left(\tau_0(T) + \eta^2\left(\frac{\nabla}{i} - \frac{2e\mathbf{A}}{c}\right)^2\right)|\Delta_{sc}|^2\,, \qquad (3)$$

where $\tau_0(T) = \bar{\tau}_0\left(1 - \frac{T}{T_c}\right)$, and $-\frac{1}{T_c}\frac{dT_c}{dH}\Big|_{H=0} = \frac{2\pi}{\Phi_0}\xi^2 = \frac{2\pi}{\Phi_0}\frac{\eta^2}{\bar{\tau}_0}$. As an estimate, one has $H_{c2}(0) \approx \Phi_0/(2\pi\xi^2)$. ($\Phi_0 = hc/2e$ is the flux quantum).

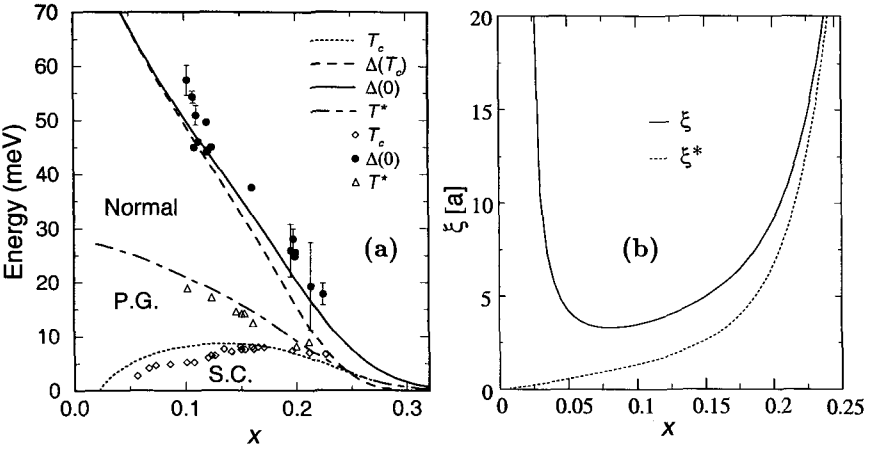

Figure 1. (a) Calculated cuprate phase diagram. T^* was estimated using the BCS mean-field solution. Experimental data are taken from: (•) Ref. 7; (◇) Ref. 8; (△) Ref. 9. For more details see Ref. 4. Note here $\Delta(0)$ has been multiplied by 2 to compare with experiment, since $\varphi_{\mathbf{k}} = 2$ at $\mathbf{k} = (\pi, 0)$. (b) Magnetic length scales associated with T_c and T^* as a function of doping concentration in the cuprates.

For 3D weak coupling (BCS), $\bar{\tau}_0 = N(0)$ and the phase stiffness $\eta^2 = N(0)7\zeta(3)/48\pi^2(v_F/T_c)^2$. Therefore $N(0)$ is canceled in $\xi^2_{BCS} = 7\zeta(3)/48\pi^2(v_F/T_c)^2$. In general, τ_0 and η^2 can be determined from the expansion of $t^{-1}(Q)$:

$$\tau_0 = \frac{1}{g} + \chi(\mathbf{0}, 0), \qquad \eta^2 = \frac{1}{2}\sqrt{\det\left[\partial_{q_i}\partial_{q_j}\chi(Q)\right]}\Big|_{Q=0}. \tag{4}$$

In weak field, $T \gg eH/mc$, we use semiclassical phase approximation to treat the single-particle and pair propagators. Both the single-particle and pair momenta can be modified by the interaction with the field. But formally, the Dyson's equation remains the same, and the superconducting transition is still determined by the pairing instability (Thouless) condition: $g^{-1} + \hat{\chi}(0) = 0 \approx \tau_0 + \eta^2 \cdot \left(\frac{2e}{c}H\right)$, where $\hat{\chi}(Q)$ is the pair susceptibility in the field. To linear order in H, we can evaluate τ_0 and η^2 at $H = 0$.

At T^*, the pseudogap is zero, only the bare Green's function is involved, $\chi_0(Q) = \sum_K G_0(K)G_0(Q-K)\,\varphi^2_{\mathbf{k}-\mathbf{q}/2}$. We have

$$-\frac{1}{T^*}\frac{dT^*}{dH}\Big|_{H=0} = \frac{\eta^{*2}}{\bar{\tau}_0^*}\frac{2\pi}{\Phi_0}, \quad \xi^{*2} = \frac{\eta^{*2}}{\bar{\tau}_0^*}, \tag{5}$$

where $\bar{\tau}_0^* = \sum_{\mathbf{k}} \varphi_{\mathbf{k}}^2 \left[-f'(\epsilon_{\mathbf{k}}) + \frac{d\mu}{dT} \frac{T}{\epsilon_{\mathbf{k}}} \left(\frac{1-2f(\epsilon_{\mathbf{k}})}{2\epsilon_{\mathbf{k}}} + f'(\epsilon_{\mathbf{k}}) \right) \right]_{T=T^*}$

At weak coupling (for s-wave $\varphi_{k_F} = 1$), we recover the BCS limit: $\mu \approx E_F$, $\bar{\tau}_0^* = -\sum_{\mathbf{k}} f'(\epsilon_{\mathbf{k}}) \varphi_{\mathbf{k}}^2 \approx N(0) \varphi_{k_F}^2 \approx N(0)$. And η^{*2} is determined by expanding $\chi_0(\mathbf{q}, 0) = \sum_{\mathbf{k}} \frac{1 - f(\epsilon_{\mathbf{k}}) - f(\epsilon_{\mathbf{k}-\mathbf{q}})}{\epsilon_{\mathbf{k}} + \epsilon_{\mathbf{k}-\mathbf{q}}} \varphi_{\mathbf{k}-\mathbf{q}/2}^2$ to the q^2 order.

At large g (for the underdoped cuprates), $\Delta_{pg}(T_c)$ is large. Noticing that T^* is very weakly H dependent in the strong pseudogap regime [see Fig. 1(b)], and that $T^* \propto \Delta_{pg}$ in zero field, we assume Δ_{pg} is only weakly H dependent. In other words, only the superconducting order parameter is strongly coupled to the field. Then we obtain $\bar{\tau}_0 \approx -\sum_{\mathbf{k}} \varphi_{\mathbf{k}}^2 f'(E_{\mathbf{k}})$, which decreases rapidly as Δ_{pg} increases. η^2 is obtained by expanding to the q^2 order

$$\chi(\mathbf{q}, 0) = \sum_{\mathbf{k}} \left[\frac{1 - f(E_{\mathbf{k}}) - f(\epsilon_{\mathbf{k}-\mathbf{q}})}{E_{\mathbf{k}} + \epsilon_{\mathbf{k}-\mathbf{q}}} u_{\mathbf{k}}^2 - \frac{f(E_{\mathbf{k}}) - f(\epsilon_{\mathbf{k}-\mathbf{q}})}{E_{\mathbf{k}} - \epsilon_{\mathbf{k}-\mathbf{q}}} v_{\mathbf{k}}^2 \right] \varphi_{\mathbf{k}-\mathbf{q}/2}^2. \quad (6)$$

At weak coupling, ξ and ξ_{BCS} coincide. But they split apart as g increases and the pseudogap opens (see Ref. 10 for details). In Fig. 1(b), we plot the doping dependence of the calculated ξ and ξ^*. At large x (overdoping, weak coupling), the two are nearly equal. But for underdoping, while ξ^* continues to decrease with decreasing x, ξ remains nearly flat for a broad range of x until its final rapid increase toward the insulator limit. Since $dT/dH \propto \xi^2$, T^* is rather insensitive and T_c is relatively more sensitive to H. These results are in agreement with experimental observations.[2,11]

This work was supported by NSF-MRSEC, grant No. DMR-9808595, and by the State of Florida (Q.C.).

References

1. S. Chakravarty *et al.*, Phys. Rev. B **63**, 094503 (2001).
2. V. M. Krasnov *et al.*, Phys. Rev. Lett. **84**, 5860 (2000); **86**, 2657 (2001); Ch. Renner *et al.*, Phys. Rev. Lett. **80**, 3606 (1998); K. Gorny *et al.*, Phys. Rev. Lett. **82**, 177 (1999); G. Zheng *et al.*, Phys. Rev. Lett. **85**, 405 (2000).
3. I. Kosztin, Q. J. Chen, B. Jankó, and K. Levin, Phys. Rev. B **58**, R5936 (1998).
4. Q. J. Chen, I. Kosztin, B. Jankó, and K. Levin, Phys. Rev. Lett. **81**, 4708 (1998).
5. Q. J. Chen, I. Kosztin, and K. Levin, Phys. Rev. Lett. **85**, 2801 (2000).
6. L. P. Kadanoff and P. C. Martin, Phys. Rev. **124**, 670 (1961).
7. N. Miyakawa, Phys. Rev. Lett. **80**, 157 (1998); **83**, 1018 (1999).
8. J. Rossat-Mignod *et al.*, Physica B **169**, 58 (1991).
9. M. Oda *et al.*, Physica C **281**, 135(1997).
10. Y.-J. Kao, A. P. Iyengar, Q.J. Chen and K. Levin, *Phys. Rev. B* **64**, 140505 (2001).
11. H. H. Wen *et al* , Phys. Rev. Lett. **85**, 2805 (2000); T. Shibauchi *et al.*, Phys. Rev. Lett. **86**, 5763 (2001).

SPECIFIC HEAT OF $Mg^{11}B_2$ IN MAGNETIC FIELDS: TWO ENERGY GAPS IN THE SUPERCONDUCTING STATE

R. A. FISHER, F. BOUQUET and N. E. PHILLIPS
LBNL and Chemistry Department, University of California, Berkeley, CA 94720, USA

D. G. HINKS and J. D. JORGENSEN
ANL, Argonne, IL 60439, USA

We present specific-heat measurements on $Mg^{11}B_2$ in magnetic fields to 9 T. The anomaly at T_c is rapidly broadened and attenuated in fields, as expected for an anisotropic, randomly oriented superconductor. At low temperature there is a strongly field-dependent feature that shows the existence of a second energy gap. The Sommerfeld constant, γ, increases rapidly and non-linearly with magnetic field, which cannot be accounted for by anisotropy. It approaches γ_n = 2.6 mJ K^{-2} mol^{-1}, the coefficient of the normal-state electron contribution, asymptotically for fields greater than 5 T. In zero magnetic field the data can be fitted with a phenomenological two-gap model, a generalization of a semi-empirical model for single-gap superconductors. Both of the gaps close at the same T_c; one is larger and one smaller than the BCS weak coupling limit, in the ratio ~ 4:1, and each accounts for ~ 50% of the normal-state electron density of states. The parameters characterizing the fit agree well with those from theory and are in approximate agreement with some spectroscopic measurements.

Soon after the discovery of superconductivity in MgB_2 with T_c ~ 40 K (see Ref. [1]), it was shown that the specific heat, C, provides compelling evidence for the existence of two distinctly different energy gaps. In this paper we will describe briefly how specific-heat measurements in magnetic fields, H, can be used to identify and quantify these energy gaps.[2-4]

The electronic specific heat, $C_e(H)$, for various H is plotted in Fig. 1 as $C_e(H)/T$ *vs.* T for a polycrystalline sample of $Mg^{11}B_2$, where $C_e(H)$ was evaluated from the difference $C(H) - C(9\ T)$ (see Refs. [2-4]). The anomaly at T_c is rapidly broadened and attenuated in H, as expected for an anisotropic, randomly oriented superconductor in the mixed state. In addition, two things are striking about the plot: 1). For $H = 0$ C_e increases much more rapidly with T than for a BCS superconductor. 2). At low T and $H \neq 0$, there is a very rapid, non-linear (nearly exponential) increase in C_e/T, with increasing H, which cannot be accounted for by anisotropy (see below). Two other reports of specific-heat measurements[5,6] give similar results, confirming that this behavior is intrinsic. The behavior is conspicuously different from that of any other known superconductor. It gives the appearance of a transition to the superconducting state in two stages that are associated with two energy gaps, one much smaller than the other.

Figure 2(a) is a plot of $\gamma(H)$ *vs.* H, where γ is the Sommerfeld constant, showing the non-linear increase. The normal state γ_n was obtained by extrapolating the data to the upper critical field $H_{c2}(0)$ = 16 T (see Fig. [7]). Anisotropy in H_{c2} cannot explain the dramatic increase in $\gamma(H)$ at low H. The dashed curve is a calculation

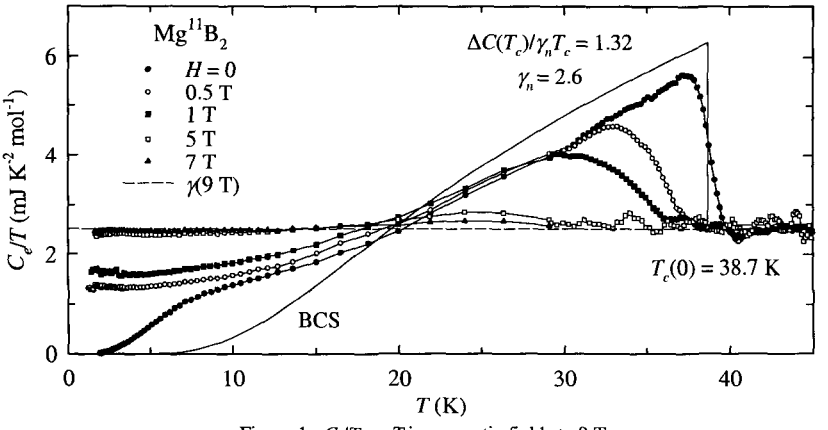

Figure 1: C_e/T *vs.* T in magnetic fields to 9 T.

using the effective-mass model with an anisotropy of 10, which is larger than reported values,[8,9] but $\gamma(H)$ cannot be fitted with *any* value of anisotropy. The rapid increase in $\gamma(H)$ at low H can be explained by the presence of a second energy gap with a small magnitude and associated small condensation energy.

In Fig 2(b) the presence of a second, smaller energy gap is shown clearly in the exponential T dependence of C_{es} for $H = 0$, where C_{es} is the electronic specific heat in the superconducting state. C_{es} is well represented by a simple exponential over a much wider range of T, $4 < T_c/T < 17$, than for a BCS superconductor. This corresponds to the fact that the smaller gap, which determines C_{es}, is much smaller than the BCS gap. A comparison of the fitted parameters, shown in Fig. 2(b), with BCS expressions valid in this temperature interval gives as a rough approximation to the $T = 0$ gap parameter $\Delta_2(0) = 0.44 k_B T_c$, about one quarter of the BCS value. For a two-band, two-gap superconductor, interband coupling ensures that both gaps open at the same T_c (see Ref. [10]). If the electron-phonon coupling is weaker in one band than the other the two gaps are likely to have similar T dependences,[11] but C_{es} will be determined by the smaller gap at low T (see Ref. [10]). Qualitatively, the T dependence of C_{es} is consistent with the expectations for such a two-gap superconductor.

A phenomenological model for a two-gap superconductor,[4] which is a generalization of a semi-empirical model for single-gap superconductors[12] – generally referred to as the "α-model"– provides the basis for a quantitative interpretation of C_{es} for $H = 0$. In a two-band, two-gap model the total C_{es} is taken as the sum of the specific heats calculated independently for each band. C_{es} is fitted with four parameters: The two gaps Δ_1 and Δ_2 plus their normalizing factors γ_1/γ_n

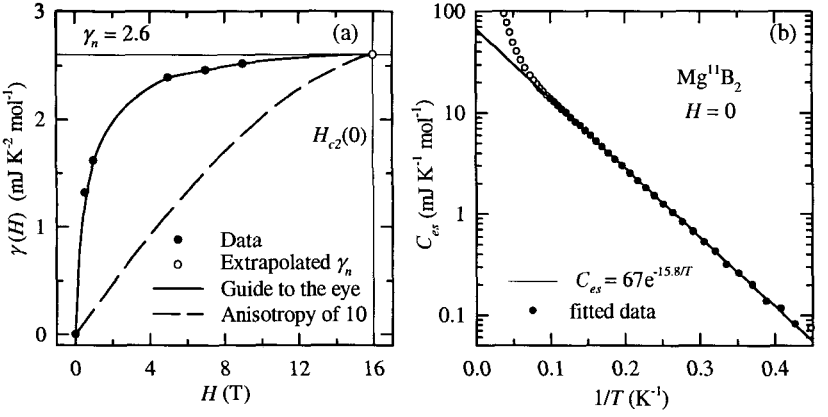

Figure 2: (a) $\gamma(H)$ *vs.* H. (b) The low-temperature exponential dependence of C_{es} *vs.* $1/T$ for $H = 0$.

and γ_2/γ_n, which are subject to the constraint that $\gamma_1 + \gamma_2 = \gamma_n$. Figure 3 shows the result of such a fit, with the four fitted parameters given in the figure. The two gaps are in the ratio ~ 4:1, and each accounts for ~ 50% of the normal-state electron density of states (see Fig. 3 for the exact fitted values of the parameters). These results are consistent with constraints imposed by the general theory of two-gap superconductors: In the low-T limit C_{es} is determined by the smaller gap;[10] $\Delta C(T_c)/\gamma_n T_c$ must be less than the BCS value (the experimental value is 1.32 and the BCS value is 1.43); one gap must be larger than the BCS gap and one smaller.[11] The derived values of the parameters are in remarkably good agreement with band-structure calculations.[13] The agreement of the parameters derived from the two-gap model with the theoretical band-structure calculations argues persuasively for both the existence of two-gaps in MgB_2 and its relation to the high value of T_c.

The phenomenological two-gap model fit of the data of Ref. [5] gives results in Ref. [4] that are similar to ours, while the data of Ref. [6] has a low-temperature exponential behavior that is very similar to that shown in Fig. 2(b).

The majority of spectroscopic determinations of the gap parameters for MgB_2 identify only one gap (some large, some small), but a significant number do show two gaps, which in some cases[14-18] are in approximate agreement with those derived from the two-gap model C_{es} fit[3,4] and band-structure calculations.[13]

Acknowledgments

The work at LBNL was supported by the Director, Office of Basic Energy Sciences, Materials Sciences Division of the U. S. DOE under Contract No. DE-AC02-

76SF00098. The work at ANL was supported by the U. S. DOE, BS-MS under Contract No. W-31-109-ENG-38.

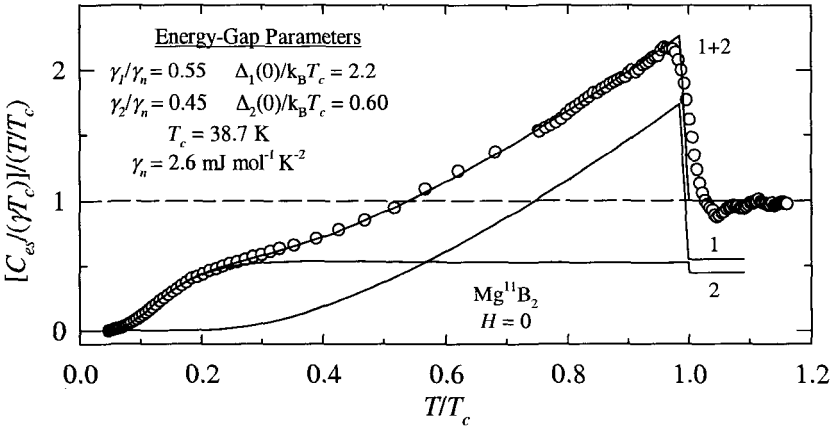

Figure 3: Results of a fit to C_{es}, for $H = 0$, with a phenomenological two-gap model.

References

1. J. Nagamatsu *et al.*, *Nature* **410**, 63 (2001).
2. F. Bouquet *et al.*, *Phys. Rev. Lett.* **87**, 47001 (2001).
3. R. A. Fisher *et al.*, *Studies of High Temperature Superconductors* **38**, ed. by A. V. Narlikar (Nova Science, Commack, NY, 2001) in press, cond-mat/0107072 (2001).
4. F. Bouquet *et al.*, *Europhys. Lett.*, in press, cond-mat/0107196 (2001).
5. Y. Wang *et al.*, *Physica C* **355**, 179 (2001).
6. H. D. Yang *et al.*, *Phys. Rev. Lett.*, in press, cond-mat/0104574 (2001).
7. S. L. Bud'ko *et al.*, *Phys. Rev. B* **63**, 220503R (2001).
8. J. M. An *et al.*, *Phys. Rev. Lett.* **86**, 4366 (2001).
9. O. F. deLima *et al.*, *Phys. Rev. Lett.* **86** (2001) 59741.
10. B. T. Geilikman *et al.*, *Sov. Phys. Solid State* **9**, 642 (1967).
11. V. Z. Kresin and S. A. Wolf, *Physica C* **169**, 476 (1990).
12. H. Padamasee *et al.*, *J. Low Temp. Phys.* **12**, 387 (1973).
13. A. Y. Liu *et al.*, *Phys. Rev. Lett.* **87**, 87005 (2001).
14. F. Giubileo *et al.*, cond-mat/0105592 (2001).
15. P. Szab *et al.*, cond-mat/0105598 (2001).
16. F. Laube *et al.*, cond-mat/0106407 (2001).
17. S. Tsuda *et al.*, *Phys. Rev. Lett.* **87**, 177006 (2001).
18. X. K. Chen *et al.*, *Phys. Rev. Lett.* **87**, 157002 (2001).

MIXING OF SINGLET AND TRIPLET PAIRING FOR SURFACE SUPERCONDUCTIVITY

L. P. GOR'KOV[1] and E. I. RASHBA[2]
[1]*NHMFL, Florida State University, Tallahassee, Florida 32310, USA*
[2]*Department of Physics, The State University of New York at Buffalo, Buffalo, New York 14260, USA*

We consider structure of the Cooper wave function for superconductivity in a surface layer. Broken space inversion at the surface results in lifted spin degeneracy and in two branches of the gapped energy spectrum as caused by the spin-orbit interaction. The pair wave function consists of a mixture of both singlet and triplet components. Anisotropy of the Knight shift measurable in the NMR experiments is calculated in the whole temperature regime. Implications for a few known experimental situations is briefly discussed.

Mg AS A MAIN SOURCE FOR THE DIVERSE MAGNETOTRANSPORT PROPERTIES OF MgB_2

K. H. KIM, J. B. BETTS, M. JAIME, A. H. LACERDA, and G. S. BOEBINGER

NHMFL, Los Alamos National Laboratory, MS E536, Los Alamos, NM 87545 USA
E-mail: khkim@lanl.gov

C. U. JUNG, H.-J. KIM, M.-S. KIM, J. Y. KIM, Z. DU, and S.-I. LEE

National Creative Research Initiative Center for Superconductivity and Department of Physics, Pohang University of Science and Technology, Pohang 790-784, Republic of Korea

Magnetotransport properties of pure Mg metal and MgB_2 samples with varying amounts of excess Mg were systematically studied in magnetic fields up to 18 T. It is found that the both the Mg and inhomogeneous MgB_2 samples show large low temperature conductivity, residual resistance ratio (RRR) and magnetoresistance (MR) under high fields. Calculations of the generalized effective medium theory show that the large RRR and MR of the inhomogeneous MgB_2 samples can be explained by unusual magnetotransport properties of pure Mg metal.

1 Introduction

The recent discovery of superconductivity in MgB_2 with $T_c \approx 39$ K (see Ref. [1]) has attracted great scientific interest among condensed matter researchers. However, there is no consensus for even some basic physical properties such as magnetotransport behaviors and superconducting gap values. Especially, transport properties of various forms of MgB_2 show very different values of resistivity, residual resistance ratio (RRR), and magnetoresistance (MR) at high fields.[3] Those diverse magnetotransport properties were attributed to microstrain, insulating impurities, and defect scattering due to off-stoichiometry. However, there is no convincing explanation for the diverse transport data. Therefore, it is quite important to clarify this intriguing issue to understand intrinsic physical properties of MgB_2.

2 Experiments

We used high pressure-synthesis technique to make high density-polycrystalline MgB_2 samples with different concentrations of Mg inside. Details for sample preparation can be found elsewhere.[4] The resulting samples were characterized with magnetization, x-ray diffraction, and scanning electron microscope (SEM). The SEM image of A-MgB_2 shows large single grains of pure MgB_2 without any impurity. The images of B-MgB_2 and C-MgB_2 showed that they are inhomogeneous

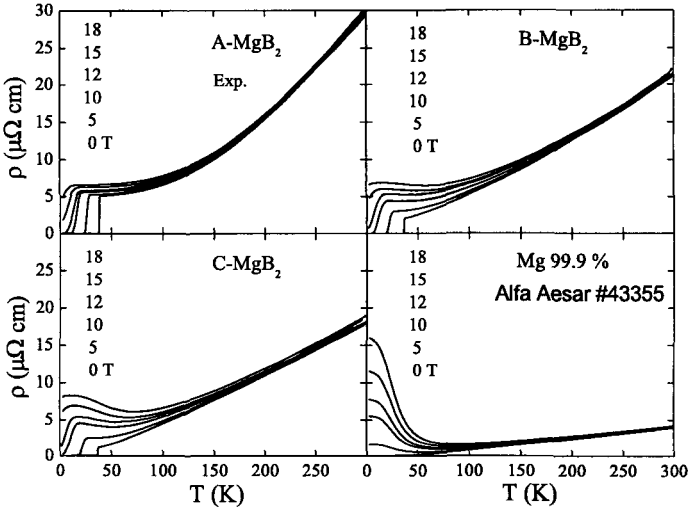

Figure 1: Temperature- and magnetic field- dependent resistivity curves for A-, B- , C-MgB_2, and Mg.

phase mixtures, mainly composed of pure MgB_2 and Mg with grain sizes as large as ~100 μm, as confirmed by energy disperse spectroscopy analysis.[5] It is noted that the volume fraction of Mg grains for C-MgB_2 was larger than for B-MgB_2.

Resistivity, ρ, of the inhomogeneous MgB_2 samples and pure Mg metal (Alfa Aesar #433355, 99.9 %) were measured with the standard four probe method in a transverse geometry between 3 and 300 K and under high fields up to 18 T.

3 Results and simulations based on generalized effective medium theory

Figure 1 displays $\rho(T,H)$ of A-, B-, C-MgB_2, and Mg at 0, 5, 10, 12, 15, and 18 T. The A-MgB_2 sample shows the highest T_c =38.8 K and the smallest $\Delta T_c \approx 0.3$ K. $\rho(T)$ of A-MgB_2 at 40 and 300 K were 5.14 and 30.0 μΩ cm, respectively, so that RRR≡ρ(300 K)/ρ(40 K) was 5.8. MR of A-MgB_2 was relatively small. These values of RRR and MR are consistent with single-crystalline MgB_2 samples which typically exhibit 4.5≤ RRR≤6 (see Ref. [5]). This suggests that A-MgB_2 is the best quality among the three samples studied.

On the other hand, $\rho(T)$ of B-MgB_2 and C-MgB_2 decreased significantly so that ρ(40 K)=2.12 (1.29) μΩ cm & ρ(300 K)=21.0 (17.9) μΩ cm for B-MgB_2 (C-MgB_2). [$T_c \approx 38.2$ K (B-MgB_2) & 38.0 K (C-MgB_2), and $\Delta T_c \approx 0.6$ (B-MgB_2) & 1.5 K (C-MgB_2).] Therefore, RRR values were 9.90 and 13.9 for B- and C-MgB_2, respectively, and MR of the two samples increased significantly below ~100 K. At

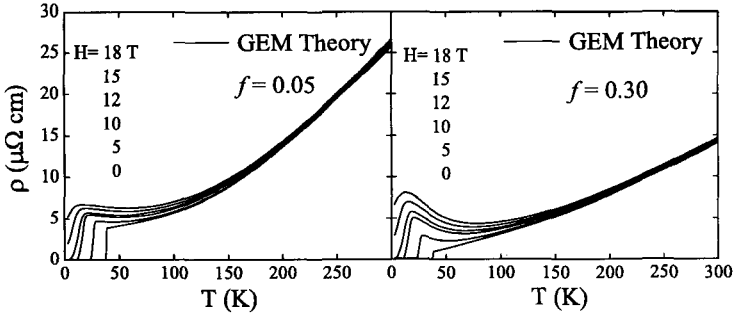

Figure 2: Predictions of resistivity from generalized effective medium (GEM) equation for the volume fraction of Mg, f=0.05 and 0.30, when the two phases are assumed to be sample A-MgB_2 and pure Mg metal, respectively.

T=40 K and H=18 T, MR values were 30 % (A-MgB2), 226 % (B-MgB_2), and 452 % (C-MgB_2). Note that the $\rho(T,H)$'s of B-MgB_2 and C-MgB_2 at high magnetic fields are characterized by an resistive upturn below 70 K, which is a common feature observed in MgB_2 with relatively large RRR values.[2,3]

We also measured $\rho(T,H)$ of pure Mg metal. The ρ at 40 and 300 K were 0.118 and 4.0 μΩ cm, respectively, so that RRR=34. Surprisingly, $\rho(T,H)$ of Mg also shows a drastic increase at finite fields below ~ 70 K. Furthermore, the upturn behavior of $\rho(T,H)$ is quite similar to those of B-MB_2 and C-MgB_2. The $\rho(T,H)$ of Mg at high fields above 10 T can be well fit with the formula explaining a simple metal in magnetic fields, $\rho(T,H)= \rho(T,0)(1+(\omega_c\tau)^2)$ with $\omega_c = eH/m^*c$ and $\rho(T,0)=a+bT^3$. Due to magnetic breakdown phenomena in Mg (see Ref. [6]), at H≤ 10 T, $\rho(T, H)$ does not follow such a simple form.

The large MR and RRR of Mg strongly suggest that the enhanced MR as well as RRR values of B-MgB_2 and C-MgB_2 could be related to the properties of pure Mg metal. Given the data from the SEM images, we model the B-MgB_2 and C-MgB_2 samples as inhomogeneous phase mixtures, composed of mainly MgB_2 and Mg phases. To quantitatively describe $\rho(T,H)$ of the inhomogeneous MgB_2 samples, we calculate the effective resistivity, ρ_E, of a binary phase mixture, based on the generalized effective medium theory,[7]

$$(1-f)\left(\frac{\rho_1^{-1/t}-\rho_E^{-1/t}}{\rho_1^{-1/t}+A\rho_E^{-1/t}}\right)+f\left(\frac{\rho_2^{-1/t}-\rho_E^{-1/t}}{\rho_2^{-1/t}+A\rho_E^{-1/t}}\right)=0\,, \qquad (1)$$

where $A \equiv (1-f_c)/f_c$. Here, the critical percolation volume fraction f_c and critical exponent t are close to 0.17 and 2 in three dimensions. Assuming that $\rho_1 = \rho(T,H)$ of A-MgB_2 & $\rho_2 = \rho(T,H)$ of Mg, simulation was performed for the volume fraction of Mg, f=0.05 & 0.30, as shown in Fig. 2, in which the characteristic ρ behaviors of B-MgB_2 and C-MgB_2 are qualitatively well captured. More detailed analysis finds quantitative agreement as well [8]. Note that the GEM analysis predicts that the

presence of even a small amount of Mg metal ($f \approx 0.05$) will dramatically change the MR and RRR measured on an inhomogeneous MgB_2 sample.

4 Discussion

The above experimental findings indicate that the existence of a pure Mg phase in MgB_2 samples can significantly affect magnetotransport properties. The low resistivity values, quasi-linear temperature dependent resistivity, and increase of RRR and MR in inhomogeneous MgB_2 samples are identified as characteristics arising from the presence of excess Mg. According to our experimental findings and previous single crystal studies,[4] the appropriate RRR of a stoichiometric sample should be about 5-7. The presence of nonstoichiometric Mg could account for the wide range of RRR and residual resistivity currently being reported for MgB_2. Care must be taken to rule out extrinsic effects due to excess Mg from intrinsic properties of MgB_2 in all future investigations.

Acknowledgments

The authors thank Dr. C. M. Varma and Prof. Y. Bang for helpful discussions. The work at National High Magnetic Field Laboratory (NHMFL) is performed under the auspices of the National Science Foundation, the State of Florida, and the U. S. Department of Energy. The work is also supported by the Ministry of Science and Technology of Korea through the Creative Research Initiative Program.

References

1. Jun Nagamatsu *et al.*, *Nature* **410**, 63 (2001).
2. S. L. Bud'ko *et al.*, *Phys. Rev. Lett.* **86**, 1877 (2001).
3. See, C. Buzea and T. Yamashita, *cond-mat*/0108265 and references therein.
4. M. Xu *et al.*, *cond-mat*/0105271; Kijoon H. P. Kim *et al.*, *cond-mat*/0105330; S. Lee *et al.*, *cond-mat*/0105545.
5. C. U. Jung *et al.*, to be published.
6. D. S. McLachlan, *J. Phys. C* **20**, 865 (1987); K. H. Kim *et al.*, *Phys. Rev. Lett.* **84**, 2961 (2000).
7. R. W. Stark, T. G. Eck and W. L. Gordon, *Phys. Rev.* **133**, A443 (1964); F. Richards, *Phys. Rev. B* **8**, 2552 (1973).
8. K. H. Kim *et al.*, to be published.

ANOMALOUS RE-ENTRANT SUPERCONDUCTIVITY IN $Sr_{0.4}K_{0.6}BiO_3$: RECOVERY OF SUPERCONDUCTIVITY WITH ELECTRIC AND MAGNETIC FIELD

D. C. KIM, J. S. KIM, A. N. BARANOV and Y. W. PARK

School of Physics and Condensed Matter Research Institute, Seoul National University, Seoul, 151-747, Korea

J. S. PSHIRKOV and E. V. ANTIPOV

Department of Chemistry, Moscow State University, Moscow 119899, Russia

Anomalous re-entrant superconducting-normal resistive transition was observed in $Sr_{0.4}K_{0.6}BiO_3$ superconductor *i.e.*, normal – supernormal behavior as temperature is increased. Contrary to previously reported re-entrant resistive behaviors in other compounds, the re-entrant resistivity appearing at zero magnetic field in $Sr_{0.4}K_{0.6}BiO_3$ is suppressed to zero by applying an external magnetic field (H) or increasing the electrical transport current (I): an observation of a zero resistive superconducting state induced by H or I. Comparisons of the normal-state resistivity data in different samples indicate an important role that disorder in the junction barriers between superconducting grains might play on the observed re-entrant resistivity behavior. Possible physical origins of this anomalous phenomenon are discussed.

1 Introduction

Among the various superconducting properties found in different superconducting systems, one of the unusual properties is an observation of the re-entrant superconducting – normal resistive transition (RRT) below T_c. There has been several experimental reports about the RRT especially in granular superconducting systems.[1,2] The general behavior of the previously reported RRT showed that the re-entrant resistivity which appears at T* below T_c increases with T* by an application of the external magnetic field (H) or an increase of the electrical transport current (I), and further increases of H or I result in the breakdown of the superconducting state, turning the system into the normal state. This RRT behavior in granular superconductors could be explained in terms of the destruction of the Josephson weak links caused by the increase of the tunneling resistance in the grain barriers at low temperatures as H or I increase.

In contrast to the previously observed RRT's, another type of the RRT has recently been reported in the $Sr_{0.4}K_{0.6}BiO_3$ (SKBO) compound.[3-5] At zero magnetic field the re-entrant resistivity (ρ_{re}) suddenly appears at a temperature below T_c, and more surprisingly it becomes zero by applying H or increasing I: an observation of the recovery of a zero resistive superconducting state induced by H or I. In this

paper, we present the magnetotransport data of various SKBO samples with discussion on possible physical origins of this anomalous RRT phenomenon.

2 Experiment

The detailed synthesis procedure of SKBO samples was discussed elsewhere.[5] The important thing to note is that the sample characterization by XRD, EDS, and SEM did not show any differences between the samples although, as shown in Fig. 1, the measured magnetotransport data and the RRT behavior varied from sample to sample. We also stress that SKBO contains only non-mangetic elements, which enables to neglect any magnetic origins for the observed anomalous RRT. For the magnetoresistance measurement, the standard 4 - probe method was used with a 7 Tesla superconducting magnet system.

3 Results and Discussion

Figure 1 clearly shows the magnetic field dependence of the observed anomalous RRT in SKBO samples. For sample 2 and sample3, ρ_{re} appeared at a temperature (T_{re} ~ 5K and T_{re} ~ 8K, respectively) below T_c is suppressed to zero as H is applied. The RRT is not found in sample 1 below T_c and sample 4 shows a quasi-RRT (RRT without zero resistivity state) with the same decreasing behavior of ρ_{re} by increasing H. Another peculiar feature is found in I-V characteristics of the samples exhibiting the RRT or quasi-RRT (Fig. 2). Below T_{re} an ohmic behavior is first found in the low current region (I ~ 100μA). As I increases further, the re-entrant voltage sharply decreases and eventually becomes zero, similar to the H dependence of ρ_{re}. If the sample temperature is increased (see the inset of Fig. 2), the overall magnitude of re-entrant voltage decreases to zero in the region $T_{re} < T < T_c$, followed by the usual ohmic behavior above T_c.

From Fig. 1 and Fig. 2, one can clearly see the anomalous RRT behavior with respect to H or I in SKBO. The magnetic field and the electric field have a similar effect –suppression of ρ_{re}– on the RRT and quasi-RRT, pointing out that the observed anomalous RRT be considered in the context of I and H simultaneously.

Through the series of measurements on various SKBO samples, we observed a systematic change from superconducting to insulating behavior via the RRT and the quasi-RRT as the normal-state transport properties of the sample changes from metallic to insulating (see Table. 1). This implies a percolating behavior of superconductivity in our system and the anomalous behaviors below T_c are related to the normal state transport property of the sample. So we analyzed the normal-state transport data of the samples in connection with the RRT or quasi-RRT behaviors by using a tunneling percolating model.[6] The analysis with an assumption of a

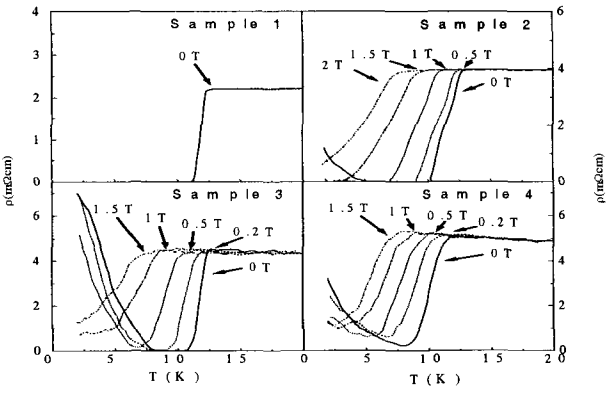

Figure 1: Temperature dependence of resistivity of SKBO samples in various H fields (I = 100μA).

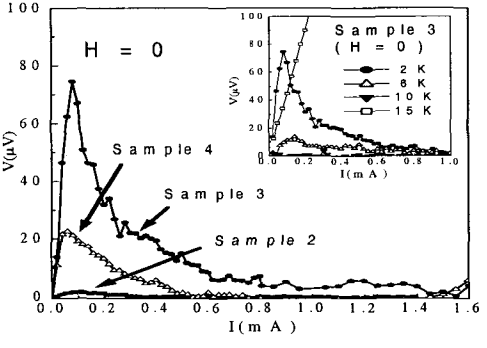

Figure 2: *I-V* curves of SKBO samples showing the RRT or quasi-RRT at T = 2 K with H = 0. Inset: *I-V* curves of sample 3 at various temperatures with H = 0.

transition rate $w(T) \sim exp[-U/(T+T_o)]$ for the tunneling junctions, where U/T_o is proportional to the barrier size at zero temperature,[7] indicated that the disorderness in junction barriers between superconducting grains conjectured from the normal transport data is important in relation to the observed RRT phenomenon (see Table.1).[5]

In regard to I dependences of the RRT, we note that the current-controlled negative differential resistivity (NDR), which is observed below T_{re} in SKBO samples, has been generally investigated in a percolating network system.[8]

Table 1: Transport properties of SKBO samples showing the RRT or quasi-RRT

	Sample 2	Sample 3	Sample 4
T_{c_onset}/T_{c_zero}	12.5/10.1	12.6/10.5	12.0/quasi-RRT
T_{re}(K)	~ 5	~ 8	~ 8
ρ_{re} (2 K) (mΩ cm)	0.95	7.00	3.23
ρ(20 K) (mΩ cm)	3.97	4.29	4.88
ρ(20 K)/ ρ(273 K)	0.81	0.97	1.29
U/T_o	12.02	31.03	19.77

Obviously the observed anomalous RRT behavior cannot be simply understood by the general Josephson coupling mechanism between superconducting grains and this requires a consideration of another special tunneling mechanism with a special character of the tunneling barriers. For the anomalous tunneling junction that becomes superconducting by *H* or *I*, disorder in the insulating barrier seems to be important specifically. If disorder in tunneling barriers is considered, one might speculate possible localized states induced by disorder in the Josephson tunneling barrier. The localized spin state in the tunneling barrier could be regarded as one form of the π junction, the Josephson junction with a spin-flip tunneling between superconducting grains,[9] which would behave differently under the magnetic field in comparison with the normal Josephson weak links.[10] Although the above scenario about the transport through the π junctions is one of possible candidates in explaining the origin of the anomalous RRT, the change of the RRT behavior below T_c synchronized with the change of the normal state transport property indicates the special role of disordered junction barrier between superconducting grains, which should be investigated theoretically .

This work was supported by the Korea Research Foundation (2000-042-D00032) in the Ministry of Education (MOE), Korea.

References

1. T. H. Lin *et al., Phys. Rev. B* **29**, 1493 (1984).
2. U. Welp *et al., Physica C* **156**, 27 (1988).
3. D. C. Kim *et al., Physica C* **341-348**, 797 (2000).
4. D. C. Kim *et al., J. Supercond.* **14**,341 (2001).
5. D. C. Kim *et al., Phys. Rev. B* **64**, 064502 (2001).
6. P. A. Pury and M. O. Caceres, *Phys. Rev. B* **55** 3841 (1997).
7. P. Sheng, *Phys. Rev. B* **21**, 2180 (1980).
8. J. Peinke *et al., Phys. B* **66**, 65 (1987).
9. B. I. Spivak and S. A. Kivelson, *Phys. Rev. B* **43**, 3740 (1991).
10. F. V. Kusmartsev, *Phys. Rev. Lett.* **69**, 2268 (1992).

THE INHOMOGENEOUS MAGNETIC FLUCTUATIONS IN THE SUPERCONDUCTING $La_{2-x}Sr_xCuO_4$

P. L. KUHNS, A. P. REYES, and W. G. MOULTON
NHMFL, 1800 E P.Dirac Dr., Tallahassee, FL 32310

E. F. KUKOVITSKII, E. L.VAVILOVA, G. B. TEITEL'BAUM
Institute for Technical Physics of the RAS, Sibirskii Trakt 10/7, Kazan 420029 Russia
E-mail: grteit@dionis.kfti.knc.ru

The NMR and ESR analysis revealed the dynamical coexistence of superconductivity and the antiferromagnetic correlations in the entire superconductivity region of $La_{2-x}Sr_xCuO_4$ with the spin stiffness enhancement near $x=0.12$.

The interest to the microscopic phase separation in the HTSC materials has received a new impetus after the observation of stripe correlations. They were observed only in the compounds doped with the rare earth ions to induce the LTT (low temperature tetragonal) phase favorable for the pinning of the stripe fluctuations.[1] Recent experiments[2] on the neutron scattering in LTO (low temperature orthogonal) phase of $La_{2-x}Sr_xCuO_4$ with $x=0.12$ reveal the presence of modulated antiferromagnetic order very similar to that observed in LTT compound $La_{1.6-x}Nd_{0.4}Sr_xCuO_4$. But at the larger time scale the magnetic fluctuations in $La_{2-x}Sr_xCuO_4$ are dynamical especially for the superconducting state and their relevance to the stripe structure is a matter of debate. Attempts to investigate the character of microscopic phase separation with the help of low frequency local methods such as NMR (see Refs. [3,4]) are hindered by its dynamical nature.

The main aim of the present work is to investigate the phase diagram and properties of magnetic fluctuations of superconducting $La_{2-x}Sr_xCuO_4$ shifting the measurements to larger frequencies by using ESR (X-band) and high field NMR.

We studied a series of $La_{2-x}Sr_xCuO_4$ powders with the Sr doping x corresponding to the superconducting region doped by 1 at. % of Gd, which served as ESR probe.[5] Such tiny concentration of Gd ensured only the small suppression of T_c via pair breaking (the T_c values are shown in Fig. 2). We analyzed the temperature and concentration dependence of the linewidth of the most intense component of Gd^{3+} ESR spectrum, consisting from several lines corresponding to the fine structure of the ion with $S=7/2$ in the crystalline electric field.[5] The typical temperature dependence of the linewidth is shown in Fig. 1.

In addition to the important but temperature independent residual inhomogeneous broadening the linewidth is given by different contributions linked to the magnetic properties of CuO_2 planes:

1) the interaction of Gs^{3+} spins with the charge carriers, that is the Korringa relaxation channel. The simplest Korringa term in the linewidth is $\delta H = a + bT$ with $b = 4\pi(JN_F)^2 P_m$ (see Ref. [6]), where $P_m = [s(s+1)-m(m+1)]$ - is the squared matrix element, N_F is the density of states at the Fermi level, J is the s - f coupling constant. For the system under study it was discussed in.[5]

2) the interaction of Gd with copper spins, giving rise to homogeneous broadening of Gd ESR line (a close analogue of nuclear spin-lattice relaxation): $\delta H = (\gamma H)^2 \tau P_m/(1+(\omega\tau)^2)$, where $\tau = \tau_\infty exp(E_A/kT)$ is the magnetic fluctuations life-time, τ_∞ is the lifetime at the infinite temperature, H – the internal magnetic field at Gd site, E_A – the activation energy.

The second contribution describes the standard Bloembergen-Purcell-Pound (BPP) behaviour: the broadening of the ESR line upon cooling down with the downturn at certain freezing temperature T_m corresponding to $\omega\tau = 1$, where ω is the resonant frequency. We observed that depending on the Sr content the linewidth behaviour transforms from the BPP-like (with the maximum) to the pure Korringa (linear) temperature dependence. It means that at low x the Gd spin probes almost magnetic state and at the high x end - almost nonmagnetic metal.

The magnetic transition temperatures T_m are shown in Fig. 2 together with superconducting temperatures T_c. It is important that the dependencies $T_m(x)$ and $T_c(x)$ are almost coincident for all x corresponding to the superconductivity region. This indicates that the magnetic and superconducting properties are strongly coupled. The fitting to the measured temperature dependence of the linewidths of

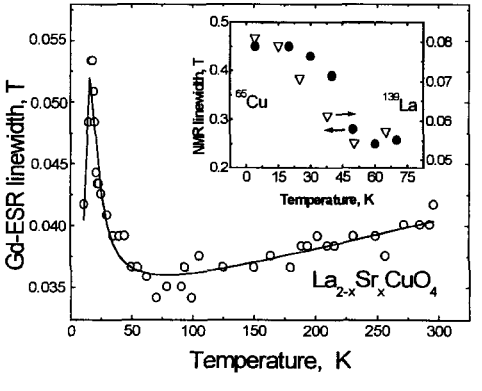

Figure 1: The typical temperature dependence of the Gd ESR linewidth. Inset: the temperature dependence of the Cu and La NMR linewidths.

the Gd ESR spectra makes it possible to obtain the values of the parameters in the expression for the linewidth: the maximal H value is about $0.02T$; $\tau_\infty = 0.3 \cdot 10^{-12}$ sec and the E_a values are plotted in Fig. 2. The activation energy for the two-dimensional spin fluctuations may be written as $E_a = 2\pi\rho_s$ The enhancement of a spin stiffness ρ_s near $x=0.12$ shown in Fig. 2 gives evidence for the developed antiferromagnetic correlations and explains both the anomalously narrow peak in inelastic neutron scattering[7] and the elastic incommensurate peak with a narrow q-width[2] reported for the superconducting $La_{2-x}Sr_xCuO_4$ for this Sr doping. At $x=1/8$ E_a is close to the value found for Nd-doped stripe-compound ($E_a = 143K$) (see Ref. [8]) whereas τ_∞ is by one order smaller. This means that for superconducting compounds the fluctuations are of more dynamical character.

The dependence $E_a(x)$ is in a controversy with the shape of the NMR wipe out boundary $T_{NQR}(x)$ (see Ref. [9]) shown in Fig. 2. Probably this gives evidence that the wipe out for $0.06<x<1/8$ is due to the slowing down of the charge fluctuations rather than the spin ones. Since the charge fluctuations for doping $x<1/8$ were not detected in the diffraction experiments it is not excluded that in this part of the phase diagram they correspond not to the stripes but to the charged droplets discussed earlier in the phase separation picture of Gorkov and Sokol.[10]

To obtain the information about the ordered magnetic moments for the compounds with the enhanced spin stiffness the NMR measurements at $20\text{-}25T$ were carried out in a high homogeneity resistive magnet of the NHMFL in Tallahassee FL. The temperature and doping dependencies of $^{63,65}Cu$ and ^{139}La NMR field sweep spectra of the oriented powders $La_{2-x}Sr_xCuO_4$ were studied. According to the previous La NQR results[11] the measurements in a magnetic field perpendicular to c axis revealed that for Sr content near $1/8$ the central lines of the observed spectra both for Cu and La exhibit the broadening upon cooling below $40\text{-}50K$ (Inset to

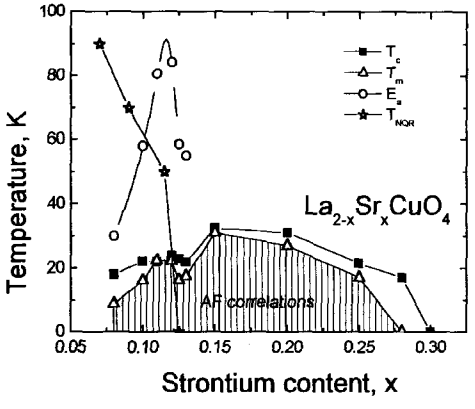

Figure 2: The phase diagram for $La_{2-x}Sr_xCuO_4$ (see text for details). The lines are guide for eyes.

Fig. 1). This is connected with the slowing down of the magnetic fluctuations, which are gradually freezing upon ordering.[11] It allows us to estimate that the additional magnetic field at La nucleus is *0.015T*. If we consider that for the antiferromagnet La_2CuO_4 the copper moment of $0.64\mu_B$ induces at the La site the field of *0.1T* (see Ref. [12)], then the effective magnetic moment in the present case is $\sim 0.09\mu_B$. Note that the manifestation of the magnetic order only in the vicinity of $x=1/8$ when the AF structure is commensurate with the lattice indicates that the magnetic inhomogeneities are of a plane character.

In conclusion our investigation reveals that:

- According to the phase diagram the inherent feature of the superconducting state in cuprates is the presence of frozen antiferromagnetic correlations. In other words the superconductivity seems to be a result of phase separation at the microscopic scale.
- In the vicinity of *1/8* doping this separation may be realized in a form of dynamical stripes - the corresponding enhancement of the spin-stiffness reveals the plane character of the spin (and charge) inhomogeneities.

The authors are grateful to V. E. Kataev for the participation in the initial stage of ESR analysis. This work is supported through the NIS/NHMFL Program and through the RFFR Grant N 01-02-17533.

References

1. J. M. Tranquada *et al., Nature* **375**, 561 (1995).
2. T. Suzuki *et al., Phys. Rev. B* **57**, R3229 (1998.
3. S. Oshugi *et al., J. Phys. Soc. Jpn.* **63**, 2057 (1994).
4. T. Goto *et al., J. Phys. Soc. Jpn.* **66**, 2870 (1997).
5. V. Kataev *et al., JETP Lett.* **56**, 385 (1992); *Phys. Rev. B* **48**, 13042 (1993).
6. S. E. Barnes, *Adv. Phys.* **30**, 801 (1981).
7. K. Yamada *et al., Phys. Rev. B* **57**, 6165 (1998).
8. G. B. Teitel'baum *et al., Phys. Rev. B* **63**, 020507(R) (2001).
9. A. W. Hunt *et al., Phys. Rev. Lett.* **82**, 4300 (1999).
10. L. P. Gorkov and A. V. Sokol, *JETP Lett.* **46**, 420 (1987).
11. M.-H. Julien *et al., Phys. Rev. B* **63**, 144508 (2001).
12. T. Tsuda *et al., J. Phys. Soc. Jpn.* **57**,, 2908 (1988).

FIELD-INDUCED ANTIFERROMAGNETISM IN THE HIGH-TEMPERATURE SUPERCONDUCTOR $La_{2-x}Sr_xCuO_4$

B. LAKE,[1] T. E. MASON,[1] G. AEPPLI,[2] K. LEFMANN,[3] N. B. CHRISTENSEN,[3] D. F. MCMORROW,[3] K. N. CLAUSEN,[3] H. M. RONNOW,[4] P. VORDERWISCH,[5] P. SMEIBIDL,[5] N. MANGKORNTONG,[6] N. E. HUSSEY,[6] T. SASAGAWA,[6] M. NOHARA,[6] H. TAKAGI,[6] and A. SCHRÖDER,[7]

[1]*Oak Ridge National Laboratory, Oak Ridge, Tennessee, USA.*
[2]*N.E.C. Research Institute, Princeton, New Jersey, USA.*
[3]*Riso National Laboratory, Roskilde, Denmark.*
[4]*CEA-Grenoble, and Institute Laue-Langevin, Grenoble, Cedex 9, France.*
[5]*BENSC, Hahn-Meitner Institute, Berlin, Germany.*
[6]*University of Tokyo, Tokyo, Japan.*
[7]*University of Karlsruhe, Karlsruhe, Germany.*

There is strong evidence that magnetic interactions play a crucial role in the mechanism driving high-temperature superconductivity in cuprate superconductors. To investigate this we have done a series of neutron scattering measurements on $La_{2-x}Sr_xCuO_4$ (LSCO) in an applied magnetic field. Below T_c the field penetrates the superconductor via an array of normal state metallic inclusions or vortices. Phase coherent superconductivity characterized by zero resistance sets in at the lower field-dependent irreversibility temperature (T_{irr}). We have measured optimally doped LSCO (x=0.16, T_c=38.5 K) and under-doped LSCO (x=0.10, T_c = 29 K); both have an enhanced antiferromagnetic response in a field. Measurements of the optimally doped system at H=7.5 T show that sub-gap spin fluctuations first disappear with the loss of finite resistivity at T_{irr}, but then reappear at a lower temperature with increased lifetime and correlation length compared to the normal state. In the under-doped system elastic antiferromagnetism develops below T_c in zero field, and is significantly enhanced by application of a magnetic field. Phase coherent superconductivity is then established within the antiferromagnetic phase at T_{irr}; thus, the situation in under-doped LSCO is the reverse of that for the optimally doped LSCO where the zero-resistance state develops first before the onset of antiferromagnetism.

MAGNETIC TESTS TO REVEAL TRIPLET SUPECONDUCTIVITY IN $(TMTSF)_2PF_6$ AND A POSSIBLE BREAKING OF A TIME REVERSAL SYMMETRY IN Sr_2RuO_4, LBCO, and YBCO

A. G. LEBED
L. D. Landau Institute for Theoretical Physics, Kosygina St. 2, 117334, Moscow

We propose methods to reveal the existence of a two-component triplet order parameter (which is recently suggested to break a time reversal symmetry in Sr_2RuO_4) and to test a possible two-component singlet d-wave order parameter in high-T_c superconductors (which may also break the time reversal symmetry). We have also determined a spin part (*i.e.*, $\mathbf{d}(\mathbf{k}) = [d_x(\mathbf{k}) \neq 0, d_y(\mathbf{k}) = 0, d_z(\mathbf{k}) = 0)]$ of a triplet order parameter[1,2] in $(TMTSF)_2PF_6$ under pressure by means of an analysis of the experimental H_{c2} measurements (I. J. Lee *et al., Phys. Rev. Lett.* 78, 3555 (1997)).

1. A. G. Lebed, *Phys. Rev. B* (Rapid Commun.), **59**, R795 (1999).
2. A. G. Lebed *et al., Phys. Rev. B* (Rapid Commun.), **62**, R795 (2000).

METAL-INSULATOR CROSSOVER IN HIGH T_C CUPRATES: GAUGE FIELD THEORY VERSUS EXPERIMENTS

P. A. MARCHETTI,[A] Z.-B. SU,[B] L. YU[C,B]

[A] *Dipartimento di Fisica "G. Galilei", INFN, I--35131 Padova, Italy*
[B] *Institute of Theoretical Physics, CAS, Beijing 100080, China*
[C] *Abdus Salam International Centre for Theoretical Physics, I-34100 Trieste, Italy*
E-Mail: yulu@ictp.trieste.it

The *U(1)×SU(2)* Chern-Simons gauge field theory, proposed by the authors to explain in a unified fashion the metal-insulator crossover of the in-plane resistivity upon temperature decrease in heavily underdoped cuprates without magnetic field and a similar phenomenon, observed in several classes of superconducting cuprates, when a strong magnetic field suppresses the superconductivity, is briefly outlined and confronted with recent experiments.

1 Introduction

There are two sets of experiments showing metal-insulator crossover (MIC) in cuprate superconductors:

1) The in-plane resistivity in heavily under-doped cuprates (LSCO and YBCO) exhibits a minimum and a crossover from metallic to insulating behavior upon the temperature decrease.[1]

2) A similar crossover was observed in several classes of superconducting cuprates,[2-4] when a strong magnetic field (up to 60 Tesla) suppresses the superconductivity. The "obvious" interpretation in terms of two-dimensional (2D) localization or 2D insulator-superconductor transition is ruled out, as the estimated product $k_F l$, where k_F is the Fermi momentum, l the mean free path, is between 12 and 25 for the superconducting case,[2-4] while it is of order 1 in the first case![1] A similar phenomenon was also observed when Zn doping suppressed the superconductivity.[5]

We believe these two sets of phenomena are of the same origin. Based on the *U(1)×SU(2)* Chern-Simons gauge field theory,[6] we have proposed to explain the MIC in the absence of magnetic field[7] and that in the presence of strong magnetic field[8] within a unified scheme. In our opinion, this crossover is due to a strong interplay between the short-range antiferromagnetic order (SRAFO) and the dissipation effect coming from the charge carriers. The theoretical framework has been presented earlier,[6-8] so here we will only briefly outline the basic idea of this scheme and compare the proposed theory with recent experiments.

2 Outline of the Basic Idea

The theoretical treatment of the *t-J* model is based on the following theorem: If we couple the fermions of the *t-J* model to a *U(1)* field B_μ gauging the global charge symmetry and to an *SU(2)* field V_μ, gauging the global spin symmetry, and we assume that the dynamics of the gauge fields is described by the Chern-Simons actions, then the gauged model so obtained is exactly equivalent to the original *t-J* model.[6] To the fermion field of the gauged model χ_α with α as spin index, we apply the spin-charge decomposition: $\chi_\alpha \sim h z_\alpha$ where h denotes a spinless fermion (holon) field and z_α a spin 1/2 hard-core boson (spinon) field satisfying the constraint $z_\alpha^* z_\alpha = 1$ which implements the "no-double" occupancy of the *t-J* model. The above spin-charge decomposition introduces a further *U(1)* gauge symmetry between h and z_α, to which is associated a self-generated gauge field A_μ, analogous to the one appearing in the slave boson and slave fermion approaches. In a "Mean-Field-Approximation" to the gauged $U(1) \times SU(2)$ *t-J* model, in the parameter region corresponding to the "pseudogap phase" of high T_c cuprates, the role of the three gauge fields is the following:

-- $B_{\{MFA\}}$ carries a flux π per plaquette, converting the spinless holon h into a Dirac fermion with a "pseudospin" structure related to the two Néel sublattices and exhibiting a ("small") Fermi surface with $\varepsilon_F \sim t\delta$, where t is the hopping, while δ being the doping concentration.

-- $V_{\{MFA\}}$ dresses the holons by spin vortices of opposite chirality in the two Néel sublattices. The spinons in the presence of this gas of "slowly moving" dressed holons acquire a mass $m_s = \sim (-\delta \ln \delta)^{1/2}$ yielding SRAFO.

--The self-generated "photon" field A_μ couples the Fermi liquid of holons to the gapped spinons, described by a massive nonlinear σ-model. The low-energy effective action for A is dominated by the contribution due to gapless holons and the propagator of the transverse component A^T of the gauge field turns out to be, for $\omega,\ q,\ \omega/q \sim 0$, of the form $\langle A^T A^T \rangle(\omega,q) \sim (-\chi q^2 + i\kappa\omega/q)^{-1}$ where χ is the diamagnetic susceptibility and κ the Landau damping.

The resistivity is given by the sum of the resistivity ρ_s due to the spinon-"photon" subsystem and the resistivity ρ_h due to the holon-"photon" subsystem (Ioffe-Larkin rule). The Fermion part ρ_h was calculated earlier,[9] while the spinon part turns out to be[7]

$$\rho_s \sim \frac{\mathrm{Im}(m_s^2 - iT/\chi)^{1/4}}{\sqrt{\delta}} \sim \frac{[m_s^4 + (T/\chi)^2]^{1/8}}{\delta^{1/2} \sin[\frac{1}{4}\arctan(T/\chi m_s^2)]}$$

In the temperature range between a few tens and hundreds K the spinon part dominates. The basic feature of the resistivity formula can be summarized as follows: For low T the effect of the spinon gap is dominating, leading to an insulating behaviour $\rho \sim 1/T$, while at higher temperatures we find a metallic behavior $\rho \sim T^{1/4}$, due to the dissipation induced by gauge fluctuactions coming, in turn, from holons with a small Fermi surface. Therefore a MIC is recovered decreasing the temperature. This crossover is determined by the interplay between the AF correlation length $\xi \sim (-\delta \ln \delta)^{-1/2}$ and the thermal de Broglie wavelength $\lambda \sim (\chi/T)^{1/2}$. When $\lambda \leq \xi$, the "peculiar" localization effect due to SRAFO is not "felt" and a metallic behavior is observed. In the opposite limit $\lambda >> \xi$, we find the insulating behavior. A magnetic field H perpendicular to the plane modifies the contribution to ρ_s via the cyclotron effect, by reducing the damping T/χ to $T/\chi(H) - H^2/(3q_0^2)$, where $q_0 \sim (\delta^2 T/t)^{1/3}$, $\chi(H)$ is the diamagnetic susceptibility in the presence of H, given by $\chi + \sigma_h(H)^2 / 4\pi^2$ with $\sigma_h(H)$ the holon Hall conductivity. This makes the de Broglie wavelength λ longer, so the MIC temperature is increased. This way the external magnetic field reveals the MIC originally hidden by the superconducting transition.

3 Comparison with experiments

The comparison with earlier experiments can be summarized as follows:[7,8]

1) The temperature dependence of resistivity (with and without magnetic field) is in semi-quantitative agreement with experiments;

2) The MIC temperature shifts down with doping concentration, while up with magnetic field, as shown by experiments;

3) A significant positive magnetoresistance at low temperatures, seen experimentally, but not following from earlier theoretical treatments.

Recently, the doping dependence of the carrier mobility in under-doped cuprates was systematically studied,[10] and the inverse mobility is found to be proportional to the AF correlation length which supports our proposal of "peculiar localization" due to SRAFO. However, a quantitative comparison is not possible now, because 300 K is beyond the validity limit of our approximation.

Following earlier work on Zn doping,[5] the magnetotransport properties of Zn doped BSLCO single crystals have been extensively studied,[11] and the authors interpret their data in terms of Kondo scattering on Zn-induced local magnetic moment, as suggested earlier to explain the NMR experiments.[12] MIC in resistivity was also observed in underdoped YBCO, exposed to irradiation.[13] The authors interpret their data as due to defects which behave like Zn impurities and again invoke the Kondo scattering to explain their results. It seems to us that these results are much more natural to understand in terms of our theoretical model. In fact, the Zn doping disturbs the AF background, so making the AF correlation length shorter, therefore shifting the MIC temperature up, as shown by experiments. We are not

able at the moment to make a quantitative estimate of this shift. However, the qualitative behavior is fully consistent with our anticipation. On the other hand, there is some doubt about the "Kondo" interpretation:

1) According to the well-known theory of the Kondo effect,[14] the logarithmic dependence of resistivity is expected only over a small range around T_k, and it should saturate quickly as $R_0\ (1-\ (T/T_k)^2)$ when $T < T_k$ which is not the case in experiments.[2,4,5,11,13] It is not clear whether the Kondo strong coupling regime (Fermi liquid behavior) is expected in these systems.

2) The recent NMR experiments on Li-doped YBCO[13] seem to show that the "Kondo" scattering (actually the local moment) survives superconducting transition. On the other hand, the Anderson impurity model study in d-wave superconductors shows that the Kondo regime does not appear,[15] in spite of the existence of the local moment.

To sum up, the existence of local moment needed to explain the NMR data may not be the origin of the MIC observed in transport measurements. It may well be that neither of them is due to the Kondo physics in the usual sense.

References

1. H. Takagi *et al., Phys. Rev. Lett.* **69**, 2975 (1992); B. Wuyts *et al. Phys. Rev. B* **53**, 9418 (1996).
2. Y. Ando *et al., Phys. Rev. Lett.* **75**, 4662 (1995); G. S. Boebinger *et al., ibid*, **77**, 5417 (1996).
3. P. Fournier *et al., Phys. Rev. Lett.* **81**, 4720 (1998).
4. S. Ono *et al., Phys. Rev. Lett.* **85**, 638 (2000).
5. Y. Fukuzumi *et al. Phys. Rev. Lett.* **76**, 684 (1996); K. Segawa and Y. Ando, *Phys. Rev. B* **59**, R3948 (1999).
6. P. A. Marchetti, Z-B. Su, L Yu, *Phys. Rev. B* **58**, 5808 (1998).
7. P. A. Marchetti, J. H. Dai, Z-B. Su, L Yu, *J. Phys. Condens. Matter* **12**, L329 (2000).
8. P. A. Marchetti, Z-B. Su, L Yu, *Phys. Rev. Lett.* **86**, 3834 (2001).
9. P. A. Lee and N. Nagaosa, *Phys. Rev. Lett.* **65**, 2450 (1990).
10. Y. Ando *et al., Phys. Rev. Lett.* **87**, 017001(2001).
11. Y. Hanaki *et al., Phys. Rev. B* **64**, 172514 (2001).
12. See, *e.g.,* J. Bobroff *et al., Phys. Rev. Lett.* **86**, 4116 (2001).
13. F. Rullier-Albenque *et al., Phys. Rev. Lett.* **87**, 157001 (2001); H. Alloul, *This Proceedings.*
14. See, *e.g.,* A. C. Hewson, *The Kondo Problem to Heavy Fermions*, Cambridge, 1993.
15. G. M. Zhang, H. Hu, L.Yu, *Phys. Rev. Lett.* **86**, 704 (2001) and to appear.

USING RADIO FREQUENCY PENETRATION DEPTH TO PROBE LAYERED SUPERCONDUCTORS

C. H. MIELKE

Los Alamos National Laboratory, MST-NHMFL, MS-E536, Los Alamos, NM 87545, E-mail: cmielke@lanl.gov

Measuring the electrical resistivity of layered superconductors yields interesting information regarding the mixed and normal state of the system. Because of the high degree of anisotropy of many systems it becomes impossible to distinguish between the relatively small resistivity associated with ρ_{xy} and the much larger ρ_{zz} using traditional 4 lead techniques. Moreover, dissipation associated with vortex pining masks the crossover from superconducting to normal state. Recent development of radio frequency (rf) techniques in milli-second pulsed high magnetic fields have resulted in a powerful tool to investigate metals and superconductors at extremes in *H-T* space. The rf technique is sensitive to changes in the most conducting regions of the sample, hence the in-plane resistivity is measured. By measuring the change in skin depth as a function of applied magnetic field and temperature, a reliable method for mapping the upper critical field is realized. Direct comparison with thermodynamic measurements such as magnetization and thermal conductivity show compelling agreement.

Determination of the upper critical field of superconductors is important for understanding the nature of the mechanism of superconductivity. Often the resistivity as a function of magnetic field is used as an indicator of the upper critical field transition. Due to intrinsic broadening of the superconducting transition in layered and inhomogeneous systems the magnetic field dependency of the magnetoresistance is poorly suited to determine the upper critical field. Further, adding to the problem is the dissipative effect of flux motion in dynamic fields or temperature. Thermodynamic measurements, such as the specific heat or thermal conductivity in magnetic field are perhaps the most clear indications of H_{c2}, however, small sample size and time constants limit the use of such techniques. By using radio frequency (rf) contactless conductivity and penetration depth techniques some of the intrinsic measurement difficulties are overcome as well as extending the usable field range of the measurement to pulsed high magnetic fields.

The radio frequency technique was pioneered by Schalow and Devlin[1] as a method of measuring the rf penetration depth of superconductors as a function of temperature. The technique is quite simple in that a self resonant circuit which consists of an inductor and capacitor in parallel (tank circuit) are driven by an external source that resonates at $\omega = (LC)^{-1/2}$. It is convenient to use a tunnel diode as the driving element. The so called tunnel diode oscillator technique is carefully treated by Van Degrif.[2] The premise of the technique is to fix either the capacitor or inductor at a constant value and couple some physical parameter to the orthogonal element. As the physical parameter changes in field or temperature the resonant frequency shifts in a proportionate manner. In the case of measuring the rf

penetration depth the sample is placed inside of the inductor of the tank circuit. Ideal sample geometry is a long cylinder. As the temperature is lowered to T_c the rf flux is expelled from the sample and the effective inductance of the circuit is lowered, thus increasing the resonant frequency. A simple relation from reference 3 uses the cylindrical sample approximation to corrolate the shift in frequency to a shift in penetration (or skin) depth. From Ref. 3:

$$\Delta\lambda = \frac{R_c^2}{r_s}\frac{\Delta f}{f_0},$$

where, R_c is the coil radii, r_s is the effective sample radii, Δf is the frequency shift and f_0 is the quiescent state resonant frequency. Use of this simple approximation leads to a good representation of the shift in either the rf penetration depth of a superconductor or the skin depth of a metal as shown in figure 1. This is valuable as one can use the shift in frequency to determine the resistivity of the sample in the metallic state. The skin depth is simply related to the resistivity by $\delta = (2\rho/\mu_0\omega)^{1/2}$ and the zero field resistivity is vanishing for a superconductor. The physical parameter that is actually being measured is a change in effective rf flux volume of the inductor. Careful measurements of the penetration depth and volumetric expressions are given by Hardy *et al.*,[4] and Prozorov *et al.*,[5] however, the above expression provides a good approximation, recently demonstrated to be within 20% of conventional methods.

We make a direct comparison between conventional magnetotransport, rf contactless results, and thermodynamic measurements for a layered superconductor. A model system for consideration is the organic superconductor κ-$(ET)_2Cu(NCS)_2$ as this is the most widely studied high temperature organic superconductor (T_c=10.4 K) and all of *H-T* phase space is accessible. Earlier comparison studies between magnetotransport and thermal conductivity show a dramatic difference between the two techniques. Belin *et al.*,[6] have shown that there exists a significant discrepancy between upper critical field determination between magnetotransport and thermal conductivity. Perhaps the most striking difference is observed in the shape of the *H-T* curves. It is also clear that the microwave penetration results track the thermodynamic measurements well while the magnetoresistance looks more like the irreversibility line. Figure 2 is an *H-T* compilation of earlier results,[3] rf penetration, and magnetization. A simple fit of $(T_c\text{-}T)^{1/2}$ provides a good fit to the data and is consistent with the 2D model

Application of the rf technique to other layered superconductors, such as the cuprates reveal a drastic contrast to the resistivity data on the same compound.[7] Almost a factor of two difference is observed in the resultant *H-T* plot. Some of this discrepancy stems from the fact that no sharp signature appears in either of the two techniques, however the same criteria are used for determination of the saturation point. Given the significant role that vortex motion plays in well pinned superconductors, it is likely to be the dominant mechanism for the additional dissipation masking the superconducting to normal state transition observed in

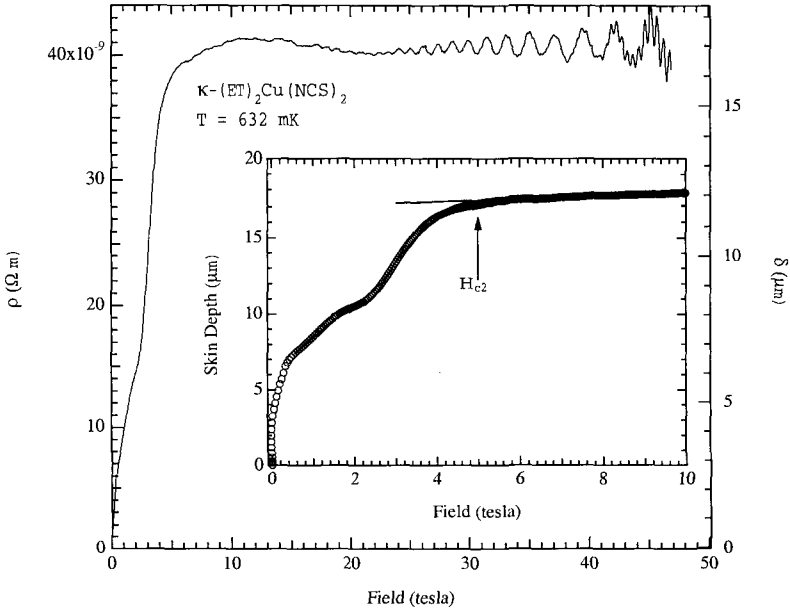

Figure 1: Radio Frequency skin depth (33 MHz) to 47 tesla taken in pulsed magnetic fields. The inset shows the superconducting transition.

magnetotransport data. The high degree of anisotropy of these materials also plays a fundamental role in the observed discrepancy. When the rf field is aligned perpendicular to the xy planes and $\rho_{zz}>>\rho_{xy}$, the rf technique is proportionately more sensitive to changes in ρ_{xy}. Therefore, the rf resistivity technique is a much more accurate means of determining the in-plane resistivity since that is where the screening occurs, i.e. $\delta_{xy} << \delta_{zz}$ if $\rho_{zz}>>\rho_{xy}$. This is equivalent to saying that since the resistivity is large in between the planes, the rf field fully penetrates this region. Despite best efforts to attach electrical contacts to the surface of a sample, the electric fields disperse through the layers. In most cases it is impossible to grow atomically flat samples with macroscopic dimensions, even if that were possible micro-cracks, dislocations, and impurities redirect some current flow through the layers. Recent simultaneous rf conductivity and ρ_{zz} magnetotransport of the highly anisotropic superconductor κ-$(ET)_2Cu(NCS)_2$ were measured.[8] Keeping the magnetic field fixed, the angle of the sample relative to the applied field was changed. Distinct signatures are observed. Conventional transport show strong oscillations associated with the corrugations of a closed Fermi surface while this ρ_{zz} effect is absent in the rf ρ_{xy} data. This proves that the rf ρ_{xy} technique is effective in

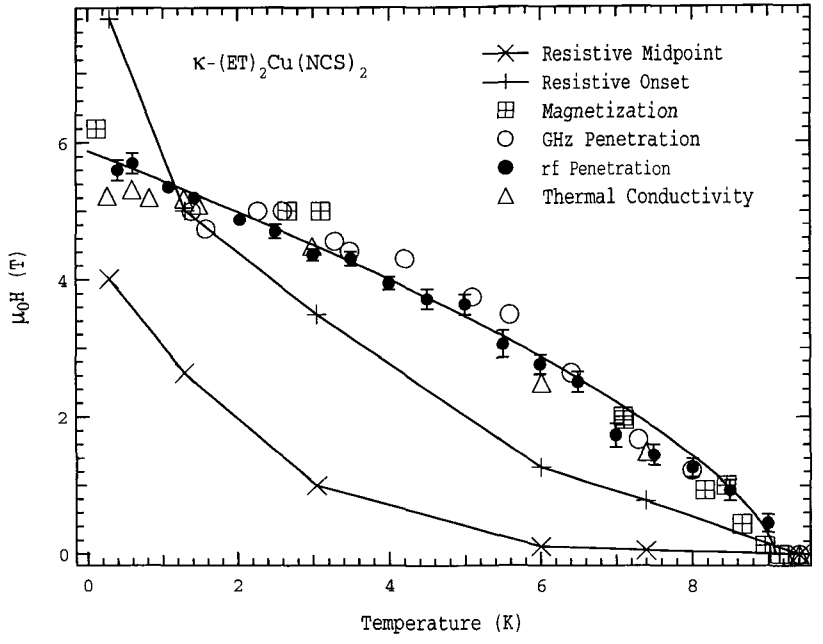

Figure 2: Recent rf penetration depth results for κ-$(ET)_2Cu(NCN)_2$ compared to other techniques.[3,6]

measuring the in-plane contribution to the magnetoresistance in a highly anisotropic metal.

The rf technique is an ideal tool for measuring highly anisotropic metals and superconductors in transient environments. With the proper rf components and techniques it is relatively easy to achieve time constants of the order of 1μsec while maintaining a signal to noise ratio of 1000:1 or better. These recent results are indicators that this technique is an excellent means for determining the upper critical field in systems in which vortex dissipation dominates transport properties. This research was carried out under the auspices of the National Science Foundation, the Department of Energy, and the State of Florida.

References

1. A. L. Shawlow and G. E. Devlin, *Physical Review* **113**, 120.(1959).
2. C. T. Van Degrift, *Rev. Sci. Instrum.* **46**, 599 (1975).
3. C. Mielke *et al., J. Phys.: Condens. Matter* **13**, 8325 (2001).
4. W. N. Hardy *et al., Phys. Rev. Lett.* **70**, 3999 (1993).
5. R. Prozorov *et al., Phys. Rev. B,* **62**, 115 (2000).
6. S. Belin *et al., J. of Superconductivity* **12** (1999).
7. B. Khaykovich *et al., in preparation.*
8. J. Singleton *et al., in preparation.*

INFLUENCE OF ELECTRON IRRADIATION DEFECTS ON THE TRANSPORT PROPERTIES OF CUPRATES

F. RULLIER-ALBENQUE,[1] R. TOURBOT[1] and H. ALLOUL[2]
[1]*SPEC/CEA, Orme des Merisiers, 91191 Gif sur Yvette Cedex, France*
[2]*Physique des Solides, UMR 8502, Universit Paris-Sud, 91405 Orsay, France*

We use electron irradiation at low temperature to introduce defects in a controlled manner in the cuprates. We have shown in $YBCO_7$ that the main influence on transport properties is due to stable defects in the CuO_2 plane. They are found analogous to Zn substitution on the copper planar site.[1] Compared to impurity substitutions, the great advantage of electron irradiation is to allow to study the physical properties of a single sample with an increasing defect content. T_c and electrical resistivity measurements have been performed on electron irradiated single crystals of different cuprates (YBCO, Bi-2212, Hg-1223, Tl-2201) for a wide range of hole dopings n_h. A simple correlation between the decrease of T_c and the increase of residual resistivity ΔR_{2D} is found, as expected for d wave superconductivity. The ratio $\Delta T_c/\ \Delta R_{2D}$, which is expected to be proportional to n_h/m^* is found to reproduce the variation of n_h from the under-doped to the over-doped regime.[2] This demonstrates that the hole content is the relevant paramter to describe the transport properties all over the phase diagram. For large defect contents, low T upturns of the resistivity are observed in under-doped $YBCO_{6.6}$ and over-doped Tl-2201 (see Ref. [3]). In the highly over-doped Tl compound the decrease of conductivity scales as expected from weak localization theory. For $YBCO_{6.6}$ the large low T contribution to the resistivity is shown to be initially proportional to the defect content. It might therefore be associated to a Kondo like spin flip scattering term. This would be consistent with the results on the magnetic properties induced by spinless defects such as Li (see Ref. [4]).

1. A. Legris, F. Rullier-Albenque *et al, J. Phys. I France* **3**, 1605 (1993).
2. F. Rullier-Albenque *et al, Europhys. Lett.* **50**, 81, (2000).
3. F. Rullier-Albenque *et al, cond-mat/*0102294, to be published in *Phys. Rev. Lett.* (2001).
4. J. Bobroff *et al., Phys. Rev. Lett.* **83**, 4381 (1999).

INTERPLAY BETWEEN SPIN AND CRYSTAL LATTICES IN ANTIFERROMAGNETIC $YBa_2Cu_3O_{6.25}$

V. SANDU,* E. CIMPOIASU and C. C. ALMASAN

Department of Physics, Kent State University, Kent, OH 44242, USA
E-mail: calmasan@physics.kent.edu

A. P. PAULIKAS and B. W. VEAL

Materials Science Division, Argonne National Laboratory, Argonne, IL 60439, USA

In-plane ρ_{ab} and out-of-plane ρ_c resistivity measurements were performed on the same antiferromagnetic $YBa_2Cu_3O_{6.25}$ single crystal over a wide range of temperatures T. $\rho_{ab}(T)$ exhibits two crossovers with decreasing T: a crossover from metallic to weak localization behavior at 175 K and a second crossover to two-dimensional chiral variable-range hopping VRH behavior at 115 K. The latter reflects the topologic excitations induced in the spin system. $\rho_c(T)$ displays an $\exp(-T^2/T^2_{c,h})$ dependence at high T and a VRH type dependence below 115 K. The T derivative of $\rho_c(T)$ shows a kink at 32.65 K which we attribute to the antiferromagnetic ordering of the Cu(1) spins.

1 Introduction

Antiferromagnetic (AFM) layered cuprates have attracted a lot of attention due to their unusual potential to change their insulating state into a superconducting one upon doping. In the last decade, a lot of effort has been dedicated to the understanding of the role of magnetism in the evolution of the physical properties as the charge carrier concentration is increased. In the case of $YBa_2Cu_3O_6$, hole doping is achieved by inserting oxygen atoms in the $Cu(1)O_x$ planes. Placed between two $Cu(1)^+$ ions in the $Cu(1)O_x$ planes and two $Cu(2)O_2$ bilayers, the inserted oxygen can supply a hole to either the bilayers or the coplanar $Cu^+(1)$. The hole inserted in the CuO_2 plane has dramatic effects on the magnetic structure even at low doping, since it locally frustrates and dilutes the spin system. The result is a local distortion of the AFM background called texture.[1,2] Shraiman and Siggia[3] have shown that, for large on-site Hubbard repulsion between carriers with opposite spins, a local distortion of the spin orientation may lower the carrier energy. Vergés *et al.*[4] have found that, for dilute hole doping, within the same approximation, a lower energy configuration consists of a vortex-like distortion of the local spins, which dresses the hole (charged topological excitation). At low doping levels, the hole is localized around the dopant atom and, due to the texture it creates in the spin system, it moves around this impurity clockwise or counterclockwise in a double

* Permanent address: National Institute of Materials Physics, Bucharest-Magurele, Romania

degenerated chiral ground state.[5] The aim of the present paper is to investigate the way in which this complex state is reflected in the electronic transport properties.

2 Experimental

$YBa_2Cu_3O_{6.25}$ single crystals with typical size 0.8×0.5×0.04 mm^3 and the c-axis along the smallest dimension were used for transport measurements. An 8-terminal lead configuration with the current applied parallel to the crystal faces allowed simultaneous measurements of both in-plane ρ_{ab} and c-axis ρ_c resistivities.

3 Results and discussion

The in-plane resistivity is metallic for T > 175 K whereas, below this T, it exhibits a transition to localization. The increase of ρ_{ab} with decreasing T is very sharp below 115 K. In the T range in which transport occurs through variable-range hopping VRH, $\rho \propto \exp(T_0/T)^{\alpha}$ with a T independent pre-exponential factor, hence $\ln(-d\ln\rho/dT)$ is linear in lnT with the slope $m = -\alpha-1$. Our in-plane resistivity data do not display the above linear dependence over any measured T range. However, a plot of $\ln\{-d[\ln(\rho_{ab}/T^{4/3})]/dT\}$ vs lnT is linear for 8 K ≤ T ≤ 115 K (Fig. 1). The linear fit of the data gives the exponent $\alpha = 0.34 \approx 1/3$ and the characteristic temperature $T_{ab,\chi} = 27{,}000$ K. Therefore, $\rho_{ab}(T)$ of $YBa_2Cu_3O_{6.25}$ follows the relationship:

$$\rho_{ab} \propto T^{4/3} \exp\left(T_{ab,\chi}/T\right)^{1/3}. \qquad (1)$$

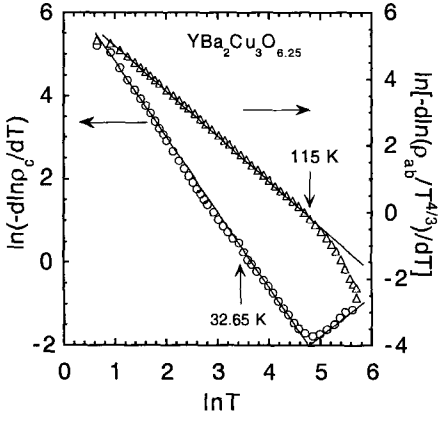

Figure 1: Temperature T dependence of the temperature derivative of in-plane ρ_{ab} (Δ) and out-of-plane ρ_c (O) resistivities.

This T dependence of ρ_{ab} is consistent with the model of hopping of localized holes in a textured magnetic system proposed by Lai and Gooding.[5] Their model is an extension of the percolation theory of localization in semiconductors of Mott, Efros, and Shklovskii[6] to the peculiarities of an AFM system with topological excitations. It differs from the original Mott-Efros-Shklovskii model by a power-law temperature dependent pre-exponential factor, with the power related to the dimensionality D of conduction. This model predicts:

$$\rho_{ab} = AT^{2D/(D+1)} \exp\left(T_{ab,\chi}/T\right)^{1/(D+1)}. \qquad (2)$$

Since the best fit of our data gives D + 1 = 3 [see Eqs. (1) and (2)], it follows that D = 2, indicating the 2 D character of the transport in this highly anisotropic material.

A similar analysis of $\rho_c(T)$ (see Fig. 1) reveals two T ranges with a well-defined crossover at 115 K. At high T, $\rho_{c,h} \propto \exp[-(T/T_{c,h})^2]$ with $T_{c,h}$ = 308 K. For T < 115 K, ρ_c has a VRH type behavior, but with an unusual exponent α = 3/4 and a very low characteristic temperature $T_{c,VRH}$ = 30.6 K. As Efros and Shklovskii have shown,[6] such an unusual exponent could be reconciled with Mott's VRH theory if, instead of considering a constant density of states (DOS) at the Fermi level μ, one takes a DOS with a power-law dependence $g(\varepsilon) \propto (\varepsilon - \mu)^n$, which vanishes at the Fermi level.

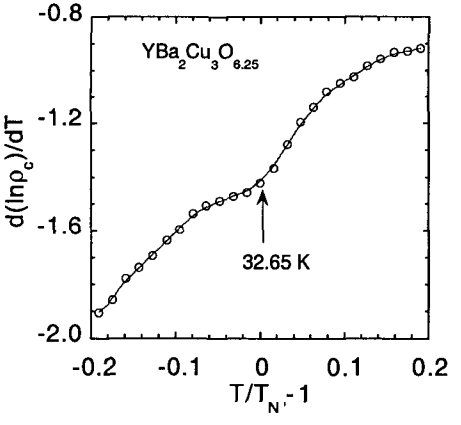

Figure 2: Temperature derivative of c-axis resistivity ρ_c vs reduced temperature T/T_N - 1

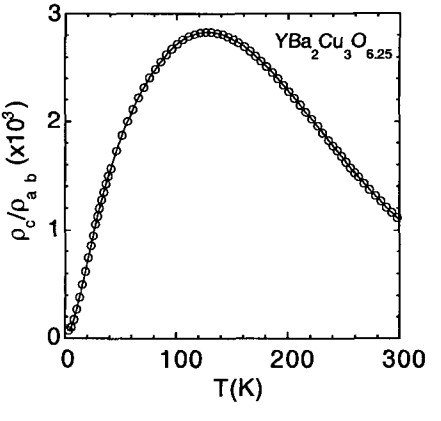

Figure 3: Temperature T dependence of the anisotropy ρ_c/ρ_{ab}.

A second striking feature of $\rho_c(T)$ is a small kink in its T derivative at 32.65 K (see Fig. 2). This kink is not visible in ρ_{ab}. Therefore, it is characteristic only to c-axis transport. We attribute this behavior to the AFM ordering of Cu^{2+} spins in the

$Cu(1)O_x$ planes based on neutron diffraction experiments by Kadowaki *et al.*[10] They have reported AFM ordering of the Cu(1) spins around 40 K. When an oxygen atom gives a hole to its co-planar Cu(1), the latter acquires a spin which, subsequently, undergoes AFM ordering. It is known that the resistivity exhibits a jump at the Néel transition temperature T_N due to the large fluctuation in the spin-spin correlation function close to T_N (see Ref. [8]). Such jumps are more visible at the first AFM ordering which takes place in the Cu spins of the $Cu(2)O_2$ planes at high temperatures.[9] The formation of $Cu(1)^{2+}$ spins is a rather rarely observed phenomenon, and this kind of AFM ordering is still controversial. The fact that ρ_{ab} does not exhibit such a jump upholds the idea that only the inter-bilayer structure is involved in this AFM ordering.

Interestingly, the T dependence of ρ_c/ρ_{ab} is nonmonotonic. It increases with decreasing T and displays a maximum around 110÷125 K, below which both resistivities cross over into the localization regime (see Fig. 3). A similar nonmonotonic T dependence was also reported by Semba and Matsuda.[7]

In conclusion, the temperature dependence of ρ_{ab} is metallic above 175 K and exhibits a strong localization below 115 K, consistent with hopping of charged spin vortices. ρ_c has a different dependence but with a sharp crossover at the same temperature between $\exp[-(T/T_{c,h})^2]$ behavior at high temperatures and a strong VRH-type dependence at low temperatures. In the latter regime, a kink in the logarithmic derivative of ρ_c vs T signals a second AFM ordering which involves the Cu(1) spins.

This research was supported by the National Science Foundation under Grant No. DMR-0102415 and by the University Research Council at KSU and the US Department of Energy under Contract No. W-31-109-ENG-38 at ANL

References

1. B. I. Shraiman and E. D. Siggia, *Phys. Rev. Lett.* **61**, 467 (1988).
2. J. R. Schrieffer, X. G. Wen and S. C. Zhang, *Phys. Rev. B* **39**, 11663 (1989).
3. B. I. Shraiman and E. D. Siggia, *Phys. Rev. B* **40**, 9162 (1988).
4. J. A. Vergés *et al., Phys. Rev. B* **43**, 6099 (1991).
5. E. Lai and R. J. Gooding, *Phys. Rev. B* **57**, 1498 (1999).
6. A. L. Efros and B. I. Shklovskii, *Electronic Properties of Doped Semiconductors*, Elsevier, (1985).
7. K. Semba and A. Matsuda, *Phys. Rev. Lett.* **86**, 496 (2001).
8. P. G. de Gennes and J. J. Friedel, *Phys. Chem. Solid.* **4**, 71 (1958).
9. A. N. Lavrov and L. P. Kozeeva, *Physica C* **248**, 365 (1995).
10. H. Kadowaki *et al., Phys. Rev. B* **37**, 7932 (1988).

MAGNETOTRANSPORT AND THE MAGNETIC PHASE DIAGRAM OF SUPERCONDUCTING $ErNi_2B_2C$

G. M. SCHMIEDESHOFF and S. TOUTON

Department of Physics, Occidental College, Los Angeles, CA 90041, USA
E-mail: gms@oxy.edu

W. P. BEYERMANN

Department of Physics, University of California, Riverside, CA 92521, USA

A. H. LACERDA

National High Magnetic Field Laboratory, Los Alamos, NM 87545, USA

S. L. BUD'KO and P. C. CANFIELD

Ames Laboratory and Iowa State University Department of Physics, Ames, IA 50011, USA

We report magnetotransport measurements made on the anisotropic magnetic superconductor $ErNi_2B_2C$. We observe a minimum in the magnetoresistance with fields along the a-axis, a behavior consistent with the high field quenching of magnetic scattering. When the field is applied along the c-axis the magnetoresistance is positive. The temperature of the antiferromagnetic phase transition is depressed by magnetic fields applied along the c-axis (as it is along the a-axis) and is suppressed near 17 T. A feature in the first derivative of the temperature dependent resistivity may be related to the weak ferromagnetic phase. We find the temperature at which this feature occurs to be independent of magnetic fields to 18 T.

1 Introduction

Materials exhibiting coexisting ferromagnetic and superconducting states are exceedingly rare. The coexistence of antiferromagnetism and superconductivity is somewhat more common and leads to a rich variety of magnetic structures as exhibited by, for example, the rare-earth nickel borocarbides.[1] One of the borocarbides, tetragonal $ErNi_2B_2C$, has a superconducting transition at T_c = 11 K, an antiferromagnetic transition at T_N = 6 K, and weak ferromagnetism occurring at T_{WFM} = 2.3 K in zero magnetic field.[2,3] In this paper we report on magnetotransport measurements made on $ErNi_2B_2C$ to complete the antiferromagnetic phase diagram and to attempt to identify and map out the onset of the weak ferromagnetic state in high magnetic fields.

2 Experimental Results

The electrical resistance was measured using a standard 4 lead, ac technique. The resistivity was determined from the dimensions of the sample with an uncertainty of about 20 %. Representative isothermal field-dependent resistivity data are shown in Figs. 1(a) and 1(b). The magnetoresistance in the normal state is positive with fields along the c-axis (Fig 1(a)); below about 6 K, a fairly sharp feature is observed when the antiferromagnetic state is destroyed. When fields are applied along the a-axis (Fig 1b) the magnetoresistance in the normal state is initially negative and exhibits a minimum which moves to lower fields as the temperature is lowered, a behavior commonly observed in antiferromagnets resulting from the quenching of magnetic scattering by high fields. Typical constant-field resistivity data are shown in Figs. 1(c) and 1(d) for fields along the c-axis and a-axis respectively. The resistivity increases monotonically with temperature and exhibits a feature as the antiferromagnetic state is destroyed.

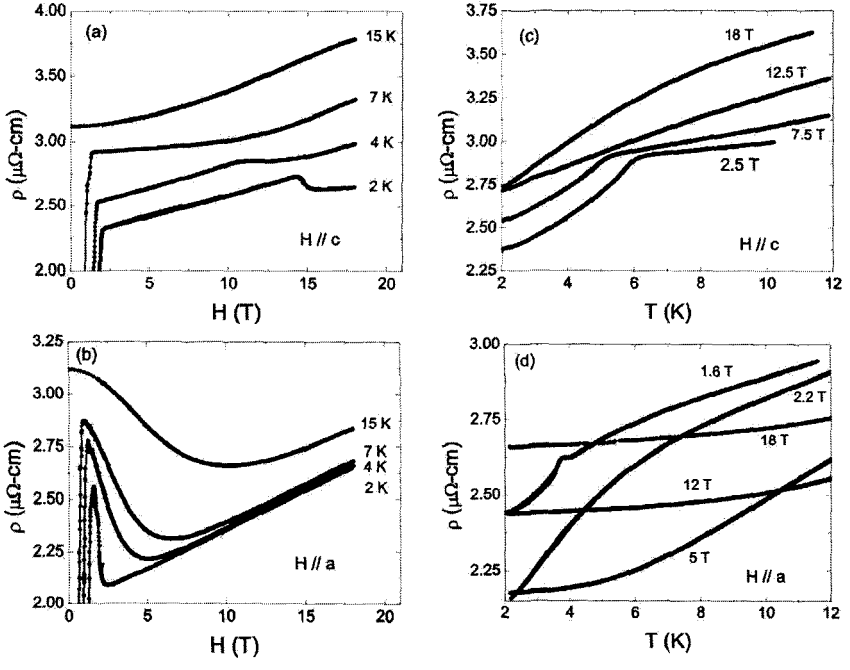

Figure 1: The electrical resistivity of $ErNi_2B_2C$ as a function of magnetic field and temperature.

Plots of the first derivative of the temperature dependent resistivity data (with fields along the c-axis) show a second feature in addition to the peak associated with $T_{N,c}$. Representative data are shown in Fig. 2(a) where a shoulder is visible near $T_o = 2.7$ K. We find T_o to be independent of field within experimental resolution (see Fig. 2(b)). We do not observe a similar shoulder with fields along the a-axis.

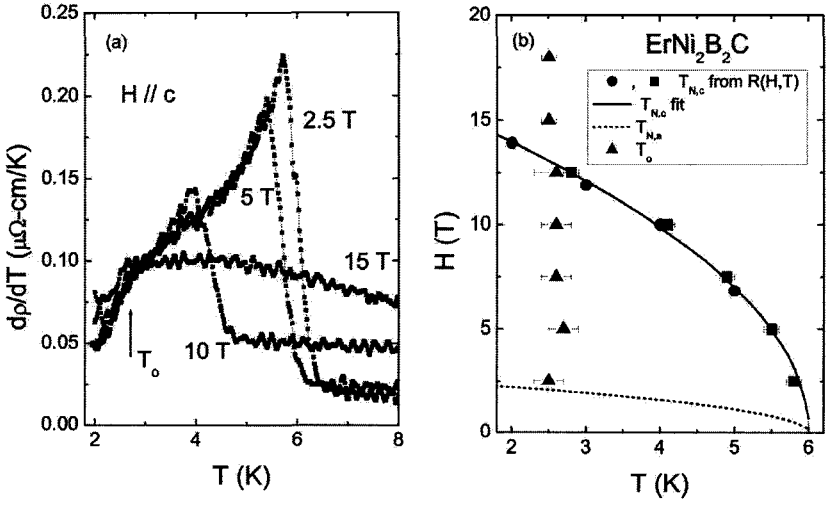

Figure 2: (a) The first derivative of the temperature dependent resistivity of $ErNi_2B_2C$ in several fixed fields as shown. A shoulder near the temperature at which weak ferromagnetism has been observed is identified with an arrow (see text). (b) The magnetic phase diagram of $ErNi_2B_2C$. Solid circles and squares denote $T_{N,c}$ (fields along the c-axis), the solid line is a quadratic fit to the data (see text). The dotted line represents the temperature dependence of $T_{N,a}$ (fields along the a-axis) from Ref. [4]. The solid triangles show the temperatures at which the "shoulders" of Fig.2(b) are observed (see text).

3 Discussion

The temperatures and fields of the features in the resistivity data associated with the onset of antiferromagnetism (with fields applied along the c-axis) are plotted in Fig. 2(b) as solid squares and circles respectively. The solid line in Fig. 2(b) is a fit to the form

$$T_{N,c}(H) = T_{N,c}(0) - \alpha H^2,$$

where $T_{N,c}(0) = 6.01 \pm 0.05$ K and $\alpha = 20.6 \pm 0.4$ mK/T^2. If the fit continues to hold, $T_{N,c} \rightarrow 0$ at H = 17.1 T. Cho *et al.*,[4] have shown that this form also describes the behavior of $T_{N,a}$ when fields are applied along the a-axis. Their results are shown as the dotted line in Fig. 2(b).

The proximity of the feature at T_o to T_{WFM} = 2.3 K where weak ferromagnetism has been observed suggests that this feature may be due to the onset of this state. If this conjecture is true it seems unlikely that the weak ferromagnetic state could be significantly coupled to the antiferromagnetic state since the applied fields that suppress antiferromagnetism do not affect T_o within our experimental resolution.

4 Conclusions

We found the shapes of the magnetoresistance curves (with fields along the a-axis) to be consistent with that expected for the quenching of magnetic scattering by high magnetic fields. When the field is applied along the c-axis the magnetoresistance is positive. T_N is quadratically depressed by magnetic fields along the c-axis (as it is along the a-axis) and is suppressed near 17 T. A shoulder in the first derivative of the temperature dependent resistivity (with fields along the c-axis only) may be related to the weak ferromagnetic phase. We find the temperature at which this feature occurs to be nearly independent of magnetic fields to 18 T.

Acknowledgments

This work was supported by the National Science Foundation under DMR-0071947. The measurements were made at the National High Magnetic Field Laboratory which is supported by NSF Cooperative Agreement No. DMR-9527035 and by the State of Florida. Ames Laboratory is operated for the U. S. Department of Energy by Iowa State University under Contract No. W-7405-Eng-82.

References

1. P. C. Canfield *et al., Phys. Today* **51**, 40-46 (1998). G. M. Schmiedeshoff *et al., J. Supercond.* **13**, 847-853 (2000).
2. P. C. Canfield *et al., Physica C.* **262**, 249-254 (1996).
3. S.-M. Choi *et al., Phys. Rev. Lett.* **87**, 1070011+1070014 (2001).
4. B. K. Cho *et al., Phys. Rev. B* **52**, 3684-3695 (1995).

HIGH-FIELD TRANSPORT PROPERTIES OF T'-$Ln_{2-x}Ce_xCuO_4$ (Ln=Nd, Pr, La)

T. SEKITANI, N. MIURA and M. NAITO*

Institute for Solid States Physics, University of Tokyo, Kashiwanoha, Kashiwa-shi, Chiba, 277-8581, Japan

**NTT Basic Research Laboratories, Morinosato-Wakamiya, Atsugi-shi, Kanagawa, 243-0198, Japan*

We report low-temperature magnetotransport in the normal state of the electron-doped superconductors, $Nd_{2-x}Ce_xCuO_4$, $Pr_{2-x}Ce_xCuO_4$, and $La_{2-x}Ce_xCuO_4$, by suppressing the superconductivity with high magnetic fields. The normal state ρ - T curve shows an up-turn at low temperatures, which has a log T dependence with saturation at lowest temperatures. The up-turn is gradually suppressed with increasing magnetic field, resulting in negative magnetoresistance. We discuss these findings on the basis of the Kondo scattering originating from the magnetic moments of Cu^{2+} ions.

The low-temperature normal state of cuprates induced by high magnetic fields, regardless the hole- or electron-doped, commonly show an insulator-metal crossover as a function of doping level.[1-3] In the insulating regime, the resistivity shows an up-turn ($d\rho/dT<0$) with a log T dependence at low temperatures in many cases. There has been much controversy on the origin of the log T dependent up-turn, but no clear explanation has been given yet. We have undertaken a systematic magnetotransport experiment on high-quality $Nd_{2-x}Ce_xCuO_4$ (NCCO), $Pr_{2-x}Ce_xCuO_4$ (PCCO), and $La_{2-x}Ce_xCuO_4$ (LCCO) films, in order to unveil the low-temperature normal state, especially the nature of the log T dependent up-turn. The measurements were performed on seven c-axis oriented films, which were grown by MBE on $SrTiO_3$ (001) substrates.[4,5]

Figure 1 shows the in-plane resistivity as a function of magnetic field applied in the direction of c-axis at various temperatures for the optimal-doped NCCO film (x=0.146). The resistivity was measured by the standard four-probe method. The DC current was supplied in plane. Negative magnetoresistance can be seen at low temperatures above the upper critical field (H_{c2}) of superconductivity, in addition to positive magnetoresistance as a background. The background positive magnetoresistance is probably due to an orbital effect, which we do not discuss in this article. Here we focus on the negative magnetoresistance component. The negative magnetoresistance component becomes more prominent with decreasing temperature, and it seems to saturate at high magnetic fields.

For convenience, experimentally obtained ρ-B curves are converted to ρ-T curves at constant magnetic fields. Figure 2 shows such converted ρ-T curves of under-doped (x=0.131), optimal-doped (x=0.146), slightly over-doped (x=0.166),

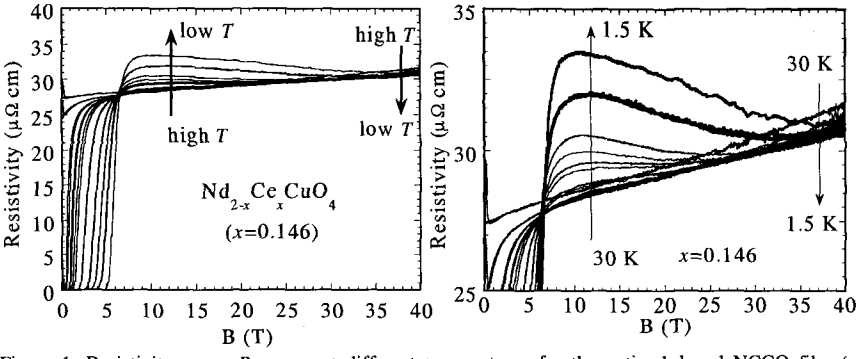

Figure 1: Resistivity-versus-B curves at different temperatures for the optimal-doped NCCO film (x =0.146). The left panel shows raw data, and the right shows an enlarged view.

and heavily over-doped (x=0.185) NCCO films. This demonstrates a systematic evolution of the normal-state resistivity with doping. Except for the heavily over-doped film that is metallic down to the lowest temperature, all the films show a low-temperature up-turn at low magnetic fields (but above H_{c2}). The up-turn follows a log T dependence (see the insets). In the under-doped film, this dependence is already seen in zero-magnetic fields above T_c. In the slightly over-doped film, however, the up-turn is very weak, and can be observed only at very low temperatures. Correspondingly, the resistivity minimum shifts to the lower temperature with increasing Ce-doping. Furthermore, in the lowest temperature region, it should be noted that the resistivity for all films tends to deviate from a simple log T dependence and to saturate toward T = 0 K. The up-turn occurs at an anomalously large value of $k_F l_{ab}$ ($=hd_c/\rho_{ab}e^2$) > 17 (x=0.131) and > 70 (x=0.166) in our experiments. Such large values of $k_F l_{ab}$ should ordinarily give metallic behavior. Thus an explanation based on variable range hopping, which should be observed only for $k_F l_{ab} < 1$, is discarded.

With increasing magnetic field, the up-turn is suppressed for all the films. In the under-doped film, the up-turn persists up to the highest magnetic field even with noticeable suppression. In the optimal-doped film, the resistivity shows metallic behavior in high magnetic fields, except for very low temperatures, where small up-turn remains. In the slightly over-doped film, the low-temperature resistivity turns to be completely metal-like in high magnetic fields. The negative magnetoresistance (suppression of the up-turn by field) is almost independent of the direction of magnetic field, namely isotropic, as demonstrated in our recent work.[6]

We can think of two candidates as its origin of up-turn: the Kondo effect and the 2D weak localization. Here from the discussion below, we believe that the Kondo effect is responsible for the observed anomalies. Typical Kondo systems such as $(La,Ce)B_6$ (see Ref. [7]) show log T dependent up-turn of resistivity that results from the second order perturbation of the spin inversion process in the scattering of conduction electrons by local magnetic impurities. Below the Kondo

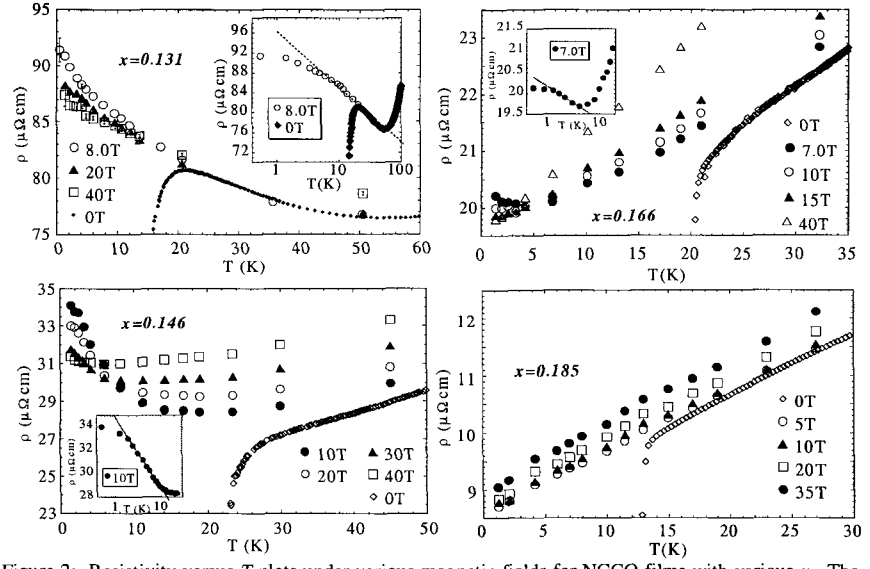

Figure 2: Resistivity-versus-T plots under various magnetic fields for NCCO films with various x. The insets show resistivity-versus-log T plots.

temperature (T_K), the AF coupling between a conduction electron spin and a local spin predominates, forming a singlet state. At 0 K, the resistivity has a finite maximum value (unitarity limit) without the divergence to infinity. High magnetic fields act to suppress the spin inversion, and this effect is expected to give isotropic negative magnetoresistance with a log B dependence. The up-turn observed in NCCO satisfies essentially all such features. On the other hand, another possible scenario of our findings based on 2D weak localization can be ruled out by the observed isotropic negative magnetoresistance.

Regarding the field dependence of negative magnetoresistance, we show ρ-versus-log B curves for very under-doped nonsuperconducting NCCO in Fig. 3. The nonsuperconducting sample was chosen so as to see the field dependence down to very low fields by avoiding the influence of superconductivity. All the data at various temperatures show straight lines between 1 T and 40 T and converge at around 1500 T. This indicates that the Kondo singlets are dissociated by magnetic fields above ~ 1500 T. The corresponding magnetic field for optimal-doped NCCO is about 30 T as shown in Fig. 1. It implies that the binding energy of Kondo singlets rapidly decreases with doping. Finally it should be noted that this behavior looks qualitatively similar to that very recently found for hole-doped $Bi_2Sr_2CaCu_2O_{8+y}$ by Shibauchi *et al.*[8]

Next we discuss the origin of the Kondo scatterer. We can exclude the Kondo scattering originating from the paramagnetic spin moment of Nd^{3+}. It is because essentially the same magnetotransport behavior is observed also in PCCO, and

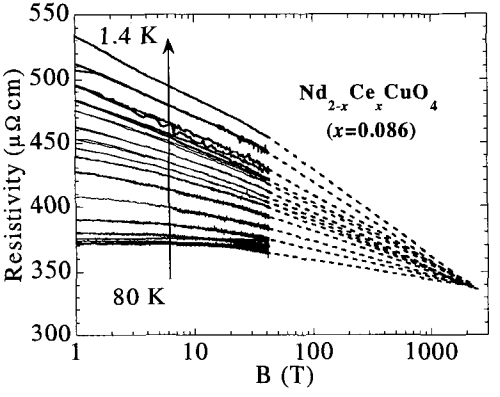

Figure 3: ρ-versus-log B plots under various temperatures for very under-doped NCCO (x=0.086) films. All lines show log B dependent negative magnetoresistance. Dotted lines are a guide to eye pointing to the limiting value of Kondo singlets.

LCCO, where Pr^{3+} or La^{3+} has no spin moment.[9] Therefore we have to resort to the other possibility, namely Cu^{2+} spins in the CuO_2 plane. Then we conclude that the low-temperature up-turn is due to the Kondo scattering caused by the Cu^{2+} spins in the CuO_2 plane. With overdoping, the Cu-3*d* orbit becomes more itinerant, resulting in reduction or eventually in loss of spin moments. As a result, the Kondo interaction between a Cu^{2+} local spin and a conduction electron essentially vanishes. This scenario explains the reduction of the up-turn or the residual resistivity with doping and also the doping dependence of the Kondo singlet binding energy as mentioned above.

In summary, our systematic magnetotransport experiments on high-quality films of NCCO, PCCO, and LCCO with various doping conclude that the Kondo scattering due to the Cu^{2+} spins in the CuO_2 plane is responsible for the low-temperature anomalous behavior in these compounds.

References

1. G. S. Boebinger *et al.*, *Phys. Rev. Lett.* **77**, 5417-5420 (1996).
2. Y. Ando *et al.*, *Phys. Rev. Lett.* **77**, 2065-2068 (1996).
3. P. Fournier *et al.*, *Phys. Rev. Lett.* **81**, 4720-4723 (1998).
4. M. Naito *et al.*, *Physica C* **293**, 36-43 (1997).
5. M. Naito and M. Hepp, *Jpn. J. Appl. Phys.* **39**, L485-L487 (2000).
6. T. Sekitani *et al.*, *Physica B* **294-295**, 358-362 (2001).
7. K. Samwer and K. Winzer, *Z. Physik B* **25**, 269-274 (1976).
8. T. Shibauchi *et al.*, *Phys. Rev. Lett.* **86**, 5763-5766 (2001).
9. T. Sekitani accepted in *J. Phys. Chem. Solids.*

PERCOLATIVE SUPERCONDUCTIVITY IN $Mg_{1-x}B_2$

P. A. SHARMA
Rutgers University, Physics Department, 136 Frelinghuysen Road, Piscataway, New Jersey 08854, USA

Using various synthesis techniques, we have obtained a number of interesting results regarding the magnesium diboride system. First, we have observed a maximum T_C of 42 K in $Mg_{1-x}B_2$ films on crystalline boron substrates, which is significantly higher than the reported value of 39 K. Furthermore, our study of Mg-vacant $Mg_{1-x}B_2$ specimens, fabricated by using high-pressure (35 MPa) sintering, provides convincing evidence for electronic phase separation, probably induced by Mg-vacancy clustering.

* This work was performed in collaboration with N. Hur, Y. Horibe, C. H. Chen, B. G. Kim, S. Guha, D. J. Werder, Marta Z. Cieplak, and S-W. Cheong.

VORTEX GLASS TRANSITION VERSUS IRREVERSIBILITY LINE IN SUPERCONDUCTING BKBO

P. SZABO,[1] P. SAMUELY,[1] J. KACMARCIK[1]
T. KLEIN,[2] A. G. M. JANSEN,[3] A. MORELLO,[3] and J. MARCUS[2]
[1]*Institute of Experimental Physics, Slovak Academy of Sciences, SK-04353 Kosice, Slovakia*
[2]*Laboratoire d'Etudes des Proprietes Electroniques des Solides, CNRS, BP166, 38042 Grenobel Cedex 9, France*
[3]*Grenoble High Magnetic Field Laboratory, Max-Planck-Institut fur Festkorperforschung and CNRS, B.P. 166, F-38042 Grenoble Cedex 9, France*

Simultaneous magnetotransport and torque magnetization measurements have been performed on superconducting (B, Ka)BiO_3 single crystals. The measurements have been carried out at very low temperatures ($0.03\ K < T < 2\ K$) and up to high magnetic fields: ($30 Tesla \sim H_{c2}(0)$). The resistivity drops below the experimental resolution for a magnetic field $H_R(T)$ which is very close to the irreversibility line deduced from torque magnetometry. Close to $H_R(H)$ the resistive transition can be well by the vortex-glass scaling formalism[1] suggesting that the vortex solid melts into a liquid for $H > H_R$. Our measurements show that the irreversibility line in *(K, Ba)BiO_3* is closely related to this vortex glass transition line but, surprisingly, a large reversible (i.e. liquid) phase can still be observed at very low temperatures (30 *m*K).

1. T. Klein, A. Conde-Gllardo, J. Marcus, P. Szabo, P. Samuely, A. G. M. Jansen and C. Escribe-Filippini *Phys. Rev. B* **58**, 12411 (1998).

TRANSPORT IN MgB_2 IN HIGH MAGNETIC FIELDS

P. SZABO,[1] P. SAMUELY,[1] A. G .M. JANSEN,[2] T. KLEIN,[3] J. MARCUS,[3]
D. FRUCHART,[4] and S. MIRAGLIA[4]
[1]*Institute of Experimental Physics, SAS Kosice, Slovakia*
[2]*Grenoble High Magnetic Field Laboratory, MPI-FKF and CNRS, France*
[3]*LEPES CNRS, Grenoble, France*
[4]*Laboratoire de Cristallographie, CNRS, Grenoble, France*

Magnetotransport measurements are presented on polycrystalline MgB_2 samples. The 'resistive' upper critical magnetic field reveals a temperature dependence with positive curvature from T_c = 39.3 K down to about 20 K, then changes to slightly negative curvature reaching 26 T at 1.5 K. The 26-Tesla upper critical field is much higher than what is known so far on polycrystals of MgB_2 but it is in agreement with the recent data obtained on epitaxial MgB_2 films.[1] The deviation of $H_{c2}(T)$ from standard BCS might be due to the proposed two-gap superconductivity in this compound.[2] Recently we have found evidence for the existence of two superconducting energy gaps in this system using Andreev reflection spectroscopy.[3] The temperature dependence of the resistivity and the normal state magnetoresistance are analyzed.

1. M. H. Jung *et al., Chem. Phys. Lett.* in press.
2. S. V. Shulga *et al., cond-mat*/0103154.
3. P. Szabo *et al., cond-mat*/0105598, accepted to *Phys. Rev. Lett.* (2001).

EVIDENCE FOR THE PAIR FORMATION FAR ABOVE T_C IN EPITAXIAL $La_{2-X}Sr_XCuO_4$ THIN FILMS

J. VANACKEN, L. WECKHUYSEN, P. WAGNER and V. V. MOSHCHALKOV

Laboratorium voor Vaste-Stoffysica en Magnetisme, Katholieke Universiteit Leuven, Celestijnenlaan 200D, B-3001Leuven, Belgium

E-mail: Johan.Vanacken@fys.kuleuven.ac.be

A large positive magnetoresistivity (up to ten percent or more) is observed for both under-doped and over-doped superconducting $La_{2-x}Sr_xCuO_4$ epitaxial thin films at temperatures far above the superconducting critical temperature T_c. This magnetoresistivity can be related to the pairs eventually forming the superconducting phase at low temperatures. Our observations support the idea of a close relation between the pseudogap and the superconducting gap and provide new indications for the presence of pre-pairs above T_c.

1 Introduction

One of the most intriguing questions about high temperature superconductors is whether the pseudogap and the superconducting gap have a common origin. If they are related, the pseudogap might be associated with the presence of electronic pairs above T_c. From this point of view, superconductivity occurs when the phase of these pairs becomes coherent and not when they are first formed in the phase incoherent state.[1] The idea of a precursory pair formation at relatively high temperatures $T \sim T^*$ and its relevance for high T_c superconductivity is supported by the experimental observation that the pseudogap evolves into the superconducting gap at low temperatures, as clearly demonstrated by scanning tunneling spectroscopy.[2] Moreover, the ARPES data[3,4] indicate, that the pseudo- and the superconducting gap both have the d-wave symmetry. If performed pairs really exist, they should also influence the normal state transport properties of high T_c superconductors at temperatures $T_c < T < T^*$. This paper will present experimental evidence for precursor pair formation effects derived from high field magneto-transport experiments.

2 Results and Discussion

The as-grown films are prepared by DC magnetron sputtering from stoichiometric targets.[5] The magnetoresistivity measurements were performed in the pulsed field facility of the Katholieke Universiteit Leuven[6] by using a homemade flow-cryostat and 50 T coil. All data reported in this paper was obtained on thin films (~150 nm), patterned (1000 × 50 μm strip) for four probe measurements in the transverse

geometry ($\mu_0 H \perp I$) with the magnetic field perpendicular to the film ($\mu_0 H$ // c) and the current sent along the ab-plane (I // ab).
Figure 1 shows the zero field resistivity while the insets show the magnetoresistivity at selected temperatures of a $La_{1.94}Sr_{0.06}CuO_4$ thin film. This $La_{1.94}Sr_{0.06}CuO_4$ sample has a T_c of 3.8 K and is therefore situated very close to the lower edge of the superconducting phase in the (T,x)-phase diagram (Fig. 3). Together with the onset of superconductivity with doping, a large positive magnetoresistivity is observed.

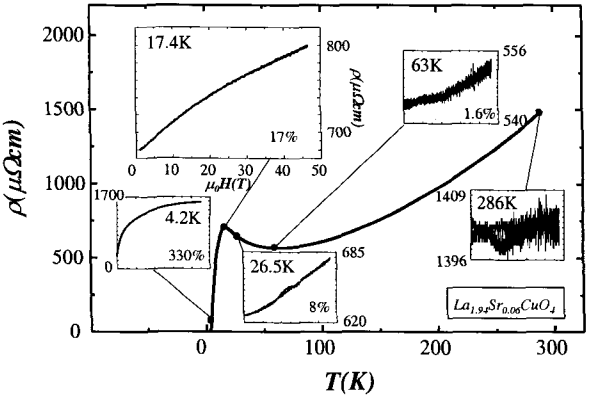

Figure 1: Resistivity as a function of the temperature at zero field for $La_{1.94}Sr_{0.06}CuO_4$. The insets show the magneto-resistivity in fields up to 50 T at different temperatures.

At first glance, one might assume that the magnetoresistivity at temperatures close to T_c is associated with the field-induced suppression of superconducting fluctuations. For conventional superconductors, typical fields for a complete suppression of fluctuations should not exceed the paramagnetic limit $\mu_0 H_p = k_B T_c/\mu_B$ in any case. However, the $La_{1.94}Sr_{0.06}CuO_4$ system shows, at 4.2 K, a magnetoresistivity is not even saturated at 50 T, a field value which is almost a decade higher than the conventional paramagnetic limit of $\mu_0 H_p$ = 6 T for this sample. The more detailed data show that at 26 K, which is 7 times T_c, the magnetoresistivity at 50 T (8%) is still substantially higher than for a non-superconducting $La_{1.955}Sr_{0.045}CuO_4$ sample (~1%) (see Ref. [7]). This observation rules out the possibility that the suppression of ordinary superconducting fluctuations causes the excess magnetoresistivity, as kinds of fluctuations typically exists only up to $2T_c$, typically.[8] It is probable that, at 4.2 K, the magnetic field destroys the superconducting regions and induces, at the same time, a magnetoresistivity of a different origin. In this respect, even the 50 T data might be not representative of the normal state of high T_c-compounds yet. At high temperatures, like at 286 K, the magnetoresistivity for superconducting and non-superconducting samples is comparable. Similar considerations are also valid for $La_{1.9}Sr_{0.1}CuO_4$ (T_c = 18 K).

Figure 2 shows the amplitude of the magnetoresistivity as a function of the temperature, presented in logarithmic coordinates for $La_{1.94}Sr_{0.06}CuO_4$, $La_{1.9}Sr_{0.1}CuO_4$ and $La_{1.8}Sr_{0.2}CuO_4$. We observe a lowering of the magnetoresistivity with temperature following a similar power-law for $La_{1.94}Sr_{0.06}CuO_4$ and $La_{1.9}Sr_{0.1}CuO_4$. The value of the power is close to 3/2, which may reflect the one-dimensional character of the system, at least this is the meaning of the power 3/2 for the temperature dependence of fluctuations in conventional superconductors.[8]

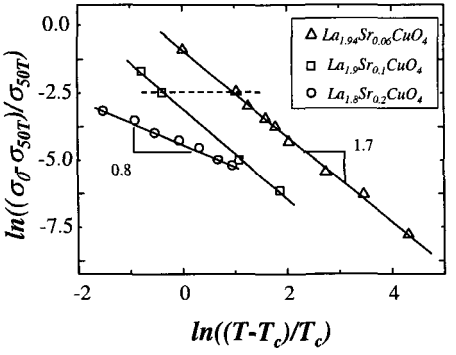

Figure 2: The change in conductivity as a function of the applied magnetic field at different temperatures for samples $La_{1.94}Sr_{0.06}CuO_4$, $La_{1.9}Sr_{0.1}CuO_4$ and $La_{1.8}Sr_{0.2}CuO_4$.

The magnetoresistivity of the weakly overdoped $La_{1.8}Sr_{0.2}CuO_4$ sample decreases more slowly with increasing temperature, but it can be described by a power-law as well. The power (0.8) is close to 1/2, referring to two-dimensional superconductivity in conventional systems. The observed dimensionalities are in good agreement with stripe models. From the above analysis, we can derive formally the temperature $T_{1\%}$ below which the magnetoresistivity amplitude at 50 T is less then 1%. $T_{1\%}$ for the different samples, together with the fitted gap data,[9] is added into the (T,x)-phase diagram shown in Figure 3. The experimentally determined minima in the temperature dependent resistivity curves T_{MI}, characterizing the metal to insulator-like transition, are also given in the figure. While $T_{1\%}$ mainly follows T_c for under-doped systems, it is noticeably diminished close to the T*-line for slightly overdoped systems in agreement with our previous results. The shaded region in the phase diagram, limited by $T_{1\%}$, corresponds to the temperature domain where an excess magnetoresistivity is observed. It has an abrupt border at the lower edge of the superconducting phase. These arguments favor the idea that the excess magnetoresistivity is related both to the superconducting phase and the pseudogap. The magnetoresistivity might, therefore, reflect the behavior of precursor pairs in a magnetic field. Emery and Kivelson[10] determine two temperatures, one temperature below which pairing becomes significant locally, one below which global phase coherence is possible.[1] In fact,

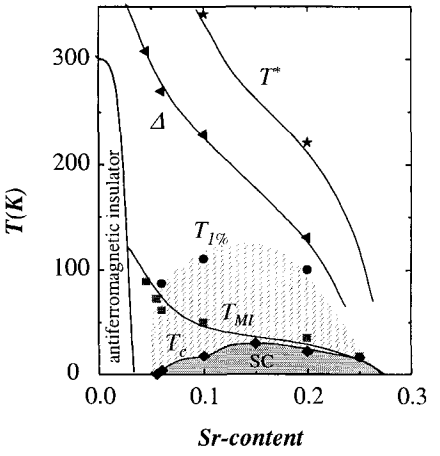

Figure 3: (T, x)-phase diagram for the $La_{2-x}Sr_xCuO_4$ system. The pseudogap Δ, the temperature at which the pseudogap opens T^*, the critical temperature T_c, the temperature of the metal to insulator-like transition T_{MI} and the temperature $T_{1\%}$ at which the magnetoresistivity at 50 T is less than 1% are indicated in the figure.

the $T_{1\%}(x)$ line could be then situated in the area below their intersecting pre-pairing and phase coherence lines.

Acknowledgments

The Belgian IUAP, the Flemish GOA and FWO-programs have supported this work. J.V. is a postdoctoral fellow of the FWO - Vlaanderen.

References

1. V. J. Emery and S. A. Kivelson, *Nature* **374**, 434 (1995).
2. M. Kugler *et al., Phys. Rev. Lett.* **86**, 4911 (2001).
3. A. G. Loeser *et al., Science* **273**, 325 (1996).
4. H. Ding *et al., Nature* **382**, 51 (1996).
5. P. Wagner *et al., Physica C* **356**, 107 (2001).
6. F. Herlach *et al., Physica B* **216**, 161 (1996).
7. L. Weckhuysen *et al.*, submitted to *Phys. Rev. B.*
8. W. Buckel, *Supraleitung Grundlagen und Anwendungen, Physik Verlag*, ISBN 3-87664-084-9 (1984).
9. V. V. Moshchalkov *et al., Europhys. Lett.* **46**, 75 (1999), *Phys. Rev. B* **64** (2001) in press.
10. V. J. Emery and S. A. Kivelson, *Cond-mat/9902179* (1999).

Part VI

Magnetism and Magnetic Phenomena

This page is intentionally left blank

RESISTIVITY AND PENETRATION DEPTH MEASUREMENTS OF ORGANIC SUPERCONDUCTORS IN HIGH MAGNETIC FIELDS USING A TUNNEL DIODE OSCILLATOR

C.C. AGOSTA, T. COFFEY, Z. BAYINDIR, I. MIHUT, and C. MARTIN
Physics Dept., Clark University, 950 Main S, Worcester MA 01610, USA
E-mail: cagosta@clarku.edu

M. TOKUMOTO
Electrotechnical Institute, Tskuba, Japan

We have made measurements of resistivity and penetration depth in dc-and pulsed-magnetic fields of the organic superconductors α-$(ET)_2NH_4Hg(SCN)_4$, and κ-$(ET)_2Cu(NCS)_2$ using a resonant rf circuit powered by a tunnel diode oscillator (TDO). We compare the critical fields as measured by resistivity, and the TDO. All the superconductors we have studied have anisotropic critical fields with a ratio $H_{C2}//$ to $H_{C2}\perp$ of 5-17. In κ-$(ET)_2Cu(NCS)_2$, we observed an almost monotonic increase in the parallel critical fields up to 24 T at 390 mK, and a sharp cusp in the critical field as a function of angle when the sample is parallel to the magnetic field. This suggests that the superconducting layers are only Josephson-coupled and the superconductivity is two-dimensional (2D). Another salt, α-$(ET)_2NH_4HG(SCN)_4$, shows similar cusp behavior, but this material shows evidence of extreme Pauli limiting when the field is turned parallel to the conducting layers.

1 Introduction

Many of the superconducting materials that are of interest in the current literature are lower dimensional, including the high temperature cuprates, the borocarbides, intercolated graphites, and the organic superconductors. We have measured critical magnetic fields in two highly anisotropic organic conductors. Under the influence of a magnetic field, superconductivity is normally destroyed by orbital effects as magnetic vortices form in the bulk. These orbital effects can be reduced in an anisotropic superconductor by orienting the conducting planes of the conductor parallel to the magnetic field. In this orientation, it is energetically favorable for the magnetic field lines to pass through the insulating layers of the sample and not form vorticies in the superconducting layers. By eliminating the orbital effects, the superconducting state can survive to higher fields. The next obvious limit to the superconducting state is the when the magnetic energy necessary needed to flip one of the spins of a Cooper pair, $\sqrt{2}\mu_B H$, equals the superconducting energy gap.[1] If this limit is reached, then H_{c2} should be directly proportional to the energy gap.

Our results show that in one of the above superconductors, the parallel critical field is Pauli paramagnetic limited over all of its field-temperature (HT) phase diagram. The other material has a more complicated phase diagram that has

prompted another group to suggest that it enters a Fulde-Ferrell-Larkin-Olchinnokov (FFLO) state,[2] although we do not interpret the data in the same way.

2 Experimental

The critical fields were measured using a tunnel diode oscillator (TDO) method that has been described elsewhere.[3] This method involves placing the sample in the coil of a self resonant tank circuit and measuring the frequency and amplitude shifts as the applied magnetic field is changed. In the normal state, the change in skin depth of the sample changes the effective inductance of the coil, which we measure as a frequency shift. In the mixed state, the oscillating magnetic field from the coil sets up screening currents that apply a force the vorticies on the surface of the sample. When the vorticies are perpendicular to the conducting planes of the sample, the vorticies can be moved easily. In the case where the vorticies are parallel to the conducting layers of the sample, the vorticies are strongly pinned and do not move easily. The movement of the vorticies is detected because the movement allows the rf field to penetrate, and again this change in penetration changes the effective area of the inductor and shifts the frequency. In all cases, we also measure the amplitude, which indicates the amount of dissipation in the system.

The samples were various irregular sizes ranging from 1 x 1 x 0.5 mm^3 to 0.5 x 0.5 x 0.1 mm^3. The experiments were carried out in three different magnet systems. At Clark University, we used a resistive dc magnet with a maximum field of 1 tesla (T) for low fields and a pulsed magnetic field capable of generating 50 T for our high field work. In both venues a ^{3}He insert cooled the samples down to 400 mK. For lower temperatures, we used the dilution refrigerator at the National High Magnetic Field Laboratory in Tallahassee. In all the apparatus the sample was placed on a rotating platform that could be positioned with a precision of 0.25° or better by turning a micrometer at the top of the cryostat. The samples were carefully placed inside the coil and help in place with packed Teflon tape. As always, we avoided using grease which tends to add stresses to the sample.

3 Results

In Fig. 1 we show the penetration depth (proportional to the frequency shift) as a function of applied magnetic field in the sample α-$(ET)_2NH_4Hg(SCN)_4$ [NH4] with the applied magnetic field parallel and perpendicular to the conducting planes. It is clear in this normalized plot that it is much harder to move the vorticies and hence penetrate the sample when the field is aligned parallel to the sample layers. A similar plot in Fig. 2 shows the amplitude signal plotted with the penetration depth signal. The initial penetration, where there is negative curvature, is a region that has been shown to have a $\sqrt{H}$ dependence.[4] Fitting to this functional form, it is possible to recover the restoring force holding the vortices to their pinning centers. We have

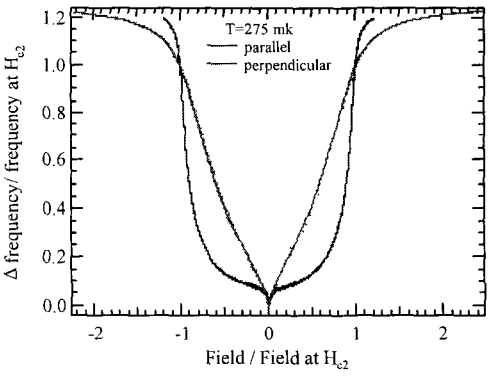

Figure 1: The penetration, perpendicular and parallel to the conducting planes.

not yet done this calculation. In contrast to the penetration depth, the amplitude follows a curve that looks similar to a resistive measurement of the critical field.

At the superconducting transition the two measurements, the penetration and the dissipation, converge. This behavior is always expected in a measurement where the skin depth is less than the sample size, because in the normal state both the penetration (frequency shift) and the dissipation (amplitude) measure the same quantity. Also, as is explained by Coffey and Clem,[5] the ratio η/κ, where κ is the restoring force and η is the viscosity, defines a characteristic relaxation time for the vorticies. The inverse of this relaxation time becomes less than the TDO frequency as the critical field is approached, which causes the frequency to be a measure of the dissipation.

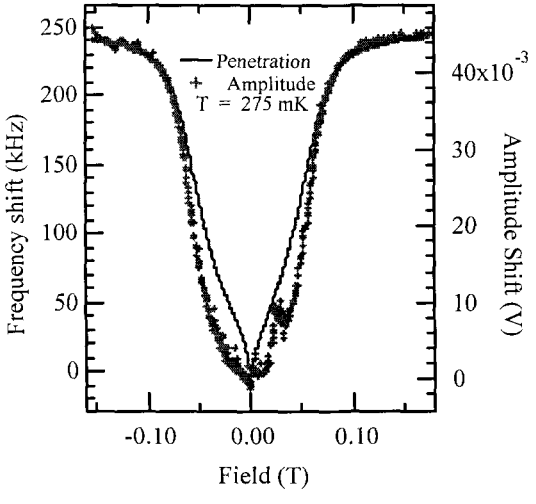

Figure 2: The penetration (frequency) and dissipation (amplitude) superimposed on each other.

The critical field as a function of angle follows the functional form derived by Tinkham[6] and is shown in in Fig. 3. From the data one can calculate that the critical field anisotropy is ~14. Normally we could use this data to calculate the anisotropy in the coherence length, but we will discuss why this is not a good idea below. Next in Fig. 4, we present the critical field as function of temperature with the applied field perpendicular the layers.

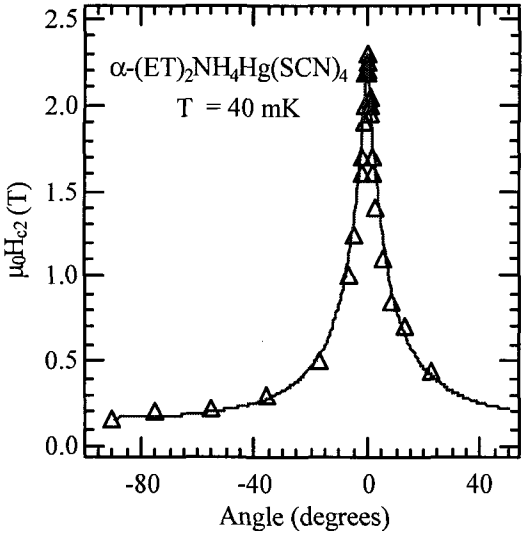

Figure 3: The critical field versus angle. The solid line is a fit using the Tinkham 2D formula.

Apart from the slight positive curvature, this data follows roughly what is expected from Ginsberg Landau theory. In the parallel direction, however, the critical field is saturated for more than half of the phase diagram as seen in Fig. 4. We interpret this saturation field as the Pauli paramagnetic limit (PPL). Apparently, we have been able to turn off the orbital effects effectively and reached the PPL, which depends only on the energy gap. Although the BCS value of the PPL, 1.8 T, is close to the measured saturation of the critical field, 2.2 T, we can use the reasoning of Zou *et al.*[7], and McKenzie[8] to calculate the PPL from other measurements of the superconducting properties. This calculation

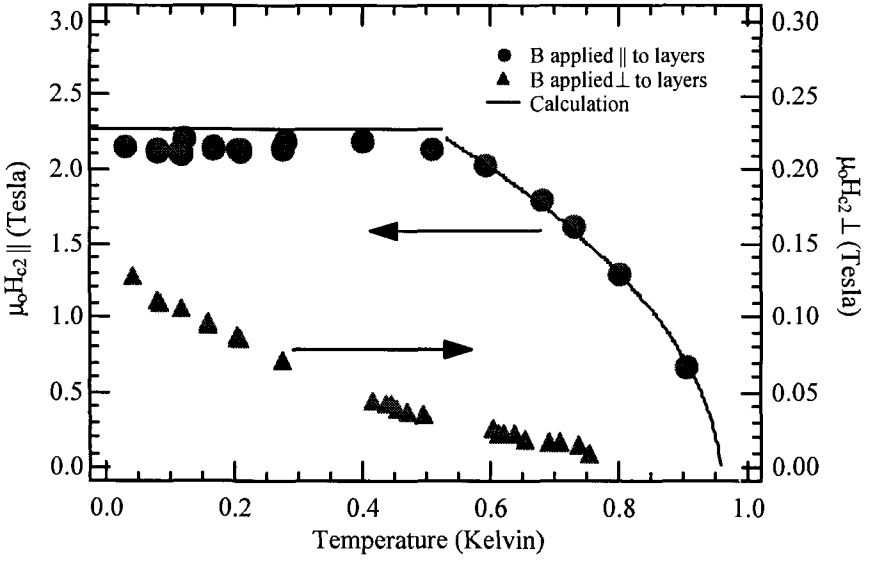

Figure 4: The critical fields with the applied magnetic field perpendicular and parallel to the conducting planes. Notice that the perpendicular data is expanded 10x in the y direction.

yields a zero temperature critical field value equal to 2.2 T within our margin of error. Starting with this zero temperature estimation, we can use the BCS energy gap function[6] to find the temperature dependence of the critical field, assuming the PPL is proportional to the energy gap over the whole temperature range. The good agreement between this theory and the experiment is shown in Fig. 4. More details of this calculation will be presented in a forthcoming paper.

In the compound κ-$(ET)_2Cu(NCS)_2$ (CuNCS) the situation is quite different. The perpendicular critical fields have been discussed at length elsewhere.[9] We find that the angular dependence follows the Tinkham formula as in NH4, but as in the case above, this does not mean that critical fields are the result of orbital processes alone. The difference between this salt and the NH4 salt is obvious in the phase diagram shown in Fig. 5. There is a change in slope near 18T, close to the BCS PPL in this material, but the critical field continues to rise as the temperature is lowered, at least down to 0.4 K, the limit of our cryogenic system.

Another group with similar data claims that the shape of the critical field phase diagram coupled with the signature of a first order phase transition in the frequency verses field sweeps suggests that the low temperature phase is the FFLO state. We do not come to the same conclusion with our data. One striking difference between this CuNCS data and the NH4 sample is seen is Fig. 6. Here it is shown that the resistance, represented by the amplitude, and the frequency shift have the same behavior as a function of field. We must conclude that we are only measuring dissipation in this sample. Furthermore, if we carefully subtract the background signal, which is significant for this large field range, we obtain the other result shown in Fig. 6, which looks like a standard superconducting transition measured using resistance, again consistent with a dissipation measurement. There is no evidence of a first order transition before H_{c2}.

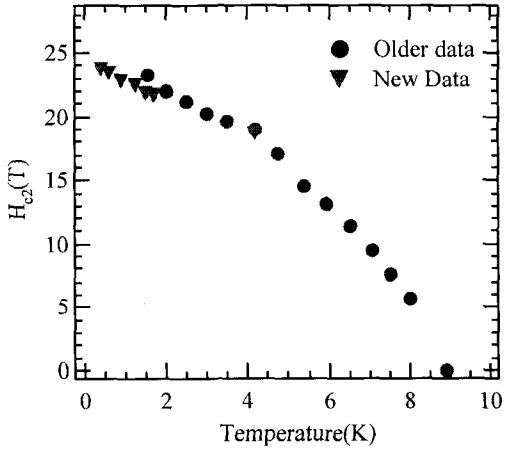

Figure 5: The parallel critical field in CuNCS.

Although it is clear from our data that the FFLO state does not exist, our samples may not be clean enough to see the FFLO state, which is sensitive to spin orbit scattering. On the other hand, the data of Singleton are not entirely consistent with the FFLO state. In particular we do not understand why the penetration depth would increase linearly and not as $\sqrt{H}$ at low fields in

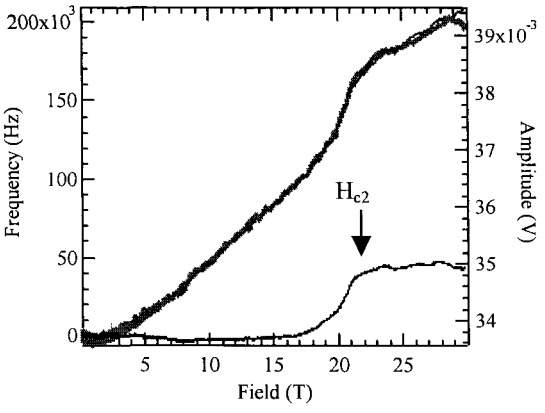

Figure 6: The lines with the large slope represent the frequency and amplitude and are barely distinguishable. When the background is subtracted from the data, it looks like a simple resistive transition as represented by the lower line that has zero slope at low fields.

Singleton's data. We look forward to doing these measurements again with cleaner samples, to see if we can understand the discrepancy between our measurements and others.

We have measured the critical fields perpendicular and parallel to the conducting planes in two organic superconductors. In the NH4 compound we were able to turn off the orbital contribution to the superconducting state and measure the Pauli paramagnetic limit. In essence, this is a measurement of the superconducting gap in this material. In the second organic superconductor the data is not as clear. We do not think we have reached the Pauli paramagnetic limit, and we also do not believe that the superconducting state at low temperatures is a FFLO state.

We would like to acknowledge the NSF Grant #9805784 and the NHMFL for support of this work.

References

1. A. M. Clogston, *Phys. Rev. Lett.* **9**, 266 (1962).
2. J. A. Symington *et al.*, *Preprint* (2000).
3. T. Coffey *et al.*, *Rev. Sci. Instrum.* **71**, 4600 (2000).
4. P. A. Mansky *et al.*, *Phys. Rev. B* **50**, 15929 (1994) and references therein.
5. M. W. Coffey and J. R. *Clem, Phys. Rev.* Lett. **67**, 386 (1991).
6. M. Tinkham, *Introduction to Superconductivity*, (McGraw-Hill, NY, 1996).
7. F. Zuo *et al.*, *Phys. Rev. B* **61**, 750 (2000).
8. R. McKenzie, *cond-mat*/9905044 v2 (1999).
9. C. Mielke *et al.*, *J. Phys.: Condens. Matt.* **13**, October (2001).

THEORETICAL OVERVIEW OF SUPERCONDUCTIVITY IN STRONTIUM RUTHENATE

D. F. AGTERBERG

Department of Physics, University of Wisconsin – Milwaukee

P.O. Box 413, Milwaukee, WI 53201

E-mail: agterber@uwm.edu

An overview of the phenomenological and microscopic theory of the superconducting state in Sr_2RuO_4 is presented. Existing experimental evidence will be used to demonstrate that the superconducting state is a 2D analogue of the Anderson Brinkman Morel superfluid ^3He state. A discussion of the microscopic theory will be presented that focuses on the recent experimental observations that line-nodes exist in superconducting Sr_2RuO_4. These nodes come as a surprise since theory would predict a spin-triplet pairing state to be nodeless for this quasi-2D material. Finally, the consequences of magnetic fields on this pairing state will be described.

1 Introduction

The oxide Sr_2RuO_4 has a layered perovskite structure and was discovered to be superconducting with a T_c=1.35 K by Maeno *et al.* in 1994.[1] Since the original proposal of Rice and Sigrist that Sr_2RuO_4 is a spin-triplet superconductor ,[2] four key experiments have been carried out that illustrate this is indeed the case.[3] The Knight shift measurements of Ishida *et al.*[4] reveal that the spin susceptibility is unchanged upon entering the superconducting state; this is consistent with spin-triplet superconductivity. The Knight shift measurements have been confirmed by the spin polarized-neutron scattering measurements of Duffy *et al.*[5] The μSR experiments of Luke *et al.*[6] indicate that the superconducting state breaks time reversal symmetry. This implies that the order parameter must have more than one component.[6] Finally, measurements of Riseman *et al.*[7] and Kealey *et al.*[8] of the field distribution of the vortex lattice for the field along the four-fold symmetry axis are not consistent with a single-component order parameter but are consistent with a two-component order parameter. The observation of a two-component order parameter implies spin-triplet superconductivity if the interactions within an individual RuO_2 plane are primarily responsible for superconductivity.

The discovery of unconventional superconductivty in Sr_2RuO_4 makes it the ideal material in which to study unconventional superconductivity. It is the only established unconventional superconductor that satisfies the following three properties: (1) the normal state is well understood; (2) the electronic properties of the normal state are simple; and (3) it is easy to grow large, high-quality samples.[3] No other unconventional superconductor satisfies all these properties. In cuprates, (1) is not satisfied, in heavy fermion materials (2) is not satisfied, and in organics (3)

is not satisfied. Consequently, focusing efforts on this material will lead to rapid progress in understanding unconventional superconductors. In the following, an overview of the superconducting state will be given.

2 Order parameter of Sr_2RuO_4

Spin-triplet superconducting gap functions are described by a vector with an odd-parity momentum dependence: $\mathbf{d}(\mathbf{k})=-\mathbf{d}(-\mathbf{k})$ (see Refs. [9-10]). The three components of the vector correspond to the spin degrees of freedom of the Cooper pairs. Physically, $\mathbf{d}$ is orthogonal to the Cooper pair spin projection. Within the group theoretical classification scheme of Ref. [9], the most natural conclusion of the experiments discussed above is that the superconducting gap function belongs to the two-dimensional Γ_5^- representation (REP) of the tetragonal point group. For this REP the gap function is given by $\mathbf{d}(\mathbf{k},\mathbf{r})=\mathbf{z}[\eta_1(\mathbf{r})f_x(\mathbf{k}) +\eta_2(\mathbf{r})f_y(\mathbf{k})]$, where f_x and f_y share the same symmetry properties as k_x and k_y under the rotations of the tetragonal point group, and $[\eta_1(\mathbf{r}),\eta_1(\mathbf{r})]$ are the spatially dependent components of the order parameter. For a Fermi surface with cylindrical topology, weak-coupling theory predicts that in the homogeneous ground state $[\eta_1(\mathbf{r}),\eta_1(\mathbf{r})] \propto [1,i]$. This bulk order parameter is favored over other possibilities because it implies that there are no nodes in the quasi-particle gap and consequently maximizes the condensation energy. The relative phase factor of $\pi/2$ between f_x and f_y implies that the ground state breaks time reversal symmetry (this state will be called the chiral p-wave state).

The chiral p-wave state is selected by the four experiments described above. In particular, it is one of only two two-dimensional REPS of the tetragonal point group. The one-dimensional REPS are ruled out by μSr measurements and by measurements of the vortex lattice. Of these two two-dimensional REPS, one (Γ_5^+) corresponds to a spin-singlet order parameter and is ruled out by the Knight shift and spin-polarized neutron scattering measurements. Furthermore, the orientation of $\mathbf{d}$ is dictated by the Knight shift measurements. These measurements were conducted with the applied field in the basal plane. Since $\mathbf{d}$ is orthogonal to the spin projection of the Cooper pair,[9-10] these measurements are consistent with the gap function aligned along $\mathbf{z}$. This is the predicted orientation of $\mathbf{d}$ for the Γ_5^- REP, provided the pairing interactions are predominantly within a single RuO_2 plane.

From a group theoretical point of view, the homogeneous chiral p-wave state $[\mathbf{d}(\mathbf{k},\mathbf{r})=\mathbf{z}(f_x(\mathbf{k})+if_y(\mathbf{k}))]$ should be gapless on a Fermi surface with cylindrical topology. It has therefore come as a surprise that many recent measurements provide evidence for nodes.[11-14] Given the strong evidence for the chiral p-wave state, an understanding of this phenomenon should not abandon the underlying symmetry properties that were outlined in the previous paragraph. All proposed theoretical suggestions are in keeping with this philosophy.[15-18] Typically, line nodes are placed in the chiral gap function. For example, by multiplying the k_x+ik_y dependence by

k_x^2-k_y^2. The proposed gap functions belong the Γ_5^- REP and are thus consistent with the four key experiments described above. Most of these proposed gap functions are introduced phenomenologically, and there is little attempt to give a microscopic origin for the nodes. Given that nodes in a chiral p-wave gap function are accidental, it is important to develop a microscopic understanding of this incongruity to give credibility to such proposals. Such a microscopic understanding arises naturally for the chiral p-wave state, once the electronic structure of the normal state in taken into account. This theory (orbital dependent superconductivity) has been developed through two papers.[18-19] This theory relies only on the well understood electronic properties of the normal state. The normal state properties and the theory will be described in the next section.

3 Normal state and orbital dependent superconductivity

Measurements of the normal state properties show that, while it is clear that correlation effects are important, Sr_2RuO_4 is well described a quasi 2-D Fermi liquid. For example, the resistivity in all directions follows a T^2 behavior and the resistivity along and perpendicular to the c-axis differ by a factor of 850 (see Ref. [1]). Quantum oscillations show three Fermi surface sheets with a 2D topology that agrees well with band structure calculations.[20] In particular, band structure calculations give the correct shape of the Fermi surface, but predict an effective mass that is factor of four smaller than that observed.[21-22] These calculations reveal that the density of states near the Fermi surface are due mainly to the four Ru 4d electrons in the t_{2g} orbitals (d_{xy}, d_{xz}, and d_{yz}). There is a strong hybridization of these orbitals with O 2p orbitals giving rise to antibonding π bands. The resulting bands have three quasi-2D Fermi surface sheets labeled α, β, and γ. The quasi-2D nature of the electronic dispersion implies that the γ Fermi surface sheet is derived from xy Wannier functions while the α and β Fermi surface sheets are derived form xz and yz Wannier functions. This is due to the reflection symmetry of the ruthenium oxygen plane; this symmetry implies that there can be no in-plane hopping between xy and {xz ,yz} Wannier functions.

This ability to attribute the particular Fermi surface sheets to xy or {xz,yz} Wannier functions is the keystone to the development of orbital dependent superconductivity.[18-19] In a multi-band system, the superconducting state is described by a gap function for each band. These gap-functions are coupled though inter-band scattering matrix elements that describe the motion of Cooper pairs from one band to another. In most materials it is difficult to say anything about such inter-band scattering matrix elements without a detailed microscopic model. However, in Sr_2RuO_4 the poor overlap between xy and {xz,yz} Wannier functions implies that the associated inter-band scattering matrix elements must be smaller than the intra-band scattering matrix elements.[19] Furthermore, it has been observed

that the magnetic interactions in Sr_2RuO_4 have a very anisotropic orbital dependence.[23] Such interactions are likely to be responsible for the spin-triplet pairing state in Sr_2RuO_4. This implies that the intra-band scattering matrix elements for the bands stemming from xy and the {xz,yz} Wannier functions will have quite different magnitudes. The emerging physical picture for Sr_2RuO_4 is one in which the bulk of the condensation energy is due to superconductivity forming on one band while the induced pairing on the other bands is small. In the following it is assumed that the dominant pairing is in the γ Fermi surface sheet (which arises from the xy Wannier functions). The pairing on the α and β Fermi sheets is therefore induced. The physics that follows does not dependent critically in this assumption.

To understand how nodes can arise within a chiral-gap function for Sr_2RuO_4, a more detailed understanding of the inter-band scattering matrix elements between the γ and the $\{\alpha,\beta\}$ bands is required. In particular, the contribution to this matrix element is small for Cooper pairs in the xy Wannier functions scattering to Cooper pairs in the {xz,yz} functions within the same ruthenium oxygen plane.[19] Consequently, the inter-band pair scattering between two adjacent ruthenium-oxygen planes can dominate the total inter-band matrix element.[18] Zhitomirsky and Rice have shown that this inter-plane, inter-band scattering matrix element, coupled with the body-centered tetragonal structure of Sr_2RuO_4, implies that the induced gap on the α and β sheets has the form $\cos(k_zc/2)[\sin(k_xa/2)\cos(k_ya/2)\pm i\sin(k_ya/2)\cos(k_xa/2)]$ (see Ref. [18]). While the γ sheet is fully gapped, the α and β sheets have a small induced gap that has nodes at $k_zc=\pi$. The resulting state has many attractive features. It accounts for nodes even within a weak-coupling theory since the bulk of the condensation energy lies on the γ sheet which is fully gapped (in accord with weak-coupling arguments). Furthermore, the nodes on the $\{\alpha,\beta\}$ sheets are stable provided the inter-plane contribution is larger than the intra-plane contribution to the inter-band scattering matrix element. In the presence of an intra-plane, inter-band scattering matrix element, the position of the nodes on the $\{\alpha,\beta\}$ sheets of the Fermi surface can lie at arbitrary k_z values.

4 Properties of Sr_2RuO_4 in a magnetic field

Some of the most exciting and new physics of Sr_2RuO_4 should occur in the presence of a magnetic field. As mentioned previously, one of the major successes of this research field is the direct evidence for a two-component order parameter from studies of the square vortex lattice for the field along the c-axis.[7-8] The physics of Sr_2RuO_4 for fields in the basal plane is also expected to be very rich. It has been shown that there must exist *two* vortex lattice phases with a second order phase transition between them for applied fields along the in-plane (1,0,0) or (1,1,0) directions.[24] This is a consequence of the Γ_5^- REP itself and does not depend upon the details of any microscopic theory.[24] Evidence has been found for multiple

phases,[26] however, it is not clear whether the observed transitions have the same origin as that predicted in Ref. [24]. A puzzling experimental result is that the in-plane anisotropy of H_{c2} has been observed to be on the order of 3% at low temperatures.[25] This is much smaller than expected from theory.[10] However, an accidental cancellation of this anisotropy may occur due to contributions of opposite sign from the different electronic bands.[26]

Reference

1. Y. Maeno *et al., Nature* **372**, 532 (1994).
2. T. M. Rice and M. Sigrist, *J. Phys.: Con. Mat.* **7**, L643 (1995).
3. Y. Maeno, T. M. Rice and M. Sigrist, *Physics Today* **54**, 42 (2001).
4. K. Ishida *et al., Nature* **96**, 658 (1998).
5. J. A. Duffy *et al., Phys. Rev. Lett.* **85**, 5412 (2000).
6. G. M. Luke *et al., Nature* **394**, 558 (1998).
7. T. M. Riseman *et al., Nature* **396**, 242 (1998).
8. P. G. Kealey *et al., Phys. Rev. Lett.* **84**, 6094 (2000).
9. M. Sigrist and K. Ueda, *Rev. Mod. Phys.* **63**, 239 (1991).
10. L. P. Gor'kov, *Sov. Sci. Rev. Sect. A* **9**, 1 (1987).
11. S. Nishizaki, Y. Maeno and Z.Q. Mao, *J. Low Temp. Phys.* **117**, 1581 (1999).
12. K. Ishida *et al., Phys .Rev. Lett.* **84**, 5387 (2000).
13. I. Bonalde *et al., Phys. Rev. Lett.* **85**, 4775 (2000).
14. C. Lupien *et al., Phys. Rev. Lett.* **86**, 5986 (2001).
15. Y. Hasegawa, K. Machida and M. Ozaki, *J. Phys. Soc. Jpn.* **69**, 336 (2000).
16. M. J. Graf and A. V. Balatsky, *Phys. Rev. B* **62**, 9697 (2000).
17. H. Won and K. Maki, *Europhys. Lett.* **52**, 427 (2000).
18. M. E. Zhitomirsky and T. M. Rice, *Phys. Rev. Lett.* **87**, 057001 (2001).
19. D. F. Agterberg, T. M. Rice and M. Sigrist, *Phys. Rev. Lett.* **78**, 3374 (1997).
20. C. Bergemann *et al., Phys. Rev. Lett.* **84**, 2662 (2000).
21. T. Oguchi, *Phys. Rev. B* **51**, 1385 (1995).
22. D. J. Singh, *Phys. Rev. B* **52**, 1358 (1995).
23. T. Imai *et al., Phys. Rev. Lett.* **81**, 3006 (1998).
24. D. F. Agterberg, *Phys. Rev. Lett.* **80**, 5185 (1998).
25. Z. Q. Mao *et al., Phys. Rev. Lett.* **84**, 991 (2000).
26. D. F. Agterberg, *Phys. Rev. B* **64**, 052502 (2001).

THE MILLIMETRE-WAVE MAGNETO-OPTICAL RESPONSE OF Sr_2RuO_4

A. ARDAVAN, E. RZEPNIEWSKI, R. S. EDWARDS and J. SINGLETON

University of Oxford, Department of Physics, Clarendon Laboratory, Parks Road, Oxford OX1 3PU, UK

E-mail: arzhang.ardavan@physics.ox.ac.uk

Y. MAENO

Department of Physics, Kyoto University, Kyoto 606-8502

We report a study of the angle-dependent millimetre-wave magnetoconductivity of the *p*-wave triplet-paired perovskite superconductor Sr_2RuO_4. We find two harmonic series. We assign the first to interlayer cyclotron resonance of the β-Fermi surface and its harmonics, yielding a cyclotron effective mass of $m^{cr}_{\beta} = 4.25\ m_e$. We assign the second series, which contains only odd harmonics, to cyclotron resonance of the γ-Fermi surface, yielding a cyclotron effective mass of $m^{cr}_{\gamma} = 12.4\ m_e$. In addition, we find a very strong absorption mode in the presence of a magnetic field component parallel to the quasi-two-dimensional (Q2D) planes of the sample. Its dependence on the orientation of the magnetic field cannot be described in the context of conventional Q2D cyclotron resonance, and the origin of this mode is not yet clear.

Since Kohn and Luttinger pointed out that electron-electron interactions could mediate the formation of Cooper pairs with non-zero angular momentum,[1] there has been great interest in physical manifestations of this effect. One case is the layered perovskite Sr_2RuO_4, which is believed to form a *p*-wave triplet-paired superconducting state below 1.5 K (see Refs. [2-5]); this state is thought to be a two-dimensional analogue of the superfluid A-phase in ^{3}He (see Refs. [6,7]). Sr_2RuO_4 was the first layered perovskite superconductor discovered that does not contain Cu (see Ref. [2]) (although it now seems clear that the superconductivity in Sr_2RuO_4 is quite different in nature from the high-T_c superconductivity). The normal-state properties have been studied extensively using d.c. experimental techniques[8-14] and theoretically.[15-17] Below about 30 K, the electron system appears to be a coherent Fermi liquid. This, combined with the availability of high quality single crystals, makes Sr_2RuO_4 an ideal test material for unconventional superconductivity.

These considerations motivated us and others[21] to study the magneto-optical response of Sr_2RuO_4. The frequency range for such a measurement must be chosen carefully; the product of the cyclotron frequency and scattering time must exceed 1 for any resonant measurement, and the resonance position in magnetic field is linearly proportional to the cyclotron frequency for cyclotron resonance. Thus the lower bound on frequency is set by sample quality (scattering time) and the upper is set by the available magnetic field range. Our experiments were performed at 70

GHz; at this frequency, a quasiparticle with an effective mass of 10 m_e undergoes cyclotron resonance at a magnetic field of 25 T (where m_e is the free electron mass). We measured the high-frequency conductivity of a single crystal of Sr_2RuO_4 (T_c = 1.42 K) (see Ref. [22]), using a cavity perturbation technique. The sample was placed in a magnetic field antinode in a rectangular cavity of dimensions 6 by 3 by 1.5 mm resonating in the TE_{102} mode at 71 GHz. The sample was polished to a thickness of 50 μm in the c-axis direction and aligned such that the millimetre-wave magnetic field was polarized parallel to the highly conducting planes (perpendicular to the c-axis). In this configuration, we estimate that the dissipation in the sample is due to both in-plane and inter-plane currents (see Refs. [23-26] for discussion of the use of this geometry with layered materials). The quality factor of the cavity changes from 2500 to 1500 and the resonant frequency shifts by 130 MHz on introducing the sample. Quasi-static magnetic fields of up to 31 T were supplied by resistive magnets at NHMFL, Florida State University; temperatures down to 0.55 K were supplied by ^{3}He and ^{4}He cryostats.

We have shown in earlier work on other metals of reduced dimensionality (organic molecular metals),[25-26] that it is imperative that the dependence of the millimetre-wave response on the orientation of the quasistatic magnetic field is studied before assignments of the cause of any magneto-optical resonances are made. For features arising from cyclotron resonance around a quasi-two-dimensional (Q2D) Fermi surface, the resonant magnetic field, B_{res}, increases as the field is tilted by an angle θ away from the axis of the Fermi cylinder according to $B_{res} \propto 1/\cos\theta$. Features with a different angle dependence cannot be assigned to traditional Q2D cyclotron resonance.

In an angle-dependent study it is necessary to maintain the orientation of the sample with respect to the millimetre-wave field in the cavity while rotating the external quasistatic magnetic field; if the sample moves in the millimetre-wave field, the components of conductivity being probed change.[26] In practice, in high-field experiments this means that the entire cavity, with the sample inside, must be rotated through the quasistatic field, since the orientation of the quasistatic field is fixed.[27] We have designed a system and demonstrated its effectiveness in such measurements; it is described in detail elsewhere.[26-28]

Figure 1 shows the cavity transmission as a function of magnetic field up to 31 T for a range of steady field orientations, θ, between 0 and 70 degrees, where θ represents the angle between the steady field and the normal to the a-b plane; at 0 degrees, the steady field is parallel to the c-axis ([001]). A decrease in cavity transmission corresponds to an increase in sample conductivity. These are raw data, offset for clarity; there has been no background subtraction. There is a sharp feature close to 2 T in all traces, independent of angle; this is an artifact of our apparatus and is present in the absence of a sample.

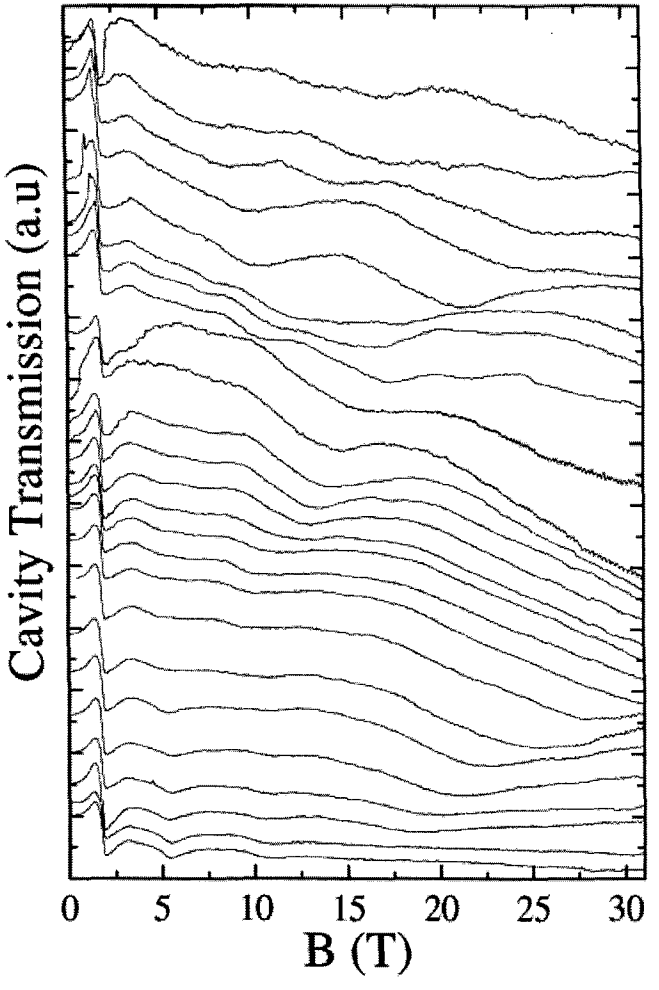

Figure 1: The cavity transmission as a function of magnetic field for 0 £ q £ 70. The temperature is 0.55 K. The millimetre-wave frequency is 71 GHz.

Several features can be seen developing with angle; their positions are plotted in Figure 2(a) as a function of θ. At low angles (lower traces in Figure 1), a series of resonances are visible below about 10 T, moving slowly to higher fields as θ increases (the θ = 0 trace is shown expanded in Figure 2(b)). These resonances are indicated by filled diamonds in Figure 2(a). At higher angles, another series (open circles on Figure 2(a)) is visible. In the θ = 7.5 degrees trace (third from the bottom

of Figure 1), a feature can be seen emerging at about 17 T; it moves very rapidly upward in field and intensifies with increasing θ (filled circles in Figure 2(a)). By θ = 22.5 degrees, the resonance moves above the accessible field range. However, its low-field tail is visible in the range 25 < θ < 40 degrees; the resonance appears to continue to intensify and move upward in field over this interval.

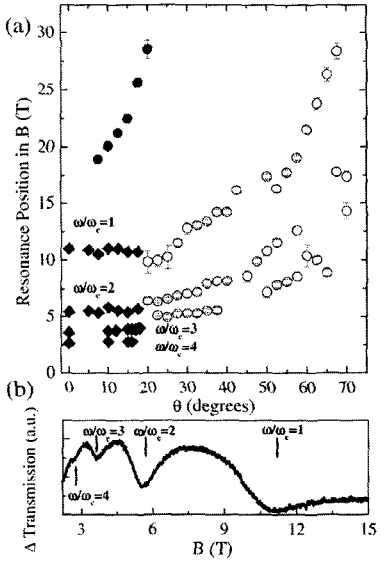

Figure 2: (a) Positions of resonances in the spectra of Figure 1 versus q. (b) A close-up of the cavity transmission as a function of magnetic field for θ = 0, showing the integer harmonic series.

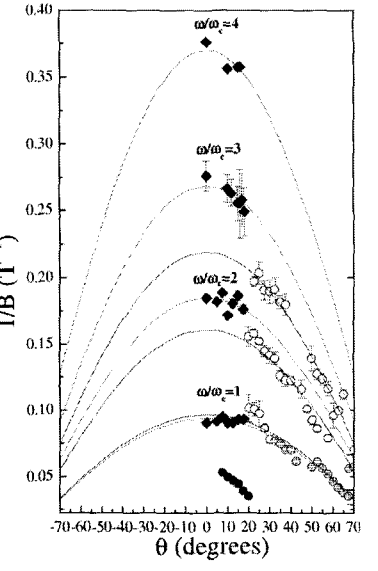

Figure 3: Resonance positions plotted against inverse magnetic field. The solid lines are fits to the equation $1/B_{res} = A_n \cos\theta$ with A_n as a parameter.

In Figure 3, the resonance positions are plotted against (1/B). The solid lines represent fits to the equation $1/B_{res} = A_n \cos\theta$ with A as a parameter, which represents the angle dependence expected for cyclotron resonance-like features. For a fundamental cyclotron resonance mode, $A = e\omega / m^{cr}$, where e is the electron charge, $\omega/2\pi$ is the measurement frequency and m^{cr} is the cyclotron mass. The open circles lie on curves described by $A_1 = 0.097 \pm 0.002$ T^{-1}, $A_2 = 0.160 \pm 0.002$ T^{-1}, $A_3 = 0.219 \pm 0.002$ T^{-1}. These lie in the ratio A_1: A_2: A_3 = 3:5:7, indicating that the open circles represent an odd-harmonic cyclotron resonance series, with a fundamental that lies above the accessible field range, and a cyclotron mass of $m^{cr}_{\gamma} = 12.4\ m_e$, where m_e is the free electron mass. The filled diamonds lie on a

curves with $A_1 = 0.094 \pm 0.002\ T^{-1}$, $A_2 = 0.185 \pm 0.002\ T^{-1}$, $A_3 = 268 \pm 0.002\ T^{-1}$, $A_4 = 0.37 \pm 0.01\ T^{-1}$. These are in the ratio A_1: A_2: A_3: A_4 = 1:2:3:4, indicating that the filled diamonds represent a harmonic series with a cyclotron mass of $m^{cr}{}_{\beta} = 4.25\ m_e$.

Harmonic series such as these are expected to occur in cyclotron resonance in materials with complex Fermi surfaces. Harmonics arise because the real-space velocity of charge carriers orbiting the Fermi surface, though periodic, is non-sinusoidal; each harmonic in the Fourier decomposition generates a cyclotron resonance harmonic.[30-32] The in-plane symmetry of the Fermi surface leads to the appearance of odd harmonics only for resonances measured in the in-plane conductivity,[31] while integer harmonic series are observed for resonances in the inter-plane conductivity.[30] Thus we can assign the first series (open circles) to an in-plane cyclotron resonance and the second (filled diamonds) to an inter-plane resonance.

The Fermi surface of Sr_2RuO_4 comprises three Q2D sections, conventionally labeled α, β, γ(see Refs. [2–5]. Band-structure calculations show that the Fermi velocity varies strongly around the γsheet.[33] Earlier studies demonstrate that the γsheet has weak interlayer dispersion,[14] a large variation of Fermi velocity [33] and a thermodynamic effective mass of $m^*_{\gamma} = 14.6\ m_e$ (see Ref. [8]). We assign the odd harmonic series, with cyclotron mass 12.4 m_e, to cyclotron resonance of the γsheet. The β sheet dominates the interlayer conductivity and is of a form that generates strong harmonic content in the interlayer velocity.[14] Its thermodynamic effective mass is $m^*_{\beta} = 7.5\ m_e$ (see Ref. [8]). We assign the integer harmonic series, with cyclotron mass 12.4 m_e, to cyclotron resonance of the β sheet. As yet, the origin of the resonance with anomalous angle dependence (filled circles in Figures 2 and 3) is unknown. The volume of the α sheet, and consequently its contribution to the conductivity, are rather small;[14] there is no strong evidence for features arising from this Fermi surface.

In summary, we have measured cyclotron resonance harmonic series arising from the two largest Fermi surfaces in Sr_2RuO_4. The cyclotron masses that we obtain are consistently lower than the thermodynamic masses obtained from transport and magnetization measurements. This is in support of the argument that the cyclotron masses are renormalized over the bare band masses by different interactions from thermodynamic effective masses.[8,15-20] In addition we observe a resonance mode with an anomalous magnetic field angle dependence. For certain field orientations, this mode dominates the high-frequency absorption in Sr_2RuO_4; it is therefore of some importance to identify its origin.

References

1. W. Kohn and J. M. Luttinger, *Phys. Rev. Lett.* **15**, 524 (1965).

2. Y. Maeno *et al.*, *Nature* **372**, 532 (1994).
3. G. M. Luke *et al.*, *Nature* **394**, 558 (1998).
4. A. P. Mackenzie *et. al*, *Phys. Rev. Lett.* **80**, 161 (1998).
5. K. Ishida *et al.*, *Nature* **396**, 658 (1998).
6. T. M. Rice and M. Sigrist, *J. Phys. Cond. Mat.* **7**, L643 (1995).
7. M. Rice, *Nature* **396**, 627 (1998).
8. A. P. Mackenzie *et al.*, *Phys. Rev. Lett.* **76**, 3786 (1996); A. P. Mackenzie *et al., J. Phys. Soc. Jpn.* **67**, 385 (1998).
9. A. P. Mackenzie *et al.*, *Phys. Rev. B* **54**, 7425 (1996).
10. Y. Maeno *et al.*, *J. Phys. Soc. Japan* **66**, 1405 (1997).
11. N. E. Hussey *et al.*, *Phys. Rev. B* **57**, 5505 (1998).
12. E. Ohmichi *et al.*, *J. Phys. Soc. Japan* **68**, 24 (1999).
13. E. Ohmichi *et al.*, *Phys. Rev. B* **59**, 7263 (1999).
14. C. Bergemann *et al.*, *Phys. Rev. Lett.* **84**, 2662 (2000).
15. T. Oguchi, *Phys. Rev. B* **51**, 1385 (1995).
16. P. K. de Boer and R.A. de Groot, *Phys. Rev. B* **59**, 9894 (1999).
17. S. R. Julian *et al.*, *Physica B* **261**, 928 (1999).
18. J. Singleton *et al.*, *Phys. Rev. Lett.* **68**, 2500 (1992).
19. K. F. Quader *et al.*, *Phys. Rev. B* **36**, 156 (1987); A. J. Leggett, Ann. Phys. **46**, 76 (1968); A. J. Leggett, *Phys. Rev.* **140A**, 1869 (1965); W. Kohn, *Phys. Rev.* **123**, 1242 (1961).
20. K. Kanki and K. Yamada, *J. Phys. Soc. Japan* **66**, 1103 (1997).
21. S. Hill *et al.*, *Phys. Rev. Lett.*, **84**, 3374 (2000).
22. Z. Q. Mao, Y. Maeno and H. Fukazawa, *Matt. Res. Bull.* **35**, 11 (2000): a detailed description of the crystal growth of Sr_2RuO_4.
23. S. Hill *et al.*, in Physical Phenomena in High Magnetic Fields-III, ed L. Gor'kov, Z. Fisk and R. Schrieffer, 218 (World Scientific, Singapore, 1999) and references therein.
24. A. Polisskii *et al.*, *J. Phys. Cond. Mat.* **8**, L195-L201 (1996).
25. J. Singleton, Rep. *Prog. Phys.* **63**, 1111 (2000).
26. A. Ardavan *et al.*, *Phys. Rev. Lett.* **81**, 713 (1998).
27. M. D. Bird *et al.*, *Physica B* **216**, 193 (1996).
28. J. M. Schrama *et al.*, *Proc. SPIE* **3828**, 311 (1999).
29. See for example *Optical Properties of Semiconductors*, ed. T. S. Moss and M. Balkanski, (Elsevier, Amsterdam), Chapters 6,7 and 11.
30. S. Hill, *Phys. Rev. B* **55**, 4931 (1997).
31. S. J. Blundell *et al.*, *Phys. Rev. B* **53**, 5609 (1997).
32. S. J. Blundell *et al.*, *Phys. Rev. B Rapid Comm.* **55**, R6129 (1997).
33. I. I. Mazin and D. J. Singh, *Phys. Rev. Lett.* **79**, 733 (1997).

MAGNETIC PROPERTIES OF HEAVY FERMION SUPERCONDUCTORS CERHIN$_5$ AND CE$_2$RHIN$_8$

WEI BAO[1], G. AEPPLI[2], A.D. CHRISTIANSON[1], Z. FISK[3,1], M.F. HUNDLEY[1], A.H. LACERDA[1], J.W. LYNN[4], P.G. PAGLIUSO[1], J.L. SARRO[1], J.D. THOMPSON[1]

[1] *Los Alamos National Laboratory, Los Alamos, NM 87545, USA*
[2] *NEC Research, 4 Independence Way, Princeton, NJ 08540, USA*
[3] *Florida State University, Tallahassee, FL 32306, USA*
[4] *National Institute of Standards and Technology, Gaithersburg, MD 20899, USA*

Some recent neutron scattering works on CeRhIn$_5$ and Ce$_2$RhIn$_8$, together with related resistivity and specific heat measurements, are summarized. In spite of its layered crystal structure, CeRhIn$_5$ is shown to be 3 dimensional both magnetically and in transport. We also find that the Fisher-Langer behavior is closely followed in CeRhIn$_5$. This may circumvent the Kondo lattice model and support applying established Fermi-liquid superconductivity theory to heavy fermion superconductors.

1 Introduction

Three materials, CeMIn$_5$ (M=Rh, Ir, Co), of the same HoCoGa$_5$ crystal structure recently have been added to the list of Ce-based heavy fermion superconductors[1,2,3]. Previously, the list contained only one ambient pressure superconductor, CeCu$_2$Si$_2$ (T_C = 0.7 K)[4]. The others, CeCu$_2$Ge$_2$ (T_C = 0.64 K at 10 GPa), CePd$_2$Si$_2$ (T_C = 0.5 K at 2.5 GPa), CeRh$_2$Si$_2$ (T_C = 0.35 K at 0.9 GPa) and CeIn$_3$ (T_C = 0.2 K at 2.5 GPa)[5,6,7,8], superconduct only under high pressures. Of the three new materials, the Ir and Co compounds are ambient pressure superconductors with T_C = 0.4 K and 2.3 K respectively, while the Rh compound superconducts at 2.1 K above 1.6 GPa[9].

CeMIn$_5$ is structurally related to the previously known superconductor CeIn$_3$ by alternately stacking CeIn$_3$ and MIn$_2$ layers. Particularly, it is interesting to compare CeIn$_3$ and CeRhIn$_5$, both of which are antiferromagnets at ambient pressure. The optimal T_C of the layered compound is 10 times that for cubic CeIn$_3$. In terms of the strength of magnetic interactions as represented by the Néel temperature, T_C/T_N of CeRhIn$_5$ is 28 times that for CeIn$_3$. In term of the Fermi energy via the Sommerfeld constant, the enhancement of $T_C/E_f \sim T_C\gamma$ from CeIn$_3$ to CeRhIn$_5$ is an even more impressive value of 35. Monthoux and Lonzarich recently argued that 2-dimensional (2D) magnetic fluctuations are superior to 3D magnetic fluctuations in elevating T_C[10]. It is,

therefore, natural to ask whether this mechanism is working for CeMIn$_5$. de Haas-van Alphen (dHvA) measurements on CeRhIn$_5$, CeIrIn$_5$ and CeCoIn$_5$ have provided evidence for the existence of 2D Fermi sheets in addition to 3D ones[11,12,13]. Aspects of magnetic measurements, such as a small β critical exponent, have been used to suggest magnetic 2-dimensionality. However, we are going to show with neutron scattering and bulk measurements that at least for CeRhIn$_5$, both magnetic and transport properties are 3D[14]. Furthermore, the close relation among resistivity, specific heat and antiferromagnetic fluctuations in the neighborhood of T_N, in the fashion illustrated by Fisher and Langer, indicates the Kondo lattice of CeRhIn$_5$ has been renormalized at low temperatures to weakly coupled subsystems of local magnetic moments and heavy fermions. If this holds true at the critical pressure for CeRhIn$_5$ and also true for CeIrIn$_5$ and CeCoIn$_5$, one can bypass theoretical difficulties possed by the Kondo lattice model, and directly treat superconductivity in these new heavy fermion materials with a Fermi liquid model using the experimentally measured magnetic fluctuation spectra for the bosons.

2 Experimental Results and Discussions

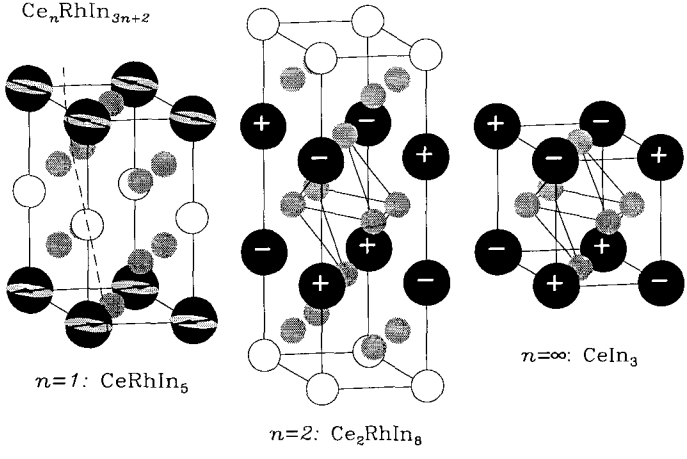

Figure 1. Magnetic structures of Ce$_n$RhIn$_{3n+2}$. The solid circle denotes Ce with arrow or signs indicating moment orientation. The shaded circle denotes In, the open circle Rh. Magnetic moment per Ce is 0.37μ_B for CeRhIn$_5$[15], 0.55μ_B for Ce$_2$RhIn$_8$[16] and 0.48-65μ_B for CeIn$_3$[17,18]. From ref. [16].

Fig. 1 shows magnetic structures of Ce_nRhIn_{3n+2} (n=1, 2 and ∞) determined with neutron diffraction. Notice that the nearest neighbor (n.n.) antiferromagnetic pairs of the three materials have identical local environments. The pairs separated by the $RhIn_2$ layer are collinear for n=2 but are incommensurate for n=1. The incommensurate magnetic structure of $CeRhIn_5$ is found to transform to a commensurate one by a 2-3 T magnetic field applied in the layer at low T[19]. An additional incommensurate antiferromagnetic component appears below 1.4 K for Ce_2RhIn_8. They suggest competing magnetic interaction between the Ce pairs. The T-H phase diagram also reveals the Néel point as a multicritical point[19]. This explains the small β critical exponent.

Now let us address the dimensionality issue. Fig. 2 shows antiferromagnetic fluctuations along the c-axis for $CeRhIn_5$. There exists strong intensity modulation in step with magnetic Bragg peaks, which are marked by the crosses. This directly contradicts the idea that $CeRhIn_5$ is a formally 2D magnetic system. Magnetic correlation lengths along the c axis and in-plane have the same order of magnitude and evolve with temperature in a similar fashion. This also contradicts a 2D magnetic model for $CeRhIn_5$. From the correlation lengths, it is deduced that the magnetic interaction for the further

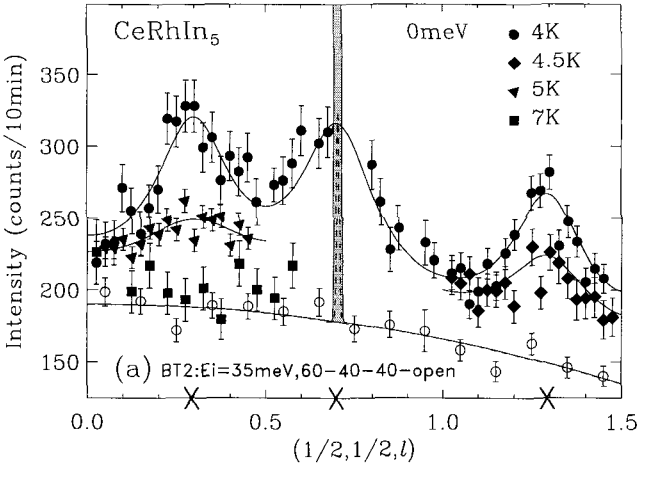

Figure 2. Instantaneous magnetic correlation function $\mathbf{S}(\mathbf{q})$ measured along the c axis at various temperatures. The open circles indicate background. From ref. [14].

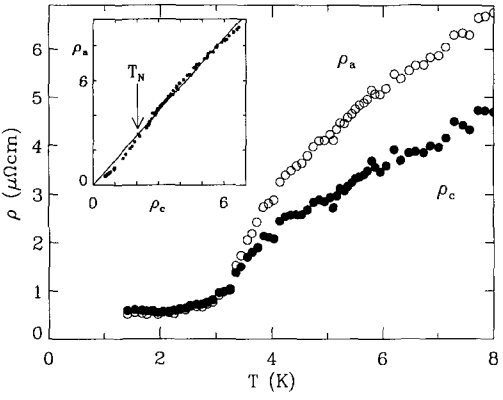

Figure 3. Resistivity measured with current along the a axis and the c axis respectively. From Ref. [14].

separated n.n. Ce pairs along the c axis is weaker than that for the n.n. Ce pairs along the a axis, consistent with a robust antiferromagnetic bond for the n.n. Ce pairs in the plane.

Fig. 3 shows resistivity measured with current in-plane and along the c axis for $CeRhIn_5$. At lowest temperatures, resistivity out of plane, ρ_c, is comparable to the in-plane ρ_a. At higher temperatures, ρ_c is even smaller than ρ_a. This clearly rules out for $CeRhIn_5$ 2D electronic transport, which requires $\rho_c \gg \rho_a$. Although there is 2D band at the Fermi energy as revealed in the dHvA experiments, 3D bands clearly dominate in transport.

The single impurity Kondo model of N electrons has very complex behavior at finite temperatures. It however renormalizes to a simple N-1 electron system at T=0. It is also possible for the Kondo lattice model, which describes a heavy fermion system, to renormalized to a simple system at low T. But a reliable theoretical prediction for possible states in a real material is difficult. Fig. 4 compares the intensity of antiferromagnetic fluctuations at magnetic Bragg point, derivative of resistivity, and magnetic part of specific heat for $CeRhIn_5$. These quantities are remarkably similar. Fisher and Langer[20] have considered a model which can be regarded as the Kondo lattice model at the small Kondo interaction limit and which can be solved with the Born approximation. They predict the behavior for the three quantities shown in Fig. 4. The Fisher-Langer theory is a great success for ferromagnets such as Fe[21] and Ni[22] and is reasonably successful for antiferromagnets such as PrB_6[23]. We

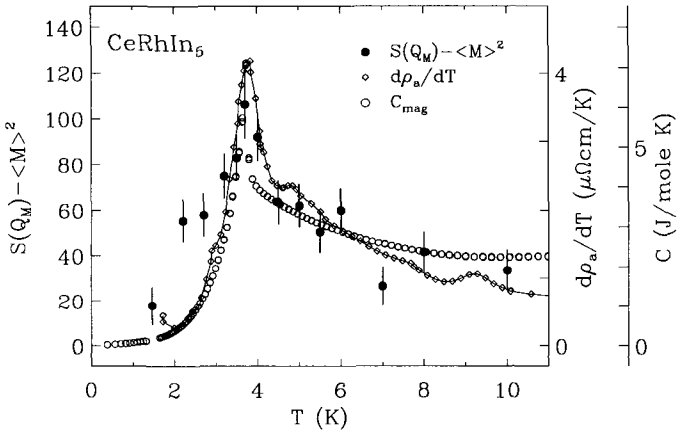

Figure 4. Intensity of magnetic fluctuations $\mathbf{S}(\mathbf{Q}_M) - \langle M \rangle^2$, derivative of resistivity, and magnetic specific heat as a function of temperature. From Ref. [14].

already know from specific heat that bare electrons are renormalized to heavy electrons in $CeRhIn_5$[1], and from neutron diffraction that magnetic moment of Ce ion has been renormalized to $0.37\mu_B$ at low temperatures[15]. The Fisher-Langer behavior in Fig. 4 indicates that the Kondo interaction in $CeRhIn_5$ has been renormalized to the small value limit at low T.

A fermion system weakly coupled to localized moments, whose magnetic excitation spectra can be measured with inelastic neutron scattering, is much easier for theoretical treatment than the Kondo lattice model. Established theory for superconductivity may be readily applied to such a system. The Fisher-Langer behavior, therefore, may be used as the indicator for heavy fermion materials which have approached such a tractable fixed point.

3 Summary

Magnetic structures of $CeRhIn_5$ and Ce_2RhIn_8 have been determined with neutron diffraction. Several phase transitions, including commensurate-incommensurate transitions, are induced by magnetic field applied in the basal plane. From neutron scattering measurement of the spatially dependent magnetic fluctuations and resistivities measured in the basal plane and along the c axis, $CeRhIn_5$ is concluded to be a 3D system both magnetically

and in transport. The Fisher-Langer behavior in $CeRhIn_5$ suggests that the Kondo lattice of this material is renormalized to heavy Fermi liquid weakly interacting with magnetic excitations of the local moments. Critical behavior of magnetic order, which exists in some heavy fermion materials, thus, can be used to probe the Kondo renormalization process.

Acknowledgments

We thank C.M. Varma, S.M. Shapiro, C. Broholm, M.E. Zhitomirsky, S.A. Trugman, J.M. Lawrence, A.V. Balatsky and D. Pines for useful discussions. Work at LANL was support by US Department of Energy. ZF acknowledges NSF support at FSU, and PGP acknowledges FAPESP-Brazil.

References

1. H. Hegger, et al., Phys. Rev. Lett. **84**, 4986 (2000).
2. C. Petrovic, et al., Europhys. Lett. **53**, 354 (2001).
3. C. Petrovic, et al., J. Phys. Condens. Mat. **13**, L337 (2001).
4. F. Steglich, et al., Phys. Rev. Lett. **43**, 1892 (1979).
5. D. Jaccard, K. Behnia, and J. Sierro, Phys. Lett. **163A**, 475 (1992).
6. R. Movshovich, et al., Phys. Rev. B **53**, 8241 (1996).
7. F.M. Grosche, et al., Physica B **223-224**, 50 (1996).
8. I.R. Walker, et al., Physica C **282-287**, 303 (1997).
9. J.L. Sarrao, et al., in this volumn.
10. P. Monthoux and G. G. Lonzarich, Phys. Rev. B **63**, 054529 (2001).
11. Y. Haga, et al., Phys. Rev. B **63**, 060503(R) (2001).
12. D. Hall, et al., Phys. Rev. B **64**, 064506 (2001).
13. D. Hall, et al., cond-mat/0102533 (2001).
14. W. Bao, et al., cond-mat/0102503, accepted by Phys. Rev. B, (2001).
15. W. Bao, et al., Phys. Rev. B **62**, R14621 (2000); **63**, 219901(E) (2001).
16. W. Bao, et al., Phys. Rev. B **64**, 020401(R) (2001).
17. J.M. Lawrence and S.M. Shapiro, Phys. Rev. B **22**, 4379 (1980).
18. A. Benoit, et al., Solid State Commun. **34**, 293 (1980).
19. W. Bao, et al., (unpublished).
20. M. E. Fisher and J. S. Langer, Phys. Rev. Lett. **20**, 665 (1968).
21. L. W. Shacklette, Phys. Rev. B **9**, 3789 (1974).
22. P. Handler, D. E. Mapother, and M. Rayl, Phys. Rev. Lett. **19**, 356 (1967); P. P. Craig, et al., ibid. **19**, 1334 (1967).
23. K. N. Lee, et al., Phys. Rev. B **2**, 4580 (1970).

SPIN CORRELATIONS IN MAGNETIZED HALDANE CHAINS*

C. L. BROHOLM
Department of Physics and Astronomy
Johns Hopkins University, Baltimore, MD 21218, USA

Neutron scattering experiments have been carried out in high magnetic fields to understand the magnetized state of the uniform spin-1 antiferromagnetic chain. In zero field this system has a cooperative singlet ground state with a gap to a propagating triplet excitation. The quasi-one-dimensional uniform spin-1 antiferromagnets NENP ($Ni(C_2D_8N_2)_2NO_2ClO4$) and NDMAP ($Ni(C_5D_{14}N_2)_2N_3PF_6$) were examined. NENP has an alternating g-tensor such that staggered magnetization is induced for arbitrarily small fields and there is no finite field phase transition. In the high field phase the lowest energy mode has a field dependent gap and an unusually small effective spin wave velocity. NDMAP has only one spin per unit cell and hence a uniform g-tensor. This system has a critical transition at a finite field. Surprisingly the high field phase has quasi-two-dimensional or three-dimensional long-range order depending on the direction of the applied field. In the paramagnetic high field phase immediately above the ordering transition of NDMAP, there are gapless magnetic excitations that are broader in Q than the higher energy gap mode. The data is compared to theoretical predictions of a gapless incommensurate phase above the critical field.

* Work performed in collaboration with Y. Chen, M. Enderle, Z. Honda, K. Katsumata, L. P. Regnault, D. H. Reich, J. Rittner, S. M. Shapiro, M. Sieling, I. Zaliznyak, and A. Zheludev.

QUANTUM OSCILLATIONS, TUNNELING MAGNETORESISTANCE AND ANGULAR DEPENDENCE OF MAGNETIZATION IN $Ca_3Ru_2O_7$*

G. CAO
National High Magnetic Field Laboratory, Tallahassee, FL 32310

$Ca_3Ru_2O_7$ has a double Ru-O layered orthorhombic structure. It is a "bad" metal characterized by various abrupt magnetic and electronic transitions that are highly anisotropic. $Ca_3Ru_2O_7$ undergoes antiferromagnetic ordering at T_N=56 K and a metal to poorer metal transition at T_M = 48 K with a unique antiferromagnetic metallic phase intermediate between the paramagnetic and antiferromagnetic phases. Our recent study reveals a few more striking features: (1) Quantum oscillations, *i.e.*, the Shubnikov-de Haas effect, of which the fast Fourier transform shows two frequencies F_1 = 23.4 and F_2 = 41 tesla, respectively; (2) Inter-plane tunneling magnetoresistance, whose ratio is more than 90% [$\rho(0)$-$\rho(H)/\rho(0)$]; (3) Anomalous angular dependence of magnetization, which leads to similar angular dependence of resistivity due to a strong spin-charge coupling. $Ca_3Ru_2O_7$ is a rare system that possesses a wide range of interesting yet complex physical properties that very often do not coexist in other materials. The results and discussions will be presented along with comparisons with other related systems.

*The work was done in collaboration with L. Balicas, Y. Xin, and J. E. Crow

SPIN DENSITY WAVE ORDER AND FLUCTUATIONS IN $(TMTSF)_2PF_6$ AT VERY HIGH MAGNETIC FIELDS

W. G. CLARK, P. VONLANTHEN, A. GOTO, K. B. TANAKA and B. ALAVI

University of California at Los Angeles, Department of Physics and Astronomy, Box 951547, Los Angeles, CA 90095-1547, USA

W. G. MOULTON, A. REYES, and P. KUHNS
National High Magnetic Field Laboratory, 1800 East Paul Dirac Drive, Tallahassee, FL 32310, USA

We report extremely high field and frequency NMR measurements of the proton spin-lattice relaxation rate ($1/T_1$) in $(TMTSF)_2PF_6$. They probe the spin density wave (SDW) fluctuations in the critical regime near the SDW transition and in the ordered phase at lower temperatures. The highest field measurements were made using the NHMFL hybrid magnet at 44.7 T and a proton NMR frequency of 1.9 GHz. A quadratic increase in the transition temperature is observed that agrees with transport measurements made at lower fields. As the field is increased above 40 T, a change in the SDW critical dynamics is seen. Also, the behavior of $1/T_1$ vs. the alignment of the magnetic field suggests a magnetic transition at moderate to high fields with the characteristics of a sharp change in the orientation of the SDW polarization, but with parameters that differ from the spin-flop transition seen at low field.

1 Introduction

Spin density wave (SDW) order and fluctuations associated with this low temperature phase of quasi one-dimensional conductors, such as $(TMTSF)_2PF_6$, have been widely investigated for a substantial length of time. In part, this is because they reflect the static and dynamic properties of the low temperature phases of low-dimensional organic conductors and provide a means to compare these properties with theoretical models for their origin. One NMR measurement of interest is the nuclear spin-lattice relaxation rate $1/T_1$ (see Refs. [1-3]).

For the ordered phase of the SDW in the temperature (T) range not far below the SDW transition temperature (T_{SDW}), it is generally agreed that thermally excited phase fluctuations of the pinned SDW (phasons) are responsible for $1/T_1$. In this regime, the phason fluctuations generate a fluctuating magnetic field whose power spectrum is frequency dependent. Since the fluctuation motion of the SDW also corresponds to polarization charge fluctuations of the condensed electrons that make up the SDW, one model[4] finds that $1/T_1$ is proportional to the sum of the imaginary part of the SDW dielectric constant over all wave vectors at the NMR frequency. Thus, through measurements of $1/T_1$ as a function of frequency, one investigates the dynamics of the pinned SDW charge fluctuations on different time scales. Another

temperature region of interest is near T_{SDW}, where $1/T_1$ is dominated by critical fluctuations.

One of the experimental goals in this field is to extend the frequency (ω) and field (B) of the measurements to the highest possible values. Part of the results reported here include proton NMR measurements using the Hybrid magnet at the NHMFL-Tallahassee. They go up to 44.7 T and 1.9 GHz, which are substantially higher than has been done before. These measurements show a quadratic increase in T_{SDW} with B, a change of $1/T_1$ with B in both the critical fluctuation and SDW regimes, and a change in both $1/T_1$ and T_{SDW} with the alignment of B relative to the crystalline axes. The angular behavior of $1/T_1$ at moderate to high fields has a sharp change that may indicate a new phase boundary in this system.

2 Field dependence of $1/T_1$

Figure 1 shows measurements of $1/T_1$ for three values of B aligned approximately 30 degrees from the c^*-axis in the b'-c^* plane. The values of B and the corresponding NMR frequency are: 44.7 T (1.90 GHz), 40.75 T (1.73 T), and 9.0 T (0.383 GHz). For all three values of B, a sharp peak is seen where $1/T_1$ is dominated by critical fluctuations near T_{SDW}. The weak, quadratic dependence of $1/T_1$ on B shown in Fig. 2 agrees with transport measurements for B along c^* at lower values of B (see Ref. [5]). The latter were interpreted using a model of imperfect nesting and showed no variation for B along b'. We have made preliminary NMR measurements of T_{SDW} vs. the alignment of B = 9.0 T in the b'-c* plane (not shown here). They indicate that the increase in T_{SDW} varies approximately as $\sin^2\theta$, where θ is the angle between B and the b' axis.

A particular challenge for the T_1 measurements at 44.7 T was that they had to be made in less than one hour of running time. This was done by using three standard, full recovery measurements followed by a large number of continuous saturation measurements. A significant problem during this period was the substantial temperature fluctuations of approximately ± 0.12 K from convection currents in the NMR probe. They are indicated by the error bars in Fig. 1. Subsequently, this condition was suppressed and the fluctuations were reduced to ± 0.01 K for the 9 T measurements.

3 Field alignment variation of $1/T_1$

The variation of $1/T_1$ as a function of field alignment in the b'-c* plane for the ordered SDW phase is shown in Figs. 3 and 4 for 7.5 K and 11.0 K at 9 T and 12.81 K at 40.75 T. The key feature evident in Fig. 3 is the jump to a higher value of $1/T_1$ over the range ~ 35 deg. starting at θ = 8 deg. In the 40.75 T data shown in Fig. 4, a qualitatively similar behavior is seen. The primary differences are that the data do

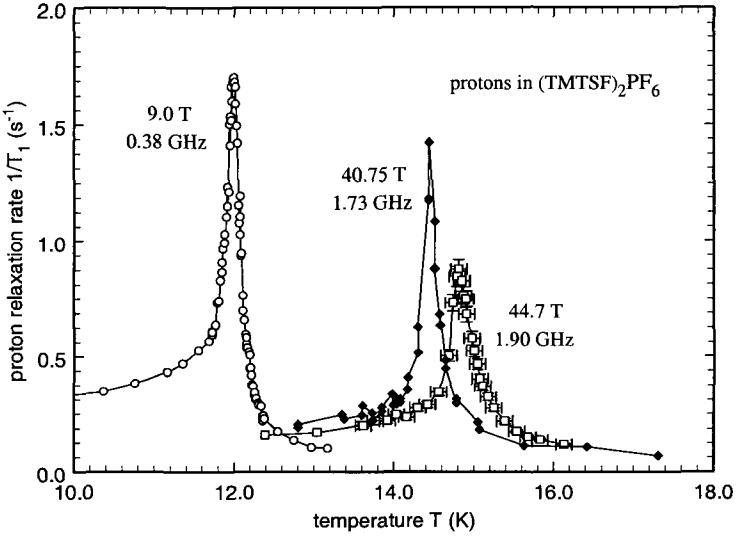

Figure 1: Proton spin-lattice relaxation rate as a function of temperature at three values of the magnetic field. The peak in $1/T_1$ occurs at T_{SDW} and the rapid variation near T_{SDW} is caused by critical fluctuations. At temperatures more than 0.5 K below T_{SDW}, the relaxation is dominated by pinned SDW phase fluctuations.

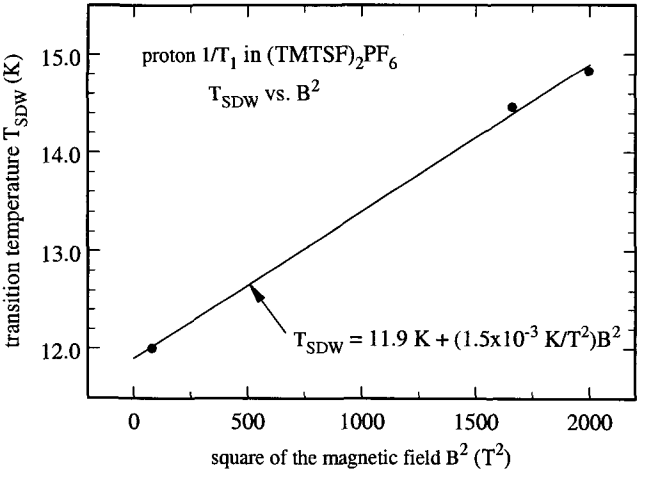

Figure 2: Transition temperature variation vs. B^2 for B in the b'-c* plane oriented approximately 30 deg from the c* axis.

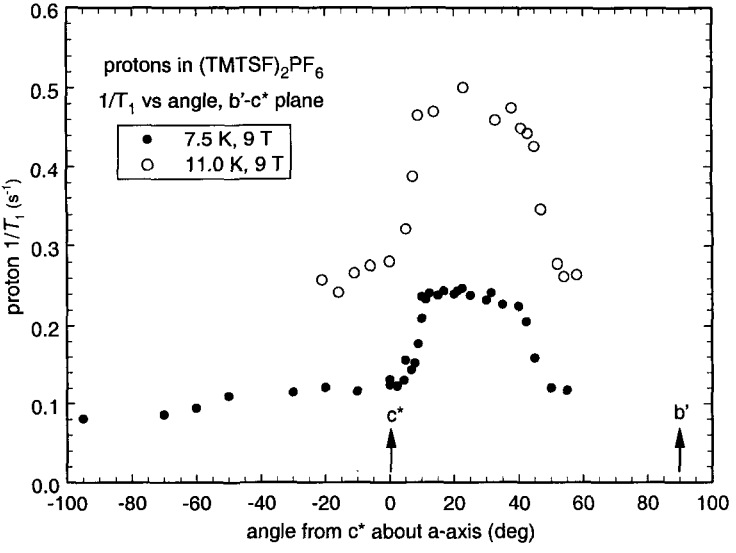

Figure 3: Relaxation rate vs. angle at 9.0 T for *B* in the b'-c* plane.

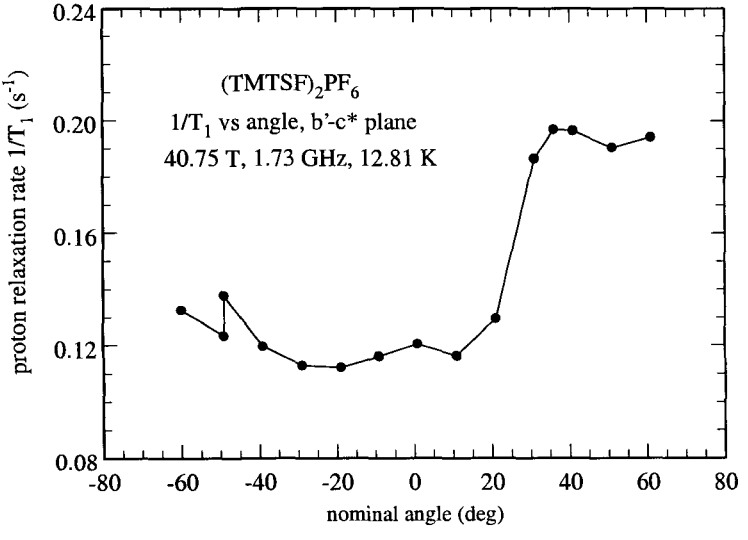

Figure 4: Relaxation rate vs. angle at 40.75 T for *B* in the b'-c* plane.

not extend far enough in θ to tell if the drop at the high angle occurs and the increase at the low angle end occurs at θ ~25 deg. instead of θ = 8 deg. For these first results, it is not known whether this difference is real or just an error in the setting of the goniometer.

4 Discussion and conclusions

First, we mention the significance of $1/T_1$ measurements for investigating the dynamic properties of the SDW. Amplitude and phase fluctuations of the SDW create at the i-th nucleus a time-dependent magnetic field $[\delta B_{\perp i}(t)]$ perpendicular to B. The Fourier transform of the ensemble average of the autocorrelation function of $\delta B_{\perp i}(t)$ corresponds to a power spectrum whose ω-dependence reflects the dynamic properties of the SDW. It is the component of this power spectrum at $\omega = \gamma B$ that drives $1/T_1$. (γ is the nuclear gyromagnetic ratio, which is 42.57 MHz/T for protons). Thus, by investigating the ω-dependence of $1/T_1$, one probes the dynamics of the SDW on different frequency/time scales. By changing T, one can study these dynamic properties in different regimes. Near T_{SDW}, they are dominated by the critical fluctuations, whereas at somewhat lower values of T they correspond to the substantially different fluctuations of the ordered SDW. An additional feature that may occur upon going to very high field is that the dynamic properties of the SDW may be modified by B. In this case, the challenge is to separate the effects on $1/T_1$ that are dependent only on ω from those that correspond to a fundamental change in the SDW properties imposed by B.

One of the most significant results indicated in Fig. 1 is that the height of the peak in $1/T_1$ decreases substantially at the very highest fields. This behavior is not seen in field-dependent measurements up to 12 T (see Ref. [3]). Because the temperature fluctuations during the measurement were a substantial fraction of the width of the peak, the possibility that it is a thermal smearing effect, though not very likely, can not be ruled out. On the other hand, the width in the divergent fluctuation regime, remains essentially constant at all values of B that have been investigated; i.e., over the entire range 0.3-44.7 T.

On the assumption that the reduction in $1/T_1$ seen at high field is not an artifact of the measurements, we mention two potential reasons for it. One is that by going to very large B, critical slowing of the fluctuations near the transition causes the power spectrum to become weaker at correspondingly high values of ω. The other is that the large value of B itself has reduced the power spectrum of the fluctuations at ω. We believe the latter mechanism is more likely, particularly since one is in a regime where T_{SDW} is changed substantially by B, as indicated in Fig. 2. In future measurements, it should be possible to test this hypothesis by carrying out measurements on different nuclear species, so that the effects of ω and B can be separated. Also, it is of interest to see if the reduction observed in $1/T_1$ has an angular dependence that mirrors that of T_{SDW}.

Now we turn to the sharp change in $1/T_1$ with field alignment displayed in Figs. 3 and 4. Since measurements (not presented here) show that in the critical regime slightly above T_{SDW}, $1/T_1$ is nearly independent of θ, it follows that the behavior below T_{SDW} is a property of the ordered SDW phase. It also is not seen at low magnetic fields slightly above the spin-flop transition near 0.45 T (see Ref. [2]). Thus, we associate it with a field- and angle-driven process in the SDW phase. It implies a sharp change of $\delta B_{\perp i}(t)$ with angle. One mechanism for that is a sharp change in the polarization direction of the SDW with θ, which would indicate a new magnetic phase boundary for this material. As mentioned above, it is not certain whether the corresponding step observed at 40.75 T a somewhat different value of θ is real or an artifact of the measurement. More measurements of this effect in the high field regime are needed to characterize this property of the SDW in $(TMTSF)_2PF_6$.

In conclusion, we have presented proton $1/T_1$ measurements of SDW fluctuations up to 1.9 GHz and 44.7 T. For the field alignment used, an increase of T_{SDW} quadratic in B is observed along with a depression of the fluctuation power spectrum at the highest values of B. We speculate that the latter may be an effect of B on the SDW state. A sharp plateau in the fluctuation power spectrum as a function of the alignment of B is also seen in the ordered phase at intermediate and high values of B. This behavior may indicate a phase boundary that corresponds to a change in the polarization direction of the SDW order parameter.

Acknowledgments

The UCLA part of this work was supported by NSF Grant DMR-0072524. We also thank S. E. Brown for helpful discussions.

References

1. T. Takahashi, Y. Maniwa, H. Kawamura and G. Saito, *J. Phys. Soc. Jpn* **55,** 1364-73 (1986).
2. W. G. Clark, W.G., Hanson, M.E. Wong and B. Alavi, *J. Phys. Paris IV* **235-242,** 235-42 (1993).
3. W. G. Clark *et al., Synth. Met.* **86** 1941-7 (1997).
4. S. E. Brown, W. G. Clark and G. Kriza, *Phys. Rev. B* **56,** 5080-3 (1997).
5. G. M. Danner, P. M. Chaikin and S. T. Hannahs, S.T., *Phys. Rev. B* **53.** 2727-31 (1996).

A METAMAGNETIC QUANTUM CRITICAL ENDPOINT IN $Sr_3Ru_2O_7$

S. A. GRIGERA and A. P. MACKENZIE
School of Physics and Astronomy, University of St. Andrews, North Haugh, St. Andrews KY16 9SS, U. K.

A. J. SCHOFIELD
School of Physics and Astronomy, University of Birmingham, Edgbaston, Birmingham B15 2TT, U. K.

S. R. JULIAN and G. G. LONZARICH
Cavendish Laboratory, Madingley Road, Cambridge, Cambridge CB3 OHE, U. K.

In this paper, we discuss the concept of a metamagnetic quantum critical end-point, consequence of the depression to zero temperature of a critical end-point terminating a line of first order first transitions. This new type of quantum critical point (QCP) is interesting both from a fundamental point of view: a study of a symmetry conserving QCP, and because it opens the possibility of the use of symmetry breaking tuning parameters, notably the magnetic field. In addition, we discuss the experimental evidence for the existence of such a QCP in the bilayer ruthenate $Sr_3Ru_2O_7$.

1 Introduction

The concept of a quantum critical point has grown to be an extensively investigated issue both theoretically[1-4] and experimentally.[5-8] The attractions of the problem are many-fold. From the fundamental point of view it allows the extension to the quantum regime of the challenges and paradigms generated by the study of critical phenomena. There is also the hope that it could offer a unified phenomenological framework for the understanding of a wide range of correlated electron behaviour. This would have technological implications, because the properties of many materials of practical interest would then be governed by their proximity to a QCP.

Recently, we have worked on a novel form of quantum criticality, identifying what we believe to be a quantum critical end-point associated with metamagnetism in $Sr_3Ru_2O_7$. In this paper we will give a qualitative discussion of the general features of quantum criticality in itinerant ferromagnets, in order to emphasise the similarities and differences between 'traditional' quantum critical points, which are associated with spontaneous symmetry breaking, and the quantum critical end-point, which is not.

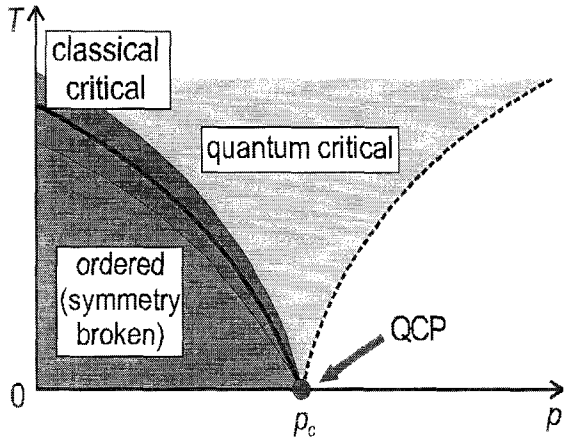

Figure 1: Schematic phase diagram of a second order phase transition giving rise to a quantum critical point at p_c.

Usually, a quantum critical point is created by the depression of a second order phase transition to zero temperature by means of a non-thermal external parameter p, as illustrated in Fig. 1. For $p = 0$, the transition at T_c is thermal, with the symmetry of the high temperature disordered phase spontaneously broken. Around the transition point, there is the well-known critical region associated with such a classical phase transition. If T_c is lowered by the application of the non-thermal parameter p, the width of the classical critical region shrinks, until it disappears altogether at $T_c = 0$. In this case criticality is purely of the quantum type, in which (since momentum and coordinates operators do not commute) the temporal and spatial components cannot be decoupled. There is a third region of criticality, that marked "quantum critical" in Fig. 1, in which fluctuations controlled by the quantum critical point are thermally excited, which explains the decrease in its width as the temperature falls. The other significant point of note is the extent of the quantum critical region up the temperature axis; fluctuations associated with quantum critical points are thought to play an important role in determining the properties of correlated electron systems even at room temperature and above. The treatment of a QCP differs from the classical one not by the introduction of new ingredients *ad hoc,* but rather from the fact that simplifications normally made when considering the latter are no longer valid.

A physically appealing way to understand the interplay between the temporal and spatial domains is provided by the relation $\Delta E \Delta T \geq \hbar$. If the characteristic thermal time $\tau_{thermal} = \hbar / k_B T$ is much less than τ, the characteristic time of the spatial fluctuations, the system appears static. This then justifies a classical treatment in the vicinity of T_c, because τ diverges during critical slowing down. Further away

from T_c, however, this is not the case, and a proper quantum mechanical treatment is required. As T_c drops to zero, $\tau_{thermal}$ itself diverges, and the system never enters the classical regime.

In treating the quantum regime, it is customary to do something like the reverse of the above: treat the temporal variation of the fluctuations as extra effective spatial dimensions (in imaginary time), and so map the quantum system to a classical one of higher dimension. In general, imaginary time plays the role of z (coupled) spatial dimensions, where z is the dynamic exponent, whose value is related to the universality class of the transition. The role of the temporal dimensions can then be understood in a finite size analysis, because the system size in any temporal direction (L_t) is determined by the inverse temperature. If $T_c = 0$, the system is infinite in all directions, and a treatment in $d+z$ dimensions is appropriate. At any finite temperature the importance of the temporal fluctuations is cut off by the finite L_t as their correlation length attempts to diverge. Closer to the transition than this, only the genuine spatial correlation lengths are diverging, signalling the crossover from the quantum $d+z$-dimensional treatment to a regime in which a classical d-dimensional treatment is adequate. Since L_t is inversely proportional to temperature, this 'saturation' of the temporal fluctuations happens further from the phase transition line as the temperature increases.

As stressed in the above discussion, the key step in producing the full quantum critical region' from Fig. 1 is to produce a phase change with associated diverging susceptibilities at $T = 0$. A standard first order phase transition would not be appropriate in this context, because it does not give a source of diverging susceptibilities. At first sight, this seems to lead to the conclusion that quantum criticality must be associated with only second order phase transitions, and hence with symmetry-broken phases.

In this context, a series of recent observations giving hints for quantum critical behaviour associated with metamagnetism[9-13] were something of a surprise. Metamagnetism is empirically defined as a sudden non-linear rise in magnetisation at some finite applied field. It cannot be a second order phase transition, because the low and high field states are of the same symmetry. It must either be a first order phase transition, with the consequent discontinuous jump in the magnetisation, or simply a crossover. The former case is in close analogy to the liquid to gas transition in water, the difference in the value of the magnetisation between the two states playing the role analogous to the difference in density of vapour and liquid water. At first sight, neither of these can be a source of the required diverging susceptibilities. However, due to the symmetry conservation between the two phases, it is possible for this first order line to end at a critical end-point (CEP), again in close analogy to the situation in water. The CEP shares the property of a second order phase transition that is the key to producing quantum criticality, since it is characterised by diverging susceptibilities and the physics is dominated by fluctuations. The main qualitative difference is the absence of any spontaneous breaking of symmetry. The possibility of a new type of quantum.

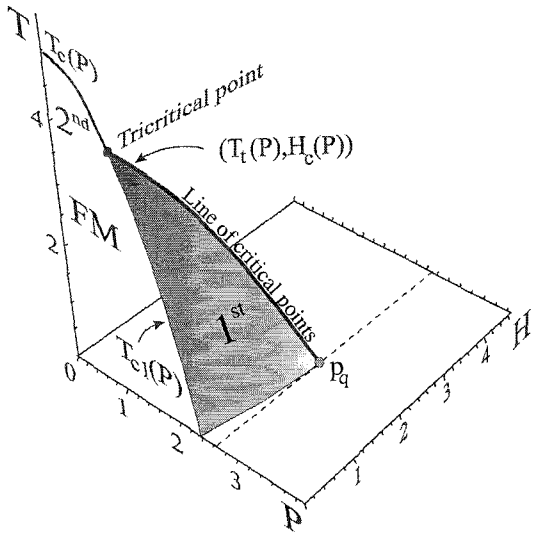

Figure 2: Schematic (P,H,T) phase diagram of an itinerant ferromagnet.

critical point is now apparent: that which would arise from the depression of the critical end-point temperature to zero by means of some tuning parameter. As we now discuss, this can occur in itinerant ferromagnets.

An itinerant ferromagnet has a rich *P,H,T* phase diagram (see Fig 2): at $H=0$ the ferromagnetic to paramagnetic phase transition is second order below a certain pressure p^*, and first order for higher pressures.[14] Any non-zero magnetic field induces a finite magnetisation in the system; the symmetry associated with the ferromagnetic transition is broken and the second order phase transition can no longer take place. On the other hand, since there are no symmetry constraints on the first order transition, it extrudes into a surface in *(P,H,T)* of first order phase transitions that separate states with quantitatively different degrees of magnetisation (the metamagnetic transition). The tricritical point at p^* extrudes in turn into a line of critical end points that bounds the surface of first order transitions. At a particular point (p_q,H_q) of the pressure and magnetic field, the line reaches $T=0$, giving rise to a quantum critical end-point (QCEP). Keeping the pressure fixed at p_q it is possible then to use the magnetic field to tune in and out of criticality.

This reasoning is appealing, but clearly in need of experimental investigation. In principle, these would be difficult experiments, requiring simultaneous application of high pressures and magnetic fields. However, it should be noted that both the *origin* and scale of the *P* axis depends on the particular compound which is being considered, if we appeal to the standard analogy between interatomic bonding and effective chemical pressure. In what follows we will argue that the magnetic behaviour of the ruthenate $Sr_3Ru_2O_7$ can be described within the framework that we

have discussed above, and furthermore, that p_q for this system sits very close to ambient pressure. This last point is an issue of considerable experimental importance: in isolation, the applied magnetic field is an extremely easy parameter to control.

2 The system $Sr_3Ru_2O_7$

The basic physical properties of $Sr_3Ru_2O_7$ have been described in various reports.[15-17] The main development of significance was the discovery by Ikeda, Maeno and co-workers of techniques for the image-furnace growth of high purity single crystals. This work was extended by Perry to produce crystals with residual resistivity $\rho_{res} \sim 2$ μΩcm. In weak applied fields these crystals are strongly enhanced paramagnets down to the lowest temperatures, and metamagnetism is seen with transition fields of approximately 7.8 tesla for H // c and 5.5 tesla for H // ab. Preliminary work on the properties in the vicinity of metamagnetism gave evidence for critical fluctuations, notably the behaviour of the resistivity exponent as a function of field and temperature, and the observation of an apparent logarithmic divergence of C/T *vs.* T in a field of approximately 7.8 tesla applied parallel to c (see Ref. [16]). This work was far from conclusive, however. Only one decade of temperature was investigated, and the results gave hints rather than proof of the existence of a QCEP. As can be seen from examination of Fig. 1, high temperature 'quantum critical' signatures can be observed if experiments are performed some distance in phase space away from a critical point, particularly at elevated temperatures.

To investigate the system in more detail, a transport study with H // c was performed at lower temperatures (Grigera *et al.* see Ref. [17]). To separate the different contributions to the resistivity the data were analysed using the expression $\rho=\rho_{res}+AT^{\alpha}$. ρ_{res} is the resistivity due to elastic scattering, the exponent α provides information about the temperature dependence of the resistivity, and A is a temperature independent coefficient related to the square of the quasi-particle effective mass. Both the temperature dependence and the residual part of the resistivity show pronounced changes when the field is swept through the metamagnetic transition, but the most significant finding concerns the behaviour of A. As seen in Fig. 3, A diverges as the metamagnetic transition is approached. The experiments and the way in which A was extracted (both described in detail in Ref. [17]) mean that it is effectively a probe for diverging susceptibilities along the T=0 axis. The fact that these were observed gives very good evidence that a QCEP of the class described above exists at ambient pressure in $Sr_3Ru_2O_7$.

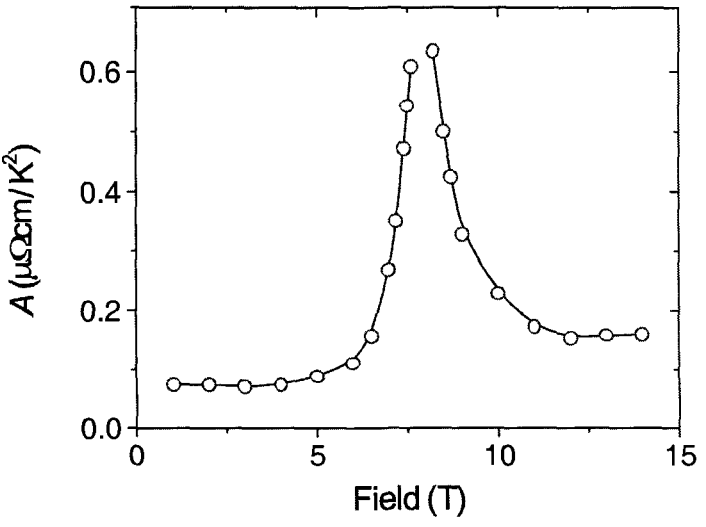

Figure 3: Divergence of the A coefficient as a function of the magnetic field in the neighbourhood of the metamagnetic field H_c=*7.785 tesla* (data from Ref. [17]).

3 Conclusions and future directions

We have discussed a new form of quantum criticality in itinerant fermionic systems based on a *quantum critical end-point* (QCEP) in which no symmetry is broken at the transition. This will hopefully open the way to new avenues of investigation. Firstly, it shows that discovery of a spontaneously-symmetry-broken phase is not a necessary step in establishing the existence of a quantum critical point. It also removes a significant restriction on tuning parameters for traditional QCP's, namely that the tuning parameter cannot break the same symmetry as the ordered phase in Fig. 1. Finally, there is the possibility of observing even more anomalous behaviour right in the vicinity of the QCEP. Novel ordered phases have been seen in this region near traditional QCP's (see Ref. [7]), and may also exist near QCEP's. In the latter case, the ability to use symmetry-breaking tuning parameters may promote genuinely new behaviour. Intriguing preliminary evidence for this has already been seen in $Sr_3Ru_2O_7$ (see Ref. [17]), and is worthy of detailed further investigation. Metamagnetism in itinerant ferromagnets is likely to be an ideal testing ground for these ideas. Magnetic field is a convenient tuning parameter, hopefully allowing the construction of a unified picture of the consequences of quantum criticality in clean itinerant systems.

Acknowledgments

We thank the Leverhulme Trust, the UK Engineering and Physics Science Research Council, and the Royal Society for valuable financial support. We also gratefully acknowledge R. Perry, Y. Maeno, A. J. Millis, M. Chiao, S. Ikeda, S. Nakatsuji, and C. Pfleiderer for collaboration and useful discussions.

References

1. J. A. Hertz, *Phys. Rev. B* **14**, 1165 (1976).
2. A. J. Millis, *Phys. Rev. B* **48**, 7183 (1993).
3. S. Sachdev, *Quantum phase transitions* (Cambridge University Press, Cambridge 1999).
4. S. L. Sondhi *et al.*, *Rev. Mod. Phys.* **69**, 315 (1997).
5. C. Pfleiderer *et al.*, *Phys. Rev. B* **55**, 8330 (1997).
6. H. v. Löhneysen *et al.*, *Phys. Rev. Lett.* **72**, 3262 (1994).
7. N. D. Mathur *et al.*, *Nature* **394**, 39 (1998).
8. D. Bitko, T. F. Rosenbaum and G. Aeppli, *Phys. Rev. Lett.* **77**, 940 (1996).
9. J. S. Kim *et al.*, *Solid State Comm.* **114**, 413 (2000).
10. H. Sugawara *et al.*, *J. Phys. Soc. Jpn.* **68**, 1094 (1999).
11. S. Kambe *et al.*, *Solid State Comm.* **95**, 449 (1995); **96** 175 (1995).
12. Y. Aoki *et al.*, *J. Magn. Magn. Mater.* **177**, 271 (1998).
13. S. R. Julian *et al.*, *J. Magn. Magn. Mater.* **177**, 265 (1998).
14. It has been argued that non analytic terms would drive all ferromagnetic transitions first order, see D. Belitz, T. R. Kirkpatrick and T. Vojta, *Phys. Rev. Lett.* **82**, 4707 (1999).
15. S. Ikeda *et al.*, *Phys. Rev. B* **62**, R6089 (2000).
16. R. S. Perry *et al.*, *Phys. Rev. Lett.* **86**, 2661 (2001).
17. S. A. Grigera *et al.*, *Science* **294**, 329 (2001).

HIGH FIELD NMR IN STRONGLY CORRELATED LOW-DIMENSIONAL FERMIONIC SYSTEMS

M. HORVATIĆ and C. BERTHIER

Grenoble High Magnetic Field Laboratory, CNRS and MPI-FKF, BP 166X, 38042 Grenoble, France

E-mail: horvatic@polycnrs-gre.fr

We review some recent NMR results obtained in Grenoble High Magnetic Field Laboratory on magnetic field induced phenomena in strongly correlated low-dimensional fermionic systems: *i*) magnetic field dependence of the soliton lattice in the IC phase of the spin-Peierls system $CuGeO_3$, *ii*) NMR study of the complete *H-T* phase diagram of the organo-metallic spin ladder $Cu_2(C_5H_{12}N_2)_2Cl_4$, and *iii*) the first "standard" NMR measurements (i.e., without optical pumping) on 2D electrons in Quantum wells, providing a detailed description of the fractional quantum Hall effect state at $\nu = 1/2$ with the first determination of the corresponding effective polarization mass of composite fermions. Latest study of the $\nu = 2/3$ state revealed, among other features, an unexpected phase transition.

1 Introduction

Rather than increasing the resolution and sensitivity in NMR spectroscopy, the use of high-field NMR in Solid State Physics at the Grenoble High Magnetic Field Laboratory is aimed at studying magnetic field induced phenomena. Examples are:

1. Low dimensional (D) quantum spin systems in which the magnetic field (*H*) can induce phase transitions by closing the singlet-triplet gap: spin-Peierls chain $CuGeO_3$ (see Refs. [1-2]), spin-ladder $Cu_2(C_5H_{12}N_2)_2Cl_4$ (see Refs. [3-5]), Haldane chain Y_2BaNiO_5 (see Refs. [6,7]), 2D Shastry-Sutherland system $SrCu_2(BO_3)_2$ (see Ref. [8]).
2. The quantum-Hall effect where *H* ensures the quantization of kinetic energy of 2D electrons (see Refs [9-11]).
3. Dimensionality cross-over in low-D organic conductors, e.g., in Bechgaard salts $(TMTSF)_2ClO_4$ (see Ref. [12]) and $(TMTSF)_2PF_6$, where strong magnetic field reduces the transversal motion of electrons and converts the dimensionality from 2D to 1D.

In all these cases we study *strongly interacting* fermionic systems in which the magnetic field is the pertinent parameter, revealing rich physics.

2 Low-D quantum spin systems

One dimensional (1D) quantum antiferromagnetic (AF) spin systems such as spin chains,[13] spin-Peierls systems[14] and spin ladders[15] have recently attracted an increasing interest, partly as a possible way to approach from a lower dimension the

physics of copper-oxide high T_c superconductors. Also, using the Jordan-Wigner canonical transformation, their magnetic Hamiltonians can be transformed into that of strongly interacting 1D spinless fermions, in which the magnetic field plays the role of the chemical potential and the band width is of the order of the coupling J. This makes quantum spin chains remarkable models for the investigation of quasi-1D physics.

2.1 Spin-Peierls system $CuGeO_3$

First example deals with the spin-Peierls chain, i.e., a Heisenberg, AF, spin 1/2 chain on an elastic lattice.[14] At low temperature, this spin chain can gain energy by spontaneous dimerization (deformation) of the lattice, which allows the opening of a gap in magnetic excitations (absent in simple Heisenberg half integer spin chains). The dimerized state is non-magnetic, with a collective singlet state and an energy gap towards triplet excitations. Application of magnetic field will reduce the gap and, above the critical field H_c, drive the system into a magnetic phase with spatially inhomogeneous magnetization (Fig. 1). In this field-induced phase, magnetization appears as an incommensurate (IC) lattice of magnetization peaks (solitons), where each soliton is bearing a total spin 1/2. The subject of our investigation was the NMR imaging of the magnetic field dependence (at nearly zero temperature) of the soliton lattice, followed from the limit of nearly independent solitons just above H_c, up to the limit of strongly overlapping solitons at high magnetic field, where the modulation of spin polarization is nearly sinusoidal.

By NMR we have studied[16,2,1] the first inorganic spin-Peierls system $CuGeO_3$ (see Ref. [17]), presenting a spin-Peierls transition at 14-10 K (depending on H), and a critical field $H_c \cong 13$ T. While in the high-temperature and in the dimerized phase symmetric NMR lines are observed[16] reflecting spatially uniform magnetization,

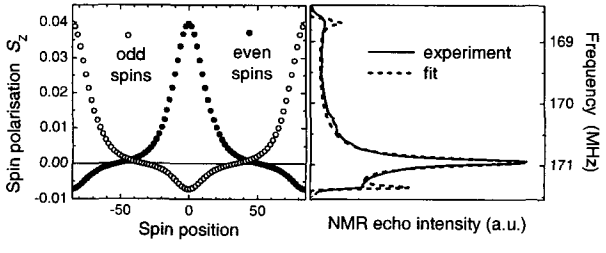

Figure 1: Reconstitution of the real space spin-polarization profile (left) and the corresponding fit to Jacobi elliptic functions [1] (right, dashed line) superposed on experimental NMR lineshape (right, full line), taken in the incommensurate high magnetic field phase of the spin-Peierls compound $CuGeO_3$ (here just above the critical field). In this way, NMR lineshape has provided the precise magnetic field dependence of average and staggered spin-polarization and the magnetic correlation length up to $2H_c$.

above H_c each line is converted to a very wide asymmetric spectrum (Fig. 1) corresponding to a non-uniform distribution of magnetization. More precisely, the NMR lineshape is in fact the density distribution of the local magnetization, i.e., of the spin polarization. In 1D (and for a periodic function) this can be directly converted to the corresponding real-space spin-polarization profile (soliton lattice, one period of which is shown in Fig. 1).[16] We have thus obtained full *quantitative* description of the H dependence of the spin-polarization profile in the range from H_c to $2H_c$ = 26 T (see Ref. [1]), which can serve as reference data for the comparison to theory. Analysis of these data proved that the staggered component of magnetization is reduced in the NMR image by phason-type motion of the soliton lattice.[18-19] The magnetic correlation length is found to be smaller than the one corresponding to the lattice deformation (measured by X-rays),[20] which is a direct consequence of the frustration, i.e., the second neighbor interaction in the system. The observed field dependence of correlation length remains to be understood.

2.2 *Spin ladder $Cu_2(C_5H_{12}N_2)_2Cl_4$*

If in the organo-metallic $Cu_2(C_5H_{12}N_2)_2Cl_4$ compound[21,4] we consider only the shortest bonds connecting copper spins, we arrive to a 1D spin-ladder structure (inset to Fig. 2). This system has been thought to be the first physical realization of a strong coupling (along rungs, $J_\perp >> J_{//}$), S = 1/2, spin ladder in which the exchange integrals $J_\perp$ and $J_{//}$ are low enough so that the full H-T phase diagram can be covered by experimentally accessible magnetic fields (Fig. 2). It is predicted that for H = 0 the ground state is a gapped spin liquid, in which the singlet ground state is separated by a gap $\Delta = J_\perp - J_{//}$ from the lowest lying triplet excitations. As long as $H < H_{c1} = \Delta/g\mu_B$, the system remains gapped with $\Delta(H) = \Delta - g\mu_B H$. The point

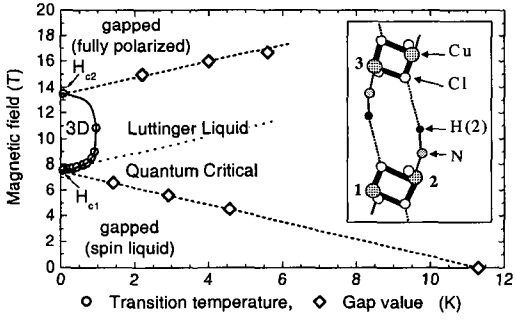

Figure 2: The phase diagram of $Cu_2(C_5H_{12}N_2)_2Cl_4$ (whose "ladder" structure is shown in the inset) determined from NMR experiments. Solid line is a phase boundary to the 3D ordered phase, determined (○) from the changes in the NMR lineshape.[5] Open diamonds give the gap value determined from the T_1 measurements.[3] The dotted lines separate different regimes.

(H_{c1}, $T = 0$) is a quantum critical point which separates the singlet spin liquid state from a magnetic state, which in a purely 1D approach is equivalent to a Luttinger liquid (LL). Within this phase, one expects a divergence of the nuclear spin-lattice relaxation rate $1/T_1 \propto T^{-\alpha(H)}$; in practice, there is always a transverse coupling between the chains, which induces a 3D transition at a finite temperature between H_{c1} and $H_{c2} = J_\perp + 2J_{//}$. The point ($H_{c2}$, $T = 0$) separates this 3D phase issued from the LL from a fully polarized phase which again is gapped with $\Delta = g\mu_B(H - H_{c2})$.

All these expected features have indeed been observed through the behavior of the spin-lattice relaxation of protons in single crystals of $Cu_2(C_5H_{12}N_2)_2Cl_4$, as shown in Fig. 2. In particular, linear dependence of the gap on magnetic field (diamonds) is confirmed both below $H_{c1} \cong 7.5$ T in a spin liquid state, and above $H_{c2} \cong 13.5$ T in a fully polarized state.[22,2,4] Between H_{c1} and H_{c2}, and above 1.5 K, $1/T_1$ indeed shows divergence associated to the LL regime, while at lower temperature appears 3D ordered state. Transition line to this state has been established by the modifications in the proton lineshape.[5] Near the H_{c1} critical point, the field dependence of transition temperature is well described by a power law with the exponent of 2/3, in agreement with the predictions of Giamarchi and Tsvelik.[23] Modifications of the proton spectra, as well as the temperature dependence of $1/T_1$, strongly suggest that below ~2 K the longitudinal couplings $J_{//}$ are modified, and finally modulated in the 3D ordered phase, in a scenario which is equivalent to the spin-Peierls transition.[5]

Finally, from recent neutron data quite *different* magnetic exchange paths have been proposed, leading to a *frustrated, 3D* quantum spin liquid.[24] However, the neutron data cannot provide complete magnetic Hamiltonian and, for the moment, it is not clear how a 3D Hamiltonian could be related to the observed phase diagram.

3 2D electron gas in GaAs/GaAlAs Quantum wells

When 2D electrons are put in a sufficiently strong magnetic field, they will all fill the lowest Landau level (LLL). We thus obtain a highly degenerate system where the only characteristic energies are the Coulomb interaction energy and the Zeeman energy. Special (Fractional Quantum Hall Effect) states and the corresponding quasiparticle excitations are formed at fractional fillings of LLL ($\nu = 2/3$, 1/2, ...) (see Ref. [25]), and the NMR technique can provide important insights in their spin configuration. The NMR hyperfine shift corresponding to electrons confined into 2D by "Quantum wells" is directly proportional to their spin-polarization P, and offers unique possibility to follow P as a function of both magnetic field (H) and temperature (T). Until recently, the NMR in these systems was performed only using "optical pumping" to increase the signal.[26] We found that on the multiple Quantum wells samples *standard* NMR provides enough signal, and is more convenient to access to low (dilution fridge) temperatures.[9,27]

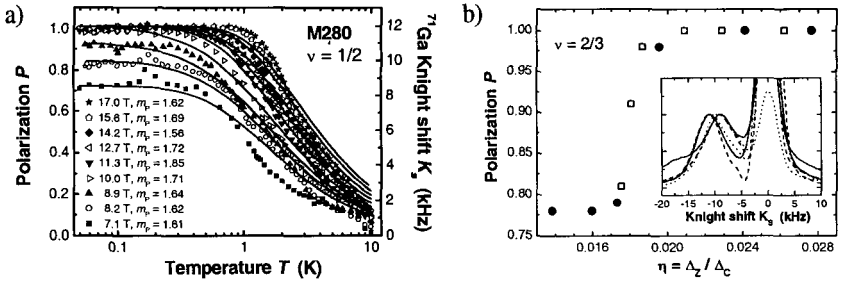

Figure 3: a): The temperature dependence of the spin-polarization $P(T)$ at $\nu = 1/2$ measured on the M280 sample for different total magnetic field values. Data are compared to the non-interacting composite fermions model (solid lines) with the polarization mass as the only fit parameter. b): The phase transition of the $\nu = 2/3$ state as revealed by the dependence of the spin polarization on the ratio of Zeeman and Coulomb energies $\eta = \Delta_Z/\Delta_C$ for samples M280 (dots) and M242 (squares) at temperatures below 100 mK. The inset shows original NMR spectra corresponding to M280 sample.

We studied two multiple (100) Quantum wells GaAs/GaAlAs samples, named "M280" and "M242", having the electronic density of $n_{2D} = 0.85$ and 1.4×10^{11} cm^{-2}, respectively.

At LLL filling $\nu = 1/2$, the system is supposed to be well described by composite fermions (CFs) made of one electron and two magnetic flux quanta (or, rather, two vortices), so that CFs keep the same spin and charge as electrons, but (as regards their orbital motion only) they see *zero* effective magnetic field. Supposing that CFs are indeed non-interacting, it is then easy to predict the spin polarization of this system as a function of H and T (see Ref. [9]); the system is described by only one parameter, the spin polarization effective mass m_p. When this prediction is compared to the NMR data[9,11] as shown in Fig. 3(a), we obtain reasonably good fits at low T, and find the value of m_p as predicted by the theory of Park and Jain.[28] However, unexpectedly, m_p turns out to be *independent* of magnetic field. Equivalently, low-T polarization is found to be linear in magnetic field until the full polarization is reached, i.e., $P(T \to 0, \eta) = \min\{45.2\eta, 1\}$. This behavior seems to be better captured by the recent "Hamiltonian theory" of Shankar.[29]

The most remarkable result at $\nu = 2/3$ is the observation of the quantum phase transition from a *partially* polarized ($P \approx 3/4$) to a fully polarized ($P = 1$) state, which is driven by increasing the ratio between the Zeeman and the Coulomb energy above a critical value $\eta = \Delta_Z/\Delta_C = 0.0185$ (Fig. 3(b)). The transition is very sharp, apparently without any change in the thermal activation energy between two states, which all suggests a first-order type of transition. While a transition from zero to full P is indeed predicted at high η (i.e., field), partial polarization is completely unexpected. Within the CF picture only zero or full polarization can be constructed, and any partial polarization can be only from inhomogeneous mixture of these two states. However, static mixture of two states is excluded, as only one NMR line is

observed. In numerical (exact) solutions k*8 electrons are needed to be able to generate $P \approx 3/4$; this exceeds the limit of state-of-the-art calculations already for $k = 2$. So far, only $P = 1/2$ state has been found in calculations on 12 electrons.

References

1. M. Horvatić *et al.*, *Phys. Rev. Lett.* **83**,420-423 (1999).
2. Y. Fagot-Revurat *et al.*, *Phys. Rev. B* **55**, 2964-2974 (1997).
3. G. Chaboussant *et al.*, *Phys. Rev. Lett.* **80**, 2713-2716 (1998).
4. G. Chaboussant *et al.*, *Eur. Phys. J. B* **6**, 167-181 (1998).
5. H. Mayaffre *et al.*, *Phys. Rev. Lett.* **85**, 4795-4798 (2000).
6. F. Tedoldi *et al.*, M., *Phys. Rev. Lett.* **83**, 412-415 (1999).
7. F. Tedoldi *et al.*, *App. Magn. Res.* **19**, 381-389 (2000).
8. M. Takigawa *et al.*, Grenoble High Magnetic Field Laboratory Annual Reports, 57 (2000) and (2001), see http://GHMFL.polycnrs-gre.fr/totalescience.htm
9. S. Melinte *et al.*, *Phys. Rev. Lett.* **84**, 354-357 (2000).
10. N. Freytag *et al.*, *Phys. Rev. Lett.* **87**,136801/1-4 (2001).
11. N. Freytag, Ph.D. *Thesis,* University Joseph Fourier, Grenoble, France, 2001.
12. K. Behnia *et al.*, *Phys. Rev. Lett.* **74**, 5272-5275 (1995); P. Carretta *et al.*, in *Proceedings of the PPHMF II Conference*, ed. by Z. Fisk *et al.,* (World Scientific, Singapore, 328-333, 1996).
13. I. Affleck, *J. Phys. Condens. Matter* **1**, 3047-3072 (1989) and Refs. therein.
14. For a review, see J. W. Bray *et al.*, in *Extended Linear Compounds*, ed. by J. C. Miller (Plenum, New York, 353-415, 1982).
15. E. Dagotto and T. M. Rice, *Science* **271**, 618-623 (1996); E. Dagotto, *Rep. Prog. Phys.* **62**, 1525-1571 (1999).
16. Y. Fagot-Revurat *et al.*, *Phys. Rev. Lett.* **77**, 1861-1864 (1996).
17. M. Hase *et al.*, *Phys. Rev. Lett.* **70**, 3651-3654 (1993).
18. G. S. Uhrig *et al.*, *Phys. Rev. B* **60**, 9468-9476 (1999).
19. H. M. Rønnow *et al.*, *Phys. Rev. Lett.* **84**, 4469-4472 (2000).
20. K. Kiryhukin *et al.*, *Phys. Rev. Lett.* **76**, 4608-4611 (1996).
21. B. Chiari *et al.*, *Inorg. Chem.* **29**, 1172 (1990).
22. G. Chaboussant *et al.*, *Phys. Rev. Lett.* **79**, 925-928 (1997).
23. T. Giamarchi and A. Tsvelik, *Phys. Rev. B* **59**, 11398-11407 (1999).
24. M. B. Stone *et al.*, preprint, cond-mat/0103023 v2.
25. H. L. Stormer. and D. C. Tsui, in *Perspectives in Quantum Hall Effects*, ed. by S. Das Sarma and A. Pinczuk (Wiley, New York, 1996).
26. S. E. Barrett *et al.*, *Phys. Rev. Lett.* **72**, 1368-1371 (1994) and *ibid.* **74**, 5112-5115 (1995).
27. S. Melinte *et al.*, *Phys. Rev. B* **64**, 085327/1-9 (2001).
28. K. Park and J. K. Jain, *Phys. Rev. Lett.* **80**, 4237-4240 (1998).
29. R. Shankar, *Phys. Rev. B* **63**, 085322/1-33 (2001).

TRIPLET SUPERCONDUCTIVITY ORDER PARAMETER IN AN ORGANIC SUPERCONDUCTOR $(TMTSF)_2PF_6$

A. G. LEBED
L. D. Landau Institute for Theoretical Physics, Kosygina St. 2, 117334, Moscow

We argue that an organic superconductor $(TMTSF)_2PF_6$ under pressure $P \simeq 6$ kbar is a triplet superconductor[1,2] with a spin part of the triplet order parameter being $\mathbf{d}(\mathbf{k}) = (d_x(\mathbf{k}) \neq 0, d_y(\mathbf{k}) = 0, d_z(\mathbf{k}) = 0)$. We obtain these results by means of an analysis of the anisotropic experimental critical fields H_{c2} (see I. J. Lee *et al.*, *Phys. Rev. Lett.* **78**, 3555 (1997)). By using symmetry arguments, we also discuss the most probably orbital part of the triplet order parameter in $(TMTSF)_2PF_6$. Our analysis is in accordance with the very recent Knight shift data obtained on $(TMTSF)_2PF_6$.

1. A. G. Lebed, *Phys. Rev. B* (Rapid Commun.), **59**, R795 (1999).
2. A. G. Lebed *et al.*, *Phys. Rev. B* (Rapid Commun.), **62**, R795 (2000).

MAGNETISM AT THE SPATIAL LIMIT

H. MANOHARAN

Department of Physics and Geballe Laboratory for Advanced Materials
Stanford University, Stanford, CA

In this talk I will survey our recent experimental results in the detection and manipulation of magnetism at the spatial limit. Our experiments rely on atom manipulation techniques and scanning tunneling microscopy at low temperatures to enable atomic-scale imaging and control.

We have observed "quantum mirages" in focusing devices of order 10 nanometers in size, built by assembling structures out of individual atoms. We have directly imaged the spin perturbations due to isolated magnetic moments on a metal surface. The detection of this localized magnetism can then be utilized in a type of teleportation experiment, in which the spectroscopic signature of an atom is sampled and projected to a remote location by means of a surrounding sea of electrons confined in an engineered nanostructure. The quantum mirage thus cast by a single magnetic atom can be coherently refocused at a distinct point where it is detected as a phantom atom around which the electronic structure mimics that at the real atom. Once materialized, this phantom can interact with real matter in intriguing ways.

We have constructed other nanoscale magnetic structures which either elucidate the coupling between isolated moments or provide a mechanism for controlling and exploiting spin coupling over long distances. We have also been developing novel communication methods based on the fundamental effects we have discovered.

FERROMAGNETIC AND STRUCTURAL INSTABILITIES IN $Ca_{2-x}Sr_xRuO_4$

S. NAKATSUJI*

Department of Physics, Kyoto University, Kyoto 606-8502, Japan
E-mail:nakatuji@magnet.fsu.edu

Y. MAENO

Department of Physics, Kyoto University, Kyoto 606-8502, Japan
CREST, Japan Science and Technology Corporation, Kawaguchi, Saitama 332-0012, Japan
E-mail:maeno@scphys.kyoto-u.ac.jp

$Ca_{2-x}Sr_xRuO_4$ is a unique quasi-two-dimensional multi-band system that connects the Mott insulator Ca_2RuO_4 with the spin-triplet superconductor Sr_2RuO_4. The isovalent Sr substitution changes the crystal distortions and thus modifies the hybridization and degeneracy of t_{2g} orbitals. Such effective change of electron correlation induces the Mott transition and rich evolution of itinerant magnetism. One of the striking features in this system is the appearance of ferromagnetic critical behavior in the metallic phase near a zero-temperature structural instability ($x_c \approx 0.5$). The low temperature susceptibility shows Curie-like diverging behavior, and the electronic specific heat (C_e) divided by temperature, C_e/T, enormously increases up to 250 mJ/mol-Ru at $x = 0.5$. Moreover, critical enhancement of Wilson ratio is attributable to a ferromagnetic instability developed near the structural instability.

1 Introduction

Multi-band strongly correlated systems such as ruthenates, manganites and vanadates have attracted much interest for their variety of ground states originated from their orbital degrees of freedom and their interaction with spin, lattice and charge. Among them, $Ca_{2-x}Sr_xRuO_4$ is a unique quasi-two-dimensional multi-band system[1] that connects the Mott insulator Ca_2RuO_4 (see Refs. [2,3,4]) with the spin-triplet superconductor Sr_2RuO_4 (see Refs. [5,6]). The isovalent substitution of Sr controls the hybridization and degeneracy of $4d$ t_{2g} orbitals (d_{xy}, d_{yz}, d_{zx}) by tuning crystal distortions.[7,8] Thus, band degeneracy tuning as well as band-width control induces the metal-insulator transition and the rich variation of metallic phases toward the spin-triplet superconductor.

In this system, adjacent to the antiferromagnetic (AF) insulating phase in region I ($0 \leq x < 0.2$), an AF correlated metallic state appears in a low temperature orthorhombic phase in region II ($0.2 \leq x < 0.5$), which we will refer to as the magnetic metallic (M-M) region. However, once the system recovers the tetragonal symmetry above T_O through a second-order structural transition, the magnetic coupling changes to be ferromagnetic (FM). The low temperature susceptibility

increases as T_O decreases, and finally shows a diverging behavior near the structural instability at $x_c \approx 0.5$, suggesting the appearance of a nearly FM metal. Further substitution of Sr in region III ($0.5 \leq x \leq 2$), on the other hand, continuously decreases the susceptibility and evolves the Fermi-liquid state of the spin-triplet superconductor at $x = 2.0$. The magnetic critical behavior observed at the structural instability implies a strong coupling between spin, lattice and orbital degrees of freedom, and its significant role in the Mott transition and even in the spin-triplet superconductivity.

In order to investigate the ground state magnetism around $x = 0.5$, we have measured the low temperature specific heat. The critical behavior at $x = 0.5$ is also found in the temperature dependence of the specific heat and in its x dependence of the electronic coefficient γ. Especially, γ shows critical enhancement at $x = 0.5$ to reach the maximum of about 250 mJ/mol-Ru. Moreover, the critical enhancement of Wilson ratio strongly suggests the ferromagnetic instability developed near the structural instability.

2 Experimental

The single crystals of $Ca_{2-x}Sr_xRuO_4$ were prepared using a floating zone method.[9] No trace of second phase was found by powder X-ray diffraction analysis at room temperature. The specific heat C_P was measured by a thermal relaxation method from 25 K to 0.4 K with a commercial system (Quantum Design PPMS). The low temperature C_P of the insulator Ca_2RuO_4 is well fitted by $\gamma T + \beta T^3$ with $\gamma \approx 0.0$ (2) mJ/molK^2 and Debye temperature $\Theta_W = 420$ K (see Ref. [4]). Since Θ_W keeps almost constant around 410–420 K through the entire system, we assume the lattice part of the specific heat C_{Lat} is well represented by C_P of the insulator Ca_2RuO_4. Thus, we define the electronic part C_e as $C_e \equiv C_P - C_P(Ca_2RuO_4)$.

3 Results and Discussion

3.1 Evolution of the temperature dependence of the specific heat

The temperature dependence of C_e/T in Fig. 1 shows continuous and critical enhancement in region III. As for Sr_2RuO_4, it exhibits a jump in C_e/T at the superconducting transition temperature $T_c \approx 1.5$ K. Reflecting its Fermi liquid ground state,[5] C_e/T above T_c is almost constant up to around 12 K. This situation is clearer in the data for $x = 1.95$, which manifests temperature independent C_e/T without any transition down to the lowest temperature 0.4 K, owing to the suppression of the superconductivity by 2.5 % Ca substitution.

With decreasing the Sr content x from $x = 2$ (Sr_2RuO_4), C_e/T gradually increases with stronger temperature dependence as in Fig. 1. While C_e/T at $x = 1.5$ is still almost temperature independent below about 5 K, those for $x = 0.9$ and 0.7 exhibit significant increase of C_e/T on cooling down to the lowest temperature 0.4 K. Moreover, C_e/T for $x = 0.5$ shows the most prominent enhancement, and finally it saturates below 0.6 K.

As this system enters the M-M region, however, C_e/T starts to form a peak in its temperature dependence. This is presumably due to the formation of AF short-range order at low temperatures in the M-M region.

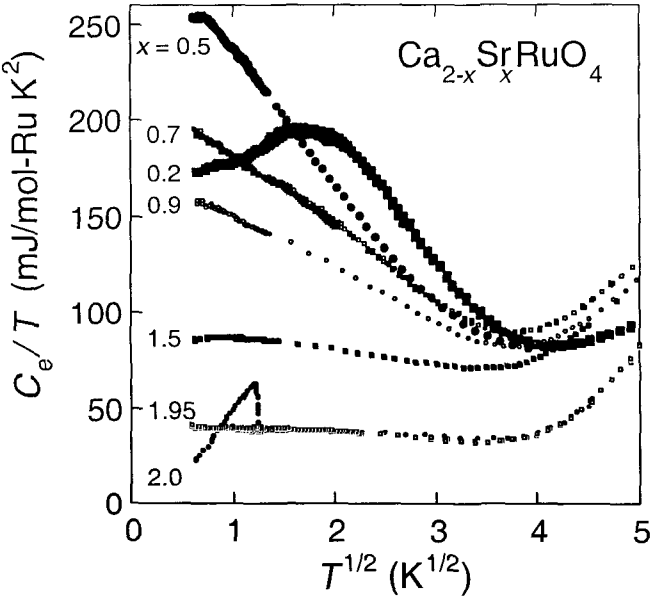

Figure 1: Temperature dependence of the electronic part of the specific heat divided by the temperature C_e/T for single crystal $Ca_{2-x}Sr_xRuO_4$ with variable x.

3.2 *Wilson Ratio*

As we can see in Fig. 1, C_e/T in region III shows a large enhancement with Ca substitution as well as on cooling. This systematic change is well summarized in Fig. 2 which displays the $\gamma = C_e/T(0.4\ \mathrm{K})$ against the Sr content x. While Sr_2RuO_4 itself has a large value about 37 mJ/mol-RuK^2, γ increases significantly with Ca substitution and it finally reaches the maximum of 255 mJ/mol-RuK^2 at $x = 0.5$.

To our knowledge, this value is the largest among those for the transition metal oxides, and surpasses $\gamma \approx 210$ mJ/mol-VK^2 for LiV_2O_4, which is known as the first heavy-fermion transition-metal oxide.[10] Taking account of the fact that the magnetic instability as well as structural instability exists just near $x = 0.5$, the large γ value at this point should be attributed to the critical enhancement due to both the spin fluctuations and the electron-phonon interaction.

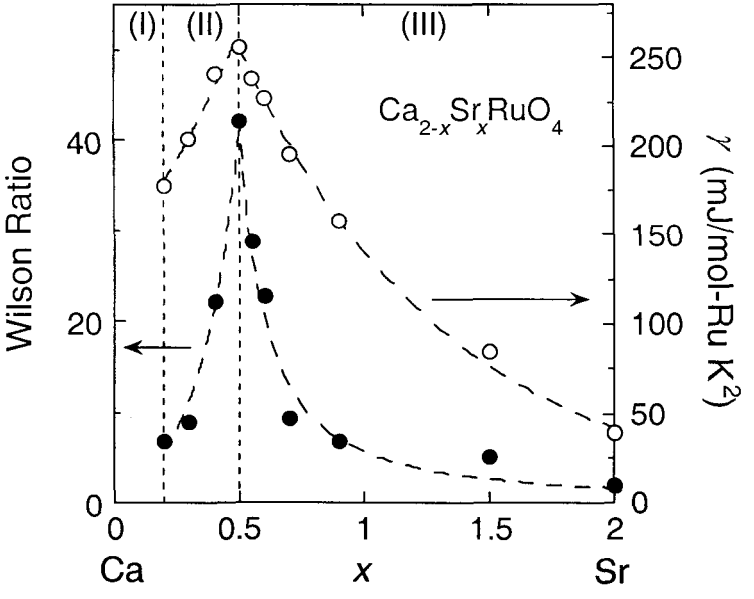

Figure 2: x dependence of the electronic specific heat coefficient γ at 0.4 K (open circle, right axis) and Wilson ratio (solid circle, left axis) for single crystal $Ca_{2-x}Sr_xRuO_4$. The broken lines are guides to the eye.

While γ decreases with Ca substitution in the M-M region, reflecting the formation of the peak in the temperature dependence of C_e/T, it is significant that the system retains a large value around 175 mJ/mol-RuK^2 near the M/NM transition point around $x = 0.2$. This may be due to electron-electron correlations enhanced near the Mott transition.

A well-defined measure to characterize the enhancement by the correlation effect is the Wilson ratio, which is defined by

$$R_W = \pi^2 k_B^2 \chi(0)/(g^2 \mu_B^2 \gamma S(S+1)) \quad (1)$$

where S, μ_B and k_B are spin, Bohr magneton and Boltzmann's constant. This ratio is scaled to be unity for a non-interacting Fermi gas, and the change in the ratio reflects the character of electron correlation in the system. The electron-phonon interaction enhances γ, but not $\chi(0)$ and reduces R_W. The electron-electron correlation enhances R_W to 2, as calculated for a Kondo system.[11] The enhancement beyond that is usually attributed to ferromagnetic spin correlation with additionally enhanced $\chi(0)$, and in fact observed in a series of nearly FM systems.[12] Although the ground state of $Ca_{2-x}Sr_xRuO_4$ may not be a Fermi liquid around $x = 0.5$, R_W is still a well-defined experimental measure to clarify how the electron correlation evolves from the Fermi liquid Sr_2RuO_4 with Ca substitution.

Figure 2 illustrates the x dependence of R_W calculated by Eq. (1). Here, $\chi(0)$ and γ in the equation are the lowest temperature values measured, that is, the susceptibility at 1.8 K in Fig. 4 in Ref. [1] and γ at 0.4 K in Fig. 2. S is fixed to 1/2 according to the result of Curie-Weiss fitting in Ref. [7]. While R_W for Sr_2RuO_4 is 1.7 corresponding to its strongly correlated Fermi liquid ground state, R_W first increases gradually with Ca substitution and then reveals critical divergence at $x = 0.5$ to reach the value more than 40. $R_W \approx 40$ is so large that it well surpasses those known for other well studied nearly FM materials, such as $R_W = 5.8$ for Pd, 5.4 for Ni_3Ga, and 12 for $TiBe_2$ (see Ref. [12]). This strongly suggests that the Ca substitution enhances ferromagnetic coupling in Sr_2RuO_4 to lead to a nearly FM state near $x = 0.5$. Once the system goes beyond $x = 0.5$ into the M-M region, however, R_W decreases and finally down to 7 at $x = 0.2$ just near the M/NM transition. The crossover of the magnetic coupling to AF should result in this decrease of R_W.

To summarize, we have revealed the critical enhancement of C_e/T around the structural instability at $x_c \approx 0.5$ in $Ca_{2-x}Sr_xRuO_4$ by low temperature specific heat measurements. Beside this, the Wilson ratio shows diverging behavior at around x_c. This strongly suggests that the system around the structural instability is also close to a ferromagnetic (FM) instability, suggestive of underlying competition between the instabilities of the structural transition and FM ordering.

Acknowledgments

The authors acknowledge T. Ishiguro for his support in many aspects. They thank H. Fukazawa for his technical support and valuable discussions. This work has been supported in part by a Grant-in-Aid for Scientific Research from the Ministry of Education, Science, Sports and Culture of Japan. One of the authors (S.N.) has been supported by JSPS Research Fellowships.

*Present address: National High Magnetic Field Laboratory, Florida State University, Tallahassee, Florida 32310, USA.

References

1. S. Nakatsuji and Y. Maeno, *Phys. Rev. Lett.* **84**, 2666 (2000).
2. S. Nakatsuji, S. Ikeda and Y. Maeno, *J. Phys. Soc. Jpn.* **66**, 1868 (1997).
3. G. Cao, S. McCall, M. Shephard, J. E. Crow and R. P. Guertin, *Phys. Rev. B* **56**, R2916 (1997).
4. H. Fukazawa, S. Nakatsuji and Y. Maeno, *Physica B* **281&282**, 613 (2000).
5. Y. Maeno, H. Hashimoto, K. Yoshida, S. Nishizaki, T. Fujita, J. G. Bednorz and F. Lichtenberg, *Nature* (London) **372**, 532 (1994).
6. K. Ishida, H. Mukuda, Y. Kitaoka, K. Asayama, Z. Q. Mao, Y. Mori and Y. Maeno, *Nature* (London) **396**, 658 (1998).
7. S. Nakatsuji and Y. Maeno, *Phys. Rev. B* **62**, 6458 (2000).
8. O. Friedt, M. Braden, G. Andrè, P. Adelman, S. Nakatsuji and Y. Maeno, *Phys. Rev. B* **63**, 174432 (2001).
9. S. Nakatsuji and Y. Maeno, *J. Solid State Chem.* **156**, 26 (2001).
10. S. Kondo, D. C. Johnston, C. A. Swenson, F. Borsa, A. V. Mahajan, L. L. Miller, T. Gu, A. I. Goldman, M. B. Maple, D. A. Gajewski, E. J. Freeman, N. R. Dilly, R. P. Dickey, J. Merrin, K. Kojima, G. M. Luke, Y. J. Uemura, O. Chmaissem and J. D. Jorgensen, *Phys. Rev. Lett.* **78**, 3729 (1997).
11. K. Yamada, *Prog. Theor. Phys.* **53**, 119 (1975).
12. S. R. Julian, A. P. Mackenzie, G. G. Lonzarich, C. Bergemann, R. K. W. Haselwimmer, Y. Maeno, S. NishiZaki, A. W. Tyler, S. Ikeda and T. Fujita, *Physica B* **259-261**, 928 (1999).

EFFECTS OF PARALLEL MAGNETIC FIELDS ON THE UNUSUAL METALLIC BEHAVIOR IN TWO DIMENSIONS

D. POPOVIC

NHMFL-Tallahassee, 1800 E. Paul Dirac Dr., Tallahassee, FL 32310-3748, USA

The fate of the metallic phase in parallel magnetic fields represents one of the major open issues in the studies of dilute, strongly interacting systems in two dimensions (2D). In this experiment, the temperature dependence of conductivity $\sigma(T)$ of a 2D electron system in silicon has been studied in parallel magnetic fields B. At $B = 0$, the system displays a new and unexpected kind of metallic behavior with $d\sigma / dT > 0$, and a novel type of a metal-insulator transition,[1] which occurs at a critical electron density $n_c(0)$. At low fields ($B \leq 2$ T), n_c increases as $n_c(B) - n_c(0) \propto B^{\beta}$ ($\beta \approx 0.9$), and the zero-temperature conductivity scales as $\sigma(n_s,B,0)/\sigma(n_s,0,0) = f(B^{\beta}/\delta_n)$ (where $\delta_n = (n_s - n_c(0))/ n_c(0)$, and n_s is electron density) as expected for a quantum phase transition. The metallic phase persists in fields up to 18 T, consistent with the saturation of n_c at high fields. These results strongly suggest that the 2D metal may exist even for spinless electrons.

1. X. G. Feng, D. Popovic, S. Washburn, and V. Dobrosavljevic, *Phys. Rev. Lett.* **86**, 2625 (2001).

GEOMETRICAL FRUSTRATION, AND RELEVANCE FOR HIGH FIELD STUDIES

A. P. RAMIREZ

Los Alamos National Laboratory, MST-10, MS K764,
Los Alamos, New Mexico 87545

Geometrical Frustration arises when the symmetry of a magnetic interaction is incompatible with the spatial symmetry of the crystalline lattice. Magnetic field can break this symmetry condition and we will illustrate different classes of behavior on the pyrochlore lattice – spin ice for Ising spins and spatial symmetry projection for Heisenberg spins.

Contributed Papers

This page is intentionally left blank

EFFECTS OF IN-PLAIN STRAIN ON MAGNETISM IN $LaMnO_3$ THIN FILMS

K. H. AHN

Theoretical Division, T-11, Los Alamos National Laboratory
Los Alamos, New Mexico, 87545, USA
E-mail: ahn@lanl.gov

A. J. MILLIS

Center for Material Theory, Department of Physics and Astronomy, Rutgers University
Piscataway, New Jersey, 08854, USA

The effects of the in-plane strain on the magnetic properties of $LaMnO_3$ thin films are calculated using an elastic energy expression and a tight binding Hamiltonian with electron-lattice coupling. Tensile uniaxial strain of the order of 2%, which is the order of the magnitude of those induced in thin films by lattice mismatch with substrates, is found to change the magnetic ground state from A-type antiferromagnetic state to purely antiferromagnetic state.

These days a lot of attention has been focused on the strain effects in thin films of perovskite manganites, so called 'colossal' magnetoresistive materials.[1] Since most of the future technological applications of this class of materials would require thin films on substrates, it is important to understand the effects of strains induced by substrates. Though the strong electron-lattice coupling, particularly the Jahn-Teller coupling, is believed to be important to understand these strain effects, theoretical study on this issue is still lacking. In this work, we study the effects of uniaxial strains in $LaMnO_3$ (undoped compound of manganites), which has a (π,π, 0) type JT distortion (or orbital ordering) below 750 K, and A-type (or (0,0,π) type) antiferromagnetic (AF) spin ordering below 140 K.

The total elastic energy per Mn ion we will consider is

$$E_{tot}^{Elastic} / N_{Mn} = (E_u + E_s + E_{JT} + E_{anh}) / N_{Mn}. \quad (1)$$

E_u and E_s are the elastic energies due to the uniform strains and the (π,π, 0) staggered strains, respectively

$$E_u / N_{Mn} = \frac{1}{2} K_B Q_{1u}^2 + \frac{1}{2} K^* (Q_{1u}^2 + Q_{3u}^2), \quad (2)$$

$$E_s / N_{Mn} = \frac{1}{2} K_{2s} Q_{2s}^2 + \frac{1}{2} K_{3s} Q_{3s}^2, \quad (3)$$

where $Q_{1u} = a_o (e_{xx} + e_{yy} + e_{zz})/\sqrt{3}$, $Q_{2u} = a_o (e_{xx} - e_{yy})/\sqrt{2}$, $Q_{3u} = a_o (2 e_{zz} - e_{xx} - e_{yy})/\sqrt{6}$, $Q_{2s} = a_o (v_{sx} - v_{sy})/\sqrt{2}$, $Q_{3s} = a_o (2 v_{sz} - v_{sx} - v_{sy})/\sqrt{6}$, v_{sa} is the (π π 0) amplitude of $v_i^a = u_i^a - u_{i-\hat{a}}^a$, and u_i^a is the displacement along the a direction of an

oxygen ion located between Mn ion at $\vec{i}$ and $\vec{i}+\hat{a}$. E_{JT} represents the Jahn-Teller coupling between Mn e_g orbital state and the lattice distortion:

$$E_{JT}/N_{Mn} = -\sqrt{3/2}\lambda[\cos 2\theta_1(Q_{3u}+Q_{3s})+\sin 2\theta_1(Q_{2u}+Q_{2s})+ \cos 2\theta_2(Q_{3u}-Q_{3s})+\sin 2\theta_2(Q_{2u}-Q_{2s})]/2 \quad (4)$$

where $\theta_{1,2}$ represent Mn e_g orbital state on the two sublattices:

$$|\theta_{\vec{i}}> = \cos\theta_{\vec{i}}\,|3z^2-r^2> + \sin\theta_{\vec{i}}\,|x^2-y^2>. \quad (5)$$

E_{anh} is the anharmonic elastic energy between the nearest neighbor Mn and O ions:

$$E_{anh} = A\frac{4}{\sqrt{3}}a_0{}^3\sum_{i,a}(e_{aa}/2+u_i^a-\delta_i^a)^3+(\delta_i^a-u_{i-a}^a-e_{aa}/2)^3, \quad (6)$$

where $\vec{\delta i}$ represents the Mn ion displacement vector at site $\vec{i}$.

We minimize E_u+E_s+E_{JT} about the orbital state (This gives $\tan(2\theta_{1,2}) = \pm Q_{2s}/Q_{3u}$.) and lattice distortions, and then treat E_{anh} as a perturbation. From this we obtain the total energy:

$$E_{tot}/N_{Mn} = K_B Q_{1u}{}^2/2 + K^* Q_{3u}{}^2/2 + K_{2s}Q_{2s}{}^2/2 - \sqrt{3/2}\lambda\sqrt{Q_{2s}{}^2+Q_{3u}{}^2} + AQ_{2s}{}^2(Q_{1u}-Q_{3u}/\sqrt{2}) \quad (7)$$

For thin films with in-plane strains, we calculate the lattice distortions in the following way: We assume that (π π 0) distortion pattern is favored even in strained films, and the film is thin enough to make the epitaxy perfect. Therefore, e_{xx} and e_{yy} are determined by substrates, and other lattice distortions and orbital states, $\theta_{1,2}$, can be found by minimizing E_{tot} (π,π,0). Parameters of the model are determined from experiments, as explained in Ref. [2].

θ_1 versus in-plane strain, $e_{\|}$, (Here, we assume square lattice for substrate.) is shown in Fig. 1. The change in θ_1 is about $\pm 5^o - 15^o$. For tensile strains, orbital states approach towards $|x^2-y^2>$. For compressive strains, towards $|3z^2-r^2>$. This can be understood from the fact that in $\theta_{1,2} = |x^2-y^2>$ state, the x-y plane Mn-O-Mn distance tends to be farthest, and in $\theta_{1,2} = |3z^2-r^2>$ state, shortest. Since the change of θ_1 by 30° would correspond to changing the orbital state from $|3x^2-r^2>$ to $|x^2-y^2>$, the 15° change predicted for 2 % strain is a very large change of the orbital state, which is the result of the strong electron-lattice coupling combined with the small effective modulus K^*-K_{2s} (see Ref. [2]).

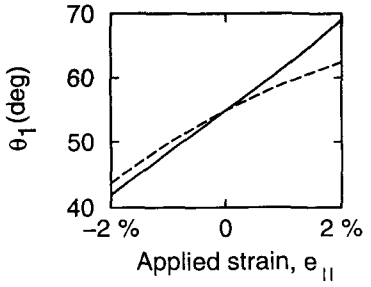

Figure 1: θ_1 versus $e_{\|}$: The solid and dashed lines are for the parameter sets determined from two experiments. (See Ref. [2] for detail).

Once the lattice distortions for thin films are determined from the elastic energy, then we use a tight-binding Hamiltonian with the Hartree-Fock approximation of the on-site Coulomb interaction to calculate total e_g electronic energy for different magnetic orderings. The tight-binding Hamiltonian for Mn e_g electron we use is explained in detail in Ref. [3]. The magnetic energy in $LaMnO_3$ has two contributions: one from an isotropic t_{2g} derived core-spin core-spin interaction, and one from the motion of the e_g electrons:[4]

$$E_{mag} = J_{t2g} \sum_{i,\delta} \hat{S}_{c,i} \cdot \hat{S}_{c,i+\delta} + E_{tb}[\{\hat{S}_c\}]. \qquad (8)$$

Here J_{t2g} is fixed by the observation that $CaMnO_3$ (the end-member with no e_g electrons) is an antiferromagnet with T_N = 120 K. E_{tb} is the energy of the e_g electron calculated by the tight binding model, $<H_{eg,\,tot}>$.

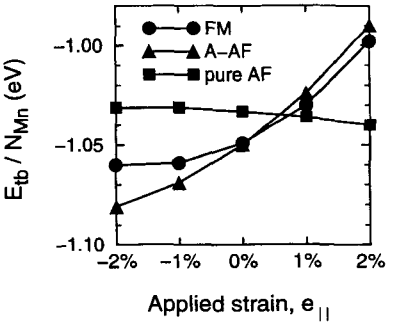

Figure 2: Total eg electronic energy versus applied strain, for ferromagnetic, A-type antiferromagnetic, and purely antiferromagnetic core spin configurations. We use t_o=0.622 eV, $2J_HS_c$=3.7 eV, λ=1.7 eV/Å, U = 1.2 eV, and lattice distortions for the solid lines in Fig.1.

For the lattice distortions in strained films obtained above, we calculate the e_g electronic energies for the competing magnetic orderings. The results are shown in

Fig. 2. It shows that as the tensile strain is applied, the purely AF ordering is favored over the A-AF, by about 50 meV, which will be increased further if we add t_{2g} exchange energy. This change is larger than the $T_N \sim 10$ meV for bulk $LaMnO_3$. Therefore, the results suggest that the magnetic order can be changed to pure AF by 2 % tensile strain.

The main reason for this is the change of the hybridization energy, $-2t^2/\Delta$, where t is the hopping amplitude between filled and empty levels with energy difference Δ. For the $3x^2-r^2/3y^2-r^2$ orbital state in bulk $LaMnO_3$, the hopping between the lower JT level ($3x^2-r^2$)at site $\vec{i}$ and the upper JT level (z^2-x^2) at site $\vec{i}+\hat{x}$ is $t=\sqrt{3}t_o/2$. This hybridization makes A-AF favored in bulk orbital ordering. As the orbital ordering changes towards x^2-y^2 / x^2-y^2 by tensile strain, the hopping between lower (x^2-y^2) and upper ($3z^2-r^2$) JT levels decreases ($t=\sqrt{3}t_o/4$). At this expense, the hopping between the two lower JT levels in different spin manifolds, which is possible for pure AF, increases. The change of the orbital state by 2 % strain is large enough to induce a pure AF ground state. Since $t_o \sim 0.6$ eV, $\Delta \sim 3$ - 7 eV, the typical change of the kinetic energy is a fraction of 100 meV, which agrees with the calculation. The result also suggests that the changes in the e_g orbital occupancy by substrate-induced strain play a crucial role in the phenomena observed in Ref. [1] for doped manganites.

In summary, we found that ± 2 % strain in $LaMnO_3$ can induce significant changes in the e_g orbital states and magnetic properties. This result shows that the strong coupling between electron and lattice is crucial to understand the effects of the substrate-induced strain in thin film perovskite manganites. This work is supported by NSF-DMR-9705182, the University of Maryland and Rutgers University MRSEC, and U.S. DOE.

References

1. T. Y. Koo *et al.*, *Appl. Phys. Lett.*, **71**, 977 (1997), J. O'Donnell *et al.*, *Phys. Rev. B* **54** , 6841 (1996), Y. Suzuki *et al.*, *Appl. Phys. Lett.* **71**, 140 (1997), B. S. Teo *et al.*, *J. Appl. Phys.* **83**, 7157 (1998), A. J. Millis *et al.*, *J. Appl. Phys.* **83**, 1588 (1998).
2. K. H. Ahn and A. J. Millis, *Phys. Rev.* B **64**, 115103 (2001).
3. K. H. Ahn and A. J. Millis, *Phys. Rev.* B. **61**, 13545 (2000).
4. I. V. Solovyev *et al.*, *Phys. Rev. Lett.* **76**, 4825 (1996), O. N. Mryasov *et al.*, *Phys. Rev. B* **56**, 7255 (1997).

OBSERVATION OF QUANTUM OSCILLATIONS IN FOUR-LAYER $BaRuO_3$

C. S. ALEXANDER, Y. XIN, Z. X. ZHOU, S. MCCALL, G. CAO, J. E. CROW
National High Magnetic Field Laboratory, Tallahassee, FL 32310
E-mail: alexande@magnet.fsu.edu

Well characterized single crystals of the four layer crystallographic form of $BaRuO_3$ were studied at low temperatures ($20 < T < 850$ mK) and high magnetic fields ($0 < H < 30$ T). Quantum oscillations have been observed via the Shubnikov - de Haas and de Haas - van Alphen effects. In marked contrast, $BaRuO_3$ with the nine-layer structure shows no similar behavior, suggesting a substantial change in the Fermi surface or quasi-particle relaxation times. The quantum oscillations provide insight into the ground state which, like those of other layered ruthenates, is characteristically sensitive to electron-lattice coupling. This observation is significant in that it represents the first example of quantum oscillations in a non-Ruddlesden–Popper type ruthenate and provides some insight into the Fermi surface even though a psuedo-gap is evident in other studies.

Introduction

Much attention has been given to the ruthenates lately, in part due to the richness of physical phenomena present in this family of materials. Over the past several years, the Ruddlesden–Popper ruthenates have been well characterized and show a wide range of behavior including non-conventional superconductivity, itinerant electron magnetism, Mott transition, and metamagnetism[1-4] More recently, some attention has been given to a chemically similar yet structurally different system $BaRuO_3$.

$BaRuO_3$ is a low dimensional transition metal oxide structurally characterized by chains of RuO_6 octahedra with both face and corner sharing between octahedra as shown in Fig. 1. $BaRuO_3$ is known to form three crystallographic structures; (1) the nine layered rhomohedral (9R), (2) the six layered hexagonal (6H), and (3) the four layered hexagonal (4H) (see Figs. [5-7]). Each of these forms are chemically equivalent. The differences arise out of the stacking sequence of RuO_6 octahedra along the c-axis. This in turn leads to a variance in the strength of the Ru-Ru interactions. For corner sharing octahedra, the Ru-Ru interaction is through exchange with the intermediary O. For face sharing octahedra, the indirect exchange through the oxygen appears to be secondary direct overlap of the Ru d-orbitals in adjacent cells. Thus the variation in the stacking sequence in these systems lead to varying relative amounts of Ru-Ru and Ru-O-Ru interaction. This work will concentrate on the 4H structure and briefly compare it to the 9R structure.

In this paper, we report on the observation of quantum oscillations in the electrical resistivity and the magnetization of 4H $BaRuO_3$. These results give a measure of the Fermi surface which may be helpful in interpreting future theoretical work on the band structure of these materials.

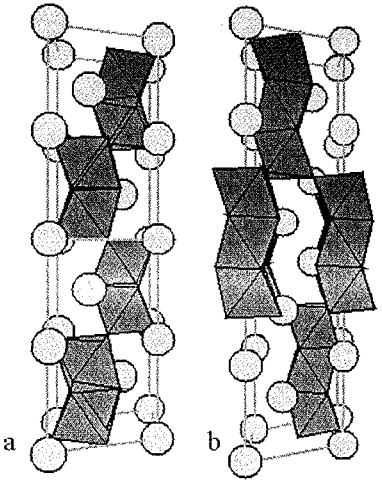

Figure 1: Crystal structure of (a) 4H and. (b) 9R $BaRuO_3$.

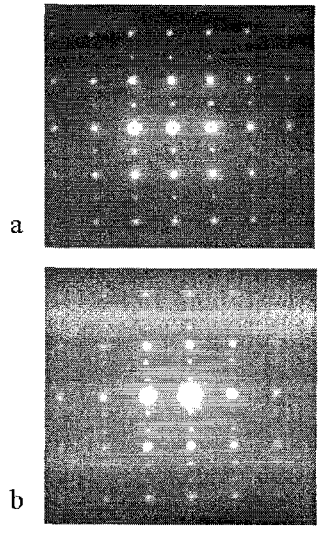

Figure 2: TEM diffraction patterns for (a) 4H and (b) 9R $BaRuO_3$.

Experimental Details

Single crystals of both 4H and 9R $BaRuO_3$ were grown in Pt crucibles from off-stoichiometric quantities of RuO_2, $BaCO_3$, and $BaCl_2$ using a self-flux technique. The different crystallographic forms are the result of different temperature profiles used. Single crystals produced in this fashion were characterized by TEM microscopy. TEM diffraction patterns for the 4H and 9R samples are shown in Fig. 2. In the data, the number of intermediate maxima indicates the number of layers in the material. The 4H structure is characterized by one intermediate maxima while the 9R structure will have two. The uniformity of the pattern and the absence of any extra maxima indicate that the samples are single phase and free from defects.

Shown in Fig. 3 is the c-axis magneto resistance for several crystal orientations relative to the applied field at 30 mK. Immediately obvious is the large anisotropy between the measurements with the applied field parallel (90°) and perpendicular (0°) to the c axis. For field applied parallel to the c axis, the magneto resistance displays an unexplained peak at low fields followed by a minimum and increasing positive magneto resistance. This positive magneto resistance is systematically reduced as the crystal is rotated away from the c-axis and in the vicinity of $\theta \approx 40°$, the magneto resistance becomes negative. These results indicate quasi one-dimensional behavior reflective of the crystal structure and Ru-Ru coupling.

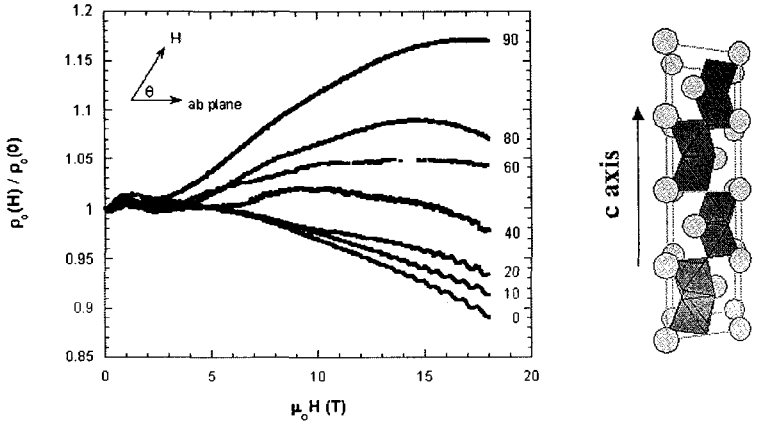

Figure 3: Magnetoresistance along the c axis for 4H $BaRuO_3$ for several crystal orientations at 30 mK. The numbers at the far right indicate the angle θ between the applied field and the c axis.

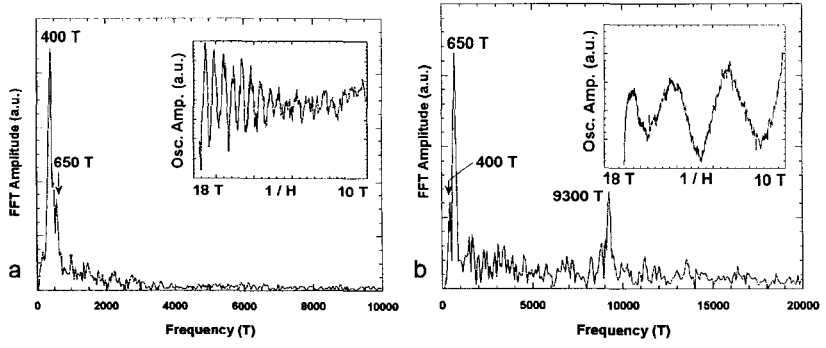

Figure 4: Fourier spectrum of (a) Shubnikov-deHass and (b) deHass-vanAlphen oscillations of 4H $BaRuO_3$ for field perpendicular to the c axis at 30 mK. The insets show the oscillations after removal of the background.

Oscillations can be seen in the magneto resistance when the applied field is within 40 degrees of being perpendicular to the c axis. In the case of applied field perpendicular to the c axis, these oscillations are shown in the inset to Fig. 4(a). Upon Fourier analysis, fundamental frequencies of 400 T and 650 T were detected in the oscillations as shown in the Fourier spectrum of Fig. 4(a). These relatively low frequencies indicate that the observed oscillations are derived from a small branch of the Fermi surface. Additionally, oscillations were seen in magnetization measurements in the same temperature and field range. These oscillations, shown in the inset to Fig. 4(b), also show fundamental frequencies of 400 T and 650 T as well as a higher fundamental frequency of 9300 T. Further study of this material at

higher magnetic field is clearly needed to gain a more complete picture of the Fermi surface.

While we cannot at this point construct a complete picture of the Fermi surface, the observation of quantum oscillations allows us to draw some conclusions about the material. Recently, Y.S. Lee *et al.*, have observed a psuedo gap opening at low temperature.[8] They suggest that the observed metallic behavior is due to a strong suppression of the scattering rate, which counteracts the effects of a gap opening. A suppression of the scattering rate is certainly consistent with the observation of quantum oscillations which depend on a long mean free path. Once again a more complete picture of the Fermi surface will provide more insight into these matters.

Acknowledgments

Support for the NHMFL is by the National Science Foundation under Cooperative Agreement No. DMR95-27035 and the State of Florida.

References

1. Y. Maeno *et al., Nature* **372**, 532 (1994)
2. G. Cao *et al., Phys. Rev. B* **56**, 321 (1997)
3. C. S. Alexander *et al., Phys. Rev. B* **60**, R8422 (1999)
4. G. Cao *et al., Phys. Rev. Lett.* **78**, 1751 (1997)
5. P. C. Donohue, L. Katz and R. Ward, *Inorg. Chem.* **4**, 306 (1965)
6. J. M. Longo and J. A. Kafalas, *MRS Bull.* **3**, 687 (1968)
7. S. T. Hong and A. W. Sleight, *J. Solid State Chem.* **128**, 251 (1997)
8. Y. S. Lee *et al., Phys. Rev. B* **64**, 165109 (2001)

HOPPING CONDUCTIVITY IN ONE-DIMENSIONAL $Ca_3Co_2O_6$ SINGLE CRYSTAL

J. M. BROTO, B. RAQUET and H. RAKOTO
Laboratoire National des Champs Magnétiques Pulsés, UMR 5830, 143, Av. de Rangueil – BP4245, 31432 Toulouse cedex 4, France

M. N. BAIBICH
Instituto de Física, UFRGS, Av. Bento Gonçalves 9500, Caixa Postal 15051, 91501-970 Porto Alegre, RS Brazil

S. LAMBERT and A. MAIGNAN
Laboratoire CRISMAT, UMR CNRS 6508, ISMRA, Boulevard du Mal Juin, 14050 Caen Cedex, France

We studied the electronic conductivity of the quasi-one dimensional $Ca_3Co_2O_6$ single crystal. The results evidence a VRH conductivity with temperature-induced crossover between 1D (intra-chain) and 3D transport and the opening of a Coulomb gap in the *d* bands. At low temperatures, an applied magnetic field induces a large negative magneto-resistance (MR) independent from the 3D magnetic ordering. Both spin-dependent hopping and field-induced suppression of the Coulomb gap are discussed.

1 Introduction

The $Ca_3Co_2O_6$ compound consists of parallel 1-D $Co_2O_6^{6-}$ chains with alternating face-sharing CoO_6 trigonal prisms and CoO_6 octahedra along the c-axis.[1] The short metal-metal intra-chain distance (0.28nm) compared to the inter-chain separation (0.53nm) reinforces the 1-D character of the structure. Magnetic studies reveal an intra-chain ferromagnetic ordering ($T_{c1} \approx 24$ K) and a weaker antiferromagnetic (AF) inter-chain coupling ($T_{c2} \approx 12$ K) (see Refs. [2-4]). Field induced transition from a ferrimagnetic (Fi) to a ferromagnetic (Fo) state suggests that it behaves as a planar Ising-like Heisenberg AF triangular lattice[3] The spin states[2] and Fo order along the chains support the idea of partially filled *d* bands with unpaired electrons on Co sites. $Ca_3Co_2O_6$ is therefore a unique candidate to study electronic transport in low dimensional frustrated magnetic systems.[4]

2 Results and Discussion

In the temperature range of AF inter-chain interactions, our magnetization measurements exhibit a step-by-step magnetization reversal with a plateau at one third of the total magnetization (1.33 μ_B/mol. of $Ca_3Co_2O_6$) followed by a Fi to Fo

ordering between chains. The sharpness of the transition confirms the mono-crystalline nature of our samples with the c-axis parallel to H.

The resistivity, from 2 K to 450 K, is measured along the c-axis (Fig.1). An activated behavior is observed over the whole temperature range with a resistivity of 4Ω.cm at 300 K, far above the metallic limit. The resistivity perpendicular to the chains is about 10^4 times larger than the longitudinal one. The resistivity behavior suggests a strong localization regime of the form $\rho(T)=\rho_0 exp(T_0/T)^n$ (Eq(1)). From the logarithmic derivative technique, we infer four conductivity regimes: below 25 K, the resistivity is well described by Eq.(1) with $\nu \approx 0.43$ and $T_0 \approx 600$ K. A transition regime (crossover) is observed between 30 K and 70 K. Above 70 K, $\rho(T)$ is thermally activated with $\nu \approx 0.9$ and $T_0 \approx 87$ K. This intermediate regime is limited by a drastic resistivity drop above 230 K, which saturates around 450 K.

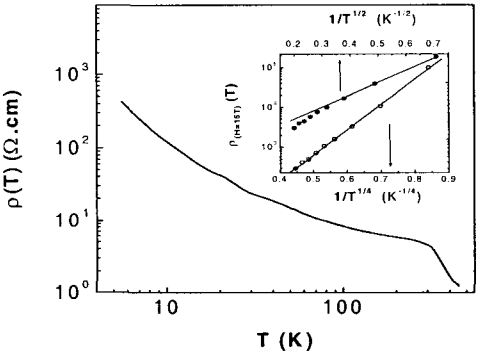

Figure 1: Resistivity versus temperature of the $Ca_3Co_2O_6$ single crystal measured along the chains. In inset, the high field resistivity at 15 T, $\rho_{(H=15T)}(T)$, versus $T^{-1/2}$ (top scale) and $T^{-1/4}$ (bottom scale). Solid lines are the best linear fits.

For the low temperature regime, below 25 K, a hopping exponent about 0.5 is consistent with the Efros-Shklovskii (ES) conductivity-type variable range hopping (VRH), i.e. a VRH with a soft Coulomb gap Δ_c due to Coulomb interactions between the localized d electrons. We estimate $\Delta_c \approx 30$ K ± 10 K from the upper temperature limit of the ES regime. This gap drives the hopping energy below 30 K and surprisingly appears with the intra-chain ferromagnetic state.

For intermediate temperatures, from 70 K to 230 K, the activated behavior ($\nu \approx 1$) of the conductivity may be associated to different electronic transport mechanisms involving either extended or localized cobalt d states. According to the Co-Co distances, a nearest-neighbor hopping hints of an intra-chain conductivity with very weakly probable transition rates perpendicular to the chains. The activation energy would be related to average energy barriers between the Co_{oct} to

Co_{trig} sites along the chains. On the other hand, extended calculations of the variable range hopping process in 1-D systems also exhibit an activated T^{-1} law for the conductivity.[5] If we sketch a 1D-VRH mechanism between 70 K and 230 K, we infer the ratio between the average hopping distance $R_{opt}(T)$ and the localization length α^{-1}: $R_{opt}(T)/\alpha^{-1} \approx 18/\sqrt{T}$, greater than 1. We also deduce $N_1(E_F) \times \alpha^{-1} \approx 60$ eV^{-1}, where $N_1(E_F)$ is the 1D density of states along the chains. The 1D conductivity assumption above 70 K holds on if $R_{opt}(T)$ remains lower than the inter-chain distance. This implies a localization length of the order of 0.25 nm, which is favorably compared to the Co-Co distance within the chains. From the above condition, we estimate the 1D density of states $N_1(E_F) \approx 2.5\ 10^{11}$ $eV^{-1}m^{-1}$. Such a high value agrees with extended Hückel calculations which predict narrow bandwidths for the Co *d* bands[6] and E_F close to its maximum.

The high temperature regime, above 230 K, represents a departure towards a more conducting regime: the inter-chain transition rate is significantly increased as the corresponding energies become accessible by phonon assisted hopping.

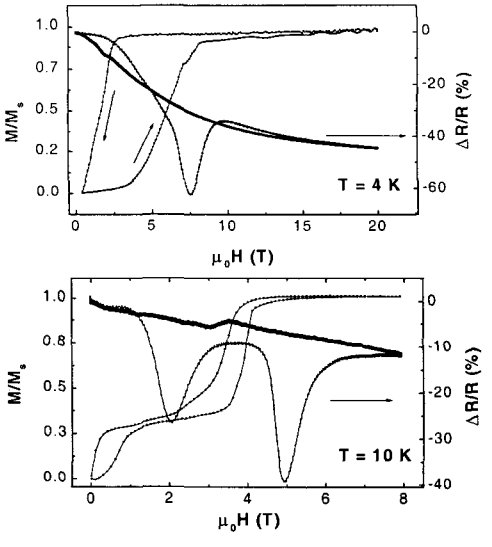

Figure 2: Magnetization and magneto-resistance of the $Ca_3Co_2O_6$ single crystal in the longitudinal configuration at 4 K (top panel) and 10 K (bottom panel).

The longitudinal high field MR measurements shows a negligible field effect above 25 K. Below the ferromagnetic ordering temperature, a negative MR appears that drastically increases with decreasing temperature, reaching around 80% at 2 K

and 20T. On the increasing pulsed field only, the $\rho(H)$ curves exhibit very deep minima corresponding to "transient" resistivity decreases (Fig.2). They are superimposed to the monotonous and reversible $\rho(H)$ decrease and they both depend on the temperature and field dynamics.[4]

The large monotonous resistivity decrease is uncorrelated to the magnetization process (Fig.2). The high field resistivity at 15 T still exhibits a weak insulating behavior following a $1/T^{1/4}$ law (see inset Fig.1). This evidences a field-induced transition from the ES conductivity to 3D-Mott VRH regime.[7] The Coulomb gap in the *d* bands in zero-field, below 30 K, is drastically affected by the Zeeman energy with a Landé factor of 3.7 (see Ref. [8]). Below 25 K and in the high field regime, we estimate the localization length comparable to that obtained above 70 K, close to the metal-metal intra-chain distance, and the average hopping distance large enough for electronic hopping between nearest and next nearest chains.[4]

The transient resistivity decreases are connected to the field-induced transitions during the magnetization (Fig.2). Simulations for an Ising-like Heisenberg AF triangular lattice have shown the appearance of a transient in-plane component of the magnetization when it is reversed from the Fi to the Fo state along the easy axis.[9] The inter-chain hopping which contributes to a conductivity enhancement, may be favored by the existence of a non-trivial component of the magnetization perpendicular to the chains when the AF coupling between chains is broken. On the other hand, the dynamic effects suggest that the internal magnetic flux variations during the magnetization jumps may also be responsible for transient induced voltages. More experiments are required, particularly in static fields.

References

1. H. Fjellvag *et al., J. Solid State Chem.* **124**, 190 (1996).
2. S. Aasland *et al., Solid States Commun.* **101**, 187 (1997).
3. A. Maignan *et al., Eur. Phys. J. B.* **15**, 657 (2000).
4. B. Raquet *et al., to be published.*
5. J. Kurkijärvi, *Phys. Rev. B* **8**, 922 (1973).
6. G. V. Vajenine *et al., Chem. Phys.* **204**, 469 (1996).
7. N. F. Mott and J. Non, Cryst. Solids **1**, 1 (1968).
8. H. Kageyama *et al., J. Phys. Soc. Jpn.* **66**, 3996 (1997).
9. S. Miyashita, *J. Phys. Soc. Jpn.* **55**, 3605 (1986).

COLOSSAL EFFECTS IN TRANSITION METAL OXIDES CAUSED BY INTRINSIC INHOMOGENEITIES

J. BURGY,[1] M. MAYR,[1] V. MARTIN-MAYOR,[2] A. MOREO[1] and E. DAGOTTO[1]
[1]*Florida State University, NHMFL, Tallahassee, Florida 32306, USA*
[2]*Dipartimento di Fisica, Universit a di Roma, La Spienza, Piazzale Aldo Moro 2, 00185 Roma, Italy*

The general aspects of the influence of quenched disorder on the competition between ordered states separated by a first-order transition are investigated. A phase diagram with features resembling quantum-critical behavior is observed. The paramagnetic phase at low temperature consists of coexisting ordered clusters, with a random orientation of the order parameter. Specializing to manganites, this state is shown to have a colossal magnetoresistance effect. A new scale T* for cluster formation is predicted. It is argued that cuprates have similar features, compatible with the large proximity effect of the very underdoped regime.[1]

1. J. Burgy *et al.*, *cond-mat*/0107300.

^{55}Mn NMR AND MAGNETIZATION STUDIES OF $La_xSr_{1-x}MnO_3$

T. CALDWELL, P. L. KUHNS, W. G. MOULTON and A. P. REYES
National High Magnetic Field Laboratory, 1800 E Paul Dirac Dr., Tallahassee, FL 32310

The ^{55}Mn NMR has been measured in $La_xSr_{1-x}MnO_3$ for x=0.2and 0.3 as a function of temperature, in zero field and in field. The samples had a room temperature resistivity of 10^{-4} ohm-cm, and the magnetizarion showed a sharp FM transition 312 K. The zero field FM frequency follows $T^{3/2}$ power law at both x values consistent with the simple magnon model. A second feature at lower frequency of uncertain origin is observed.

1 Introduction

Recent interest in Lanthanum manganites $La_{1-x}A_xMnO_3$ (A = Alkali metals) has been primarily due to the discovery of colossal magnetoresistance (CMR) in the appropriately substituted compounds. However, the manganese perovskites also reveal interesting magnetic and electronic properties as a function of dopant and doping levels giving a rich phase diagram with antiferromagnetic (AFM), ferromagnetic (FM), metallic, and charge ordered regions.[1]

While there have been a number of NMR studies of other Manganites, notably the Ca doped system, the only previous NMR studies on the Sr doped system has been only at 4.2 K showing a single spectrum for 3 samples in the doping range x-0.1 to 0.25 (see Ref. [2]). In the metallic or semiconducting phase a single FM line is observed, over all ranges of A and doping levels, around 390 MHz due to the fast exchange, produced by the double exchange, of the Mn^{3+} and Mn^{4+} sites. In the insulating phase with slow exchange the Mn^{+3} line is observed near 410 MHz while the Mn^{4+} line appears at around 330 MHz. In many of the manganites (Ca doped (see Ref. [3]), Tb+Ca doped, $Ca_xPr_{1-x}MnO_3$ (see Ref. [4]) and several others.) both FM and AF lines are observed with the AF lines around 260 MHz. The FM spectra are easily distinguished from the AF spectra. The FM spectra exhibit a large enhancement factor of order 100 to 1000 outside the domain walls and an even larger enhancement within the domain walls, while there is no enhancement in the AF phase.

2 Experimental

The samples used in this work, $La_xSr_{1-x}MnO_3$, have the rhombohedral structure, as determined by TEM studies, and no evidence of a second phase. The rhombohedral structure is ferromagnetic at x>0.125 while the orthorhombic is antiferromagnetic for x<0.1 and ferromagnetic for x>0.1 (see Ref. [5]). The single crystal samples (~100mg) were grown by the floating zone method under ambient pressure of

oxygen.[6] The low temperature resistance was10^{-4} ohm-cm indicating the high purity of the bulk sample, and the x=0.2 shows a very sharp FM transition at 315 K. Figure 1 shows the hyperfine field (H_{hyp}=frequency/γ) as measured by the ^{55}Mn NMR in zero external field as a function of temperature. The internal field (proportional to M through the contact hyperfine interaction) decreases slightly more rapidly in the x=0.2 than x=0.3 with reduced temperature. The zero temperature magnetization M_0 is 399 T and 391 T for the x=0.2 and x=0.3 samples respectively. This difference is due to different contributions from the Mn to the internal field.

The fractional change in magnetization is: $\Delta M/ M_0= (0.0587/SQ)(k_BT/2JS)^{3/2}$ from the thermal excitation of magnons in a simple spin wave model. The fit of the data to this power law is shown in Fig. 3. The data for x=0.2 and x=0.3 converted to the reduced magnetization was fit to this function, giving J=2.7679meV and J=1.9690meV respectively. J was then calculated from the mean field theory equation ($J=(3k_BT_C)/(2zS(S+1))$) for x=0.3 assuming z=8, S=1.7, T_c=370 K giving a J~2.5 and for x=0.2 assuming z=8, S=1.8, T_c=312 K giving J~1.92 which are both in good agreement with the values obtained from the spin wave theory. The difference in S for the two $T^{3/2}$ fits indicates a difference in the admixture of Mn^{4+} and Mn^{3+} with a corresponding spins of 2 and 3/2, with the ratio determined from M_0. The hybridization of the charge between the two Mn ions is such that x=0.2 has a higher contribution from the Mn^{4+} ion than in the x=0.3.

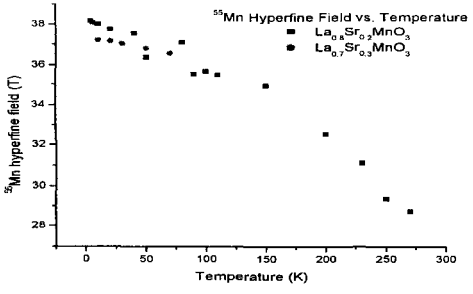

Figure 1: 55Mn Hyperfine field as a function of T, proportional to M. H_{hyp}=F/γ

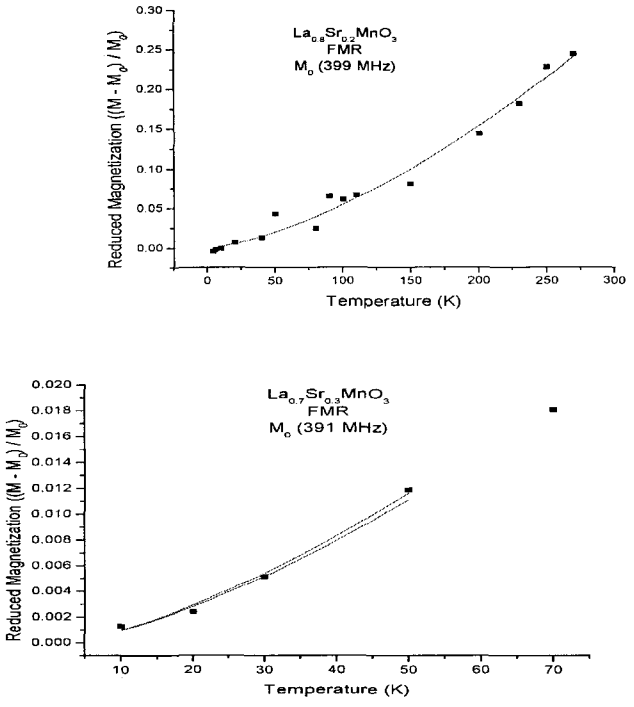

Figure 2: The fractional change in magnetization (M/M_0) versus temperature. The solid curve is a fit to $T^{3/2}$. The upper is 0.3, the lower x=0.2.

Both the x=0.2 and x=0.3 samples show a weak line centered at 330 MHz. The ^{55}Mn NMR of the x=0.3 spectrum is shown in Fig. 4, the large line is from the predominant FM phase, whose frequency varies with field as H_{int}- $\gamma * H_0$ and requires very low power due to the FM enhancement. This line broadens with increasing field. The frequency of the lower frequency line is nearly field independent and requires two orders of magnitude more power in order to be observed. The low frequency signal broadens rapidly with field and is lost as the field is increased beyond 0.5 T. A possible interpretation of this second line could be a canted state, or due to the small enhancement, may possibly be an AF state, although the frequency is higher than the AF phase in other Manganites or it possibly, but unlikely, due to an impurity phase. Work is in progress to elucidate this.

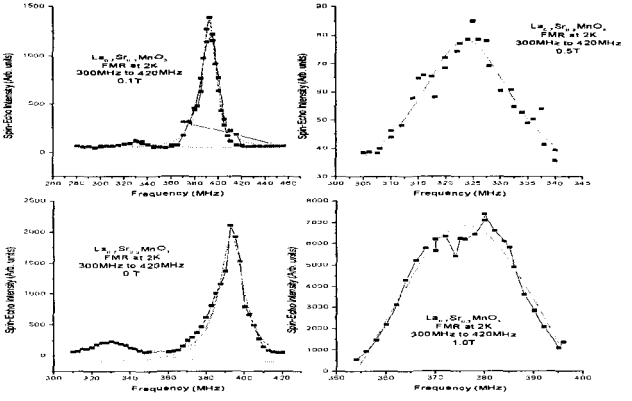

Figure 3: ^{55}Mn NMR spectra for x=0.3 showing the two observed lines as a function of externally applied field. The strong, high frequency line is clearly the FM conducting phase. The weak lower frequency line is of uncertain origin (see text).

The experimental results presented completely rule out microscopic inhomogeniety (or microscopic phase mixture) but do not conclusively rule out either a canted state system, AF state, or macroscopic impurities within the sample. The primary reason for the difference in previous results obtained in $La_{1-x}Ca_xMnO_3$ (see Ref. [2]) is the larger size of the Ca atom versus Sr has effect on the structure in terms of increased Mn-O bond angles for Ca which in turn has effect on whether a Jahn-Teller distortion can occur.[7]

References

1. G. Papavassiliou *et al., Phys. Rev Lett.* **84**, 761 (2000).
2. A. M. de Leon-Guevara, *Phys. Rev B* **56**, 6031 (1997).
3. G. Papavassiliou *et al., Phys. Rev. B* **59**, 6390 (1999).
4. M. M. Savosta *et al., Phys. Rev. B* **62**, 9532 (2000).
5. J. F. Mitchell *et al., Phys. Rev B.* **54**, 6172 (1996).
6. D. Shulyatev, MISA, for providing sample.
7. P. Schlottman *et al., Phys. Rev B.* **60**, 7911 (1999).

HIGH FIELD NMR STUDIES OF NaV_2O_5 TO 44.7 T

T. CALDWELL,[1] P. L. KUHNS,[1] W. G. MOULTON,[1]
A. P. REYES,[1] P. N. ROGERS,[2] and R. N. SHELTON, [1]
[1] *National High Magnetic Field Laboratory, 1800 E Paul Dirac Dr. Tallahassee, FL 32310*
[2] *University of California, 918 Drake Dr., Davis, CA 95616*

^{23}Na NMR studies have been carried out to map the uniform to dimerized phase boundary up to 44.7 T in the NHMFL hybrid. The transition is observed by the splitting of the NMR line (H//*a* axis) by the lattice distortion. The field dependence of T_c up to 44.7 T, in agreement with previous magnetization data to 30 T, is very small (α=0.092) compared to 0.4 for conventional SP systems and shows no deviation within experimental error from the h^2 dependence, while optical data show a decrease of the slope in the H-T phase diagram beginning around 40 T. The region of an anomaly near T 33 T and 32 K observed in optical data taken in the long pulse magnet at LANL[1] was also explored. The only evidence in the NMR of the observed optical anomaly near 33 T and 32 K was line broadening over a 2 T interval.

1 Introduction

There has been much interest in systems which exhibit a strong interplay of the charge, spin, and phonon degrees of freedom. Such interplay can lead to many interesting phenomena including systems exhibiting spin-Peierls (SP) phenomena. While there are a number of organic spin-Peierls systems. $CuGeO_3$ was the only inorganic until the discovery of α-NaV_2O_3 by Hase.[1] Since then it has become clear that if α-NaV_2O_3 is a spin- Peierls system, it falls into a different class. Below T_c there are two distinct V sites in the unit cell, chains of V^{4+} AF coupled along the b axis, and decoupled by non-magnetic V^{5+} chains in between. It has been variously described as a ¼ filled ladder system and a zig-zag chain system.[2,3] The opening of a spin gap of ~100 K, nearly 4 times that of $CuGeO_3$, and a distortion that at least doubled the unit cell indicated this was a new SP system.[3] However, there are a number of differences which indicate this is not a simple SP system: a) the BCS ratio ($2\Delta_0/k_BT_c$) is about 6, more than twice that of other SP systems,[3] b) the dependence of T_c on field is much smaller than other SP systems, c) there is no evidence of an incommensurate phase, and d) the transition appears to be associated with a charge ordering of the V^{4+} and V^5. Recent optical studies[5] show an unusual, not understood, feature just below T_c around 32 T and a "bending" of the phase boundary above about 40 T. Previous NMR work was at 4.2 T.

2 Experimental

The single crystal samples (~50mg) were grown by solid state reaction. The x-ray data showed no signs of a second phase and the T_c as measured by magnetization

was 34.7 K. The ^{23}Na NMR spectrum at temperatures above T_c consists quadrupolar triplet, which splits into 8 lines below the lattice distortion, corresponding to the development of 4 non-equivalent sites for $H_0 \| a$. The spectrum above and below the transition at 40 T are shown in Fig. 1

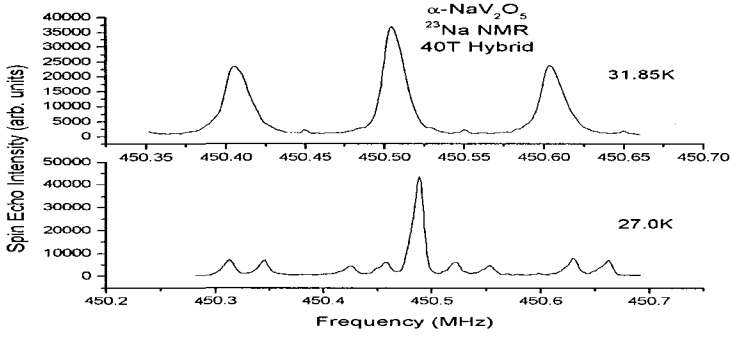

Figure 1: ^{23}Na NMR spectrum above and below the SP transition at 40 T. These spectra show the site splitting at the transition into 4 inequivalent Na sites, $H_0 \| a$.

The frequency of the individual sites as a function of temperature are shown in Fig. 1, along with the spin part of the Knight shift K_{spin}. The rounding of the splitting with temperature shows the lattice distortion develops gradually, and that the transition is second order in agreement with the low field work.[4] The spin part of the Knight shift, K_{spin}, is shown in the lower part of Fig. 3. K_{spin} is obtained by subtracting K_{orb}, the value of K_{tot} at 6 K, where K_{spin} is near zero for the dimerized phase. Note that K_{spin} starts to decrease at about 3 K above where the splitting occurs and where the charge ordering appears. We associate this with charge ordering since temperature of the initial decrease in K_{spin} is independent of field. This behavior is in contrast to previous NMR work where the ^{27}Na K_{spin} does not start to decrease until the lattice distortion occurs.[4] In that work only the ^{51}V K_{spin} shows a decrease where charge ordering occurs, about 3 K above the lattice distortion and dimerization. The reason for this difference in behavior is not currently understood.

The frequency shift of the outermost line was fit to the scaling relation: $f(T)=f(T_c)+\delta f(1-T/T_c)^{\beta}$ where β is the critical exponent, δf is the frequency difference between low temperature (6 K) and the frequency just above the transition. The best fit resulted in $\beta=0.20$, in agreement with the 4.2 T NMR value[4] and neutron data. A similar fit to the 40 T data resulted in the same value of β, showing β is field independent as expected.

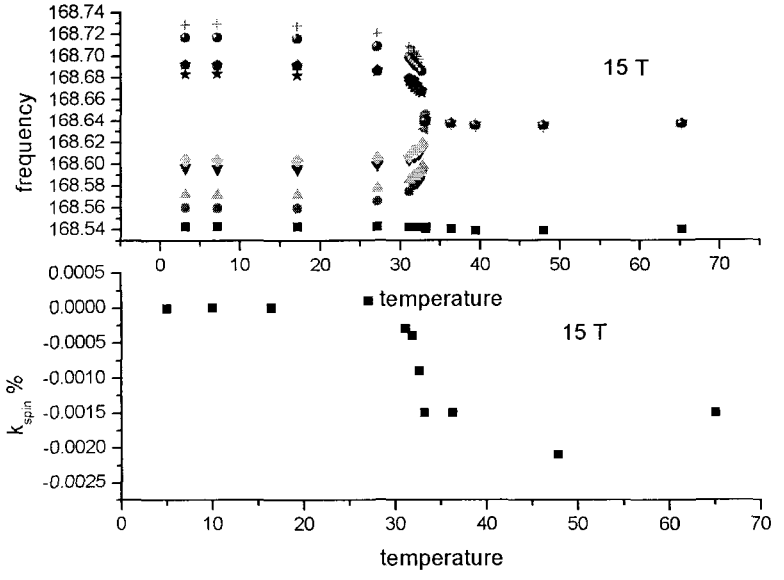

Figure 2: Site splitting of the quadrupole satellite of the ^{23}Na NMR spectrum and spin part of the Knight shift (K_{spin}) as a function of temperature at 15 T. The appearance of the splitting signals the lattice distortion, while the K_{spin} starts to decrease about three degrees above the distortion, which we ascribe to the onset of charge ordering.

The dependence of T_c on magnetic field for SP systems has been calculated by Cross[6] using the Luther-Peschel formalism in the weak coupling approximation and leads to the behavior: $\Delta T_c/T_c(0)=-\alpha h^2$, with the reduced field $h=g\mu_B H/2kT_c(0)$. The g factor was taken as 2, consistent with that used to fit the magnetization data of Bompadre *et al.*[7]

The data to H=44.7 T, along with the magnetization data[7] to 30 T, are shown in Fig. 3. A fit to these data gives $\alpha=0.093$, with no deviation from the h^2 dependence within experimental error. This value is slightly larger than that from the magnetization data alone (0.072) but in agreement with specific heat data, and much smaller than that predicted and observed, 0.32 to 0.44, in conventional SP systems, This clearly shows that NaV_2O_5 falls outside the class of conventional SP systems.

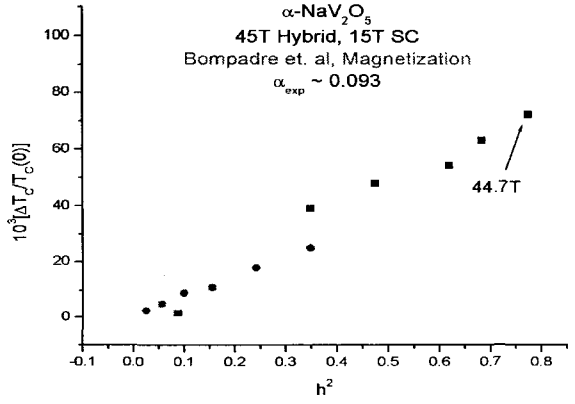

Figure 3: Plot of T_{sp} vs. h^2 showing the h^2 dependence is maintained to 44.7 T. No evidence of an incommensurate phase was observed.

Careful studies of the NMR from 28 T to 34 T just below the transition showed no evidence of the anomaly observed in optical data except for a small increase in line width. It appears that whatever anomalies the optical experiments are seeing show only weakly, if at all, in the NMR data.

References

1. M. Hase *et al., Phys. Rev Lett.* **70**, 3651 (1993).
2. M. Isobe *et al., J. Phys. Soc. Jpn* **65**, 1178 (1996).
3. Y. Fuji *et al., J. Phys. Soc. Jpn* **66**, 326 (1997).
4. Y. Fagot-Revurat *et al., Phys. Rev. Lett.* **84**, 4176 (2000).
5. A. B. Sushkev *et al., Phys. Rev. B* **63**, 220401 (2001).
6. M. C. Cross, *Phys. Rev. B* **20**, 4606.
7. Bompadre *et al., Phys. Rev. B*, **60** 15721 (1999).

TRIPLET MODES IN A QUANTUM SPIN LIQUID ACROSS THE CRITICAL FIELD

N. CAVADINI, CH. RÜEGG and A. FURRER
Laboratory for Neutron Scattering,, ETH Zurich & PSI, CH-5232 Villigen PSI
E-mail: nordal.cavadini@psi.ch

H. U. GÜDEL and K. KRÄMER
Dept. for Chemistry and Biochemistry, University of Berne, CH-3000 Bern 9

H. MUTKA and A. WILDES
Institut Laue-Langevin, B.P. 156, F-38042 Grenoble Cedex 9

K. HABICHT, and P. VORDERWISCH
BENSC, Hahn-Meitner-Institut, D-14109 Berlin Wannsee

S=1/2 $TlCuCl_3$ is a magnetic insulator with a singlet ground state and a finite spin gap to triplet excited states. At finite fields, the degeneracy of the triplet states is lifted according to the Zeeman interaction term. Field-induced magnetic ordering occurs in $TlCuCl_3$ at the critical field H_c~6T, when the Zeeman interaction overcomes the spin gap at the antiferromagnetic zone center. A detailed characterization of the elementary excitations realized at $H>H_c$ is obtained by means of inelastic neutron scattering on single crystals. The general framework of field-induced quantum criticality in a three-dimensional spin liquid is illustrated on the complete dynamic range for the first time.

1 Introduction

Quantum spin pairs minimize their exchange energy forming a valence bond (VB). The VB limit is a robust starting point for notable model systems of quantum magnetism, characterized by a singlet ground state and a finite spin gap to triplet excited states. Exploration of the latter by inelastic neutron scattering (INS) unambiguously allows the determination of the VB network through the system specific energy dispersion of the triplet spectrum.

S=1/2 $TlCuCl_3$ has a quantum spin gap $\Delta=g\mu_B H_c$ of the order H_c~6T, (see Refs. [1, 2]) and references therein. Its dynamic properties above the gap were recently investigated by INS on single crystals,[3] spectra collected along the main symmetry directions of reciprocal space were well reproduced by a model based on three-dimensional (3D) Heisenberg interactions. The absence of classical magnetic order in spite of 3D interactions is ascribed to a dominant VB quantitatively determined in.[3,4] This illustrates an interesting régime where collective correlations on the one

side and quantum fluctuations on the other side compete at "T=0". Upon application of a finite external field H, the triplet excited states are split according to the Zeeman energy $g\mu_B H$ between distinct $|11\rangle$, $|10\rangle$ and $|1{-}1\rangle$ modes. At the 3D antiferromagnetic zone center the lowest Zeeman mode reduces and eventually overcomes the spin gap at $H{=}H_c$. In $TlCuCl_3$ the observed INS spectra for $H{\rightarrow}H_c$ confirm the progressive splitting of the triplet states throughout reciprocal space, certifying the ideal realization of "first principles".

2 High-Field Phase

In S=1/2 $TlCuCl_3$ the modest critical field H_c~6 T is well within the accessible experimental range. Static measurements evidence field-induced magnetic ordering above H_c in accordance with the 3D nature of the magnetic interactions.[3,4] The measured phase boundary $H_c(T)$ is successfully reproduced by a theory assuming Bose-Einstein condensation of the diluted triplet gas,[5] and references therein. At the AF zone center elastic neutron scattering investigations unambiguously show the appearance of magnetic Bragg reflections for $H{>}H_c$, substantiating the picture of the soft Zeeman mode driving the quantum phase transition. The high-field phase is described by commensurate ordering perpendicular to the external field direction.[6]

Less is known about the elementary excitations in this novel state. The lack of spectral information in the field-induced ordered phase of S=1/2 spin liquids notably limits their description and – in the end – their complete rationalization. To our knowledge, the INS investigations in $TlCuCl_3$ single crystals to be introduced below constitute the first microscopic contribution directly addressing this issue. Measurements were performed at the cold neutron spectrometers V2 (HMI, Berlin) and IN14 (ILL, Grenoble), with preliminaries at TASP (SINQ, Villigen PSI). All instruments were equipped with vertical cryomagnets and operated in standard configurations to be detailed elsewhere. Applied temperatures down to T=50 mK were chosen according to the different aspects of our concern. For the purpose of the present contribution, salient results restricted to the AF zone center at $H{>}H_c$ are summarized as follows:

- At high energy, the correspondings of the $|00\rangle{\rightarrow}|10\rangle$ and $|00\rangle{\rightarrow}|1{-}1\rangle$ Zeeman transitions smoothly renormalize as a function of the applied field according to a perturbative VB model.
- At low energy, the corresponding of the $|00\rangle{\rightarrow}|11\rangle$ Zeeman transition is replaced by classic-like modes emerging from the field-induced magnetic Bragg reflections.

The latter is most clearly observed at the maximum field applied H=14 T by k scans at constant energy transfer (Fig. 1). A perturbative correction of the aforementioned VB model to account for staggered internal fields on a mean-field basis captures the high energy features discussed in.[7] However, this approach is less

accurate in the low energy, long wavelength limit most sensitive to the nature of the quantum phase transition. A mapping of the ground state and lowest excited state to exact quantum models has proven adequate for the description of the high-field phase observed in $S=1/2$ $CuGeO_3$. Field-dependent incommensurability (IC) of the soft modes is reported in[8,9] and references therein. Similar observations are recently claimed in the 1D high-field phase of a Haldane system.[10] We remark that estimates along these lines can be formulated in the title compound from the uniform magnetization m experimentally reported in:[1] with $(2/g)m\sim0.05\mu_B/Cu^{2+}$ at $H=14$ T a putative overall IC shift $2k_F=g\mu_B m\sim0.05$ r.l.u. is predicted. This value exceeds the resolution of the Bragg reflections observed at the AF zone center. Linear extrapolation of the low energy spectrum previously described further supports a gapless commensurate origin of the soft modes. Though we are not aware of appropriate model generalizations for the 3D high-field phase realized in $S=1/2$ $TlCuCl_3$, we speculate that given the upper quantum critical dimension theoretical support might be expected in favor of these novel results (Fig. 1).

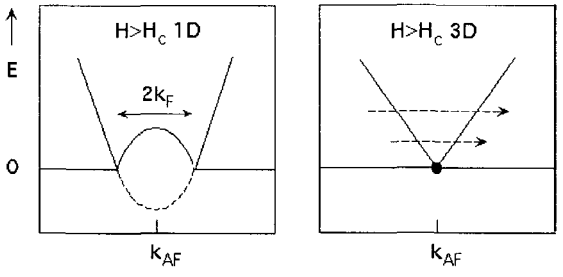

Figure 1: Ideal sketch of the low lying spectrum distinguishing the high-field phase of a one-dimensional and a three-dimensional VB system, as described in the text. The latter applies to $S=1/2$ $TlCuCl_3$, showing field-induced Bragg reflections at the antiferromagnetic zone center k_{AF} (right panel, full circle) and sharp emerging excitation modes. Dashed arrows qualitatively illustrate the constant energy technique adopted in the measurements.

3 Outlooks

For the first time, a complete investigation of the elementary excitations in the field-induced ordered phase of a $S=1/2$ spin liquid is performed. Results at $H>H_c$ determine the qualitative separation of the spectrum in quantum- and classic-like excitations as previously described, compare also.[11] These findings are highly nontrivial because:

- The underlying ground state is manifestly tuned at fixed "$T=0$" by the applied field $H>H_c$ only, demonstrating a clean quantum phase transition.

- Both the addressed quantum- and classic-like excitations originate from magnetic fluctuations at the same spin site.

A severe lack of microscopic studies limits the general discussion of the spin dynamics in 3D VB compounds at $H>H_c$. Above investigations constitute a remarkable exception, hopefully motivating additional efforts towards a complete understanding. We speculate that the conditions encountered in $S=1/2$ $TlCuCl_3$ might be representative for many 3D VB compounds of less favorable parameter range, as exemplified in[12,13] and references therein. An extension of the experimental input is mandatory to fully characterize this novel phase.

Acknowledgments

We gratefully thank M. Meissner, S. Kausche and F. Thomas for helpful assistance during part of the experiments.

References

1. W. Shiramura *et al., J. Phys. Soc. Jpn.* **66**, 1900 (1997).
2. A. Oosawa M. Ishi and H. Tanaka, *J. Phys.: Condens. Matter* **11**, 265 (1999).
3. N. Cavadini *et al., Phys. Rev. B* **63**, 172414 (2001).
4. N. Cavadini N *et al., J. Phys.: Condens. Matter* **12**, 5463 (2000).
5. A. Nikuni *et al., Phys. Rev. Lett.* **84**, 5868 (2000).
6. H. Tanaka *et al., J. Phys. Soc. Jpn.* **70**, 939 (2001).
7. Ch. Rüegg *et al., Appl. Phys. A* (accepted for publication)
8. H. M. Rønnow *et al., Phys. Rev. Lett.* **84**, 4469 (2000).
9. M. Enderle *et al., cond-mat/0008202* (unpublished).
10. A. Zheludev *et al., cond-mat/0107416* (unpublished).
11. A. Zheludev *et al., Phys. Rev. Lett.* **85**, 4799 (2000).
12. B. Leuenberger *et al., Phys. Rev. B* **31**, 597 (1985).
13. G. Xu *et al., Phys. Rev. Lett.* **84**, 4465 (2000).

CRYSTAL-FIELD EFFECTS IN THE FIRST-ORDER VALENCE TRANSITION IN $YbInCu^4$ INDUCED BY EXTERNAL MAGNETIC FIELD

M. DZERO
Florida State University, NHMFL and Physics Department, Tallahassee, Florida 32310, USA

As it was shown earlier [Dzero, Gor'kov and Zvezdin, *J. Phys.: Condens. Matt.* **12**, L711 (1000)], the properties of the first-order valence phase transition in $YbInCu_4$ in the wide range of magnetic fields and temperatures are perfectly described in terms of a simple entropy transition for free Yb ions. Within this approach, the crystal field effects have been taken into account and we show that the phase diagram in the B - T plane acquires some anisotropy with respect to the direction of an external magnetic field.

1. M. O. Dzero, L. P. Gor'kov, and A. K. Zvezdin, *J. Phys.: Condens. Matt.* **12**, 1711 (2000).

TAMM-TYPE OF STATES AT THE INTERFACE IN $LA_{1-X}SR_XMNO_3$ (X=0.4, 0.55) SUPERLATTICES

M. DZERO and L.P. GOR'KOV

National High Magnetic Field Laboratory, Florida State University, Tallahassee, FL 32310

We address some of the results of the recent experiments by Izumi *et. al.* where the properties of heterostructures composed of $La_{1-x}Sr_xMnO_3$ (x=0.4, 0.55) layers have been investigated. Anomalies in conductivity and large magnetoresistance measurements for several heterostructures with thin constituent ferromagnetic (x=0.4) and antiferromagnetic (x=0.55) layers are explained in terms of existence of the localized (Tamm-type) of states at the interface.

Generally, as it is well known, the phase diagram for the perovskite manganites $A_{1-x}B_xMnO_3$ (A=La, Pr, Nd; B=Sr, Ca) consists of several different phases, with a crossover from one phase to another upon change in temperature T or doping concentration x (see, for example [1,2,3] and references therein). $A_{1-x}Sr_xMnO_3$ manganites deserve special attention for an appearence of ferro- or antiferro-magnetic orderings depending on temperature and concentration without a charge ordering (CO-phase).

In this paper we will focus on results obtained in [4] for manganites superlattices where a systematic study of physical properties of $La_{1-x}Sr_xMnO_3$ (x=0.4, 0.55) single-layer films and heterostructures composed of alternating stacks of these layers has been presented. It has been observed that the magnetization measurements indicate that the constituent x=0.4 and x=0.55 layers essentially keep their magnetic properties ($M \simeq (4-x)\mu_B$ per x=0.4 layer) which means that magnetization is simply proportional to the volume fraction of the FM layers. Conductivity also has been measured with and without applied external magnetic field for type of heterostructures, symbolically denoted as $[A_n,F_m]$ (here $[A_n,F_m]$ is a notation, which represents the number of unit cells (u.c.) of the constituent ferromagnetic (FM) x=0.4 and antiferromagnetic (AFM) x=0.55 layers of the superlattices; schematic presentation of these structures is shown on Fig. 1.). The suprising observation is that the conductivity for $[A_3, F_3]$ structure turns out to be much larger then the one for $[A_{10}, F_{10}]$ structure, while both these structures having the same ratio $\Delta_{0.4}/(\Delta_{0.4}+\Delta_{0.55})$, where the $\Delta_{0.4}$ and $\Delta_{0.55}$ represent the thicknesses of the constituent x=0.4 and x=0.55 respectively. Then, in order to elucidate the carrier motion at the interface, the magnetoconductivity measurements have been carried out. As a result, the magnetoconductivity for the case of

thin ($\leq$ 5u.c.) x=0.55 layers was observed to be considerable and the largest for the [A_3, F_3] structure, while the magnetoconductivity for the [A_3, F_{10}] structure is field independent. These experimantal observations are very in-

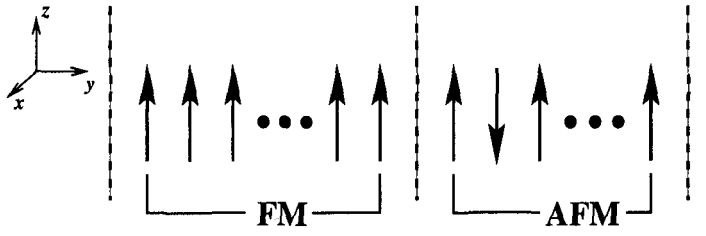

Figure 1. The schematic representation of our system: superlattice consisting of ferromagnetic and antiferromagnetic layers separated by an interface. In this paper, we consider the number of antiferromagnetic layers to be odd.

teresting because of quite unexpected conductivity behaviour for that type of systems with controlled magnetic structure.

In what follows, we would like to explain the results [4] by implying the existence of the localized states at the interface between the AF and FM layers. The so-called parallel circuit model (PCM), which is usually used for qualitative explanation of transport properties in various types of magnetic superstructures. In the PCM all layers are considered as an independent resistors but as it was shown in [4] it does not explain the magnetotransport results. Thus we can expect that interface adds essentially new features to the electronic transport. Transport in manganites is generally described in terms of the double-exchange (DE) model [5], in which for the antiferromagnetically alligned core spins, the phase will be always an insulating one.

As it was first shown by Tamm [6], even perfect crystals due to their finite size[a] may have energy levels laying in the energy gaps between the different energy bands. These energy levels are associated with the localized states at the surface of a crystal, and a decay rate of the localized electronic wave-functions along the perpendicular to the plane direction (y axis) must be finite. In our case, the last condition is provided by the dominant FM interactions between the adjucent FM and AFM layers at the interface.

In what follows we neglect the exchange interactions between the core spins in AFM and FM layers as well as at the interface and will adopt a

[a]By "finite size" we mean that generally one has to take explicitly surface type of effects into account

model, described by the double-exchange (DE) Hamiltonian:

$$\hat{H}^{\sigma}_{DE} = -\hat{t}^{x,z}_{i,j} - \hat{T}^{y}_{i,j} + J_H \cdot (1 - \delta_{e_i,\sigma})\delta_{ij}, \ (e_i = \uparrow, \downarrow), \tag{1}$$

where J_H is a Hund's coupling constant (in the DE limit: $J_H \to \infty$).

The variables which describe the electron's motion parallel and perpendicular to the layers can be separated. The charge is assumed to be homogeneously distributed in each layer. Thus, the electron energy will be equal to:

$$E_m(k_x, k_z) = -t_{xz}(\cos k_x + \cos k_z) + \lambda_m, \tag{2}$$

where λ_m is a solution of an eigenvalue equation:

$$\sum_{j=1}^{N} \hat{T}^{y}_{ij} \Psi_m(j) = \lambda_m \Psi_m(i), \tag{3}$$

(where $\Psi_m(i)$ is an electron's wave-function in i-th layer, and $\hat{T}^{y}_{ij}$ is the hopping matrix, describing motion of electrons along the y-direction and $N-2$ is a total number of FM layer). Let us consider how the effective width of the surface localized states depends on the value of E_0, with E_0 being an energy of an electron at the interface and t an a hopping amplitude between the neighboring layers. We can now write $\hat{T}^{y}_{ij}$ in (3) as:

$$\hat{T}^{y}_{ij} = \begin{bmatrix} E_0 & t & 0 & 0 & \cdots & 0 & 0 \\ t & 0 & t & 0 & \cdots & 0 & 0 \\ 0 & t & 0 & t & \cdots & 0 & 0 \\ \cdots & \cdots & \cdots & \cdots & \cdots & \cdots & \cdots \\ 0 & 0 & 0 & 0 & \cdots & 0 & t \\ 0 & 0 & 0 & 0 & \cdots & t & E_0 \end{bmatrix}, \tag{4}$$

As it turns out, for the case when $N \geq 4$, the eigenvalues can not be found analytically.

Since the electrons can not hop onto an AFM layer, the interface energy, E_0, is lower compared to the one at the FM layers. Thus, the charge will be distributed inhomogeneously along the y direction. As a next step, we include the Coulomb interaction between the electrons hopping along the y-axis by means of Kohn-Sham equations:

$$\hat{T}^{y}_{ij} \Psi_k(j) + \varphi(i)\Psi_k(i) = \lambda_k \Psi_k(i), \tag{5}$$

$$\varphi(i+1) - 2\varphi(i) + \varphi(i-1) = -\sum_{k<k_F} |\Psi_k(i)|^2. \tag{6}$$

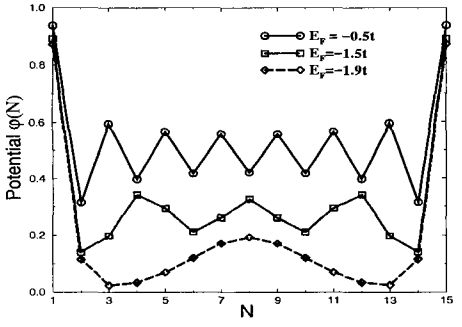

Figure 2. The results of the numerical solution of the Kohn-Sham equations for the potential distribution. The results are given for different values of the Fermi level relatively to the position of the localized states E_0. The oscillations in the potential are due to the change in the number of states under the Fermi level, when the latter is shifted.

The equations (5,6) have been solved numerically. As a result, the potential distribution along the y-axis is given on Fig. 1. As we see from Fig. 1, the lower the position of E_0 with respect to the energy band $[-t, t]$, the larger is the number of electrons which are localized at the interface. We suggest this fact as a qualitative explanation of data, published in [4]: electrons are localized at the interface, so that the overlap between the wave-functions at two neighboring interfaces is the stronger the smaller is the number of ferromagnetic layers in a slab. An understanding of magnetoresistance effect, which is highly pronounced in $[A_3, F_3]$ structure, needs an ability to calculate transport properties in a given film. We do not discuss that question here since it is very complicated. Besides, in order to fully understand physical behavior of electrons in thin magnetic films, one has to take into account an exchange interaction between the core spins, particularly focusing on a magnetic ground state at the interface.

To summarize, the results of recent experiments [4] on transport properties in superlattice composed of different numbers of FM and AFM layers of $La_{1-x}Sr_xMnO_3$ (x=0.44, 0.55) can be understood in terms of the localized states at the interface, which extend deep into the bulk of the FM layers. We have to emphasize, that experimental data [4] do not allow one to make a judgement regarding a magnetic structure of the interface layer at the very boundary. We leave this question for further discussion.

This work was supported by the NHMFL through the NSF cooperative

agreement DMR-9527035 and the State of Florida and (MD) by DARPA through the Naval Research Laboratory Grant No. N00173-00-1-6005.

References

1. Y. Tokura *et. al.*, J. Phys. Soc. Jpn. 63, 3931 (1994).
2. A. Urushibara *et. al.* Phys. Rev. B 51, 14103 (1995).
3. H. Fujishiro, M. Ikebe, and Y. Kohno, J. Phys. Soc. Jpn. 67, 1799 (1998).
4. M. Izumi *et. al.*, Phys. Rev. B 61, 12187 (2000).
5. C. Zener, Phys. Rev. 82, 403 (1951); P. W. Andreson, H. Hasegawa, Phys. Rev. 100, 675 (1955).
6. I. E. Tamm, Phys. Z. Sowjetunion 1, 733 (1932).

MAGNETIC RESONANCES OBSERVED IN THE HIGH-FIELD MAGNETO-OPTICAL ABSORPTION OF THE QUANTUM ISING FERROMAGNET $LiHoF_4$

R. S. EDWARDS, A. NARDUZZO, E. LYONS, L. CHILDRESS, S. J. BLUNDELL, J. SINGLETON and R. C. C. WARD

Clarendon Laboratory, Parks Road, Oxford, OX1 3PU, UK
E-mail: r.edwards1@physics.ox.ac.uk

The magneto-optical absorption of the quantum Ising ferromagnet $LiHoF_4$ has been measured in the frequency range 38 to 140 GHz, the temperature range 0.5 to 20 K and magnetic fields of up to 15 T. The sample was studied in two orientations, with the external magnetic field aligned perpendicular or parallel to the uniaxial direction, *i.e.*, along the quantum and classical directions. In each case, several families of resonances are observed, including linear EPR branches and a series of non-linear fast moving resonances. We present this data and propose an interpretation for the origin of these resonances.

We report experiments performed on the quantum Ising ferromagnet $LiHoF_4$ (see Refs. [1-4]). Below 1.53 K (at zero applied magnetic field) $LiHoF_4$ is ferromagnetic.[4] The ferromagnetism can be destroyed by heating the sample above 1.53 K, or by applying a magnetic field perpendicular to the spin axis.[4]

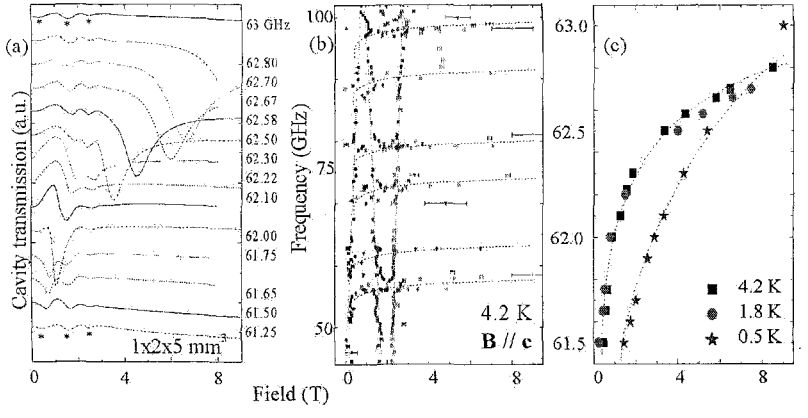

Figure 1: Results from the larger sample of $LiHoF_4$ (1x2x5 mm^3) taken at 4.2 K, with the magnetic field parallel to the **c** (1mm) direction, i.e. in the "classical" direction. (a) shows results taken at frequencies around 60 GHz, normalized and offset for clarity; (b) shows the positions of the resonances for all frequencies studied, with dashed lines showing the standard ESR branches and curves showing the fast-moving resonances; (c) shows the temperature dependence of the fast moving resonance at 62 GHz.

Electron spin resonance (ESR) has been measured in this material by several groups[3,5] in different frequency ranges. Several ESR branches have been measured, with a fundamental doublet with g=13.8. This work was done in a frequency range of approximately 70 to 600 GHz in large steps.[6]

We have extended these experiments to study the behaviour of the resonances in very small frequency steps. Firstly, a sample of $LiHoF_4$ was measured in a tuneable cylindrical cavity (tuneable between 45 and 55 GHz) (see Ref. [7]) and three ESRs were found, corresponding to resonances measured previously.[6] This was then extended to higher frequencies using millimetre-wave transmission techniques. Millimetre-waves were provided by a Millimetre-wave Vector Network Analyser (MVNA) (see Ref. [8]), which acts as a continuous source and detector of microwaves between 8 and 350 GHz. A superconducting magnet was used to provide magnetic fields between 0 and 15 T with an insert that enabled the experiment to be held at temperatures between 0.5 K and 300 K.

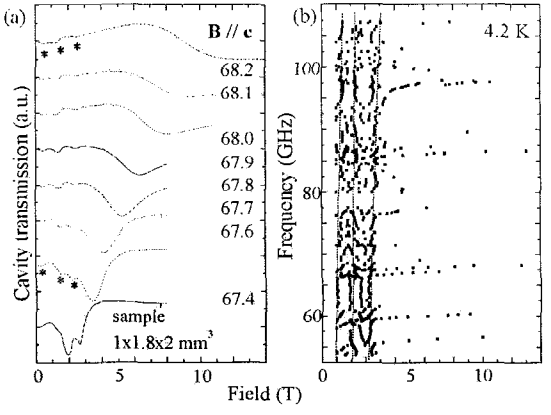

Figure 2: (a,b) A repeat of Fig. 1 showing data taken on a small sample of $LiHoF_4$ (1x1.8x2 mm^3, where **c** is the 1mm side).

Figure 1(a) shows magnetic field sweeps on a sample of $LiHoF_4$ (1x2x5mm^3) for frequencies around 60 GHz at a temperature of 4.2 K, i.e. above the transition temperature for zero applied field. The three basic ESR can be seen at low field (shown by stars on two sweeps). However, a new, strong feature can be seen which shifts non-linearly and extremely rapidly with changing frequency. This moves from zero field to above the range of the magnet in about 1 GHz.

Figure 1(b) shows the positions of all the resonances seen in the frequency range 44 to 104 GHz at 4.2 K for this orientation. The three linear ESR are shown (marked by dashed lines). The first line corresponds to transitions between the lines of the fundamental doublet.[6] The second and third have equal gradients but with opposite sign, and meet at 2.0 ± 0.3 T at zero frequency, indicating that they are the same transition measured above and below the crossing field of 2 T (this was not reported in the previous measurements).[6]

The fast moving resonance can be seen to repeat regularly (shown by dotted curved lines as an aid to the eye). Taking the frequency at 6 T for each resonance, it is found that they are acting as harmonics of two fundamental frequencies, 14.55 and 15.65 GHz.

We have studied these fast moving resonances at temperatures above and below the transition temperature. Figure 1(c) shows results for the resonance around 62 GHz at temperatures of 4.2, 1.8 and 0.5 K (shown by squares, circles and stars respectively). There is almost no difference between the results at the higher temperatures; the points start out moving almost linearly (c.f. ESR), then curve over towards some limiting frequency. Below 1.53 K the fast moving resonances are still visible (however, the three standard ESR vanish), but tail off to the limiting frequency slower and start off moving in a less ESR-like fashion. Remnants of these resonances persist to around 25 K.

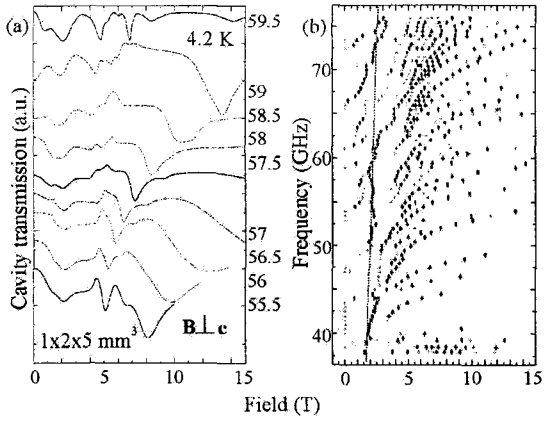

Figure 3: Results from the larger sample of $LiHoF_4$, taken at 4.2 K but with the magnetic field perpendicular to the c axis (1mm side), i.e. in the "quantum" direction.

Figure 2 shows data taken on a smaller sample (1x1.8x2 mm^3) in the same orientation, at 4.2 K. Again, the three ESR and several fast-moving resonances are seen. However, the resonances appear to reduce to harmonics of just one

fundamental frequency, 5.1 GHz at 6 T. The experiments have recently been repeated with the samples mounted in a different direction, i.e. B $\perp$ c. Figure 3 shows some of the data taken on the larger sample. As expected,[6] one ESR can be seen, but there are also many fast moving resonances visible. The results taken on the smaller sample in this orientation behave in a qualitatively similar.[9]

It is suggested[9] that these fast moving resonances are a remnant of the ordered state of the material. An external magnetic field can align the dipoles, leading to a state similar to a ferromagnet above a certain field. Above the transition temperature at low fields, the dipoles will behave as paramagnets, and so an ESR-like branch would be visible. At intermediate fields the dipoles will coalesce and begin to form domains, leading to a change in the field vs. frequency behaviour. At high fields all the domains will be aligned and the sample will behave as a ferromagnet and exhibit ferromagnetic-like resonance with a limiting frequency when all domains are aligned. Below the transition temperature the domains will already be part aligned at low field and the resonance will not be paramagnetic-like at low field. The dependence of these resonances on sample size and magnetization is being calculated.[9] This behaviour may be an observation of the Griffiths phase, in which features of the ordered (low-temperature) state of a material persist to higher temperature.[1,9,10]

References

1. D. Bitko, T. F. Rosenbaum and G. Aeppli, *Phys. Rev. Lett.* **77**, 940-943 (1996).
2. T. F. Rosenbaum, *J. Phys.:Cond. Mat.* **8**, 9759 (1996).
3. A. H. Cooke, D. A. Jones, J. F. A. Silva and M. Wells, *J. Phys. C* **8**, 4083-4095 (1975).
4. S. Sachdev, *Physics World* 33-38(April 1999).
5. H. P. Christensen, *Phys. Rev. B* **19**, 12 (1979).
6. J. Magarino, J. Tuchendler, J. P. D'Haenens, A. Linz, *Phys. Rev. B* **13, 7,** 2805 (1976); J. Magarino, J. Tuchendler, P. Beauvillain, I. Laursen, *Phys. Rev. B* **21, 1,** 18 (1980).
7. A. Ardavan, D. Phil, *thesis*, Clarendon Laboratory, University of Oxford.
8. MVNA built by *ABmm*, 52 Rue Lhomond, Paris, France. More details of its use can be found in J.M. Schrama *et al., J. Phys.:Cond. Mat.* **13**, (10) (2001) and references therein.
9. R.S. Edwards *et al., to be published.*
10. C. Binek and W. Kleemann, *Phys. Rev. Lett.* **72**, 1287 (1994); C. Binek, S. Kuttler and W. Kleemann, *Phys. Rev. Lett.* **75**, 2412 (1995).

LARGE EFFECTS OF MAGNETIC FIELD ON JOSEPHSON CURRENTS THROUGH ANTIFERROMAGNETIC BARRIERS

L. P. GOR'KOV[1] and V. Z. KRESIN[2]
[1]*NHMFL-Tallahassee, Florida State University, Tallahassee, Florida 32310, USA*
[2]*Lawrence Berkeley Laboratory, University of California-Berkeley, Berkeley, California 94720*, USA

Ferromagnetism being known to have a detrimental effect on superconductivity, we consider the Josephson current amplitude for junctions built up of antiferromagnetic metallic weak links. It is assumed that the latter consist of ferromagnetic layers with magnetizations aligned alternatively along perpendicular-to-the-layers direction. Currents between two superconducting electrodes flow along the layers. Such antiferromagnetic structure realizes itself in mixed valence manganites (the so-called A-phase), in an array of parallel ferromagnetic domains, or even in artificial GMR heterostructures. It is shown that even minor canting of magnetic moments in the presence of magnetic fields causes remarkable oscillations in the value of the Josephson current amplitude.

PRESSURE DEPENDENT MAGNETIZATION AND MAGNETIC ORDERING IN RARE EARTH RUTHENATES, Sm_2RuO_5, Gd_2RuO_5, Tb_2RuO_5, AND Nd_3RuO_7

R.P. GUERTIN
Department of Physics and Astronomy, Tufts University, Medford, MA 02155

S. McCALL,
National High Magnetic Field Laboratory, 1800 East Paul Dirac Dr., Tallahassee, FL 32310

The antiferromagnetic ordering temperatures of Sm_2RuO_5, Tb_2RuO_5 and the ferromagnetic ordering temperature of Nd_3RuO_7 are reduced by the application of high hydrostatic pressure, whereas that of antiferromagnetic Gd_2RuO_5 remains unchanged. The results are discussed in terms of the enhancement of the crystalline electric field interaction on the Ln cation constituents. A versatile method of measuring magnetization in high fields and high pressure is presented.

1 Introduction

We present the first experimental results obtained from a newly enhanced technique for measurement of the full magnetic moment of samples under the simultaneous influence of high magnetic fields and high hydrostatic pressure. The samples chosen for these first measurements are members of the lanthanide-transition metal oxide series[1], Ln_2RuO_5 and the weak ferromagnet, Nd_3RuO_7. The ground state of the three Ln_2RuO_5 members selected is antiferromagnetic, with T_N = 19.1 K, 9.8 K and 13.1 K for Ln = Sm, Gd and Tb, respectively. The magnetic entropy removed below T_N for Gd_2RuO_5, obtained from the specific heat, is nearly $2Rln(2S+1)$ = 34.6 J/mol-K, as expected for full ordering of the Gd cations.[1]

Ln_2RuO_5 has a complex orthorhombic structure with the Ru cations coupled via chains of corner-sharing RuO_5 square pyramids, and the Ln cations in two inequivalent seven-fold coordinated sites.[2] The signature of antiferromagnetism is clear–a peak in the temperature dependence of the low field magnetization, which is how we operationally define T_N. Based on the difference between field-cooled (FC) and zero field-cooled (ZFC) measurements we believe these systems order as canted antiferromagnets.

The magnetization of all three Ln_2RuO_5 samples was measured over a wide range of field, temperature and pressure: $0 < B < 9$ T, $2 < T < 300$ K, and $0 < P < 7$ kbar (0.7 GPa). We present the salient results of the pressure dependence of T_N in this paper. The basic technique for determination of M(H,T,P) adapts a high purity beryllium-copper piston cylinder pressure clamp to a vibrating sample magnetometer (VSM) (see Ref. [3]). An essential requirement for this technique is

to employ a highly homogeneous magnetic field in order to minimize eddy currents in the vibrating clamp. While the 13 gm clamp outweighs the sample by over 1000:1, the moment of the clamp is minimized by using high purity, cobalt-free, beryllium-copper. Most of the residual moment of the clamp cancels due to its highly symmetric nature within the VSM pickup coils as first demonstrated by Guertin and Foner[4] in 1974. The empty clamp background is diamagnetic and < 0.01 emu for $B < 2$ T, rising to about 0.1 emu at 9 T. The VSM allows continuous data recording, so hundreds of data points can be collected in a few minutes, thus revealing high detail of $M(T,P)|_B$ or $M(H,P)|_T$. The differential between T_c of a superconducting Pb manometer inside and outside the clamp determines pressure and is accurate to about 0.2 kbar[5].

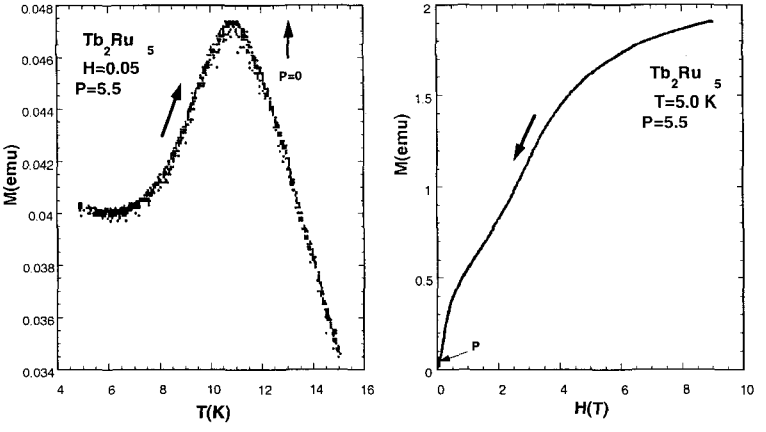

Figure 1: a) Temperature dependence of the magnetization of Tb_2RuO_5 in a 500 G measuring field, and at 5.5 kbar hydrostatic pressure. b) Isothermal magnetization at 5.0 K and at 5.5 kbar of Tb_2RuO_5. The very small anomaly at low fields is the irreversible magnetization of the superconducting Pb manometers inside and outside the clamp.

In Fig. 1(a), we show the temperature dependence of the ZFC magnetization, M(T), in a 500 G field with the sample under a pressure of 5.5 kbar. The peak in M(T, P=0) is also indicated in Fig. 1, so there is a clear pressure-induced shift ($\Delta T_C = -2.2$ K). A smaller but still negative shift was also found for Sm_2RuO_5, but T_N was independent of pressure for Gd_2RuO_5.

Figure 1(b) shows isothermal magnetization at T=5.0 K for Tb_2RuO_5 for B up to 9 T and at the same 5.5 kbar pressure. Over 500 data points were collected in only 13 minutes. The two weak field-induced transition-like features were also found at ambient pressure and may result from spin reorientation, though the resolution is limited because of the polycrystalline nature of the samples. There is

no zero field hysteresis in M(T) for any Ln_2RuO_5 sample, supporting antiferromagnetic rather than ferromagnetic ordering.

Figure 2(a) summarizes the pressure-dependence of T_N for all three samples investigated. While $dT_N/dP < 0$ for Sm_2RuO_5 and Tb_2RuO_5, and is indeed non-linear for Tb_2RuO_5, T_N for Gd_2RuO_5 shows no pressure dependence. In principle, both cation constituents of Ln_2RuO_5 can carry a magnetic moment, but because of the pyramidally coordinated symmetry for the Ru ion, the moment should be very small. Assuming full quenching of the orbital contribution to the Ru^{4+} ($4d^4$ configuration) magnetic moment (L=0), the four 4d electrons will populate only the crystalline electric field (CEF) ground state doublet, with d_{xy} and d_{yz} symmetry, including twofold spin degeneracy. Nevertheless, there is compelling evidence, based on the non-magnetic behavior of isomorphic Gd_2TiO_5, that the Ru ion promotes ordering in Ln_2RuO_5 despite possessing a negligible local moment itself.

For the lanthanide cations, the CEF effect is much smaller. However, in the very low Ln ion symmetry the free ion 2J+1 degeneracy for Tb^{3+} ($4f^8$ configuration), for example, is entirely lifted so the ground state is a CEF split singlet. For Sm^{3+}($4f^5$ configuration), which has an odd number of f electrons, and is thus a Kramers ion, the ground state is a doublet. For Gd^{3+} ($4f^7$ configuration), the CEF effect is negligible, because it is an S-state ion (L=0).

The lack of pressure dependence to T_N for Gd_2RuO_5 has several implications. First, it indicates little pressure dependence to the complex superexchange mechanism, J_{ex}, which gives rise to the magnetic ordering in Ln_2RuO_5. Secondly, the Ru moment itself, which is close to zero, must not be significantly pressure dependent. Finally, the lack of pressure dependence of T_N, compared to the other Ln members suggests the significant decrease in T_N for those members is a single Ln

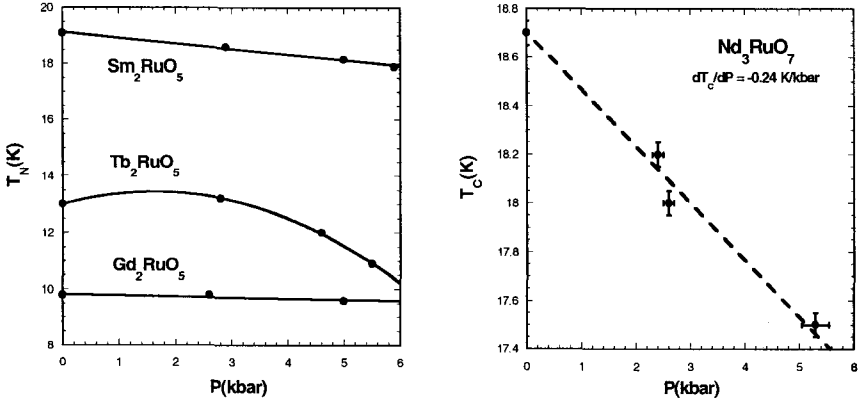

Figure 2: a) Pressure dependence of the antiferromagnetic ordering temperature of three Ln_2RuO_5 samples. b) Pressure dependence of the ferromagnetic ordering temperature of Nd_3RuO_7.

ion effect. Thus, the results of this work show the CEF interaction itself is pressure dependent. This is easy to understand in that the CEF interaction strength should increase with decreasing lattice constant as pressure increases. While the relationship between T_N and the CEF interaction in this system is considerably more complex than those previously studied[6], we expect an enhancement of the CEF to decrease the magnetic coupling, as $T_N \propto f(J_{ex}/\Delta)$, Δ being proportional to the CEF interaction strength.

Finally, in Fig. 2(b) we show the pressure dependence of the ferromagnetic (Curie) temperature, T_C, for Nd_3RuO_7, a rare earth-ruthenate with a different complex orthorhombic structure.[7] Unlike the Ln_2RuO_5 systems, Nd_3RuO_7 shows hysteresis at $B = 0$ for $T < T_C$. Low field ZFC measurements again enabled determination of T_c. We attribute the decrease of T_c in this system also to an enhancement of the CEF interaction under pressure, though in this instance there is no comparable data on a Gd based system to rule out a pressure dependence of the exchange interaction.

Acknowledgments

The authors are grateful to Z. X. Xhou and G. Cao for providing the samples for these measurements and to J. E. Crow for interesting discussions. S. McCall was supported by the Research Corporation and the National High Magnetic Field Laboratory, which is supported by the National Science Foundation under Cooperative Agreement No. DMR-0084173and the State of Florida. R. Guertin was supported by Research Corporation Research Opportunity Award RA0265 and by the Keck Foundation.

References

1. G. Cao *et al., Phys. Rev. B* **63**, (2001).
2. W. G. Mumme and A. D. Wadsley, *Acta Crystallogr., Sect. B: Struct. Crystallogr. Cryst. Chem.* **24**, 1327 (1967); L. L. Cochergina *et al., J. Inorg. Chem.* **27**, 638 (1982).
3. See for example, J. Diederichs, A. K. Gangopadhyay and J. S. Schilling, *Phys. Rev. B* **54**, R9662 (1996) (SQUID method). Dyakonov and G. Levchenko, *Pribory i Technika Eksperimenta* **5**,250 (1983).
4. R. P. Guertin and S. Foner, *Rev. Sci. Instrum* **45**, 863 (1974).
5. T. F. Smith, C. W. Chu and M. B. Maple, *Cryogenics* **9** 53 (1969).
6. R. P. Guertin *et al.,Phys. Rev. B* **12**, 1005 (1975).
7. F. P. F. van Berkel and D. J. W. Ijdo, *Mater. Res. Bull.* **21**, 1103 (1986).

DYNAMICAL PROPERTIES OF FIELD-INDUCED ORDERED-STATES IN S = 1/2 ONE-DIMENSIONAL QUANTUM SPIN SYSTEMS

N. HAGA and S.-I. SUGA
Department of Applied Physics, Osaka University,
Suita, Osaka 565-0871, Japan
E-mail: haga@tp.ap.eng.osaka-u.ac.jp

We calculate the dynamical structure factors of the magnetization-plateau state in the S = 1/2 bond-alternating spin chain with a next-nearest-neighbor interaction. The results show characteristic behaviors depending on the next-nearest-neighbor interaction and the bond-alternation. We discuss the lower excited states in comparison with the exact excitation spectrums of an effective Hamiltonian.

1 Introduction

Recently, it was shown theoretically that there appears a plateau region on the magnetization curve at half of the saturation value in the S = 1/2 bond-alternating spin chain with a next-nearest-neighbor (NNN) interaction.[1-3] This magnetization-plateau state can be regarded as a field-induced ordered state. In this paper, we calculate the dynamical structure factors (DSF) of the half-magnetization-plateau state in the S = 1/2 bond-alternating spin chain with a NNN interaction.

Let us consider the following Hamiltonian,

$$H = J\sum_{i=1}^{N}\{[1-(-1)^{\delta}]\vec{S}_i\cdot\vec{S}_{i+1}+\alpha\vec{S}_i\cdot\vec{S}_{i+2}\}-g\mu_B H\sum_{i=1}^{N}S_i^z\ , \qquad (1)$$

where δ denotes the bond-alternation, α denotes the NNN interaction, N is the total number of the site, and H is magnetic field. We set J = 1 and $g\mu_B = 1$. The periodic boundary condition is applied. Using a continued fraction method based on Lanczos algorithm,[4] the DSF of the magnetization-plateau state can be calculated numerically

2 Numerical Results

In Fig. 1, the transverse DSF $S^x(q,\omega)$ in the half-magnetization-plateau state is shown for N = 28 and $\alpha = 0.2$. In larger δ, the separation of the excitation bands becomes apparent, and we can see nearly three excitation bands in the region $\omega < 1$, $\omega \sim 2$, and $\omega \geq 3$. An almost dispersionless mode appears in the lowest excited states for $\delta = 0.64$, where the elementary excitation is well localized in the real space. The wave number of the largest intensity in given α shifts from π to $\pi/2$, as δ increases. The results indicate that the effect of the bond-alternation becomes dominant.

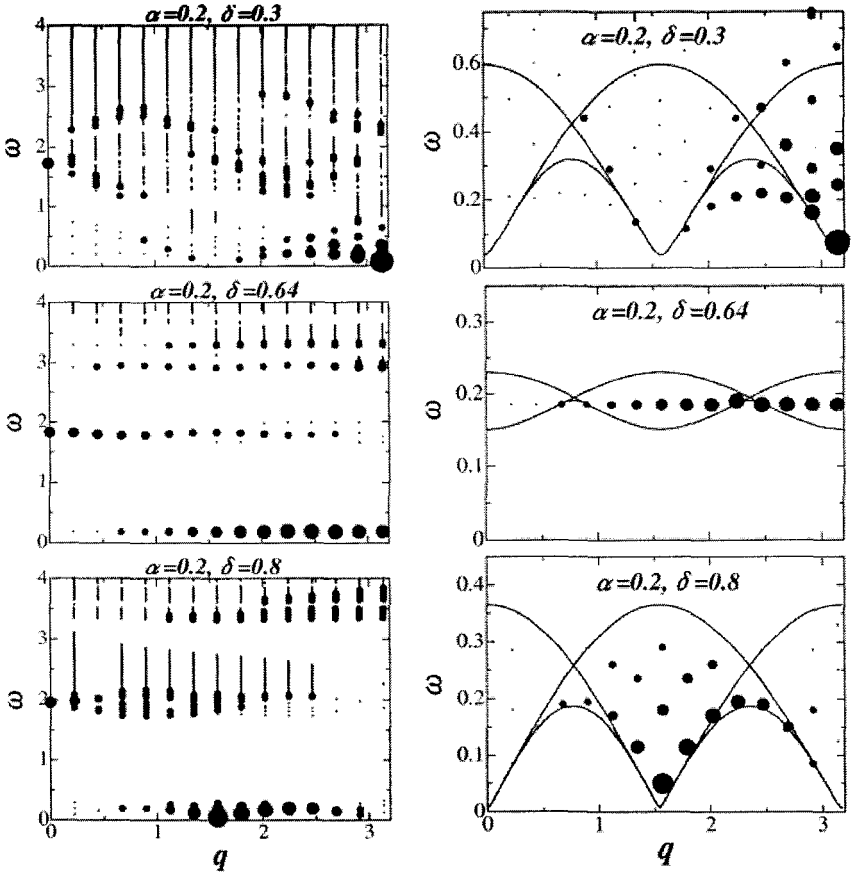

Figure 1: The left-hand side: $S^x(q,\omega)$ in the half-magnetization-plateau state for N = 28 in $\alpha = 0.2$. The intensity is proportional to the area of the circle. The right-hand side: the lowest excitation of $S^x(q,\omega)$ corresponding to the results of the left-hand side. The solid lines represent the exact bounds of the excitation continuum for the effective Hamiltonian obtained by the Bethe ansatz method.

For $\delta \sim 1$ and $\alpha \sim 0$, the model described by (1) can be mapped onto the one-dimensional (1D) S=1/2 Heisenberg-Ising model in zero field.[3,5] In the right-hand side of Fig. 1, we compare the distribution of the intensity in the lowest excitation band with the exact excitation spectrums of the effective Hamiltonian. In smaller δ, the intensity distributes beyond the upper and lower bounds of the excitation continuum of the effective Hamiltonian. In larger δ, on the other hand, the intensity

distributes within the excitation continuum of the effective Hamiltonian. In the latter case, therefore, the ground state can be given by the singlet and triplet pairs occupying strong (1+δ)-bonds alternately, and the elementary excitation can be described by a superposition of massive two kinks and anti-kinks which have $S^z = \pm 1/2$.

To see whether the excited states belong to a continuum or form an isolated mode, we investigate the size dependence of the lowest excited states. Using the method developed in Ref. [6], we conclude that the lowest excitation in $\delta = 0.64$ is the isolated mode and the others are probably the lower edge of the excitation continuum.

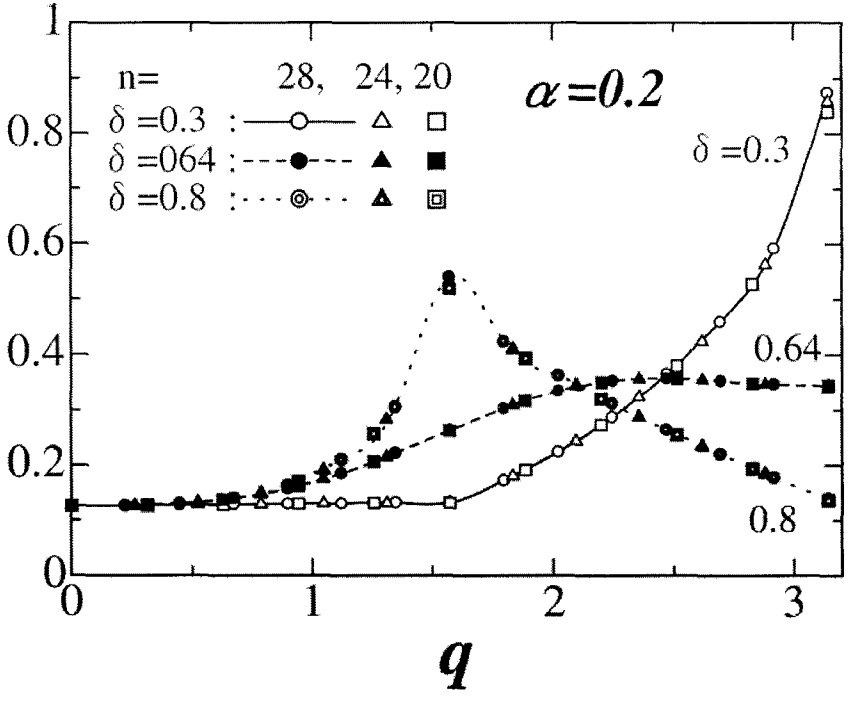

Figure 2: SSF in the half-magnetization-plateau state for N = 20, 24, and 28 in $\alpha = 0.2$.

Next, we calculate the static structure factors (SSF) in the half-magnetization-plateau state. As shown in Fig. 2, the finite-size effects slightly appear only at $q = \pi$ or $q = \pi/2$, where the intensity takes the maximum. The largest intensity is located at $q = \pi$ in the small δ region. As δ increases, the wave number of the largest

intensity shifts towards $q = \pi/2$, taking the incommensurate value of q. In other 1D spin-gapped system, the incommensurate mode between $\pi/2$ and π is difficult to observe. The dominant incommensurate mode of the transverse spin correlation may be characteristic of the magnetization-plateau states in the present system.

We have further calculated the DSF and SSF for $\alpha = 0.1$, 0.2, 0.3 and 0.4 with many choices of δ. It is interesting that even in $\alpha > 0.1$, the intensity of the DSF in the lowest excitation band distributes within the excitation continuum of the effective Hamiltonian, although the mapping can be successful for $\delta \sim 1$ and $\alpha \sim 0$. From the finite-size analysis, we have conclude that the lowest excited states in such a parameter region are the lower bound of the excitation continuum. Details will be published elsewhere.[7]

Acknowledgments

We would like to thank I. Harada ,T. Tonegawa and M. Takahashi for useful comments and valuable discussions. Our computational programs are based on TITPACK Ver. 2 by H. Nishimori. Numerical computation was partly carried out at the Yukawa Institute Computer Facility, Kyoto University, and the Supercomputer Center, the Institute for Solid State Physics, University of Tokyo.

References

1. T. Tonegawa, T. Nishida and M. Kaburagi, *Physica B* **246-247**, 368 (1998); private communication.
2. T. Tonegawa, T. Hikihara, K. Okamoto and M. Kaburagi, *Physica B* **294-295**, 39 (2001).
3. K. Totsuka, *Phys. Rev. B* **57**, 3454 (1998).
4. E. R. Gagliano and C. A. Balseiro, *Phys. Rev. Lett.* **59**, 2999 (1987).
5. F. Mila, *Eur. Phys. J. B* **6**, 201 (1998).
6. M. Takahashi, *Phys. Rev. B* **50**, 3045 (1994).
7. N. Haga and S. Suga, to appear in *Phys. Rev. B* (2001).

DYNAMICAL STRUCTURE FACTORS OF THE S = 1/2 SPIN LADDER SYSTEMS WITH A DIAGONAL INTERACTION IN THE MAGNETIZATION-PLATEAU STATE

N. HAGA and S. SUGA
Department of Applied Physics, Osaka University, Suita, Osaka 565-0871, Japan

We investigate the dynamical structure factors of the S = 1/2 spin ladder systems with a diagonal interaction in the magnetization-plateau state. The results show characteristic behaviors depending on the chain interaction α, the ladder interaction $1 + \delta$ and the diagonal interaction $1 - \delta$. The large weights are located at $q = \pi$, when δ is small. With increasing δ, the wavenumber of the large weights shifts towards $q = \pi/2$, taking the incommensurate value. The almost dispersionless behavior comes out at several combinations of α and δ, indicating that the elementary excitation is localized spatially. We discuss our results in comparison with the exact excitation spectrums of the S = 1/2 XXZ model which is an effective Hamiltonian of the present system in $\alpha \sim 0$ and $\delta \sim 1$.

Dynamical structure factors of some S = 1/2 one-dimensional quantum spin systems in the magnetic fields were measured by inelastic neutron-scattering experiments[1,2] and it has been shown the theoretical results from the numerical diagonalization of finite systems can explain them.[3-5]

1. I. U. Heilmann, G. Shirane, Y, Endoh, R. J. Birgeneau and S. L. Holt, *Phys. Rev. B* **18**, 3530 (1978).
2. R. Coldea, D. A. Tennant, R. A. Cowley, D. F. McMorrow, B. Dorner and Z. Tylczynski, *Phys. Rev. Lett.* 79, 151 (1997).
3. N. Ishimura and H. Shiba, *Prog. Theor. Phys.* 64, 479 (1980).

D-STRAIN, g-STRAIN, AND DIPOLAR INTERACTIONS IN THE Fe_8 AND Mn_{12} SINGLE MOLECULE MAGNETS: AN EPR LINESHAPE ANALYSIS

S. HILL
Department of Physics, University of Florida, Gainesville, FL 32611
E-mail: hill@phys.ufl.edu

S. MACCAGNANO
Department of Physics, Montana State University, Bozeman, MT 59717

R. ACHEY and N. DALAL
Department of Chemistry and National High Magnetic Field Laboratory, Florida State University, Tallahassee, FL 32306

K. PARK
School of Computational Science and Information Technology, Florida State University, Tallahassee, FL 32306

We report high sensitivity, high field/frequency (up to 9 tesla/210 GHz) EPR measurements on the Fe_8 and Mn_{12} single molecule magnets. Oriented single crystal studies, carried out in well defined experimental geometries, enable very accurate determinations of EPR lineshapes; we note that this is not possible when studying aligned powders or polycrystals. Analysis of individual resonances, which we can assign to known transitions, reveal complex nonlinearities in the linewidths as functions of energy eigenstate, frequency, and temperature. Our findings compare favorably with recent calculations which introduce distributions in the uniaxial anisotropy parameter D, the Landé g-factor, and dipolar interactions.

1 Introduction

Single molecule magnets (SMMs) such as $[Fe_8O_2(OH)_{12}(tacn)_6]Br_8.9H_2O$ (Fe_8) and $[Mn_{12}O_{12}(CH_3COO)_{16}(H_2O)_4]\cdot 2CH_3COOH \cdot 4H_2O$ (Mn_{12}-acetate, or Mn_{12}), have aroused considerable interest due to their novel quantum properties and their possible future use in computational devices. Both materials may be thought of as consisting of 3D arrays of identical high-spin ($S = 10$) clusters (magnetic quantum dots) with the same magnetic properties and characteristic energies.[1]

To lowest order, the effective spin Hamiltonian for the Mn_{12} and Fe_8 systems has the form:[1-8]

$$\hat{H} = D\hat{S}_z^2 + g\mu_B \mathbf{B}\cdot\hat{\boldsymbol{S}} + \hat{H}' \qquad (1)$$

where $\hat{\boldsymbol{S}}$ is the spin operator and $\hat{S}_z$ is its projection along the magnetic easy axis; D is the uniaxial spin-spin coupling parameter; g is the Landé factor and $\mathbf{B}$ is the applied magnetic field vector. $\hat{H}'$ represents perturbations such as those which lead to EPR line broadening and magnetic quantum tunneling (see below). D is negative

for both Mn_{12} (−0.457 cm^{-1} (see Ref. [3])) and Fe_8 (−0.203 cm^{-1} (see Ref. [4])). For $\mathbf{B}//z$ and $\hat{H}' = 0$, the energy eigen states may be labeled by the quantum number M_S ($-S < M_S < S$), which represents the projection of $\hat{\boldsymbol{S}}$ on to the easy axis. The energy eigenvalues are then given by the expression $\varepsilon = DM_S^2$, resulting in an energy barrier separating doubly degenerate ($M_S = \pm i$, i = integer) spin "up" and "down" states;[1] hence the potential for magnetic memory elements. Terms in $\hat{H}'$ that do not commute with $\hat{S}_z$ mix different M_S states, giving rise to the situation in which any given eigenstate may be made up from coherent superpositions of unperturbed states on either side of the barrier. Under these circumstances, a spin-up state may evolve (quantum tunnel) with time into a spin down state. Although detrimental in terms of magnetic memory applications, this process may prove useful for quantum computation.

Both Fe_8 and Mn_{12} exhibit magnetic quantum tunneling (MQT) at low temperatures ($k_BT << DS^2$) (see Refs. [1,2]), yet the origin of this effect remains unclear. For Fe_8, a rhombic distortion gives rise to a term in $\hat{H}'$ of the form $E(\hat{S}_x^2 - \hat{S}_y^2)$, where $E = 0.032$ cm^{-1} (see Ref. [4]). However, current leading theories additionally invoke inter-SMM dipolar and nuclear hyperfine fields in order to fully explain the observed MQT (see Ref. [4]). For the uniaxial Mn_{12} SMM, the rhombic term is zero, and the MQT mechanism is not well understood. Recent high-field EPR studies[5,6] have provided indications that 4th order single-ion transverse anisotropy ($\hat{S}_x^4$ and $\hat{S}_y^4$) may be generic to all SMMs, and that such terms in $\hat{H}'$ play a crucial role in the MQT. However, there is considerable disagreement as to the magnitudes of these 4th-order terms,[3-8] and fits to EPR spectra are generally poor.[5,6] Furthermore, 4th-order transverse anisotropy cannot explain many other key experimental facts associated with MQT. In this study, we present EPR linewidth data for Fe_8 and Mn_{12}. D and g-strain contribute significantly to the linewidths in both systems, and a significant inter-SMM dipolar broadening is observed for Fe_8 (see Ref. [9]). We discuss the implications of these findings in the light of recent theories of MQT (see Ref. [10]).

2 Experimental

We use a cavity perturbation technique (described elsewhere)[11] to study oriented single crystals of Fe_8 and Mn_{12}, in the frequency range from 40 to 211 GHz and at temperatures from 50 K down to 2 K. All of the data presented in this article were obtained with the field applied approximately parallel to the samples' easy axes. Details of the experiments, and representative raw data may be found in refs.[7,8]

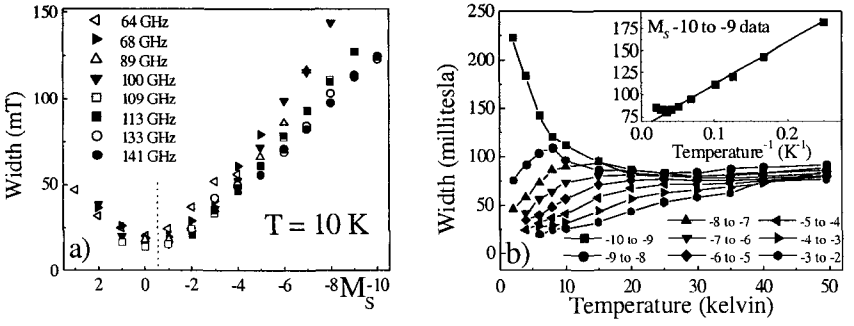

Figure 1: Linewidth data for the Fe_8 SMM as a function of a) the M_S value from which the transition was excited, and b) temperature (frequency = 116 GHz). The inset in b) shows the 1/T dependence of the width of the $M_S = -10$ to -9 transition, which is observed very close to zero field at this frequency.

3 Results and discussion

Figure 1(a) shows linewidth data for Fe_8, as a function of M_S (the level from which the transition was excited), obtained at different frequencies (fields). The pronounced (almost linear) increase in EPR linewidth with M_S is due to *D*-strain. Since $\varepsilon \propto M_S^2$, energy differences (*i.e.* EPR transition frequencies) scale as M_S; hence *D*-strain produces a linear width ($\Delta\varepsilon$) dependence on M_S, which projects onto a width in field (ΔB) that also scales linearly with M_S. The rounding close to $M_S = 0$ is due to a convolution of the intrinsic lifetime broadening and the M_S dependent contribution. The slight narrowing as a function of increasing frequency, and the weak asymmetry about $M_S = -1/2$, is due to the fact that higher (lower) frequency (M_S) transitions are observed at higher magnetic fields, where the inter-SMM dipolar broadening is weaker (see discussion below).For Fe_8, no measurable g-strain is observed. Qualitatively similar *D*-strain effects were obtained for Mn_{12}, together with a slight g-strain, which produces the opposing dependence on M_S compared to *D*-strain, since higher M_S transitions are observed at lower fields. A theoretical treatment of these effects may be found in Ref. [9].

The temperature dependent contribution to the linewidths for Fe_8 (Fig. 1(b)) is dominated by fluctuating dipolar fields at each SMM site due to the moments of the surrounding SMMs. At 116 GHz, the $M_S = -10$ to -9 transition occurs very close to zero field (≈0.1 T). Hence, in the superparamagnetic regime above the blocking temperature, the fluctuating dipole fields at each SMM site reflect the spin susceptibility, which should follow a Curie (1/T) law, as demonstrated for the $M_S = -10$ to -9 transition in the inset to Fig. 1(b). The same should also be true for the other transitions, provided that k_BT exceeds the Zeeman splitting of the ground

state. For k_BT less than the ground state Zeeman splitting, the system polarizes and the dipole fluctuations are suppressed, leading to an EPR line narrowing, as confirmed for all but the $M_S = -10$ to -9 transition in Fig. 1(b). The crossover occurs when k_BT is equal to the ground state Zeeman splitting. For the $M_S = -9$ to -8 transition, where the resonance occurs at 0.5 T, the ground state splitting is $7k_B$; hence the crossover in temperature dependence is seen at $\approx$7 K (Fig. 1(b)). Corresponding shifts are observed in the temperature dependence of the line positions.[12] Weaker, though finite, dipolar broadening is observed for Mn_{12} (see Ref. [12]).

Based on theoretical calculations by Park *et al.*,[9] we estimate distributions in D and g of: 0.01 D and negligible g-strain for Fe_8; and 0.02 D and 0.008 g for Mn_{12}. The dipolar contribution, which is much more significant in Fe_8 than Mn_{12}, also agrees with predictions taking into account inter-SMM distances. We can fit all of our data (many frequencies and temperatures) using the same set of parameters.

The pronounced D strain observed for these two systems highlights the fact that there are strains in the samples, possibly caused by dislocations. These strains may locally distort the (axial) crystal fields, and therefore give rise to the necessary symmetry breaking terms in $\hat{H}'$ that cause MQT, thus providing an alternative plausible explanation for this effect.[9,10]

This work was supported by the National Science Foundation (DMR 0103290). S.H. is a Cottrell scholar of the Research Corporation.

References

1. G. Christou *et al., MRS Bull.* **25**, 66 (2000).
2. W. Wernsdorfer *et al., Phys. Rev. Lett.* **83**, 628 (1999).
3. R. Caciuffo *et al., Phys. Rev. Lett.* **81**, 4744 (1998).
4. A-L. Barra *et al.,Chem-Eur. J.* **6**, 1608 (2000); also *cond-mat*/00023869.
5. A-L. Barra *et al., cond-mat*/0101216.
6. S. Maccagnano *et al.,Polyhedron* **20**, 1441 (2001).
7. S. Hill *et al., Phys. Rev. Lett.* **80**, 2453 (1998).
8. K. Park *et al., Phys. Rev. B* (in press); also *cond-mat*/0106276 (14 Jun2001).
9. E. M. Chudnovsky *et al., cond-mat*/0107586.
10. M. Mola, *et al., Rev. Sci. Inst.* **71** (2000) 186.
11. S. Hill, *to be published.*

HIGH PRESSURE APPARATUS FOR TRANSPORT PROPERTIES STUDY IN HIGH MAGNETIC FIELD

F. HONDA and V. SECHOVSKÝ

Department of Electronic Structures, Charles University, 121 16 Prague 2, The Czech Republic
E-mail: sech@mag.mff.cuni.cz

O. MIKULINA and J. KAMARÁD

Institute of Physics, Academy of Sciences of CR, 182 21 Prague 8, The Czech Republic
E-mail: kamarad@fzu.cz

A. M. ALSMADI and H. NAKOTTE

Physics Department, New Mexico State University, Las Cruces, NM88003, USA
E-mail: hnakotte@nmsu.edu

A. H. LACERDA

National High Magnetic Field Laboratory, LANL, MS E 536 Los Alamos, NM87545, USA
E-mail: lacerda@lanl.gov

We have designed a high pressure apparatus for measuring electrical-transport properties at low temperatures, high magnetic field and hydrostatic pressure up to 10 kbar. Details of the high-pressure cell and an exemplary study on UNiAl are described and discussed briefly.

1 Introduction

The measurement of physical properties of solids in multi-extreme conditions, under high-pressure, low temperature and high magnetic field, occupies attention in many fields of science and engineering. At multi-extreme conditions, the relationship of atom configuration and electronic structure can be tested and, moreover, there is a chance that some induced exotic electronic states can become a seed of new phenomena. Here, we describe the design and operation of the high-pressure apparatus for electrical-transport properties measurements under hydrostatic pressure to 10 kbar and magnetic field to 20 Tesla at low temperatures. We will discuss recent results of relevant pressure measurement of the electrical resistivity of the UNiAl single crystal.

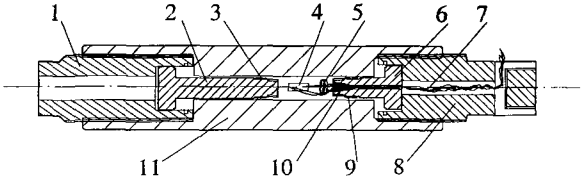

Figure 1: Cross-section of the clamp type pressure CuBe cell up to 1 GPa. (1), (8) nuts; (3), (9) seals; (2) piston; (4) sample; (5) manganin coil; (6), (10) obturator with a conical lead-through; (7) electrical leads sealed with epoxy; (11) cell body.

2 Experimental procedure

The schematic picture of hydrostatic high-pressure CuBe cell, which we designed and build for the 20-T superconducting magnet at the Pulse Field Facility, NHMFL, LANL, is shown in Fig.1. This clamped high-pressure cell can be put into the ^{4}He cryostat with 20-T superconducting magnet. The sample (4) is placed in a chamber with inner diameter of 7 mm and height of 30 mm. The chamber is filled by a liquid pressure transmitting medium (mineral oil). The sample space is closed by piston (2) and obturator (10) and sealed by rubber (3) and copper (9) sealing rings. Copper wires are sealed by epoxy resin in the obturator for measuring the electrical resistance of two samples and manganin manometer (5) by standard AC four probe method. For the electrical-transport studies, we typically use gold or copper wires of 50 μm in diameter which are glued by silver paste on the surface of the metallic samples to ensure reliable electrical contacts even under the extreme conditions.

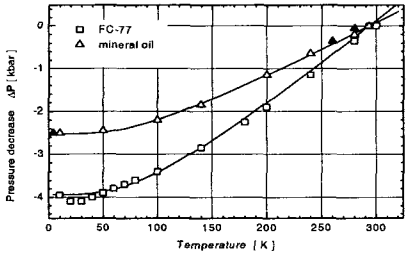

Figure 2: Pressure variation of $\Delta P=P(T)-P_{RT}$, (P_{RT}=10 kbar) inside the pressure cell with respect to temperature.

Due to different thermal expansion of the pressure medium and the CuBe bronze, the pressure inside the clamped cell decreases with decreasing temperature. The actual pressure at any given temperature is determined by measuring the

electrical resistance of a manganin wire . The pressure coefficient of the manganin resistance is almost constant (+ 2.465×10^{-3} $kbar^{-1}$) for the temperature range of interest (1.5-300 K), and the measured change of pressure as a function of temperature with mineral oil as a pressure medium is shown in Fig. 2. Pressure decreases gradually of about 2.6 kbar as the cell filled by mineral oil is cooled from room temperature to 50 K. For temperatures below 50 K, any further pressure decrease is practically negligible. Compared to mineral oil as a pressure medium, a substantially large pressure decrease of about 4 kbar was found if Fluorinert FC-77 is used (see Fig.2).

Next, we present an exemplary study on UNiAl at multi-extreme conditions using the high-pressure apparatus described above.

3 Magnetoresistance of UNiAl at high pressures

UNiAl belongs to isostructural *UTX* (*T* = transition metal, *X* - *p*-electron metal) compounds crystallizing in the hexagonal ZrNiAl-type structure.[1] UNiAl is an itinerant 5*f*-electron antiferromagnet with T_N = 19.3 K. At low temperatures, this material undergoes a metamagnetic transition[2] to a high-field ferromagnetic state for magnetic fields applied along the *c*-axis, and B_c = 11.35 T at 1.7 K. We measured low temperature electrical resistance on single crystalline UNiAl under hydrostatic pressures to 10 kbar and in magnetic field to 18T in a wide range of temperature in order to clarify the effect of pressure onto the electronic structure in this material.

The temperature dependence of the electrical resistance, *R*, of UNiAl at 0 kbar and 10 kbar is displayed in Fig.3. At ambient pressure, *R* (*T*) in 10 T (< B_c) shows

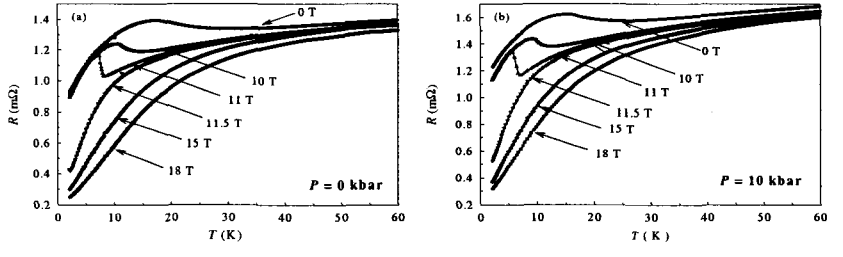

Figure 3: Electrical resistance of UNiAl for current along c-axis, at 0 kbar (a) and 10 kbar (b).

anomaly around T_N, and it can be ascribed to a magetic scattering due to strong antiferromagnetic (AF) correlations. The resistance anomaly around T_N is sharpens with increasing magnetic field until reaching B_c, above which *R*(*T*) decreases monotonically with decreasing temperature. UNiAl exhibits giant magnetoresistance (GMR) effects at the metamagnetic transition. At 1.5 K, the GMR effect is as large as 80%. On the hand, large magnetoresistance effects were found to exist also well

above T_N (ex. 14% GMR at 30 K, 18 T), which supports the idea that AF correlations are suppressed by an applied magnetic field.

Under hydrostatic pressure of 10 kbar (room-temperature value), we find that the anomaly at T_N broadens and shifts to the lower temperature which is in good agreement with previous data.[3,4] Compared to the ambient-pressure results, the GMR effect in the antiferromagnetic and paramagnetic states were found to be somewhat reduced. Thus, we speculate that AF correlations are suppressed by increased *f-d* hybridization due to pressure, and a detailed analysis is in progress.

We have constructed a high-pressure apparatus that can be used with a large superconducting magnet. As an example, the resistivity of the single crystals of UNiAl has been measured under multi-extreme conditions (high pressure, high magnetic field, low temperature).

To better understand the nature of the magnetic correlations under pressure in this material measurements at higher pressure (to 30 kbar) and lower temperatures (down to 20 mK) are now under development.

This work is partly supported by the Grant Agency of the Czech Republic (grant number: D202/01/D045). The work was also supported by a grant from NSF (grant number: DMR-0094241). Work at the National High Magnetic Field Laboratory in Los Alamos was performed under the auspices of the NSF (INT-9722777), the US Department of Energy and the State of Florida.

References

1. V. Sechovský and L. Havela, in: *Handbook of Magnetic Materials*, ed. K. H. J. Buschow (North Holland, Amsterdam, 1998), Vol. 11, 1 and references therein.
2. E. Brück *et al., Phys.Rev.B* **49**, 8852 (1994).
3. O. Mikulina *et al., Science and Technology of High Pressure*, eds M. H. Manghnani, W. J. Nellis and M. F. Nicol, Vol. 2, 730-733 (2000).
4. K. Prokes *et al.,Phys.Rev.B* **59**, 8720 (1999).

HIGH-FIELD HALL EFFECT AND BAND STRUCTURE OF HALF-METALLIC CrO_2 FILMS

S. M. WATTS and S. VON MOLNÁR
MARTECH, Florida State University, Tallahassee, FL 32306

M. JAIME
NHMFL, Los Alamos National Laboratory, Los Alamos, NM 87545

The Hall effect of (100)- and (110)-oriented films of the half-metallic ferromagnetic oxide CrO_2, fabricated by both chemical vapor deposition and high pressure, thermal decomposition methods, has been examined in large magnetic fields up to 60 T. In all cases the Hall effect exhibits a sign reversal from positive to negative with increasing field, which we take as evidence for multi-band behavior. (110) films fabricated by both methods exhibit this sign reversal at relatively low fields. The data may be fit with a simple two-band model, which indicates the existence of highly mobile holes of p-like parentage, along with a much larger number of heavy, d-like electrons. In the (100) film the sign reversal is at much higher field. The parameters obtained from the fits allow us (with help from band structure calculations) to infer the band structure near the Fermi level and how it depends on sample strain and other structural characteristics. These details will be important for understanding carrier transport through interfaces such as for spin injection or other "spintronics" applications.

Chromium dioxide is the only known binary oxide to be both ferromagnetic and metallic. It is also a member of the rare class of compounds known as "half-metals," in which the conduction band is completely spin-polarized—the minority spin band structure has a insulating bandgap at the Fermi energy.[1] This feature is attractive in the field of "spintronics," where CrO_2 could see applications as a spin-polarized electron source.

We have characterized films produced by both a high-pressure method (Hi-P) as well as a chemical vapor deposition (CVD) method onto different substrates with x-ray diffraction in order to examine epitaxy both in-plane and out-of-plane[2] and with magnetotransport measurements to examine the band structure near the Fermi level and to infer the evolution of spin-flip scattering with temperature.[3] The Hall effect is particularly interesting in that the normal Hall slope changes sign from positive to negative in relatively low fields at low temperatures. This sort of sign-reversal is often a hallmark of two-band conduction, and the data were analyzed within a simple two-band model. In the high-field limit of the two-band model, the normal Hall constant reverts to the simple dependence on inverse carrier concentration (in this case the difference between the concentration of holes and electrons). It is therefore necessary to use quite high fields to obtain an accurate assessment of the carrier concentrations.

The Hi-P film was made onto (110)-oriented TiO_2 substrates as described previously.[4,5] Magnetotransport measurements on these films, including Hall effect

data to 18 T, were reported earlier.[3] We now present Hall data measured in pulsed magnetic fields up to 60 T. This data, spanning the range from 80 K to 200 K, is shown in Fig. 1. Also included in this plot is the earlier 18 T data at 5, 80, and 100 K. In addition we plot the data after subtracting the anomalous Hall contribution and dividing by the magnetic field, versus the field squared. In this form, the two-band model predicts the simple dependence:[3]

$$R_0 = \frac{\rho_H}{B} = \frac{b - cx}{1 + ax},$$

where a, b and c are functions of the two band conductivities σ_e and σ_h and the two band Hall coefficients R_e and R_h (the subscript indicates either electron or hole), and $x = B^2$. If the Fermi surfaces are spherical then these parameters have no field dependence. The fits of (1) to the data are shown as black solid curves in Fig. 1.

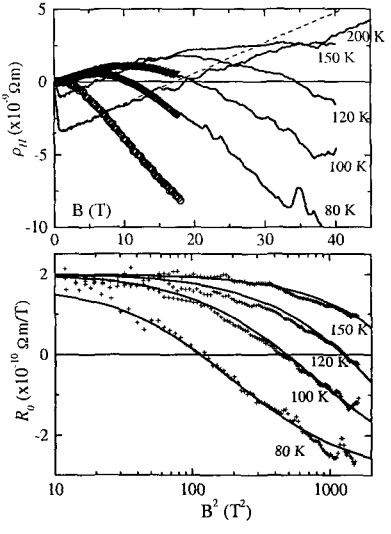

Figure 1: Top panel: Hall resistivity vs. field for the high-pressure (110) oriented sample measured in pulsed magnetic fields (solid lines). The symbols are the data collected previously[3] in dc field, shown for comparison. Bottom panel: the normal Hall coefficient vs. the square of the magnetic field. The solid black lines are fits of the two-band model.

The fits give the three parameters a, b and c, which can be transformed to the four band parameters given the additional equation $1 / \rho = \sigma_e + \sigma_h$. The band parameters are plotted in Fig. 2, where the mobility is defined as $\mu = \sigma R$. Both the

carrier concentration and the mobility are quite different between the bands, implying the parentage of the different carriers is different in character.

Recently, the CVD method was used to prepare single-crystal films onto (100) TiO_2 substrates[6] We obtained a similarly prepared film from A. Gupta, IBM T. J. Watson Research Center, and measured the Hall effect in magnetic fields up to 28 T at the NHMFL, Tallahassee. The Hall effect was found to change sign in this sample but at much higher field. We have therefore produced our own films of both the (100) and (110) orientation by the CVD method in order to examine more closely the structural characteristics. Because the CVD films are single-crystal, there are fewer relaxation mechanisms for strain relief, and so they show significant lattice strain compared to bulk CrO_2 or the more granular, but highly textured Hi-P CrO_2 films.[2]

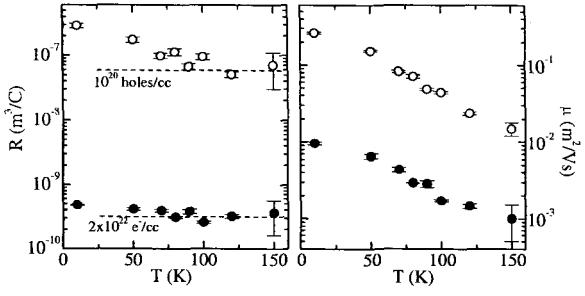

Figure 2: Band parameters extracted from fits of (1) to the data in Fig. 1. The left panel shows the Hall coefficient vs. temperature; solid symbols are for the electron band, open symbols are for the hole band. The dashed line indicates the carrier concentration in the simple case that $R = (ne)^{-1}$. The right panel shows the mobilities vs. temperature.

The high-field data from the IBM, CVD (100) film is plotted along with pulsed-field data for a CVD (110) film in Fig. 3. Two-band fits to some of the data are also shown in Fig. 3. We find that the two-band model adequately accounts for the Hall effect behavior in all of the films. The electron concentration is similar for all films, around 10^{22}, and independent of temperature; however, there are many more holes in the (100) CVD film than in the others. Furthermore, there is a marked difference between the electron and hole mobilities in all of the films.

As discussed in our earlier analysis,[3] the disparity in the magnitude of the mobilities is likely due to the effective mass rather than the scattering rate. Based on the band structure calculation of Korotin, *et al.*,[7] we assign the heavier, more numerous electrons to a narrow d-band at the Fermi level and the lighter holes to an O 2p-band edge. For the CVD (100) film the holes can still be ascribed to the oxygen band, if it is assumed that the strain has decreased slightly the bandwidth and shifted the band up in energy relative to the Fermi level.

We are grateful to A. Gupta for providing the CVD sample for the high-field measurements. We would also like to acknowledge our collaborators A. Barry and

J. M. D. Coey, who produced the high-pressure samples and initiated the work on CrO_2, and P. A. Stampe and R. J. Kennedy for the detailed x-ray diffraction measurements. This research was sponsored by DARPA through the Office of Naval Research, ONR Grant No. N00014-99-1-1094.

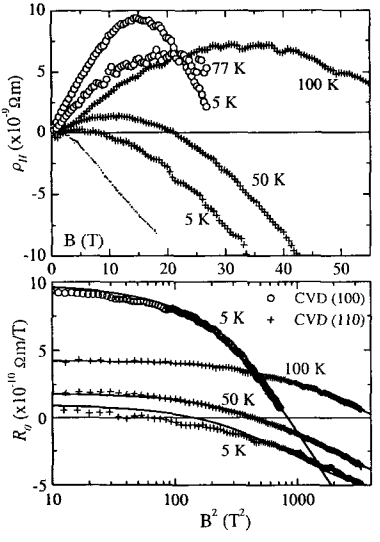

Figure 3: Hall data for the CVD films (as in Fig. 1). In the top panel the 5 K curve for the high pressure (110) film is shown for comparison (solid line).

References

1. K. Schwarz, *J. Phys. F* **16**, L211 (1986).
2. P. A. Stampe, R. J. Kennedy, S. M. Watts and S. von Molnár, *J. Appl. Phys.* 89, 7696 (2001).
3. S. M. Watts, S. Wirth, S. von Molnár, A. Barry and J. M. D. Coey, *Phys. Rev. B* 61, 9621 (2000).
4. L. Ranno, A. Barry and J. M. D. Coey, *J. Appl. Phys.* 81, 5774 (1997).
5. A. Barry, J. M. D. Coey, L. Ranno and K. Ounadjela, *J. Appl. Phys.* 83, 7166 (1998).
6. X. W. Li, A. Gupta, T. R. McQuire, P. R. Duncombe and G. Xiao, *J. Appl. Phys.* 85, 5585 (1999).
7. M. A. Korotin, V. I. Anisimov, D. I. Khomskii and G. A. Sawatzky, *Phys. Rev. Lett.* 80, 4305 (1998).

PHASE TRANSITIONS IN INSULATING VANADIUM OXIDE

A. JOSHI,[1,2] M. MA,[2] and F. C. ZHANG[2]
[1]*NHMFL, 1800 E Paul Dirac Dr., Tallahassee, FL 32310*
[2]*Department of Physics, University of Cincinnati, Cincinnati, OH 45221*

The magnetic phase transition from the paramagnetic to antiferromagnetic state in insulating V_2O_3 shows some very interesting features. Not only is the magnetic order ng pattern anomalous, but the magnetic transition shows other surprises: I) the magnetic and orbital ordering occur at the same transition temperature; II) the transition is strongly first order; III) above the transition temperature, neutron scattering observes features in wave vectors different from the ordering wave vector. We study this system using the recently proposed S=2 bond model (*Phys. Rev. Lett.* **85,** 1714 (2000)) for insulating V_2O_3. We show that this model not only explains the anomalous magnetic ordering, but also resolves the other questions associated with the magnetic phase transition (*Phys. Rev. Lett.* 86, 5743 (2001)). We further point out the possibility of changes in the phase transition phenomenology in presence of a magnetic field, and another orbital phase transition at lower temperatures.

MAGNETIZATION CURVES OF QUASI-ONE-DIMENSIONAL HALDANE SYSTEMS

A. KAWAGUCHI, A. KOGA and N. KAWAKAMI

Department of Applied Physics, Osaka University, Suita, Osaka 565-0871 JAPAN

K. OKUNISHI

Department of Physics, Niigata University, Igarashi 2, Niigata 950-2181 JAPAN

We study the magnetization process of a quasi-one-dimensional S=1 antiferromagnet with bond alternation by using the density matrix renormalization group method combined with interchain mean-field approximation. Particularly, we discuss how the interchain couplings affect the magnetization curve around a plateau structure in both of the Haldane phase and the dimer phase. It is shown that the antiferromagnetic correlation induced by the interchain couplings reduces the region of the plateau significantly, which will play an important role when the theoretical results are compared with actual measurements of the magnetization.

Recently low-dimensional quantum spin systems with the spin gap have attracted much interest. A remarkable example is the Haldane system,[1] which is described by the one-dimensional (1D) antiferromagnetic Heisenberg model with integer spins. It is known that the effects of the bond alternation[2-7] result in further interesting properties of the system. In order to analyze the experimental results in real compounds, it is indispensable to incorporate three-dimensional (3D) effects due to the finite interchain coupling, as is the case for $CsNiCl_3$, NENP, etc. Such 3D effects have been studied by various theoretical methods. Among others, Sakai and Takahashi[8,9] have investigated the effects of the interchain coupling on the ground-state phase diagram by combining the finite-size calculation of the 1D system with mean-field treatment of the interchain coupling. More recently, magnetic properties of the compound [Ni (333-tet)(μ -NO_2)](ClO_4) (see Ref. [10]) have been experimentally studied by Y. Narumi *et al.*,[11] which suggest that the interchain coupling is important to understand the magnetization process in this compound.

Motivated by the above experimental suggestions, we study the effects of the interchain coupling on magnetic properties of an S=1 antiferromagnetic spin-chain system with bond alternation. We obtain the phase diagram of the quasi-1D system in an applied magnetic field. In particular, we discuss how the plateau structure of the magnetization curve is affected by the interchain coupling.

In order to study magnetic properties of a quasi-1D S=1 antiferromagnet, we consider the following Hamiltonian,

$$\mathrm{H} = J\sum_{j,i}\{1-(-1)^i\,\delta\}\mathbf{S}_{j,i}\cdot\mathbf{S}_{j,i+1} + J'\sum_{<j,j'>,i}\mathbf{S}_{j,i}\cdot\mathbf{S}_{j',i} - H\sum_{j,i}S^z_{j,i}\quad , \qquad (1)$$

where $S_{j,i}$ is the spin operator at the i –th site in the j –th chain. The summation with $<j,j'>$ is done over the z' nearest-neighbor chains (e.g. $z'=4$ for simple cubic lattice). Here δ is the bond-alternation parameter, and $J(=1)$ and J' denote the intrachain and interchain couplings, respectively.

We now compute the magnetization for the above quasi-1D Haldane spin system by exploiting the density matrix renormalization group (DMRG) method,[12] which is combined with interchain mean-field treatment. To this end, we first introduce the mean field defined as $<S_i>=(-1)^i m_s$, where m_s is an effective staggered moment induced by the interchain coupling. We then have to consider the reduced 1D spin system subjected to an effective staggered field $h_s(=z'J'm_s)$. The staggered magnetization m_s should be determined by the self-consistent equation, $m_s=\phi(h_s, \delta, H)$, where h_s is replaced with the mean field: $h_s=z'J'm_s$. By applying the DMRG method to the effective quantum spin chain with both of uniform and staggered magnetic fields, we can compute the function ϕ precisely, which allows us to discuss the competition between the spin-gap phase and the magnetically ordered phase.

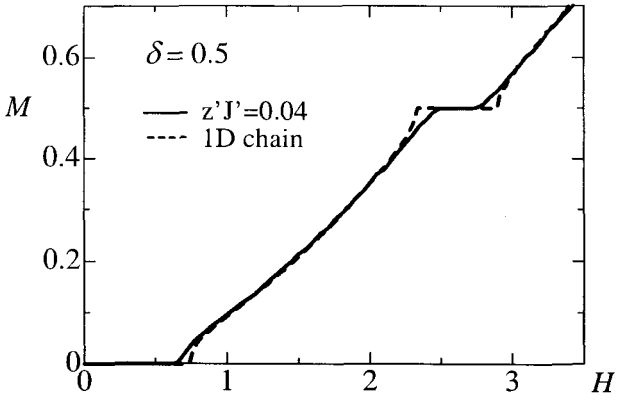

Figure 1: Magnetization curves in the dimer phase: the solid and broken lines correspond to those computed for $z'J'=0.04$ and 0, respectively.

Let us now discuss the obtained results. In Fig. 1, we show typical magnetization curves in the singlet-dimer phase, by choosing the bond-alternation parameter $\delta=0.5$. Note that in the limit of isolated chains $J'=0$, the ground state is either in the singlet-dimer phase ($\delta > 0.25$) or in the Haldane phase ($\delta < 0.25$). In both phases, the profile of the magnetization is essentially the same, as shown in Fig. 1. Namely, the spin gap at $H=0$ disappears at a certain critical field, and the system is driven to a gapless phase often called as the Tomonaga-Luttinger liquid phase. Further increase in a magnetic field induces the plateau structure at half of

the saturated magnetization, as shown by Tonegawa *et al.*[6] When the interchain coupling is introduced, magnetic correlations are enhanced, and thus the gapless Tomonaga-Luttinger liquid phase is immediately driven to a magnetically ordered phase. On the other hand, the spin gap phases with the magnetization M=0 and M=1/2, still persist for weak interchain couplings although the corresponding spin-gap regions are reduced as shown in Fig. 1. We have checked that the above characteristic properties of the magnetization process are also found in the quasi-1D Haldane phase.

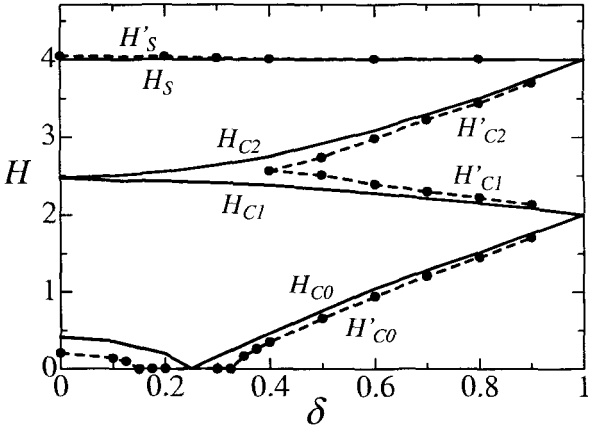

Figure 2: Phase diagram for the quasi-1D Haldane system with bond-alternation δ under an applied field H: the solid and broken lines are the results for $z'J'$=0 (isolated chain) and $z'J'$=0.04, respectively. The magnetization takes the quantized value at M=0 in the region from 0 to H_{c1} (H'_{c1}), M=1/2 in the region from H_{c2} (H'_{c2}) to H_{c3} (H'_{c3}), and M=1 above H_s (H'_s). In other regions, the magnetization is changed continuously.

To see the stability of the spin-gap phases against the interchain coupling, we show the phase diagram calculated for $z'J'$=0 and 0.04 in Fig. 2. Note that the present results reproduce the phase diagram known for an isolated Haldane chain with bond alternation (J'=0), where the quantum phase transition between the dimer and Haldane phases occurs at the critical value $\delta \sim 0.25$ in the absence of a magnetic field.[6] It is seen that the spin-gap state around this critical point is unstable against the introduction of the interchain coupling. On the other hand, it is seen that the stability of the magnetic plateau depends on the strength of the bond alternation. Namely, the plateau in the Haldane phase (for smaller δ) is rather unstable and disappears even for weak interchain couplings, while the plateau in the dimer phase (for larger δ) is stable, which persists up to a reasonably large interchain coupling. This is also seen in Fig. 1.

In summary, we have investigated the magnetization process of a quasi-1D S=1 antiferromagnet with bond alternation. By combining DMRG with interchain mean-field approximation, we have discussed the 3D effects on the phase diagram in a magnetic field. It has been shown that the introduction of the interchain coupling enhances antiferromagnetic correlation, making the spin-gap phases unstable beyond a certain critical value. In particular, the plateau region in the magnetization curve is reduced rather significantly by the interchain coupling, which will play a crucial role when we analyze the magnetization curves quantitatively for quasi-1D S=1 antiferromagnetic spin compounds.

Acknowledgments

We would like to thank Y. Narumi and K. Kindo for valuable discussions. This work was partly supported by a Grant-in-Aid from the Ministry of Education, Science, Sports and Culture of Japan. A part of computations was done at the Supercomputer Center at the Institute for Solid State Physics, University of Tokyo and Yukawa Institute Computer Facility. A. Kawaguchi was supported by Japan Society for the Promotion of Science.

References

1. F. D. M. Haldane, Phys. Lett. **93A**, 646 (1983); *Phys. Rev. Lett.* **50**, 1153 (1983).
2. I. Affleck and F. D. M. Haldane, *Phys. Rev. B* **36**, 5291 (1987).
3. R. R. P. Singh and M. P. Gelfand, *Phys. Rev. Lett.* **61**, 2133 (1988).
4. Y. Kato, and A. Tanaka, *J. Phys. Soc. Jpn.* **63**, 1277 (1994).
5. K. Totsuka, Y. Nishiyama, N. Hatano and M. Suzuki, *J. Phys.: Condens. Matter* **7**, 4895 (1995).
6. T. Tonegawa, T. Nakao and M. Kaburagi, *J. Phys. Soc. Jpn.* **65**, 3317 (1996).
7. W. Chen, K. Hida and B. C. Sanctuary, *J. Phys. Soc. Jpn.* **69**, 237 (2000).
8. T. Sakai, and M. Takahashi, *Phys. Rev. B.* **42**, 4537 (1990).
9. T. Sakai, *Phys. Rev. B.* **62**, R9240 (2000).
10. A. Escuer, R. Vincente and X. Solans, *J. Chem. Soc.* Dalton Trans. 531 (1997); Y. Narumi, M. Hagiwara, M. Kohno,and K. Kindo, *Phys. Rev. Lett.* **86**, 324 (2001).
11. Y. Narumi, M. Hagiwara and K. Kindo: *preprint.*
12. S. R. White, *Phys. Rev. Lett.* **69**, 2863 (1992); *Phys. Rev. B.* **48**, 10345 (1993).

NEGATIVE MAGNETORESISTANCE IN PbTe(Mn,Cr)

D. KHOKHLOV, I. IVANCHIK, A. KOZHANOV and A. MOROZOV
Physics Department, Moscow State University, Moscow, Russia

E. SLYNKO and V. SLYNKO
Chernovtsy Division, Institute of Materials Science Problems, Chernovtsy, Ukraine

W. DOBROWOLSKI and T. STORY
Insitute of Physics, Polish Academy of Sciences, Warsaw, Poland

We have observed the negative magnetoresistance effect in the narrow-gap PbTe(Mn,Cr) semiconductor, in which the Fermi level is pinned within the gap nearby the conduction band edge. Previously the giant negative magentoresistance effect has been reported in PbTe(Mn,Yb), in which the Fermi level is pinned in the gap nearby the valence band edge. It is known that in the case of Yb doping the Fermi level pinning results from the 2+ - 3+ valence instability of an impurity. The same sort of the valence instability provides the Fermi level pinning in PbTe(Mn,Cr), but the conductivity is of the *n*-type, not of the *p*-type as in PbTe(Mn,Yb). Introduction of magnetic field leads to substantial drop of the PbTe(Mn,Cr) resistivity of about 30% at T = 4.2 K. This is however much lower than in PbTe(Mn,Yb), where the effect amplitude reached 3 orders of magnitude. The effect disappears at T = 15 K. Possible mechanisms of the effect are discussed.

1 Introduction

Lead chalcogenides are well-known materials for the infrared optoelectronics. Applications of the lead salts are restricted by the fact that they grow with high deviation from stoikhiometry, and all growth defects are electrically active. Doping of the lead telluride and some other narrow-gap IV-VI semiconductors with certain impurities results in appearance of a range of strong and unusual effects that are not characteristic for the undoped material.[1] In particular, doping of the lead telluride-based alloys with some of the group III impurities, such as In or Ga, leads to the Fermi level pinning effect and to appearance of long-term non-equilibrium phenomena at low temperatures. In certain range of alloy composition, the Fermi level may be pinned within the gap, providing appearance of a semi-insulating state at low temperatures.

Formation of analogous impurity states has been reported for the Cr - and Yb - doped PbTe. The Fermi level is pinned in the conduction band in PbTe(Cr) (see Ref. [2]), and in the valence band in PbTe(Yb) (see Ref. [3]).

Doping of PbTe with Mn gives rise to the bandgap with the rate $\partial E_g/\partial x \approx 40$ meV/mol.%MnTe, but does not provide appearance of local or quasilocal levels in the vicinity of the actual bands.

The giant negative magentoresistance effect has been observed in PbTe(Mn,Yb) (see Ref. [12]), when the alloy conductivity dropped by 3 orders of magnitude in magnetic field. The effect observed in[12] was attributed to the peculiarities of impurity band transport in magnetic field. It was interesting to learn how would this effect transform in the case of the *n*-type semi-insulating state expected in PbTe(Mn,Cr).

2 Samples

The PbTe(Mn,Cr) bulk crystal was grown by the Bridgman technique. Concentration of the dopants varies along the growth axis: whereas the N_{Mn} increases from the top to the end of the ingot, the concentration of Cr, instead, drops. The ingot was cut into slices perpendicular to the growth direction. The concentration of dopants in each slice was determined using energy dispersive X-ray fluorescence analysis. Samples of the size 5×1×1 mm^3 were cut from the slices. Contacts to the samples were soldered with indium. DC galvanomagnetic measurements have been done using the 4-probe technique.

3 Experimental Results

Application of magnetic field results in appearance of negative magnetoresistance effect at temperatures T < 15 K (Fig. 1).

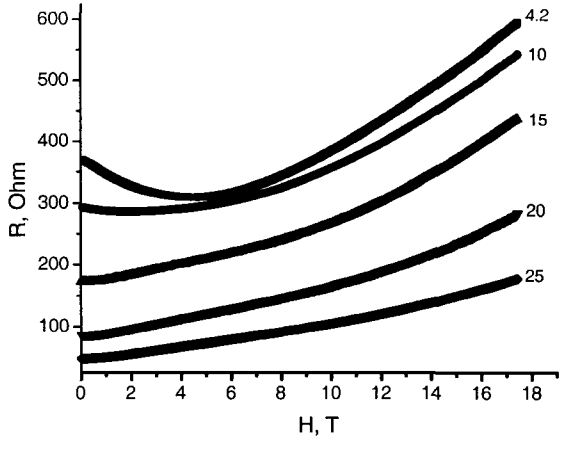

Figure 1: Magnetoresistance in $Pb_{1-x}Mn_xTe(Cr)$. Figures near the curves – temperature in K; x = 0.091.

The effect amplitude is much lower that in the case of PbTe(Mn,Yb), but is still about 30% that is much higher than the negative magnetoresistance normally observed in disordered systems. The drop of resistance in magnetic field decreases with increasing temperature, and disappears at T > 15 K. It can be seen from the Fig. 1 that the resistivity gradually rises with lowering temperature in the field intervals H < 5 T and H > 7 T. However the sample resistance almost saturates at T < 10 K in the field interval 5 T < H < 7 T.

This fact is most clearly seen in the temperature dependence of resistivity taken in different fields (Fig.2).

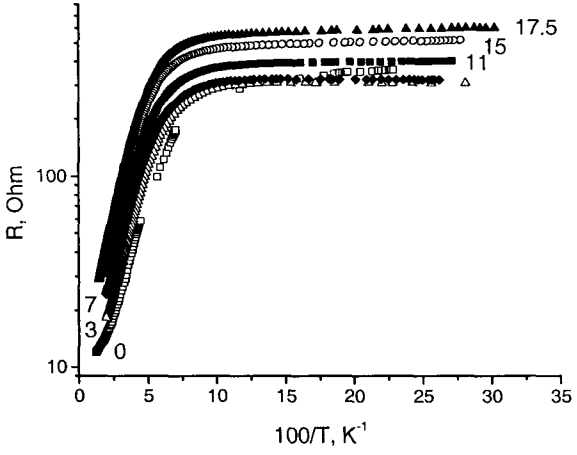

Figure 2: Temperature dependence of resistance in different magnetic fields. Open squares – H = 0 T, open triangles – H = 3 T, diamonds – H = 7 T, solid squares – H = 11 T, circles – H = 15 T, solid triangles – H = 17.5 T

It is important to note that the resistivity temperature dependence consists of two activation parts at H < 5 T . The activation energy corresponding to relatively high temperatures T> 15 K is about 5-6 meV and slightly rises with increasing H. At the same time the low-temperature activation energy decreases with field going down to zero at H ~ 5 T. At H > 7 T the conductivity rise with lowering temperature at T < 15 K appears again.

The low field Hall mobility rises with lowering temperature, reaches a maximum at T ≈ 35 K and then quickly drops. This drop in the mobility temperature dependence is normally observed in the disordered systems, or in the situations when the conductivity is defined by percolation. The maximal value of mobility $\mu \sim 10^3$ cm^2/V·s is typical for the conduction band electrons in this temperature range.

Data taken for the other samples demonstrate the same trends.

4 Discussion

The high-temperature resistivity activation observed at T > 15 K most likely corresponds to the thermal activation of free electrons from the pinned Fermi level to the conduction band, as suggested by high mobility of carriers. It means that the free holes may give contribution to the positive magnetoresistance in the low fields at elevated temperatures, but not to the negative magnetoresistance.

The activation energy corresponding to the process observed at the low temperatures and in the low fields is much smaller than the distance between the impurity level that pins the chemical potential and the valence band. Besides that, the Hall data suggest that the charge carriers responsible for this activation have much lower mobility. It is natural to assume therefore that the mechanism of this low-temperature activation is the following. There may exist a considerable widening of the impurity level in Cr-doped PbTe. In certain cases this widening may lead to the possibility of percolative transport as long as the Fermi level is inside the middle part of the respective density of states profile. If it stays in the "tails" of this profile, the conductivity is defined by the thermal activation from the Fermi level to the mobility edge. Apparently the Fermi level shifts in magnetic field with respect to the mobility edge in PbTe(Mn,Cr).

The possible mechanism of the effect is the following. Application of magnetic filed may result in splitting of impurity states with different spin directions. Under these conditions the overall filling of the band does not change, but filling of each of the spin-polarized impurity sub-bands may change and result, in turn, in a shift of the Fermi level with respect to the mobility edge in each sub-band. In any case, it is clear that the effect is defined by peculiarities of the magnetotransport via the impurity band, not by conduction band carriers, as in II-VI semiconductors.[6]

Acknowledgments

The research described in this paper has been supported in part by the supplemental funds to the NSF core grant at the NHMFL DMR 008 4173.

References

1. B. A. Akimov *et al., Phys. Status Solidi A*, **137**, 9 (1993).
2. L. M. Kashirskaya *et al., Sov. Phys. Semicond.*, **24**, 848 (1990).
3. I. I. Ivanchik *et al., Proc. 24 Int. Conf. Phys. Semicond., ed. D. Gershoni, World Scientific,* CD-ROM, VIII B-8 (1999).
4. J. Niewodniczska-Zawadzka *et al., Physica B*, **117B**, 458 (1983).
5. I. I. Ivanchik *et al., Phys. Rev. B*, **61**, R14889 (2000).
6. A. Mycielsky and J. Mysielski, *J. Phys. Soc. Jp*, **49A**, 807 (1980).

NEW NON-COOPERATIVE QUANTUM PHENOMENON IN A FERRIMAGNET WITH ANTIFERROMAGNETIC IMPURITY

A. S. LAGUTIN, A. SEMENO, J. VANACKEN and Y. BRUYNSERAEDE

Laboratorium voor Vaste-Stoffysica en Magnetisme Katholieke Universiteit Leuven, Celestijnenlaan 200D, B-3001, Leuven, Belgium

E-mail: sascha.lagutin@fys.kuleuven.ac.be

The differential magnetic susceptibility of $Gd_{0.01}Y_{2.99}Fe_5O_{12}$ polycrystalline compounds is studied at the temperature range from 0.6 to 4.2 K in pulsed magnetic fields up to 50 T. It was observed that the magnetization of the compound with x=0.01 shows a quantum (stepwise) behavior at T = 0.6 K in magnetic fields around 33 T. The Heisenberg model of a ferrimagnet with weakly coupled antiferromagnetic impurities is used to explain the obtained results. Following this model, the energy levels of the impurity ions become not equally spaced due to the magnon-magnon interaction between the iron spins and the rare earth spins. Increase of the external field leads to the crossover of the excited states with the ground one, which takes place in different fields. In result, several peaks of the magnetic susceptibility appear under a variation of magnetic field in the vicinity of a field, which is equal to the effective field of the Gd-Fe exchange interaction.

1 Introduction

In the early seventies a new type of macroscopic quantum phenomena was predicted giving rise to field induced oscillations in the specific heat and susceptibility of materials with a ferromagnetic matrix and antiferromagnetic impurities.[1,2] These oscillations are the direct consequence of the magnon - magnon interaction between the matrix and the impurity, which causes an unequal spacing of the $2S_0+1$ impurity energy levels where S_0 denotes the impurity spin. The first attempt to discover these oscillations was made shortly after the theoretical prediction,[3] but no evidence of oscillations was found in $Gd_xY_{3-x}Fe_5O_{12}$ ($x < 0.2$) polycrystalline samples even at the lowest impurity content ($x = 0.01$) and temperature (1.6 K). On the other hand, the experiments did not reveal the classical result for low impurity content ($x \leq 0.05$), because in that case the field interval ΔH, where the spin reversal takes place, did not depend on the impurity content. This result contradicts the classical molecular-field theory, but is in accord with the microscopic model.[1,2]

In this work we present the direct observation of field induced oscillations of the impurity susceptibility in a ferrimagnetic matrix. The main aim of this work is to demonstrate that under certain conditions, as predicted in.[1,2] these oscillations appear due to quantum transitions between discrete $2S_0+1$ energy levels of the impurity spin.

2 Results and discussion

The differential magnetic susceptibility of $Gd_xY_{3-x}Fe_5O_{12}$ (x = 0.01) was studied in pulsed magnetic fields up to μ_0H=50 T in the temperature range 0.6 < T < 4.2 K. The $Gd_xY_{3-x}Fe_5O_{12}$ ferrite-garnet was the same as used in Ref. [3]. The impurity content was measured after the final annealing of the ingots by X-ray luminescence analysis and mass-spectrometer analysis. The susceptibility was measured using a pulsed inductive magnetometer of an "open" type.[5]

Figure 1 shows the field dependences of the differential magnetic susceptibility for the $Gd_{0.01}Y_{2.99}Fe_5O_{12}$ compound, measured at three different temperatures. The temperature decrease leads to a reduction of ΔH, but its value at T=0.6 K is still much larger than predicted by the classical model (~ 1 T). This is an essential deviation from the classical approach, as noted in Ref. [3]. Moreover, the temperature produces substantial changes in the susceptibility of the mixed garnet: the initial broad peak begins to split at T=1.5 K and there are already two well defined peaks at T=0.6 K. Small anomalies of the dM/dH at this temperature in field below 29 T and above 38 are not reproducible (in contrast with two central peaks). This is the noise caused by mechanical vibration of the measuring cell, and it becomes larger with the temperature decrease. To improve the signal/noise ration, the data were averaged over seven pulses.

To explain the observed splitting of the susceptibility peak, we use the model developed in.[1,2] These simulations show qualitative agreement with our experiments, confirming the new quantum phenomenon. Following,[1,2] we consider a model, where a two-sublattice iron matrix with the spins S_1 and S_2 respectively becomes equivalent to a ferromagnet with total spin $S = S_2 - S_1$, and real location of the impurity spins doesn't play an important role. The impurity spins S_0 are weakly coupled with the matrix $|J_0| << |J|$, where J>0 is the exchange integral between the matrix spins S_1 and S_2, coupled antiferromagnetically, and J_0 is the exchange integral between S_0 and S_1 or S_2 (these matrix spins are also coupled antiferromagnetically with the impurity spin). According to,[2] the solution of the Schrödinger equation at $J_0>0$ shows that there is no damping of the impurity states and that the impurity energy levels are given by:

$$\varepsilon_{ml} = m\varepsilon_1 + \frac{1}{2}l(l-1)\alpha + \frac{1}{2}(m-l)(m-l-1)\alpha \mp (l+1)\left(1-\frac{l}{2S'}\right)\varepsilon_R\delta_{m,2l+1}. \qquad (1)$$

where $\gamma = zSJ_0 + S_0\alpha$, $\alpha = z(J_0)^2(I_W - 1)/$, z is the number of nearest neighbors, g_0 is g-factor of the impurity ion, I_w is the Watson integral and $m = S_0 - M_0$. The term α describes the magnitude of the magnon-magnon interaction between the matrix and the impurity; $\delta_{m,2l+1}$ is the Kronecker symbol. For given m ($0 \le m \le 4S_0$ for a pair),

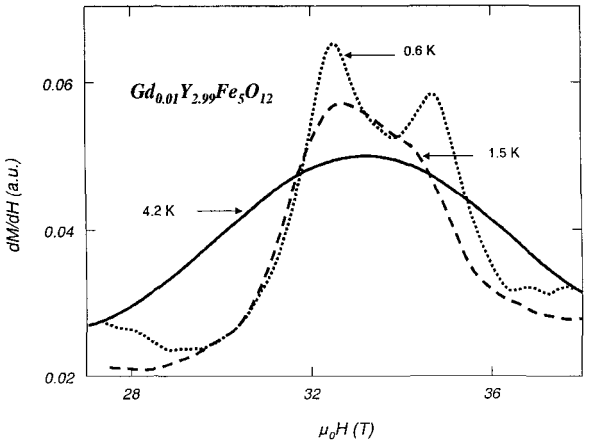

Figure 1: Field dependences of the differential magnetic susceptibility of a $Gd_{0.01}Y_{2.99}Fe_5O_{12}$ sample at different temperatures.

some of the levels break into a number of sublevels corresponding to a different distribution of magnons over the pair of impurities. The parameter l describes a number of magnons for one impurity ($0 < l < 2S_0$). The parameters ε_1 and ε_R are given by formulas

$$\varepsilon_1 = g_0\mu_B H - zSJ_0 - S_0\alpha, \tag{2}$$

$$\varepsilon_R = zS_0\frac{(J_0)^2}{J}\frac{n}{4\pi}\frac{e^{-\kappa R}}{R}, \quad \kappa^2 = n\frac{J_0}{J}. \tag{3}$$

Here n is equal to 2 and 3 for the BCC and FCC lattices respectively. Figure 2 shows the results of the calculated field dependence of the differential magnetic susceptibility of the $Gd_{0.01}Y_{2.99}Fe_5O_{12}$ sample, taking into account the concentration broadening. It is evident that this model approaches the experiment well; one initial peak of susceptibility at T = 4.2 K splits into two peaks at T = 1.5 K and T = 0.6 K. Further temperature decrease causes additional splitting at T = 0.2 K. One can conclude that interaction between impurities drastically changes the susceptibility pattern. Instead of 7 susceptibility peaks it is possible to observe two or four peaks depending on temperature. Nevertheless, the stepwise character of the magnetization curve remains and the differential magnetic susceptibility manifests quantum oscillations in fields near μ_0H ~ 32 T. The discovered in the $Gd_{0.01}Y_{2.99}Fe_5O_{12}$ sample effect has a general character and may be observable under certain conditions (see Refs [1,2]) in a large number of ferro- or ferrimagnets with antiferromagnetic impurities.

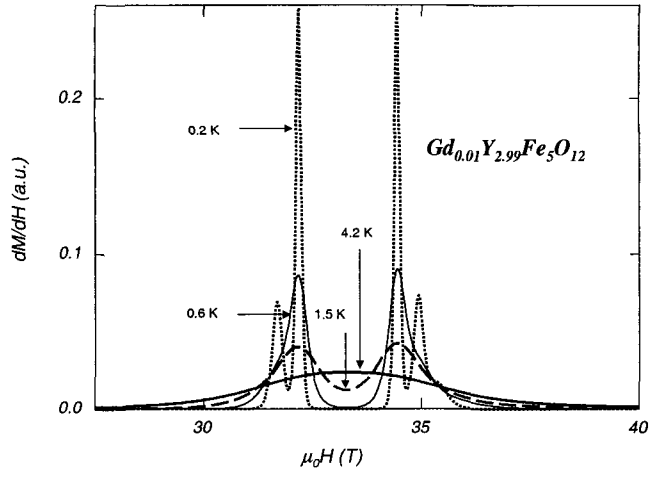

Figure 2: The differential magnetic susceptibility versus field for $Gd_{0.01}Y_{2.99}Fe_5O_{12}$ shown at different temperatures calculated within the framework of model.[7] The parameters used in the calculations are: α = 1.2 cm^{-1}, J_0 = 3.5 cm^{-1}, J = 25 cm^{-1}, z = 7, κ = 0.59, R = 200 Å

Acknowledgments

The authors are thankful to B.V. Mill for preparation of the specimens, V.A. Ivanov for fruitful discussions and L. Weckhuysen for assistance during the experiments. The Belgian IUAP, the DWTC, the Flemish GOA and FWO-programs are supporting this work.

References

1. B. Ya. Balagurov and V. G. Vaks, *Sov. Phys. JETP* **39**, 554 (1974).
2. B. Ya. Balagurov and M. B. Geilikman, *Sov. Phys. JETP* **43**, 964 (1976).
3. .K. G. Gurtovoi, A. S. Lagutin and V. I. Ozhogin, *Sov. Phys. JETP* **51**, 425 (1980).
4. S. Krupièka, Physik der Ferrite und der Verwandten Magnetischen Oxyde, *Akademie der Wissenschaften*, Prag, 1973.
5. A. S. Lagutin, J. Vanacken, N. Harrison and F. Herlach, *Rev. Sci. Instrum.* **N8**, 4267 (1995).

FERROMAGNETIC RESONANCES IN POLYCRYSTALLINE $La_{0.8}Li_{0.2}MnO_3$

R. A. LEWIS, X. L. WANG and S. X. DOU

Institute for Superconducting and Electronic Materials,

University of Wollongong, NSW 2522, Australia

E-mail: roger_lewis@uow.edu.au

N. BISKUP and J. S. BROOKS

National High Magnetic Field Laboratory, Tallahassee, FL 32310, USA

We report on magnetic resonances observed in the doped lanthanum manganite $La_{0.8}Li_{0.2}MnO_3$ (LLMO) below the Curie temperature T_c ~ 235 K. Fields up to 30 T were employed. The data are compared with that from the archetypal colossal magnetoresistance perovskite $La_{0.7}Ca_{0.3}MnO_3$ (LCMO) taken under similar conditions. In contrast to LCMO, LLMO exhibits two resonances, one above and one below the LCMO resonant field. These are attributed to a ferromagnetic interaction and a canted ferromagnetic interaction.

1 Introduction

Many perovskite manganites exhibit a phase transition from paramagnetic insulator (PMI) to ferromagnetic metal (FMM) when cooled through characteristic temperature T_c. The most studied example is $La_{0.67}Ca_{0.33}MnO_3$ (LCMO), for which T_c ~ 270 K. Magnetic resonance investigations have proved valuable in three temperature regimes: high ($T > T_c$), intermediate ($T \sim T_c$), and low ($T < T_c$).

For $T > T_c$ the electron spin resonance (ESR) linewidth is given by $\Delta H_{pp}(T) = \Delta H_{pp}(\infty)[C/T\chi_{dc}(T)]$ (see Refs. [1-3]). Linewidths and intensities for ^{16}O and ^{18}O isotope-substituted compounds suggest a bottleneck model of spin relaxation.[4,5] High-temperature linewidths depend on superexchange interactions and are insensitive to double-exchange interactions due to the relatively long time scale of the latter.[6,7]

Lowering the temperature towards T_c results in a reduction of the linewidth which reaches a minimum at $T_{min} \sim 1.1\ T_c$. Further lowering of temperature results in the linewidth increasing. Broadening is negligible in polished single crystals but is large, and follows the same T dependence as magnetization, in ceramic or polished crystal samples, suggesting the broadening mechanism is demagnetization fields associated with intergranular pores or surface cavities.[8]

For $T < T_c$ the $g \sim 2$ resonance weakens and another resonance arises, moving to lower fields as T decreases, as expected for a second-order phase transition.[9,10] Different resonances are observed for field parallel or perpendicular to (a) the length of bulk samples[11,12] and (b) the plane of thin film samples.[13]

Here we examine $La_{0.8}Li_{0.2}MnO_3$ (LLMO) in which Li rather than Ca substitutes for La. For given atom fraction, the number of Mn^{3+} ions oxidized to Mn^{4+} by Li^+ is double that oxidized by Ca^{2+}. Also, Li introduces greater lattice distortion than Ca.

2 Experiment

Ceramic samples of LCMO and LLMO were prepared by conventional sintering. Neutron powder diffraction of the LLMO indicates a rhombohedral perovskite structure with Li substituting for La. Resistivity-temperature data show an insulator-metallic transition around 235 K. Large magnetoresistance (to 80%) is observed over a wide temperature range. Details of preparation and characterisation of LLMO are given elsewhere.[14] Far-infrared spectroscopy identified the three principal phonon modes - external beating of the La/Li against the MnO_3 octahedra, Mn-O-Mn bending and Mn-O stretching. The shift to lower frequency of the external mode in LLMO relative to LCMO further confirms the substitution of Li for La (see Ref. [15]). Magnetic resonances were detected by a cavity perturbation method using a microwave network analyzer. The general principles of the technique have been described elsewhere.[16] Data were taken in DC fields to 30 T at the NHMFL, Tallahassee, over temperature range 4 to 100 K and frequency range 30 to 110 GHz.

3 Results and Discussion

Figure 1 gives data for LLMO at f = 29.48 GHz over the field range 0 to 30 T.

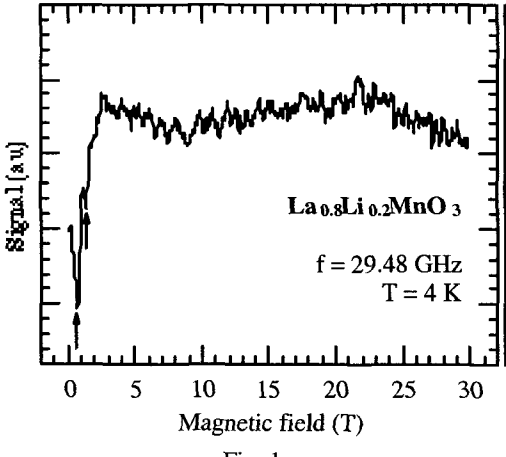

Fig. 1

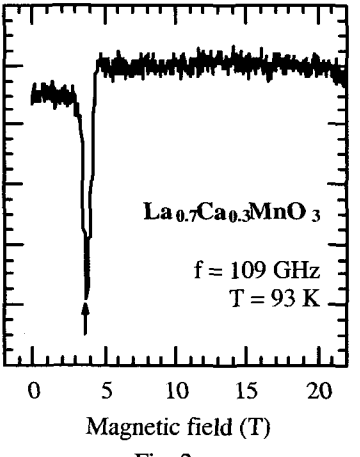

Fig. 2

Two low-field resonances are evident, but no features beyond this. In contrast, LCMO (Fig. 2) exhibits a single resonance in all spectra. The linewidth ΔH_{pp} in these experiments for both compounds was typically 0.3 T. Such a linewidth is comparable to previously measured linewidths in manganites below T_c, for example, 0.3 T in the case of $La_{0.5}Pb_{0.5}MnO_3$ (see Ref. [9]), and 0.21 - 0.28 T in the case of $La_{0.6}M_{0.07}Ca_{0.33}MnO_3$ (M = Er, Yb, Bi) (see Ref. [11]). These are much larger than the minimum linewidth observed around $T_{min} = 1.1\ T_c$ of ~ 0.013 T (see Ref. [8]), but comparable to $\Delta H_{pp}(\infty) = 0.24$ T for LCMO (see Ref. [1]).

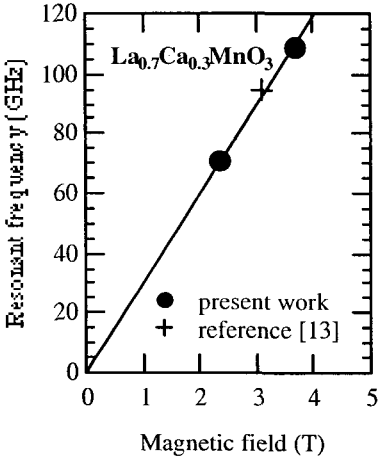

Figure 3

For comparison with the LLMO data and with earlier work, some reference data for the field dependence of the LCMO resonances are given in Fig. 3. Also shown in Fig. 3 is 95 GHz data for LCMO film below T_c (see Ref. [13]). The points lie at lower fields than for data taken above T_c due to the internal field in the ferromagnetic phase. Relating the angular frequency ω, gyromagnetic ratio γ, applied field H_0, and magnetization M by

$$\omega = \gamma(H_0 - M)$$

it is deduced that M ~ 0.7 T, in agreement with the estimate based on all or most Mn ions contributing to the magnetization.

Data for LLMO is given in Fig. 4. In contrast to LCMO, there are now two resonances. These lie at greater and lesser fields than the LCMO resonances at the corresponding frequencies. There are several possible origins of the split resonance. For example, given that the LCMO resonance corresponds to $M \| H_0$ a second resonance might arise with $M \perp H_0$, for which

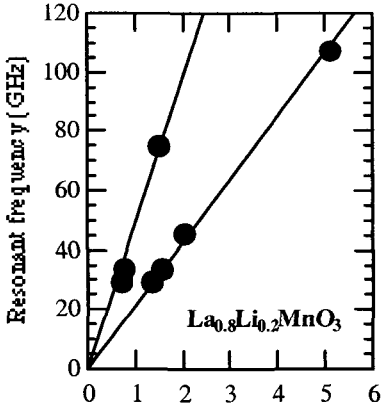

Figure 4

$$\omega^2 = \gamma^2(H_0^2 + MH_0).$$

While such an identification yields a reasonable value of $M_{\parallel} \sim 1$ T it yields an unreasonable value of $M_{\perp} > 3$ T. Alternatively, the lines may be due to impurity phases. However, they do not behave as the impurity phase lines identified in previous work.[3] The frequencies are too low for the direct observation of antiferromagnetic resonances.[17] The most likely explanation that remains is that one resonance corresponds to a ferromagnetic interaction and the second to a canted ferromagnetic (or antiferromagnetic) interaction, as has been proposed to account for data from $La_{0.6}Bi_{0.07}Ca_{0.33}MnO_3$ (see Refs. [11,12]). This explanation is consistent with the observation of only a single line in LCMO. It is also plausible in view of the transition from ferromagnetic order to canted ferromagnetic order observed in LCMO when Li nominally substitutes for Mn (see Ref. [18]).

This work was supported in part by the Australian Research Council and the University of Wollongong. A part of this work was performed at the National High Magnetic Field Laboratory, which is supported by NSF Cooperative Agreement No. DMR-9527035 and by the State of Florida. JSB acknowledges support from DMR 99-71474 and NHMFL/IHRP 5033.

References

1. M. T. Causa *et al.*, *Phys. Rev. B* **58**, 3233 (1998).
2. S. B. Oseroff *et al.*, *J. App. Phys.* **87**, 5810 (2000).
3. N. O. Moreno *et al.*, *Phys. Rev. B* **63**, 174413-1 (2001).
4. A. Shengelaya *et al.*, *Phys. Rev. Lett.* **77**, 5296 (1996).
5. A. Shengelaya *et al.*, *Phys. Rev. B* **61**, 5888 (2000).
6. D. L. Huber *et al.*, *Phys Rev. B* **60**, 12 155 (1999).
7. F. Rivadulla *et al.*, *Physica B* **284-288**, 1418 (2000).
8. F. Rivadulla *et al.*, *Phys. Rev. B* **60**, 11 922 (1999).
9. A. I. Shames *et al.*, *Solid State Commun.* **107**, 91 (1998).
10. O. Yanagisawa *et al.*, *J. Magn. Magn. Mat.* **211**, 254 (2000).
11. D. Bahadur *et al.*, *J. Alloys and Comp.* **256**, 76 (1997).
12. M. C. Walsh *et al.*, *Physica B* **253**, 103 (1998).
13. F. Dupont *et al.*, *Solid State Commun.* **133**, 499 (2000).
14. X. L. Wang *et al.*, *J. Appl. Phys.* **83**, 7177 (1998).
15. R. A. Lewis *et al.*, *Aust. J. Phys.* **52**, 197 (1999).
16. M. Boonman, *Thesis,* University of Nijmegen (1998).
17. A. Pimenov *et al.*, *Phys. Rev. B.* **62**, 5685 (2000).
18. F. Gao *et al.*, *J. Alloys and Compounds* **325**, 281 (2001).

THE STUDY OF THE MAGNETIC BREAKDOWN EFFECT AS A FUNCTION OF ANGLE IN THE ORGANIC CONDUCTOR K- (BEDT-TTF)$_2$Cu(NCS)$_2$ IN HIGH MAGNETIC FIELDS

I. MIHUT and C. C. AGOSTA
Department of Physics, Clark University, Worcester, Massachusetts, 01610,USA
E-mail: imihut@clarku.edu

C. H. MIELKE
National High Magnetic Field Laboratory, Los Alamos National Laboratory, Los Alamos, New Mexico 87545, USA

M. TOKOMOTO
Electrotechnical Laboratory, Tsukuba, Ibaraki 305, Japan

The magnetic breakdown effect can be seen by the growth of new frequencies in the quantum oscillations in clean metals as a function of magnetic field. We have studied the variation of the amplitudes in the quantum oscillations in the resistance (the Shubnikov-de Haas effect) as a function of angle in the quasi-two dimensional-organic conductor κ-(BEDT-TTF)$_2$Cu(NCS) $_2$. The measurements were made by means of a radio frequency (rf) tank circuit (~50 MHz) at very high magnetic fields(50T-60T) and low temperature(500 mK). The geometry of the rf excitation we used excited in-plane currents, and therefore we measured the in-plane resistivity. In contrast to conventional transport measurements that measure the inter-plane resistivity, the in-plane resistivity is dominated by the magnetic breakdown frequencies. As a result we measured much higher breakdown frequency amplitudes than conventional transport experiments. As is expected, the angular dependence of the Shubnikov-de Haas frequencies have a 1/cosθ behavior. This is due to the change of the cross sectional area of the tubular Fermi surface as the angle with respect to the magnetic field is changed. The amplitude of the oscillations changes due to the spin splitting factor which takes into account the ratio between the spin splitting and the energy spacing of the Landau levels which also has 1/cosθ behavior. We show that our data agree with the semi-classical theory (Lifshitz-Kosevich formula) .

1 Introduction

Many efforts have been made to understand and explain the mechanism of magnetic breakdown phenomena. Semi-classical and quantum models have been developed, but there is still not complete agreement with the experimental data. One of the most studied materials where magnetic breakdown frequencies have been observed is the quasi-two dimensional organic superconductor κ-(BEDT-TTF)$_2$Cu(NCS)$_2$. The Fermi surface (FS) of κ-(BEDT-TTF)$_2$Cu(NCS)$_2$ consists of a quasi-one-dimensional (1D) and a quasi-two-dimensional (2D) FS sections. It has been shown that the fundamental frequency F_α seen in Shubnikov de Haas or de Haas van Alphen oscillations, is associated with the 2D FS while the magnetic breakdown frequency F_β is related to the tunneling across the gap between the 2D and 1D FS. The tunneling between the two FS occurs when the magnetic energy is greater than the gap, in this case about 35 T. As the magnetic field increases more combinations ($F_{\beta-\alpha}$, $F_{\beta+\alpha}$, $F_{\beta-2\alpha}$ etc.) of original frequencies are observed. When the sample is

rotated in the magnetic field the amplitude of the frequencies changes due to the geometry of the Fermi surface and the effects of electron spin.

We have studied the magnetic breakdown effect by measuring the quantum oscillations in the resistance in the organic conductor κ- (BEDT-TTF)$_2$ Cu(NCS)$_2$ using a contact-less measurement method, called the TDO method.[1] In the TDO method the sample is placed in the coil of a rf tank circuit oscillating at 50 MHz. We then applied magnetic fields to the sample and measured the frequency shift of the oscillations. The sample could be rotated about the axis perpendicular to the magnetic field. We made all measurements at low temperature, below 500 mk. In contrast to conventional transport measurements that measure the inter-plane component of the resistivity, the TDO method measures the in-plane resistivity. Using the TDO method we found that the magnetic breakdown frequencies are much more dominant than in conventional transport measurements. Our goal was to measure ratio of the amplitudes of quantum oscillations as a function of angle.

2 Experimental Details

The sample was placed in the one of two1 mm dia. counter –wound coils of the self-resonant tank circuit.[1] The angle was changed by fixing the set of balanced coils on a platform, which had the flexibility of rotating approximately (+ 30^0,-30^0) with respect to the magnetic field. The frequencies and the amplitudes of the circuit oscillations were measured after the signal from the TDO circuit was routed through a series of amplifiers and mixer.[1] The measurements were done in 50 T pulse magnet at the NHMFL with 38 ms rise-time and decay over 500 ms and at temperature below 500 mK.

3 Results and Discussion

3.1 Contact-less measurement method versus 4-lead conventional measurement method.

Oscillations in the resistance using both a conventional four lead transport technique and a contact-less TDO measurement technique are shown in Fig 1. The measurements are taken close to zero angle meaning the conducting planes are perpendicular to the field. It can be clearly seen that at the same temperature and at high magnetic field, the amplitude of breakdown SdH oscillations as compared to α-oscillations are much stronger using the TDO technique. It is not well understood why this is true.

3.2 Magnetic breakdown frequencies as a function of angle

In order to investigate the magnetic breakdown effect we carried out angle dependent measurements. The SdH frequencies were calculated by a fast Fourier transform (FFT). It has already been determined that the angular dependence of the

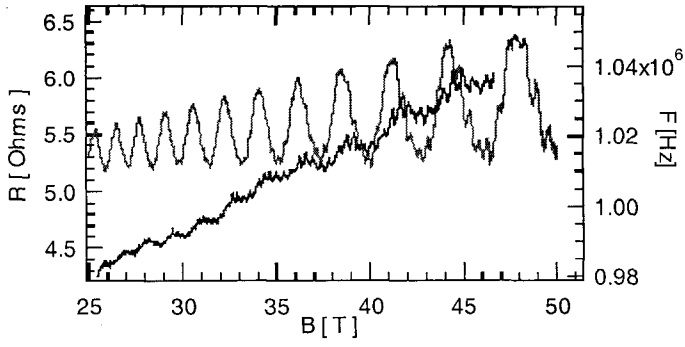

Figure 1: The large oscillations were measured using the 4-lead measurement method and the predominant frequency is the α-frequency. The small oscillations were taken using the TDO method besides the α-frequency in the magnetic breakdown oscillations were clearly seen.

α -frequency (F_α) obeys a (1/cos θ)–law.[3] We used this result to measure the orientation of our sample. The magnetic breakdown frequencies as a function of angle are shown in Fig. 2 (a-c). Previous work done by Meyer *et al.*,[4] shows that the breakdown frequency F_β follows the (1/cos θ)–law. Our data suggest the same behavior (Fig. 2(a)). In addition to the angular dependency of the F_β we present the angular dependency of the breakdown frequencies $F_{\beta-\alpha}$ and $F_{\beta+\alpha}$. The (1/cos θ)–law is also suggested for these frequencies(Fig 2 (b-c)).

3.3 Amplitude of magnetic breakdown frequencies versus angle

To study the evolution of the amplitudes of the breakdown frequencies as a function of angle we measured the amplitude of the oscillations using a FFT. The amplitudes of each of the frequencies were normalized by the amplitude of the α frequency to allow us to compare results with different samples and runs. In Fig. 3, we present the ratio of the (β–α)/α– , β/α– and (β+α)/α - amplitudes versus angle. At high angles, the amplitude of the (β–α) –orbit is larger than the amplitude of (β+α) –orbit, but smaller than the amplitude of the the β–orbit. As the sample is rotated towards the perpendicular direction on the magnetic field, the amplitude of the (β–α–orbit increases while the amplitude of the β-orbit decreases considerably. At zero angle, the dominant amplitude is the (β–α) –orbit. The amplitude of the (β+α) –orbit does not vary dramatically and it has a minimum around 17°.

3.4 Comparasion of the experimental data to the semi-classical theory

The changes in the quantum oscillations of the resistance when the magnetic field is tilted can be explained as a consequence of the spin splitting of the Landau levels. In the calculated amplitudes for different orbits, this effect is included by the well-

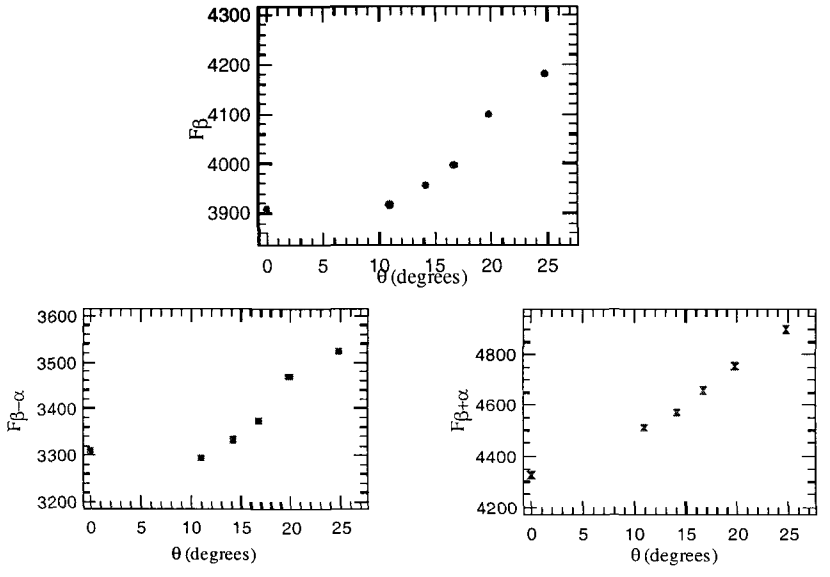

Figure 2(a-c): Magnetic breakdown frequencies versus angle

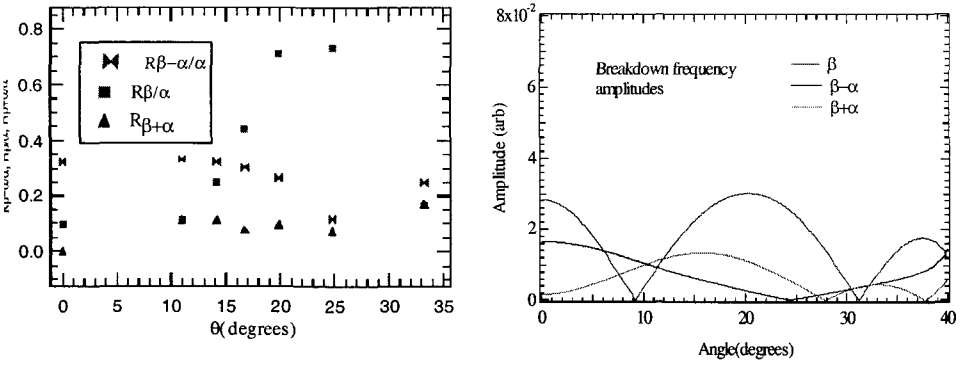

Figure 3: Ratio of the amplitudes versus angle.
Figure4: The calculated Ratio of the amplitudes versus angle.

nown spin splitting factor of the Lifshitz-Kosevich (LK) formula.[3]

$$A(\theta) \sim R_D R_T R_S \qquad (1)$$

where Rs is the spin splitting factor and R_D, R_T are other damping factors.[3] The equation below shows the spin splitting term:

$$R_s = \cos(1/2p\pi\ g\ m/m_e) \text{ and } m/m_e \sim 1/\cos\theta. \quad (2)$$

R_D, R_T also depend on m/m_e ,but they are not periodic. The amplitudes of the magnetic breakdown frequencies calculated using the LK formula are presented in Fig. 4. The values of the parameters used for simulation are given in Table 1.

m_α =3.22	m_β =7..25	$m_{\beta-\alpha}$ =3.6	$m_{\beta+\alpha}$ =8.49
g_α =1.62	g_β = 1.77	$g_{\beta-\alpha}$ =1.77	$g_{\beta+\alpha}$ =1.77

These values are in good agreement with the experimental values found by Meyer *et al.*,[4] Harrison *et al.*,[5] shown in Table 2.

Meyer et al.	m_α =3.22	m_β = 7.13	$m_{\beta-\alpha}$ =n/a	$m_{\beta+\alpha}$ =10.4
Harrison et al.	m_α =3.59	m_β = 7.29	$m_{\beta-\alpha}$ =3.69	$m_{\beta+\alpha}$ =8.42

Given the above values for the effective mass of each orbit we found good agreement between experiment and semi-classical theory prediction.

4 Conclusion

We have studied the quantum oscillations in the in-plane resistance in the organic conductor κ-(BEDT- TTF)$_2$Cu(NCS)$_2$ in a tilted magnetic field. We showed that using the contact-less measurement method the magnetic breakdown frequencies are much more dominant. We found 1/cosθ behavior for the magnetic breakdown frequencies versus angle. We studied the changes of the amplitudes of the magnetic breakdown frequencies as a function of magnetic field and we found good agreement between the experiment and the predicted semi-classical behavior.

Support came from the NSF and the experiments were done at the NHMFL in Los Alamos.

References

1. C. Agosta *et al., PPHMF II Proceeding* (1995).
2. T. Coffey *et al., Rev. Sci. Instr.*, **71**, 4600 (2000).
3. J. Wosnitza, Fermi *Surfaces of Low-Dimensional Organic Metals and Superconductors.*
4. F. A. Meyer *et al., Europhysics Lett.*, **32**, (8), 681(1995).
5. N. Harrison *et al., J. Phys;Cond. Matt.* **8**, 415 (1996).

ELECTRONIC SCATTERING AND SPIN DISORDER IN 3d-FERROMAGNETS IN THE PARAPROCESS REGIME

B. RAQUET and J.M. BROTO

Laboratoire National des Champs Magnétiques Pulsés, UMR 5830, 143, Av. de Rangueil – BP4245, 31432 Toulouse cedex 4, France

M. VIRET and E. SONDERGARD

CEA, Saclay, Service de l'Etat Condensé, Orme des merisiers, 91191 Gif sur Yvette, France

O. CESPEDES

Physics Department, Trinity College, Dublin 2, Ireland

We determine the collective spin excitations and their contribution to the intrinsic resistivity in 3d-ferromagnets by high field magneto-transport experiments. In the paraprocess regime, the longitudinal magneto resistance has a non saturating negative slope of about 0.02-0.05$\mu\Omega$.cm.T^{-1} at 300 K for Fe, Co and Ni. We demonstrate its magnetic origin and assign the effect to a decrease of the electron-magnon scattering due to the damping of spin waves in high field. We provide a unique estimate of the pure magnetic resistivity in *3d*-ferromagnets. Our analysis also gives an insight into the low energy spin waves, i.e. the theoretical magnon saturation field and the magnon mass renormalization.

1 Introduction

Even in pure metallic ferromagnets, the magnitude of the *s-d* exchange and its contribution to the magnetic resistivity via spin-flip electronic transitions remain poorly known.[1,2] No experiment has inferred a direct estimate of the pure spin-flip electronic scattering contribution to the resistivity in a temperature range where both spin excitations, electron-phonon scattering and inter-electronic collisions coexist. In this paper, we report on an original manner to determine the nature of the spin disorder and its contribution to the intrinsic resistivity for 3d-ferromagnets up to $T_c/2$.

2 Results and Discussion

We measure the longitudinal magneto resistance (MR) in 40 T pulsed magnetic field, in the paraprocess regime for epitaxial Fe, Co and Ni thin films, between 1.8 and 500 K. For the three magnets, the low temperatures are dominated by the normal MR resulting from the Lorentz force. For higher temperatures, but still well below the Curie temperature T_c, a negative MR, $\Delta\rho(T,B)\approx\rho(T,0)-\rho(T,B)$, dominates the

high field signal and its magnitude significantly increases with temperature (Fig. 1 for Fe).

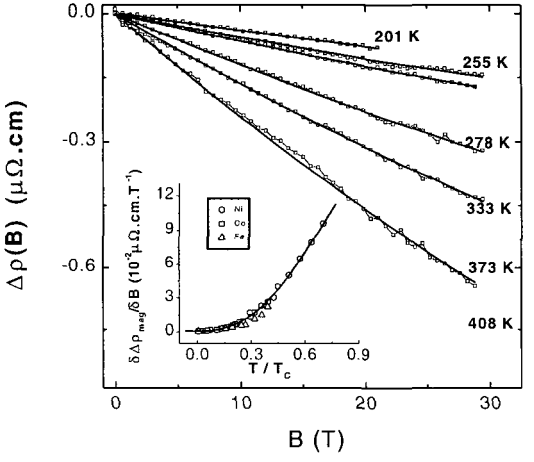

Figure 1: Longitudinal high field resistivity decrease for epitaxial Fe films -Fe_{80nm}/MgO. The solid lines are the theoretical curves deduced from the electron-magnon scattering model.[8] In inset, the high field magnetic resistivity slopes versus the normalized temperature by T_c for the 3 magnets.

In the frame of the two current mode,[3] the resistivity $\rho(1/\tau)$ is conveniently expressed by:[4] $\rho(1/\tau)=\rho_{imp}+\rho_{e\text{-}e}(T)+\rho_{ph}(T)+\rho_{mag}(T,B)+\rho_{dev}(T,B)$. Here, ρ_{imp} is the residual resistivity, $\rho_{e\text{-}e}(T)$ is due to the electron-electron interactions and $\rho_{ph}(T)$ is the electron-phonon scattering. These first three terms are little dependent on an applied magnetic field in the paraprocess regime. $\rho_{mag}(T,B)$ is the magnetic resistivity originating from the spin disorder and $\rho_{dev}(T,B)$ represents the deviation to Matthiessen's rule inherent to the inter band mixing. However, for pure metals, above the low temperature regime, let us say 50 K, $\rho_{dev}(T,B)$ is about one order of magnitude lower than $\rho_{mag}(T,B)$ (see Ref. [4]). Therefore, in a high enough temperature range, the negative MR in high field is mainly related to the $\Delta\rho_{mag}(T,B)$ term. The inset Fig. 2 shows the negative MR slopes $\partial\Delta\rho_{mag}(T,B)/\partial B$ above technical saturation for the three ferromagnets versus the normalized temperatures T/T_c. They surprisingly scale on a unique curve. This unambiguously demonstrates that the high field longitudinal MR is of magnetic origin. It probes the electron-spin disorder scattering processes in the paraprocess regime and in a temperature range well below T_c, once the normal MR is negligible. Despite a tremendous number of papers on magneto transport in ferromagnets, very few mention the coupling of magnetic excitations to the resistivity in paraprocess.[5-7]

A 40 T magnetic field certainly reduces the spin disorder and therefore increases the spin-flip electronic relaxation time. On the other hand, assuming a rigid band model, the corresponding Zeeman energy is approximately 4meV in high field. We do not expect the field induced band shift large enough to affect the electron-phonon diffusion and the Baber scattering. However, the 4meV magnetic energy introduces a non negligible gap in the dispersion relation of long wavelength magnons. So the magnetic resistivity is essentially dominated by the spin-flip electronic scattering via electron-magnon interactions and our magneto transport measurements probe the high field spin waves damping.

We propose a calculation of the electron-spin waves scattering contribution to the magnetic resistivity $\rho_{mag}(T,B)$ in a two polarized *s* and *d* bands model, including high magnetic field effects on the spin-flip diffusion plus the magnon mass renormalization.[8] Our experimental MR measurements expressed in term of magnetic resistivity variation are compared to the model. We set the band structure parameters for Fe, Co and Ni to the most commonly admitted values;[8] only the magnon mass and its renormalization are free parameters to fit the $\Delta\rho_{mag}(B)$ curves. Results of the fit procedure for Fe are plotted on Fig. 1 (solid lines). An excellent agreement is obtained between the high field electron-magnon model and the experimental MR for the three magnets. We infer the magnon stiffness and their temperature renormalization for Fe, Co and Ni :

$$D_{Fe}(T) = (350\pm20)\times\left[1-(2.5\pm0.2)\times10^{-6}T^2\right] meVA^2 ,$$

$$D_{Co}(T) = (470\pm20)\times\left[1-(1.57\pm0.2)\times10^{-6}T^2\right] meVA^2 ,$$

$$D_{Ni}(T) = (390\pm20)\times\left[1-(1.5\pm0.2)\times10^{-6}T^2+(6.4\pm0.2)\times10^{-8}T^{5/2}\right] meVA^2 .$$

The extrapolated magnon masses at 0°K and their temperature dependence are fully consistent with experimental values obtained by neutron scattering.[9-11] If we extrapolate the theoretical $\Delta\rho_{mag}(B)$ curves to the very high field regime, we estimate the saturation fields around 80T, 500T and 1500T for temperatures of 20, 100 and 300K to fully damp the magnons.

The consistency of the $\Delta\rho_{mag}(B)$ fits with relevant parameters provides a unique manner to estimate the magnetic resistivity $\rho_{mag}(T)$. The predicted $\rho_{mag}(T)$ curves (Fig.2) are deduced from Eq. (15) in Ref. [8] with adequate band structure parameters and where the characteristics of the spin waves are extracted from the high field fits. This is the first accurate determination of the magnetic resistivity over a large temperature range with a clear distinction from the other electronic scattering processes. At room temperature, the electron-magnon scattering contribution to the resistivity reaches 1.8, 2 and 10.5$\mu\Omega$.cm for Co, Fe and Ni respectively.

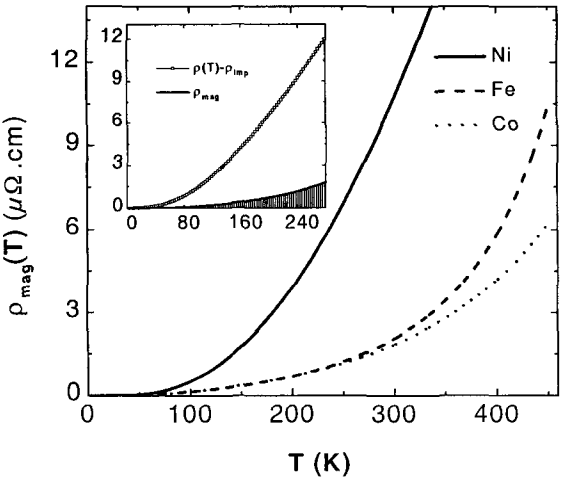

Figure 2: Determination of the magnetic resistivity due to electron-magnon scattering for Fe, Co and Ni relying on the adequate band structure parameters and the collective spin excitations inferred from the high field MR measurements. In inset, the estimated magnetic contribution to the experimental resistivity after subtraction of the residual resistivity for Fe.

The estimated $\rho_{mag}(T)$ and the experimental resistivity $\{\rho(T)-\rho_{imp}\}$ for Fe are plotted in the inset of Fig. 2. At 300 K, the magnon induced spin-flip scattering is responsible for 15% of the total resistivity (after subtraction of the residual resistivity). Our approach can be extended to other magnets like weak ferromagnets or half metallic ferromagnets to probe the spin disorder and their coupling to the conductivity.

References

1. B. Loegel and F. Gautier, *J. Phys. Chem. Solids*, **32**, 2723 (1971).
2. N. V. Volkenshtein *et al., Phys. Stat. Sol.* (b) **57**, 9 (1973).
3. N. F. Mott, *Adv. Phys.* **13**, 325 (1964).
4. A. Möbius *et al., Phys. Stat. Sol.* (b) **95**, 203 (1979).
5. A. B. Pippard, *Magnetoresistance in Metals*, Cambridge University Press.
6. S. N. Kaul and M. Rosenberg, *Phys. Rev. B* **27**, 5698 (1983).
7. K. B. Vlasov and V. V. Ustino, *Low. Temp. Phys.* **22**, 728 (1996).
8. B. Raquet *et al., to be published.*
9. M. W. Stringfellow, *J. Phys. C* **2**, 950 (1968).
10. X. Liu *et al., Phys. Rev. B* **53**, 12166 (1996).
11. D. M. Edwards and R. B. Muniz, *J. Phys. F : Met. Phys.* **15**, 2339 (1985).

RAMAN SCATTERING STUDY OF TEMPERATURE- AND FIELD-DEPENDENT MAGNETIC POLARON FORMATION IN (Eu,Gd)O

H. RHO,[1] C. S. SNOW,[1] S. L. COOPER,[1] Z. FISK,[2]
A. COMMENT[1,3] and J-PH. ANSERMET[1,3]

[1] *Department of Physics and Frederick Seitz Materials Research Laboratory, University of Illinois, Urbana, Illinois 61801*
[2] *National High Magnetic Field Laboratory, Florida State University, Tallahassee, Florida 32306*
[3] *Ecole Polytechnique Fédérale de Lausanne, CH-1015 Lausanne, Switzerland*

We use Raman scattering to investigate magnetic polarons and spin-carrier interaction effects in the (Eu,Gd)O system. Raman scattering studies reveal great richness in the phase behavior of this system: a spin-fluctuation-dominated paramagnetic (PM) phase regime for $T > T^* > T_C$, a two-phase regime for $T < T^*$ in which magnetic polarons develop below T^* and coexist with a remnant of the PM phase, and an inhomogeneous ferromagnetic phase regime for $T < T_C$. We will discuss how these phase regimes evolve as functions of magnetic field, temperature, and Gd-substitution, and will compare the results with less disordered systems such as EuB_6.

1 Introduction

Eu-based magnetic semiconductors and perovskite-based oxides have attracted great interest due to their intriguing magnetic properties, such as colossal magnetoresistance (CMR) behavior[1] and ferromagnetic (FM) cluster formation.[2-5] For example, conductivity measurements have revealed that Eu-rich EuO exhibits a large negative magnetoresistivity and an activated behavior with decreasing temperature in the paramagnetic (PM) phase regime.[2,6] Upon decreasing temperature further below T_C, the conductivity increases by 13 orders-of-magnitude, and a metal-insulator (MI) transition occurs. This MI transition has motivated many theoretical explanations, such as the formation of magnetic polarons.[2]

In this paper, we use Raman scattering to demonstrate that magnetic polarons indeed develop near the MI transition in (Eu,Gd)O, and hence likely play a significant role in the CMR-type behavior observed in this system. Moreover, we further explore the manner in which magnetic polarons evolve through the various phase regimes as functions of temperature, magnetic field, and Gd-substitution.

2 Experiment

Raman scattering from (Eu,Gd)O samples mounted inside a variable temperature, continuous Helium-flow cryostat was measured in a true-backscattering geometry using a 614.5 nm Kr-ion laser. For H = 0 measurements, linearly polarized light was

employed.[3] For magnetic-field-dependent measurements, circularly polarized light was employed, in order to avoid symmetry mixing due to Kerr rotation of polarized light in a magnetic field. Magnetic susceptibility measurements using a SQUID-based magnetometer show T_C ~ 70 K for EuO and 0.6% Gd-doped EuO, and T_C ~ 115 K for 3.5% Gd-doped EuO.

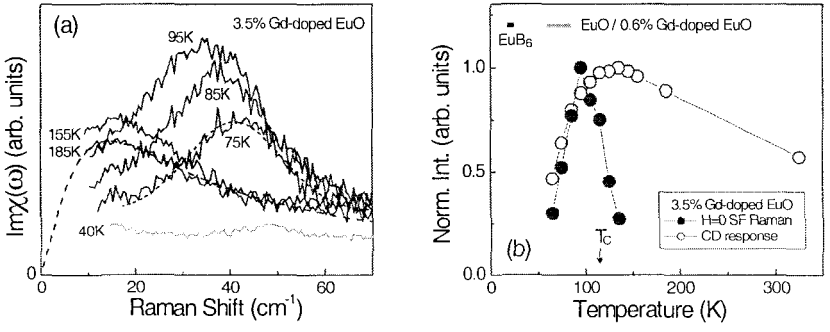

Figure 1: (a) Temperature dependent Raman scattering from 3.5% Gd-doped EuO. The dashed line is a fit to the data using Eq. 1. The short-dashed line is a Gaussian fit to the data. (b) Integrated intensity changes of H = 0 SF Raman response and CD response. The solid bars at the top denote the temperature ranges over which magnetic polarons are stable in EuB_6, EuO, and 0.6% Gd-doped EuO.

3 Results and Discussion

As shown in Fig. 1(a), Raman scattering spectra of (Eu,Gd)O exhibit much richer phase behavior than has been observed previously in transport measurements: a high temperature PM regime for $T > T^* > T_C$, a magnetic polaron regime for $T < T^*$, where T^* is a temperature below which magnetic polarons develop, and an inhomogeneous FM regime for $T < T_C$ with a diminishing magnetic polaron response. The PM phase regime, in which spin fluctuations dominate carrier scattering, can be characterized by a collision-dominated (CD) scattering response,

$$S_L(\omega) \propto (1+n(\omega))\mathrm{Im}\,\chi(\omega) = (1+n(\omega))|\gamma_L|^2 \frac{\omega\Gamma_L}{\omega^2+\Gamma_L^2}, \qquad (1)$$

where $S_L(\omega)$ is the electronic scattering response in channel L, $1+n(\omega)$ is the Bose thermal factor, γ_L is the Raman scattering vertex, and Γ_L is the carrier scattering rate.[3,4,7] The CD response increases with decreasing temperature toward T_C, likely indicating increased electronic scattering from spin fluctuations as T approaches T_C. Significant changes in the Raman scattering response occur below T^*: the Raman

spectrum at 95 K in Fig. 1(a) shows the development of a large Gaussian-shape inelastic scattering response in the crossed-polarization ($E_i \perp E_s$) scattering configuration, but not in the parallel ($E_i \parallel E_s$) scattering configuration. This distinctive scattering response is indicative of H=0 spin-flip (SF) Raman scattering, associated with the development of FM clusters (i.e., magnetic polarons).[3,4,8,10] The peak energy of the H=0 SF response gradually increases with decreasing temperature, indicating that the carrier spins and magnetic polarons are cooperatively aligned in the FM clusters.[8,9] Importantly, careful analysis of the Raman spectra in this magnetic polaron regime clearly shows that the SF Raman response is superimposed on a remnant CD response, as summarized in Fig. 1(b), revealing two-phase behavior in which FM clusters coexist with remnants of the PM phase. This result supports recent theoretical studies in which mixed-phase behavior should be ubiquitous in CMR-type magnetic systems.[5] Note that T^*, as well as the temperature range over which magnetic polarons are stable, increase with increasing Gd-substitution. Additionally, magnetic polarons in the (Eu,Gd)O system are stable over a 5–10 times greater temperature range than in EuB_6, which has a substantially higher mobility than (Eu,Gd)O. These results illustrate the importance of spin-disorder for stabilizing magnetic polaron formation in these systems. Indeed, both the magnetic polaron and CD Raman responses diminish as the system transitions into the FM metal phase, due to the increase in spin-order and to the consequent increase in the localization length of the magnetic polarons.

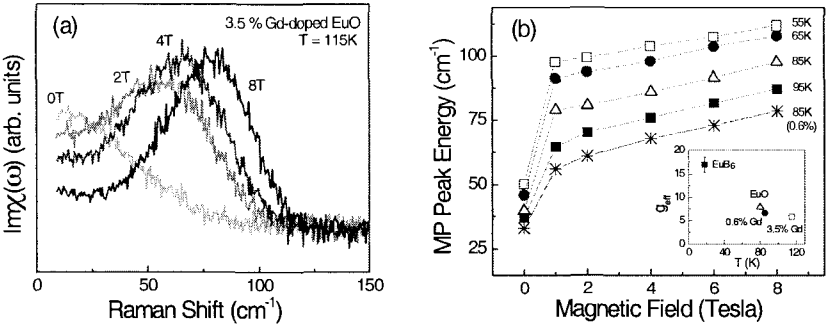

Figure 2: (a) Field dependent Raman scattering from 3.5% Gd-doped EuO at 115 K. The signature of the CD response underlying the SF Raman response is most clearly seen in the low frequency regime with increasing field. (b) Change in the SF Raman peak energy as a function of magnetic field. The inset shows the effective g-value obtained from linear fits of the linear-in-field range, $1 \leq H \leq 8T$.

When an external magnetic field is applied, both the SF Raman response and the CD response experience significant changes. As displayed in Fig. 2(a) and summarized in Fig. 2(b), the SF Raman response increases in energy with increasing field, reflecting an increase in the effective exchange energy within the FM clusters. Also, the CD response exhibits a diminishing intensity with increasing magnetic

field due to the suppression of spin fluctuations. Interestingly, in the magnetic polaron regime, the application of a small field (H < 1 T) causes an abrupt jump in the energy of the SF Raman response. We speculate that this abrupt increase in energy originates from the field-induced mutual alignment of the net moments associated with individual FM clusters, which are randomly oriented at H=0. With increasing field for H > 1 T, the SF Raman energy increases linearly. In this linear-in-field regime ($1 \leq H \leq 8T$), we can estimate an effective g-value of g_{eff} ($=\Delta E/\mu_B \Delta H$) ~ 6 for (Eu,Gd)O near T_C. By contrast, higher mobility EuB_6 has an effective g-value of g_{eff} ~ 17, as shown in the inset of Fig. 2(b). At a given field, the SF Raman energy increases with decreasing temperature and with increasing Gd-substitution, indicating increased stability of the magnetic polarons.

4 Summary

We have used Raman scattering to study magnetic polarons and spin-carrier interactions in various phase regimes of (Eu,Gd)O. Raman scattering reveals a rich phase behavior associated with the magnetic interactions and carrier dynamics. We conclude that spontaneously-occurring electronic inhomogeneity, in the form of FM clusters, and intrinsic two-phase behavior are not unique to complex perovskite-related oxides,[5] but occur even in structurally simple systems, such as (Eu,Gd)O, which are characterized by a complex interplay among the carrier kinetic energy, the carrier/local-moment exchange energy, and the local Coulomb energy.

Acknowledgment

We acknowledge support of this work by the Department of Energy (DEFG02-96ER45439) and the National Science Foundation (DMR97-00716).

References

1. E. L. Nagaev, *Physics Reports* **346**, 387 (2001).
2. J. B. Torrance *et al.*, *Phys. Rev. Lett.* **29**, 1168 (1972).
3. C. S. Snow *et al.*, *Phys. Rev. B* **64**, 174412 (2001).
4. P. Nyhus *et al.*, *Phys. Rev. B* **56**, 2717 (1997).
5. J. Burgy *et al.*, *arXiv:cond-mat/*0107300 (2001).
6. M. R. Oliver *et al.*, *Phys. Rev. B* **5**, 1078 (1972).
7. A. Zawadowski and M. Cardona, *Phys. Rev. B* **42**, 10732 (1990).
8. E. D. Isaacs *et al.*, *Phys. Rev. B* **37**, 7108 (1988).
9. D. Heiman *et al.*, *Phys. Rev. B* **27**, 4848 (1983).
10. D. L. Peterson *et al.*, *Phys. Rev. B* **32**, 323 (1985).

NUCLEAR MAGNETISM OF HELIUM-3 PRECIPITATES

V. A. SHVARTS,[1] K. J. KLESS,[1] N. MATSUNAGA,[1] E. D. ADAMS,[1] J. X. XIA,[1]
and E. A. SCHUBERTH[2]
[1]*Department of Physics and High B/T Facility, NHMFL, University of Florida, Gainesville, Florida 32611-8440, USA*
[2]*Walther-Meissner Institut, D-85748 Garching, Germany*

Simultaneous measurements of magnetic susceptibility from 0.5 to 10 mK and pressure from 2.88 to 3.54 MPa have been made in ^{3}He nanoclusters embedded in a ^{4}He matrix, following phase separation. The susceptibility of the 3.54 MPa, all –solid sample behaves similarly to that of bulk ^{3}He for v = 21.3 cm^3/mole, with a Weiss constant θ = -250μK. For the 2.88 MPa, liquid-droplet sample, θ = 140μK, indicating a ferromagnetic tendency, similar to 2-D films at some coverages. At intermediate pressures, χ has a peak near 1.05 mK, but without a discontinuity. For all samples, χ had a solid-like contribution to the lowest temperatures. Magnetic ordering in nano-clusters appears to be different than the U2D2 phase of bulk ^{3}He.

PULSE-FIELD EXPERIMENTS ON THE SPIN-LATTICE INTERACTION IN LOW-DIMENSIONAL SPIN SYSTEMS

B. WOLF, S. ZHERLITSYN, S. SCHMIDT, B. LÜTHI and M. LANG
Physikalisches Institut, Universität Frankfurt,
D-60054 Frankfurt,Germany
E-mail: wolf@physik.uni-frankfurt.de

Low-dimensional spin systems reveal new and unexpected physical phenomena such as distinct plateaus in the magnetization as a function of magnetic field. In this paper we present ultrasonic measurements for the quasi-two-dimensional spin system $SrCu_2(BO_3)_2$ in magnetic fields up to 50 T. From this technique we obtained detailed information about the spin state, the magnetic excitations and their interaction with phonons. The dimerized quantum-spin system $SrCu_2(BO_3)_2$ exhibits plateaus in the magnetization and shows surprisingly strong magneto-elastic effects as a function of temperature and magnetic field. The pronounced elastic anomalies indicate a resonant interaction between the sound wave and the magnetic excitations.

1 Introduction

To determine the interaction between the sound wave and the magnetic excitations in low-dimensional spin systems, we developed a new method of measuring simultaneously the ultrasound velocity and attenuation in pulsed fields up to 50T. In a series of papers,[1-6] we have shown that with this spectroscopic method, that beside the soft magnetic modes, we can also investigate magneto-acoustic quantum oscillations and different phase transitions in pulsed fields up to 50 T. For soft magnetic excitations this technique is complementary to ESR in pulsed fields[4] because it covers the low-frequency region.

2 Pulse-field experiments on $SrCu_2(BO_3)_2$

$SrCu_2(BO_3)_2$ is a two-dimensional coupled dimer system with remarkable properties. This tetragonal compound consists of alternately stacked $CuBO_3$ and Sr layers. Within the $CuBO_3$ plane, the Cu^{2+} - Cu^{2+} dimers are coupled with an exchange constant J. The dimers are orthogonally connected with a second coupling constant J', giving rise to an exact orthogonal dimer ground state[9] corresponding to the Shastry Sutherland model.[10] In a magnetic field, $SrCu_2(BO_3)_2$ exhibits plateaus in the magnetization at 1/8, 1/4 and 1/3 of the saturation magnetization.[11,12] Furthermore, the system is close to a quantum critical point (QCP) because the exchange parameters are J = 100 K, J' = 68 K (see Refs. [9,13]). At zero magnetic field, the singlet - triplet splitting is $\Delta \cong 35$ K as deduced from different

experimental techniques.[14-16] Recently, Oshikawa *et al.*,[8] proposed a condition for the occurrence of magnetization plateaus in quantum-spin chains: $n(S\text{-}m)$ = integer, where n is the period of the spin ground state, S the spin quantum number and m the magnetization per magnetic ion. A similar condition is also valid for two-dimensional systems like $SrCu_2(BO_3)_2$ where such magnetization plateaus are also observed.[7]

In Fig. 1 we show our results of the relative elastic constant changes for the elastic modes c_{11}, c_{44} and c_{66} as a function of magnetic field for **B** // a up to 50 T at 1.5 K. All three modes propagate in the [100]-direction with the polarisation vectors **e** along [100] for the longitudinal c_{11} mode, along [001] out of the tetragonal plane for the shear c_{44} mode and along [010] for the shear c_{66} mode. Clearly, the in plane mode c_{66} shows a dramatic softening of more than 25% compared to 2.5% for c_{11} with increasing field between the plateaus. On the scale of Fig. 1, there is no softening at all for the c_{44} mode. For c_{66} and c_{11} we notice sharp spikes at these critical-field values where the magnetization changes discontinuously from one plateau to the next one, i.e. at 27, 36 and 43 T for **B** // a.

The above findings raise the question for the reason for this dramatic softening of c_{66} which is so different from the other modes. Just as in the c_{11} investigated previously in detail,[4] the exchange-striction coupling is responsible for these phenomena. This coupling arises from the strain dependence of the exchange interaction. Usually shear waves propagating along symmetry directions do not couple via this mechanism whereas longitudinal waves do. However, because of the spatial orientation between the dimers and the displacement for the shear modes, it is evident that the c_{66} mode can couple linearly to the spin system whereas c_{44} can couple only at higher order. The exchange-striction coupling describes the temperature dependence of the various elastic modes quantitatively,[4] which is not discussed here. Experimentally the c_{44} mode does not show any magnetic field dependence except for a small hardening between each plateau of 0.01%. Note that this behaviour indicates the absence of large magnetostriction effects in $SrCu_2(BO_3)_2$, because all elastic modes shown in Fig.1 are propagating in the same direction.

The large elastic anomalies in $SrCu_2(BO_3)_2$ at the critical fields are due to a resonant interaction between phonons and magnetic excitations at the edges of the different plateaus where there is a jump in the magnetization. Such a resonant interaction close to the crossover leads to coupled phonon-magnon modes.

The difference between the effects of the c_{11} and c_{66} modes, which amount to an order of magnitude, must be explained by a detailed microscopic consideration of the exchange-striction coupling constant. Simple length change effects give the same magnitude for the two modes. Angular dependencies of the exchange and other factors have to be taken into account for a full description of such a coupling.

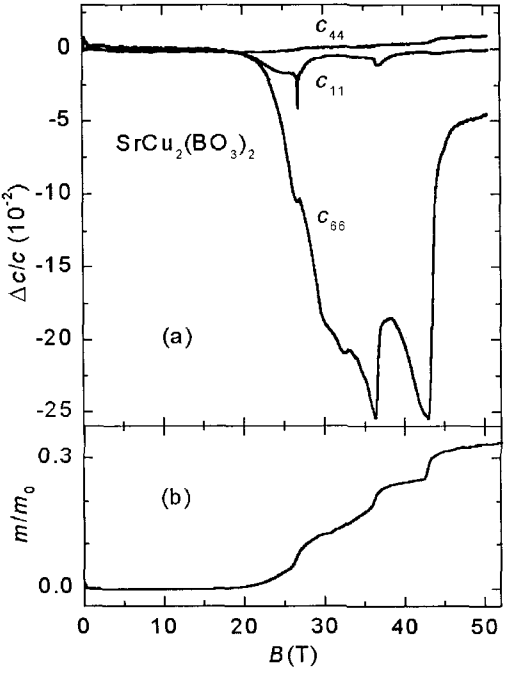

Figure 1: Relative change of the elastic constant c_{ij} (a) as a function of high magnetic field in $SrCu_2(BO_3)_2$ at T = 1.5 K. Magnetic field direction was **B**//[100]. The ultrasonic frequency was 10 MHz (c_{44} and c_{66} modes) and 86 MHz (c_{11} mode). Also shown is the magnetization (b) for **B**//[100] from Ref. [12].

Yet, we analyse the different behaviour of the elastic constants c_{11} and c_{66} in terms of the soft mode concepts. In the case of $SrCu_2(BO_3)_2$, we argue that the soft c_{66} mode reflects the symmetry of the resonantly coupled magnetic excitation and consequently of the triplet condensation for the corresponding plateaus. We compare our results with the theoretical predictions.[9] Based on the data of Fig. 1, we predict - especially for the plateaus ¼ (above B = 36 T) and $^1/_3$ (above 43 T) - a B_{2g} type symmetry arrangement. Indeed, calculations of such an arrangement for the ¼ plateau are given in Ref.[9] for the square unit cell model. The hard core boson model favours an arrangement of B_{1g} symmetry for the ¼ plateau. The $^1/_8$ plateau should obtain a mixture of B_{1g} and B_{2g} symmetry.

3 Summary

In summary, measurements of the elastic constants reveal evidence for a very strong spin-lattice coupling in the two-dimensional dimer substance $SrCu_2(BO_3)_2$. We have shown that an exchange-striction coupling can describe the field dependence of the three acoustic modes, it can also explain the absence of a magnetic field effect for c_{44} and it can explain the resonant coupling of the sound-wave with the magnetic excitations for the c_{11} and c_{66} modes. The c_{66} shear mode exhibits a very strong softening at magnetic field values between the magnetization plateaus. For $SrCu_2(BO_3)_2$, this means that the Cu^{2+}-Cu^{2+} dimers are very strain dependent especially for the ε_{xy} strain. Any theory attempting to describe the magnetism of this system has to include the strong spin-phonon coupling. This has to be done for describing the magnetic excitations, the general phase diagram and especially for parameter choices which include the quantum critical point.

Acknowledgments

We thank H.Kagayama for providing us with the single crystals. This research was supported via the DFG Schwerpunktprogramm 1073.

References

1. B. Wolf *et al., Europhys. Lett.* **48**, 182 (1999).
2. B. Lüthi *et al., Physica B* **294-295**, 20 (2001).
3. S. Zherlitsyn *et al., Phys. Rev. B* **62**, R6097 (2000).
4. B.Wolf *et al., Phys. Rev. Lett.* **86**, 4847 (2001).
5. S. Schmidt *et al., Europhys. Lett.* **53**, 591 (2001).
6. B.Wolf *et al., J. Appl. Phys.* **87**, (2000).
7. M. Oshikawa, *Phys. Rev. Lett.*, **84**, 1535 (2000).
8. M. Oshikawa *et al., Phys. Rev. Lett.*, **78**, 1984 (1998).
9. S. Miyahara *et al., Phys. Rev. Lett.* **82**, 3701 (1999); *Phys. Rev. B* **61**, 3417 (2000).
10. B. S. Shastry *et al., Physica* **108**B, 1069 (1981).
11. H. Kageyama *et al., Phys. Rev. Lett.* **82**, 3168 (1999).
12. K. Onizuka *et al., J. Phys. Soc. Jpn.*, **69** 1016 (2000).
13. Z. Weihong *et al., Phys. Rev. B* **60**, 6608 (1999).
14. H. Kageyama *et al., Phys. Rev. Lett.* **84**, 5876 (2000).
15. H. Nojiri *et al., J. Phys. Soc. Jpn.* **68**, 2906 (1999).
16. P. Lemmens *et al., Phys. Rev. Lett.* **85**, 2605 (2000).

ELECTRON-SPIN RESONANCE EVIDENCE OF THE QUANTUM SPIN GAP IN THE $LiCu_2O_2$

S. A. ZVYAGIN, G. CAO, L.-C. BRUNEL and J. CROW
National High Magnetic Field Laboratory, 1800 E. Paul Dirac Drive, Tallahassee, FL 32310 , USA
E-mail: zvyagin@magnet.fsu.edu

Results of the high-frequency/field electron spin resonance investigation of the quantum S=1/2 chain compound $LiCu_2O_2$ are presented. Spin-singlet ground state (which occurs in $LiCu_2O_2$ as a result of the spin-dimerization) is revealed at a temperature above $T \sim 23$ K. The size of the gap between the spin-singlet ground state and the excited triplet is found to be $\Delta = 72$ K. Electron spin resonance study confirms a magnetic phase transition in $LiCu_2O_2$, which results in the collapse of the spin-singlet ground state at $T < 23$ K.

1 Introduction

Recently, a considerable amount of attention has been given to theoretical and experimental investigation of low-dimensional frustrated spin systems. This interest has been stimulated by theoretical predictions of a rich phase diagram and novel magnetic properties, which originate from the intensive interplay of geometrical frustrations and quantum fluctuations in low-dimensions. Quantum S=1/2 chains with competing nearest- and next-nearest-neighbor interactions have been studied most intensively. Depending on the ratio between the nearest- and next-nearest-neighbor interactions (J_1 and J_2, respectively) this class of materials may exhibit a gapless collinear phase ($J_2/J_1 < \alpha_{c1}$), a dimmer phase ($\alpha_{c1} < J_2/J_1 < \alpha_{c2}$), or a spiral phase ($J_2/J_1 > \alpha_{c2}$). The critical value α_{c1} runs from ~ 0.33 in the XY case[1] to ~ 0.2411 in the Heisenberg chain case.[2] The critical value α_{c2} increases from ~ 1.26 (in the XY case)[1] to about 1.8 in the Heisenberg chain case.[3] One of the most challenging goals in this area is to experimentally prove the rich variety of magnetic properties of the quantum chain systems, predicted theoretically.

2 Structure and magnetic properties of $LiCu_2O_2$

$LiCu_2O_2$ (see Ref. [4]) has orthorhombic crystal structure with a *Pmna* space group. The lattice constants at room temperature are a = 5.72 Å, b = 2.86 Å, c = 12.4 Å. There are two linear Cu^{2+}-chains, which form a zigzag ladder-like structure. The ladders are isolated from each other by both Li-ions and the layers of non-magnetic Cu^{1+} ions. The distance between the next-nearest neighbor Cu^{2+}-ions (along the ladder) is about of 2.86 Å, and between the nearest-neighbor Cu^{2+}-ions (that is length of the rungs) is about of 3.38 Å and 3.08 Å. The magnetic susceptibility of

$LiCu_2O_2$ demonstrates typical low-dimensional magnetic material behavior with a broad maximum around $T \sim 40 - 50$ K (see Refs. [5 and 6]. A phase transition to the state with long-range order occurs at $T \sim 23$ K (see Refs. [6 and 7]. This transition hides low-temperature features of the magnetic susceptibility, which would arise from the low-dimensional character of the system in the absence of the long-range order in AFM correlations and are of special importance when studying the ground state in low-dimensional phase ($T > 23$ K) of $LiCu_2O_2$. Thus, the question about the ground state in the high-temperature/low-dimensional phase in $LiCu_2O_2$ remains open. The main motivation of this work is to determine the nature of ground state in $LiCu_2O_2$ in the low-dimensional magnetic phase using high-frequency/field electron spin resonance (ESR) spectroscopy.

3 Electron-spin resonance study of $LiCu_2O_2$

The experiments have been performed on the transmission-type mm-wavelength-band ESR spectrometer in a frequency range of 90 – 370 GHz and in fields up to 14 T. The magnetic field was applied along the crystallographic *c*-axis. A strong resonance absorption with a linear frequency-field dependence has been observed at a temperature larger than 23 K. The integrated intensity of the resonance has been calculated using a Lorentzian fit and is depicted as a function of the temperature in Fig. 1. One can see a pronounced maximum at the temperature of around $T \sim 45$ K. This maximum is a clear signature of the transitions within the excited states. Due

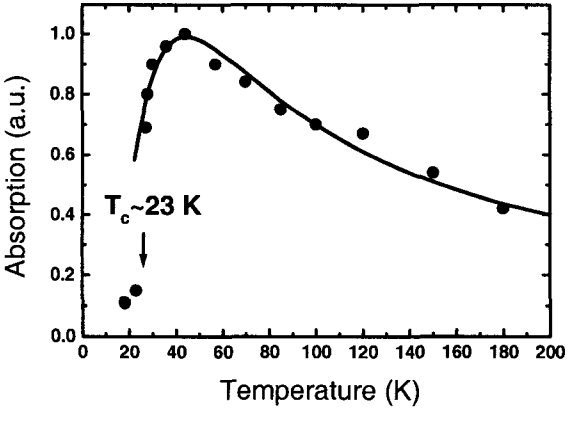

Figure 1: Integrated resonance intensity vs temperature at a frequency of 277 GHz (a resonance field is about 8.5 T). The solid line is a fit with the energy gap $\Delta = 72$ K.

to the spin-dimerization, which occurs in the S=1/2 spin chain with alternating exchange interactions in the intermediate range of the J_2/J_1-ratio ($\alpha_{c1} < J_2/J_1 < \alpha_{c2}$), an energy gap Δ in the elementary excitation spectrum is open; the ground state is a spin-singlet, separated from the first excited triplet by Δ. The Boltzman distribution was included to analyze the temperature dependence of the ESR signal and to determine the energy gap. The best fit of the experimental data in the temperature range of 23 – 180 K corresponds to the energy gap Δ of 72 K.

The resonance intensity suddenly drops below $T_c \sim 23$ K. We associate this drop with a collapse of the spin-singlet ground state, which is accompanied by the collapse of the singlet-triplet energy scheme at low temperature. This temperature corresponds to the transition to the long-range ordered magnetic state. The problem concerning the detailed investigation of the low-temperature magnetic structure in $LiCu_2O_2$ still remains open and might be of special interest for our future broad-frequency-band high-field ESR and nuclear magnetic resonance studies.

A significant broadening (about six times) of the resonance line has been observed in $LiCu_2O_2$ with a decrease in temperature from 180 K to 23 K. This broadening can be associated with an enhancement of the short-range order AFM correlations, followed by a transition into long-range ordered state. A transition into long-range ordered state in quasi-low-dimensional magnetic materials is usually accompanied by an enhancement of the three-dimensional magnetic correlations at low temperatures due to inter-chain interactions.

ESR reveals a pronounced change of the g-factor with a temperature change (from 2.35 at T = 23 K to 2.29 at T = 180 K). We associate this change with two possible factors. First, an enhancement of the short-range order correlations might significantly change the local field on the Cu^{2+}-ion sites that eventually causes a change of the g-factor. Second, the change of the g-factor can be attributed to the significantly large (~2 times) change in the orthorhombic strain $(a - 2b)/(a + 2b)$, observed in $LiCu_2O_2$ in the temperature range of 10 K – 300 K, using high-resolution X-ray diffraction.[7] Thus, an intensive interplay between the lattice and spin degrees of freedom might play an important role in the dynamics of $LiCu_2O_2$.

4 Conclusion

In conclusion, we have reported on high-frequency/field ESR investigation of single-crystalline $LiCu_2O_2$. The ESR results showed, that at $T > 23$ K $LiCu_2O_2$ had a spin-single ground state, separated from the excited states by the finite energy gap of $\Delta \sim 72$ K and could be regarded as a quantum S=1/2 chain with competing nearest- and next-nearest-neighbor interactions in the intermediate range of the J_2/J_1-ratio ($\alpha_{c1} < J_2/J_1 < \alpha_{c2}$). A collapse of the spin-singlet ground state has been revealed at $T < 23$ K. Inelastic neutron scattering study will be extremely helpful to determine

coupling parameters and the exact magnetic structure of $LiCu_2O_2$ in the different regions of its phase diagram.

Acknowledgments

We acknowledge the help of Y. Xin in the analysis of the $LiCu_2O_2$ crystal structure. We would like to appreciate a discussion with W. Moulton and T. Caldwell. This work was supported through the NHMFL by NSF DMR 9527035 and State of Florida.

References

1. T. Hikahara, M. Kaburagi, and H. Kawamura, *Phys. Rev. B* **63**, 174430-1-11 (2001).
2. K. Okamoto and K. Nomura, *Phys. Lett.* **169**,433-437 (1992).
3. R. D. Somma and A. A. Aliga, *Phys. Rev. B* **64**, 024410-1-4 (2001).
4. R. Berger, J. *Less-Common Metals* **169**, 33-43 (1991), R. Berger, P. Önnerud and R. Tellgren, *J. Alloys Compd.* **184**, 315-322 (1992).
5. F. C. Fritschij, H. B. Brom and R. Berger, *Solid St. Comm.* **107**, 719-723 (1998).
6. A. M. Vorotinov, A. I. Pankrats, G. A. Petrakovkii and K. A. Sablina, *JETP* **86**, 1020-1025 (1998).
7. B. Roessli, U. Staub, A. Amato, D. Herlach, P. Pattison, K. Sablina, G. A. Petrakovskii, *Physica B* **296**, 306-311 (2001).

Part VII

Other Aspects of Studies in High Magnetic Fields

This page is intentionally left blank

ELECTRON CORRELATION EFFECTS IN BIOLOGICAL MOLECULES

D. L. COX, R. ENDRES, R. V. KULKARNI, M. LABUTE and R. R. P. SINGH
Department of Physics, University of California-Davis, 1 Shields Avenue, Davis, California 95616, USA

Allosteric (conformation changing) proteins with transition metal atoms are at the heart of much important biological function (e.g., myoglobin hemoglobin used for storing and transporting oxygen in the bloodstream). In the case of myoglobin and hemoglobin, oxygen ligation to the iron center induces a spin crossover (high to low) coupled to a structural change; apart from the role of Hunds' exchange in the spin crossover, electron interaction effects have been ignored. We argue that the spin crossover/structure change observed in the similarly structured but far simpler cobalt valence tautomer molecules[1] necessitates an inclusion of underscreened Kondo like correlations for a complete description of the energetics of the transition and dynamics, e.g., for x-ray absorption data. We carry this study out with Varma-Yafet-Gunnarsson-Schonhammer wave functions, which, in chemistry language, are basis set restricted configuration interaction in character. We briefly review the applicability of such wave functions to the description of the putative Kondo molecules cerocene ($Ce[(CH)_5]_2$) and ytterbocene bipyridine ($Yb[(CH)_5]_2(bipy)$) and to the problem of electron transfer in biological molecules and organic conductors, where anomalous long range tunneling may occur.

Research supported by the U.S. Department of Energy, Office of Science, Basic Energy Sciences, Division of Materials Research.

1. D. M. Adams and D. J. Hendrickson, *J. Am. Chem. Soc.* **118**, 11515 (1996).

FORCE-DETECTED SCANNED PROBE MAGNETIC RESONANCE MICROSCOPY

P. C. HAMMEL
Los Alamos National Laboratory, Los Alamos, New Mexico 87545, USA

Magnetic Resonance Force Microscopy (MRFM) is a novel scanned probe technique that combines the three-dimensional imaging capabilities of magnetic resonance imaging (MRI) with the high sensitivity and resolution of atomic force microscopy (AFM). This emerging technology holds clear potential for resolution at the atomic scale. When fully realized, MRFM will provide a unique method for non-destructive, chemically specific, subsurface imaging with applicability to a wide variety of materials. I will review results to date spanning applications of MRFM to nuclear spin, electron spin, and ferromagnetic resonance. I will outline the MRFM technique, discuss its present status and indicate future directions of our effort.

ADVANCES IN MEGAGAUSS FIELD GENERATION AND APPLICATION AT ISSP

N. MIURA, Y. H. MATSUDA, K. UCHIDA, S. IKEDA and F. HERLACH*

Institute for Solid State Physics, University of Tokyo, Kashiwa, Chiba, Japan

E-mail: miura@issp.u-tokyo.ac.jp

We report recent progress in the generation and application of megagauss fields at the new Megagauss Laboratory of ISSP in Kashiwa. New facilities for studying physics in ultra-high magnetic fields were built at the new campus of the University of Tokyo at Kashiwa, where pulsed high magnetic fields are produced by three different techniques: electromagnetic flux compression, the single-turn coil technique and non-destructive long pulse magnets. Considerable progress has been made in each of these techniques, as compared with the old facilities at Roppongi. For electromagnetic flux compression, the rise time of the primary current was reduced by decreasing the residual inductance of the capacitor bank. The cylindrical symmetry of the liner implosion was remarkably improved by inserting a "feed gap compensator" between the primary coil and the liner. So far, a maximum field of 622T has been achieved. By the single-turn coil technique, very high fields exceeding 300T have been obtained depending on the coil bore, in two systems with horizontal and vertical coil axes. These fields are successfully applied in many different kinds of experiments. Non-destructive long pulse fields up to 60T are available from wire-wound coils.

1 Introduction

Generation of magnetic fields exceeding 100T (1megagauss) requires special facilities and techniques. The electromagnetic force exerted on the magnet is proportional to the square of the magnetic field; in the megagauss range it exceeds the material strength of the magnet, leading to inevitable coil destruction in this field range. Since its establishment in 1972, the Megagauss Laboratory (MGL) of the Institute for Solid State Physics (ISSP) of the University of Tokyo has a long tradition in the generation and application of extremely high pulsed magnetic fields produced by electromagnetic flux compression and the single-turn coil technique.[1] At the occasion of the move to the new campus at Kashiwa, a new MGL was completed in 1999 with entirely new facilities.[2] The new MGL has three main facilities: for electromagnetic flux compression (up to 622T), for the single-turn coil technique (up to 302T) and for non-destructive long pulse fields (up to 60T). Magnetic fields generated by each technique have different characteristics and advantages, such that users can choose the facilities that are best suited for their experiments. These fields are employed for many experiments on a variety of materials, and many novel results are obtained.[3-5] In this paper, we present the recent progress in the generation and application of megagauss fields at the new MGL.

2 Electromagnetic flux compression

At the old Roppongi campus of ISSP, we have generated magnetic fields up to 606T by electromagnetic flux compression, using a main capacitor bank with a stored energy of 5MJ when charged to 40kV (see Ref. [1]). In the new facilities at Kashiwa, the residual inductance and resistance of the capacitor bank was substantially decreased while keeping the total energy and the voltage at the same magnitudes. The resulting fast current rise and corresponding higher implosion speed is the most essential factor for obtaining higher magnetic fields.[6] To this end, the number of coaxial cables connecting the capacitor bank with the collector plates was increased from 240 to 480. As a result, the residual inductance and resistance were decreased from 28.7nH to 19.97nH, and from 0.72mΩ to 0.57mΩ, respectively. Since the load inductance is fairly small, this resulted in a substantial increase of the energy transferred to the load while decreasing the rise time of the primary current resulting in more efficient energy transfer.[2]

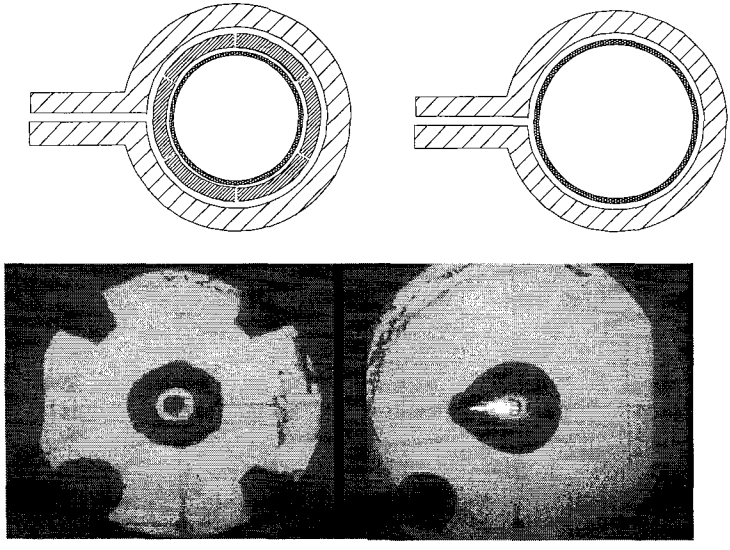

Figure 1: Arrangement of the primary coil (top) and corresponding high speed photographs of the liner (bottom). Left: with the feed gap compensator (FC), right: without FC. High speed photographs were taken at 44.74μs (left) and at 53.36μs (right) after the start of the primary current.

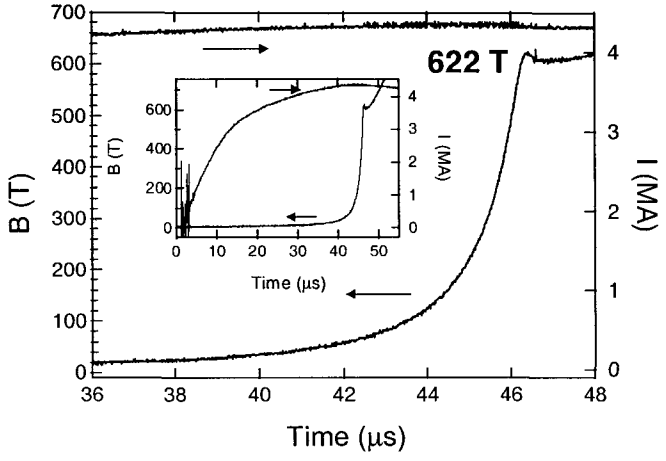

Figure 2: Waveforms of the primary current and of the compressed magnetic field obtained with the feed gap compensator.

There is a crucial problem in generating high magnetic fields by electromagnetic flux compression, the "feed gap effect": the magnetic field that drives the implosion is locally reduced by about 10% in the vicinity of the feed gap in the primary coil, resulting in a reduced acceleration of the adjacent part of the liner. Thus the symmetry of the cylindrical implosion is deteriorated; towards the end of the implosion this results in a bulge on the outside and the associated formation of a discharge and a plasma jet on the inside of the disturbance. This jet affects premature destruction of the sample and probe before the implosion is complete and peak field has been reached. The effect becomes more prominent as the liner speed is increased, thus wiping out the benefit of the higher speed that is needed to obtain a higher field. In order to solve this problem, we designed a "feed gap compensator" as shown in Fig.1(a). This is a thick-walled copper cylinder with 6 narrow radial slits. The device functions like a flux concentrator; due to the skin effect flux is excluded from the copper that now acts as a primary coil with 6 very narrow feed gaps (the feed gap in the primary coil cannot be made small because electrical breakdown at this place could result in serious damage). The resulting driving field has 6-fold rotational symmetry, and in the vicinity of the narrow gaps the reduction of the driving field is much smaller. Figure 1 shows the arrangement of the primary coil and the liner with and without the compensator, together with corresponding high speed photographs of the liner deformation at the end of the implosion. The photographs show that the cylindrical symmetry of the liner deformation is much improved by the compensator, with the liner in slightly hexagonal shape. The improvement of implosion symmetry resulted in a sizeable

increase of the maximum field. Figure 2 shows an example of the experimental traces of the magnetic field and the primary current. In this case, a maximum field of 622T was obtained. The speed of the liner was 2.0km/s. An important point is that with the new system a real "field turnaround" was achieved for the first time in electromagnetic flux compression: the field goes through a well defined maximum before the probe is destroyed. This is essential for further optimization of the device for obtaining higher fields.

3 Single-turn coil technique

The single-turn coil technique is a useful means to generate megagauss fields for experiments, because samples and cryostats are usually not destroyed. Moreover, it is much easier to do experiments than with flux compression. At Roppongi, we have produced magnetic fields up to 150T in a bore of 10mm, 200T in 6mm and 246T in 4mm.[7]

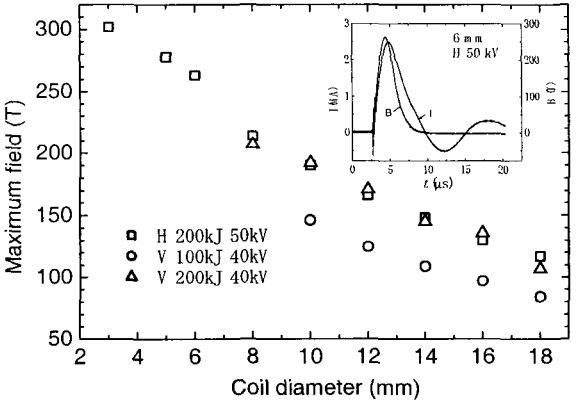

Figure 3: Maximum magnetic field obtained by the single-turn coil technique as a function of the bore of the coil. H and V denote the horizontal and the vertical system, respectively. The inset shows the waveforms of the magnetic field and of the current obtained for a bore of 6.0mm with the horizontal system.

At Kashiwa, we built two new capacitor banks with a stored energy of 200kJ each; this is twice as much as at Roppongi. One of the capacitor banks is used for a coil system with horizontal axis; this is useful for optical measurements. The maximum charging voltage is 50kV. The other bank is used for a coil system with

vertical axis, which is well suited for inserting a bath cryostat to refrigerate the sample directly by immersion in liquid helium. The maximum voltage is 40kV; this capacitor bank is divided into two parts that can be used individually at one half of the total energy. In both systems, we can obtain very high magnetic fields depending on the coil dimension. Figure 3 shows the maximum field obtained from coils with different bore (inner diameter). The length of the coils was equal to the bore. The inset shows an example of current and field waveforms. With a coil bore of 3.0 mm, a maximum field of 302T was obtained by the horizontal system. As the samples are not destroyed in the experiments, many different types of experiments have been performed. For the vertical system, a liquid helium cryostat with a plastic tail was designed and built; this enables convenient cooling of the samples to 4.2K. Many optical and transport experiments have been performed in these megagauss fields at low temperatures.

4 Long pulse fields

Non-destructive long pulse fields are generated by conventional types of wire wound magnets. A capacitor bank with a stored energy of 900kJ (5kV/10kV convertible) is installed. In addition to magnets reinforced by ice and glass fiber cloth[8] and wet-wound magnets,[9] which have been usually employed at ISSP, different types of magnet construction were implemented: Herlach-type[10] and Kindo-type.[11] Figure 4 shows typical waveforms of the magnetic fields obtained by these coils.

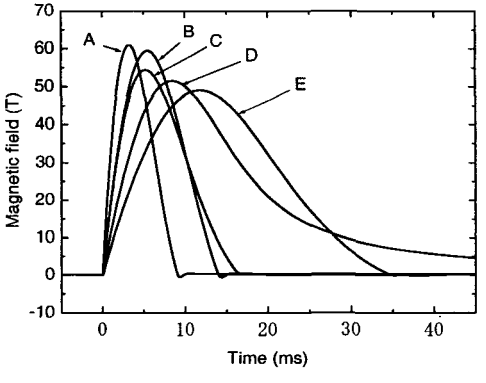

Figure 4: Typical waveforms of non-destructive long pulse fields obtained with different types of magnets. A: Recent wet-wound type,[9] B: Herlach-type,[10] C: Kindo-type,[11] D: Kindo-type with a crowbar circuit, E: Ice-reinforced type.[8]

References

1. N. Miura *et al.*, *J.Phys. Condens. Matt.* **11**, 5917-5928 (1999).
2. N. Miura *et al.*, *Physica B* **294-**295, 562-567 (2001).
3. S. Sasaki *et al.*, *J. Phys. Soc. Jpn.* **62**, 2490-2500 (1993).
4. H. Arimoto *et al.*, *Phys. Rev.* B **58**, 4560-4565 (1998).
5. H. Nakagawa *et al.*, Y., *J. Phys. Condens. Matt.* **10**, 11571-11576 (1998).
6. N. Miura and F. Herlach., in *Strong and Ultrastrong Magnetic Fields and Their Applications,* ed. F. Herlach (Springer-Verlag, 1985), Ch. 6, 247-350
7. K. Nakao *et al.*, *J.Phys. E, Sci. Instrum.* **18**, 1018-1026 (1985).
8. S. Takeyama *et al.*, *Meas. Sci. Technol.* **3**, 662-666 (1992).
9. E. Ohmichi *et al.* to be published.
10. L. Li and F. Herlach, *J. Phys.* D **31** 1320 (1998).
11. K. Kindo, *Physica* B **294-295**, 585-590 (2001).

* On leave of absence from the Katholieke Universiteit Leuven, Belgium

Contributed Papers

This page is intentionally left blank

ULTRAFAST COHERENT TERAHERTZ SPECTROSCOPY IN HIGH MAGNETIC FIELDS

S. A. CROOKER

NHMFL, Los Alamos National Laboratory, MS E536, Los Alamos, NM 87545 USA
E-mail: crooker@lanl.gov

A. J. TAYLOR

MST-10, Los Alamos National Laboratory, MS E536, Los Alamos, NM 87545 USA

With an aim towards measuring the high-frequency complex conductivity of correlated electron materials in the regime of low temperatures and high magnetic fields, we introduce a method for performing time-domain terahertz spectroscopy directly in the cryogenic bore of existing dc and pulsed-field magnets. Miniature, fiber-coupled THz emitters and receivers are constructed and are demonstrated to work down to 5 K and up to 6 Tesla, for eventual use in higher-field magnets. Maintaining the sub-micron alignment between fiber and antenna during thermal cycling, and obtaining ultrafast (<200fs) optical gating pulses at the end of long optical fibers constitute the major technical challenges of this project. Preliminary data on YBCO superconducting thin films is shown.

1 Introduction

Time-domain terahertz spectroscopy is a well-established technique for the measurement of high-frequency conductivity in the range between 100 GHz and ~3000 GHz (see Ref. [1]). This frequency range lies between that which is readily accessible by microwave cavity techniques (on the low frequency side), and Fourier-transform infrared (FTIR) spectroscopies (on the high frequency side). This frequency range corresponds to energies between 0.4meV and ~12meV, or alternatively temperatures between 4 K and 140 K and magnetic fields between 8 Tesla and 200 Tesla. This is precisely the energy scale relevant to many novel correlated-electron systems of interest today, including the high-T_c superconductors, heavy-fermion materials, manganites, and related exotic metals. Thus it is of keen interest to perform measurements of the THz complex conductivity in this regime of low temperatures and high magnetic fields. However, the conventional "table-top" transmission terahertz spectrometer is a rather complicated and physically large setup, typically utilizing several micropositioners to align the THz antennas with respect to the laser beams, and off-axis parabolic optics to collimate and focus the terahertz pulses over short distances. These traditional methods are not compatible with high-field magnets, which are generally solenoids with narrow, low-temperature bores accessible primarily via meters-long experimental probes.

To this end we have developed extremely sensitive, miniaturized, optical fiber-coupled THz emitters and detectors for use directly in the low-temperature bore of a high-field (dc or pulsed) magnet. The primary challenges include maintaining sub-micron alignment between fiber and antenna upon repeated thermal cycling, achieving ultrafast (<200fs) optical pulses at the end of tens of meters of singlemode optical fiber, and obtaining complete time-domain scans with signal:noise >100 using only milliwatts of optical power, no lock-in detection, and (for pulsed magnets) only ~100 ms of integration time.

2 Methods

The basic idea for performing THz transmission spectroscopy in high-field magnets is illustrated in Fig. 1(a). The sample of interest is positioned between the THz emitter and receiver in the center of the magnet. A single-mode optical fiber carries ultrafast optical excitation pulses (centered at 800 nm) from the laboratory to the lithographically-defined biased THz stripline emitter, whereby a pulse of THz radiation is generated and launched into free space through a silicon hyperhemispherical substrate lens. After passing through the sample, the THz pulse is incident on the stripline receiver, where the 'instantaneous' electric field is gated by a second ultrafast optical pulse, generating a measurable current. The complete time-dependent THz electric field is mapped by rapidly scanning the delay between the excitation and gating optical pulses, and the amplified signal is sent directly to a digitizing oscilloscope. A photograph of the actual apparatus is shown in Fig. 1(b). A rotating copper stage enables the sample to be moved out of the THz beam path, so that a reference scan (crucial for quantitative interpretation of data) may be taken at each new temperature or field.

THz pulses may only be launched (and detected) using ultrafast (~100fs) optical pulses, and for this reason it is necessary to compensate for the group-velocity-dispersion (GVD) in optical fibers so that fast pulses may be obtained at the ends of the long optical fibers. Silica optical fiber exhibits a GVD of roughly -120fs/m-nm at 800nm, so that without compensation, a 100fs optical pulse with a bandwidth of 10nm broadens, in the best case, to >10 picoseconds after a typical 10 meter length of fiber. Such a long pulse in time is useless for generating or detecting THz radiation. Thus it is necessary to precompensate and impart positive GVD on the optical pulses before launching into the optical fibers, so that the optical pulses shorten in time as they travel through the fiber and achieve a minimum value right at the THz devices. In this way we achieve <200fs optical pulses after 20meters of fiber. It is also important that the effects of self-phase-modulation of the optical pulse (caused by high instantaneous optical power) are minimized by using very low-power optical pulses, typically of order 10-20pJ only. These stringent power requirements make it necessary to utilize specially-designed

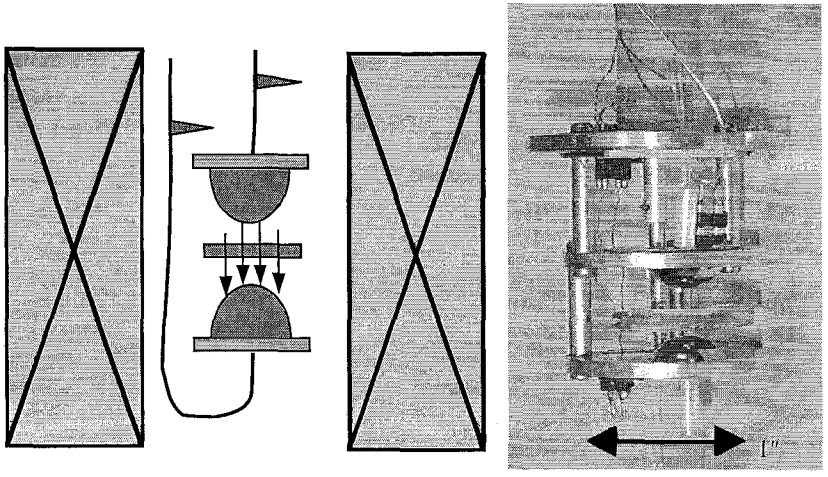

Figure 1: Schematic of the apparatus (left). THz emitter and receiver face each other in the bore of the magnet, and the sample may be positioned in between. Single-mode optical fibers couple the excitation and gating ultrafast optical pulses to the antennas. On the right is shown a photograph of the low-temperature, high-field THz probe.

lithographic antennas to maximize the efficiency of THz generation and the sensitivity of detection. We find that commonly-used emitters based on semi-insulating GaAs exhibit a strong temperature and magnetic field dependence (likely due to the long carrier lifetimes and temperature-dependent mobility in GaAs). Further, THz receivers based on implanted silicon-on-sapphire are not particularly sensitive when only milliwatts of average optical power are used. To boost sensitivity and achieve performance that is relatively independent of temperature and field, we fabricate devices on ErAs/GaAs superlattices.[2] This material is similar to low-temperature-grown GaAs in that it is ideal for fast photo-mixing applications as the carrier lifetime is extremely fast due to the presence of trapping sites.

The utility of the method is shown in the preliminary data of Fig. 2, where the imaginary part of the high-frequency conductivity of a YBCO thin film is shown (50 nm thick, T_c ~ 85 K). These data were taken in a 7 Tesla superconducting solenoid using the probe shown in Fig. 1. At low temperatures, the $1/\omega$ conductivity from the Drude-like response of superconducting particles with infinite scattering time is clearly observed. With increasing temperature, this conductivity falls rapidly above T_c, indicating the disappearance of phase coherent superconductivity, in agreement with previous works.[3] As a function of magnetic field for temperatures slightly below T_c, similar behavior is observed, indicating again that superconductivity is being suppressed, but this time by the application of magnetic field rather than temperature.

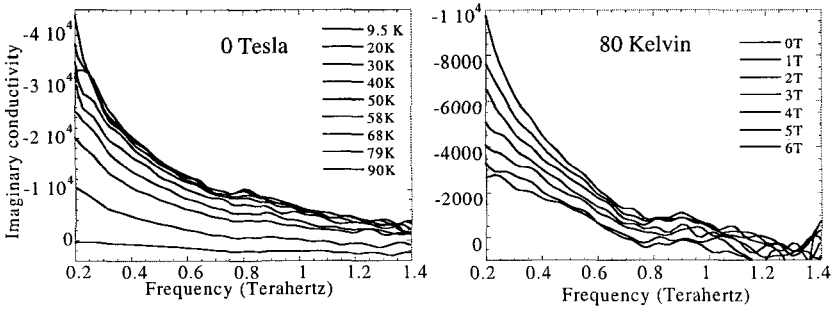

Figure 2: Terahertz imaginary conductivity of a 50 nm thick YBCO film (Tc~85 K), taken in the cryogenic bore of a superconducting solenoid. The conductivity drops above T_c, indicating the suppression of superconductivity above T_c (left). On the right, a similar quenching of the conductivity with increasing magnetic field is observed for temperatures near T_c.

These and other proof-of-principle studies will naturally be extended to higher dc magnetic fields, and ultimately, to the 60 Tesla pulsed magnetic fields at the NHMFL-LANL. We anticipate that the study of THz conductivity in high magnetic fields will find much use for the study of a variety of correlated - electron materials.

Acknowledgments

This work was supported primarily by a grant under the National High Magnetic Field Laboratory In-House Research Program.

References

1. M. van Exter, Ch. Fattinger, D. Grischkowsky, *App. Phys. Lett.* **55**, 337 (1989).
2. Courtesy of A. Gossard and M. Hanson, UCSB.
3. R. D. Averitt *et al.*, *Phys. Rev. B. Rap. Comm.* **63**, 140502 (2001).

RECENT ADVANCES IN LOW TEMPERATURE THERMOMETRY IN HIGH MAGNETIC FIELDS

E. C. PALM, T. P. MURPHY, S. W. TOZER and S. T. HANNAHS
Florida State University, NHMFL, Tallahassee, Florida, 32310 USA

The accurate determination of the temperature of an experiment at low temperatures in high magnetic fields is difficult. We present the results of measurements made using a number of new techniques developed over the last few years. In particular we discuss the results of measurements made using a unique capacitor made with Kapton and copper in a cylindrical geometry.[1] This capacitance thermometer, dubbed the "Kapacitor", is different from other low temperature thermometers in that the minimum in capacitance vs. temperature can be moved to lower temperatures (to below 20 mK) by changing the construction technique. In addition, we discuss measurements on Coulomb blockade thermometers (CBT's) that offer the possibility of true primary thermomemtry at low temperatures without any magnetic field dependence. Both of these new techniques will be compared to the standard technique of resistance thermometry using RuO chip resistors. The crucial issues of accuracy and precision, usefulness for control, and noise sensitivity will be discussed for each of these technologies. In addition, recent measurements on the magnetic behavior of RuO thermometers at low temperatures and its relationship to anomalous low field peaks in the resistance that develop at temperatures below 50 mK are also presented.

1. T. P. Murphy, E. C. Palm, L. Peabody and S. W. Tozer, Accepted for publication in *RSI.*

NEUTRON SCATTERING IN MAGNETIC FIELDS UP TO 17 T

K. PROKES, P. SMEIBIDL and M. MEISSNER
Hahn-Meitner-Institute, Glienicker Str. 100, 141 09 Berlin, Germany

Neutron scattering in magnetic fields can provide important information regarding the magnetism of a system under study on microcsopic scale. Although pulse magnets are capable to reach very high fields, for neutron scattering mostly superconducting magnets are used. At present, a split-pair 14.5 T superconducting magnet used for user-program experiments at HMI offers the highest magnetic field for neutron scattering. With Dy-pole tips placed symmetrically around the sample position a 2.5 T enhancement is achieved. The temperature range accessible with such an insert is between 1.8 and 100 K. Temperatures down to 30 mK can be achieved with a dilution stick, which can be inserted into the 14.5 T cryomagnet. In the contribution we report on the latest neutron scattering achievements in magnetic fields obtained at HMI.

ULTRASONIC SPECTROMETERS FOR CONDENSED MATTER STUDIES AT VERY HIGH MAGNETIC FIELDS

A. SUSLOV,* D. DASGUPTA, J.R. FELLER and BIMAL K. SARMA

Department of Physics, University of Wisconsin-Milwaukee, P.O. Box 413 Milwaukee, WI 53201, U.S.A.
E-mail: alexei@uwm.edu

J. B. KETTERSON

Department of Physics and Astronomy, Northwestern University, Evanston, IL 60208, U.S.A.

Three ultrasonic spectrometers have been constructed for use with the continuous and pulsed magnetic field facilities of the NHMFL at the Tallahassee and Los Alamos sites. The first of these, designed for use with the dc magnets, is a heterodyne spectrometer with the capabilities of high velocity resolution and near-simultaneous measurements at several frequencies (typically near transducer harmonics). The other two spectrometers are designed for the short-pulsed magnets, with the capability of fast data acquisition. These spectrometers have been used in the study of metamagnetism in the heavy fermion materials.

1 Introduction

Ultrasonic velocity and attenuation measurements are a powerful spectroscopic tool to study condensed matter systems,[1] especially various phase transitions and collective phenomena. In such measurements the magnetic field is a useful parameter to vary.

We have constructed ultrasonic spectrometers specifically for the study of condensed matter systems using the dc and pulsed high magnetic fields at the NHMFL sites in Tallahassee and Los Alamos. The spectrometers are being used to study metamagnetism in UPt_3 (see Ref. [2]) and URu_2Si_2 (see Ref. [3]).

Three experimental setups have been assembled from commercially available r.f. components. Each of these spectrometers consists of two parts: (1) a pulser, used to generate high-power, high-repetition-rate r.f. bursts of about 0.5 μs in duration and (2) a quadrature phase-sensitive detector. The principal difference between the three spectrometers lies in the design of the detector, and depends very much on the experimental conditions and needs.

2 Instrumentation

2.1 The Pulser

The principle of the pulser is as follows: the continuous (c.w.) r.f. output of a signal generator is split into two channels by a power splitter. These two channels form the two arms of an ultrasonic interferometer. One of the channels is a continuous sinusoidal reference signal at frequency F.

A pulsed r.f. signal is obtained by means of a pulse generator and an r.f. switch in the second channel. This gated and amplified r.f. signal is applied to a piezoelectric transducer (quartz or $LiNbO_3$) bonded (with some form of epoxy) to the end faces of the crystal sample under study. The r.f. signal is converted to an acoustic signal and travels through the sample at the speed of sound. It is received, attenuated and delayed, at the other end of the sample, and converted back into an electric signal with a second transducer. The end faces of the sample are made flat and parallel, and it is often possible to see many echoes and work at many harmonics of the fundamental transducer frequency. Multiple echo trains may be observed for good quality samples. Many pulses are generated per second with repetition rates ranging from 100 Hz – 1 kHz permitting one to do signal averaging (in a slowly varying environment – temperature or magnetic field) to improve the signal to noise ratio.

2.2 Technique for dc magnetic fields using an analog detector

A super-heterodyne receiver is an integral part of the ultrasonic detector. As a local oscillator (LO) we use a standard c.w. r.f. signal generator. The output frequency of the latter is equal to F+60 MHz. This c.w. sinusoidal output signal is split into two channels. A signal from one of them is mixed with the preamplifier output signal, and a signal from the second is mixed with the pulser reference signal. Mixers in both channels shift the frequency of the signals to the intermediate frequency, 60 MHz, whereby detection can be accomplished using low-noise narrow-band-width modules. In the reference channel a power splitter creates in–phase and quadrature signals and these two are mixed with a signal from the sample. This gives us two trains of video pulses, the amplitudes of which are measured by boxcar integrators. These amplitudes are proportional to sin ϕ (train A) and cos ϕ (train B), where ϕ is a phase shift between the signals in the reference channel and the sample. In the standard configuration, measurement precision is increased by using the quadrature signal in a feed back loop, which changes the frequency of the signal generator driving the pulser. In that case the frequency shift is proportional to ultrasound velocity shift, and the amplitude change of the in-phase signal then gives directly the ultrasound attenuation. This technique is identical to the one reported earlier in.[4]

Measurements at several frequencies can be done simultaneously. While the field is being swept slowly and the temperature held constant, the computer quickly sequences through the different frequencies. Each data point typically involves signal averaging over 50-100 pulses. The magnetic field is sensed before and after these pulses and averaged. This mode of measurement allowed us to measure the dispersion in the velocity at the metamagnetic transition in UPt_3 (see Ref. [5].

2.3 Technique for pulsed magnetic field using an analog detector

Current d.c. magnets can produce fields up to about 33 T, but with a huge consumption of electric power and cooling water. Higher fields can be achieved with a hybrid magnet (45 T); but the cost is often prohibitive for routine measurements. Pulsed magnets are suitable alternatives that can easily produce fields up to 60 T (higher magnetic fields 80-100 T will soon be available) at a modest cost. However, these magnets involve short pulses and the spectrometer has to be suitably adapted for fast data acquisition.

The commercial r.f. components that go into our spectrometers have relatively fast response/recovery times, typically less than a microsecond, and can be used in pulsed fields. However, to get a sufficiently large number of data points, one has to use a repetition rate of the ultrasonic pulses of about 100kHz. Basically one initiates a new pulse train soon after the secession of the previous one. At this high sampling rate signal averaging (or measurements using a feedback loop) are not possible. It is more straight-forward to sample, digitize and store the amplitudes of each video pulse (from trains A and B). The amplitudes are measured by boxcar integrators and the output signals of the latter are digitized by A/D converter and stored in a computer. From the arctangent of the ratio of these signals one can obtain the phase and by comparing successive pulses, the ultrasound velocity change. Computing the square root of the sum of the squares of these signals give signal amplitude and, again by comparing successive pulses, the change of ultrasound attenuation.

2.4 Technique for pulsed magnetic fields using a digital detector

Recent developments in digital hardware allow fast digitizing and storage of giant data arrays; the associated high-speed computations allow the use of software for quick processing of the data. A novel approach we have exploited is to *directly digitize* the (undetected) signal from the transducer, at a minimum sampling rate corresponding to about four samples per cycle. For higher frequencies the signal can be mixed down to a value that can suitably digitized. In contrast to the analog methods mentioned above, the frequency of LO signal applied to the f mixer was equal to f = F+12.5 MHz and the intermediate frequency of the mixer output was F_I = 12.5 MHz. A CompuSscope 1250 oscilloscope card of GaGe Applied Inc., which had a sampling rate of 50 MHz, was used to digitize the signal; our choice of IF

frequency allows us to measure four points per IF period. The signal is stored in the memory of the oscilloscope card and later transferred to a computer.

To calculate the phase shift and attenuation our original software was used. The signal is multiplied by $\sin(F_I t)$ and $\cos(F_I t)$, where t is the time. These operations are the numerical analog of the phase detection used above to extract the in-phase and quadrature signals. As a result we again have signals which are proportional to $\sin \phi$ and $\cos \phi$. Ultrasound velocity and attenuation changes as a function of magnetic field were obtained from these values by the same method as for the analog devices.

The digital ultrasound detector consists of just four commercially available minicircuits, is easy to assemble, does not require tuning and is the main innovation of this work.

Acknowledgments

This work is supported by the National Science Foundation under grant numbers DMR-9971123 and DMR-9704020. We are thankful to A. Migliori and F. Balakirev for useful discussions and help.

*) Permanent address: A.F.Ioffe Physical-Technical Institute, Russian Academy of Sciences, St.-Petersburg, Russia.

References

1. Physical Acoustics, v. XX, *Ultrasonics of High-Tc and other Unconventional Superconductors*, ed. by M. Levy (Academic Press, 1992).
2. A. Suslov *et al., Ultrasonic studies at the metamagnetic transition in UPt_3, these proceedings.*
3. A. Suslov *et al., Ultrasonic measurements at the metamagnetic transition in URu_2Si_2, these proceedings.*
4. B. Wolf *et al., Physica B* **294-295**, 612-617 (2001).
5. J. R. Feller *et al.,* J.R., *Phys. Rev. B* **62**, 11538-11544 (2000).

HIGH PRESSURE TECHNIQUES FOR LOW TEMPERATURE STUDIES IN DC AND PULSED MAGNETIC FIELDS

S.W. TOZER
National High Magnetic Field Laboratory, Tallahassee, Florida, 32310 USA

Pressure can be used to expand the parameter space available in almost any experiment and allows for the continuous tuning of the electrical and orbital properties of a material. When combined with low temperatures and high magnetic fields, it becomes a powerful tool for the exploration of the band structure and defect levels in semiconductors, exotic transport mechanisms in molecular conductors, and the coexistence of magnetism and superconductivity. We have developed a variety of miniature pressure cells to allow the user to take full advantage of these opportunities. Metallic diamond anvil cells as small as 6 mm in diameter and 8 mm in height allow the sample to be rotated in field at millikelvin temperatures. Miniature plastic DACs and sapphire ball cells, rotators, and specialized He-4 and He-3 systems have also been developed to provide similar experimental capabilities in pulsed magnetic fields. Methods and designs to generate hydrostatic pressure and techniques to perform optical and electrical measurements in DC and pulsed fields will be presented.

We would like to acknowledge the technical assistance of Richard Desilets, Howard Kolb, John Farrell, and Mike Pacheco. A portion of this work was performed at the National High Magnetic Field Laboratory, which is sponsored by NSF Cooperative Agreement No. DMR-9527035 and by the State of Florida.

This page is intentionally left blank

Part VIII

Instrumentation and Facility Development of High Magnetic Fields

This page is intentionally left blank

THE DRESDEN 100 T/10 ms PROJECT: A HIGH MAGNETIC FIELD FACILITY AT AN IR-FEL

M. DÖRR,[1] D. ECKERT,[2] H. ESCHRIG,[2] F. FISCHER,[2] P. FULDE,[3] R. GROESSINGER,[4] W. GRÜNBERGER,[2] A.HANDSTEIN,[2] D. HINZ,[2] R. KRATZ,[5] H. KRUG,[5] M. LOEWENHAUPT,[1] K.-H. MÜLLER,[2] F. POBELL,[5] L. SCHULTZ,[2] H. SIEGEL,[2] F. STEGLICH,[6] and P. VERGES,[2]

[1]*Institut für Angewandte Physik, TU Dresden, 01062 Dresden (Germany)*
[2]*IFW Dresden, 01171 Dresden (Germany)*
[3]*MPI für Physik komplexer Systeme, 01187 Dresden (Germany)*
[4]*Institut für Experimentalphysik, TU Wien, 1040 Wien (Austria)*
[5]*Forschungszentrum Rossendorf, P. O. B. 51 01 19, 01314 Dresden (Germany)*
[6]*MPI für Chemische Physik fester Stoffe, 01187 Dresden (Germany)*

We have proposed to build a 100 T/10 ms, 70 T/100 ms, 60 T/1 s pulsed field user facility with a 50 MJ capacitor bank at the Forschungszentrum Rossendorf near Dresden. This would provide the appealing possibility to have access to Zeeman energies in the energy range of the infrared free-electron-lasers (5 μm to 150 μm; 2 ps; cw; > 10 W) now under construction at the radiation source ELBE (superconducting electron linear accelerator; 40 MeV; 1 mA; 2 ps; cw) in Rossendorf. The work is accompanied by computer simulations of the planned coil systems, of the power supply, and by the development of high-strength conductors aiming at a tensile strength of about 1.5 GPa at $\sigma \approx \sigma_{Cu}/2$ (microcomposite CuAg alloys and Cu-steel macro compounds).

With a view of gaining experience in the construction and operation of pulsed magnets, a pilot pulsed field laboratory was established at the Institute of Solid State and Materials Research Dresden (IFW Dresden). The laboratory includes short pulse magnets with peak field up to 60 T in a 24 mm bore and a rise time of about 10 ms (coil from NHMFL, Tallahassee), and a 40 T long pulse magnet with 24 mm bore and rise time of about 80 ms (coil from METIS, Leuven). The repetition rate of 20 min between pulses is limited by the cooling time of the coils. The coils are energized by a 1 MJ, 10 kV capacitor bank with some special features. With this set-up measurements of magnetization and magnetotransport on 4f-electron systems, for example $RECu_2$, have been carried out in the temperature range of 1.5 to 300 K and at fields up to 52 T using high precision pick-up coils.

DEVELOPMENT OF ADVANCED INSTRUMENTATION FOR STATIC AND PULSED FIELDS

A. MIGLIORI, F. F. BALAKIREV, J. B. BETTS, G. S. BOEBINGER, C. H. MIELKE and D. RICKEL
Los Alamos National Laboratory, NHMFL, MS E536, Los Alamos, New Mexico 87545, USA

The DC and pulsed magnets now available at the NHMFL provide routine access to high magnetic fields in cryogenic environments (down to even dilution refrigerator levels), that are world-record unique. This uniqueness comes with a price that reflects constraints of the magnets and the low temperatures, including limited volume and time at peak magnetic field, cryogenic power limits on electronics, and, particularly for pulsed magnets, increased noise. In effect, the instrumentation constraints are similar for NHMFL superconducting, resistive and pulsed magnets. An NHMFL experimentalist therefore has a simple goal: acquisition of all the information produced by a measurement in the shortest time permitted by information theory, with minimum sensitivity to noise and interference. To assist with this, we propose here to eliminate commercial general-purpose lock-in amplifiers, preamplifiers and digitizers and replace them with commercial-quality custom building blocks optimized for NHMFL measurements, that are faster, quieter, more versatile, and cheaper. We will use these new instruments to support users by improving present measurements as well as adding new capabilities, including specific heat for materials that suffer adiabatic effects in pulsed fields, and thermal conductivity in both dc and pulsed magnets based on 3rd harmonic methods. We will use these techniques to measure the thermal conductivity of high T_c superconductors at high field in the normal state, and to test the Weideman-Franz relationship between electronic thermal conductivity and electrical conductivity in the extreme high-field limit.

MEGAGAUSS CYCLOTRON RESONANCE IN SEMICONDUCTOR NANOSTRUCTURES AND DILUTED MAGNETIC SEMICONDUCTORS

N. MIURA, Y. H. MATSUDA and T. IKAIDA

Institute for Solid State Physics, University of Tokyo, Kashiwa, Chiba, Japan
E-mail: miura@issp.u-tokyo.ac.jp

We report the latest results of cyclotron resonance experiments on semiconductor nanostructures and diluted magnetic semiconductors (DMS) in very high magnetic fields up to 600 T produced by magnetic flux compression and the single turn coiled technique. Many new features were observed in the very high field range, such as characteristic behavior of low dimensional electrons, carrier dynamics or electron-electron interaction effects in quantum wells and quantum dot samples. In PbSe/PbEuTe quantum dots, which were regularly arranged to form an fcc superlattice, we observed an absorption peak with a splitting and a wavelength dependence of the absorption intensity. In DMS, such as CdMnTe and InMnAs, change of the carrier effective mass with Mn doping was studied in detail. We found anomalous mass increase with doping of magnetic ions. The amount of the observed mass increase cannot be explained by the $\boldsymbol{k \cdot p}$ theory and suggests the importance of d-s or d-p hybridization.

1 Introduction

At MGL (Megagauss Laboratory) of the ISSP, we generate pulsed high magnetic fields well above 100 T (megagauss fields) by electromagnetic flux compression and the single turn coil technique and employ them for different kinds of experiments.[1-3] Cyclotron resonance (CR) is one of the most suitable experiments in the megagauss range, since accurate measurements can be performed even in short pulse duration time.[4,5] CR in high magnetic fields is a powerful tool to investigate new aspects of electronic states in the high energy region with high resolution. It is also very useful for relatively low mobility materials.

Recently, many investigations have been done on electronic states in low dimensional electron systems quantized in quantum wells, wires and dots. We have studied electronic states and carrier dynamics in quantum wells by means of CR, and found many new features for a highly quantized regime.[6] In this paper we present the recent results on quantum dots of PbSe embedded in PbEuTe matrix.[7]

Diluted magnetic semiconductors (DMS) are another class of materials which attracted much attention, in view of the spintronics and the carrier induced ferromagnetism. It is urgently necessary to obtain a difference in the effective mass of carriers from the host crystal in order to know the details of the sp-d exchange interaction. In DMS, the carrier mobility is usually very low because of the high doping of the magnetic ions. In megagauss fields, well-defined absorption peaks are observed, and anomalous mass increase has been found.[8,9] We present here the recent results on the change of the effective mass by the magnetic ion doping in CdMnTe and InMnAs.

2 Experimental Technique

Pulsed high magnetic fields are produced by electromagnetic flux compression and the single turn coil technique.[1] We can obtain high magnetic fields exceeding 600 T by the former technique and more than 200 T depending on the coil bore by the latter. In both cases, the rise time or the duration of the fields is several microseconds. Therefore, we need a high speed detection of the infrared (IR) and far-infrared (FIR) radiation. As radiation sources, we use a CO laser, CO_2 laser, pulsed H_2O laser, and a CO_2 laser-pumped molecular gas FIR laser. As fast detectors of the radiation, we use a photovoltaic detector of HgCdTe for a CO and CO_2 laser (5-11 μm) at 77 K, and a Ga-doped or Cu-doped Ge detector cooled to liquid helium temperatures for longer wavelengths (16.9–500 μm). The radiation is focused on the sample and collected by using an optical system with mirrors on both sides of the sample. Fast preamplifiers and an E/O (Electric to Optical) converter are employed to transmit the signal from the experimental room to a shield room where transient recorders are installed to acquire the data. The samples are set at the center of the magnetic field, and refrigerated by liquid helium flow through a hand-made disposal cryostat made from insulating materials. Inside the high field magnet, all the parts of the cryostat and the sample holder are made from plastics such as phenolic tubes or capton sheets and tubes. They are glued so as to ensure a vacuum tight seal at low temperatures. Slightly different types of cryostats are used for electromagnetic flux compression and the single-coil technique. Temperature is measured by a thermocouple set near the sample. Low temperatures down to about 10 K are obtained

3 PbSe/PbEuTe Quantum Dots

Samples of PbSe/PbEuTe quantum dots were grown by the group of Bauer at the Johannes Kepler University at Linz. The quantum dots of PbSe are of Pyramid shape with a size of about 40 nm in base sides. Many layers are stacked on a BaF_2 substrate. A characteristic point of the samples is that the dots are regularly arranged forming an fcc-like superlattice.[9] It is of interest to explore the effect of the regular ordering of the quantum dots. Figure 1 shows experimental traces of the CR at different wavelengths for a regularly spaced superlattice sample. Both the electron-active and hole-active spectra are shown in the same figure on both sides of the ordinate axis. The absorption peaks arising from the quantum dots are observed for the electron-active polarization. As the magnetic field is applied to the growth direction (<111> axis of PbSe crystal), there is one valley whose principal axis is along the field and three valleys whose principal axis is tilted from the field by the same angle. CR peaks from these valleys are the light electron and the heavy electron peak, respectively. The peak at 75.0 T for 10.6 μm is assigned as the heavy electron peak. At shorter wavelengths, three peaks are observed in the neighborhood. The reason of the splitting of the peak is not clear at present, but it

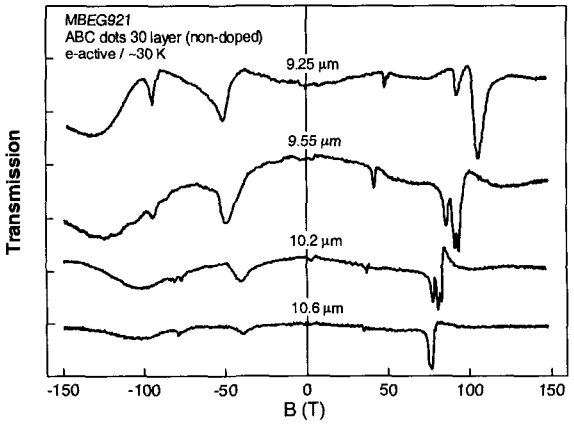

Figure 1: Cyclotron resonance traces for PbSe/PbEuTe quantum dot samples at different wavelengths. The dot layers are stacked with a ABCABC stacking forming an fcc-like superlattice. The radiation is circularly polarized so that the positive and negative magnetic fields stand for the electron-active and hole-active polarization, respectively.

comes probably from the strain due to the dot formation, which should give rise to a splitting of the three degenerate peaks. Another interesting feature is that the absorption intensity of the peaks is drastically increased as the wavelength is reduced. This may be due to the effect of the regular spacing of the quantum dots.

The splitting and the wavelength dependence of the absorption intensity are also observed for vertically aligned quantum dots (AAA stacking). A peak at 35-46 T is considered to be the light electron peak. The broad absorption peaks for the hole-active polarization are considered to arise from the PbEuTe matrix. Details of the origin of the peaks and their photon energy dependence will be published elsewhere.

4 CdMnTe

Samples of $Cd_{1-x}Mn_xTe$ with x = 0.041-0.098 were provided by the group of the Tsukuba University. They were grown by the MBE on substrates of GaAs. Figure 2 shows the CR spectra for samples with different x at T = 250 K. For each trace, a calculated curve is superimposed by a dashed line using the best fit parameters for cyclotron mass, mobility and carrier density as shown on the right. It was found that the effective mass increases significantly with increasing doping of Mn. To analyze

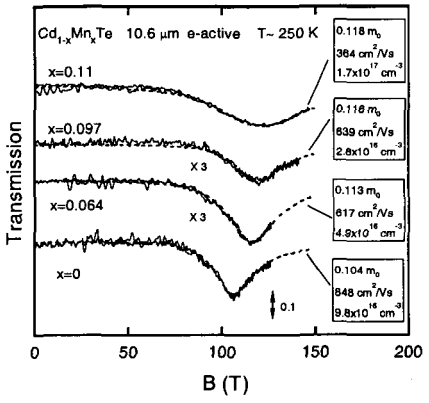

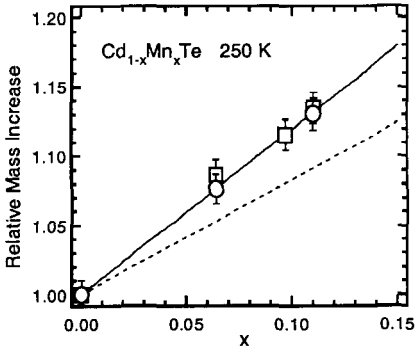

Figure 2: (left). Cyclotron resonance traces for $Cd_{1-x}Mn_xTe$ with different x. The dashed lines are theoretical lines calculated with parameters shown in the right side of each figure.
Figure 3: (right) Relative increase of the cyclotron mass at 10.6 mm (squares) and the deduced band edge mass (circles) as a function of x. The solid and dashed lines are theoretically calculated lines by Hui *et al.*,[11] with and without the sp-d interaction, respectively.

the x-dependence of the effective mass, the Landau level energies were calculated by the modified Pidgeon-Brown model.[10] The large increase of the effective mass with x cannot be explained simply by the increase of the band gap with x. Namely, the enhancement of the effective mass with x is much larger than expected from the band gap (E_g) increase with Mn doping. We compared the x dependence of the mass increase between $Cd_{1-x}Mn_xTe$ and $Cd_{1-x}Mg_xTe$. Although both Mn and Mg increases the lattice constant and thus the band gap when doped into CdTe, the E_g dependence of the mass increase is much larger in $Cd_{1-x}Mn_xTe$ than in $Cd_{1-x}Mg_xTe$. This implies that in $Cd_{1-x}Mn_xTe$, the sp-d interaction should have a significant effect on the enhancement of the effective mass. Hui *et al.*, theoretically studied the effect of the sp-d hybridization including a set of d-levels in calculation.[11] They concluded is that the main effect of the sp-d hybridization is the reduction of the momentum matrix element P. The magnetic field dependence of the resonant photon energy for each x can be explained only when we assume that P is decreased significantly with increasing x (see Ref. [12]). Figure 3 shows the relative increase of the effective mass as a function of x as compared with CdTe. Theoretical lines predicted by Hui et al. are also shown for comparison. We found that our experimental results are well explained by the theory of Hui *et al.*, including the p-d interaction.

5 InMnAs

The samples of p-type $In_{1-x}Mn_xAs$ were grown by the MBE on GaAs substrates. x was varied from 0 to 0.025. Figure 4 shows the CR traces for various samples with different x. As the samples are p-type, cyclotron resonance in the valence band is observed. The observed main peak is assigned as the light hole peak. It is apparent

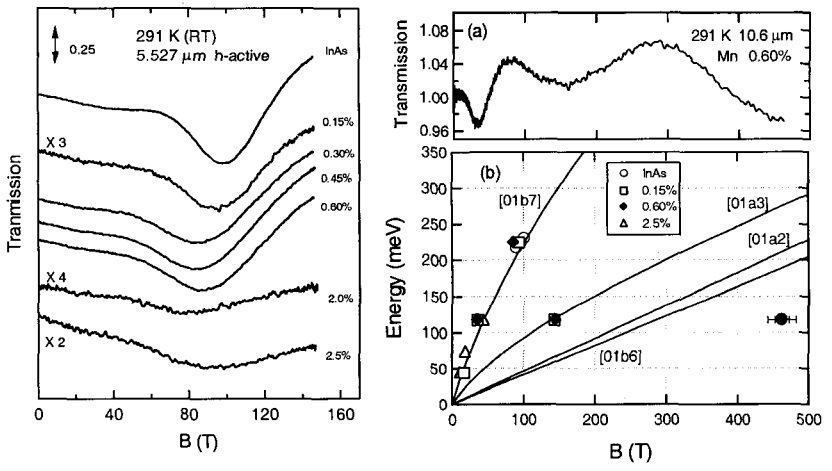

Figure 4: (left). Cyclotron resonance traces for p-type $In_{1-x}Mn_xAs$ with different x.
Figure 5: (right) (a) Cyclotron resonance trace for $In_{1-x}Mn_xAs$ with x = 0.006 up to 500 T. (b) Resonant photon energy as a function of magnetic field. Theoretical lines calculated by the ***kp*** theory are also shown for comparison.

that the cyclotron mass decreases with increasing x to the contrary to the case of CdMnTe. This is due to the decrease of the band gap with increasing x. When x exceeds 0.02, the mobility deterioration is such that peak is prominently broadened. When we lowered the temperature to 30-40 K, a large decrease of the effective mass was observed, which is contrary to the case of InAs. Figure 5(a) shows a CR trace in a very high field up to about 500 T generated by electromagnetic flux compression. Three large absorption peaks are observed. The peak at the lowest field corresponds to the light hole transition (same as those in Fig. 4). The peak at around 140 T is the transition between the light hole levels with an opposite spin. The absence of this peak in lower fields is probably due to the fact that the Fermi level is above the final states. The peak at the highest field is likely to arise from heavy holes. In Fig. 5(b), we demonstrate the magnetic field dependence of the resonant photon energy. Solid lines are the theoretical lines calculated from the ***k·p*** theory. The agreement between theory and the experimental data is excellent for the light holes but there is a considerable discrepancy for the heavy holes. The reason of the discrepancy is not clear at present.

This work was done in collaboration with a number of different groups who contributed through the supply of the samples and valuable discussion. We are indebted to Prof. G. Bauer and Prof. G. Springholz for the work on PbSe quantum

dots, to Prof. K. Takita, Prof. S. Kuroda for the work on CdMnTe, and Prof. S. Katsumoto, Prof. H. Munekata and Prof. J. Kono for the work on InMnAs.

References

1. N. Miura *et al., J. Phys.: Condens. Matter* **11**, 5917–5928 (1999).
2. N. Miura *et al., Physica B* **294-295**, 562-567 (2001).
3. N. Miura *et al.*, This Proceedings.
4. N. Miura *et al., Phys. Rev. B* **55**, 13598-13604 (1997).
5. H. Arimoto *et al.*, J. *Phys. Rev.* B **58**, 4560-4565 (1998).
6. H. Arimoto N. Miura and R. A. Stradling, *Proc. 25th Int. Conf. Phys. Semiconductors*, (Osaka, 2000) eds. N. Miura and T. Ando (Springer-Verlag, 2001) 899-900 (2001).
7. T. Ikaida *et al., Proc. 25th Int. Conf. Phys. Semiconductors*, (Osaka, 2000) eds. N. Miura and T. Ando (Springer-Verlag, 2001) 1057-1058 (2001).
8. Y. H. Matsuda *et al., Proc. 25th Int. Conf. Phys. Semiconductors*, (Osaka, 2000) eds. N. Miura T. and Ando (Springer-Verlag, 2001) 246-247(2001).
9. G. Springholz *et al., Science* **282**, 734 (1998).
10. J. Kossut J., in *Semiconductors and Semimetals* **25** eds. J. K. Furdyna and J. Kossut (Academic Press, **5**, 183-227(1988)).
11. P. M. Hui *et al., Phys. Rev.* B **40**, 12346-12352 (1989).
12. Y. H. Matsuda *et al.,* submitted to *Phys. Rev. B*

FEASIBILITY STUDIES FOR THE IMPLEMENTATION OF NUCLEAR MAGNETIC RESONANCE IN A 25T HYBRID MAGNET

P. J. M. VAN BENTUM,[1] and J. C. MAAN,[1]
J. W. M. VAN OS,[2] and A. P. M. KENTGENS,[2]
[1]*High Field Magnet Laboratory and Research Institute for Materials, University of Nijmegen, Roernooiveld 1, NL-6525 ED Nijmegen, the Netherlands*
[2]*Department of Physical Chemistry and NSR-RIM Center, University of Nijmegen, Toernooiveld 1, NL-6525 ED Nijmegen, the Netherlands*

As an exploratory study for NMR experiments in the future 20 MW Nijmegen high field magnet laboratory, the possibilities of field stabilization and field gradient compensation in a 25 T hybrid magnet in the present installation were evaluated. High frequency field fluctuations from the power supply can be compensated to better than 10^{-3} ppm in the 10 Hz-10 kHz range using a computer controlled feedback system. Field mapping by ^{2}H magnetic resonance using a homebuilt device not only showed that there are substantial axial but also strong radial field gradients. It can be shown that for any cylindrical multicoil Bitter magnet the main components of these gradients can be compensated with simple ferromagnetic inserts. In this way we achieved a linewidth under 5 ppm in 1 mm^3 without further shimming or optimization. The low frequency drift of the field due to instabilities of the present power supply and the effects of temperature fluctuations of the coil are determined by simultaneous acquisition of an in-situ deuterium reference signal together with the signal of interest. This allows for a full compensation of the field fluctuations by deconvolution techniques. We will report preliminary NMR results on solid ^{27}Al samples in fields up to 25 T.

World Scientific
www.worldscientific.com
4915 hc

ISBN 981-02-4896-2
9 789810 248963